

Proximity-based Therapeutic Modalities for Precise Modulation of Histone Deacetylases

Dissertation

zur

Erlangung des Doktorgrades (Dr. rer. nat.)

der

Mathematisch-Naturwissenschaftlichen Fakultät

der

Rheinischen Friedrich-Wilhelms-Universität Bonn

vorgelegt von

Tao Sun

aus

Wuhu (China)

Bonn, 2025

Angefertigt mit Genehmigung der Mathematisch-Naturwissenschaftlichen Fakultät der Rheinischen Friedrich-Wilhelms-Universität Bonn

Gutachter und Betreuer: Prof. Dr. Finn K. Hansen

Gutachter: Prof. Dr. Michael Gütschow

Tag der Promotion: 09.10.2025

Erscheinungsjahr: 2025

Table of Contents

Eidesstattliche Erklärung	I
List of Abbreviations	III
Chapter 1. Introduction	1
1.1 Epigenetics and Epigenetic Modifications	1
1.2 Histone Deacetylases (HDACs)	4
1.2.1 HDAC1, HDAC2, and HDAC3	5
1.2.2 HDAC4	6
1.2.3 HDAC6	7
1.2.4 SIRT6	8
1.3 HDACs-based Drug Discovery	9
1.3.1 HDAC Inhibitors	9
1.3.2 Hybrid HDAC Inhibitors	11
1.3.3 HDAC Proteolysis-targeting Chimeras (HDAC PROTACs)	13
1.4 Innovative Proximity-based Therapeutic Modalities	18
1.4.1 Molecular Glue Degraders	19
1.4.2 Bypassing E3 ligase Targeting Chimeras (BYETACs)	19
1.4.3 Deubiquitinase-targeting Chimeras (DUBTACs)	20
1.5 Scope of Thesis	22
1.6 References	25
Chapter 2. DCAF16-based Covalent Molecular Glues for Targe Degradation of Histone Deacetylases	
2.1 Publication Summary	35
2.2 Author Contribution	37
2.3 References	38
Chapter 3. Targeted Degradation of Histone Deacetylases <i>via</i> Bypassi Targeting Chimeras (BYETACs)	
3.1 Publication Summary	43
3.2 Author Contribution	45
3.3 References	46
Chapter 4. Deubiquitinase-targeting Chimeras (DUBTACs) for Stabilization of SIRT6	

4.1 Background	49
4.1.1 Discovery of Deubiquitinase-targeting Chimeras (DUBTACs)	49
4.1.2 SIRT6 Activators	52
4.2 Design, Synthesis and Evaluation of SIRT6 DUBTACs	54
4.2.1 Rational Design of SIRT6 DUBTACs	54
4.2.2 Synthesis of SIRT6 DUBTACs	55
4.2.3 SIRT6 Stabilization by OTUB1-recruiting DUBTACs	61
4.2.4 Further Testing of SIRT6 DUBTACs	63
4.3 Conclusion and Outlook	66
4.4. Experimental Section	67
4.4.1 General Information	67
4.4.2 Synthesis	68
4.4.3 Cell Culture	91
4.4.4 Western Blot Assay	92
4.4.5 CellTiter-Glo® Cell Viability Assay	92
4.5 References	94
Chapter 5. Summary	97
Chapter 6. Appendix	103
6.1 Appendix I. Publication I: DCAF16-based Covalent Molecular C Targeted Protein Degradation of Histone Deacetylases	
6.2 Appendix II. Publication II: Targeted Degradation of Histone Deacety Bypassing E3 Ligase Targeting Chimeras (BYETACs)	
6.3 Appendix III. Supporting Information of chapter 4 "Deubiquitinase-Chimeras (DUBTACs) for Targeted Stabilization of SIRT6	
Acknowledgments	109

Eidesstattliche Erklärung

Die vorliegende Arbeit wurde im Zeitraum von Oktober 2021 bis Juli 2025 unter der Leitung von Herrn Prof. Dr. Finn K. Hansen am Pharmazeutischen Institut der Rheinischen Friedrich-Wilhelms-Universität Bonn angefertigt.

Ich versichere an Eides statt, dass ich die vorliegende Dissertation "Proximity-based Therapeutic Modalities for Precise Modulation of Histone Deacetylases" selbstständig, ohne unzulässige Hilfe Dritter und ohne Benutzung anderer als der von mir angegebenen Hilfsmittel angefertigt habe. Alle aus fremden Quellen direkt oder indirekt übernommenen Gedanken wurden in der vorliegenden Arbeit als solche kenntlich gemacht. Weiterhin versichere ich, dass ich nicht die Hilfe eines Promotionsberaters in Anspruch genommen habe und, dass Dritte von mir weder unmittelbar noch mittelbar geldwerte Leistungen für Arbeiten erhalten haben, die im Zusammenhang mit dem Inhalt der vorgelegten Dissertation stehen. Ich versichere, dass die vorliegende Dissertation in gleicher oder in ähnlicher Form an keiner anderen wissenschaftlichen Einrichtung im In- oder Ausland zum Zwecke einer Promotion oder eines anderen Prüfungsverfahrens vorgelegt und veröffentlicht wurde. Ich habe bisher keine Promotionsversuche unternommen.

Ich bestätige die Richtigkeit der vorstehenden Erklärung und versichere, dass ich nach bestem Wissen die Wahrheit erklärt und nichts verschwiegen habe.

	<u> </u>
(Ort, Datum)	(Unterschrift)
	Tao Sun

List of Abbreviations

A

ATP: Adenosine triphosphate

ADP: Adenosine diphosphate

AR: Androgen receptor

B

BYETAC(s): Bypassing E3 ligase targeting chimera(s)

 \mathbf{C}

CRBN: Cereblon

CNS: Central nervous system

CFTR: Cystic fibrosis transmembrane conductance regulator

cGAS: Cyclic GMP-AMP synthase

CTCL: Cutaneous T-cell lymphoma

D

DNA: Deoxyribonucleic acid

DMB: Dynein motor binding

DUBTAC(s): Deubiquitinase-targeting Chimera(s)

DCAF16: DDB1- and CUL4-associated factor 16

DUB: Deubiquitinase

CDCl₃: Deuterated chloroform

DMSO-*d*₆: Deuterated dimethyl sulfoxide

DAD: Diode-array detector

F

FDA: Food And Drug Administration

H

HAT(s): Histone acetyltransferase(s)

HDAC(s): Histone deacetylase(s)

HSP90: Heat shock protein 90

HCC: Human hepatocellular carcinoma

HPLC: High performance liquid chromatography

\mathbf{M}

MG(s): Molecular glue(s)

MEF2: Myocyte enhancer factor-2

mRNA: Messenger RNA

N

NF-κB: Nuclear factor-κB

NAD⁺: Nicotinamide adenine dinucleotide

NLS: Nuclear localization sequence

NES: Nuclear export sequence

NCS: N-Chlorosuccinimide

NMR: Nuclear magnetic resonance spectroscopy

P

PTM(s): Post-translational modification(s)

PROTAC(s): Proteolysis-targeting chimera(s)

PTCL: Peripheral T-cell lymphoma

PEG: Polyethyleneglycol

POI: Protein of interest

PSA: Polar surface area

ppm: Parts per million

R

RNA: Ribonucleic acid

Rb: Retinoblastoma

ROS: Reactive oxygen species

\mathbf{T}

TSG(s): Tumor suppressor gene(s)

TPS: Targeted protein stabilization

TPD: Targeted protein degradation

TLC: Thin-layer chromatography

U

UPS: Ubiquitin-proteasome system

Ub: Ubiquitin

USP14: Ubiquitin-specific protease 14

UTX: Ubiquitously transcribed tetratricopeptide repeat X chromosome

V

VHL: Von Hippel-Lindau

 \mathbf{Z}

ZBG(s): Zinc-binding group(s)

ZnF-UBP: Zinc finger ubiquitin binding domain

Chapter 1. Introduction

1.1 Epigenetics and Epigenetic Modifications

Epigenetics, a pivotal discipline in modern biology, investigates heritable modifications in gene expression which occur independently of alterations in the primary DNA sequence.^[1] To elucidate the molecular mechanisms that govern cellular processes and the regulatory factors modulating gene activity states, a comprehensive exploration of epigenetic phenomena becomes imperative.^[2] The genetic blueprint of all organisms is encoded in nucleic acids, with deoxyribonucleic acid (DNA) serving as the hereditary archive, while ribonucleic acid (RNA) functions as the transcriptional intermediary. These macromolecules ultimately direct the synthesis of functional proteins and regulatory molecules.

Structurally, DNA polymers are composed of purine (adenine and guanine) and pyrimidine (cytosine and thymine) nucleobases, which are covalently linked to a deoxyribose sugar-phosphate backbone. Two complementary strands intertwine through specific base pairing to form the characteristic antiparallel double helix. [1] RNA differs from DNA in several key biochemical respects, notably the substitution of thymine with uracil and ribose for deoxyribose. The central dogma of molecular biology dictates that protein-coding genes are first transcribed into messenger RNA (mRNA), which subsequently orchestrates translation through the ribosomal biosynthesis of polypeptides. [1,3]

In eukaryotes, genomic DNA is compacted into chromatin structures, with the nucleosome representing the fundamental repeating unit. Each nucleosome contains approximately 146-147 base pairs of DNA wrapped around an octameric core of histone proteins.^[4] The nucleus harbors five major histone classes: the core histones (H2A, H2B, H3, and H4) that form the nucleosomal octamer, and the linker histone H1. The canonical nucleosome structure consists of a (H3-H4)₂ tetramer flanked by two H2A-H2B dimers (**Figure 1-1**).^[5] Unlike core histones, H1 primarily functions to stabilize higher-order chromatin folding through its

binding to linker DNA, thereby maintaining nucleosomal integrity.^[6] Although DNA sequences encode the complete genetic information from parental organisms, genetic alterations alone cannot fully explain numerous pathological conditions, such as cancer and neurodegenerative diseases.^[7,8] Emerging evidence demonstrates that epigenetic dysregulation can induce profound alterations in gene expression patterns and drive malignant cellular transformation.^[8,9]

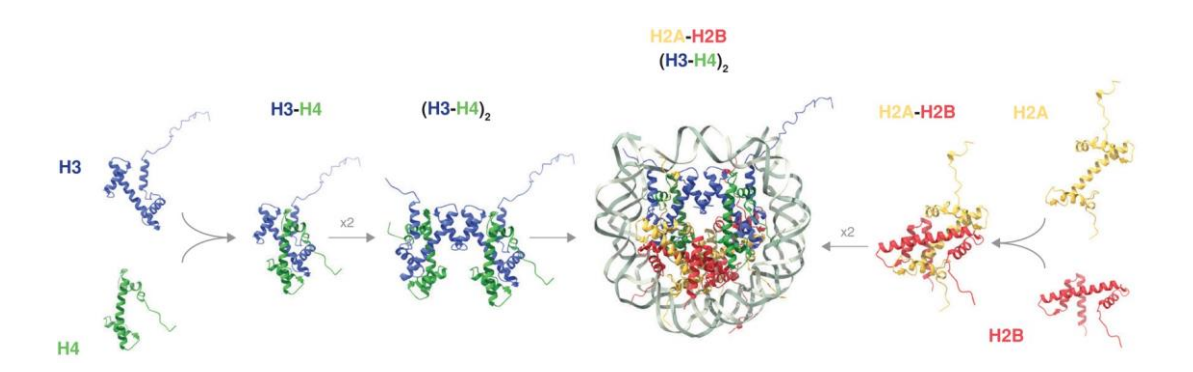


Figure 1-1. Histone–DNA complexes in eukaryote. Reprinted with permission from: Hocher A, Warnecke T. Nucleosomes at the Dawn of Eukaryotes. *Genome Biol Evol.* **2024**, *16*(3), evae029.^[5] Copyright 2024, The Author(s) 2024. Published by Oxford University Press on behalf of Society for Molecular Biology and Evolution.

Epigenetic modifications dynamically regulate gene expression without altering the underlying DNA sequence. These reversible mechanisms encompass DNA methylation, post-translational histone modifications (e.g., acetylation, methylation), and non-coding RNA-mediated regulation.^[2,4,8] A fundamental unifying feature of these processes is their ability to remodel chromatin architecture, thereby modulating DNA accessibility for the transcriptional machinery.^[1]

The eukaryotic genome employs chromatin architecture as a fundamental regulatory mechanism for controlling transcription. This nucleoprotein complex, which orchestrates genomic compaction within the nucleus and exhibits structural plasticity that directly correlates with functional demands. There are two predominant chromatin states that exist in a dynamic equilibrium: (1)

transcriptionally silent heterochromatin with condensed nucleosomal packing, and (2) transcriptionally active euchromatin characterized by decompacted chromatin fibers. This interconversion between the two states represents a crucial epigenetic switch that governs gene expression profiles and cellular homeostasis.^[10]

When chromatin transitions to a transcriptionally permissive euchromatic state, it undergoes structural decompaction that significantly enhances DNA accessibility for transcriptional regulators. In this open configuration, RNA polymerase II and associated basal transcription factors demonstrate an increased binding affinity to core promoter elements because diminished nucleosomal density reduces the steric constraints imposed by histone octamers. This chromatin accessibility is dynamically regulated through two synergistic mechanisms: (1) adenosine triphosphate (ATP)-dependent chromatin remodeling complexes that mediate nucleosome sliding or ejection, and (2) post-translational histone modifications (e.g., H3K27ac and H4K16ac) that attenuate histone-DNA binding affinity. Collectively, these epigenetic modifications establish a permissive chromatin landscape that facilitates unimpeded progression of the transcription elongation complex through previously nucleosome-occupied regions This enables precise spatiotemporal control of gene expression networks, which is critical for cellular homeostasis.^[1]

This accessible chromatin state is established through a sophisticated repertoire of post-translational modifications (PTMs) that predominantly occur on conserved residues within the *N*-terminal tails of core histones (H2A, H2B, H3, and H4). These biochemically distinct modifications collectively modulate histone charge distribution and steric properties, including lysine acetylation, arginine/lysine methylation, serine/threonine phosphorylation, and lysine ubiquitination. These alterations effectively reduce electrostatic interactions between histone basic residues and DNA phosphate backbones, thereby destabilizing nucleosomal architecture.^[5,9,11,12]

1.2 Histone Deacetylases (HDACs)

The dynamic equilibrium of histone acetylation is precisely regulated by opposing enzymatic activities. Histone acetyltransferases (HATs) catalyze the transfer of acetyl groups to lysine ε-amino residues on histone tails, while histone deacetylases (HDACs) mediate their removal. [13-15] This reversible modification system serves as a critical epigenetic switch. HDACs play particularly pivotal roles in modulating cellular signaling cascades and maintaining homeostatic balance. Dysregulation of HDAC activity has been implicated in various pathological conditions, including neurodegeneration (e.g., Alzheimer's disease *via* HDAC2 overexpression), chronic inflammation (e.g., rheumatoid arthritis through HDAC3-mediated NF-κB activation), metabolic disorders (e.g., type 2 diabetes involving HDAC4/5), and oncogenesis. [15] In cancer biology, specific HDAC isoforms (particularly HDAC1-3) are frequently overexpressed, leading to epigenetic silencing of tumor suppressor genes (e.g., p21 and PTEN) and the activation of oncogenic pathways. [8] Consequently, HDACs are regarded as important regulators of transcription and have been identified as valuable targets in cancer therapy. [8,15]

The human genome encodes 18 HDAC isoforms that are phylogenetically classified into two distinct families based on their catalytic mechanisms and cofactor requirements. The classical zinc-dependent HDAC family (HDAC1-11) comprises 11 metalloenzymes that utilize a conserved zinc ion in their active site to facilitate amide bond hydrolysis through water-mediated nucleophilic attack. [16,18] In contrast, the seven sirtuin (SIRT1-7) isoforms represent a separate class of nicotinamide adenine dinucleotide (NAD)⁺-dependent deacetylases that catalyze a unique reaction mechanism involving the transfer of the acyl group to adenosine diphosphate (ADP)-ribose, resulting in the formation of 2'-O-acetyl-ADP-ribose as a byproduct. [17,18]

The human HDACs are further classified into four major groups based on sequence homology and subcellular localization: Class I (HDAC1, 2, 3, 8), Class IIa (HDAC4, 5, 7, 9), Class IIb (HDAC6, 10), Class III (SIRT1–7), and Class IV

(HDAC11) (**Figure 1-2**).^[18]

While HDACs are named for their canonical role in removing acetyl groups from lysine residues, emerging research demonstrates that many HDAC isoforms also catalyze the hydrolysis of diverse acyl modifications. This functional versatility extends to post-translational modifications such as succinylation, malonylation, crotonylation, and long-chain fatty acylation, significantly expanding their regulatory roles in cellular physiology.^[19]

Given the scope of this thesis, the following subsections will primarily focus on introducing HDAC1-4, HDAC6 and SIRT6.

Class	Isoform	localisation	Amino acids
ı	HDAC1	nucleus	481
	HDAC2	nucleus	488
	HDAC3	nucleus	428
	HDAC8	nucleus, cytoplasm	377
	HDAC4	nucleus, cytoplasm	1084
lla	HDAC5	nucleus, cytoplasm	1121
IIa	HDAC7	nucleus, cytoplasm	952
	HDAC9	nucleus, cytoplasm	1011
IIb	HDAC6	cytoplasm	1215
	HDAC10	cytoplasm	669
	SIRT1	nucleus, cytoplasm	747
	SIRT2	nucleus	389
	SIRT3	mitochodria	399
III	SIRT4	mitochodria	314
	SIRT5	mitochodria	310
	SIRT6	nucleus	355
	SIRT7	nucleus	400
IV	HDAC11	nucleus, cytoplasm	347

Figure 1-2. The classification of HDACs. Adapted in a modified version from Huang M et *al*. 2019.^[18]

1.2.1 HDAC1, HDAC2, and HDAC3

Extensive research has documented HDAC mutations and dysregulated expression patterns linked to tumorigenesis.^[20,21] Notably, HDAC1, 2, and 3 are overexpressed in aggressive malignancies including gastric, esophageal, colorectal, and breast cancers.^[22] Class I HDACs are particularly compelling targets due to their ability to epigenetically silence tumor suppressor genes (TSGs) and associated

proteins.^[23] One key example is p53, which is a major TSG substrate of HDAC1. The MDM2-HDAC1 complex orchestrates p53 deacetylation and subsequent degradation. HDAC1 overexpression also drives TSG suppression, including p53 and von Hippel Lindau (VHL), as well as tumor angiogenesis.

Class I HDACs further promote oncogenesis by downregulating cyclin-dependent kinase inhibitors (e.g., p21/WAF1, p27/KIP1), which normally enforce G2 cell cycle arrest. HDAC2 knockdown studies demonstrated restored acetylation and reactivation of retinoblastoma (Rb)-regulated genes. The Rb-E2F axis, a critical cell cycle checkpoint, is functionally impaired by HDAC recruitment to E2F-responsive promoters, leading to direct or indirect suppression of these transcription factors (**Figure 1-3**).^[24]

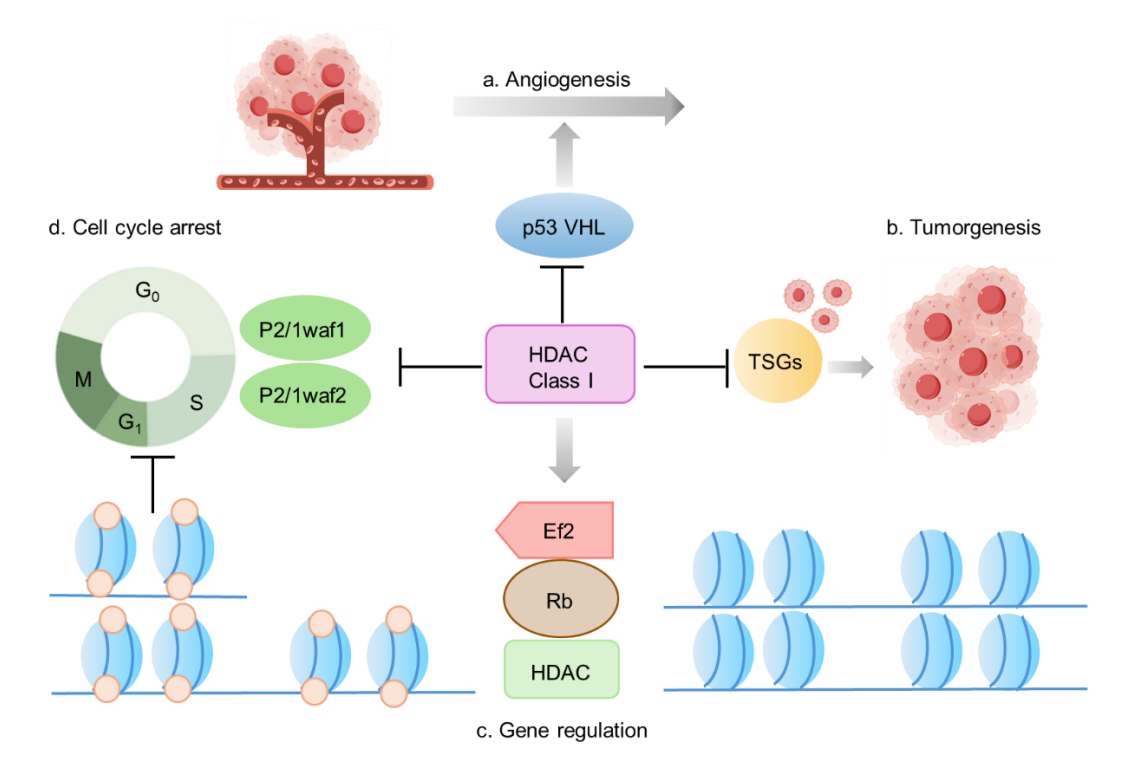


Figure 1-3. The role of class I HDACs in cancer progression. Adapted in a modified version from Huang Z et *al.* 2024.^[25]

1.2.2 HDAC4

Intriguingly, HDAC4 lacks intrinsic enzymatic activity when isolated. Instead, it functions by forming transcriptional repression complexes with transcription/non-

transcription factors to silence target genes.^[26] Structurally, HDAC4 contains a nuclear localization sequence (NLS) and a nuclear export sequence (NES), which enable nucleocytoplasmic shuttling.^[27] Emerging evidence suggests that HDAC4 may act as an epigenetic reader due to its low catalytic activity; however, this role remains underexplored. Beyond histones, HDAC4 interacts with non-histone proteins, such as myocyte enhancer factor-2 (MEF2), to suppress gene expression by occluding promoter regions.^[28-30]

1.2.3 HDAC6

HDAC6, the largest HDAC enzyme, is structurally unique in possessing two catalytic deacetylase domains (CD1 and CD2) with similar amino acid sequences and three-dimensional architecture. [31] Although the two domains exhibit structural homology, the CD2 serves as the primary catalytic center with a significantly broader substrate specificity than CD1. [32] Beyond its catalytic domains, HDAC6 contains specialized functional regions including a dynein motor binding (DMB) domain that connects CD1 and CD2, a NES that maintains cytoplasmic localization, an SE14 tetrapeptide motif that anchors the protein in the cytoplasm, and a C-terminal zinc finger ubiquitin-binding domain (ZnF-UBP) that recognizes both mono- and polyubiquitinated proteins.

The functional diversity of HDAC6 stems from this unique domain architecture. Its catalytic domains primarily mediate the deacetylation of key cytoplasmic substrates including α -tubulin, cortactin, and heat shock protein 90 (HSP90).^[31] These substrate interactions are critical for HDAC6's role in regulating cellular motility, protein homeostasis, pathways. The and stress response pathophysiological importance of HDAC6 is evident by its involvement in diverse disease states, ranging from enhanced tumor invasiveness in cancer to neurodegenerative processes in Alzheimer's and Parkinson's diseases, as well as fibrotic disorders and chronic inflammatory conditions.[33]

1.2.4 SIRT6

SIRT6 is a ubiquitously expressed, NAD⁺-dependent class III HDAC that serves as a critical regulator of diverse physiological processes including genomic stability, metabolic homeostasis, and inflammatory signaling.^[34-37] Its therapeutic potential is exemplified by the suppression of NF-κB-mediated inflammatory responses and protection against hypoxia-induced oxidative damage by scavenging reactive oxygen species (ROS). Emerging evidence positions SIRT6 as a potent tumor suppressor, with frequent downregulation observed across multiple malignancies. Preclinical studies using SIRT6 knockout models demonstrate that genetic ablation induces lethal metabolic dysregulation, while clinical data reveal improved prognosis in cancer patients with preserved SIRT6 expression.^[38-41] These findings strongly support the therapeutic rationale for the pharmacological activation of SIRT6 as a novel class of anticancer agents.

1.3 HDAC-based Drug Discovery

As previously discussed, the pharmacological modulation of HDAC expression and activity has profound effects on key oncogenic pathways across multiple cancer types. This compelling biological rationale has firmly established HDACs as clinically validated therapeutic targets in oncology. To date, multiple HDAC inhibitors have gained regulatory approval for cancer treatment, and there is an expanding pipeline of investigational agents in clinical development. The field continues to advance through global drug discovery efforts focused on next-generation HDAC-targeting strategies. These strategies include the rational design of dual/multi-target HDAC inhibitors and the development of novel HDAC proteolysis-targeting chimeras (HDAC PROTACs). [43,44]

1.3.1 HDAC Inhibitors

In October 2006, the Food And Drug Administration (FDA) approved vorinostat as the first HDAC inhibitor for the treatment of rare cutaneous T-cell lymphoma. Subsequently, romidepsin, belinostat and panobinostat have also received FDA approval for several cancers, including cutaneous T-cell lymphoma (CTCL), peripheral T-cell lymphoma (PTCL), and multiple myeloma. Additionally, the class I HDAC-selective inhibitor tucidinostat was approved in China for the treatment of relapsed or refractory PTCL and hormone receptor-positive breast cancer in combination with exemestane. The majority of these inhibitors have been approved for the treatment of hematological malignancies. Notably, givinostat gained approval in 2024 as the first HDAC inhibitor indicated for Duchenne muscular dystrophy. (**Figure 1-4**).^[42,45]

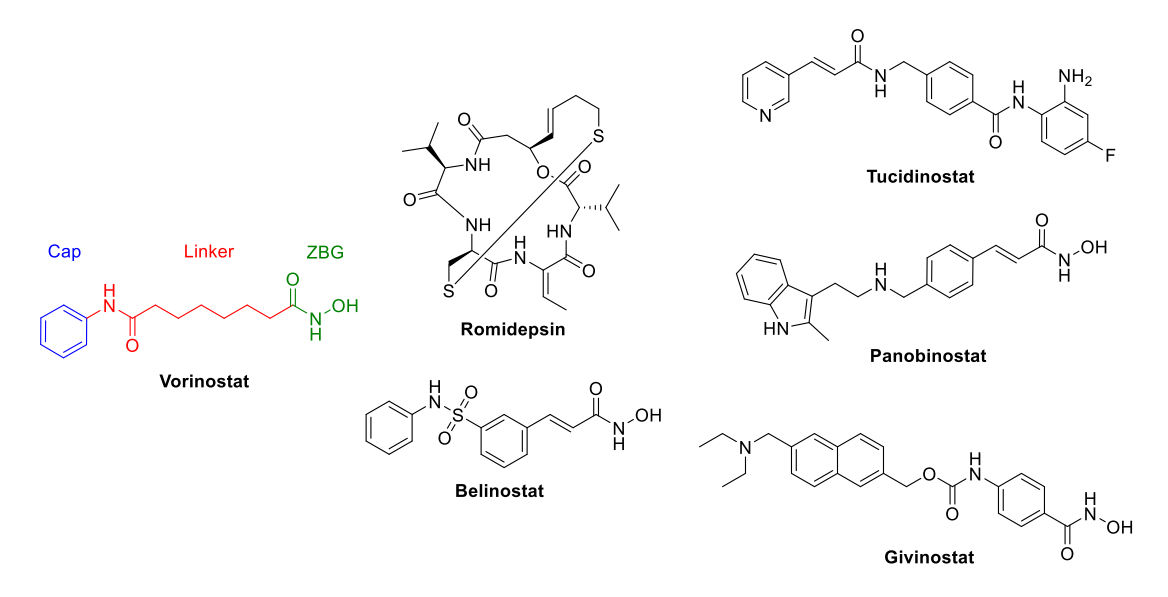


Figure 1-4. Six approved HDAC inhibitors and structures.

The prototypical HDAC inhibitor pharmacophore consists of three essential structural motifs (**Figure 1-4**): (1) a surface-binding cap group that interacts with residues surrounding the active site entrance; (2) a zinc-binding group (ZBG) that coordinates the catalytic zinc ion; (3) a hydrophobic linker spanning the channel of enzyme to connect these domains.^[42] Notably, the cap region demonstrates remarkable structural plasticity, enabling the development of chemically diverse HDAC inhibitors through rational modification of this moiety.

Beyond the currently approved HDAC inhibitors, an expanding pipeline of novel candidates is under clinical evaluation across multiple cancer indications. The analysis of available clinical data highlights several promising HDAC inhibitors currently in development (**Table 1-1**). [46,47] The robust clinical pipeline underscores the continued importance of HDACs as validated molecular targets in oncology drug discovery.

Table 1-1. Representative examples of clinical trials conducted with HDAC inhibitors.

Compd	Structure	Organization	Indication	Status
tefinostat	THE THE PART OF TH	GlaxoSmithKline	hepatocellular carcinoma	phase 1/2, no. 02759601
pracinostat	N N N N N N N N N N N N N N N N N N N	Helsinn, Menarini	acute myeloid leukemia, +azacitidine	phase 3, no. 03151408
abexinostat	N N N N N N N N N N N N N N N N N N N	Xynomics	follicular lymphoma; renal carcinoma, + pazopanib	phase 2, no. 03934567; phase 3, no. 03592472
entinostat	NH2	Syndax	breast cancer, +exemestane; renal carcinoma, +IL-2	phase 3, no. 02115282 and no. 03538171; phase 2, no. 03501381
domatinostat	N NH2	4SC	GI cancers, +avelumab	phase 2, no. 03812796

^{*}For combination trials, the other drugs involved are indicated with "+". The clinical trial is specified by the ClinicalTrials.gov NCT number.

1.3.2 Hybrid HDAC Inhibitors

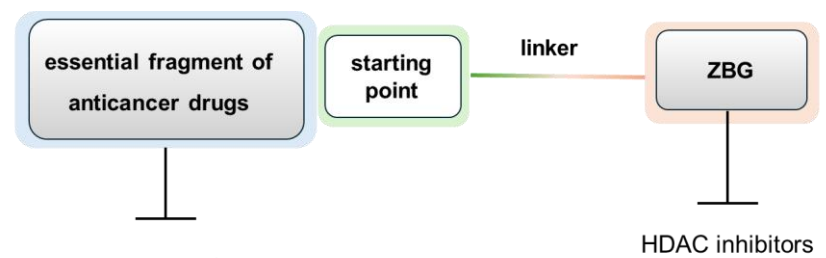
The pathogenesis of cancer involves intricate molecular mechanisms characterized by dynamic interactions among diverse enzymes, structural proteins, and transcription factors. Although single-target therapeutic agents are a mainstay of anticancer treatment, their efficacy is often limited by tumor cell adaptability. Malignant cells can quickly activate compensatory survival pathways, leading to acquired drug resistance and a diminished therapeutic response. [42,48]

One approach that can be employed to address this challenge is the combination drug strategy. However, while the conventional combination therapy strategy is theoretically sound, it presents significant clinical limitations including compromised patient adherence, unpredictable pharmacokinetic profiles, and undesirable drug-drug interactions that may diminish therapeutic outcomes.

Therefore, an innovative approach is the rational design of single molecular entities that incorporate multiple pharmacophores. These multitargeting agents offer three distinct advantages: (1) simultaneous modulation of interconnected oncogenic pathways; (2) improved pharmacokinetic properties compared to drug combinations; and (3) reduced developmental complexity and associated costs. [49,50] Such hybrid molecules are a promising frontier in anticancer drug development and merit extensive investigation of their therapeutic potential and clinical applicability. [51]

The established anticancer efficacy of HDAC inhibitors, coupled with their demonstrated capacity for synergistic activity with diverse therapeutic modalities, has motivated the development of hybrid HDAC inhibitors. These bifunctional agents incorporate two pharmacologically active moieties, representing a validated strategy for concurrent modulation of multiple oncogenic pathways.^[52-54]

The principal characteristics of the published hybrid HDAC inhibitors include: (1) a critical fragment that targets an additional cancer-related pathway and typically serves as the cap group of the hybrid HDAC inhibitor, (2) a suitable ZBGs, and (3) a linker that is crucial for influencing the activity against both targets. Following this design, these hybrids often demonstrate potent and balanced inhibitory activities against both HDACs and the complementary cancer target. The fragments of the cap groups in reported hybrid HDAC inhibitors are mainly from kinase inhibitors, cytotoxic compounds, hormone receptor modulators, epigenetic modulators, natural products, and other anticancer agents (**Figure 1-5**).^[42]



- 1. Kinase inhibitors; 2. Cytotoxic compounds;
- 3. Hormone receptor modulators; 4. Epigenetic modulators;
- 5. Natural products; 6. Other anticancer agents.

Figure 1-5. Structural features of hybrid HDAC inhibitors. Adapted in a modified version from

1.3.3 HDAC Proteolysis-targeting Chimeras (HDAC PROTACs)

Although significant progress has been made in targeted cancer therapeutics, the development of novel, well-tolerated, and effective agents remains a substantial challenge. A major limitation of current targeted therapies is the frequent emergence of resistance mechanisms that often compromise clinical outcomes. This therapeutic gap underscores the critical need for innovative treatment strategies with novel mechanisms of action. The proteolysis-targeting chimera (PROTAC) technology has recently emerged as a particularly promising approach, offering a paradigm-shifting strategy for targeted cancer therapy. Given the established clinical utility of HDAC inhibitors and the encouraging preliminary data from PROTAC clinical trials, the development of HDAC-targeting PROTACs represents a compelling therapeutic opportunity.

The human ubiquitin-proteasome system (UPS) is orchestrated by three classes of enzymes working in concert. The process initiates when the E1 ubiquitin-activating enzyme ATP-dependently activates ubiquitin (Ub), forming a high-energy thioester bond and transferring Ub to an E2 ubiquitin-conjugating enzyme. Subsequently, the Ub-charged E2 recruits a specific E3 ubiquitin ligase, which serves as a critical scaffold mediating substrate recognition and ubiquitin transfer. The E3 ligase binds its target protein through specialized substrate-binding domains, forming a transient but highly coordinated ternary E2-E3-substrate complex. The E3 ligase precisely positions the substrate and Ub-charged E2 to catalyze ubiquitin transfer onto the substrate. Polyubiquitinated substrates are then recognized by the 26S proteasome, leading to proteasomal degradation (**Figure 1-6**).^[44]

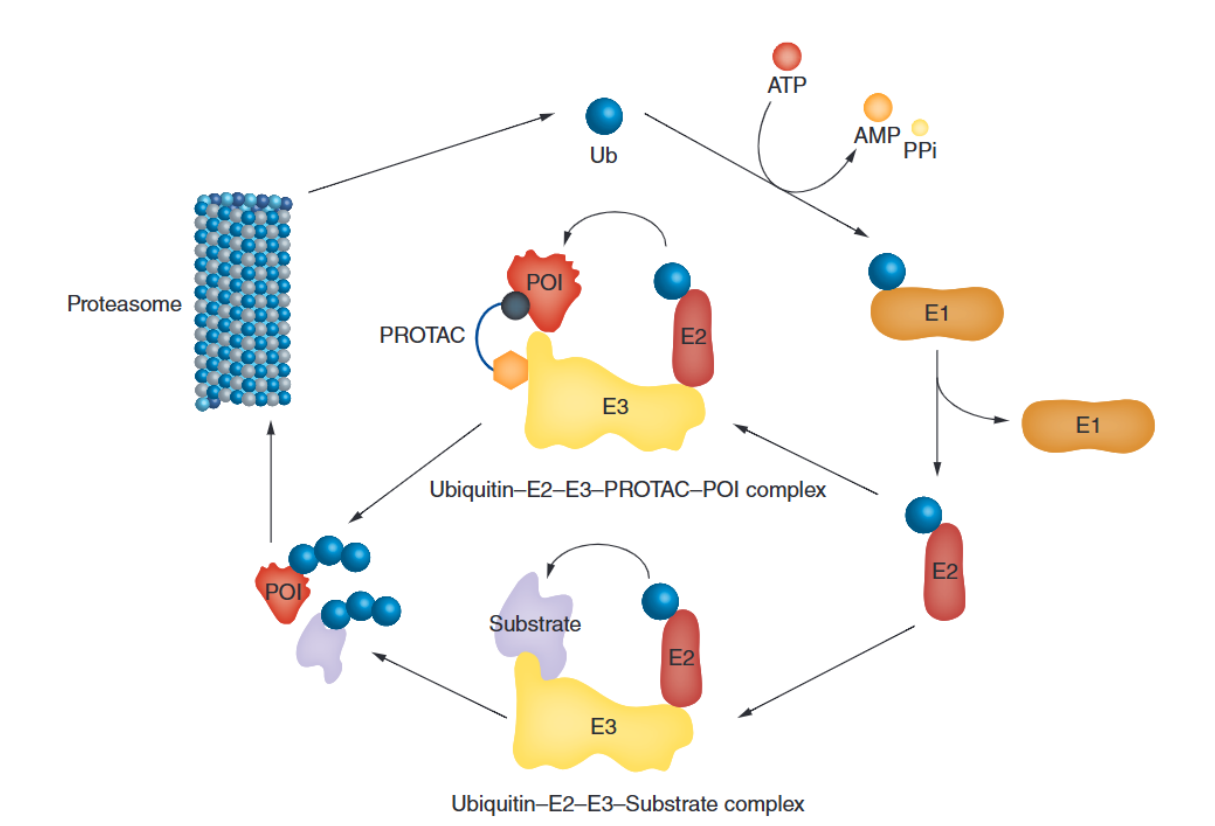


Figure 1-6. Schematic overview of the UPS and the general mechanism of PROTAC-mediated targeted protein degradation. Reprinted with permission from: Fischer F, Alves Avelar LA, Murray L, Kurz T. Designing HDAC-PROTACs: lessons learned so far. *Future Med Chem*. **2022**, *14*(3):143-166. © 2022 Heinrich-Heine-Universität Düsseldorf. [44]

The canonical architecture of HDAC-targeting PROTACs comprises three key components: an HDAC inhibitor warhead, a suitable linker, and an E3 ubiquitin ligase recruiting moiety (**Figure 1-7**).^[44] Current literature documents approximately 100 reported HDAC PROTACs,^[55,56] showcasing structural diversity through: (1) utilization of different E3 ligase ligands (cereblon (CRBN) and VHL being most prevalent), (2) selective targeting of various HDAC isoforms (including but not limited to HDAC1, 2, 3, 6, 8, and 10), and (3) incorporation of chemically diverse linker architectures. This structural versatility highlights the broad therapeutic potential of HDAC PROTACs in precision medicine applications.

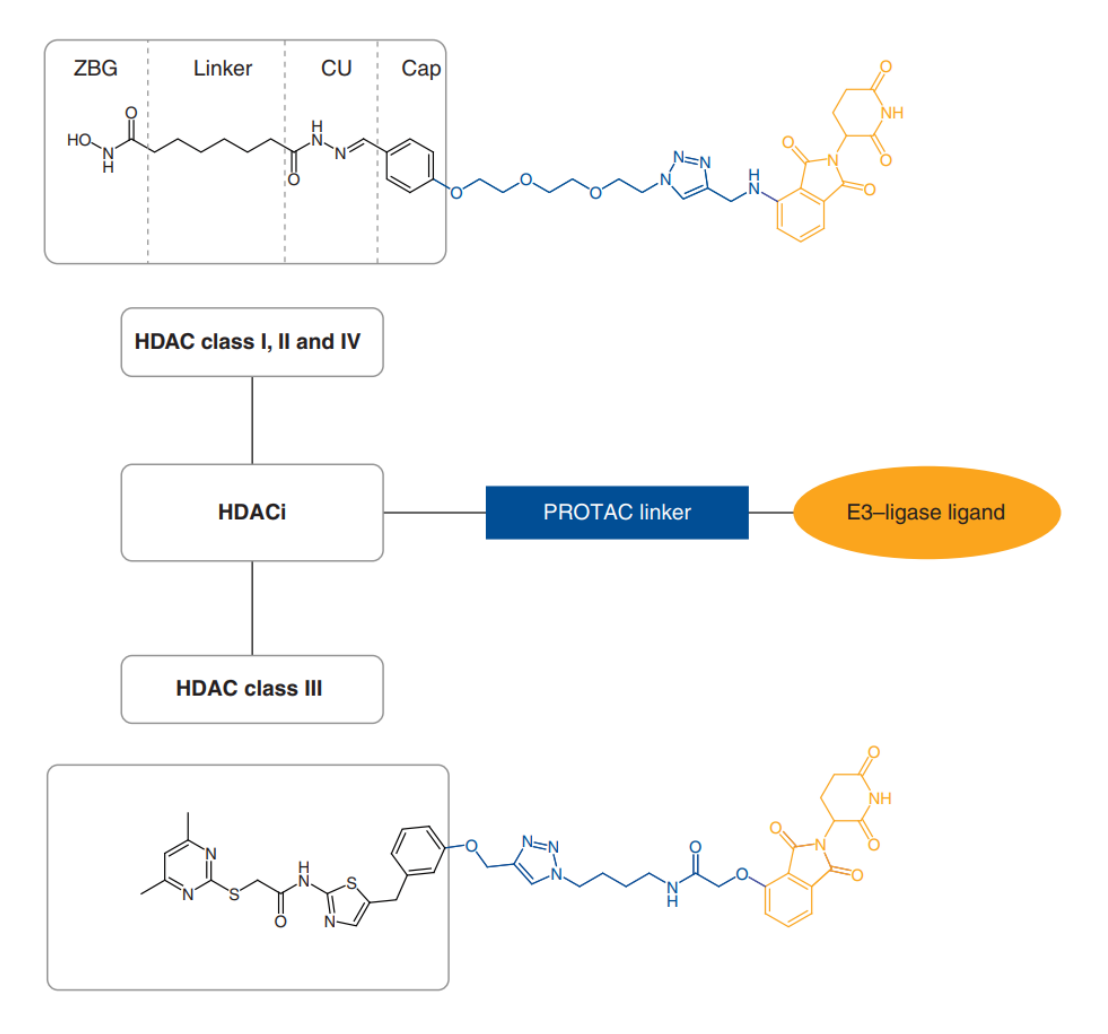


Figure 1-7. General design principle of an HDAC PROTAC. CU: Connecting unit. Reprinted with permission from: Fischer F, Alves Avelar LA, Murray L, Kurz T. Designing HDAC-PROTACs: lessons learned so far. *Future Med Chem.* **2022**, *14*(3):143-166. © 2022 Heinrich-Heine-Universität Düsseldorf. [44]

In recent years, there have been significant breakthroughs in the development of HDAC PROTACs and researchers have successfully developed potent and selective HDAC PROTAC degraders. These achievements validate the PROTAC strategy as a transformative approach in epigenetic drug discovery and highlight its ability to overcome the limitations associated with conventional HDAC inhibitors.

The canonical three-component architecture of PROTACs, comprising an E3 ligase recruiter, an HDAC ligand, and a carefully optimized linker, has been successfully applied in HDAC PROTAC design. Each structural element contributes critically to the PROTAC molecule's overall performance.

Firstly, the development of HDAC-targeting PROTACs has successfully leveraged several E3 ligases, most notably CRBN and VHL. The choice of E3 ligase ligand is critical because it affects degradation efficiency but also degradation selectivity, on-target specificity, stability, and potential off-tissue effects. Studies have shown that HDAC PROTACs that recruit CRBN or VHL exhibit superior degradation efficacy compared to IAP-based PROTACs. This is likely due to differences in ubiquitination kinetics, ternary complex stability, and the cellular abundance of the respective E3 ligases. [44,55] Notably, CRBN has proven highly effective in designing degraders against class I, II, and III HDACs. However, HDAC11, the sole class IV isoform, remains largely unexplored in PROTAC-mediated degradation, possibly due to structural constraints or insufficient ligand binding affinity. [44,55,57,58]

Secondly, the linker component serves as a critical structural determinant governing the degradation efficacy of HDAC-targeting PROTACs, with emerging evidence suggesting its additional role in modulating degradation selectivity. [44,55] While flexible alkyl chains and polyethyleneglycol (PEG)-based linkers dominate current designs due to their conformational adaptability, more constrained architectures incorporating alkyne, piperidine or piperazine moieties have demonstrated viability in CRBN-recruiting systems.^[57,59] The absence of universal design principles stems from the multifaceted nature of linker optimization, which must simultaneously accommodate the structural characteristics of both the target HDAC isoform and the recruited E3 ligase, while also maintaining a productive ternary complex. Even subtle modifications in linker length or composition can profoundly influence degradation outcomes, as demonstrated by structure-activity relationship studies showing that single-atom variations may dramatically alter proteasomal degradation efficiency. [60-62] This exquisite sensitivity underscores the necessity of optimizing linker parameters, including length, flexibility, and attachment vector, to achieve optimal engagement of both the HDAC active site and the E3 ligase ligand-binding domain. Recent structural biology insights reveal that ideal linkers must not only span the physical distance between binding moieties but also maintain appropriate solvent exposure of critical interaction surfaces while avoiding steric clashes in the ternary complex.^[44,55] The growing appreciation of linker-dependent selectivity profiles further complicates this design challenge because minor structural perturbations can affect degradation differently across HDAC family members. Consequently, PROTAC development requires systematic exploration of linker space through comprehensive structure-activity studies, with each target-ligase combination demanding customized optimization to achieve maximal degradation potency and selectivity.^[44]

Lastly, the study demonstrated that the selection of the HDAC-binding motif significantly influences the selectivity of HDAC-targeting PROTACs, yielding degraders with exquisite specificity for particular isoforms. Intriguingly, HDAC PROTACs derived from nonselective HDAC inhibitors exhibited surprising isoform selectivity, suggesting that HDAC inhibitory activity is not always a reliable predictor of degradation profiles.^[63,64] This discrepancy extends beyond the comparison between the PROTAC's degradation profile and the parent inhibitor's binding properties, it also applies to the inherent HDAC inhibitory activity of the PROTAC itself.

Collectively, PROTACs demonstrate distinct advantages over conventional occupancy-driven HDAC inhibitors due to their unique catalytic mechanism of action. These benefits include sustained pharmacological effects, reduced dosing requirements, and potentially improved safety profiles. Notably, the PROTAC technology can circumvent common cancer resistance mechanisms, such as target amplification or overexpression. These characteristics position HDAC-targeting PROTACs as promising therapeutic modalities for protein-driven pathologies.^[65]

1.4 Innovative Proximity-based Therapeutic Modalities

As discussed above, remarkable advances have been made in HDAC-targeted anticancer drug discovery in recent years. These advances include approved HDAC inhibitors, hybrid HDAC inhibitors, and HDAC PROTACs. These innovations underscore the considerable therapeutic potential of HDAC modulation in oncology. However, despite their potent antitumor efficacy, current HDAC-based therapies frequently induce dose-limiting toxicities, including hematological (thrombocytopenia, neutropenia), gastrointestinal (diarrhea, nausea, and vomiting), constitutional (fatigue), and cardiovascular adverse effects. [48,66,67] Such toxicities may cause severe and potentially irreversible harm to patients, ultimately compromising treatment adherence. These limitations largely stem from poor HDAC isoform selectivity. Therefore, a central challenge in HDAC-targeted anticancer drug development lies in achieving isoform-selective modulation to enable precise epigenetic control that maintains therapeutic potency while mitigating off-target toxicities.

The inherent limitations of conventional HDAC-based drugs necessitate alternative therapeutic strategies to address unmet clinical challenges. Proximity-based therapeutic modalities offer a transformative approach by fundamentally altering pharmacological intervention paradigms. Unlike traditional occupancy-driven inhibition, these engineered systems harness the endogenous cellular machinery to achieve catalytic and sustained protein modulation. [44,65]

While PROTACs represent a significant advancement among proximity-based therapeutic modalities by to some extent mitigating adverse effects and improving HDAC isoform selectivity, several pharmacological challenges still exist. To overcome these limitations, researchers are exploring innovative and advanced proximity-based strategies that could provide enhanced HDAC isoform selectivity, precise epigenetic modulation, and improved druggability compared to PROTACs.

1.4.1 Molecular Glue Degraders

Although targeted protein degradation represents a compelling therapeutic paradigm, the pharmacological profile of current PROTAC presents significant translational challenges. The need to incorporate both a target protein ligand and an E3 ligase recruiting element leads to heterobifunctional PROTACs with high molecular weight and polar surface area (PSA), typically in the range 800–1000 g/mol and ~200 Ų, respectively. These characteristics frequently impair membrane permeability, aqueous solubility, and ultimately, bioavailability, which limits central nervous system (CNS) penetration. Furthermore, linker optimization demands target-specific empirical refinement. Insufficient linker length can lead to steric clashes that compromise ternary complex formation, while excessive length can hinder productive ubiquitination proximity.^[68]

Similar to the mechanism of PROTACs, molecular glue degraders have emerged as a powerful therapeutic modalities that promote the degradation of disease-relevant proteins by inducing proximity between an E3 ubiquitin ligase and a neosubstrate. This interaction facilitates polyubiquitination and the subsequent proteasomal degradation of the target protein. Compared to heterobifunctional PROTACs, molecular glue degraders offer several potential advantages, including a lower molecular weight and more favorable drug-like properties. Additionally, they may better exploit shallow protein–protein interaction interfaces between E3 ligases and challenging targets that lack well-defined binding pockets.^[69,70] As a result, molecular glue degraders are considered highly promising modalities for the development of therapeutics targeting previously undruggable proteins.

1.4.2 Bypassing E3 ligase Targeting Chimeras (BYETACs)

To date, the application of PROTAC technology has largely been restricted to the use of E3 ligases from the cullin-RING family, particularly CRBN and VHL. While these ligases have demonstrated robust efficacy in multiple contexts, the overall effectiveness of PROTAC-mediated degradation is significantly influenced by the expression levels and subcellular localization of the E3 ligase in target tissues.

These constraints limit the diversity of proteins that can be ubiquitinated and subsequently degraded *via* the UPS, especially for targets that are poorly expressed or reside in cellular compartments where E3 ligases are absent or with low expression.

As a result, there is a growing interest in developing alternative targeted protein degradation strategies that bypass these limitations and expand the range of degradable proteins. One promising approach involves directly engaging subunits of the 26S proteasome to induce degradation, thereby eliminating the dependency on E3 ligase recruitment. This emerging class of degraders, referred to as bypassing E3 ligase targeting chimeras (BYETACs), offers a novel mechanism for degrading proteins that either lack accessible ubiquitination sites or are intrinsically resistant to E3 ligase-mediated recruitment. By directly tethering target proteins to the proteasome, BYETACs could potentially enable the degradation of previously undruggable targets and expand the therapeutic reach of TPD technologies.^[71]

1.4.3 Deubiquitinase-targeting Chimeras (DUBTACs)

Despite significant progress in the field of targeted protein degradation, the pharmacological stabilization of proteins through small molecule—mediated deubiquitination remains a largely untapped therapeutic strategy. To date, there are no clinically validated approaches in this area yet, and the concept remains underexplored in comparison to protein degradation platforms such as PROTACs and molecular glue degraders.

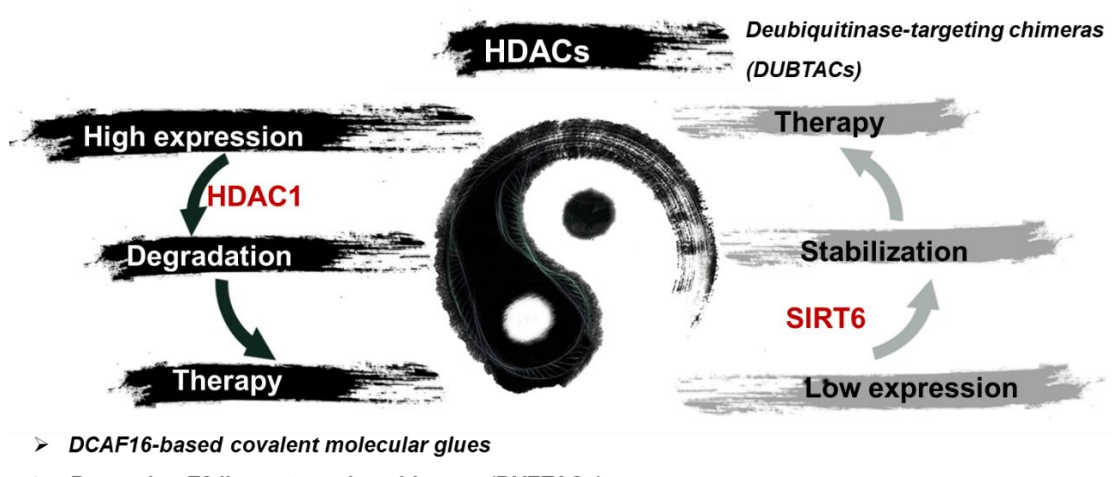
HDAC isoforms exhibit distinct expression profiles across different cancer types. Certain isoforms, such as HDAC1 and HDAC6, are frequently overexpressed in cancer cells, while others, including SIRT1 and SIRT6, usually have low expression levels. For highly expressed HDAC isoforms, targeted protein degradation can be achieved using PROTACs or molecular glue degraders. Conversely, strategies to induce targeted protein stabilization may be more appropriate for low-abundance HDAC isoforms.

To address this gap, deubiquitinase-targeting chimeras (DUBTACs) have been proposed as a novel class of heterobifunctional small molecules designed to selectively stabilize proteins. Similar to the structure of PROTACs, DUBTACs consist of two functional moieties connected *via* a tunable chemical linker: a ligand that recruits a specific deubiquitinase (DUB) and a ligand that binds to a targeted protein. By bringing a DUB into proximity with a ubiquitinated target protein, DUBTACs facilitate the removal of ubiquitin chains, thereby rescuing the protein from proteasomal degradation and restoring its steady-state levels.

This strategy holds particular promise for diseases driven by the loss or abnormal degradation of functional proteins. Examples include certain genetic disorders or neurodegenerative conditions, where enhancing protein stability could offer a therapeutic benefit. As such, DUBTACs represent a mechanistically distinct and potentially complementary approach to traditional TPD technologies, broadening the scope of druggable targets through protein stabilization rather than elimination.^[72]

1.5 Scope of Thesis

In light of recent advances in proximity-based therapeutic modalities and the fundamental challenges inherent in HDAC-based drug discovery, three innovative strategies were rationally designed to enable precise control over HDAC regulation (**Figure 1-8**). These novel approaches represent first-of-their-kind mechanisms for enhancing HDAC isoform selectivity, which could advance the clinical applicability of HDAC modulators in cancer treatment.



> Bypassing E3 ligase targeting chimeras (BYETACs)

Figure 1-8. Proximity-based therapeutic modalities to achieve precise modulation of HDACs.

Chapter 2 describes the rational design and development of novel DCAF16based covalent molecular glues. Molecular glue degraders demonstrate several therapeutic advantages over heterobifunctional PROTACs, particularly their lower molecular weight and enhanced drug-like characteristics that may translate to better pharmacokinetic profiles Recent findings have identified a vinylsulfonyl piperazine moiety as a DCAF16 binder that successfully induces the degradation of CDK4, the androgen receptor, BTK, SMARCA2/4, and BCR-ABL/c-ABL. [69] Therefore, it is worthwhile verify whether this covalent warhead could be repurposed for the potential HDAC degradation. In this project, the classical HDAC inhibitor vorinostat was chosen as the HDAC binding moiety, and the established covalent DCAF16 warhead will be connected to the cap group of vorinostat. In additiona selection of ZBGs will be incorporated for potentially

selective HDAC degradation. The synthesized molecular glues will undergo biological evaluation to assess their degradation efficacy and isoform selectivity. Additionally, their antiproliferative activity, HDAC inhibition, and ability to induce apoptosis will be evaluated in MM.1S cells.

Chapter 3 presents the development of heterobifunctional bypassing E3 ligase targeting chimeras (BYETACs) for selective HDAC degradation. A key regulatory checkpoint is mediated by USP14, a deubiquitinase that reversibly associates with the proteasome and selectively edits or removes ubiquitin chains from substrates. USP14 further interacts with RPN1, forming a stable complex that localizes it to the 26S proteasome's regulatory particle. USP14 actively trims polyubiquitin chains, thereby modulating substrate fate prior to proteasomal degradation. The treatment of cells with the USP14 inhibitor IU1 resulted in enhanced degradation of several proteasome substrates implicated in neurodegenerative diseases. Therefore, the USP14 inhibitor IU1 was identified as a direct proteasome recruiter. In this project, the conjugation of IU1 with an HDAC ligand vorinostat was intended to generate HDAC BYETACs. The synthesized compounds will be biologically evaluated for HDAC inhibitory activity, degradation efficiency, and isoform selectivity. Furthermore, their antiproliferative effects and apoptotic induction will be assessed in MM.1S cells.

Chapter 4 investigates a novel therapeutic strategy employing deubiquitinase-targeting chimeras (DUBTACs) for the targeted stabilization of SIRT6. Unlike PROTACs that mediate protein degradation, DUBTACs exploit the ubiquitin-proteasome system to promote protein deubiquitination and subsequent stabilization, offering potential therapeutic intervention for diseases driven by pathological protein destabilization.^[72] In this project, a novel class of heterobifunctional small molecules will be developed, so-called SIRT6 DUBTACs, which consist of a DUB OTUB1 recruiter and a SIRT6 activator. The synthesized SIRT6 DUBTACs will undergo biological evaluation to assess their stabilization

potency at different concentrations against SIRT6, and antiproliferative effects in MM.1S cells.

1.6 References

- (1) Hamilton JP. Epigenetics: principles and practice. *Dig Dis.* **2011**, *29*(2), 130-135. DOI: 10.1159/000323874.
- (2) Berger SL, Kouzarides T, Shiekhattar R, Shilatifard A. An operational definition of epigenetics. *Genes Dev.* **2009**, *23*(7), 781-783. DOI: 10.1101/gad.1787609.
- (3) Minchin S, Lodge J. Understanding biochemistry: structure and function of nucleic acids. *Essays Biochem.* **2019**, *63*(4), 433-456. DOI: 10.1042/EBC20180038.
- (4) Zhang Y, Wang H, Zhan Z, Gan L, Bai O. Mechanisms of HDACs in cancer development. Front Immunol. 2025, 16, 1529239. DOI: 10.3389/fimmu.2025.1529239.
- (5) Hocher A, Warnecke T. Nucleosomes at the Dawn of Eukaryotes. *Genome Biol Evol.* **2024**, *16*(3), evae029. DOI: 10.1093/gbe/evae029.
- (6) Izzo A, Kamieniarz K, Schneider R. The histone H1 family: specific members, specific functions? *Biol Chem.* **2008**, *389*(4), 333-343. DOI: 10.1515/BC.2008.037.
- Jackson M, Marks L, May GHW, Wilson JB. The genetic basis of disease. *Essays Biochem*.
 2018, 62(5), 643-723. DOI: 10.1042/EBC20170053.
- (8) Roche J, Bertrand P. Inside HDACs with more selective HDAC inhibitors. *Eur J Med Chem.* **2016**, *121*, 451-483. DOI: 10.1016/j.ejmech.2016.05.047.
- (9) Sharma S, Kelly TK, Jones PA. Epigenetics in cancer. *Carcinogenesis*. 2010, 31(1), 27-36.DOI: 10.1093/carcin/bgp220.
- (10) Liu J, Ali M, Zhou Q. Establishment and evolution of heterochromatin. *Ann N Y Acad Sci.* **2020**, *1476*(1), 59-77. DOI: 10.1111/nyas.14303.
- (11) Liu R, Wu J, Guo H, Yao W, Li S, Lu Y, Jia Y, Liang X, Tang J, Zhang H. Post-translational modifications of histones: Mechanisms, biological functions, and therapeutic targets. *MedComm.* **2023**, *4*(3), e292. DOI: 10.1002/mco2.292.
- (12) Rossetto D, Avvakumov N, Côté J. Histone phosphorylation: a chromatin modification involved in diverse nuclear events. *Epigenetics*. 2012, 7(10), 1098-1108. DOI: 10.4161/epi.21975.
- (13) Schäker-Hübner L, Haschemi R, Büch T, Kraft FB, Brumme B, Schöler A, Jenke R, Meiler J, Aigner A, Bendas G, Hansen FK. Balancing Histone Deacetylase (HDAC) Inhibition

- and Drug-likeness: Biological and Physicochemical Evaluation of Class I Selective HDAC Inhibitors. *ChemMedChem.* **2022**, *17*(9), e202100755. DOI: 10.1002/cmdc.202100755.
- (14) Ho TCS, Chan AHY, Ganesan A. Thirty Years of HDAC Inhibitors: 2020 Insight and Hindsight. *J Med Chem.* **2020**, *63*(21), 12460-12484. DOI: 10.1021/acs.jmedchem.0c00830.
- (15) Banerjee S, Adhikari N, Amin SA, Jha T. Histone deacetylase 8 (HDAC8) and its inhibitors with selectivity to other isoforms: An overview. Eur J Med Chem. 2019, 164, 214-240. DOI: 10.1016/j.ejmech.2018.12.039.
- (16) Porter NJ, Christianson DW. Structure, mechanism, and inhibition of the zinc-dependent histone deacetylases. *Curr Opin Struct Biol.* 2019, 59, 9-18. DOI: 10.1016/j.sbi.2019.01.004.
- (17) Jiang Y, Liu J, Chen D, Yan L, Zheng W. Sirtuin Inhibition: Strategies, Inhibitors, and Therapeutic Potential. *Trends Pharmacol Sci.* **2017**, *38*(5), 459-472. DOI: 10.1016/j.tips.2017.01.009.
- (18) Huang M, Zhang J, Yan C, Li X, Zhang J, Ling R. Small molecule HDAC inhibitors: Promising agents for breast cancer treatment. *Bioorg Chem.* **2019**, *91*, 103184. DOI: 10.1016/j.bioorg.2019.103184.
- (19) Yang XJ, Seto E. Lysine acetylation: codified crosstalk with other posttranslational modifications. *Mol Cell.* **2008**, *31*(4), 449-461. DOI:10.1016/j.molcel.2008.07.002.
- (20) Hayakawa T, Nakayama J. Physiological roles of class I HDAC complex and histone demethylase. *J Biomed Biotechnol.* **2011**, *2011*, 129383. DOI: 10.1155/2011/129383.
- (21) Das Gupta K, Shakespear MR, Iyer A, Fairlie DP, Sweet MJ. Histone deacetylases in monocyte/macrophage development, activation and metabolism: refining HDAC targets for inflammatory and infectious diseases. *Clin Transl Immunology*. 2016, 5(1), e62. DOI: 10.1038/cti.2015.46.
- (22) Glozak MA, Sengupta N, Zhang X, Seto E. Acetylation and deacetylation of non-histone proteins. *Gene.* **2005**, *363*, 15-23. DOI: 10.1016/j.gene.2005.09.010.
- (23) Sanaei M, Kavoosi F. Effect of Valproic Acid on the Class I Histone Deacetylase 1, 2 and 3, Tumor Suppressor Genes p21WAF1/CIP1 and p53, and Intrinsic Mitochondrial Apoptotic Pathway, Pro- (Bax, Bak, and Bim) and anti- (Bcl-2, Bcl-xL, and Mcl-1)

- Apoptotic Genes Expression, Cell Viability, and Apoptosis Induction in Hepatocellular Carcinoma HepG2 Cell Line. *Asian Pac J Cancer Prev.* **2021**, *22*(S1), 89-95. DOI: 10.31557/APJCP.2021.22.S1.89.
- (24) Ferreira R, Naguibneva I, Mathieu M, Ait-Si-Ali S, Robin P, Pritchard LL, Harel-Bellan A. Cell cycle-dependent recruitment of HDAC-1 correlates with deacetylation of histone H4 on an Rb-E2F target promoter. *EMBO Rep.* 2001, 2(9), 794-799. DOI: 10.1093/embo-reports/kve173.
- (25) Huang Z, Zeng L, Cheng B, Li D. Overview of class I HDAC modulators: Inhibitors and degraders. *Eur J Med Chem.* **2024**, *276*, 116696. DOI: 10.1016/j.ejmech.2024.116696.
- (26) Lee HA, Song MJ, Seok YM, Kang SH, Kim SY, Kim I. Histone deacetylase 3 and 4 complex stimulates the transcriptional activity of the mineralocorticoid receptor. *PLoS One.* 2015, 10(8), e0136801. DOI: 10.1371/journal.pone.0136801.
- (27) Grozinger CM, Schreiber SL. Regulation of histone deacetylase 4 and 5 and transcriptional activity by 14-3-3-dependent cellular localization. *Proc Natl Acad Sci U S A.* **2000**, *97*(14), 7835-7840. DOI: 10.1073/pnas.140199597.
- (28) Hohl M, Wagner M, Reil JC, Müller SA, Tauchnitz M, Zimmer AM, Lehmann LH, Thiel G, Böhm M, Backs J, Maack C. HDAC4 controls histone methylation in response to elevated cardiac load. *J Clin Invest.* **2013**, *123*(3), 1359-1370. DOI: 10.1172/JCI61084.
- (29) Zhang CL, McKinsey TA, Olson EN. Association of class II histone deacetylases with heterochromatin protein 1: potential role for histone methylation in control of muscle differentiation. *Mol Cell Biol.* 2002, 22(20), 7302-7312. DOI: 10.1128/MCB.22.20.7302-7312.2002.
- (30) Miska EA. HDAC4 deacetylase associates with and represses the MEF2 transcription factor. *EMBO J.* **1999**, *18*(18), 5099-5107. DOI: 10.1093/emboj/18.18.5099.
- (31) Hubbert C, Guardiola A, Shao R, Kawaguchi Y, Ito A, Nixon A, Yoshida M, Wang XF, Yao TP. HDAC6 is a microtubule-associated deacetylase. *Nature*. **2002**, *417*(6887), 455-458. DOI: 10.1038/417455a.
- (32) Hai Y, Christianson DW. Histone deacetylase 6 structure and molecular basis of catalysis and inhibition. *Nat Chem Biol.* **2016**, *12*(9), 741-747. DOI: 10.1038/nchembio.2134.
- (33) Asaad L, Pepperrell B, McErlean E, Furlong F. Regulation of HDAC6 Catalytic Activity

- in Cancer: The Role of Post-Translational Modifications and Protein-Protein Interactions. *Int J Mol Sci.* **2025**, *26*(3), 1274. DOI: 10.3390/ijms26031274.
- (34) Fiorentino F, Mai A, Rotili D. Emerging Therapeutic Potential of SIRT6 Modulators. *J Med Chem.* **2021**, *64*(14), 9732-9758. DOI: 10.1021/acs.jmedchem.1c00601.
- (35) Feldman JL, Baeza J, Denu JM. Activation of the protein deacetylase SIRT6 by long-chain fatty acids and widespread deacylation by mammalian sirtuins. *J Biol Chem.* **2013**, *288*(43), 31350-31356. DOI: 10.1074/jbc.C113.511261.
- (36) Tasselli L, Zheng W, Chua KF. SIRT6: Novel Mechanisms and Links to Aging and Disease. *Trends Endocrinol Metab.* **2017**, *28*(3), 168-185. DOI: 10.1016/j.tem.2016.10.002.
- (37) Michishita E, McCord RA, Berber E, Kioi M, Padilla-Nash H, Damian M, Cheung P, Kusumoto R, Kawahara TL, Barrett JC, Chang HY, Bohr VA, Ried T, Gozani O, Chua KF. SIRT6 is a histone H3 lysine 9 deacetylase that modulates telomeric chromatin. *Nature*. 2008, 452(7186), 492-496. DOI: 10.1038/nature06736.
- (38) Yang B, Zwaans BM, Eckersdorff M, Lombard DB. The sirtuin SIRT6 deacetylates H3 K56Ac in vivo to promote genomic stability. *Cell Cycle.* **2009**, *8*(16), 2662-2663. DOI: 10.4161/cc.8.16.9329.
- (39) Jiang H, Khan S, Wang Y, Charron G, He B, Sebastian C, Du J, Kim R, Ge E, Mostoslavsky R, Hang HC, Hao Q, Lin H. SIRT6 regulates TNF-α secretion through hydrolysis of long-chain fatty acyl lysine. *Nature.* **2013**, *496*(7443), 110-113. DOI: 10.1038/nature12038.
- (40) Fiorentino F, Carafa V, Favale G, Altucci L, Mai A, Rotili D. The Two-Faced Role of SIRT6 in Cancer. *Cancers (Basel)*. **2021**, *13*(5), 1156. DOI:10.3390/cancers13051156.
- (41) Chang AR, Ferrer CM, Mostoslavsky R. SIRT6, a Mammalian Deacylase with Multitasking Abilities. *Physiol Rev.* **2020**, *100*(1), 145-169. DOI: 10.1152/physrev.00030.2018.
- (42) Luan Y, Li J, Bernatchez JA, Li R. Kinase and Histone Deacetylase Hybrid Inhibitors for Cancer Therapy. *J Med Chem.* **2019**, *62*(7), 3171-3183. DOI: 10.1021/acs.jmedchem.8b00189.
- (43) Chen S, Zheng Y, Liang B, Yin Y, Yao J, Wang Q, Liu Y, Neamati N. The application of PROTAC in HDAC. *Eur J Med Chem.* **2023**, *260*, 115746. DOI: 10.1016/j.ejmech.2023.115746.

- (44) Fischer F, Alves Avelar LA, Murray L, Kurz T. Designing HDAC-PROTACs: lessons learned so far. *Future Med Chem.* **2022**, *14*(3), 143-166. DOI: 10.4155/fmc-2021-0206.
- (45) Mullard A. FDA approves an HDAC inhibitor for Duchenne muscular dystrophy. *Nat Rev Drug Discov.* **2024**, *23*(5), 329. DOI: 10.1038/d41573-024-00066-8.
- (46) Parveen R, Harihar D, Chatterji BP. Recent histone deacetylase inhibitors in cancer therapy. *Cancer.* **2023**, *129*(21), 3372-3380. DOI: 10.1002/cncr.34974.
- (47) Zagni C, Floresta G, Monciino G, Rescifina A. The Search for Potent, Small-Molecule HDACIs in Cancer Treatment: A Decade After Vorinostat. *Med Res Rev.* **2017**, *37*(6), 1373-1428. DOI: 10.1002/med.21437.
- (48) Fu RG, Sun Y, Sheng WB, Liao DF. Designing multi-targeted agents: An emerging anticancer drug discovery paradigm. *Eur J Med Chem.* **2017**, *136*, 195-211. DOI: 10.1016/j.ejmech.2017.05.016.
- (49) Morphy R, Rankovic Z. Designed multiple ligands. An emerging drug discovery paradigm. *J Med Chem.* **2005**, 48(21), 6523-6543. DOI: 10.1021/jm058225d.
- (50) Fortin S, Bérubé G. Advances in the development of hybrid anticancer drugs. Expert Opin Drug Discov. **2013**, 8(8), 1029-1047. DOI: 10.1517/17460441.2013.798296.
- (51) Bérubé G. An overview of molecular hybrids in drug discovery. *Expert Opin Drug Discov.*2016, 11(3), 281-305. DOI: 10.1517/17460441.2016.1135125.
- (52) Bolden JE, Peart MJ, Johnstone RW. Anticancer activities of histone deacetylase inhibitors.

 Nat Rev Drug Discov. 2006, 5(9), 769-784. DOI: 10.1038/nrd2133.
- (53) Bots M, Johnstone RW. Rational combinations using HDAC inhibitors. *Clin Cancer Res.* **2009**, *15*(12), 3970-3977. DOI: 10.1158/1078-0432.CCR-08-2786.
- (54) Frew AJ, Johnstone RW, Bolden JE. Enhancing the apoptotic and therapeutic effects of HDAC inhibitors. *Cancer Lett.* **2009**, *280*(2), 125-133. DOI: 10.1016/j.canlet.2009.02.042.
- (55) Xiong Y, Donovan KA, Eleuteri NA, Kirmani N, Yue H, Razov A, Krupnick NM, Nowak RP, Fischer ES. Chemo-proteomics exploration of HDAC degradability by small molecule degraders. *Cell Chem Biol.* 2021, 28(10), 1514-1527. DOI: 10.1016/j.chembiol.2021.07.002.
- (56) Weng G, Shen C, Cao D, Gao J, Dong X, He Q, Yang B, Li D, Wu J, Hou T. PROTAC-DB: an online database of PROTACs. *Nucleic Acids Res.* **2021**, *49*(D1), D1381-D1387.

- DOI: 10.1093/nar/gkaa807.
- (57) Yang K, Zhao Y, Nie X, Wu H, Wang B, Almodovar-Rivera CM, Xie H, Tang W. A Cell-Based Target Engagement Assay for the Identification of Cereblon E3 Ubiquitin Ligase Ligands and Their Application in HDAC6 Degraders. *Cell Chem Biol.* 2020, 27(7), 866-876. DOI: 10.1016/j.chembiol.2020.04.008.
- (58) Xiao Y, Wang J, Zhao LY, Chen X, Zheng G, Zhang X, Liao D. Discovery of histone deacetylase 3 (HDAC3)-specific PROTACs. *Chem Commun.* 2020, 56(68), 9866-9869. DOI: 10.1039/d0cc03243c.
- (59) Smalley JP, Adams GE, Millard CJ, Song Y, Norris JKS, Schwabe JWR, Cowley SM, Hodgkinson JT. PROTAC-mediated degradation of class I histone deacetylase enzymes in corepressor complexes. *Chem Commun.* 2020, 56(32), 4476-4479. DOI: 10.1039/d0cc01485k.
- (60) Wu H, Yang K, Zhang Z, Leisten ED, Li Z, Xie H, Liu J, Smith KA, Novakova Z, Barinka C, Tang W. Development of Multifunctional Histone Deacetylase 6 Degraders with Potent Antimyeloma Activity. *J Med Chem.* 2019, 62(15), 7042-7057. DOI: 10.1021/acs.jmedchem.9b00516.
- (61) Troup RI, Fallan C, Baud MGJ. Current strategies for the design of PROTAC linkers: a critical review. *Explor Target Antitumor Ther.* **2020**, *1*(5), 273-312. DOI: 10.37349/etat.2020.00018.
- (62) Yang K, Wu H, Zhang Z, Leisten ED, Nie X, Liu B, Wen Z, Zhang J, Cunningham MD, Tang W. Development of Selective Histone Deacetylase 6 (HDAC6) Degraders Recruiting Von Hippel-Lindau (VHL) E3 Ubiquitin Ligase. ACS Med Chem Lett. 2020, 11(4), 575-581. DOI: 10.1021/acsmedchemlett.0c00046.
- (63) Yang K, Song Y, Xie H, Wu H, Wu YT, Leisten ED, Tang W. Development of the first small molecule histone deacetylase 6 (HDAC6) degraders. *Bioorg Med Chem Lett.* **2018**, 28(14), 2493-2497. DOI: 10.1016/j.bmcl.2018.05.057.
- (64) Sinatra L, Yang J, Schliehe-Diecks J, Dienstbier N, Vogt M, Gebing P, Bachmann LM, Sönnichsen M, Lenz T, Stühler K, Schöler A, Borkhardt A, Bhatia S, Hansen FK. Solid-Phase Synthesis of Cereblon-Recruiting Selective Histone Deacetylase 6 Degraders (HDAC6 PROTACs) with Antileukemic Activity. J Med Chem. 2022, 65(24), 16860-

- 16878. DOI: 10.1021/acs.jmedchem.2c01659.
- (65) Feller F, Weber H, Miranda M, Honin I, Hanl M, Hansen FK. Replacing a Cereblon Ligand by a DDB1 and CUL4 Associated Factor 11 (DCAF11) Recruiter Converts a Selective Histone Deacetylase 6 PROTAC into a Pan-Degrader. *ChemMedChem.* 2025, 20(10), e202500035. DOI: 10.1002/cmdc.202500035.
- (66) Thurn KT, Thomas S, Moore A, Munster PN. Rational therapeutic combinations with histone deacetylase inhibitors for the treatment of cancer. *Future Oncol.* **2011**, 7(2), 263-283. DOI: 10.2217/fon.11.2.
- (67) Rosik L, Niegisch G, Fischer U, Jung M, Schulz WA, Hoffmann MJ. Limited efficacy of specific HDAC6 inhibition in urothelial cancer cells. *Cancer Biol Ther.* 2014, 15(6), 742-757. DOI: 10.4161/cbt.28469.
- (68) Lebraud H, Wright DJ, Johnson CN, Heightman TD. Protein Degradation by In-Cell Self-Assembly of Proteolysis Targeting Chimeras. ACS Cent Sci. 2016, 2(12), 927-934. DOI: 10.1021/acscentsci.6b00280.
- (69) Lim M, Cong TD, Orr LM, Toriki ES, Kile AC, Papatzimas JW, Lee E, Lin Y, Nomura DK. DCAF16-Based Covalent Handle for the Rational Design of Monovalent Degraders. ACS Cent Sci. 2024, 10(7), 1318-1331. DOI: 10.1021/acscentsci.4c00286.
- (70) Scholes NS, Mayor-Ruiz C, Winter GE. Identification and selectivity profiling of small-molecule degraders via multi-omics approaches. *Cell Chem Biol.* 2021, 28(7), 1048-1060. DOI: 10.1016/j.chembiol.2021.03.007.
- (71) Loy CA, Ali EMH, Seabrook LJ, Harris TJ Jr, Kragness KA, Albrecht L, Trader DJ. ByeTAC: Bypassing E-Ligase-Targeting Chimeras for Direct Proteasome Degradation. J Med Chem. 2025, 68(9), 9694-9705. DOI: 10.1021/acs.jmedchem.5c00485.
- (72) Henning NJ, Boike L, Spradlin JN, Ward CC, Liu G, Zhang E, Belcher BP, Brittain SM, Hesse MJ, Dovala D, McGregor LM, Valdez Misiolek R, Plasschaert LW, Rowlands DJ, Wang F, Frank AO, Fuller D, Estes AR, Randal KL, Panidapu A, McKenna JM, Tallarico JA, Schirle M, Nomura DK. Deubiquitinase-targeting chimeras for targeted protein stabilization. *Nat Chem Biol.* 2022, 18(4), 412-421. DOI: 10.1038/s41589-022-00971-2.
- (73) Wang Y, Jiang Y, Ding S, Li J, Song N, Ren Y, Hong D, Wu C, Li B, Wang F, He W, Wang J, Mei Z. Small molecule inhibitors reveal allosteric regulation of USP14 *via* steric

- blockade. Cell Res. 2018, 28(12), 1186-1194. DOI: 10.1038/s41422-018-0091-x.
- (74) Lee, B.-H.; Lee, M. J.; Park, S.; Oh, D.-C.; Elsasser, S.; Chen, P.-C.; Gartner, C.; Dimova, N.; Hanna, J.; Gygi, S. P.; Wilson, S. M.; King, R. W.; Finley, D. Enhancement of Proteasome Activity by a Small-Molecule Inhibitor of USP14. *Nature*. 2010, 467(7312), 179-184. DOI: 10.1038/nature09299.

Chapter 2. DCAF16-based Covalent Molecular Glues for Targeted Protein Degradation of Histone Deacetylases

Tao Sun,¹ Shiyang Zhai,¹ Stephan Lepper,¹ Beate König,¹ Mateo Malenica,¹ Irina Honin,¹ Finn K. Hansen¹

Arch Pharm (Weinheim). **2025**, *358*(7), e70045. DOI: https://doi.org/10.1002/ardp. 70045

Please refer to Appendix I for the publication manuscript and supporting information.

¹ Department of Pharmaceutical and Cell Biological Chemistry, Pharmaceutical Institute, University of Bonn, 53121 Bonn, Germany.

2.1 Publication Summary

The dynamic equilibrium of histone acetylation is maintained through the opposing actions of histone deacetylases (HDACs) and histone acetyltransferases (HATs). HDAC modulation has been demonstrated to significantly impact critical cellular processes such as cell growth, cell cycle, and chromatin decondensation.^[1] The frequent overexpression of HDACs in various malignancies positions them as compelling therapeutic targets in cancer treatment. The pharmacological intervention through HDAC inhibition or targeted degradation represents a promising strategy for anticancer therapy. Currently, four HDAC inhibitors have received FDA approval for clinical use in T-cell lymphomas and multiple myeloma.^[2] Recent advances have further expanded the therapeutic landscape, with innovative HDAC-targeting approaches demonstrating remarkable potential across diverse cancer indications.^[3-5]

Targeted protein degradation (TPD), mainly mediated by molecular glues (MGs) and proteolysis-targeting chimeras (PROTACs), has emerged as a transformative therapeutic strategy for the selective elimination of disease-relevant proteins. [6] Molecular glue degraders offer distinct advantages over heterobifunctional PROTACs, including lower molecular weights and improved drug-like properties. However, unlike PROTACs which can be rationally designed, most molecular glues have been discovered serendipitously or through phenotypic screening. Therefore, *de novo* design of MGs for specific targets remains an important challenge, hindering broader clinical translation. [7-9]

In addition to the complex design of molecular glues, they have several other limitations compared to small molecule inhibitors. For instance, not all proteins are amenable to degradation due to poor E3 ligase recognition or absence of ubiquitinated lysine residues. Moreover, their therapeutic impact may be marginal for proteins with inherently short half-lives and rapid turnover rates. However, despite these challenges associated with the development of molecular glues, they also possess advantages over small molecule inhibitors: Molecular glues (1) can

exploit shallow protein—protein interfaces between E3 ligases and therapeutic proteins that may lack deep binding pockets, which presents a significant advantage in drug development, (2) act *via* a catalytic mode of action, (3) remove all functions of the target protein, not just enzymatic activity, but also scaffolding or non-catalytic roles, and (4) exhibit sustained effects, particularly for proteins with moderate and long half-lives.^[10,11]

Recent studies have identified a covalent DCAF16-targeting scaffold that enables linker-free protein degradation. The vinylsulfonyl piperazine warhead, originally discovered by Nomura's group, represents a versatile covalent handle that can be conjugated to various protein-targeting ligands. Remarkably, this approach has proven effective across multiple protein classes, successfully inducing degradation of diverse targets including CDK4, the androgen receptor, BTK, SMARCA2/4, and BCR-ABL/c-ABL, demonstrating its broad applicability in targeted protein degradation strategies.^[12]

Capitalizing on this finding, a new class of DCAF16-based covalent molecular glues utilizing different ZBGs were designed, synthesized, and characterized for the targeted degradation of HDACs. Western blot analysis demonstrated that the hydroxamate-based degrader 10a effectively reduced HDAC1 levels in MM.1S cells in a potent and preferential manner, while the control compound 10a-nc did not affect HDAC1 levels. Subsequent cell viability assays and apoptosis induction analysis further confirmed the promising anticancer activity of 10a.

Taken together, the vinylsulfonyl piperazine moiety emerges as a highly versatile covalent warhead that successfully transformed the conventional HDAC inhibitor vorinostat into molecular glue degrader 10a, enabling preferential HDAC1 degradation. This proof-of-concept not only validates the strategic repurposing of existing pharmacophores but also underscores the broader potential of this adaptable covalent chemistry platform in rational degrader design. The demonstrated ability to convert non-degradative inhibitors into targeted protein degradation tools opens new avenues for therapeutic development across multiple target classes.

2.2 Author Contribution

<u>Tao Sun</u>: Conceptualization, synthesis and characterization of target compounds, immunoblot analysis, CellTiter-Glo[®] cell viability assay, annexin V/PI assay, writing – original draft.

Shiyang Zhai: CellTiter-Glo® cell viability assay, annexin V/PI assay.

Stephan Lepper: Synthesis and characterization of starting materials.

Beate König: Biochemical HDAC inhibition assays.

Mateo Malenica: Biochemical HDAC inhibition assays.

Irina Honin: Biochemical HDAC inhibition assays.

<u>Finn K. Hansen</u>: Conceptualization, data analysis, funding acquisition, project administration, supervision, writing – review & editing.

2.3 References

- (1) Ho TCS, Chan AHY, Ganesan A. Thirty Years of HDAC Inhibitors: 2020 Insight and Hindsight. *J Med Chem.* **2020**, 63(21), 12460-12484. DOI: 10.1021/acs.jmedchem.0c00830.
- (2) Parveen R, Harihar D, Chatterji BP. Recent histone deacetylase inhibitors in cancer therapy *Cancer*. **2023**, *129*(21), 3372-3380. DOI: 10.1002/cncr.34974.
- (3) Chen S, Zheng Y, Liang B, Yin Y, Yao J, Wang Q, Liu Y, Neamati N. The application of PROTAC in HDAC. *Eur J Med Chem.* **2023**, *260*, 115746. DOI: 10.1016/j.ejmech.2023.115746.
- (4) Huang Z, Zeng L, Cheng B, Li D. Overview of class I HDAC modulators: Inhibitors and degraders. *Eur J Med Chem.* **2024**, *276*, 116696. DOI: 10.1016/j.ejmech.2024.116696.
- (5) Lamb YN. *Drugs*. Givinostat: First Approval. **2024**, *84*(7), 849-856. DOI: 10.1007/s40265-024-02052-1.
- (6) Li K, Crews CM. PROTACs: past, present and future. Chem Soc Rev. 2022, 51(12), 5214-5236. DOI: 10.1039/d2cs00193d.
- (7) Krönke J, Udeshi ND, Narla A, Grauman P, Hurst SN, McConkey M, Svinkina T, Heckl D, Comer E, Li X, Ciarlo C, Hartman E, Munshi N, Schenone M, Schreiber SL, Carr SA, Ebert BL. Lenalidomide causes selective degradation of IKZF1 and IKZF3 in multiple myeloma cells. *Science*. 2014, 343(6168), 301-305. DOI: 10.1126/science.1244851.
- (8) Słabicki M, Kozicka Z, Petzold G, Li YD, Manojkumar M, Bunker RD, Donovan KA, Sievers QL, Koeppel J, Suchyta D, Sperling AS, Fink EC, Gasser JA, Wang LR, Corsello SM, Sellar RS, Jan M, Gillingham D, Scholl C, Fröhling S, Golub TR, Fischer ES, Thomä NH, Ebert BL. The CDK inhibitor CR8 acts as a molecular glue degrader that depletes cyclin K. *Nature*. 2020, 585(7824), 293-297. DOI: 10.1038/s41586-020-2374-x.
- (9) Słabicki M, Yoon H, Koeppel J, Nitsch L, Roy Burman SS, Di Genua C, Donovan KA, Sperling AS, Hunkeler M, Tsai JM, Sharma R, Guirguis A, Zou C, Chudasama P, Gasser JA, Miller PG, Scholl C, Fröhling S, Nowak RP, Fischer ES, Ebert BL. Small-molecule-induced polymerization triggers degradation of BCL6. *Nature*. 2020, 588(7836), 164-168. DOI: 10.1038/s41586-020-2925-1.

- (10) Dong G, Ding Y, He S, Sheng C. Molecular Glues for Targeted Protein Degradation: From Serendipity to Rational Discovery. *J Med Chem.* **2021**, *64*(15), 10606-10620. DOI: 10.1021/acs.jmedchem.1c00895.
- (11) Vetma V, Perez LC, Eliaš J, Stingu A, Kombara A, Gmaschitz T, Braun N, Ciftci T, Dahmann G, Diers E, Gerstberger T, Greb P, Kidd G, Kofink C, Puoti I, Spiteri V, Trainor N, Weinstabl H, Westermaier Y, Whitworth C, Ciulli A, Farnaby W, McAulay K, Frost AB, Chessum N, Koegl M. Confounding Factors in Targeted Degradation of Short-Lived Proteins. ACS Chem Biol. 2024, 19(7), 1484-1494. DOI: 10.1021/acschembio.4c00152.
- (12) Lim M, Cong TD, Orr LM, Toriki ES, Kile AC, Papatzimas JW, Lee E, Lin Y, Nomura DK. DCAF16-Based Covalent Handle for the Rational Design of Monovalent Degraders. ACS Cent Sci. 2024, 10(7), 1318-1331. DOI: 10.1021/acscentsci.4c00286.

Chapter 3. Targeted Degradation of Histone Deacetylases *via*Bypassing E3 Ligase Targeting Chimeras (BYETACs)

Tao Sun,¹ Shiyang Zhai,¹ Beate König,¹ Irina Honin,¹ Cindy-Esther Kponomaizoun,¹ Finn K. Hansen¹

ACS Med. Chem. Lett. **2025**, 16(6), 1155-1162. DOI: 10.1021/acsmedchemlett.5c0 0193

Please refer to Appendix II for the publication manuscript and supporting information.

¹ Department of Pharmaceutical and Cell Biological Chemistry, Pharmaceutical Institute, University of Bonn, 53121 Bonn, Germany

3.1 Publication Summary

Cellular protein homeostasis is principally maintained through the ubiquitinproteasome system (UPS), which selectively eliminates senescent or misfolded
proteins.^[1] Harnessing this endogenous quality control mechanism, researchers
have developed UPS-dependent protein degraders, including proteolysis-targeting
chimeras (PROTACs) and molecular glues (MGs), as innovative therapeutic
modalities for targeted protein degradation (TPD).^[2,3] Compared to conventional
small molecule inhibitors, UPS-dependent degraders offer several advantages,
including the ability to target undruggable proteins*via* acting through a catalytic
mode of action, and overcoming drug resistance. The remarkable therapeutic
potential of UPS-dependent degraders is evidenced by the rapid clinical translation
of this technology, with over 25 UPS-dependent degraders currently under
investigation in clinical trials.^[4,5]

Current TPD strategies face several critical limitations in E3 ligase utilization. First, the repertoire of exploitable E3 ligases remains predominantly restricted to two cullin-RING ligase family members von Hippel-Lindau (VHL) and cereblon (CRBN). [6-10] Second, degradation efficiency is intrinsically dependent on the endogenous expression levels of these E3 ligases in target tissues. These fundamental constraints significantly limit the druggable proteome accessible *via* UPS-mediated degradation. This unmet need has driven growing pharmaceutical interest in developing novel degradation platforms capable of targeting a more diverse range of disease-relevant proteins through alternative mechanisms.

An emerging strategy to bypass E3 ligase dependency involves direct engagement of the 26S proteasome subunits to induce TPD. This approach offers a potentially universal degradation platform for proteins that are refractory to ubiquitination or lack E3 ligase recognition. Recent research first demonstrated the viability of this approach by establishing a binding interaction with the 26S proteasome subunit RPN1, thereby promoting the degradation of BRD4.^[11] Building on this proof-of-concept, a novel class of non-covalent heterobifunctional

degraders, termed bypassing E3 ligase targeting chimeras (BYETACs), was subsequently developed to mediate BRD4 degradation through RPN13 engagement.^[12] These examples validate the feasibility of directly binding to a 26S proteasome subunit for TPD.

The ubiquitin-proteasome system maintains precise control over protein degradation through several regulatory checkpoints, one of which involves the ubiquitin-specific protease 14 (USP14). This critical deubiquitinating enzyme dynamically associates with the 19S regulatory particle of the 26S proteasome, where it serves as a gatekeeper by editing ubiquitin chains and potentially rejecting substrates from degradation. Structural elucidation of human USP14 in complex with the proteasome has revealed that its interaction with the RPN1 subunit is crucial for proper positioning at the proteasomal entry site. This strategic localization enables USP14 to directly access incoming substrates and modulate their fate through selective trimming of polyubiquitin chains.^[13]

Meanwhile, the small molecule IU1 was identified as a preferential USP14 inhibitor in a high-throughput screening campaign. The treatment of cells with IU1 resulted in enhanced degradation of several proteasome substrates implicated in neurodegenerative diseases.^[14]

Building upon these discoveries, a novel class of heterobifunctional BYETACs were designed and synthesized specifically engineered for HDAC degradation. This approach features the first implementation of a USP14 inhibitor as a proteasome-targeting warhead. Through strategic conjugation of this USP14-binding moiety IU1 with the HDAC inhibitor vorinostat, HDAC-targeting BYETACs demonstrated potent and selective reduction of HDAC1 protein levels in multiple myeloma MM.1S cells. Furthermore, subsequent apoptosis induction analysis confirmed its promising anticancer activity. This proof-of-concept study establishes that bypassing E3 ligases *via* BYETACs is a viable strategy for HDAC knockdown, potentially expanding the scope of protein degradation in the future.

3.2 Author Contribution

 $\underline{\text{Tao Sun}}$: Conceptualization, synthesis and characterization of all compounds, Immunoblot analysis, CellTiter-Glo® cell viability assay, annexin V/PI assay, writing – original draft.

Shiyang Zhai: CellTiter-Glo® cell viability assay, annexin V/PI assay.

Beate König: Biochemical HDAC inhibition assays.

Irina Honin: Biochemical HDAC inhibition assays.

Cindy-Esther Kponomaizoun: Biochemical HDAC inhibition assays.

<u>Finn K. Hansen</u>: Conceptualization, data analysis, funding acquisition, project administration, supervision, writing – review & editing.

3.3 References

- (1) Kwon YT, Ciechanover A. The Ubiquitin Code in the Ubiquitin-Proteasome System and Autophagy. *Trends Biochem Sci.* **2017**, *42*(11), 873-886. DOI: 10.1016/j.tibs.2017.09.002.
- (2) Churcher I. Protac-Induced Protein Degradation in Drug Discovery: Breaking the Rules or Just Making New Ones? *J Med Chem.* **2018**, *61*(2), 444-452. DOI: 10.1021/acs.jmedchem.7b01272.
- (3) Zhang L, Riley-Gillis B, Vijay P, Shen Y. Acquired Resistance to BET-PROTACs (Proteolysis-Targeting Chimeras) Caused by Genomic Alterations in Core Components of E3 Ligase Complexes. *Mol Cancer Ther.* 2019, 18(7), 1302-1311. DOI: 10.1158/1535-7163.MCT-18-1129.
- (4) Liu X, Ciulli A. Proximity-Based Modalities for Biology and Medicine. ACS Cent Sci.2023, 9(7), 1269-1284. DOI: 10.1021/acscentsci.3c00395.
- (5) Chirnomas D, Hornberger KR, Crews CM. Protein degraders enter the clinic a new approach to cancer therapy. *Nat Rev Clin Oncol.* **2023**, *20*(4), 265-278. DOI: 10.1038/s41571-023-00736-3.
- (6) Buckley, D. L., Van Molle, I., Gareiss, P. C., Tae, H. S., Michel, J., Noblin, D. J., Jorgensen, W. L., Ciulli, A., & Crews, C. M. Targeting the von Hippel–Lindau E3 ubiquitin ligase using small molecules to disrupt the VHL/HIF-1α interaction. *J. Am. Chem. Soc.* 2012, 134(10), 4465-4468. DOI: 10.1021/ja209924v.
- (7) Winter, G. E., Buckley, D. L., Paulk, J., Roberts, J. M., Souza, A., Dhe-Paganon, S., Bradner, J. E. Phthalimide conjugation as a strategy for in vivo target protein degradation. *Science* **2015**, *348*(6241), 1376-1381. DOI: 10.1126/science.aab1433.
- (8) Bondeson DP, Mares A, Smith IE, Ko E, Campos S, Miah AH, Mulholland KE, Routly N, Buckley DL, Gustafson JL, Zinn N, Grandi P, Shimamura S, Bergamini G, Faelth-Savitski M, Bantscheff M, Cox C, Gordon DA, Willard RR, Flanagan JJ, Casillas LN, Votta BJ, den Besten W, Famm K, Kruidenier L, Carter PS, Harling JD, Churcher I, Crews CM. Catalytic in vivo protein knockdown by small-molecule PROTACs. *Nat. Chem. Biol.* 2015, 11(8), 611-617. DOI: 10.1038/nchembio.1858.
- (9) Raina K, Lu J, Qian Y, Altieri M, Gordon D, Rossi AM, Wang J, Chen X, Dong H, Siu K, Winkler JD, Crew AP, Crews CM, Coleman KG. PROTAC-induced BET protein

- degradation as a therapy for castration-resistant prostate cancer. *Proc. Natl Acad. Sci. USA* **2016**, *113*(26), 7124-7129. DOI: 10.1073/pnas.1521738113.
- (10) Zengerle, M., Chan, K.-H., Ciulli, A. Selective small molecule induced degradation of the BET bromodomain protein BRD4. ACS Chem. Biol. 2015, 10(8), 1770-1777. DOI: 10.1021/acschembio.5b00216.
- (11) Bashore C, Prakash S, Johnson MC, Conrad RJ, Kekessie IA, Scales SJ, Ishisoko N, Kleinheinz T, Liu PS, Popovych N, Wecksler AT, Zhou L, Tam C, Zilberleyb I, Srinivasan R, Blake RA, Song A, Staben ST, Zhang Y, Arnott D, Fairbrother WJ, Foster SA, Wertz IE, Ciferri C, Dueber EC. Targeted degradation *via* direct 26S proteasome recruitment. *Nat Chem Biol.* 2023, 19(1), 55-63. DOI: 10.1038/s41589-022-01218-w.
- (12) Loy CA, Ali EMH, Seabrook LJ, Harris TJ Jr, Kragness KA, Albrecht L, Trader DJ. ByeTAC: Bypassing E-Ligase-Targeting Chimeras for Direct Proteasome Degradation. J Med Chem. 2025, 68(9), 9694-9705. DOI: 10.1021/acs.jmedchem.5c00485.
- (13) Wang Y, Jiang Y, Ding S, Li J, Song N, Ren Y, Hong D, Wu C, Li B, Wang F, He W, Wang J, Mei Z. Small molecule inhibitors reveal allosteric regulation of USP14 *via* steric blockade. *Cell Res.* **2018**, *28*(12), 1186-1194. DOI: 10.1038/s41422-018-0091-x.
- (14) Lee, B.-H.; Lee, M. J.; Park, S.; Oh, D.-C.; Elsasser, S.; Chen, P.-C.; Gartner, C.; Dimova, N.; Hanna, J.; Gygi, S. P.; Wilson, S. M.; King, R. W.; Finley, D. Enhancement of Proteasome Activity by a Small-Molecule Inhibitor of USP14. *Nature*. 2010, 467(7312), 179-184. DOI: 10.1038/nature09299.

Chapter 4. Deubiquitinase-targeting Chimeras (DUBTACs) for Targeted Stabilization of SIRT6

4.1 Background

4.1.1 Discovery of Deubiquitinase-targeting Chimeras (DUBTACs)

Therapeutic targeting of "undruggable" proteins demands both innovative technologies to identify ligandable binding sites and novel modalities to modulate protein function through unconventional mechanisms. [1,2] Targeted protein degradation (TPD) has emerged as a transformative strategy to address this challenge, enabling selective ubiquitination and proteasomal elimination of disease-relevant proteins. Within the TPD landscape, proteolysis-targeting chimeras (PROTACs) have emerged as a groundbreaking class of heterobifunctional degraders. These rationally designed molecules consist of two pharmacophores: (1) an E3 ligase-binding moiety and (2) a targeted protein-binding ligand, connected through a suitable linker. PROTACs facilitate the formation of productive ternary complexes that sterically position the E3 ligase in proximity to the targeted protein. This spatial arrangement enables the polyubiquitination of the POI, marking it for recognition and subsequent degradation by the 26S proteasome. [3-5] However, despite these significant advances in TPD, the pharmacological stabilization of proteins through small molecule-mediated deubiquitination remains an unexplored therapeutic strategy, with no clinically viable approaches reported to date. [6,7]

To achieve this goal, Nomura and co-workers pioneered the development of deubiquitinase-targeting chimeras (DUBTACs). These are novel, heterobifunctional small molecules composed of a deubiquitinase (DUB) recruiter conjugated to a protein-targeting ligand *via* variable linkers (**Figure 4-1**). DUBTACs are engineered to restore steady-state levels of disease-relevant proteins that undergo aberrant degradation through ubiquitin-dependent mechanisms. Using chemoproteomic strategies, the researchers discovered the covalent ligand EN523, which selectively engages a non-catalytic allosteric cysteine (C23) in OTUB1, a K48-ubiquitin-specific deubiquitinase.

Nomura and co-workers then constructed a DUBTAC by tethering EN523 to lumacaftor, a therapeutic agent for cystic fibrosis that binds to the Δ F508-cystic fibrosis transmembrane conductance regulator (CFTR). This DUBTAC effectively increased Δ F508-CFTR protein levels, resulting in improved chloride channel function in human cystic fibrosis bronchial epithelial cells.

Additionally, the Nomura group extended the application of DUBTACs to stabilize the tumor suppressor kinase WEE1 in hepatoma cells, further validating the versatility of this platform. This groundbreaking study not only underscored the power of chemoproteomics in developing proximity-based therapeutic modalities but also established DUBTACs as a transformative targeted protein stabilization (TPS) strategy with broad therapeutic potential.^[8]

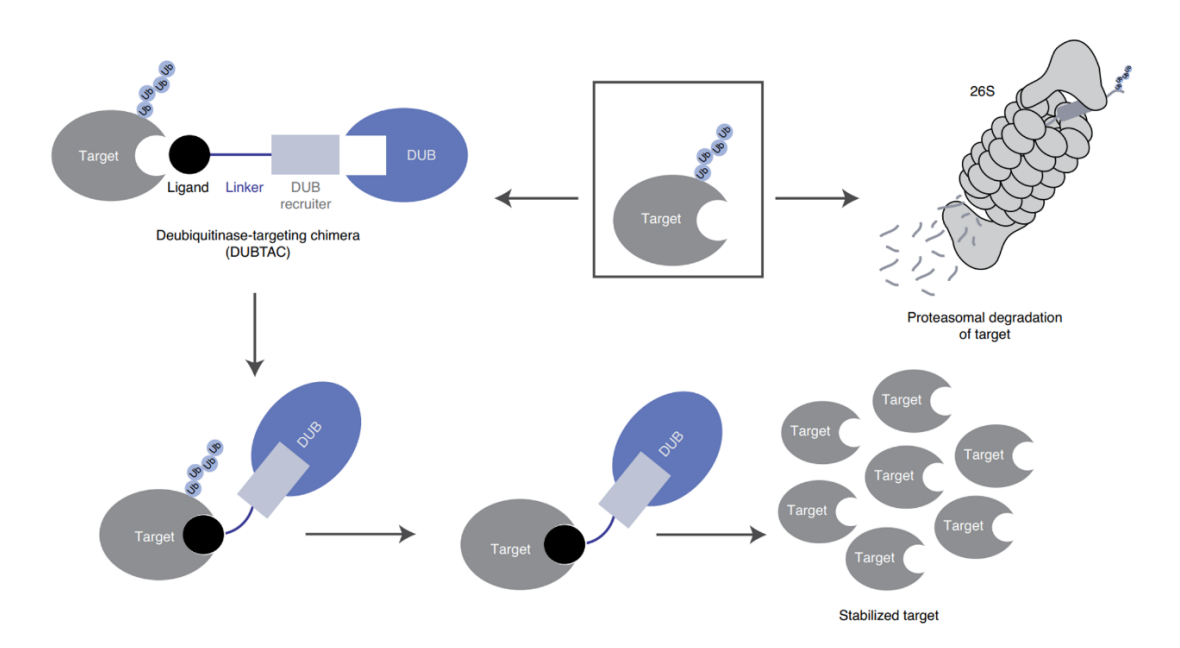


Figure 4-1. DUBTACs are heterobifunctional molecules composed of a protein-targeting ligand connected to a DUB recruiter *via* a chemical linker. Through induced proximity, DUBTACs facilitate the recruitment of DUBs to their target proteins, enabling site-specific removal of polyubiquitin chains. This process effectively blocks proteasomal degradation pathways, resulting in stabilization of disease-relevant proteins. Adapted in a modified version from Henning NJ et *al.* 2019.^[8]

Building upon the therapeutic concept of DUBTACs for CFTR stabilization in cystic fibrosis, Wei, Jin, and colleagues developed an advanced platform called TF-DUBTAC.^[9] This novel strategy employs click chemistry to conjugate a DNA oligonucleotide with EN523, the covalent OTUB1-targeting ligand, enabling selective stabilization of tumor-suppressive transcription factors. The authors developed three series of TF-DUBTACs: FOXO-DUBTAC, p53-DUBTAC and IRF-DUBTAC, which effectively stabilize FOXO3A, p53, and IRF3 in an OTUB1-dependent manner.

Building on their previous work with EN523, Wei, Jin, and co-workers first optimized the OTUB1-targeting covalent ligand to develop the improved thiophene analog MS5105. This advancement led to the development of MS7829 and MS8588, representing the first reported DUBTACs targeting cyclic GMP-AMP synthase (cGAS), a pivotal mediator of the cGAS-STING innate immune pathway. Notably, while these DUBTACs were derived from a cGAS inhibitor scaffold, they effectively stabilize cGAS and activate the cGAS/STING/IRF3 signaling cascade.^[10]

Expanding beyond OTUB1-targeting strategies, Wei, Jin, and collaborators pioneered the development of DUBTACs that utilize alternative deubiquitinases. They established proof-of-concept for this approach by developing USP7-based DUBTACs using a noncovalent USP7 ligand, which achieved stabilization of Δ F508-CFTR comparable to that of their OTUB1-targeting counterparts. Notably, they developed the first AMPK DUBTACs, which selectively stabilize different AMPK β isoforms, resulting in enhanced AMPK signaling.^[11]

Shortly afterwards, by utilizing a noncovalent small-molecule inhibitor of USP28 as a USP28 binder, Wei, Jin and co-workers developed CFTR, cGAS, and PPARγ DUBTACs that effectively stabilized these respective target proteins.^[12]

Very recently, Wei and Jin *et al.* demonstrated for the first time that USP1, a DUB which is overexpressed in multiple cancers, can be harnessed to stabilize CFTR and Ubiquitously transcribed tetratricopeptide repeat X chromosome (UTX), thus expanding the repertoire of DUBs that can be leveraged for DUBTAC development.^[13]

Collectively, these studies identified novel DUB-recruiting ligands and validated the therapeutic paradigm of TPS *via* induced proximity between deubiquitinases and

disease-relevant proteins. The successful stabilization of multiple functionally distinct targets, including CFTR, tumor suppressors, and epigenetic regulators, demonstrates the remarkable versatility of the DUBTAC platform. Given the successful applications demonstrated for several proteins, it is evident that DUBTACs can be employed for the targeted stabilization of a diverse array of protein substrates.

4.1.2 SIRT6 Activators

The class III HDACs, also known as sirtuins, represent an evolutionarily conserved family of NAD⁺-dependent epigenetic regulators that modulate critical cellular processes in organisms ranging from prokaryotes to eukaryotes. In mammals, the sirtuins consist of seven members (SIRT1-7) that catalyze the deacylation of proteins, including both histones and non-histones, through their characteristic NAD⁺-dependent enzymatic mechanism. Among these, SIRT6 is particularly notable for its ubiquitous expression in nearly all mammalian tissues and its crucial role in various biological processes such as DNA repair, glucose and lipid metabolism, inflammation, and aging.^[14-21]

Accumulating clinical and preclinical evidence established SIRT6 as a potent tumor suppressor. Importantly, downregulation of SIRT6 expression is frequently observed across multiple cancer types and SIRT6 overexpression delays tumorigenesis in immunocompromised mouse models. Furthermore, cancer patients with higher SIRT6 expression exhibit significantly improved relapse-free survival. These findings provide compelling evidence that SIRT6 plays a role in inhibiting tumor formation. [22] These insights position pharmacological SIRT6 activation and stabilization as a promising therapeutic strategy for primary cancer treatment and prevention of tumor recurrence.

The multifaceted biological functions of SIRT6 deacetylation have stimulated significant interest in developing pharmacological activators of this enzyme. Beyond endogenous regulators include Lamin A and long-chain fatty acids, Steegborn and coworkers synthesized and screened pyrrolo[1,2-a]quinoxaline derivatives, resulting in the identification of the first synthetic SIRT6 activators.^[23] Their findings demonstrated the potential for potent SIRT6 activation by small molecules and established a structural

basis for the further development of SIRT6 activators.

However, previous efforts have yielded only a limited number of nonspecific sirtuin activators with restricted potency, and no selective SIRT6 activator has been successfully employed to regulate its functions. Zhang and co-workers recently overcame this challenge by discovering MDL-800, the first selective SIRT6 activator. MDL-800 binds to an allosteric site, boosting SIRT6 deacetylase activity by up to 22-fold and leading to a global reduction in H3K9ac and H3K56ac levels in human hepatocellular carcinoma (HCC) cells [23]

4.2 Design, Synthesis and Evaluation of SIRT6 DUBTACs

4.2.1 Rational Design of SIRT6 DUBTACs

The pathological degradation of critical regulatory proteins contributes to numerous diseases, suggesting that the targeted stabilization or activation of these proteins could modulate disease mechanisms. Notably, SIRT6 deficiency has been implicated in various pathologies, and the pharmacological activation of SIRT6 is emerging as a promising anticancer strategy. Based on the success of DUBTACs in protein stabilization and the established therapeutic potential of SIRT6 modulation, the goal of this project was to develop SIRT6 DUBTACs to demonstrate the feasibility of enhancing SIRT6 stability and function.

SIRT6 DUBTACs represent a class of heterobifunctional small molecules designed to achieve targeted SIRT6 stabilization through three key components: (1) a SIRT6-binding ligand, (2) a DUB recruiter, and (3) a connecting linker. The known SIRT6 activators UBCS039^[22] and MDL-800^[23] were employed as the SIRT6-binding moieties. The DUB-recruiting element was carefully selected to engage allosteric sites without disrupting catalytic activity. Based on previous findings, OTUB1-targeting EN523 was identified as a suitable candidate. (**Figure 4-2**).^[8]

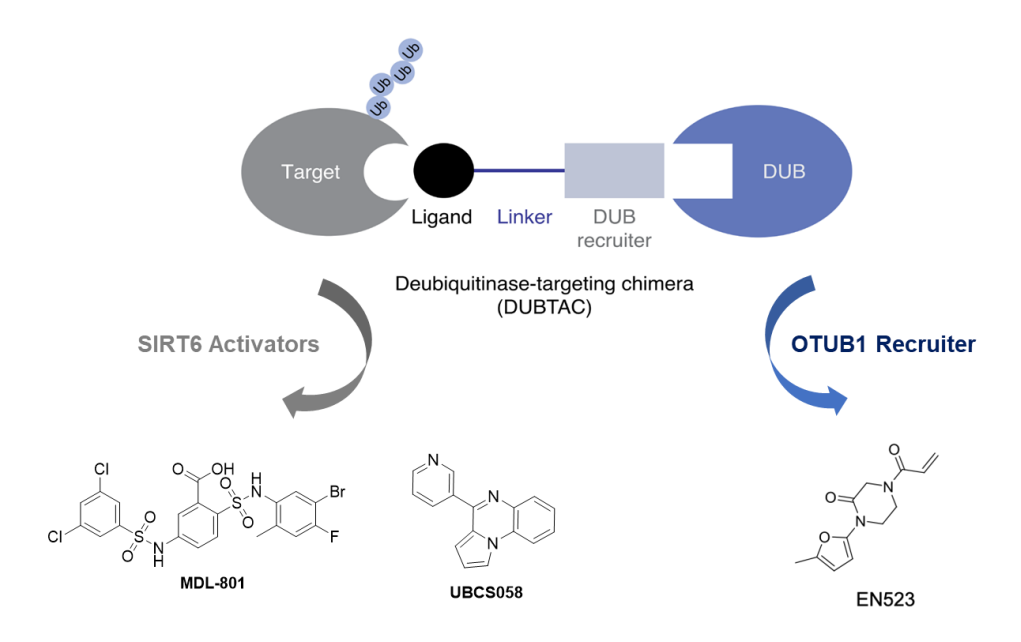


Figure 4-2. SIRT6 DUBTACs are heterobifunctional molecules consisting of a SIRT6 activator linked to a DUB OTUB1 recruiter *via* different linkers.^[8]

Leveraging available crystal structures, first-in-class SIRT6 DUBTACs were designed by conjugating the OTUB1-recruiting small molecule EN523 with established SIRT6 activators (MDL-800 or UBCS039) through a selection of linkers. These bifunctional compounds are engineered to promote targeted deubiquitination and subsequent stabilization of SIRT6 through induced proximity (**Figure 4-3**).

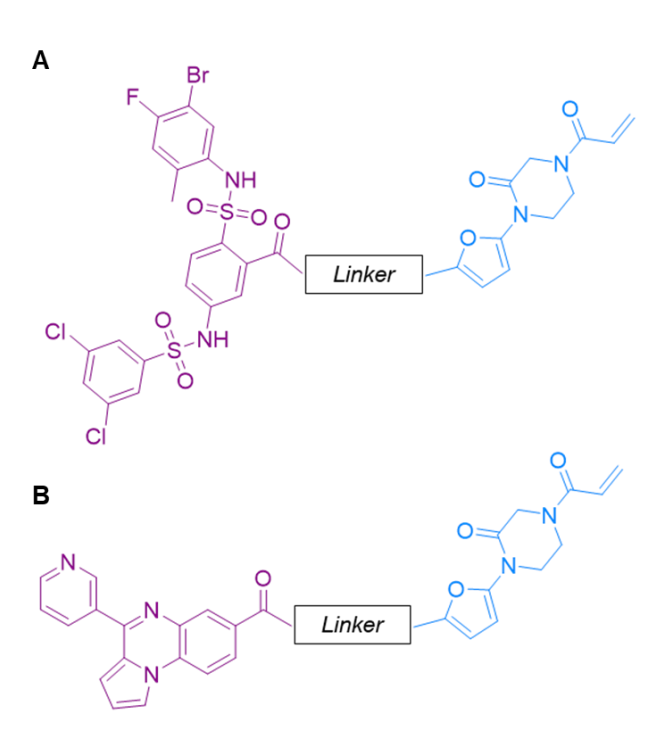


Figure 4-3. Structures of the designed MDL-800 (A) and UBCS039 (B) derived SIRT6 DUBTACs.

4.2.2 Synthesis of SIRT6 DUBTACs

The synthesis of the OTUB1 recruiter commenced with a Horner-Wadsworth-Emmons reaction between 5-bromofuran-2-carbaldehyde (1) and *tert*-butyl diethylphosphonoacetate using sodium hydride in THF. This yielded intermediate 2, which was then treated with benzyl 3-oxopiperazine-1-carboxylate to afford the protected intermediate 3. Final deprotection under standard hydrogenolysis conditions followed by acylation with acryloyl chloride provided the OTUB1 recruiter 4 (Scheme 4-1).^[8]

Scheme 4-1. Synthesis of the DUB OTUB1 recruiter **4**. *Reagents and conditions:* i) *tert*-butyl diethylphosphonoacetate, NaH, THF, 0 °C, 2 h, 89% yield. ii) Benzyl 3-oxopiperazine-1-carboxylate, K₂CO₃, CuI, *N*,*N*-dimethydiaminoethane, dioxane, 100 °C, 96 h, 43% yield. iii) Pd/C, H₂, EtOH, rt, 16 h. iv) Acryloyl chloride, TEA, DCM, 0 °C, 2 h, 60% yield for step iii) and iv).

Scheme 4-2 summarizes the synthetic route for the SIRT6 activator MDL-800, which is conjugated with a selection of different linkers. The Cs₂CO₃-mediated reaction of compound 5 with thioacetic acid and glycylglycine in DMF afforded intermediate 6, which was treated *N*-chlorosuccinimide (NCS) to yield the sulfonyl chloride 7. The subsequent reaction of 7 with 5-bromo-4-fluoro-2-methylaniline in pyridine provided compound 8, followed by reduction of the nitro group using iron powder in acetic acid to generate 9. The hydrolysis of 9 with LiOH·H₂O yielded the key carboxylic acid intermediate 10, which was then functionalized *via* amide coupling reaction with various linker moieties to produce analogs 11a-e. Finally, the treatment of 11a-e with 3,5-dichlorobenzene-1-sulfonyl chloride in pyridine furnished the target compounds 12a-e. [23]

Scheme 4-2. Synthesis of SIRT6 activator MDL-800 with different linkers. *Reagents and conditions*: i) CH₃COSH, glycylglycine, Cs₂CO₃, DMF, rt, 12 h, 76% yield. ii) NCS, 2M HCl, CH₃CN, 0 °C, 3 h, 85% yield. iii) 5-Bromo-4-fluoro-2-methylaniline, pyridine, 0 °C-rt, 16 h, 75% yield. iv) Fe, CH₃COOH, 50 °C, 12 h, 69% yield. v) LiOH·H₂O, THF/H₂O(v/v, 1:1), rt, 16 h, 56% yield. vi) NH₂-R¹-NH-Boc, HATU, DIPEA, DMF, 45 °C, 48 h, 44-96% yield. vii) 3,5-Dichlorobenzene-1-sulfonyl chloride, pyridine, 0 °C-rt, 16 h, 10-36% yield.

The synthetic route for the second SIRT6 activator UBCS058 variable linkers is outlined in Scheme 4-3. The synthesis started with a Clauson-Kaas synthesis of material 13 with pyrrole the starting 2.5dimethoxytetrahydrofuran in acetic acid to afford the pyrrole intermediate 14. The subsequent catalytic hydrogenation using Pd/C under a hydrogen atmosphere yielded compound 15. Next, 15 was converted to the intended tricyclic pyrrolo[1,2a]quinoxaline system with pyridine-3-carboxaldehyde in ethanol to generate the key intermediate 16. The final diversification was achieved through amide coupling reactions of 16 with various linker moieties to produce the target compounds 17a**e**.^[22]

Scheme 4-3. Synthesis of another SIRT6 activator UBCS058 with different linkers. *Reagents and conditions:* i) 2,5-Dimethoxytetrahydrofuran, acetic acid, 120 °C, 12 h, 78% yield. ii) Pd/C, H₂, EtOAc/MeOH, 25 °C, 16 h, 94% yield. iii) Pyridine-3-carboxaldehyde, EtOH, cat. glacial CH₃COOH, 50 °C, 74% yield. iv) NH₂-R²-NH-Boc, HATU, DIPEA, DMF, 10-43% yield.

Finally, compounds 4 and 12a-e were treated with TFA in DCM to remove the respective protecting groups without purification. These intermediates were then coupled *via* HATU-mediated amide bond formation in the presence of DIPEA to yield the first series of SIRT6 DUBTACs 18a-e (Scheme 4-4).

Scheme 4-4. Synthetic route for the first type of SIRT6 DUBTACs **18a-e**. *Reagents and conditions:* i) TFA, DCM, 1 h, rt. ii) HATU, DIPEA, DMF, rt, 16 h, 7-23% yield for two steps.

The same procedures were applied for the synthesis of the second type of DUBTACs **19a-e** (see **Scheme 4-5**).

Scheme 4-5. Synthetic route for the second type of DUBTACs **19a-e**. *Reagents and conditions:* i) TFA, DCM, 1 h, rt. ii) HATU, DIPEA, DMF, rt, 16 h, 8-16% yield for two steps.

To sum up, ten DUBTACs were totally synthesized using different linkers (**Table 4-1**).

Table 4-1. Structures of SIRT6 DUBTACs 18a-e and 19a-e.

DUBTAC Structure

18c

Br NH OSSO CI CI CI CI OSSO CI HI OSSO CI OSSO CI OSSO CI OSSO OSSO

18d

O NH NH NH NN N

18e

19a

19b

4.2.3 SIRT6 Stabilization by OTUB1-recruiting DUBTACs.^a

In the first step, 4 prototypic DUBTACs **18a-b** and **19a-b** were first evaluated in western blot experiments. The multiple myeloma cell line MM.1S was treated with varying concentrations (0.1, 1, 10, and 25 μM) of **18a-b** and **19a-b** for 24 hours, respectively. SIRT6 protein levels were subsequently evaluated using western blot analysis. As summarized in **Figure 4-4**, SIRT6 levels were to some extent increased at concentrations of 1 μM for all compounds compared to vehicle control. Furthermore, compound **18b** demonstrated the most potent stabilization of SIRT6 when treated at a concentration of 25 μM. In contrast, when treated with 0.1 μM and 10 μM of the respective DUBTAC, all the compounds showed minimal effects on SIRT6 expression. Consequently, treatment with 1 μM and 25 μM were selected for further biological evaluations based on the initial screening results.

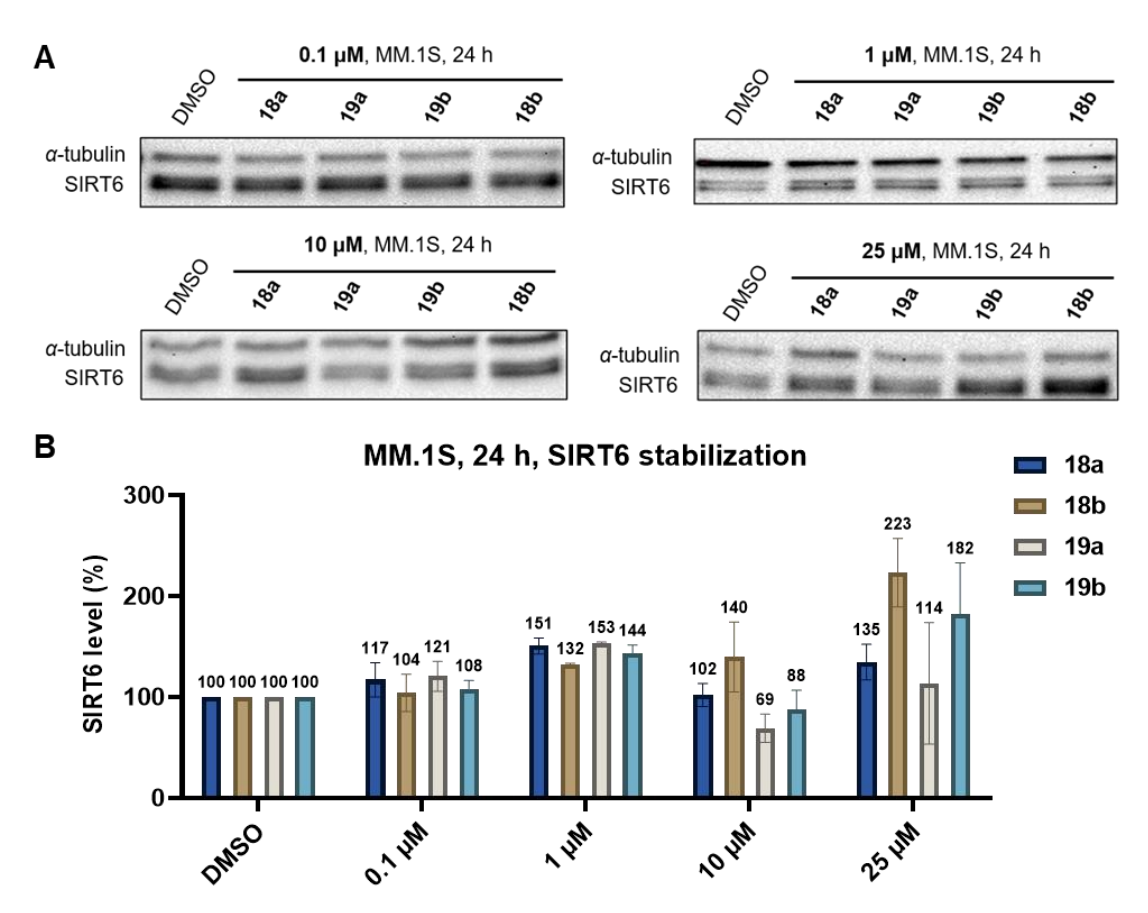


Figure 4-4. Analysis of SIRT6 protein levels after treatment of MM.1S cells with DUBTACs **18a-b** and **19a-b**. **(A)** MM.1S cells were treated with compounds at concentrations of 0.1, 1, 10, and 25 μ M for 24 h, with serving as DMSO as vehicle control. SIRT6 levels were detected by immunoblot analysis. α -tubulin was used as the loading control. Representative images from a total of n = 2 replicates. **(B)** Densitometric analysis of SIRT6 levels after treatment with **18a-b** and **19a-b** for 24 h. Data from n = 2 replicates.

^a Western blot experiments were performed by Cindy-Esther Kponomaizoun (Rheinische Friedrich-Wilhelms-Universität Bonn, Hansen Group).

To evaluate potential cell-type dependent effects, these four DUBTACs were examined in adherent MCF-7 breast cancer cells at the previously identified optimal concentrations (1 μ M and 25 μ M) that showed robust SIRT6 stabilization in MM.1S cells. Western blot analysis revealed markedly reduced stabilization efficacy in MCF-7 cells compared to the pronounced effects observed in MM.1S cells (**Figure 4-5**). These results verify MM.1S cells as the more responsive model system for further investigation of SIRT6 DUBTACs.

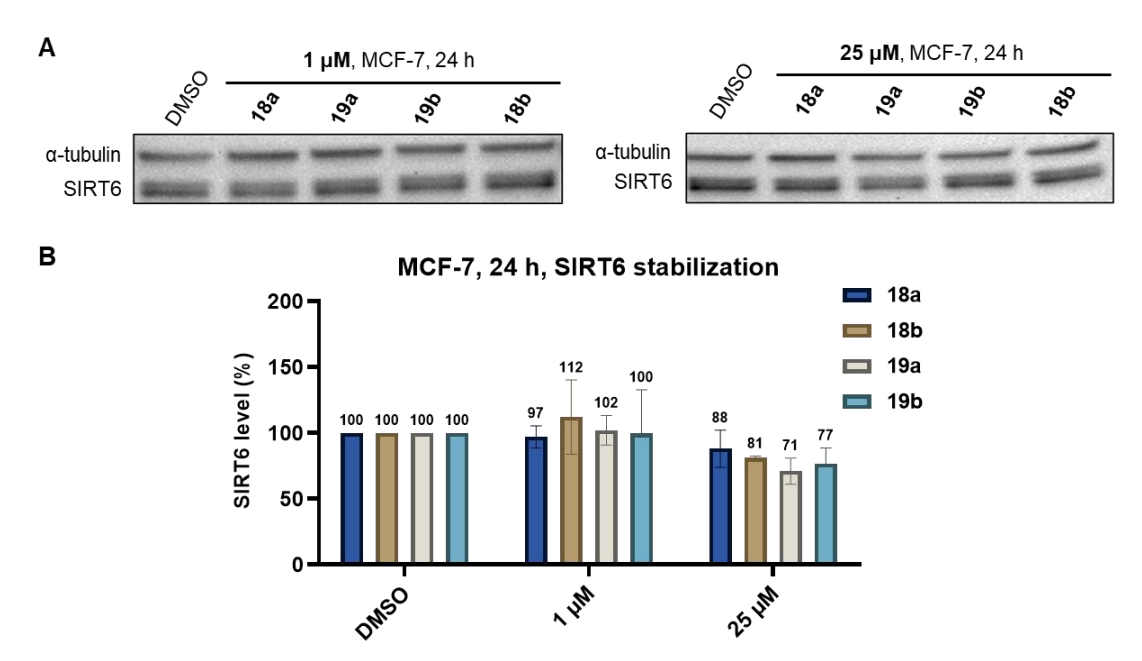


Figure 4-5. Analysis of SIRT6 protein levels after treatment of MCF-7 cells with DUBTACs **18a-b** and **19a-b**. **(A)** MCF-7 cells were treated with compounds at concentrations of 1 and 25 μ M for 24 h, with DMSO serving as vehicle control. SIRT6 levels were detected by immunoblot analysis. α -tubulin was used as the loading control. Representative images from a total of n = 2 replicates. **(B)** Densitometric analysis of SIRT6 levels after treatment with **18a-b** and **19a-b** for 24 h. Data from n = 2 replicates.

4.2.4 Further Testing of SIRT6 DUBTACs.^b

Subsequent studies were planned to evaluate the remaining DUBTACs (18c-e and 19c-e) (Table 4-1). Building upon the preliminary western blot data demonstrating optimal SIRT6 stabilization at 1 μM in MM.1S cells with initial four

DUBTACs, the remaining SIRT6 DUBTACs were evaluated at this concentration. Contrary to our expectations, western blot analysis revealed no significant enhancement in SIRT6 protein levels following 24-hour treatment with any of the new DUBTAC derivatives at 1 µM (**Figure 4-6**).

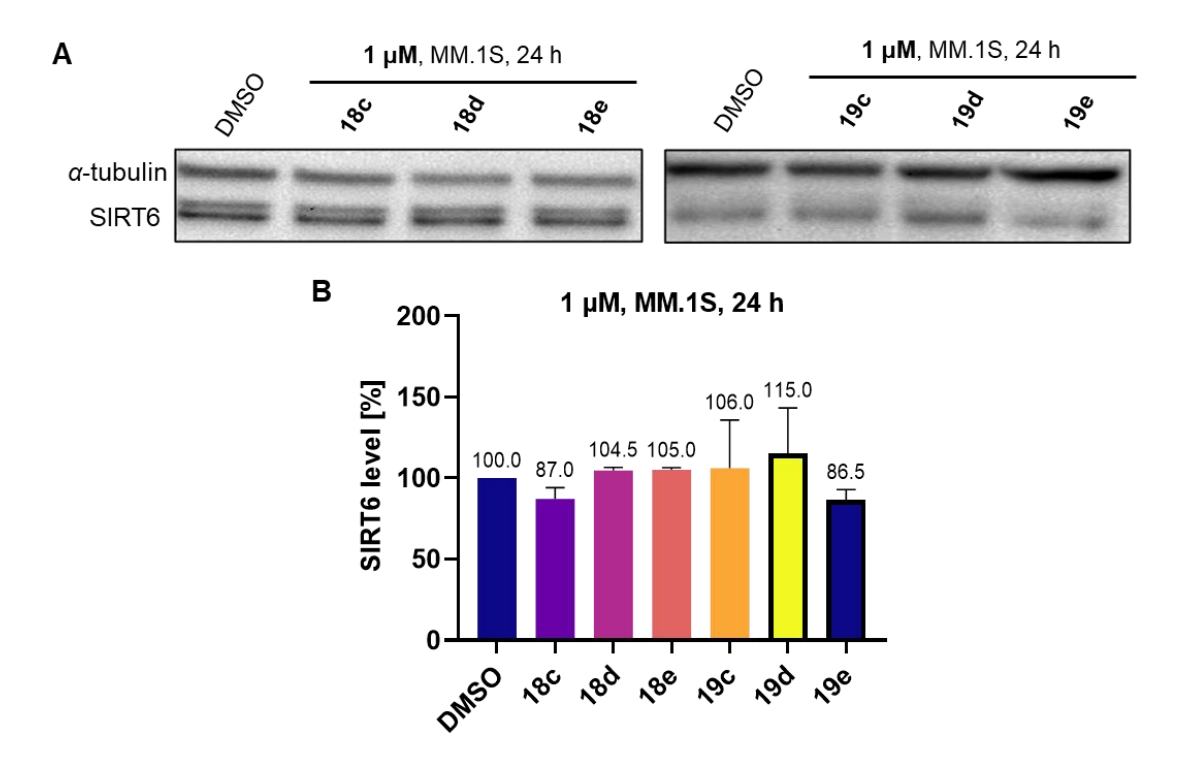


Figure 4-6. Analysis of SIRT6 protein levels after treatment of MM.1S cells with DUBTACs **18c-e** and **19c-e**. (**A**) MM.1S cells were treated with compounds at concentrations of 1 μ M for 24 h, with DMSO serving as vehicle control. SIRT6 levels were detected by immunoblot analysis. α -tubulin was used as the loading control. Representative images from a total of n = 2 replicates. (**B**) Densitometric analysis of SIRT6 levels after treatment with **18c-e** and **19c-e** for 24 h. Data from n = 2 replicates.

Following the western blot characterization, the antiproliferative potential of the SIRT6 DUBTACs **18a-e** and **19a-e** were evaluated in MM.1S cells. As illustrated in **Table 4-2**, compound **19d** exerted to some extent antiproliferative activity (EC₅₀ = 9.88 μ M), while the other DUBTACs exhibited minimal antiproliferative effects.

Table 4-2. Results of the CellTiter Glo 2.0 assay performed for DUBTACs and vorinostat $(n \ge 2)$.

DUBTAC	EC ₅₀ [μM]
18a	37.29 ± 23.12
18b	> 50
18c	> 50
18d	< 50
18e	> 50
19a	22.07 ± 0.99
19b	> 50
19c	> 50
19d	9.88 ± 2.38
19e	> 50
Vorinostat	$0.33 ~\pm~ 0.02$

^b Western blot experiments and CellTiter Glo 2.0 assay were performed by Cindy-Esther Kponomaizoun (Rheinische Friedrich-Wilhelms-Universität Bonn, Hansen Group).

4.3 Conclusion and Outlook

Pathological protein ubiquitination and subsequent degradation underlie numerous disease states, creating a compelling therapeutic rationale for TPS strategies that restore physiological protein homeostasis. Herein, the development of SIRT6 DUBTACs, a novel class of heterobifunctional molecules comprising an OTUB1-recruiting moiety tethered to a SIRT6 activator, was reported. Western blot analyses demonstrated that SIRT6 levels were successfully stabilized by the DUBTACs, especially for 18b. Preliminary cell viability assessment in MM.1S cells revealed concentration-responsive antiproliferative activity for DUBTAC 19d, supporting the therapeutic potential of this approach. Current efforts focus on structurally optimizing the DUBTAC system by replacing its OTUB1 recruiting moiety with modified MS5105 derivatives to improve both target stabilization efficiency and tissue selectivity. Overall, the heterobifunctional DUBTACs presented in this chapter could provide new therapeutic modalities in treating SIRT6-driven diseases.

4.4 Experimental Section

4.4.1 General Information

Chemicals were obtained from BLDpharm, Sigma-Aldrich, TCI Chemicals and aber GmbH used without purification. Air-sensitive reactions were carried out under argon atmosphere utilizing standard *Schlenk* techniques. Thin-layer chromatography (TLC) was carried out on prefabricated plates (silica gel 60, F254, Merck). Components were visualized by irradiation with ultraviolet light (254 nm). Column Chromatography was carried out on silica gel (60 Å, 40–60 μ m, *Acros Organics*).

Nuclear magnetic resonance spectroscopy (NMR): Proton (¹H) and carbon (¹³C) NMR spectra were recorded either on a Bruker AvanceDRX 500 (500 MHz ¹H NMR, 126 MHz ¹³C NMR) or a BrukerAvance III 600 (600 MHz ¹H NMR, 151 MHz ¹³C NMR). The chemical shifts are given in parts per million (ppm). Deuterated chloroform (CDCl₃) and deuterated dimethyl sulfoxide (DMSO-*d*₆) were used as solvents.

Mass Spectrometry: High resolution electrospray ionization mass spectra (HRMS-ESI) were acquired with *Bruker Daltonik GmbH* micrOTOF coupled to a an *LC Packings* Ultimate HPLC system and controlled by micrOTOFControl3.4 and HyStar 3.2-LC/MS, with a *BrukerDaltonik GmbH* ESI-qTOF Impact II coupled to a *Dionex* UltiMateTM 3000 UHPLC system and controlled by micrOTOFControl 4.0 and HyStar 3.2-LC/MS or with a micrOTOF-Q mass spectrometer (*Bruker*) with ESI-source coupled with an HPLC Dionex UltiMate 3000 (*Thermo Scientific*). Low resolution electrospray ionisation mass spectra (LRMS-ESI) were acquired with an *Advion* expression® compact mass spectrometer (CMS) coupled with an automated TLC plate reader Plate Express® (*Advion*).

High performance liquid chromatography (HPLC): A *Thermo Fisher Scientific* UltiMate 3000 UHPLC system with a Nucleodur 100–5 C18 (250 mm × 4.6 mm, *Macherey Nagel*) with a flow rate of 1 mL/min and a temperature of 25 °C or a

100–5 C18 (100 mm × 3 mm, *Macherey Nagel*) with a flow rate of 0.5 mL/min and a temperature of 25°C with an appropriate gradient were used. For preparative purposes a AZURA Prep. 500/1000 gradient system with a Nucleodur 110–5 C18 HTec (250 mm × 32 mm, *Macherey Nagel*) column with 20 mL/min was used. Detection was implemented by UV absorption measurement at a wavelength of λ = 220 nm and λ = 250 nm. Bidest. H₂O (A) and CH₃CN (B) were used as eluents with an addition of 0.1% TFA for eluent A. The purity of all final compounds was 95% or higher. Purity was determined *via* HPLC with the Nucleodur 100–5 C18 (250mm × 4.6 mm, *Macherey Nagel*) at 250 nm.

Flash chromatography was performed on an Interchim puriFlash XS 520 Plus with a diode-array detector (DAD) from 200-400 nm using prepacked silica gel cartridges (PF-30SIHP-F0012-F0040) or C18 reversed-phase cartridges (PF-30C18HP-F0004-F0012).

4.4.2 Synthesis

Synthesis of tert-butyl (E)-3-(5-bromofuran-2-yl)acrylate (2)

tert-Butyl diethylphosphonoacetate (971 mg, 3.85 mmol, 1.0 eq.) was dissolved in THF (20 mL) and the solution was cooled to 0 °C. Next, NaH (300 mg, 12.50 mmol, 2.0 eq.) was added slowly and the reaction mixture was stirred at 0 °C for 30 min. Then, 5-bromofuran-2-carbaldehyde (613 mg, 3.50 mmol, 0.9 eq.) was added portion-wise over 5 minutes. The reaction was stirred for 2 h at 0 °C and a gummy solid precipitated. Water was added and the resulting mixture was extracted with ethyl acetate (3 × 30 mL). Combined organic extracts were washed with brine (25 mL), dried over Na₂SO₄, and concentrated. The crude product was purified by silica gel chromatography (hexane: EA = 5:1, v/v) to provide the title compound 2 as a light yellow oil (936 mg, 89% yield). 1 H NMR (ppm, 500 MHz, DMSO- d_6): δ 7.27 (d, J = 16.0 Hz, 1H), 6.98 (d, J = 3.5 Hz, 1H), 6.74 (d, J = 3.5 Hz, 1H), 6.10 (d, J = 16.0 Hz, 1H), 1.46 (s, 9H).

Synthesis of benzyl (E)-4-{5-[3-(tert-butoxy)-3-oxoprop-1-en-1-yl]furan-2-yl}-3-oxopiperazine-1-carboxylate (3)

tert-Butyl (*E*)-3-(5-bromofuran-2-yl)acrylate (1.62 g, 5.94 mmol, 1.0 eq.) was dissolved in dioxane (30 mL) and benzyl 3-oxopiperazine-1-carboxylate (1.40 g, 5.94 mmol, 1.0 eq.), K_2CO_3 (2.46 g, 17.8 mmol, 3.0 eq.), N_iN^i -dimethyldiaminoethane (0.167 mL, 1.49 mmol, 0.25 eq.), and CuI (114 mg, 0.59 mmol, 0.1 eq.) were added. The mixture was stirred under nitrogen at reflux for 96 h, then cooled to rt. Saturated aq. NH₄Cl (5 mL) was added and the mixture stirred for 30 min. Then the mixture was diluted in ethyl acetate, filtered through celite, water was added, the mixture partitioned, and the aqueous layer extracted with ethyl acetate (2 × 25 mL). The extracts were combined, washed with brine (25 mL), dried over Na₂SO₄, concentrated, and purified by silica gel chromatography (hexane: EA = 3:1, v/v) to provide the title compound **3** as yellow solid (1.13 g, 43% yield). ¹H NMR (ppm, 500 MHz, DMSO- d_6): δ 7.41-7.32 (m, 5H), 7.30 (d, J = 15.5 Hz, 1H), 6.96 (d, J = 3.5 Hz, 1H), 6.56 (d, J = 3.5 Hz, 1H), 6.06 (d, J = 15.5 Hz, 1H), 5.13 (s, 2H), 4.23 (s, 2H), 4.00 (t, J = 5.0 Hz, 2H), 3.77 (s, 2H), 1.46 (s, 9H). ESI-MS m/z: 425.1, [M - H]⁻.

Synthesis of tert-butyl 3-[5-(4-acryloyl-2-oxopiperazin-1-yl)furan-2-yl]propanoate
(4)

Benzyl (*E*)-4-{5-[3-(tert-butoxy)-3-oxoprop-1-en-1-yl]furan-2-yl}-3-oxopiperazine-1-carboxylate (1.13 g, 2.65 mmol, 1.0 eq.) was dissolved in EtOH (25 mL) and Pd/C (232 mg, 5% wt. Pd, 0.05 eq.) was added. The reaction was placed under an atmosphere of H_2 and stirred vigorously overnight, before being

filtered through celite twice and then concentrated. The crude product was then redissolved in DCM (25 mL), cooled to 0 °C and treated with TEA (0.742 mL, 5.32 mmol, 2.0 eq.) before a solution of acryloyl chloride (258 μ L, 3.19 mmol, 1.2 eq.) in DCM (5 mL) was added over 2 minutes. After stirring for 2 h, water was added, and the mixture extracted with DCM (3 × 30 mL). Combined organic extracts were washed with brine (25 mL), dried over Na₂SO₄, concentrated, and the resulting crude oil was purified by silica gel chromatography (hexane: EA = 2:1, v/v) to obtain the title compound 4 as a light yellow oil (553 mg, 60% yield over two steps). ¹H NMR (ppm, 600 MHz, CDCl₃): δ 7.26 (s, 1H), 6.39 (dd, J = 1.8, 1.8 Hz, 1H), 6.28 (d, J = 3.0 Hz, 1H), 6.03 (d, J = 4.2 Hz, 1H), 5.80 (d, J = 10.8 Hz, 1H), 4.38 (d, J = 41.4 Hz, 2H), 3.87 (d, J = 72.6 Hz, 4H), 2.87 (t, J = 7.2 Hz, 2H), 2.53 (t, J = 7.8 Hz, 2H), 1.43 (s, 9H). ESI-MS m/z: 347.3, [M - H]⁻.

Synthesis of methyl 2-mercapto-5-nitrobenzoate (6)

To a stirred solution of thioacetic acid (267 μ L, 3.74 mmol, 1.5 eq.) and glycine-glycine (245 mg, 3.26 mmol, 1.3 eq.) in dry DMF (10 mL) was added cesium carbonate (2.43 g, 7.55 mmol, 3.0 eq.) at rt. After 10 min, a solution of the methyl 2-fluoro-5-nitrobenzoate (5, 500 mg, 2.51 mmol, 1.0 eq.) in dry DMF (10 mL) was added slowly after which the reaction mixture and stirred for 12 h. The reaction mixture was diluted with ethyl acetate (30 mL) and washed with 1 M HCl (30 mL), water (30 mL) and brine (30 mL), dried over sodium sulfate and concentrated to give 6 without further purification. (408 mg, yellow solid, 76% yield). ¹H NMR (600 MHz, DMSO- d_6) δ 8.62 (d, J = 2.4 Hz, 1H), 8.24 (dd, J = 1.8, 2.4 Hz, 1H), 7.87 (q, J = 10.8 Hz, 1H), 4.01 (s, 1H), 3.91 (s, 3H). ESI-MS m/z: 211.8, [M - H]⁻.

Synthesis of methyl 2-(chlorosulfonyl)-5-nitrobenzoate (7)

To a stirred solution of *N*-chlorosuccinimide (251 mg, 1.88 mmol, 4.0 eq.) in 2M HCl (0.8 mL) and acetonitrile (10 mL) was added methyl 2-mercapto-5-nitrobenzoate (**6**, 100 mg, 0.47 mmol, 1.0 eq.) slowly at 0 °C after which the reaction mixture was stirred for 3 h keeping the temperature below 20 °C. The reaction mixture was diluted with ethyl acetate (25 mL) and washed with water (25 mL) and brine (25 mL), dried over sodium sulfate and concentrated to give **7** (112 mg, light yellow oil, 85% yield). ¹H NMR (600 MHz, DMSO- d_6) δ 8.26 (dd, J = 2.4, 2.4 Hz, 1H), 8.12 (d, J = 2.4 Hz, 1H), 7.96 (d, J = 8.4 Hz, 1H), 3.76 (s, 3H). ESI-MS m/z: 259.9, [M – Cl + OH]⁻.

Synthesis of methyl 2-[N-(5-bromo-4-fluoro-2-methylphenyl)sulfamoyl]-5-nitrobenzoate (8)

$$O_2N$$

$$O_2N$$

$$O_3$$

$$O_4$$

$$O_5$$

$$O_7$$

$$O_8$$

$$O_8$$

To a solution of 5-bromo-4-fluoro-2-methylaniline (304 mg, 1.50 mmol, 1.0 eq.) in 20 mL pyridine was added methyl 2-(chlorosulfonyl)-5-nitrobenzoate (500 mg, 1.79 mmol, 1.2 eq.) under 0 °C and the reaction was stirred at the same temperature for 1 hour. Then the reaction was moved to room temperature and stirred for overnight. The reaction was cooled to 0 °C and adjusted the pH to 3~4 with 1N hydrochloric acid solution. The precipitate formed was filtered, washed with water (25 mL) and dried to yield crude intermediate product **8** which was directly used to the next step without purification (530 mg, yellow solid, 66% yield). 1 H NMR (600 MHz, DMSO- 2 d₆) δ 10.03 (s, 1H), 8.47 (t, 2 = 1.8 Hz, 2H), 7.96 (d, 2 = 8.4 Hz, 1H), 7.32 (d, 2 = 6.6 Hz, 1H), 7.26 (d, 2 = 9.0 Hz, 1H), 3.78 (s, 3H), 1.96 (s, 3H). ESI-MS m/z: 447.0, [M - H]⁻.

Synthesis of methyl 5-amino-2-[N-(5-bromo-4-fluoro-2-methylphenyl)sulfamoyl]benzoate (9)

To the crude intermediate product **8** (1.19 g, 2.67 mmol, 1.0 eq.) dissolved in acetic acid, iron powder (895 mg, 16.0 mmol, 6.0 eq.) was added at 50 °C. Then, the solution was stirred at the same condition for 12 h. The system was filtered and the solvent was evaporated under reduced pressure. The residue was purified by silica gel chromatography (hexane: EA = 2:1) to afford intermediate product **9** as a light yellow powder (818 mg, 74% yield). ¹H NMR (500 MHz, DMSO- d_6) δ 8.84 (s, 1H), 7.27-7.19 (m, 3H), 6.63-6.59 (m, 2H), 6.26 (s, 2H), 3.72 (s, 3H), 2.01 (s, 3H). ESI-MS m/z: 415.0, [M - H]⁻.

Synthesis of 5-amino-2-[N-(5-bromo-4-fluoro-2-methylphenyl)sulfamoyl]benzoic acid (10)

To a solution of 5-amino-2-[N-(5-bromo-4-fluoro-2-methylphenyl)sulfamoyl]benzoate (192 mg, 0.46 mmol, 1.0 eq.) in THF/H₂O (v:v, 1:1, 30 mL) was added LiOH·H₂O (83 mg, 1.84 mmol, 4.0 eq.) and the homogenous system was stirred at room temperature for 16 h. The solvent was removed under reduced pressure and the crude product was purified by flash column chromatography (C18 reversed phase, MeCN/H₂O 5-95%) to give **10** (107 mg, white solid, 56% yield). ¹H NMR (600 MHz, DMSO- d_6) δ 12.18 (s, 1H), 7.18-7.14 (m, 3H), 6.86 (d, J = 1.8 Hz, 1H), 6.33 (dd, J = 2.4, 2.4 Hz, 1H), 5.76 (s, 2H), 2.18 (s, 3H). ¹³C NMR (151 MHz, DMSO- d_6) δ 169.46, 155.28, 152.95, 136.12, 135.10, 133.28, 131.04, 130.14, 121.79, 118.21, 113.58, 113.07, 104.32, 17.36. ESI-MS m/z: 402.9, [M + H]⁺.

General procedure for the synthesis of 11a-e

To a mixture of **10** (107 mg, 0.27 mmol, 1.0 equiv.) and DIPEA (139 μ L, 0.81 mmol, 3.0 eq.) in anhydrous DMF (25 mL) was added HATU (152 mg, 0.41 mmol, 1.5 eq.), and the reaction mixture was stirred at room temperature for 30 min. Then tert-butyl (6-aminohexyl)carbamate (117 mg, 0.54 mmol, 2.0 eq.), tert-butyl (3-aminopropyl)carbamate (94 mg, 0.54 mmol, 2.0 eq.), tert-butyl (10-aminodecyl)carbamate (147 mg, 0.54 mmol, 2.0 eq.), tert-butyl (4-aminobutyl)carbamate (102 mg, 0.54 mmol, 2.0 eq.), or tert-butyl (5-aminopentyl)carbamate (109 mg, 0.54 mmol, 2.0 eq.) was added, and the mixture was stirred at room temperature for 30 min and heated this reaction mixture at 45 °C for another 48 h. The reaction mixture was distilled under vacuum to remove DMF. The obtained residue was purified by silica gel chromatography (hexane: EA = 1:1) to obtain the products **11a-e**.

tert-Butyl (6-{5-amino-2-[N-(5-bromo-4-fluoro-2-methylphenyl)sulfamoyl]benzamido}hexyl)carbamate (11a)

71 mg, light yellow oil, 44% yield. ¹H NMR (600 MHz, CDCl₃) δ 8.06 (s, 1H), 7.33 (d, J = 8.4 Hz, 1H), 7.25 (d, J = 4.8 Hz, 1H), 6.87 (d, J = 9.0 Hz, 1H), 6.79 (s, 1H), 6.60 (s, 1H), 6.52 (d, J = 8.4 Hz, 1H), 3.42 (q, J = 6.6 Hz, 2H), 3.13 (s, 2H), 2.18 (s, 3H), 1.69-1.62 (m, 2H), 1.53-1.48 (m, 2H), 1.44-1.38 (m, 13H). ¹³C NMR (151 MHz, CDCl₃) δ 169.62, 157.87, 156.24, 150.50, 136.94, 136.12, 132.48, 131.43, 130.44, 117.99, 117.84, 114.21, 105.31, 105.16, 79.15, 39.96, 29.71, 28.90, 28.40, 18.03. ESI-MS m/z: 601.5, [M - H]⁻.

tert-Butyl (3-{5-amino-2-[N-(5-bromo-4-fluoro-2-methylphenyl)sulfamoyl]benzamido}propyl)carbamate (11b)

99 mg, yellow solid, 66% yield. 1 H NMR (600 MHz, CDCl₃) δ 8.10 (s, 1H), 7.35 (d, J = 8.4 Hz, 1H), 7.28-7.25 (m, 2H), 6.86 (t, J = 9.0 Hz, 2H), 6.57 (dd, J = 1.8, 2.4 Hz, 1H), 3.46 (q, J= 6.0 Hz, 2H), 3.26 (s, 2H), 2.18 (s, 3H), 1.80-1.76 (m, 2H), 1.40 (s, 9H). 13 C NMR (151 MHz, CDCl₃) δ 169.81, 157.83, 156.19, 150.29, 136.93, 135.97, 132.51, 131.43, 130.38, 117.98, 117.83, 114.29 , 105.31, 105.16, 79.49, 38.61, 29.45, 28.35, 18.00. ESI-MS m/z: 559.0, [M - H]⁻.

tert-Butyl (10-{5-amino-2-[N-(5-bromo-4-fluoro-2-methylphenyl)sulfamoyl]benzamido}decyl)carbamate (11c)

116 mg, light yellow oil, 66% yield. ¹H NMR (600 MHz, CDCl₃) δ 8.09 (s, 1H), 7.23 (q, J = 7.8 Hz, 2H), 6.84 (d, J = 9.0 Hz, 1H), 6.69 (d, J = 1.2 Hz, 2H), 6.44 (dd, J = 1.8, 1.8 Hz, 1H), 3.37 (q, J = 6.6 Hz, 2H), 3.05 (s, 2H), 2.14 (s, 3H), 1.63-1.58 (m, 2H), 1.42 (s, 2H), 1.40 (s, 9H), 1.38-1.33 (m, 2H), 1.29 (d, J = 6.6 Hz, 2H), 1.25 (s, 8H). ¹³C NMR (151 MHz, CDCl₃) δ 169.47, 157.84, 156.20, 150.49, 136.84, 136.08, 132.43, 131.26, 130.45, 117.96, 117.81, 114.21, 113.97, 105.27,

105.12, 79.00, 40.39, 29.97, 29.34, 29.13, 28.38, 26.86, 26.69, 17.97. ESI-MS m/z: 657.4, [M - H]⁻.

tert-Butyl

(4-{5-amino-2-[N-(5-bromo-4-fluoro-2-

methylphenyl)sulfamoyl]benzamido}butyl)carbamate (11d)

11d

132 mg, light yellow solid, 87% yield. ¹H NMR (500 MHz, CDCl₃) δ 8.04 (s, 1H), 7.40 (d, J = 8.5 Hz, 1H), 7.27 (d, J = 6.5 Hz, 1H), 6.87 (d, J = 9.0 Hz, 2H), 6.63 (t, J = 7.0 Hz, 1H), 3.47 (q, J = 6.5 Hz, 2H), 3.17 (t, J = 7.0 Hz, 2H), 2.19 (s, 3H), 1.72-1.66 (m, 2H), 1.65-1.60 (m, 2H), 1.42 (s, 9H). ¹³C NMR (151 MHz, CDCl₃) δ 169.66, 157.84, 156.21, 150.46, 136.78, 136.01, 132.43, 131.33, 130.43, 117.98, 117.83, 114.44, 114.01, 105.30, 105.16, 79.30, 39.77, 36.57, 28.38, 27.24, 17.98. ESI-MS m/z: 573.2, [M - H]⁻.

 $(5-\{5-amino-2-[N-(5-bromo-4-fluoro-2-methylphenyl)sulfamoyl] benzamido\} pentyl) carbamate ~\it (11e) \\$

150 mg, light yellow oil, 96% yield. ¹H NMR (500 MHz, CDCl₃) δ 8.11 (s, 1H), 7.33 (d, J = 9.0 Hz, 1H), 7.25 (s, 1H), 6.86 (t, J = 9.5 Hz, 2H), 6.58-6.54 (m, 1H), 3.41 (q, J = 6.0 Hz, 2H), 3.12 (q, J = 2.5 Hz, 2H), 2.16 (s, 3H), 1.69-1.63 (m, 2H),

1.55-1.49 (m, 2H), 1.43 (t, J = 3.5 Hz, 2H), 1.40 (s, 9H). ¹³C NMR (126 MHz, CDCl₃) δ 169.55, 158.06, 156.09, 150.41, 136.87, 136.08, 132.38, 131.32, 130.46, 118.03, 117.85, 114.75, 105.35, 105.18, 79.27, 40.23, 29.67, 28.38, 23.81, 18.01. ESI-MS m/z: 587.2, [M - H]⁻.

General procedure for the synthesis of 12a-e

A solution of tert-butyl **11a** (168 mg, 0.28 mmol, 1.0 eq.), **11b** (156 mg, 0.28 mmol, 1.0 eq.), **11c** (184 mg, 0.28 mmol, 1.0 eq.), **11d** (161 mg, 0.28 mmol, 1.0 eq.), or **11e** (164 mg, 0.28 mmol, 1.0 eq.) in 20 mL pyridine was added 3,5-dichlorobenzene-1-sulfonyl chloride (137 mg, 0.56 mmol, 2.0 eq.) under 0 °C and the reaction was stirred at 0 °C for about 1 h. Then, the reaction was stirred for another 12 hours at room temperature. The reaction was cooled to 0 °C, and adjusted the pH to 3~4 with 1N hydrochloric acid solution. The precipitate formed was filtered and subsequently purified by silica gel chromatography (hexane: EA = 1.5:1) to afford **12a-e**.

tert-Butyl (6-{2-[N-(5-bromo-4-fluoro-2-methylphenyl)sulfamoyl]-5-[(3,5-dichlorophenyl)sulfonamide]benzamido}hexyl)carbamate (12a)

74 mg, light yellow oil, 33% yield. ¹H NMR (600 MHz, CDCl₃) δ 8.98 (s, 1H), 8.01 (s, 1H), 7.73 (d, J = 6.0 Hz, 2H), 7.55 (t, J = 1.8 Hz, 1H), 7.48 (d, J = 7.2 Hz, 1H), 7.39-7.35 (m, 2H), 7.16 (d, J = 6.0 Hz, 1H), 6.88 (d, J = 8.4 Hz, 1H), 6.40 (s, 1H), 3.49 (q, J = 5.4 Hz, 2H), 3.20 (t, J = 6.6 Hz, 2H), 2.09 (s, 3H), 1.55 (q, J = 6.6 Hz, 3H), 1.47 (s, 14H). ¹³C NMR (151 MHz, CDCl₃) δ 168.58, 158.20, 156.56, 141.96, 141.18, 136.27, 133.41, 131.62, 130.97, 130.84, 125.51, 119.38, 118.17, 118.02, 105.56, 105.41, 79.99, 40.07, 39.48, 29.19, 28.48, 25.65, 25.42, 17.84. ESI-MS m/z: 809.0, [M - H]⁻.

tert-Butyl (3-{2-[N-(5-bromo-4-fluoro-2-methylphenyl)sulfamoyl]-5-[(3,5-dichlorophenyl)sulfonamide]benzamido}propyl)carbamate (12b)

38 mg, yellow solid, 17% yield. ¹H NMR (600 MHz, CDCl₃) δ 8.59 (s, 1H), 8.18 (s, 1H), 7.73 (s, 2H), 7.54 (t, J = 1.2 Hz, 1H), 7.50 (d, J = 7.2 Hz, 1H), 7.37 (s, 1H), 7.28 (s, 1H), 7.18 (d, J = 6.6 Hz, 2H), 6.86 (d, J = 9.0 Hz, 1H), 3.50 (s, 2H), 3.29 (q, J = 6.0 Hz, 2H), 2.08 (s, 3H), 1.66 (d, J = 4.2 Hz, 2H), 1.42 (s, 9H). ¹³C NMR (151 MHz, CDCl₃) δ 168.67, 158.15, 156.51, 141.65, 140.83, 136.35, 133.59, 131.66, 131.03, 130.84, 125.48, 119.44, 119.04, 118.14, 117.99, 105.57, 80.07, 37.24, 36.95, 29.37, 28.38, 17.84. ESI-MS m/z: 767.0, [M - H]⁻.

tert-Butyl $(10-\{2-[N-(5-bromo-4-fluoro-2-methylphenyl)sulfamoyl]-5-[(3,5-dichlorophenyl)sulfonamide]benzamido\}decyl)carbamate (12c)$

89 mg, light yellow solid, 36% yield. 1 H NMR (600 MHz, CDCl₃) δ 9.17 (s, 1H), 8.16 (s, 1H), 7.71 (d, J = 1.8 Hz, 2H), 7.53 (s, 1H), 7.39 (s, 1H), 7.34 (d, J = 1.2 Hz, 1H), 7.15 (d, J = 6.6 Hz, 1H), 7.10 (d, J = 6.6 Hz, 1H), 6.86 (d, J = 9.0 Hz, 1H), 6.60 (s, 1H), 3.41 (q, J = 6.0 Hz, 2H), 3.10 (s, 2H), 2.07 (s, 3H), 1.65-1.60 (m, 2H), 1.44 (s, 9H), 1.37 (t, J = 7.2 Hz, 2H), 1.27 (s, 12H). 13 C NMR (151 MHz, CDCl₃)

δ 168.51, 158.15, 156.51, 141.84, 140.99, 136.31, 133.48, 131.61, 130.83, 125.45, 119.29, 118.14, 117.99, 105.54, 105.39, 79.43, 40.53, 29.86, 28.87, 28.45, 26.70, 17.84. ESI-MS m/z: 865.3, [M - H]⁻.

tert-Butyl (4-{2-[N-(5-bromo-4-fluoro-2-methylphenyl)sulfamoyl]-5-[(3,5-dichlorophenyl)sulfonamide]benzamido}butyl)carbamate (12d)

23 mg, light yellow oil, 10% yield. ¹H NMR (500 MHz, CDCl₃) δ 9.27 (s, 1H), 8.11 (s, 1H), 7.71 (d, J = 2.5 Hz, 2H), 7.53 (t, J = 2.0 Hz, 1H), 7.37 (t, J = 2.0 Hz, 2H), 7.15 (t, J = 6.5 Hz, 2H), 7.01 (t, J = 5.5 Hz, 1H), 6.86 (d, J = 9.0 Hz, 1H), 3.44 (q, J = 6.0 Hz, 2H), 3.17 (t, J = 7.0 Hz, 2H), 2.05 (s, 3H), 1.69-1.61 (m, 4H), 1.44 (s, 9H). ¹³C NMR (126 MHz, CDCl₃) δ 168.66, 158.32, 156.35, 141.77, 141.03, 136.30, 133.49, 132.69, 131.59, 130.81, 125.45, 119.52, 118.75, 118.15, 117.97, 105.55, 105.38, 79.91, 39.92, 28.43, 27.61, 27.25, 17.81. ESI-MS m/z: 781.3, [M - H]⁻.

tert-Butyl $(5-\{2-[N-(5-bromo-4-fluoro-2-methylphenyl)sulfamoyl]-5-[(3,5-dichlorophenyl)sulfonamide]benzamido\}pentyl)carbamate (12e)$

31 mg, light yellow oil, 21% yield. ¹H NMR (500 MHz, CDCl₃) δ 8.10 (s, 1H), 7.73 (d, J = 1.5 Hz, 2H), 7.52 (t, J = 1.5 Hz, 1H), 7.10 (q, J = 6.0 Hz, 2H), 6.96 (s, 1H), 6.86 (d, J = 9.0 Hz, 1H), 3.43 (d, J = 5.0 Hz, 2H), 3.14 (d, J = 8.5 Hz, 2H), 2.06 (s, 3H), 1.70-1.64 (m, 2H), 1.54 (t, J = 7.0 Hz, 2H), 1.44 (s, 11H). ¹³C NMR (126 MHz, CDCl₃) δ 168.68, 158.35, 156.38, 141.84, 141.19, 136.56, 136.29, 133.46, 131.57, 130.82, 125.48, 118.17, 117.99, 105.52, 105.35, 79.91, 40.59, 39.84, 29.66, 28.42, 17.82. ESI-MS m/z: 795.2, [M - H]⁻.

Synthesis of 3-nitro-4-(1H-pyrrol-1-yl)benzoic acid (14)

To a solution of 4-amino-3-nitrobenzoic acid (1.0 g, 5.50 mmol, 1.0 eq.) in glacial acetic acid (25 mL) was add 2,5-dimethoxytetrahydrofuran (3.5 mL, 5.50 mmol, 1.0 eq.). Heating the reaction mixture to 120 °C for 12 h and cool the reaction mixture to room temperature. Then remove the solvent and purified the residue by silica gel chromatography (MeOH/CHCl₃ = 1 : 20) to obtain **14** (990 mg, red solid, yield 78%). ¹H NMR (600 MHz, DMSO- d_6) δ 13.69 (s, 1H), 8.45 (d, J = 1.8 Hz, 1H), 8.26 (dd, J = 1.8, 1.8 Hz, 1H), 7.77 (d, J = 8.4 Hz, 1H), 7.01 (t, J = 1.8 Hz, 2H), 6.32 (t, J = 1.8 Hz, 2H). ESI-MS m/z: 233.0, [M + H]⁺.

Synthesis of 3-amino-4-(1H-pyrrol-1-yl)benzoic acid (15)

To a mixture of **14** (990 mg, 4.26 mmol, 1.0 eq.) and a catalytic amount of 5% palladium on carbon (452 mg, 0.05 eq.) in EA/MeOH (v/v = 1:1, 20 mL) at 25°C under H₂ atmosphere for 16 h. Then the reaction mixture was filtered through celite and concentrated to obtain **15** for next step without further purification. (806 mg, brown solid, 94% yield). ¹H NMR (500 MHz, DMSO- d_6) δ 12.76 (s, 1H), 7.47 (d, J = 2.0 Hz, 1H), 7.19 (dd, J = 2.0, 2.0 Hz, 1H), 7.11 (d, J = 8.0 Hz, 1H), 6.95 (t, J = 2.0 Hz, 1H), 7.19 (dd, J = 2.0, 2.0 Hz, 1H), 7.11 (d, J = 8.0 Hz, 1H), 6.95 (t, J = 2.0)

 $= 2.0 \text{ Hz}, 2\text{H}, 6.26 \text{ (t, } J = 2.0 \text{ Hz}, 2\text{H}), 5.06 \text{ (s, 2H)}. ESI-MS m/z: 203.0, [M + H]^+.$

Synthesis of 4-(pyridin-3-yl)pyrrolo[1,2-a]quinoxaline-7-carboxylic acid (16)

A solution of **15** (500 mg, 2.48 mmol, 1.0 eq.) and the commercial pyridine-3-carboxaldehyde (360 mg, 3.36 mmol, 1.4 eq.) in dry ethanol (20 mL) was heated to 50 °C for 6 h in the presence of a catalytic amount of glacial acetic acid (15 drops). After cooling to room temperature, the reaction was quenched with water (25 mL) and stirred for 1 h. The resulting solid in suspension was then filtered off, washed with water (25 mL) and purified by silica gel chromatography (chloroform/MeOH = 40:1, v/v) to afford **16**. (536 mg, yellow solid, 74% yield). ¹H NMR (500 MHz, DMSO- d_6) δ 12.68 (s, 1H), 8.56 (d, J = 2.0 Hz, 1H), 8.50 (dd, J = 1.5, 1.5 Hz, 1H), 7.70 (dt, J = 2.4, 2.4 Hz, 1H), 7.61 (d, J = 9.6 Hz, 1H), 7.55 (q, J = 1.8 Hz, 1H), 7.49 (d, J = 1.8 Hz, 1H), 7.39-7.33 (m, 1H), 6.94 (s, 1H), 6.27 (t, J = 4.2 Hz, 1H), 5.73-5.71 (m, 1H). ¹³C NMR (151 MHz, DMSO- d_6) δ 167.25, 149.07, 148.67, 138.17, 136.07, 134.97, 128.51, 127.64, 127.07, 123.83, 115.72, 114.69, 106.24. ESI-MS m/z: 290.2, [M + H]⁺.

General procedure for the synthesis of 17a-e

To a mixture of **16** (750 mg, 2.60 mmol, 1.0 eq.) and DIPEA (1.35 mL, 7.78 mmol, 3.0 eq.) in anhydrous DMF (25 mL) was added HATU (1.98 g, 5.20 mmol, 2.0 eq.), and the reaction mixture was stirred at room temperature for 30 min. Then tert-butyl (6-aminohexyl)carbamate (1.12 g, 5.20 mmol, 2.0 eq.), tert-butyl (3-aminopropyl)carbamate (906 mg, 5.20 mmol, 2.0 eq.), tert-butyl (4-aminobutyl)carbamate (979 mg, 5.20 mmol, 2.0 eq.), tert-butyl (10-aminodecyl)carbamate (1417 mg, 5.20 mmol, 2.0 eq.), or tert-butyl (5-aminopentyl)carbamate (1052 mg, 5.20 mmol, 2.0 eq.) was added, and the mixture was stirred at the room temperature for 12 h. The reaction mixture was distilled under vacuum to remove DMF. The obtained residue was purified by flash column

chromatography (C18 reversed phase, MeCN/H₂O 5-95%) to obtain the products **17a-e**.

tert-Butyl {6-[4-(pyridin-3-yl)pyrrolo[1,2-a]quinoxaline-7-carboxamido]hexyl}carbamate (17a)

356 mg, yellow solid, 43% yield. ¹H NMR (600 MHz, DMSO- d_6) δ 9.18 (d, J = 2.4 Hz, 1H), 8.78 (dd, J = 1.2, 1.2 Hz, 1H), 8.67-8.64 (m, 2H), 8.50 (d, J = 1.8 Hz, 1H), 8.42-8.39 (m, 2H), 8.09 (dd, J = 1.8, 1.8 Hz, 1H), 7.63 (q, J = 3.0 Hz, 1H), 7.11 (dd, J = 0.6, 1.2 Hz, 1H), 7.06 (q, J = 1.2 Hz, 1H), 6.75 (t, J = 5.4 Hz, 1H), 3.29 (q, J = 6.6 Hz, 2H), 2.90 (q, J = 6.0 Hz, 2H), 1.55 (q, J = 7.2 Hz, 2H), 1.40-1.27 (m, 15H). ¹³C NMR (151 MHz, DMSO- d_6) δ 165.12, 155.73, 151.56, 151.06, 149.08, 136.10, 135.01, 133.45, 131.76, 128.60, 127.25, 124.29, 123.89, 117.60, 115.25, 114.99, 109.08, 77.42, 29.61, 29.22, 28.42, 26.38, 26.19. ESI-MS m/z: 488.1, $[M + H]^+$.

tert-Butyl {3-[4-(pyridin-3-yl)pyrrolo[1,2-a]quinoxaline-7-carboxamido]propyl}carbamate (17b)

156 mg, yellow solid, 30% yield. ¹H NMR (600 MHz, DMSO- d_6) δ 9.18 (d, J = 1.8 Hz, 1H), 8.79 (dd, J = 1.8, 1.8 Hz, 1H), 8.67-8.65 (m, 2H), 8.51 (d, J = 1.8 Hz, 1H), 8.43-8.39 (m, 2H), 8.09 (dd, J = 1.8, 2.4 Hz, 1H), 7.63 (q, J = 3.0 Hz, 1H), 7.12 (dd, J = 0.6, 1.2 Hz, 1H), 7.06 (q, J = 1.2 Hz, 1H), 6.82 (t, J = 4.8 Hz, 1H),

3.32 (t, J = 6.6 Hz, 2H), 3.01 (q, J = 6.6 Hz, 2H), 1.71-1.66 (m, 2H), 1.38 (s, 9H). ¹³C NMR (151 MHz, DMSO- d_6) δ 165.24, 155.76, 151.59, 151.07, 149.08, 136.11, 135.01, 133.44, 131.63, 128.65, 128.53, 127.23, 124.29, 123.89, 117.63, 115.27, 115.03, 109.12, 77.64, 37.93, 37.29, 29.67, 28.41. ESI-MS m/z: 446.1, [M + H]⁺.

tert-Butyl {4-[4-(pyridin-3-yl)pyrrolo[1,2-a]quinoxaline-7-carboxamido]butyl}carbamate (17c)

118 mg, yellow oil, 10% yield. ¹H NMR (500 MHz, DMSO- d_6) δ 9.18 (q, J = 1.5 Hz, 1H), 8.78 (dd, J = 1.5, 2.0 Hz, 1H), 8.67 (t, J = 5.5 Hz, 1H), 8.63 (dd, J = 1.0, 1.0 Hz, 1H), 8.50 (d, J = 2.0 Hz, 1H), 8.41-8.38 (m, 2H), 8.09 (dd, J = 2.0, 2.0 Hz, 1H), 7.64-7.62 (m, 1H), 7.10 (dd, J = 1.0, 1.5 Hz, 1H), 7.05 (q, J = 1.5 Hz, 1H), 6.79 (t, J = 5.0 Hz, 1H), 3.29 (d, J = 7.0 Hz, 2H), 2.95 (q, J = 6.0 Hz, 2H), 1.58-1.52 (m, 2H), 1.48-1.43 (m, 2H), 1.37 (s, 9H). ¹³C NMR (126 MHz, DMSO- d_6) δ 165.17, 155.75, 151.53, 151.04, 149.07, 136.08, 134.99, 133.44, 131.73, 128.56, 127.23, 124.28, 123.86, 117.57, 115.22, 114.96, 109.06, 77.47, 28.41, 27.26, 26.66. ESI-MS m/z: 460.3, [M + H]⁺.

tert-Butyl {10-[4-(pyridin-3-yl)pyrrolo[1,2-a]quinoxaline-7-carboxamido]decyl}carbamate (17d)

278 mg, yellow oil, 20% yield. ¹H NMR (500 MHz, DMSO- d_6) δ 9.17 (d, J = 1.5 Hz, 1H), 8.78 (dd, J = 1.0, 1.5 Hz, 1H), 8.66-8.62 (m, 2H), 8.50 (d, J = 2.0 Hz, 1H), 8.41-8.38 (m, 2H), 8.09 (dd, J = 2.0, 2.0 Hz, 1H), 7.62 (q, J = 3.0 Hz, 1H),

7.11-7.04 (m, 2H), 6.70 (s, 1H), 3.28 (d, J = 6.5 Hz, 2H), 2.86 (q, J = 6.0 Hz, 2H), 1.56 (t, J = 6.5 Hz, 2H), 1.35 (s, 9H), 1.22 (d, J = 2.0 Hz, 14H). ¹³C NMR (126 MHz, DMSO- d_6) δ 165.11, 155.70, 151.51, 151.02, 149.07, 136.07, 135.00, 133.44, 131.75, 128.55, 127.22, 124.28, 123.85, 117.55, 115.20, 114.94, 109.04, 77.37, 29.60, 29.20, 29.08, 28.93, 28.39, 26.68, 26.40. ESI-MS m/z: 544.5, [M + H]⁺.

tert-Butyl {5-[4-(pyridin-3-yl)pyrrolo[1,2-a]quinoxaline-7-carboxamido]pentyl}carbamate (17e)

321 mg, yellow solid, 26% yield. ¹H NMR (600 MHz, DMSO- d_6) δ 9.18 (d, J = 0.6 Hz, 1H), 8.78 (d, J = 4.8 Hz, 1H), 8.66 (t, J = 6.0 Hz, 1H), 8.62 (d, J = 1.2 Hz, 1H), 8.50 (s, 1H), 8.39 (q, J = 3.6 Hz, 2H), 8.08 (d, J = 9.0 Hz, 1H), 7.62 (q, J = 3.0 Hz, 1H), 7.10 (d, J = 4.2 Hz, 1H), 7.04 (t, J = 2.4 Hz, 1H), 6.75 (d, J = 4.8 Hz, 1H), 3.30 (t, J = 6.0 Hz, 2H), 2.92 (q, J = 6.0 Hz, 2H), 1.59-1.54 (m, 2H), 1.45-1.40 (m, 2H), 1.35 (s, 9H), 1.32 (t, J = 7.2 Hz, 2H). ¹³C NMR (151 MHz, DMSO- d_6) δ 165.15, 155.74, 151.51, 151.03, 149.08, 136.08, 134.99, 133.44, 131.74, 128.56, 127.24, 124.28, 123.86, 117.56, 115.20, 114.94, 109.04, 77.42, 29.38, 28.94, 28.41, 23.98. ESI-MS m/z: 474.3, $[M + H]^+$.

General procedure for the synthesis of 18a-e and 19a-e

To a solution of **4**, **12a-e** or **17a-e** in DCM (10 mL) was added TFA (2.5 mL) dropwise and reaction mixture was stirred at room temperature for 2 h. Then DCM was removed to provide compounds **4'**, **12a-e'** or **17a-e'** directly for next step without purification. Next, to a mixture of **4'** (292 mg, 1.0 mmol, 1.0 eq.) and DIPEA (1.74 mL, 10.0 mmol, 10.0 eq.) in anhydrous DMF (25 mL) was added HATU (760 mg, 2.0 mmol, 2.0 eq.) and the reaction mixture was stirred at room temperature for 30 min. Then **12a'** (708 mg, 1.0 mmol, 1.0 eq.), **12b'** (668 mg, 1.0 mmol, 1.0 eq.), **12c'** (766 mg, 1.0 mmol, 1.0 eq.), **12d'** (682 mg, 1.0 mmol, 1.0 eq.),

12e' (696 mg, 1.0 mmol, 1.0 eq.), or **17a'** (387 mg, 1.0 mmol, 1.0 eq.), **17b'** (345 mg, 1.0 mmol, 1.0 eq.), **17c'** (359 mg, 1.0 mmol, 1.0 eq.), **17d'** (343 mg, 1.0 mmol, 1.0 eq.), **17e'** (373 mg, 1.0 mmol, 1.0 eq.) treated with TFA was individually added, and the mixture was stirred at the room temperature for 12 h. The reaction mixture was distilled under vacuum to remove DMF. The obtained residue was purified by preparative HPLC (MeCN/H₂O 5-95%) for eluting to obtain final product **18a-e** or **19a-e**.

N-(6-{3-[5-(4-Acryloyl-2-oxopiperazin-1-yl)furan-2-yl]propanamido}hexyl)-2-[N-(5-bromo-4-fluoro-2-methylphenyl)sulfamoyl]-5-[(3,5-dichlorophenyl)sulfonamide]benzamide (18a)

226 mg, white solid, 23% yield. ¹H NMR (600 MHz, CDCl₃) δ 10.82 (s, 1H), 8.08 (s, 1H), 7.75 (d, J = 1.8 Hz, 2H), 7.51 (q, J = 1.8 Hz, 2H), 7.42 (dd, J = 1.8, 1.2 Hz, 1H), 7.29 (s, 1H), 7.14 (d, J = 6.6 Hz, 1H), 6.87 (q, J = 3.6 Hz, 1H), 6.68 (s, 1H), 6.50 (s, 1H), 6.40 (dd, J = 1.2, 1.8 Hz, 1H), 6.15 (s, 1H), 6.08 (d, J = 3.0 Hz, 1H), 5.81 (q, J = 1.8 Hz, 1H), 4.53-4.28 (m, 2H), 3.94 (t, J = 4.2 Hz, 2H), 3.79 (s, 2H), 3.48 (t, J = 4.8 Hz, 2H), 3.33 (s, 2H), 3.03 (s, 2H), 2.70 (t, J = 6.0 Hz, 2H), 2.07 (s, 3H), 1.59 (q, J = 3.0 Hz, 2H), 1.51 (t, J = 6.0 Hz, 2H), 1.44-1.39 (m, 2H), 1.33 (d, J = 6.6 Hz, 2H). ¹³C NMR (151 MHz, CDCl₃) δ 173.53, 168.77, 165.09, 158.12, 156.48, 149.51, 145.08, 142.20, 141.90, 136.68, 136.23, 136.12, 133.20, 131.84, 130.91, 130.71, 126.13, 125.58, 119.64, 118.12, 117.97, 107.69, 105.48, 105.34, 101.27, 49.25, 48.26, 47.52, 40.08, 39.88, 34.91, 28.82, 28.44, 25.71, 25.10,

24.53, 17.86. ESI-MS m/z: 985.3, $[M + H]^+$. HRMS (ESI): calcd for $C_{40}H_{42}BrCl_2FN_6O_9S_2$, $[M + H]^+$ 983.1072; found, 983.1072. HPLC: $t_R = 13.79$ min (99.69% purity).

N-(3-{3-[5-(4-Acryloyl-2-oxopiperazin-1-yl)furan-2-yl]propanamido}propyl)-2[N-(5-bromo-4-fluoro-2-methylphenyl)sulfamoyl]-5-[(3,5-dichlorophenyl)sulfonamide]benzamide (18b)

160 mg, white solid, 17% yield. 1 H NMR (600 MHz, CDCl₃) δ 8.21 (s, 1H), 7.74 (t, J = 1.8 Hz, 2H), 7.54-7.49 (m, 2H), 7.35-7.32 (m, 1H), 7.27 (s, 1H), 7.19 (t, J = 6.6 Hz, 1H), 6.87 (t, J = 9.6 Hz, 1H), 6.61-6.51 (m, 2H), 6.40 (q, J = 16.2 Hz, 1H), 6.12 (d, J = 37.8 Hz, 1H), 6.01 (d, J = 3.0 Hz, 1H), 5.87-5.81 (m, 1H), 4.55-4.27 (m, 2H), 4.03-3.82 (m, 4H), 3.45 (dd, J = 4.2, 4.8 Hz, 2H), 3.36 (s, 2H), 2.83 (dt, J = 6.0, 5.4 Hz, 2H), 2.54 (s, 2H), 2.06 (t, J = 20.4 Hz, 3H), 1.77 (q, J = 7.2 Hz, 2H). 13 C NMR (151 MHz, CDCl₃) δ 174.13, 168.71, 165.35, 159.51, 158.22, 156.58, 144.65, 141.87, 136.27, 133.46, 132.70, 131.67, 130.93, 130.30, 126.36, 126.08, 125.50, 119.88, 118.18, 118.03, 107.52, 105.59, 105.45, 49.42, 48.76, 47.85, 38.57, 36.58, 33.54, 29.58, 24.39, 17.78. ESI-MS m/z: 943.3, [M + H] $^+$ HRMS (ESI): calcd for C₃₇H₃₆BrCl₂FN₆O₉S₂, [M + H] $^+$ 941.0602; found, 941.0573. HPLC: t_R = 13.38 min (99.88% purity).

N-(4-{3-[5-(4-Acryloyl-2-oxopiperazin-1-yl)furan-2-yl]propanamido}butyl)-2-[N-(5-bromo-4-fluoro-2-methylphenyl)sulfamoyl]-5-[(3,5-dichlorophenyl)sulfonamide]benzamide (18c)

95 mg, white solid, 10% yield. 1 H NMR (600 MHz, DMSO- d_6) δ 11.27 (s, 1H), 8.84 (t, J = 5.4 Hz, 1H), 8.75 (s, 1H), 8.02 (s, 1H), 7.87 (t, J = 5.4 Hz, 1H), 7.79 (d, J = 1.8 Hz, 2H), 7.41 (d, J = 9.0 Hz, 1H), 7.27 (d, J = 8.4 Hz, 1H), 7.23 (s, 1H), 7.16 (q, J = 7.2 Hz, 2H), 6.85-6.77 (m, 1H), 6.19 (q, J = 4.2 Hz, 2H), 6.09 (d, J = 3.0 Hz, 1H), 5.75 (d, J = 9.0 Hz, 1H), 4.34 (d, J = 93.6 Hz, 2H), 3.82 (q, J = 37.8 Hz, 4H), 3.24 (q, J = 6.0 Hz, 2H), 3.09 (q, J = 5.4 Hz, 2H), 2.80 (t, J = 7.8 Hz, 2H), 2.39 (t, J = 7.2 Hz, 2H), 1.87 (s, 3H), 1.54-1.45 (m, 4H). 13 C NMR (151 MHz, DMSO- d_6) δ 170.75, 167.87, 164.32, 157.26, 155.64, 149.80, 145.15, 137.11, 136.66, 135.49, 133.29, 132.57, 130.84, 130.55, 128.42, 127.78, 125.41, 119.51, 118.46, 118.30, 118.14, 106.61, 104.39, 104.25, 100.21, 49.01, 47.28, 46.55, 42.15, 39.12, 38.29, 33.50, 26.64, 26.13, 23.67, 17.13. ESI-MS m/z: 957.1, [M + H] $^+$. HRMS (ESI): calcd for C_{38} H₃₈BrCl₂FN₆O₉S₂, [M + H] $^+$ 955.0759; found, 955.0732. HPLC: t_R = 13.38 min (99.00% purity).

N-(10-{3-[5-(4-Acryloyl-2-oxopiperazin-1-yl)furan-2-yl]propanamido}decyl)-2-[N-(5-bromo-4-fluoro-2-methylphenyl)sulfamoyl]-5-[(3,5-dichlorophenyl)sulfonamide]benzamide (18d)

145 mg, white solid, 14% yield. ¹H NMR (500 MHz, DMSO- d_6) δ 11.26 (s, 1H), 8.80 (t, J = 6.0 Hz, 1H), 8.75 (s, 1H), 8.03 (t, J = 2.0 Hz, 1H), 7.79 (q, J = 6.0 Hz, 3H), 7.42 (d, J = 8.5 Hz, 1H), 7.29-7.24 (m, 2H), 7.15 (q, J = 3.5 Hz, 2H), 6.79 (q, J = 10.5 Hz, 1H), 6.18 (t, J = 3.0 Hz, 2H), 6.07 (d, J = 3.0 Hz, 1H), 5.74 (d, J = 10.0 Hz, 1H), 4.40 (s, 1H), 4.25 (s, 1H), 3.84 (q, J = 31.5 Hz, 4H), 3.22 (q, J = 6.0 Hz, 2H), 3.01 (q, J = 6.0 Hz, 2H), 2.77 (t, J = 7.5 Hz, 2H), 2.35 (t, J = 7.5 Hz, 2H), 1.86 (s, 3H), 1.54-1.49 (m, 2H), 1.38-1.24 (m, 14H). ¹³C NMR (126 MHz, DMSO- d_6) δ 170.62, 167.73, 164.31, 157.43, 155.49, 149.76, 145.15, 141.95, 141.35, 137.19, 136.70, 135.55, 133.49, 132.54, 131.75, 130.89, 130.56, 128.40, 127.78, 125.43, 119.34, 118.53, 118.30, 118.12, 106.56, 104.40, 104.22, 100.11, 48.99, 47.23, 46.54, 38.62, 33.45, 29.26, 29.13, 28.91, 28.73, 26.54, 23.64, 17.11. ESI-MS m/z: 1041.2, [M + H]⁺. HRMS (ESI): calcd for C₄₄H₅₀BrCl₂FN₆O₉S₂, [M + H]⁺ 1039.1698; found, 1039.1693. HPLC: t_R = 22.85 min (95.60% purity).

N-(5-{3-[5-(4-Acryloyl-2-oxopiperazin-1-yl)furan-2-yl]propanamido}pentyl)-2-[N-(5-bromo-4-fluoro-2-methylphenyl)sulfamoyl]-5-[(3,5-dichlorophenyl)sulfonamide]benzamide (18e)

68 mg, white solid, 7% yield. ¹H NMR (600 MHz, DMSO- d_6) δ 11.26 (s, 1H), 8.81 (t, J = 5.4 Hz, 1H), 8.75 (s, 1H), 8.03 (t, J = 1.8 Hz, 1H), 7.83 (t, J = 5.4 Hz, 1H), 7.79 (d, J = 1.8 Hz, 2H), 7.42 (d, J = 8.4 Hz, 1H), 7.28 (dd, J = 2.4, 1.8 Hz, 1H), 7.23 (d, J = 2.4 Hz, 1H), 7.15 (q, J = 6.6 Hz, 2H), 6.84-6.75 (m, 1H), 6.18 (q, J = 6.0 Hz, 2H), 6.08 (d, J = 3.0 Hz, 1H), 5.73 (d, J = 9.6 Hz, 1H), 4.33 (d, J = 93.6 Hz, 2H), 3.81 (q, J = 36.6 Hz, 4H), 3.22 (q, J = 6.6 Hz, 2H), 3.04 (q, J = 6.0 Hz, 2H), 2.77 (t, J = 7.2 Hz, 2H), 2.37 (q, J = 4.2 Hz, 2H), 1.85 (s, 3H), 1.54-1.49 (m,

2H), 1.44-1.39 (m, 2H), 1.34-1.29 (m, 2H). 13 C NMR (151 MHz, DMSO- d_6) δ 170.69, 167.74, 164.32, 157.29, 155.66, 149.78, 145.15, 141.93, 141.36, 137.18, 136.72, 135.56, 133.51, 132.50, 131.72, 130.94, 130.59, 128.41, 128.00, 127.77, 125.45, 119.36, 118.47, 118.29, 118.14, 106.58, 104.40, 104.25, 100.18, 49.00, 47.28, 46.55, 38.58, 38.45, 33.46, 28.94, 28.37, 23.83, 23.64, 17.11. ESI-MS m/z: 971.1, [M+H]⁺. HRMS (ESI): calcd for C₃₉H₄₀BrCl₂FN₆O₉S₂, [M+H]⁺ 969.0915; found, 969.0890. HPLC: $t_R = 21.11 \text{ min } (96.43\% \text{ purity}).$

N-(6-{3-[5-(4-Acryloyl-2-oxopiperazin-1-yl)furan-2-yl]propanamido}hexyl)-4-(pyridin-3-yl)pyrrolo[1,2-a]quinoxaline-7-carboxamide (**19a**)

106 mg, yellow solid, 16% yield. ¹H NMR (600 MHz, DMSO- d_6) δ 9.23 (d, J = 1.8 Hz, 1H), 8.83 (dd, J = 1.2, 1.2 Hz, 1H), 8.68-8.67 (m, 2H), 8.52-8.49 (m, 2H), 8.42 (t, J = 4.8 Hz, 1H), 8.11 (dd, J = 1.8, 1.8 Hz, 1H), 7.84 (t, J = 5.4 Hz, 1H), 7.73 (q, J = 3.0 Hz, 1H), 7.16-7.14 (m, 1H), 7.09-7.06 (m, 1H), 6.86-6.75 (m, 1H), 6.18 (q, J = 12.0 Hz, 2H), 6.08 (d, J = 3.6 Hz, 1H), 5.74 (d, J = 9.6 Hz, 1H), 4.33 (d, J = 92.4 Hz, 2H), 3.92-3.74 (m, 4H), 3.30 (q, J = 6.6 Hz, 2H), 3.04 (q, J = 6.0 Hz, 2H), 2.78 (t, J = 7.8 Hz, 2H), 2.37 (t, J = 7.8 Hz, 2H), 1.55 (q, J = 7.2 Hz, 2H), 1.39 (q, J = 6.6 Hz, 2H), 1.35-1.27 (m, 4H). ¹³C NMR (151 MHz, DMSO- d_6) δ 170.68, 165.12, 164.33, 151.11, 150.02, 149.79, 148.14, 145.14, 137.43, 134.87, 133.77, 131.83, 128.52, 127.97, 127.36, 124.43, 124.23, 117.81, 115.38, 115.05, 109.26, 106.58, 100.18, 49.01, 47.28, 46.55, 42.15, 38.58, 33.47, 29.24, 26.38, 23.66. ESI-MS m/z: 662.6, [M + H]⁺. HRMS (ESI): calcd for C₃₇H₃₉N₇O₅, [M + H]⁺ 662.3085; found, 662.3074. HPLC: t_R = 14.82 min (95.36% purity).

N-(3-{3-[5-(4-Acryloyl-2-oxopiperazin-1-yl)furan-2-yl]propanamido}propyl)-4-(pyridin-3-yl)pyrrolo[1,2-a]quinoxaline-7-carboxamide (**19b**)

93 mg, yellow solid, 15% yield. ¹H NMR (600 MHz, DMSO- d_6) δ 9.23 (d, J = 1.8 Hz, 1H), 8.83 (dd, J = 1.2, 1.2 Hz, 1H), 8.66 (t, J = 3.0 Hz, 2H), 8.53-8.50 (m, 2H), 8.43 (d, J = 8.4 Hz, 1H), 8.10 (dd, J = 1.8, 1.8 Hz, 1H), 7.93 (t, J = 6.0 Hz, 1H), 7.73 (q, J = 3.0 Hz, 1H), 7.15 (d, J = 3.6 Hz, 1H), 7.08 (t, J = 4.2 Hz, 1H), 6.79 (t, J = 10.8 Hz, 1H), 6.19-6.09 (m, 3H), 5.72 (d, J = 10.2 Hz, 1H), 4.32 (d, J = 93.0 Hz, 2H), 3.80 (q, J = 34.2 Hz, 4H), 3.31 (q, J = 6.0 Hz, 2H), 3.14 (q, J = 6.6 Hz, 2H), 2.79 (t, J = 7.2 Hz, 2H), 2.39 (t, J = 7.2 Hz, 2H), 1.71-1.66 (m, 2H). ¹³C NMR (151 MHz, DMSO- d_6) δ 170.95, 165.21, 164.32, 151.08, 149.89, 149.75, 148.02, 145.17, 137.61, 134.87, 133.80, 131.71, 128.69, 128.51, 128.40, 127.76, 127.34, 124.50, 124.22, 117.85, 115.41, 115.11, 109.31, 106.64, 100.21, 49.00, 47.26, 46.55, 42.15, 37.34, 33.54, 29.35, 23.66. ESI-MS m/z: 620.4, [M + H]⁺. HRMS (ESI): calcd for $C_{34}H_{33}N_{7}O_{5}$, [M + H]⁺ 620.2616; found, 620.2609. HPLC: t_{R} = 14.18 min (98.72% purity).

N-(4-{3-[5-(4-Acryloyl-2-oxopiperazin-1-yl)furan-2-yl]propanamido}butyl)-4-(pyridin-3-yl)pyrrolo[1,2-a]quinoxaline-7-carboxamide (**19c**)

95 mg, yellow solid, 15% yield. ¹H NMR (500 MHz, DMSO- d_6) δ 9.23 (d, J = 1.5 Hz, 1H), 8.83 (dd, J = 1.5, 1.5 Hz, 1H), 8.69-8.67 (m, 2H), 8.52-8.50 (m, 2H), 8.43 (d, J = 8.5 Hz, 1H), 8.11 (dd, J = 2.0, 2.0 Hz, 1H), 7.88 (t, J = 5.5 Hz, 1H), 7.72 (q, J = 3.0 Hz, 1H), 7.15 (q, J = 3.0 Hz, 1H), 7.08 (q, J = 1.0 Hz, 1H), 6.87-

6.73 (m, 1H), 6.18 (q, J = 3.0 Hz, 2H), 6.08 (d, J = 3.5 Hz, 1H), 5.73 (d, J = 10.5 Hz, 1H), 4.40 (s, 1H), 4.25 (s, 1H), 3.81 (q, J = 30.5 Hz, 4H), 3.31 (q, J = 6.0 Hz, 2H), 3.09 (q, J = 5.5 Hz, 2H), 2.79 (t, J = 7.5 Hz, 2H), 2.38 (t, J = 7.5 Hz, 2H), 1.58-1.53 (m, 2H), 1.49-1.44 (m, 2H). ¹³C NMR (126 MHz, DMSO- d_6) δ 170.71, 165.14, 164.31, 151.14, 150.08, 149.77, 148.19, 145.19, 137.31, 134.87, 133.72, 131.77, 128.63, 128.51, 128.37, 127.77, 127.34, 124.37, 124.23, 117.79, 115.36, 115.04, 109.24, 106.59, 100.18, 47.25, 46.53, 42.13, 38.44, 33.49, 26.87, 26.73, 23.64. ESI-MS m/z: 634.3, [M + H]⁺. HRMS (ESI): calcd for C₃₅H₃₅N₇O₅, [M + H]⁺ 634.2772; found, 634.2752. HPLC: t_R = 14.16 min (97.26% purity).

N-(10-{3-[5-(4-Acryloyl-2-oxopiperazin-1-yl)furan-2-yl]propanamido}decyl)-4-(pyridin-3-yl)pyrrolo[1,2-a]quinoxaline-7-carboxamide (**19d**)

79 mg, yellow solid, 11% yield. ¹H NMR (500 MHz, DMSO- d_6) δ 9.21 (d, J = 2.0 Hz, 1H), 8.81 (dd, J = 1.5, 1.5 Hz, 1H), 8.66 (t, J = 3.0 Hz, 2H), 8.51 (d, J = 2.0 Hz, 1H), 8.48-8.45 (m, 1H), 8.42 (d, J = 8.5 Hz, 1H), 8.10 (dd, J = 2.0, 2.0 Hz, 1H), 7.81-7.78 (m, 1H), 7.69 (q, J = 3.0 Hz, 1H), 7.14 (dd, J = 1.0, 1.0 Hz, 1H), 7.07 (q, J = 1.0 Hz, 1H), 6.81 (t, J = 10.5 Hz, 1H), 6.19 (t, J = 3.0 Hz, 2H), 6.07 (d, J = 3.0 Hz, 1H), 5.74 (d, J = 9.5 Hz, 1H), 4.41 (s, 1H), 4.25 (s, 1H), 3.84 (q, J = 31.5 Hz, 4H), 3.30 (q, J = 6.0 Hz, 2H), 3.00 (q, J = 5.5 Hz, 2H), 2.77 (d, J = 7.5 Hz, 2H), 2.35 (t, J = 7.5 Hz, 2H), 1.59-1.54 (m, 2H), 1.36-1.32 (m, 6H), 1.24 (s, 8H). ¹³C NMR (126 MHz, DMSO- d_6) δ 170.61, 165.10, 164.30, 151.29, 150.46, 149.75, 148.54, 145.13, 136.83, 134.92, 133.61, 131.80, 128.60, 128.51, 128.38, 127.79, 127.30, 124.25, 124.17, 117.70, 115.31, 115.01, 109.17, 106.55, 100.09, 49.00, 47.23, 46.54, 42.14, 38.60, 33.44, 29.23, 29.09, 28.91, 26.66, 26.52, 23.63. ESI-MS m/z: 718.5, $[M + H]^+$ HRMS (ESI): calcd for C₄₁H₄₇N₇O₅, $[M + H]^+$ 718.3711;

found, 718.3709. HPLC: $t_R = 16.88 \text{ min } (98.54\% \text{ purity})$.

N-(5-{3-[5-(4-Acryloyl-2-oxopiperazin-1-yl)furan-2-yl]propanamido}pentyl)-4-(pyridin-3-yl)pyrrolo[1,2-a]quinoxaline-7-carboxamide (**19e**)

52 mg, yellow solid, 8% yield. 1 H NMR (500 MHz, DMSO- d_6) δ 9.23 (d, J = 2.0 Hz, 1H), 8.83 (dd, J = 1.5, 1.5 Hz, 1H), 8.66 (t, J = 2.0 Hz, 2H), 8.52 (t, J = 2.0 Hz, 2H), 8.42 (d, J = 8.5 Hz, 1H), 8.11 (dd, J = 2.0, 2.0 Hz, 1H), 7.85 (t, J = 5.5 Hz, 1H), 7.73 (q, J = 3.0 Hz, 1H), 7.15 (dd, J = 1.0, 1.0 Hz, 1H), 7.08 (q, J = 1.0 Hz, 1H), 6.84-6.76 (m, 1H), 6.19-6.16 (m, 2H), 6.06 (d, J = 3.0 Hz, 1H), 5.74 (d, J = 10.0 Hz, 1H), 4.41 (s, 1H), 4.25 (s, 1H), 4.00-3.67 (m, 4H), 3.30 (q, J = 6.0 Hz, 2H), 3.05 (q, J = 5.5 Hz, 2H), 2.77 (t, J = 7.5 Hz, 2H), 2.36 (t, J = 7.5 Hz, 2H), 1.60-1.54 (m, 2H), 1.47-1.41 (m, 2H), 1.35-1.29 (m, 2H). 13 C NMR (126 MHz, DMSO- d_6) δ 170.69, 165.13, 164.32, 151.10, 150.03, 149.76, 148.15, 145.13, 137.38, 134.87, 133.75, 131.80, 128.62, 128.52, 128.39, 127.78, 127.36, 124.40, 124.22, 117.79, 115.36, 115.03, 109.24, 106.55, 100.12, 49.00, 47.24, 46.53, 42.13, 38.57, 33.49, 28.99, 28.90, 24.02, 23.66. ESI-MS m/z: 648.3, [M+H] + HRMS (ESI): calcd for $C_{36}H_{37}N_{7}O_{5}$, [M+H] + 648.2929; found, 648.2919. HPLC: t_{R} = 14.44 min (97.18% purity).

4.4.3 Cell Culture

The MM.1S and MCF-7 were obtained from ATCC (Manassas, VA, USA). MM.1S cells were cultivated in RPMI 1640 medium supplemented with 10% FBS, 100 IU/mL penicillin, 0.1 mg/mL streptomycin and 1 mM sodium pyruvate at 37°C in a 5% CO₂ atmosphere. MCF-7 cells were cultivated in DMEM medium supplemented with 10% FBS, 100 IU/mL penicillin, 0.1 mg/mL streptomycin and 1 mM *L*-Glutamin at 37°C in a 5% CO₂ atmosphere.

4.4.4 Western Blot Analysis

The MM.1S cells (3×10^6 cells/mL) were seeded into cell culture flasks and after 72 h treated with the indicated concentration of compound or DMSO for the given time. Cell lysis was performed with Cell Extraction Buffer and addition of Halt Protease Inhibitor Cocktail and phenylmethanesulfonyl fluoride. Protein content was determined by PierceTM BCA Protein Assay Kit. Samples were denatured by Laemmli 2× Concentrate, and Precision Plus Protein Unstained Standard was used as molecular weight marker in all cases. SDS-PAGE was performed with 10% Mini-PROTEAN TGX Stain-Free Gel (Catalog# 458035, Bio-Rad, Hercules, CA, USA) at 200 V for 50 min (Catalog# 458035, Bio-Rad). Afterwards, proteins were transferred with the Trans-Blot Turbo Transfer System to Immobilon-FL PVDF membranes at 1.0 A for 30 min and incubated with 5% milk-powder solution for 1 h at room temperature under slight agitation. Subsequently, the membranes were incubated with anti-SIRT6 (Catalog# 12486S, Cell Signaling Technology, Denver, MA, USA) or anti-α-tubulin (Catalog# sc-8035, Santa Cruz, Dallas, TX, USA) antibody solutions in 1:250-1:1000 dilutions at room temperature under slight agitation for 1 h, then put membranes at 4°C for overnight. Incubation with HRPconjugated secondary anti-mouse (Catalog# sc-516102, Santa Cruz, Dallas, TX, USA) and anti-rabbit (Catalog# HAF008, R&D Systems, Inc., Minneapolis, MN, USA) antibody solutions were performed for 1.5 h, and membranes were developed with clarity western ECL substrate. The ChemiDoc XRS+ System was used for detection and Image Lab Software 6.1 (Bio-Rad, Hercules, CA, USA) for quantification.[24-26]

4.4.5 CellTiter-Glo® Cell Viability Assay

The MM.1S cells $(2.5 \times 10^3 \text{ cells/well})$ were seeded in white 384-well plates and incubated with the respective compounds at increasing concentrations. For this purpose, the dilution series were prepared at $200 \times$ concentration in DMSO and then further diluted to $10 \times$ concentration in medium. The final DMSO concentration was 0.5%. The toxicity of compounds was assessed after 72 h using the CellTiter-Glo

2.0 cell viability assay. Luminescence was then measured, and the EC₅₀ was determined by plotting dose-response curves and performing nonlinear regression using GraphPad Prism.^[27]

4.5 References

- (1) Dixon SJ, Stockwell BR. Identifying druggable disease-modifying gene products. *Curr Opin Chem Biol.* **2009**, *13*(5-6), 549-555. DOI: 10.1016/j.cbpa.2009.08.003.
- (2) Spradlin JN, Zhang E, Nomura DK. Reimagining Druggability Using Chemoproteomic Platforms. *Acc Chem Res.* **2021**, *54*(7), 1801-1813. DOI: 10.1021/acs.accounts.1c00065.
- (3) Nalawansha DA, Crews CM. PROTACs: An Emerging Therapeutic Modality in Precision Medicine. *Cell Chem Biol.* **2020**, *27*(8), 998-1014. DOI: 10.1016/j.chembiol.2020.07.020.
- (4) Burslem GM, Crews CM. Proteolysis-Targeting Chimeras as Therapeutics and Tools for Biological Discovery. *Cell.* **2020**, *181*(1), 102-114. DOI: 10.1016/j.cell.2019.11.031.
- (5) Farnaby W, Koegl M, McConnell DB, Ciulli A. Transforming targeted cancer therapy with PROTACs: A forward-looking perspective. *Curr Opin Pharmacol.* 2021, 57, 175-183. DOI: 10.1016/j.coph.2021.02.009.
- (6) Yamazoe S, Tom J, Fu Y, Wu W, Zeng L, Sun C, Liu Q, Lin J, Lin K, Fairbrother WJ, Staben ST. Heterobifunctional Molecules Induce Dephosphorylation of Kinases-A Proof of Concept Study. *J Med Chem.* 2020, 63(6), 2807-2813. DOI: 10.1021/acs.jmedchem.9b01167.
- (7) Siriwardena SU, Munkanatta Godage DNP, Shoba VM, Lai S, Shi M, Wu P, Chaudhary SK, Schreiber SL, Choudhary A. Phosphorylation-Inducing Chimeric Small Molecules. J Am Chem Soc. 2020, 142(33), 14052-14057. DOI: 10.1021/jacs.0c05537.
- (8) Henning NJ, Boike L, Spradlin JN, Ward CC, Liu G, Zhang E, Belcher BP, Brittain SM, Hesse MJ, Dovala D, McGregor LM, Valdez Misiolek R, Plasschaert LW, Rowlands DJ, Wang F, Frank AO, Fuller D, Estes AR, Randal KL, Panidapu A, McKenna JM, Tallarico JA, Schirle M, Nomura DK. Deubiquitinase-targeting chimeras for targeted protein stabilization. *Nat Chem Biol.* 2022, 18(4), 412-421. DOI: 10.1038/s41589-022-00971-2.
- (9) Liu J, Yu X, Chen H, Kaniskan HÜ, Xie L, Chen X, Jin J, Wei W. TF-DUBTACs Stabilize Tumor Suppressor Transcription Factors. J Am Chem Soc. 2022, 144(28), 12934-12941. DOI: 10.1021/jacs.2c04824.
- (10) Deng Z, Chen L, Qian C, Liu J, Wu Q, Song X, Xiong Y, Wang Z, Hu X, Inuzuka H, Zhong Y, Xiang Y, Lin Y, Dung Pham N, Shi Y, Wei W, Jin J. The First-In-Class Deubiquitinase-

- Targeting Chimera Stabilizes and Activates cGAS. *Angew Chem Int Ed Engl.* **2025**, *64*(3), e202415168. DOI: 10.1002/anie.202415168.
- (11) Liu J, Hu X, Luo K, Xiong Y, Chen L, Wang Z, Inuzuka H, Qian C, Yu X, Xie L, Muneer A, Zhang D, Paulo JA, Chen X, Jin J, Wei W. USP7-Based Deubiquitinase-Targeting Chimeras Stabilize AMPK. *J Am Chem Soc.* 2024, 146(16), 11507–11514. DOI: 10.1021/jacs.4c02373.
- (12) Wang Z, Qian C, Xiong Y, Zhang D, Inuzuka H, Zhong Y, Xie L, Chen X, Jin J, Wei W. USP28-Based Deubiquitinase-Targeting Chimeras for Cancer Treatment. *J Am Chem Soc.* 2025, 147(16), 13754-13763. DOI: 10.1021/jacs.5c01889.
- (13) Qian C, Wang Z, Xiong Y, Zhang D, Zhong Y, Inuzuka H, Qi Y, Xie L, Chen X, Wei W, Jin J. Harnessing the Deubiquitinase USP1 for Targeted Protein Stabilization. *J Am Chem Soc.* **2025**, *147*(17), 14564-14573. DOI: 10.1021/jacs.5c01662.
- (14) Fiorentino F, Mai A, Rotili D. Emerging Therapeutic Potential of SIRT6 Modulators. *J Med Chem.* **2021**, *64*(14), 9732-9758. DOI: 10.1021/acs.jmedchem.1c00601.
- (15) Feldman JL, Baeza J, Denu JM. Activation of the protein deacetylase SIRT6 by long-chain fatty acids and widespread deacylation by mammalian sirtuins. *J Biol Chem.* **2013**, *288*(43), 31350-31356. DOI: 10.1074/jbc.C113.511261.
- (16) Tasselli L, Zheng W, Chua KF. SIRT6: Novel Mechanisms and Links to Aging and Disease. *Trends Endocrinol Metab.* **2017**, *28*(3), 168-185. DOI: 10.1016/j.tem.2016.10.002.
- (17) Michishita E, McCord RA, Berber E, Kioi M, Padilla-Nash H, Damian M, Cheung P, Kusumoto R, Kawahara TL, Barrett JC, Chang HY, Bohr VA, Ried T, Gozani O, Chua KF. SIRT6 is a histone H3 lysine 9 deacetylase that modulates telomeric chromatin. *Nature*. 2008, 452(7186), 492-496. DOI: 10.1038/nature06736.
- (18) Yang B, Zwaans BM, Eckersdorff M, Lombard DB. The sirtuin SIRT6 deacetylates H3 K56Ac in vivo to promote genomic stability. *Cell Cycle*. **2009**, *8*(16), 2662-2663. DOI: 10.4161/cc.8.16.9329.
- (19) Jiang H, Khan S, Wang Y, Charron G, He B, Sebastian C, Du J, Kim R, Ge E, Mostoslavsky R, Hang HC, Hao Q, Lin H. SIRT6 regulates TNF-α secretion through hydrolysis of long-chain fatty acyl lysine. *Nature*. **2013**, *496*(7443), 110-113. DOI: 10.1038/nature12038.
- (20) Fiorentino F, Carafa V, Favale G, Altucci L, Mai A, Rotili D. The Two-Faced Role of

- SIRT6 in Cancer. Cancers (Basel). 2021, 13(5), 1156. DOI: 10.3390/cancers13051156.
- (21) Chang AR, Ferrer CM, Mostoslavsky R. SIRT6, a Mammalian Deacylase with Multitasking Abilities. *Physiol Rev.* **2020**, *100*(1), 145-169. DOI: 10.1152/physrev.00030.2018.
- (22) Huang Z, Zhao J, Deng W, Chen Y, Shang J, Song K, Zhang L, Wang C, Lu S, Yang X, He B, Min J, Hu H, Tan M, Xu J, Zhang Q, Zhong J, Sun X, Mao Z, Lin H, Xiao M, Chin YE, Jiang H, Xu Y, Chen G, Zhang J. Identification of a cellularly active SIRT6 allosteric activator. *Nat Chem Biol.* **2018**, *14*(12), 1118-1126. DOI: 10.1038/s41589-018-0150-0.
- (23) You W, Rotili D, Li TM, Kambach C, Meleshin M, Schutkowski M, Chua KF, Mai A, Steegborn C. Structural Basis of Sirtuin 6 Activation by Synthetic Small Molecules. Angew Chem Int Ed Engl. 2017, 56(4), 1007-1011. DOI: 10.1002/anie.201610082.
- (24) Schäker-Hübner L, Haschemi R, Büch T, Kraft FB, Brumme B, Schöler A, Jenke R, Meiler J, Aigner A, Bendas G, Hansen FK. Balancing Histone Deacetylase (HDAC) Inhibition and Drug-likeness: Biological and Physicochemical Evaluation of Class I Selective HDAC Inhibitors. *ChemMedChem.* 2022, 17(9), e202100755. DOI: 10.1002/cmdc.202100755.
- (25) Sinatra L, Vogelmann A, Friedrich F, Tararina MA, Neuwirt E, Colcerasa A, König P, Toy L, Yesiloglu TZ, Hilscher S, Gaitzsch L, Papenkordt N, Zhai S, Zhang L, Romier C, Einsle O, Sippl W, Schutkowski M, Gross O, Bendas G, Christianson DW, Hansen FK, Jung M, Schiedel M. Development of First-in-Class Dual Sirt2/HDAC6 Inhibitors as Molecular Tools for Dual Inhibition of Tubulin Deacetylation. *J Med Chem.* 2023, 66(21), 14787-14814. DOI: 10.1021/acs.jmedchem.3c01385.
- (26) Feller F, Hansen FK. Targeted Protein Degradation of Histone Deacetylases by Hydrophobically Tagged Inhibitors. *ACS Med Chem Lett.* **2023**, *14*(12), 1863-1868. DOI: 10.1021/acsmedchemlett.3c00468.
- (27) Ahmed IA, Hafiz S, van Ginkel S, Pondugula SR, Abdelhaffez AS, Sayyed HG, El-Aziz EAA, Mansour MM. Augmentation of Docetaxel-Induced Cytotoxicity in Human PC-3 Androgen-Independent Prostate Cancer Cells by Combination With Four Natural Apoptosis-Inducing Anticancer Compounds. *Nat Prod Commun.* **2023**, *18*(5), 10.1177/1934578x231175323. DOI: 10.1177/1934578x231175323.

Chapter 5. Summary

Histone deacetylases (HDACs) serve as critical epigenetic regulators that modulate gene expression through catalytic removal of acetyl groups from histone substrates. By controlling the acetylation status of both histone and non-histone proteins, HDACs orchestrate fundamental cellular processes including cell cycle, chromatin decondensation, apoptosis and angiogenesis. These pleiotropic functions have established HDACs as validated therapeutic targets in oncology, evidenced by the FDA and CFDA approval of five HDAC inhibitors for various cancer indications to date.

Despite their clinical utility, currently available HDAC inhibitors suffer from significant off-target effects, including nausea, vomiting, fatigue, and cardiotoxicity, that largely result from their pan-HDAC inhibitory activity across multiple isoforms. Developing isoform-selective HDAC modulators represents a promising strategy to overcome these limitations, as targeted pharmacological regulation of specific HDAC family members could potentially maintain therapeutic efficacy while substantially reducing adverse effects.

To address these limitations, three innovative proximity-based therapeutic modalities were designed to achieve precise control of HDAC activity. These approaches leverage targeted protein modulation to enhance isoform specificity while minimizing off-target effects, potentially overcoming the key challenges that have constrained the clinical utility of conventional HDAC inhibitors in oncology applications.

5.1 DCAF16-based Covalent Molecular Glues for Targeted Protein Degradation of Histone Deacetylases

The vinylsulfonyl piperazine warhead, originally developed by Nomura et al.,^[1] shows promise for targeted protein degradation but requires substantial optimization to enhance its potency, selectivity, and drug-like properties. While the authors successfully incorporated this warhead into a range of small molecule degraders targeting proteins such as BRD4, CDK4, the androgen receptor (AR), BTK, SMARCA2/4, and BCR-

ABL/c-ABL, selectivity remained a significant challenge. Specifically, off-target degradation was observed across the reported degraders, likely due to non-specific interactions of the covalent handle. Despite its lack of optimization, this chemotype represents a valuable starting point for developing molecular glue degraders.

In this study, a novel series of DCAF16-based covalent molecular glues incorporating different zinc-binding groups (ZBGs) were developed for targeted HDAC degradation. The hydroxamate-containing degrader 10a exhibited potent and selective reduction of HDAC1 protein levels in MM.1S cells, as confirmed by western blot analysis, while the non-covalent control 10a-nc showed no activity. The promising anticancer activity of 10a was further validated through antiproliferative effects and apoptosis induction assays. Notably, this work establishes the vinylsulfonyl piperazine moiety as a versatile warhead capable of transforming the classical HDAC inhibitor vorinostat into a targeted degrader. These findings underscore the broader potential of strategic warhead incorporation in advancing targeted protein degradation therapeutics (Figure 5-1).

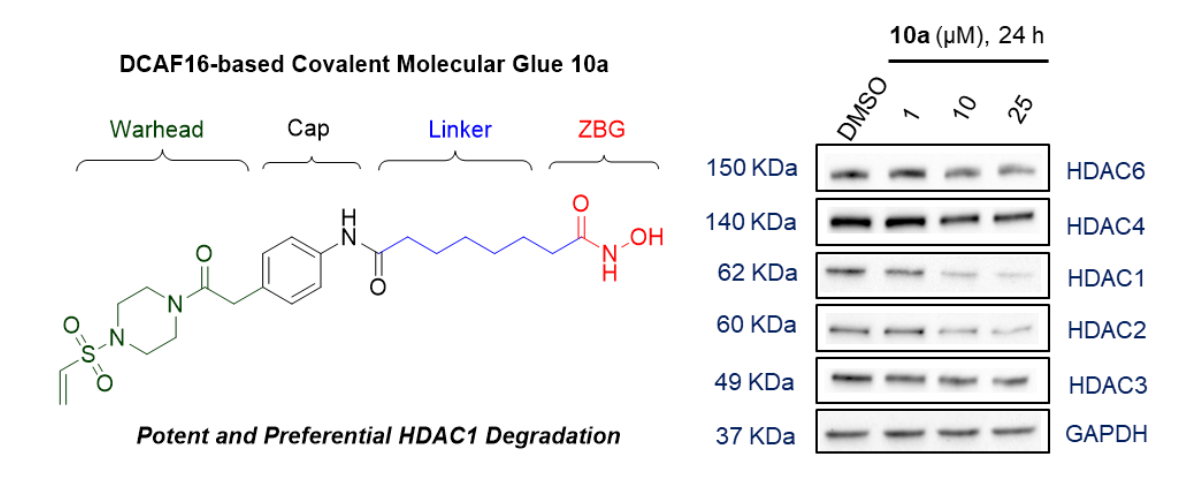


Figure 5-1. Inspired by the recently identified vinylsulfonyl piperazine handle, which enables conjugation to protein of interest ligands for targeted protein degradation, a novel class of DCAF16-based covalent molecular glues was proposed to degrade HDACs. This strategy yielded an effective molecular glue (**10a**) that significantly and preferentially reduced HDAC1 levels in MM.1S cells.

5.2 Targeted Degradation of Histone Deacetylases *via* Bypassing E3 Ligase Targeting Chimeras (BYETACs)

Targeted protein degradation (TPD) through heterobifunctional molecules to initiate ubiquitination and facilitate subsequent degradation has emerged as a powerful therapeutic strategy. Most heterobifunctional molecules designed for TPD function primarily through a limited set of E3 ligases, which restricts this therapeutic approach to specific tissues that express the necessary ligases.^[2,3]

Capitalizing on the interaction between USP14 and the 26S proteasome subunit RPN1, BYETACs were developed as a novel class of degraders that directly engage the proteasome for HDAC elimination. The lead compound **10c** demonstrated potent and selective reduction of HDAC1 protein levels in MM.1S cells, as evidenced by western blot analysis. Furthermore, subsequent apoptosis induction analysis confirmed its promising anticancer activity. These findings open new avenues for expanding the protein degradation toolbox beyond conventional E3-dependent approaches (**Figure 5-2**).

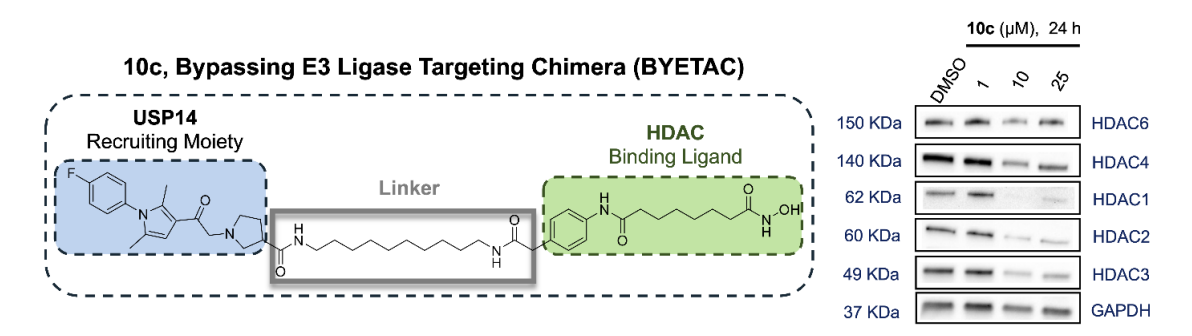


Figure 5-2. Structure of the designed HDAC BYETACs with the USP14 recruiting moiety attached to the HDAC binding ligand *via* linker.

5.3 Deubiquitinase-targeting Chimeras (DUBTACs) for Targeted Stabilization of SIRT6

Many diseases are driven by the aberrant ubiquitination and further degradation of proteins. Targeted protein stabilization (TPS) offers a promising approach to address these issues, as it can potentially restore the normal function of key proteins involved in disease pathways. [4] Herein, the development of SIRT6 DUBTACs was reported, heterobifunctional molecules comprising an OTUB1-recruiting moiety linked to a SIRT6 activator. Western blot analysis confirmed upregulation of SIRT6 protein levels, and cellular assays demonstrated corresponding antiproliferative effects in MM.1S cells. Current efforts focus on structurally optimizing the DUBTAC system by replacing its OTUB1 recruiting moiety with modified MS5105 derivatives to improve both target stabilization efficiency and tissue selectivity. Overall, the heterobifunctional DUBTACs provide a new therapeutic modality for TPS in treating diseases associated with dysfunctional protein ubiquitination (Figure 5-3).

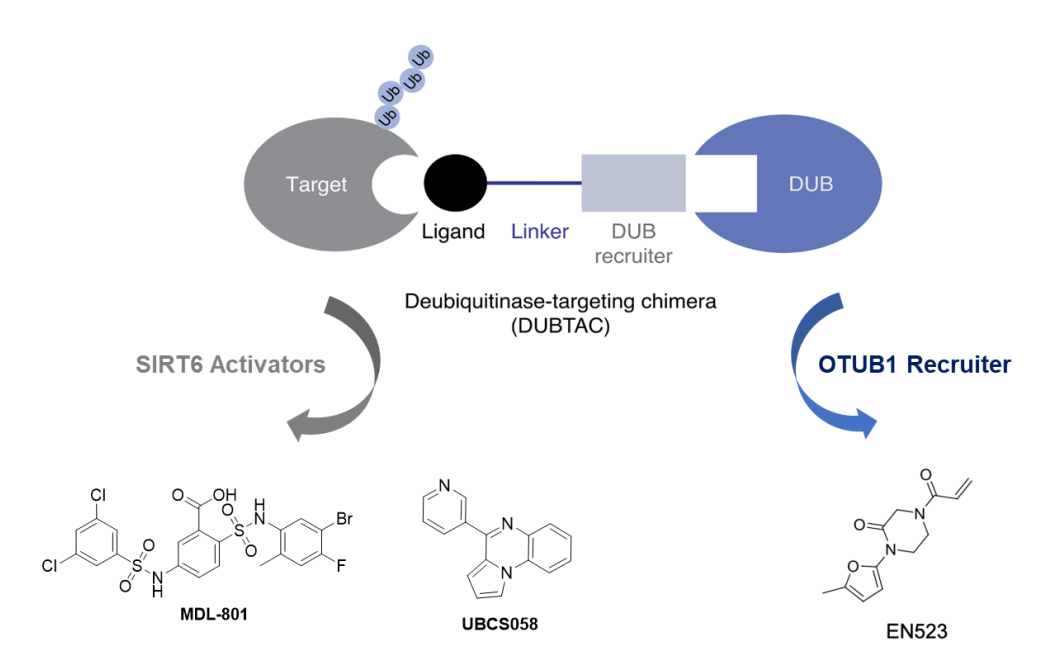


Figure 5-3. Rational design for SIRT6 DUBTACs. SIRT6 DUBTACs are heterobifunctional molecules consisting of a SIRT6 activator linked to a DUB OTUB1 recruiter *via* different linker.

In summary, this thesis advances the development of proximity-based therapeutic modalities that achieve significant HDAC isoform selectivity, offering novel paradigms for targeted protein modulation. Current efforts are directed toward lead compound optimization and mechanistic elucidation to facilitate the translation of these novel modalities into viable oncology therapeutics.

5.4 References

- (1) Lim M, Cong TD, Orr LM, Toriki ES, Kile AC, Papatzimas JW, Lee E, Lin Y, Nomura DK. DCAF16-Based Covalent Handle for the Rational Design of Monovalent Degraders. ACS Cent Sci. 2024, 10(7), 1318-1331. DOI: 10.1021/acscentsci.4c00286.
- (2) Bashore C, Prakash S, Johnson MC, Conrad RJ, Kekessie IA, Scales SJ, Ishisoko N, Kleinheinz T, Liu PS, Popovych N, Wecksler AT, Zhou L, Tam C, Zilberleyb I, Srinivasan R, Blake RA, Song A, Staben ST, Zhang Y, Arnott D, Fairbrother WJ, Foster SA, Wertz IE, Ciferri C, Dueber EC. Targeted degradation *via* direct 26S proteasome recruitment. *Nat Chem Biol.* 2023, 19(1), 55-63. DOI: 10.1038/s41589-022-01218-w.
- (3) Loy CA, Ali EMH, Seabrook LJ, Harris TJ Jr, Kragness KA, Albrecht L, Trader DJ. ByeTAC: Bypassing E-Ligase-Targeting Chimeras for Direct Proteasome Degradation. J Med Chem. 2025, 68(9), 9694-9705. DOI: 10.1021/acs.jmedchem.5c00485.
- (4) Henning NJ, Boike L, Spradlin JN, Ward CC, Liu G, Zhang E, Belcher BP, Brittain SM, Hesse MJ, Dovala D, McGregor LM, Valdez Misiolek R, Plasschaert LW, Rowlands DJ, Wang F, Frank AO, Fuller D, Estes AR, Randal KL, Panidapu A, McKenna JM, Tallarico JA, Schirle M, Nomura DK. Deubiquitinase-targeting chimeras for targeted protein stabilization. *Nat Chem Biol.* 2022, 18(4), 412-421. DOI: 10.1038/s41589-022-00971-2.

Chapter 6. Appendix

6.1 Appendix I. Publication I: DCAF16-based Covalent Molecular Glues for Targeted Protein Degradation of Histone Deacetylases

The following part contains the research article "DCAF16-based Covalent Molecular Glues for Targeted Protein Degradation of Histone Deacetylases", including the supporting information, as it was published in *Archiv Der Pharmazie* by Wiley-VCH GmbH, Weinheim.

The article is reprinted with permission from:

Sun T, Zhai S, Lepper S, König B, Malenica M, Honin I, Hansen FK. DCAF16-Based Covalent Molecular Glues for Targeted Protein Degradation of Histone Deacetylases. *Arch Pharm (Weinheim)*. **2025**, *358*(7), e70045. DOI: https://doi.org/10.1002/ardp.70045

Copyright 2025. The Author(s). Published under the license CC BY 4.0: https://creativecommons.org/licenses/by/4.0/



Check for updates



DCAF16-Based Covalent Molecular Glues for Targeted **Protein Degradation of Histone Deacetylases**

Tao Sun | Shiyang Zhai | Stephan Lepper | Beate König | Mateo Malenica | Irina Honin | Finn K. Hansen



Department of Pharmaceutical and Cell Biological Chemistry, Pharmaceutical Institute, University of Bonn, Bonn, Germany

Correspondence: Finn K. Hansen (finn.hansen@uni-bonn.de)

Received: 14 January 2025 | Revised: 22 May 2025 | Accepted: 15 June 2025

Funding: S.L. and F.K.H. acknowledge financial support from the Deutsche Forschungsgemeinschaft (HA 7783/4-1). T.S. (grant no. 202107060004) and S.Z. (grant no. 202106150022) are funded by the China Scholarship Council. The new NMR console for the 500-MHz NMR spectrometer used in this research was funded by the Deutsche Forschungsgemeinschaft (DFG, German Research Foundation) under project number 507275896. M.M. and F.K.H. acknowledge financial support from the Deutsche Forschungsgemeinschaft (HA 7783/5-1). The work of M.M., I.H., and F.K.H. is funded by the Deutsche Forschungsgemeinschaft (DFG, German Research Foundation) - GRK2873 (494832089).

Keywords: cancer | DCAF16 | histone deacetylases (HDACs) | molecular glues | targeted protein degradation (TPD)

ABSTRACT

Histone deacetylases (HDACs) are intriguing cancer targets due to their high expression in many tumors. Consequently, inhibition or degradation of HDACs can be beneficial for cancer therapy. Targeted protein degradation using molecular glues represents a promising therapeutic approach, enabling the specific degradation of numerous disease-causing proteins. However, the rational design of molecular glues in a target-based manner remains challenging. A recent study has described the identification of a DCAF16-based covalent linker-less chemical handle for molecular glues. This covalent warhead can be attached to protein of interest ligands to induce the targeted degradation of various protein classes. Inspired by this, we designed and synthesized a new class of DCAF16-based covalent molecular glues utilizing different zinc-binding groups for the targeted degradation of HDACs. This approach led to the discovery of an efficient molecular glue (10a) that reduced HDAC1 levels in multiple myeloma MM.1S cells in a potent and preferential manner.

1 | Introduction

Histone acetylation is regulated by histone deacetylases (HDACs) and histone acetyltransferases (HATs). Modulating HDAC levels has been shown to influence many cellular processes including cell growth, cell cycle, and chromatin decondensation [1]. The HDAC family encompasses 18 isoforms classified into four groups: Class I (HDAC1, 2, 3, and 8), Class IIa (HDAC4, 5, 7, and 9), Class IIb (HDAC6 and 10), Class III (Sirt1-7), and Class IV (HDAC11) [1]. HDACs are intriguing cancer targets due to their overexpression in many tumors. Consequently, inhibition or degradation of HDACs can be beneficial for cancer treatment. To date, four anticancer HDAC inhibitors have been approved by the FDA for the treatment of T-cell lymphoma and multiple myeloma [2]. Additionally, novel HDAC-based therapeutic strategies have

emerged in recent years, underscoring the broad potential applications of HDAC-targeted therapies [3-5].

Targeted protein degradation (TPD) using molecular glues and proteolysis-targeting chimeras (PROTACs) represents a promising therapeutic strategy, enabling the selective degradation of numerous disease-causing proteins [6]. Compared to heterobifunctional PROTACs, molecular glue degraders are particularly promising due to their lower molecular weights and favorable drug-like properties. However, unlike PROTACs, which can be rationally designed, the majority of molecular glue degraders have been identified serendipitously or through phenotypic screening methods. The rational design of molecular glue degraders in a target-specific context remains a significant challenge, limiting the broader applications of molecular glues [7–9]. In addition to the complex design of molecular

This is an open access article under the terms of the Creative Commons Attribution License, which permits use, distribution and reproduction in any medium, provided the original work is properly

© 2025 The Author(s). Archiv der Pharmazie published by Wiley-VCH GmbH on behalf of Deutsche Pharmazeutische Gesellschaft.

glues, they have several other limitations compared to small-molecule inhibitors. For instance, not all proteins are degradable because they are poorly recognized by E3 ligases or lack a suitable ubiquitination site. In addition, for proteins with short half-lives and high turnover rates, the relative advantage of a molecular glue may be less pronounced. However, despite these challenges associated with the development of molecular glues, they also possess advantages over small-molecule inhibitors: Molecular glues (1) can exploit shallow protein—protein interfaces between E3 ligases and therapeutic proteins that may lack deep binding pockets, which presents a significant advantage in drug development, (2) act via a catalytic mode of action, (3) remove all functions of the target protein, not just enzymatic activity, but also scaffolding or non-catalytic roles, and (4) exhibit sustained effects, particularly for proteins with moderate and long half-lives [10, 11].

A recent study has described the identification of a DDB1- and CUL4-associated factor 16 (DCAF16)-based covalent, degradative, and linker-less chemical handle [12]. This vinylsulfonyl piperazine handle can be conjugated to protein of interest (POI) ligands to induce the degradation of various proteins. Building on the successful applications of this chemical handle, we designed and synthesized a novel class of DCAF16-based covalent molecular glues utilizing various zinc-binding groups (ZBGs) for the targeted degradation of HDACs. We then investigated the degradation efficacy and isoform selectivity of the molecular glue degraders. Additionally, the antiproliferative activity, HDAC inhibition, and induction of apoptosis were further evaluated in MM.1S cells.

2 | Results and Discussion

2.1 | Chemistry

To investigate whether the DCAF16-based covalent handle can convert nondegrading HDAC inhibitors into degraders, we designed a series of molecular glues for targeting HDACs. Traditionally, HDAC inhibitors, such as vorinostat, consist of three key components: a cap structure, a ZBG, and a linker connecting the cap to the ZBG [1]. Among these components, the cap structure can exhibit considerable structural diversity, allowing for the design of HDAC inhibitors with a wide range of structures [13]. Accordingly, the covalent handle was introduced to the cap group of the HDAC inhibitor vorinostat. Additionally, the hydroxamic acid of vorinostat was substituted with three different ZBGs for further explorations (Figure 1).

The synthetic routes for the target Compounds 10a-d are outlined in Schemes 1-3. Briefly, for the synthesis of the HDAC ligands (Scheme 1), 4-aminophenylacetic acid (1) was first activated with thionyl chloride and esterified with methanol to yield intermediate 2, which was further treated with suberic anhydride to afford 3. Subsequently, Compound 3 was subjected to amide coupling reactions with various ZBG precursors to produce Compounds 4a-d. The protected HDAC ligands 5a-d with a free phenylacetic acid moiety were prepared by the treatment of 4a-d with LiOH·H₂O [14].

For the synthesis of the DCAF16 warhead (Scheme 2), Compound 6 was reacted with 2-chloroethanesulfonyl chloride in the presence of triethylamine (TEA) in dry dichloromethane to give 7, which was then directly treated with trifluoroacetic acid (TFA) to yield precursor 8 [12].

Next, **5a-d** were conjugated with **8** using HATU and DIPEA as amide coupling system to produce **9a-d**. Finally, deprotection of **9a-d** with TFA afforded the target Compounds **10a-d** (Scheme 3).

2.2 | Biological Evaluation

2.2.1 | HDAC Degradation by DCAF16-Recruiting Covalent Molecular Glues 10a-d

First, the multiple myeloma cell line MM.1S was treated with varying concentrations (1, 10, and 25 µM) of degraders 10a-d for 6 and 24 h, respectively. HDAC1 and HDAC6 were selected for investigation due to their critical roles in various diseases such as cancer [15]. HDAC1 and HDAC6 protein levels were subsequently evaluated using western blot analysis. As summarized in Figure 2A and Supporting Information S2: Figure S1, all compounds exhibited either no or weak degradation efficacy for HDAC1 and HDAC6 at different concentrations after 6 h. This limited efficacy could be due to insufficient incubation time of the compounds with MM.1S cells. To address this, the incubation time was extended to 24 h to investigate whether 10a-d displayed enhanced degradation of HDAC1 and HDAC6 after longer treatment times (Figure 2B and Supporting Information S2: Figure S2). All compounds still exerted no degradation of HDAC6 at different concentrations after 24 h of treatment.

FIGURE 1 | Rational design of DCAF16-based HDAC molecular glues.

2 of 12 Archiv der Pharmazie, 2025

SCHEME 1 | Synthesis of HDAC ligands 5a-d. Reagents and conditions: (i) SOCl₂, CH₃OH, 80°C, 16 h, 97% yield. (ii) Suberic anhydride, NaHCO₃, THF, rt, 16 h, 63% yield. (iii) R¹-NH₂, HATU, DIPEA, DMF, rt, 16 h, 28%–88% yield. (iv) LiOH·H₂O, THF/H₂O (v/v = 1:1), rt, 2–12 h, 26%–84% yield.

SCHEME 2 | Synthesis of the DCAF16 warhead **8**. Reagents and conditions: (v) 2-chloroethanesulfonyl chloride, TEA, DCM, $0^{\circ}C \rightarrow rt$, 16 h. (vi) TFA, DCM, rt, 1 h, 95% yield (over two steps).

However, different from **10b-d**, degrader **10a**, which contains a hydroxamic acid as ZBG, achieved substantial degradation of HDAC1 with a maximal degradation ($D_{\rm max}$) value of 74% at 25 μ M. Consequently, Compound **10a** was selected for further biological evaluations based on the initial screening results.

2.2.2 | Preferential HDAC1 Degradation and DC_{50} Value Determination for 10a

Subsequently, degrader 10a was investigated at various concentrations (1, 10, and 25 µM) for degradation effects on different HDAC isoforms, including HDAC2, HDAC3, and HDAC4. As shown in Figure 3A and Supporting Information S2: Figure S3A, none of the used concentrations resulted in the degradation of HDAC2, HDAC3, or HDAC4 when MM.1S cells were treated with 10a for 6 h. Meanwhile, treatment with 10a for 24 h had minimal impact on HDAC3 and HDAC4 protein levels, whereas HDAC2 levels were slightly affected (Figure 3B and Supporting Information S2: Figure S3B). In detail, **10a** induced a modest degradation of HDAC2 $(D_{\text{max}} = 46\% \text{ at } 25 \,\mu\text{M})$, which may be attributed to the high structural similarity between HDAC1 and HDAC2, particularly in their catalytic domains [16]. In summary, the results presented above clearly confirm that 10a exhibits potent degradation activity and high preference for HDAC1 among the various tested HDAC isoforms.

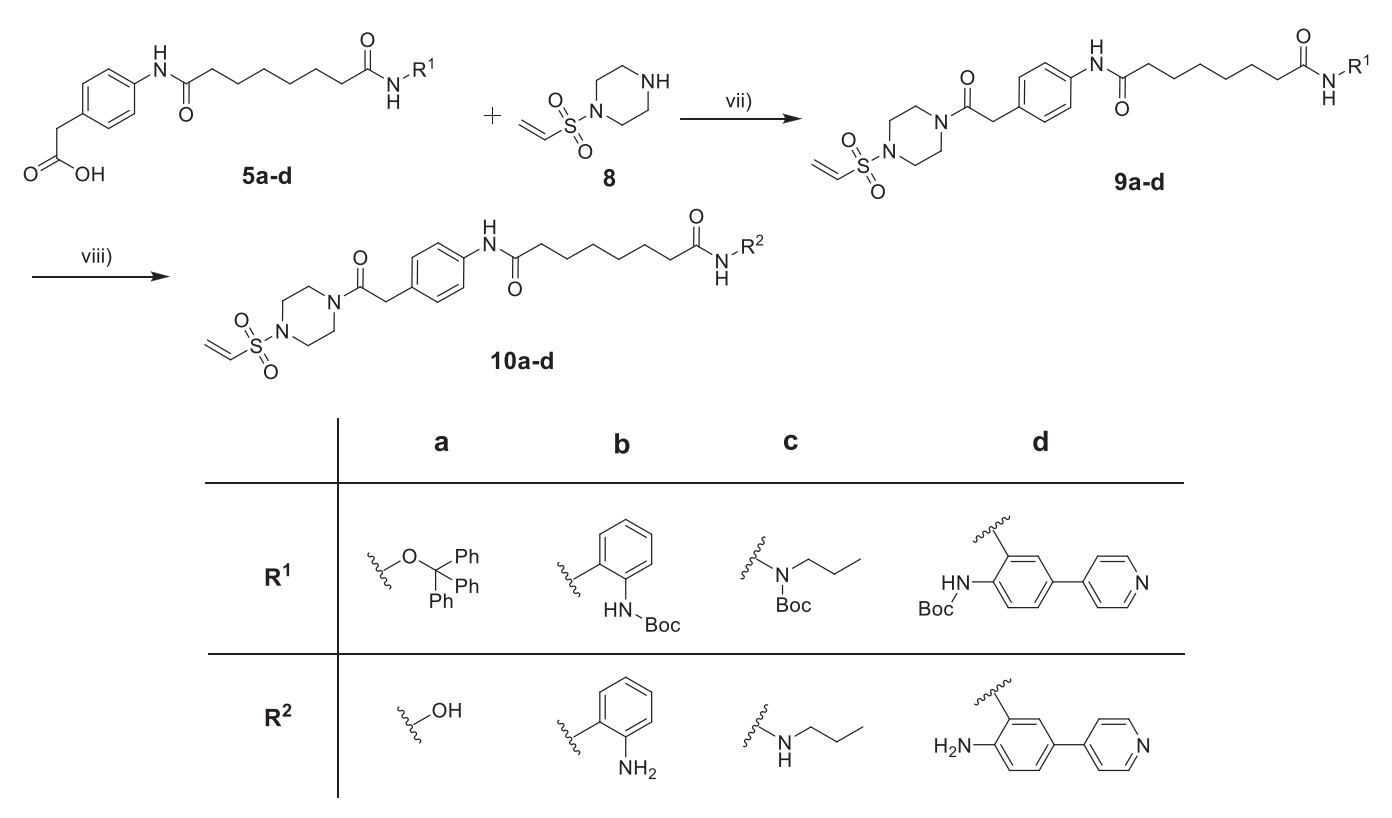
Following the observation that Compound 10a preferentially induced degradation of HDAC1 in MM.1S cells, we proceeded to determine its half-maximal degradation concentration (DC₅₀) for HDAC1 (Supporting Information S2: Figure S4). When MM.1S cells were treated with increasing concentrations of 10a for 24 h, HDAC1 levels gradually decreased in a dose-dependent manner (DC₅₀ = $8.8 \pm 4.4 \,\mu\text{M}$).

2.2.3 | Antiproliferative Activity, HDAC Enzyme Inhibition of 10a, and Cellular Target Engagement Studies

Building on the results obtained from western blot analysis, we subsequently assessed **10a** for its antiproliferative activity in MM.1S cells and for its inhibitory activity against HDAC1 and HDAC6. As shown in Table 1, Compound **10a** exhibited substantial antiproliferative activity (half-maximal inhibitory concentration, $IC_{50} = 6.48 \,\mu\text{M}$) against MM.1S cells. The possible mechanism of antiproliferative activities is the induction of HDAC1 degradation by **10a**, which supports the critical role of HDAC1 as one of the most relevant isoforms in cancer. Regarding HDAC inhibition, **10a** displayed notable inhibitory activity against HDAC1 ($IC_{50} = 0.017 \,\mu\text{M}$) and HDAC6 ($IC_{50} = 0.027 \,\mu\text{M}$).

Based on the HDAC6 inhibition data, the lack of efficient HDAC6 degradation by **10a** (Figure 2) is surprising. However, efficient TPD depends not only on binding affinity and ternary complex formation but also on subcellular localization. Since DCAF16 is predominantly localized in the nucleus [17], a DCAF16-recruiting degrader is more likely to target nuclear HDACs, such as HDAC1, rather than cytoplasmic isoforms like HDAC6.

To assess the cellular target engagement of degrader 10a of HDACs in MM.1S cells, we conducted western blot experiments to analyze the levels of acetylated histone H3 (an indicator of reduced HDAC1-3 activity) and acetylated α -tubulin (a marker of decreased HDAC6 activity) using vorinostat as a control. Consistent with the results of the biochemical HDAC inhibition assays, degrader 10a resulted in a pronounced upregulation of acetylated H3 histone and acetylated α-tubulin after 24-h treatment, indicating that 10a exhibited significant inhibition or degradation of both HDAC1 and HDAC6 in MM.1S cells. As expected, the DCAF16-targeting chemical handle 8 exhibited no effects on the levels of acetylated histone H3 and acetylated α-tubulin (Figure 4). Interestingly, Compound 10a induced hyperacetylation of α -tubulin comparable to its parent inhibitor, vorinostat, thereby indicating sufficient cellular permeability. However, its effect on histone H3 acetylation was markedly lower than that of vorinostat. This discrepancy may suggest reduced nuclear permeability of 10a, which could also account for its diminished activity in the viability assays (Table 1).



SCHEME 3 | Synthesis of DCAF16-based HDAC molecular glues 10a-d. Reagents and conditions: (vii) HATU, DIPEA, DMF, rt, 16 h, 33%–47% yield. (viii) TFA, DCM, rt, 1 h, 25%–85% yield.

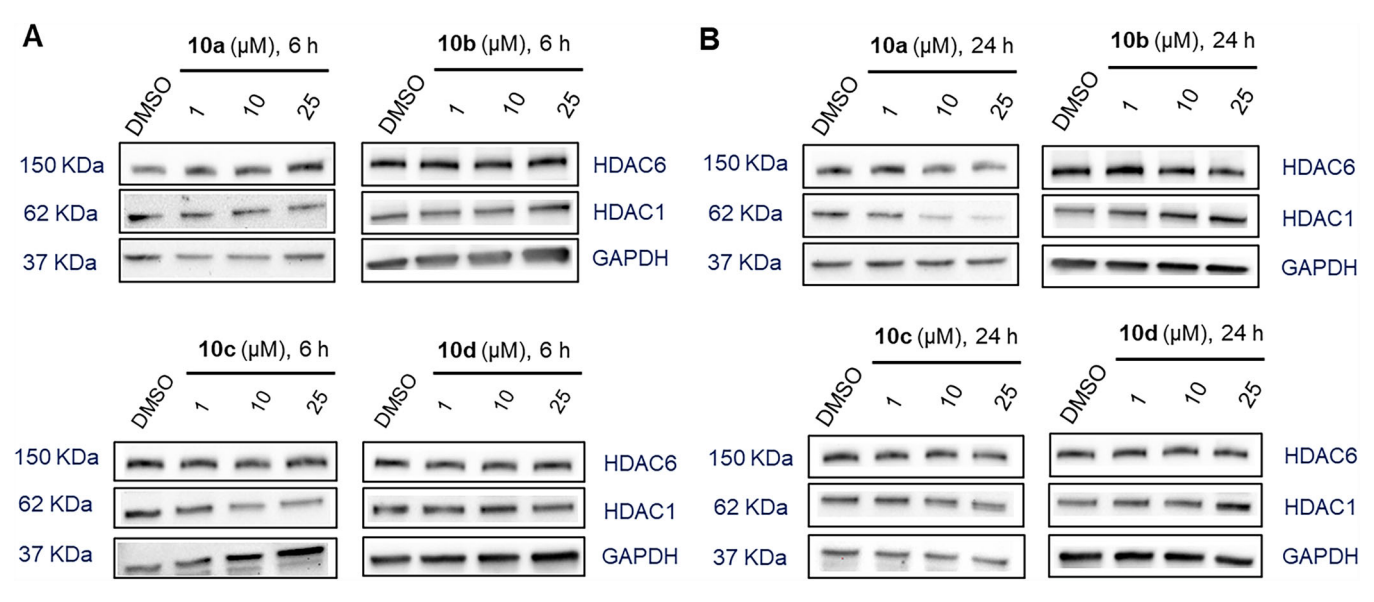


FIGURE 2 | Degradation of HDAC1 and HDAC6 mediated by 10a-d. MM.1S cells were treated with Compounds 10a-d at concentrations of 1, 10, and 25 μ M for 6 h (A) or for 24 h (B), with DMSO as vehicle control. HDAC1 and HDAC6 levels were detected by immunoblot analysis. GAPDH was used as the loading control. Representative images from a total of n=2 replicates.

2.2.4 | Negative Control Compound and HDAC1-3 Inhibition

To assess the functional relevance of the covalent vinylsulfonyl piperazine moiety in mediating HDAC1 degradation, we synthesized a noncovalent control compound, designated **10a-nc**, in which the vinylsulfonyl warhead was replaced by an unreactive ethylsulfonyl analog (see Supporting Information S2: Scheme S1,

for synthetic details). Biochemical HDAC inhibition assays showed that 10a-nc, while less potent than 10a, effectively inhibits HDAC1–3 with submicromolar IC₅₀ values (Table 2). The subsequent immunoblot analysis revealed that only 10a, and not 10a-nc, induced a reduction of HDAC1 protein levels (Figure 5). These findings underscore the essential role of the electrophilic vinylsulfonyl piperazine handle for the knockdown of HDAC1.

4 of 12 Archiv der Pharmazie, 2025

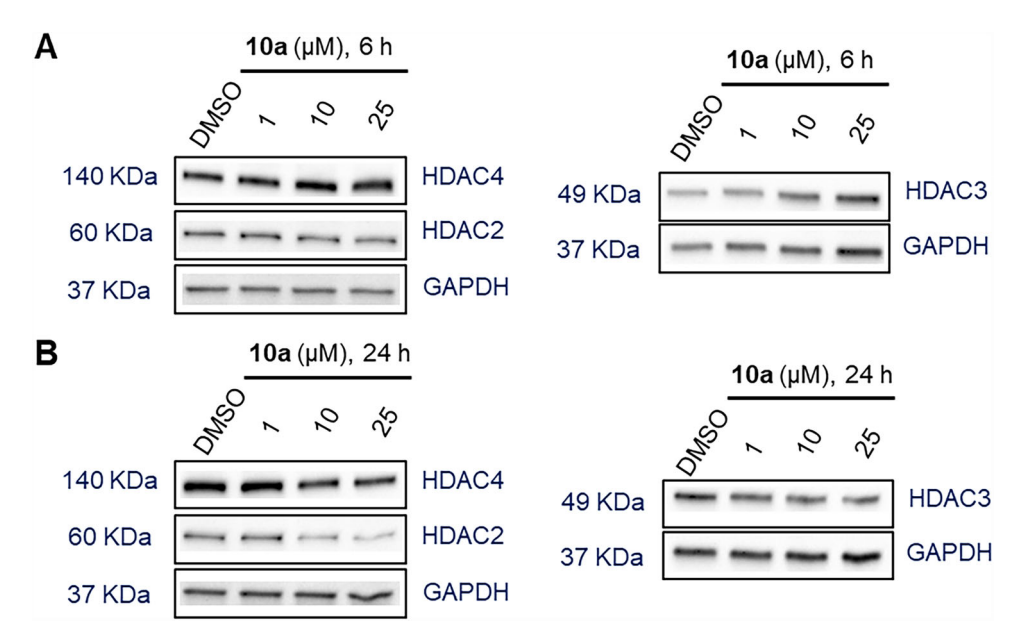


FIGURE 3 | Degradation selectivity of **10a**. MM.1S cells were treated with Compound **10a** at concentrations of 1, 10, and 25 μ M for 6 h (A) or for 24 h (B). DMSO was used as a vehicle control. HDAC2, HDAC3, and HDAC4 levels were detected by immunoblot analysis. GAPDH was used as a loading control. Representative images from a total of n = 2 replicates.

TABLE 1 | Antiproliferative activities against MM.1S cells and HDAC1 and 6 enzyme inhibition of 10a.

Compound	IC ₅₀ (μM) Cell viability ^a	IC ₅₀ (μΜ) HDAC1 ^b	IC ₅₀ (μM) HDAC6 ^b
10a	6.48 ± 1.18	0.017 ± 0.001	0.027 ± 0.008
Ricolinostat	2.59 ± 0.27	n.d.	n.d.
Vorinostat	0.79 ± 0.13	0.064 ± 0.012	0.030 ± 0.017

^a n = 3 biologically independent replicates. MM.1S cells were treated with the indicated compounds in increasing concentration for 72 h followed by a CellTiter-Glo cell viability assay.

 $^{^{\}rm b}n=2$ biologically independent replicates. In all cases, mean \pm standard deviation is shown. n.d. = not determined.

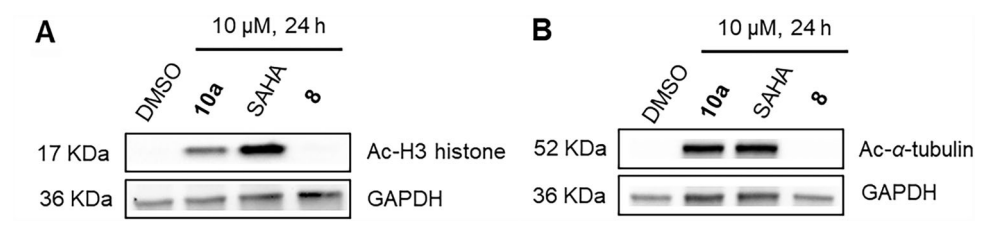


FIGURE 4 | Cellular target engagement by **10a**, vorinostat (SAHA), and **8**. Immunoblot analysis of acetylated histone H3 (A) and α -tubulin (B) in MM.1S cell lysates after treatment with the indicated compounds (10 μ M) or vehicle (DMSO) for 24 h. Representative images from a total of n = 2 replicates.

TABLE 2 | HDAC1-3 enzyme inhibition of 10a and 10a-nc.

Compound	IC ₅₀ (μM) HDAC1 ^a	IC ₅₀ (μM) HDAC2 ^a	IC ₅₀ (μM) HDAC3 ^a
10a	0.017 ± 0.001	0.088 ± 0.007	0.051 ± 0.004
10a-nc	0.229 ± 0.004	0.423 ± 0.063	0.323 ± 0.022
Vorinostat	0.064 ± 0.012	0.203 ± 0.055	0.129 ± 0.002

 $^{^{}a}n = 2$ biologically independent replicates, mean \pm standard deviation is shown.

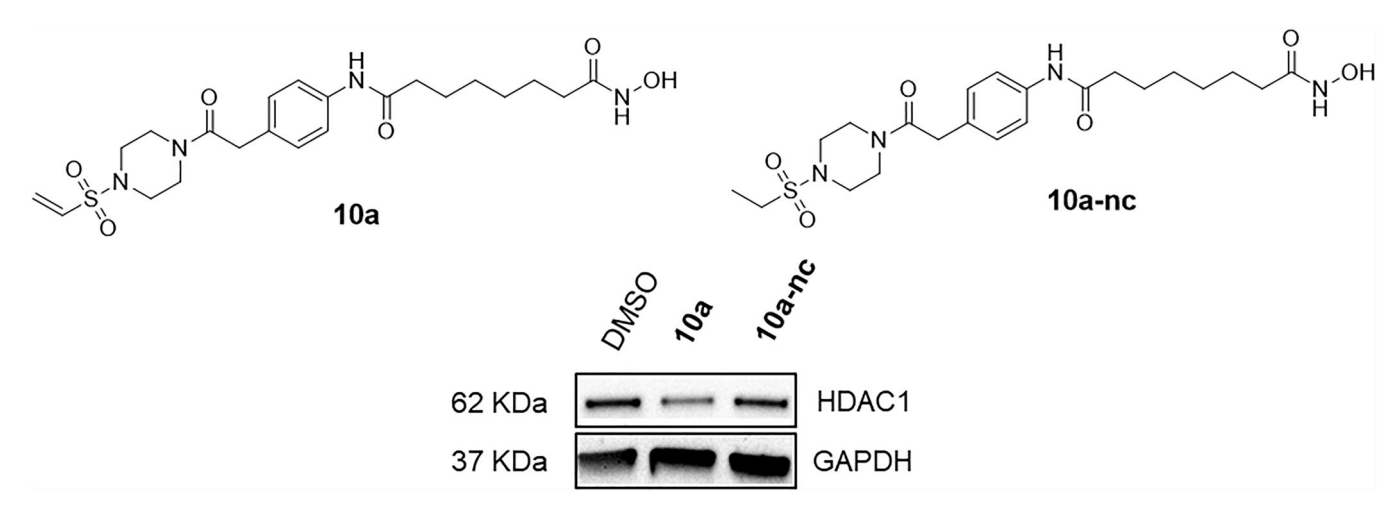


FIGURE 5 | Degradation of HDAC1 mediated by 10a and negative control 10a-nc. MM.1S cells were treated with Compounds 10a and 10a-nc at a concentration of $25 \,\mu\text{M}$ for $24 \,\text{h}$. DMSO was used as a vehicle control. HDAC1 levels were detected by immunoblot analysis. GAPDH was used as the loading control. Representative images from a total of n=2 replicates.

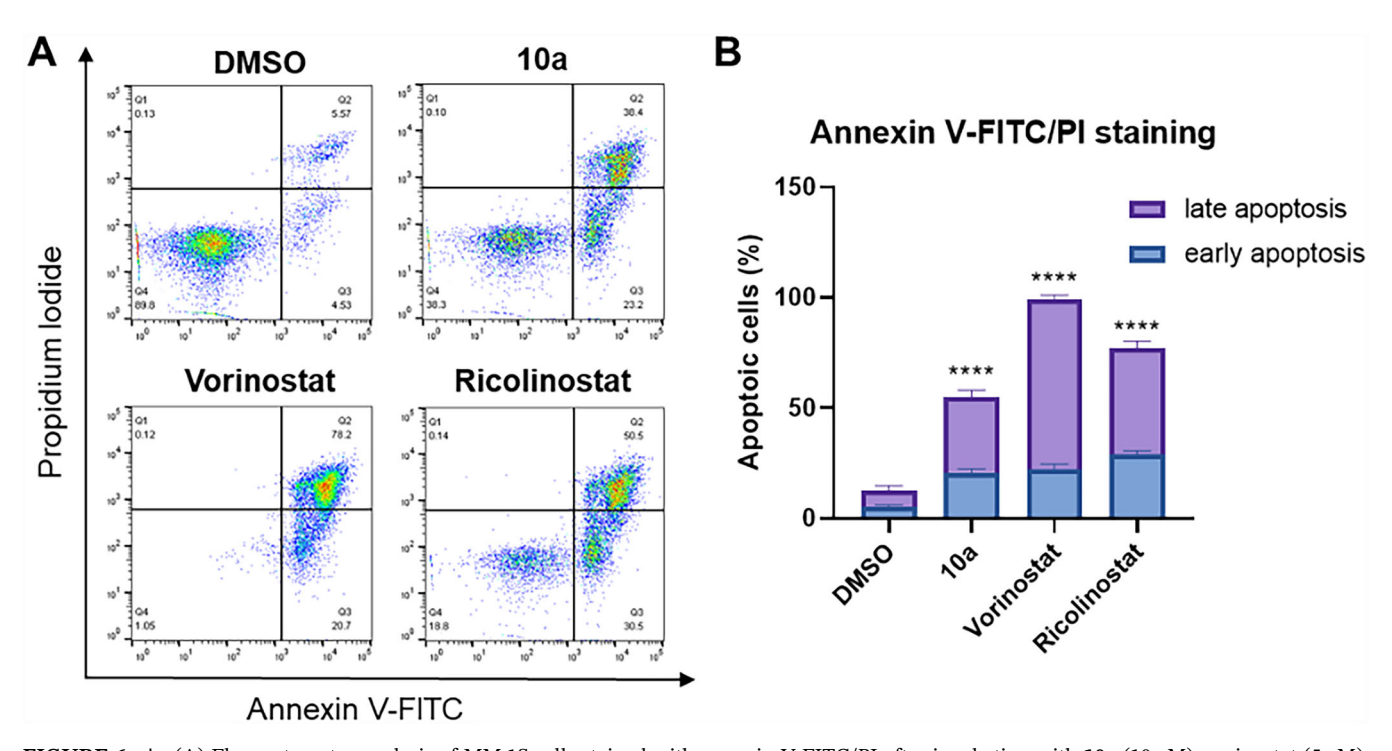


FIGURE 6 | (A) Flow cytometry analysis of MM.1S cells stained with annexin V-FITC/PI after incubation with 10a ($10 \mu M$), vorinostat ($5 \mu M$), ricolinostat ($5 \mu M$), or DMSO for 48 h. Representative images are shown. (B) Quantification of early and late apoptotic cells. The percentage of cells that were annexin V-positive but PI-negative was considered as early apoptotic, whereas the percentage of cells that were both annexin V- and PI-positive was considered as late apoptotic. Data are presented as mean \pm standard deviation (n=2 biological replicates, each performed in duplicates). Statistical analysis was performed by using one-way ANOVA in GraphPad Prism 8. Statistical significance was indicated with asterisks (**** $p \le 0.0001$).

2.2.5 | Apoptosis Induction in MM.1S Cells After 10a Treatment

Finally, following a 48-h incubation of MM.1S cells with **10a**, along with vorinostat and ricolinostat as positive controls, apoptosis induction was evaluated using annexin V-FITC/ propidium iodide (PI) staining and flow cytometry (Figure 6). As expected, **10a** markedly increased the proportions of both early and late apoptotic cells, confirming its anticancer activity

via apoptosis induction. This potency in triggering apoptosis aligned with the findings from the cell viability assays (Table 1).

3 | Conclusion

The covalent vinylsulfonyl piperazine handle, first reported by Nomura and co-workers, requires further optimization to improve its potency, selectivity, and pharmacokinetic properties [12].

6 of 12 Archiv der Pharmazie, 2025

Although the authors successfully incorporated this warhead into a range of small-molecule degraders targeting proteins such as BRD4, CDK4, the androgen receptor, BTK, SMARCA2/4, and BCR-ABL/c-ABL, selectivity remained a significant challenge. Specifically, off-target degradation was observed across the reported degraders, likely due to nonspecific interactions of the covalent handle [12]. Despite its lack of optimization, the covalent vinylsulfonyl piperazine handle presents a promising avenue for developing molecular glue-like molecules. Although off-target effects or nonselective HDAC inhibition cannot be ruled out as contributors to the observed phenotypic effects of 10a, we demonstrated that the vinylsulfonyl piperazine handle's target scope can be successfully extended to HDACs.

In summary, we designed, synthesized, and characterized a new class of DCAF16-based covalent molecular glues utilizing different ZBGs for the targeted degradation of HDACs. Western blot analysis demonstrated that the hydroxamate-based degrader 10a effectively reduced HDAC1 levels in MM.1S cells in a potent and preferential manner, whereas the control Compound 10a-nc did not affect HDAC1 levels. Subsequent cell viability assays and apoptosis induction analysis further confirmed the promising anticancer activity of 10a. Taken together, the vinylsulfonyl piperazine handle serves as a versatile covalent warhead, enabling the conversion of the nondegradative HDAC inhibitor vorinostat into the molecular glue degrader 10a for targeted HDAC1 degradation. This approach highlights the potential of this adaptable covalent chemical handle in drug development.

4 | Experimental

4.1 | Chemistry

4.1.1 | General

Chemicals were obtained from BLDpharm, Sigma-Aldrich, TCI Chemicals, and abcr GmbH and used without purification. Airsensitive reactions were carried out under argon atmosphere utilizing standard *Schlenk* techniques. Thin-layer chromatography (TLC) was carried out on prefabricated plates (silica gel 60, F254, Merck). Components were visualized by irradiation with ultraviolet light (254 nm). Column chromatography was carried out on silica gel (60 Å, $40-60\,\mu\text{m}$, *Acros Organics*).

Nuclear magnetic resonance (NMR) spectroscopy: Proton (1 H) and carbon (13 C) NMR spectra were recorded either on a Bruker AvanceDRX 500 (500 MHz 1 H NMR, 126 MHz 13 C NMR) or a BrukerAvance III 600 (600 MHz 1 H NMR, 151 MHz 13 C NMR). The chemical shifts are given in parts per million (ppm). Deuterated chloroform (CDCl₃) and deuterated dimethyl sulfoxide (DMSO- d_6) were used as solvents.

High-performance liquid chromatography (HPLC): A *Thermo Fisher Scientific* UltiMate 3000 UHPLC system with a Nucleodur 100-5 C18 ($250 \, \text{mm} \times 4.6 \, \text{mm}$, *Macherey Nagel*) with a flow rate of $1 \, \text{mL/min}$ and a temperature of 25°C or a 100-5 C18 ($100 \, \text{mm} \times 3 \, \text{mm}$, *Macherey Nagel*) with a flow rate of $0.5 \, \text{mL/min}$ and a temperature of 25°C with an appropriate gradient were used. For preparative purposes a AZURA Prep. $500/1000 \, \text{gradient}$ system with a Nucleodur $110-5 \, \text{C18} \, \text{HTec}$ ($250 \, \text{mm} \times 32 \, \text{mm}$,

Macherey Nagel) column with 20 mL/min was used. Detection was implemented by UV absorption measurement at a wavelength of $\lambda=220\,\mathrm{nm}$ and $\lambda=250\,\mathrm{nm}$. Bidest. $\mathrm{H_2O}$ (A) and $\mathrm{CH_3CN}$ (B) were used as eluents with an addition of 0.1% TFA for Eluent A. The purity of all final compounds was 95% or higher. Purity was determined via HPLC with the Nucleodur 100–5 C18 (250 mm \times 4.6 mm, Macherey Nagel) at 250 nm.

Flash chromatography was performed on an Interchim puri-Flash XS 520 Plus with a diode-array detector (DAD) from 200 to 400 nm using prepacked silica gel cartridges (PF-30SIHP-F0012-F0040) or C18 reversed-phase cartridges (PF-30C18HP-F0004-F0012).

The InChI codes of the investigated compounds, together with some biological activity data, are provided as Supporting Information S1.

4.1.2 | Synthesis of Methyl 2-(4-Aminophenyl) acetate (2)

Thionyl chloride (787 mg, 6.60 mmol, 1.0 eq.) was added dropwise to a solution of 4-aminophenylacetic acid (1, 1000 mg, 6.60 mmol, 1.0 eq.) in anhydrous methanol (25 mL). The mixture was stirred at 80°C for 16 h. The resulting solution was cooled, and the solvent was removed under reduced pressure. The brown solid hydrochloride salt of the title compound was triturated with Et₂O (2× 30 mL) to remove impurities. The free amine was liberated from its hydrochloride salt by the addition of aqueous NaHCO₃, followed by extraction into CHCl₃ (3× 30 mL). The organic layers were combined, dried over MgSO₄, and the solvent removed to get Compound 2 as a light brown oil (1.10 g, yield 97%). ¹H NMR (ppm, 500 MHz, DMSO-d₆): δ 6.90–6.88 (m, 2H), 6.51–6.48 (m, 2H), 4.94 (s, 2H), 3.58 (s, 3H), 3.43 (s, 2H). ESI-MS m/z: 166.1, [M+H]⁺.

4.1.3 | Synthesis of 8-{[4-(2-Methoxy-2-Oxoethyl) phenyl]amino}-8-Oxooctanoic Acid (3)

Compound **2** (700 mg, 4.69 mmol, 1.0 eq.), suberic anhydride (560 mg, 3.59 mmol, 0.8 eq.), and NaHCO₃ (200 mg, 2.38 mmol, 0.5 eq.) were dissolved in anhydrous THF (25 mL) and stirred at room temperature for 16 h. Solid impurities were removed by filtration, and the solvent was removed under reduced pressure. The obtained residue was purified by flash column chromatography (C18 reversed phase, MeCN/H₂O 5%–95%) to obtain **3** as a white solid (860 mg, 63% yield). ¹H NMR (ppm, 600 MHz, CDCl₃): δ 7.47–7.46 (m, 2H), 7.22–7.21 (m, 2H), 3.68 (s, 3H), 3.59 (s, 2H), 2.34 (q, J = 7.2 Hz, 4H), 1.73 (t, J = 7.2 Hz, 2H), 1.65 (t, J = 6.6 Hz, 2H), 1.39–1.36 (m, 4H). ESI-MS m/z: 322.2, [M + H]⁺.

4.1.4 | General Procedure for the Synthesis of 4a-d

To a mixture of 3 (321 mg, 1.0 mmol, 1.0 eq.) and DIPEA (522 μ L, 3.0 mmol, 3.0 eq.) in anhydrous DMF (25 mL) was added HATU (570 mg, 1.5 mmol, 1.5 eq.), and the reaction mixture was stirred at room temperature for 30 min.

Then *O*-tritylhydroxylamine (275 mg, 1.0 mmol, 1.0 eq.), *tert*-butyl (2-aminophenyl)carbamate (312 mg, 1.5 mmol, 1.5 eq.), *tert*-butyl 1-propylhydrazine-1-carboxylate (216 mg, 1.5 mmol, 1.5 eq.), or *tert*-butyl (2-amino-5-(pyridin-4-yl)phenyl)carbamate (428 mg, 1.5 mmol, 1.5 eq.) was added, and the mixture was stirred at room temperature for 16 h. The reaction mixture was distilled under vacuum to remove DMF. The obtained residue was purified by flash column chromatography (C18 reversed phase, MeCN/H₂O 5%–95%) to obtain **4a–d**.

Methyl 2-(4-{8-oxo-8-[(trityloxy)amino]octanamido}phenyl)acetate (4a): Yellow solid, 163 mg, 28% yield. 1 H NMR (ppm, 500 MHz, DMSO- d_6): δ 10.14 (s, 1H), 9.80 (s, 1H), 7.53–7.52 (m, 2H), 7.33–7.30 (m, 15H), 7.17–7.16 (m, 2H), 3.60 (s, 5H), 2.24 (t, J = 7.5 Hz, 2H), 1.78 (s, 2H), 1.52–1.46 (m, 2H), 1.19–1.14 (m, 4H), 1.00 (t, J = 7.5 Hz, 2H). 13 C NMR (ppm, 126 MHz, DMSO- d_6): δ 174.56, 171.85, 171.28, 142.63, 138.25, 129.64, 129.11, 128.89, 127.62, 119.21, 91.88, 51.75, 36.48, 33.74, 32.12, 28.48, 25.09. ESI-MS m/z: 577.5, [M – H] $^-$.

Methyl 2-{4-[8-({2-[(*tert*-butoxycarbonyl)amino]phenyl}amino)-8-oxooctanamido]phenyl}acetate (**4b**): Yellow solid, 436 mg, 85% yield. 1 H NMR (ppm, 500 MHz, DMSO- d_6): δ 9.82 (s, 1H), 9.42 (s, 1H), 8.29 (s, 1H), 7.53–7.52 (m, 3H), 7.40 (d, J= 7.5 Hz, 1H), 7.17–7.11 (m, 3H), 7.08–7.05 (m, 1H), 3.60 (s, 5H), 2.34 (t, J= 7.5 Hz, 2H), 2.30 (t, J= 7.5 Hz, 2H), 1.63–1.57 (m, 4H), 1.45 (s, 9H), 1.35 (d, J= 3.0 Hz, 4H). 13 C NMR (ppm, 126 MHz, DMSO- d_6): δ 171.84, 171.24, 153.20, 138.25, 131.25, 129.84, 129.63, 128.88, 125.16, 124.98, 124.02, 123.81, 119.19, 79.46, 51.75, 36.50, 36.09, 28.62, 28.49, 28.18, 25.26. ESI-MS m/z: 510.2, [M — H] $^-$.

tert-Butyl 2-(8-{[4-(2-methoxy-2-oxoethyl)phenyl]amino}-8-oxooctanoyl)-1-propylhydrazine-1-carboxylate (**4c**): Light yellow oil, 421 mg, 88% yield. 1 H NMR (ppm, 500 MHz, DMSO- d_6): δ 9.81 (d, J=5.5 Hz, 2H), 7.52–7.51 (m, 2H), 7.17–7.15 (m, 2H), 3.60 (s, 5H), 3.25 (s, 2H), 2.28 (t, J=7.5 Hz, 2H), 2.06 (t, J=7.5 Hz, 2H), 1.58–1.50 (m, 4H), 1.45–1.35 (m, 11H), 1.30 (t, J=7.0 Hz, 4H), 0.83 (t, J=7.5 Hz, 3H). 13 C NMR (ppm, 126 MHz, DMSO- d_6): δ 171.85, 171.26, 171.02, 138.23, 129.63, 128.89, 119.20, 79.44, 51.75, 50.08, 36.47, 33.21, 28.52, 28.02, 25.13, 25.00, 20.39, 11.23. ESI-MS m/z: 476.2, [M – H] $^-$.

Methyl 2-{4-[8-({2-[(tert-butoxycarbonyl)amino]-5-(pyridin-4-yl)phenyl}amino)-8-oxooctanamido]phenyl}acetate (4d): Yellow oil, 533 mg, 77% yield. 1 H NMR (ppm, 500 MHz, DMSO- d_6): δ 9.82 (s, 1H), 9.52 (s, 1H), 8.61 (q, J = 3.0 Hz, 2H), 8.51 (s, 1H), 7.88 (d, J = 1.5 Hz, 1H), 7.74 (d, J = 8.5 Hz, 1H), 7.63–7.58 (m, 3H), 7.53–7.51 (m, 2H), 7.17–7.15 (m, 2H), 3.60 (s, 5H), 2.39 (t, J = 7.0 Hz, 2H), 2.30 (t, J = 7.5 Hz, 2H), 1.65–1.60 (m, 4H), 1.47 (s, 9H), 1.37 (d, J = 3.0 Hz, 4H). 13 C NMR (ppm, 126 MHz, DMSO- d_6): δ 172.13, 171.85, 171.26, 153.04, 150.39, 146.34, 138.25, 132.37, 129.94, 129.64, 128.89, 123.73, 123.53, 123.27, 120.89, 119.20, 79.86, 51.75, 36.51, 36.13, 28.64, 28.55, 28.17, 25.20. ESI-MS m/z: 587.4, [M – H] $^-$.

4.1.5 | General Procedure for the Synthesis of 5a-d

4a-d (1.0 mmol, 1.0 eq.) were dissolved in THF/ H_2O (20 mL, v/v=1:1). LiOH· H_2O (2.0 eq.) was added, and the homogenous solution was stirred at room temperature for 2–12 h. The

solvent was removed under reduced pressure and purified by flash column chromatography (C18 reversed phase, MeCN/ H_2O 5%–95%) to obtain **5a–d**.

2-(4-{8-Oxo-8-[(trityloxy)amino]octanamido}phenyl)acetic acid (**5a**): White solid, 401 mg, 71% yield. ¹H NMR (ppm, 600 MHz, DMSO- d_6): δ 10.24 (s, 1H), 9.81 (s, 1H), 7.43–7.42 (m, 2H), 7.33–7.28 (m, 15H), 7.12–7.11 (m, 2H), 3.18 (s, 2H), 2.22 (t, J=7.2 Hz, 2H), 1.77 (s, 2H), 1.50–1.45 (m, 2H), 1.17 (t, J=7.8 Hz, 4H), 0.99 (s, 2H). ¹³C NMR (ppm, 151 MHz, DMSO- d_6): δ 174.80, 171.06, 142.76, 136.76, 134.45, 129.41, 129.13, 127.61, 118.76, 91.79, 45.45, 36.47, 32.16, 28.54, 28.33, 25.18, 24.89. ESI-MS m/z: 563.4, [M – H]⁻.

2-{4-[8-({2-[(*tert*-Butoxycarbonyl)amino]phenyl}amino)-8-oxooctanamido]phenyl}acetic acid (**5b**): Yellow solid, 415 mg, 84% yield. 1 H NMR (ppm, 500 MHz, DMSO- d_6): δ 7.56 (d, J= 8.0 Hz, 1H), 7.51 (d, J= 7.5 Hz, 1H), 7.43–7.42 (m, 2H), 7.13–7.11 (m, 2H), 6.96 (s, 1H), 6.89 (s, 1H), 3.20 (s, 2H), 2.26 (t, J= 7.5 Hz, 4H), 1.57 (q, J= 6.5 Hz, 4H), 1.43 (s, 9H), 1.32 (s, 4H). 13 C NMR (ppm, 126 MHz, DMSO- d_6): δ 175.10, 171.70, 171.09, 154.15, 136.83, 134.38, 129.39, 123.62, 122.53, 122.25, 118.80, 78.19, 36.49, 31.47, 28.66, 28.53, 28.40, 25.56, 25.31. ESI-MS m/z: 496.2, [M – H] $^-$.

2-(4-{8-[2-(*tert*-Butoxycarbonyl)-2-propylhydrazinyl]-8-oxooctanamido}phenyl)acetic acid (**5c**): White solid, 505 mg, 82% yield. 1 H NMR (ppm, 500 MHz, DMSO- d_6): δ 9.82 (d, J = 4.0 Hz, 2H), 7.42–7.40 (m, 2H), 7.11–7.10 (m, 2H), 3.25 (s, 2H), 3.16 (s, 2H), 2.26 (t, J = 7.5 Hz, 2H), 2.05 (t, J = 7.5 Hz, 2H), 1.57–1.50 (m, 4H), 1.45–1.35 (m, 11H), 1.29 (s, 4H), 0.82 (t, J = 7.5 Hz, 3H). 13 C NMR (ppm, 126 MHz, DMSO- d_6): δ 174.57, 171.02, 155.02, 136.68, 134.69, 129.36, 118.75, 79.41, 45.70, 36.45, 33.26, 28.55, 28.05, 25.22, 25.07, 20.43, 11.26. ESI-MS m/z: 462.3, [M - H] $^-$.

2-{4-[8-({2-[(tert-Butoxycarbonyl)amino]-5-(pyridin-4-yl)phenyl} amino)-8 oxooctanamido]phenyl}acetic acid (**5d**): Brown solid, 148 mg, 26% yield. ¹H NMR (ppm, 500 MHz, DMSO- d_6): δ 10.15 (s, 1H), 9.75 (s, 1H), 8.98 (s, 1H), 8.59 (q, J = 2.5 Hz, 2H), 7.94 (d, J = 1.5 Hz, 1H), 7.75 (d, J = 8.5 Hz, 1H), 7.62 (q, J = 3.0 Hz, 2H), 7.56 (dd, J = 2.0, 2.0 Hz, 1H), 7.40–7.39 (m, 2H), 7.11–7.09 (m, 2H), 3.16 (s, 2H), 2.34 (t, J = 7.5 Hz, 2H), 2.27 (t, J = 7.5 Hz, 2H), 1.59 (s, 4H), 1.47 (s, 9H), 1.32 (s, 4H). ¹³C NMR (ppm, 126 MHz, DMSO- d_6): δ 173.91, 172.23, 171.02, 153.21, 150.36, 146.48, 136.59, 134.93, 132.42, 132.05, 130.17, 129.26, 123.65, 123.16, 120.88, 118.68, 79.59, 46.02, 36.53, 36.04, 28.65, 28.50, 28.20, 25.28. ESI-MS m/z: 573.5, [M – H] $^-$.

4.1.6 | Synthesis of 1-(Vinylsulfonyl)piperazine (8)

tert-Butyl piperazine-1-carboxylate (6, 200 mg, 1.1 mmol, 1.0 eq.) was dissolved in DCM, and TEA (448 μ L, 3.3 mmol, 3.0 eq.) was added at 0°C. 2-Chloroethanesulfonyl chloride (133 μ L, 1.3 mmol, 1.2 eq.) in DCM was added dropwise, and the resulting reaction mixture was stirred at room temperature overnight. The reaction was quenched with water (3 × 30 mL) and extracted with DCM (3 × 30 mL). The organic extracts were washed once with brine, dried over Na₂SO₄, vacuum filtered, and concentrated in vacuo. The resultant

residue **7** was directly dissolved in DCM (20 mL). TFA (2 mL) was added, and the reaction mixture was stirred at room temperature for 1 h. The volatiles were removed in vacuo to give **8** for the next step without purification (light yellow oil, 179 mg, 95% yield over the two steps). ¹H NMR (ppm, 600 MHz, DMSO- d_6): δ 6.91 (q, J = 6.0 Hz, 1H), 6.26 (d, J = 9.6 Hz, 1H), 6.17 (d, J = 16.8 Hz, 1H), 3.25 (q, J = 3.6 Hz, 4H), 3.21 (d, J = 4.8 Hz, 4H), 1.18 (t, J = 7.8 Hz, 1H). ESI-MS m/z: 177.0, [M + H]⁺.

4.1.7 | General Procedure for the Synthesis of 9a-d

A mixture of **5a** (564 mg, 1.0 mmol, 1.0 eq.), **5b** (497 mg, 1.0 mmol, 1.0 eq.), **5c** (463 mg, 1.0 mmol, 1.0 eq.), or **5d** (574 mg, 1.0 mmol, 1.0 eq.) and HATU (570 mg, 1.5 mmol, 1.5 eq.) were dissolved in DMF, DIPEA (522 μ L, 3.0 mmol, 3.0 eq.) was added, and the reaction mixture was allowed to stir at room temperature for 30 min. **8** (264 mg, 1.5 mmol, 1.5 eq.) dissolved in DMF (15 mL) was added dropwise, and the reaction mixture was stirred at room temperature for 16 h. Solvents were removed under vacuum and extracted with ethyl acetate (3 × 20 mL). The organic layers were dried over Na₂SO₄, vacuum filtered, and concentrated in vacuo. The resultant residue was purified by flash column chromatography (C18 reversed phase, MeCN/H₂O 5%–95%) to afford **9a–d**

 N^1 -(4-{2-Oxo-2-[4-(vinylsulfonyl)piperazin-1-yl]ethyl}phenyl)- N^8 -(trityloxy)octanediamide (**9a**): Yellow solid, 239 mg, 33% yield. 1 H NMR (ppm, 600 MHz, DMSO- d_6): δ 10.14 (s, 1H), 9.78 (s, 1H), 7.51–7.50 (m, 2H), 7.33–7.29 (m, 15H), 7.12–7.11 (m, 2H), 6.77 (q, J = 6.6 Hz, 1H), 6.15 (d, J = 9.6 Hz, 1H), 6.09 (d, J = 16.2 Hz, 1H), 3.66 (s, 2H), 3.56 (s, 4H), 3.00 (s, 2H), 2.93 (s, 2H), 2.23 (t, J = 7.8 Hz, 2H), 1.77 (s, 2H), 1.48 (t, J = 7.2 Hz, 2H), 1.16 (q, J = 7.2 Hz, 4H), 1.00 (s, 2H). 13 C NMR (ppm, 151 MHz, DMSO- d_6): δ 171.25, 170.45, 169.35, 142.63, 137.89, 132.68, 130.10, 129.79, 129.31, 129.11, 127.64, 119.23, 91.87, 45.49, 45.21, 44.96, 40.79, 36.48, 32.12, 30.83, 28.49, 28.30, 25.11, 24.81. ESI-MS m/z: 721.2, [M – H] $^-$.

tert-Butyl (2-{8-oxo-8-[(4-{2-oxo-2-[4-(vinylsulfonyl)piperazin-1-yl] ethyl}phenyl)amino]octanamido}phenyl)carbamate (**9b**): Light yellow solid, 155 mg, 36% yield. 1 H NMR (ppm, 600 MHz, DMSO- d_6): δ 9.79 (s, 1H), 9.41 (s, 1H), 8.28 (s, 1H), 7.52–7.49 (m, 3H), 7.38 (d, J= 7.8 Hz, 1H), 7.13–7.04 (m, 4H), 6.76 (q, J= 6.6 Hz, 1H), 6.15 (d, J= 10.2 Hz, 1H), 6.08 (d, J= 16.8 Hz, 1H), 3.64 (s, 2H), 3.55 (t, J= 6.0 Hz, 4H), 2.99 (s, 2H), 2.92 (s, 2H), 2.33 (t, J= 7.2 Hz, 2H), 2.28 (t, J= 7.2 Hz, 2H), 1.59 (q, J= 7.2 Hz, 4H), 1.44 (s, 9H), 1.33 (d, J= 3.0 Hz, 4H). 13 C NMR (ppm, 151 MHz, DMSO- d_6): δ 171.92, 171.22, 169.36, 153.21, 137.90, 132.69, 131.26, 130.10, 129.80, 129.31, 125.19, 125.00, 124.04, 123.83, 119.23, 79.49, 45.50, 45.21, 44.97, 40.80, 38.98, 36.51, 36.09, 28.65, 28.50, 28.20, 25.27. ESI-MS m/z: 654.2, [M – H] $^-$.

tert-Butyl 2-{8-oxo-8-[(4-{2-oxo-2-[4-(vinylsulfonyl)piperazin-1-yl] ethyl}phenyl)amino]octanoyl}-1-propylhydrazine-1-carboxylate (**9c**): Light yellow solid, 218 mg, 47% yield. 1 H NMR (ppm, 600 MHz, DMSO- d_6): δ 9.83 (s, 1H), 9.79 (s, 1H), 7.51–7.49 (m, 2H), 7.12–7.10 (m, 2H), 6.78 (q, J = 6.6 Hz, 1H), 6.16 (d, J = 10.2 Hz, 1H), 6.09 (d, J = 16.8 Hz, 1H), 3.66 (s, 2H), 5.56

(t, J = 6.0 Hz, 4H), 3.25 (s, 2H), 3.00 (s, 2H), 2.93 (s, 2H), 2.27 (t, J = 7.2 Hz, 2H), 2.05 (t, J = 7.2 Hz, 2H), 1.58–1.51 (m, 4H), 1.43–1.29 (m, 15H), 0.83 (t, J = 7.8 Hz, 3H). ¹³C NMR (ppm, 151 MHz, DMSO- d_6): δ 171.23, 171.00, 169.35, 155.00, 137.89, 132.69, 130.11, 129.79, 129.31, 119.24, 79.46, 50.09, 45.50, 45.21, 44.97, 40.80, 38.99, 36.49, 33.22, 28.54, 28.03, 25.16, 25.02, 20.41, 11.25. ESI-MS m/z: 620.3, $[M-H]^-$.

tert-Butyl (2-{8-oxo-8-[(4-{2-oxo-2-[4-(vinylsulfonyl)piperazin-1-yl]ethyl}phenyl)amino]octanamido}-4-(pyridin-4-yl)phenyl) carbamate (**9d**): Yellow solid, 282 mg, 39% yield. ¹H NMR (ppm, 500 MHz, DMSO- d_6): δ 9.79 (s, 1H), 9.51 (s, 1H), 8.59 (q, J=3.0 Hz, 2H), 8.50 (s, 1H), 7.86 (d, J=2.0 Hz, 1H), 7.72 (d, J=8.5 Hz, 1H), 7.62–7.57 (m, 3H), 7.50–7.48 (m, 2H), 7.11–7.09 (m, 2H), 6.76 (q, J=6.0 Hz, 1H), 6.14 (d, J=10.0 Hz, 1H), 6.07 (d, J=16.5 Hz, 1H), 3.64 (s, 2H), 3.55 (t, J=4.5 Hz, 4H), 2.98 (d, J=4.0 Hz, 2H), 2.93 (d, J=4.5 Hz, 2H), 2.38 (t, J=7.0 Hz, 2H), 2.29 (t, J=7.5 Hz, 2H), 1.64–1.59 (m, 4H), 1.46 (s, 9H), 1.35 (t, J=3.0 Hz, 4H). ¹³C NMR (ppm, 126 MHz, DMSO- d_6): δ 172.13, 171.22, 169.35, 153.04, 150.39, 146.34, 137.89, 132.70, 132.37, 130.10, 129.94, 129.76, 129.30, 123.74, 123.54, 123.27, 120.90, 119.23, 79.86, 45.48, 45.20, 44.96, 40.79, 38.97, 36.51, 36.12, 28.65, 28.54, 28.18, 25.21. ESI-MS m/z: 731.8, $[M-H]^-$.

4.1.8 | General Procedure for the Synthesis of 10a-d

9a–d were dissolved in DCM ($10\,\mathrm{mL}$) and triisopropylsilane (TIPS, $0.5\,\mathrm{mL}$). TFA ($1\,\mathrm{mL}$) was added dropwise, and the reaction mixture was stirred at room temperature for $1\,\mathrm{h}$. Solvents were removed in vacuo, and the residue was purified by flash column chromatography (C18 reversed phase, MeCN/H₂O 5%–95%) to give **10a–d**.

 N^1 -Hydroxy- N^8 -(4-{2-oxo-2-[4-(vinylsulfonyl)piperazin-1-yl] ethyl}phenyl)octanediamide (**10a**): Yellow solid, 28 mg, 25% yield. ¹H NMR (ppm, 600 MHz, DMSO- d_6): δ 10.31 (s, 1H), 9.80 (s, 1H), 8.63 (s, 1H), 7.55–7.46 (m, 2H), 7.17–7.10 (m, 2H), 6.77 (q, J = 6.6 Hz, 1H), 6.16 (d, J = 10.2 Hz, 1H), 6.09 (d, J = 16.2 Hz, 1H), 3.65 (s, 2H), 3.56 (t, J = 6.0 Hz, 4H), 3.00 (s, 2H), 2.93 (s, 2H), 2.27 (t, J = 7.2 Hz, 2H), 1.94 (t, J = 7.2 Hz, 2H), 1.55 (q, J = 7.2 Hz, 2H), 1.48 (q, J = 7.2 Hz, 2H), 1.27 (s, 4H). ¹³C NMR (ppm, 151 MHz, DMSO- d_6): δ 171.27, 169.37, 169.26, 137.90, 132.69, 130.12, 129.81, 129.32, 119.25, 45.50, 45.22, 44.98, 40.81, 38.99, 36.49, 32.40, 28.56, 25.18. ESI-MS m/z: 479.2, [M – H]⁻. HRMS (ESI): calcd for $C_{22}H_{32}N_4O_6$ S, [M + H]⁺ 481.2115; found, 481.2097. HPLC: $t_R = 10.82$ min (98.1% purity).

 N^1 -(2-Aminophenyl)- N^8 -(4-{2-oxo-2-[4-(vinylsulfonyl)piperazin-1-yl] ethyl}phenyl)octanediamide ($\bf 10b$): White solid, 138 mg, 85% yield. 1 H NMR (ppm, 500 MHz, DMSO- d_6): δ 9.81 (s, 1H), 9.57 (s, 1H), 7.53–7.49 (m, 2H), 7.23 (d, J=7.5 Hz, 1H), 7.12–7.08 (m, 3H), 7.03 (d, J=7.5 Hz, 1H), 6.94 (t, J=7.5 Hz, 1H), 6.77 (q, J=1.5 Hz, 1H), 6.16 (d, J=10.0 Hz, 1H), 6.09 (d, J=16.5 Hz, 1H), 3.66 (s, 2H), 3.56 (t, J=4.5 Hz, 4H), 3.00 (s, 2H), 2.94 (s, 2H), 2.35 (t, J=7.5 Hz, 2H), 2.29 (t, J=7.5 Hz, 2H), 1.60 (q, J=7.0 Hz, 4H), 1.35 (q, J=3.5 Hz, 4H). 13 C NMR (ppm, 126 MHz, DMSO- d_6): δ 171.91, 171.26, 169.35, 154.65, 137.89, 132.70, 130.94, 130.11, 129.77, 129.31, 126.20, 125.67, 125.59, 119.24, 45.49, 45.20, 44.96, 40.80, 38.97, 36.49, 35.77, 28.63, 28.26, 25.19. ESI-MS m/z: 554.3, [M - H] $^-$. HRMS (ESI): calcd for

 $C_{28}H_{37}N_5O_5S$, $[M + H]^+$ 556.2588; found, 556.2577. HPLC: $t_R = 10.82 \text{ min } (99.1\% \text{ purity})$.

8-Oxo-*N*-(4-{2-oxo-2-[4-(vinylsulfonyl)piperazin-1-yl]ethyl}phenyl)-8-(2-propylhydrazinyl)octanamide (**10c**): White solid, 126 mg, 60% yield. 1 H NMR (ppm, 600 MHz, DMSO- d_6): δ 10.88 (s, 1H), 9.82 (s, 1H), 7.51–7.50 (m, 2H), 7.12–7.10 (m, 2H), 6.78 (q, J=6.6 Hz, 1H), 6.16 (d, J=10.2 Hz, 1H), 6.09 (d, J=16.2 Hz, 1H), 3.66 (s, 2H), 3.56 (q, J=3.0 Hz, 4H), 3.00–2.94 (m, 6H), 2.28 (t, J=7.2 Hz, 2H), 2.20 (t, J=7.2 Hz, 2H), 1.59–1.53 (m, 6H), 1.29 (t, J=3.6 Hz, 4H), 0.90 (t, J=7.2 Hz, 3H). 13 C NMR (ppm, 151 MHz, DMSO- d_6): δ 171.44, 171.24, 137.89, 132.70, 130.14, 129.81, 129.34, 119.24, 51.60, 45.50, 45.22, 44.97, 40.81, 38.98, 36.44, 32.98, 28.46, 25.13, 24.67, 17.96, 10.96. ESI-MS m/z: 520.4, [M – H] $^-$. HRMS (ESI): calcd for $C_{25}H_{39}N_5O_5S$, [M + H] $^+$ 522.2745; found, 522.2750. HPLC: $t_R=10.71$ min (97.5% purity).

8-Oxo-*N*-(4-{2-oxo-2-[4-(vinylsulfonyl)piperazin-1-yl]ethyl} phenyl)-8-(2-propylhydrazinyl)octanamide (**10d**): solid, 21 mg, 40% yield. ¹H NMR (ppm, 600 MHz, DMSO- d_6): δ 9.82 (s, 1H), 9.16 (s, 1H), 8.49 (q, $J = 3.0 \,\text{Hz}$, 2H), 7.71 (d, J = 1.8 Hz, 1H), 7.53-7.50 (m, 4H), 7.41 (dd, J = 1.8, 1.8 Hz,1H), 7.12-7.11 (m, 2H), 6.83-6.76 (m, 2H), 6.16 (d, J = 9.6 Hz, 1H), 6.09 (d, J = 16.2 Hz, 1H), 5.27 (s, 2H), 3.66 (s, 2H), 3.56 (t, J = 6.0 Hz, 4H), 3.00 (s, 2H), 2.94 (s, 2H), 2.35 (t, J = 7.8 Hz,2H), 2.30 (t, J = 7.8 Hz, 2H), 1.61 (q, J = 7.2 Hz, 4H), 1.36 (t, J = 3.0 Hz, 4H). ¹³C NMR (ppm, 151 MHz, DMSO- d_6): δ 171.61, 171.28, 169.36, 150.15, 147.06, 143.47, 137.90, 132.69, 130.11, 129.80, 129.32, 124.28, 123.88, 123.62, 119.82, 119.25, 116.15, 45.50, 45.21, 44.97, 40.80, 38.98, 36.52, 35.95, 28.68, 25.27. ESI-MS m/z: 631.3, $[M-H]^-$. HRMS (ESI): calcd for $C_{33}H_{40}N_6O_5S$, $[M + H]^+$ 633.2854; found, 633.2845. HPLC: $t_{\rm R} = 10.68 \, \text{min} \, (98.3\% \, \text{purity}).$

4.1.9 | Synthesis of Negative Control N^1 -(4-{2-[4-(Ethylsulfonyl)piperazin-1-yl]-2-Oxoethyl}phenyl)- N^8 -Hydroxyoctanediamide (10a-nc)

A mixture of 5a (564 mg, 1.0 mmol, 1.0 eq.) and HATU (570 mg, 1.5 mmol, 1.5 eq.) was dissolved in DMF, DIPEA (522 µL, 3.0 mmol, 3.0 eq.) was added, and the reaction mixture was allowed to stir at room temperature for 30 min. 11 (356 mg, 2.0 mmol, 2.0 eq.) dissolved in DMF (15 mL) was added dropwise, and the reaction mixture was stirred at room temperature for 16 h. Solvents were removed under vacuum, and the residue was directly dissolved in DCM (10 mL) without purification. TFA (1 mL) was added dropwise, and the reaction mixture was stirred at room temperature for 1 h. Solvents were removed in vacuo, and the residue was purified by flash column chromatography (C18 reversed phase, MeCN/ H_2O 5%–95%) to give **10a-nc** (light yellow oil, 61 mg, 10% yield over two steps). ¹H NMR (ppm, 500 MHz, DMSO- d_6): δ 10.31 (s,1H), 9.80 (s, 1H), 7.52-7.36 (m, 2H), 7.27-7.13 (m, 2H), 3.67 (s, 2H), 3.54 (s, 4H), 3.09 (t, J = 19.5 Hz, 6H), 2.27 (s, 2H), 1.94 (s, 2H), 1.49 (d, $J = 39.0 \,\mathrm{Hz}$, 4H), 1.19 (d, J = 43.0 Hz, 7H). ¹³C NMR (ppm, 126 MHz, DMSO- d_6): δ 171.26, 169.36, 169.25, 137.90, 130.15, 129.31, 119.25, 45.48, 45.14, 42.94, 41.25, 36.49, 32.40, 28.55, 25.18, 7.60. ESI-MS *m/z*: 481.4, $[M - H]^-$. HPLC: $t_R = 14.19 \text{ min } (98.3\% \text{ purity})$.

4.2 | Pharmacological/Biological Assays

4.2.1 | Cell Culture

The MM.1S was obtained from ATCC (Manassas, VA, USA). MM.1S cells were cultivated in RPMI 1640 medium supplemented with 10% FBS, 100 IU/mL penicillin, 0.1 mg/mL streptomycin, and 1 mM sodium pyruvate at 37°C in a 5% $\rm CO_2$ atmosphere.

4.2.2 | Western Blot Analysis

The MM.1S cells $(3 \times 10^6 \text{ cells/mL})$ were seeded into cell culture flasks and, after 72 h, treated with the indicated concentration of compound or DMSO for the given time. Cell lysis was performed with Cell Extraction Buffer and the addition of Halt Protease Inhibitor Cocktail and phenylmethanesulfonyl fluoride. Protein content was determined by Pierce BCA Protein Assay Kit. Samples were denatured by Laemmli 2x Concentrate, and Precision Plus Protein Unstained Standard was used as a molecular weight marker in all cases. SDS-PAGE was performed with 10% Mini-PROTEAN TGX Stain-Free Gel (Catalog# 458035, Bio-Rad, Hercules, CA, USA) at 200 V for 50 min (Catalog# 458035, Bio-Rad). Afterwards, proteins were transferred with the Trans-Blot Turbo Transfer System to Immobilon-FL PVDF membranes at 1.0 A for 30 min and incubated with 5% milkpowder solution for 1 h at room temperature under slight agitation. Subsequently, the membranes were incubated with anti-HDAC1 (Catalog# 5356S, Cell Signaling Technology, Denver, MA, USA), anti-HDAC2 (Catalog# 9959S, Cell Signaling Technology, Denver, MA, USA), anti-HDAC3 (Catalog# 85057S, Cell Signaling Technology, Denver, MA, USA), anti-HDAC4 (Catalog# 7628S, Cell Signaling Technology, Denver, MA, USA), anti-HDAC6 (Catalog# 7558S, Cell Signaling Technology, Denver, MA, USA), anti-acetyl-histone H3 (Catalog# 9677S, Cell Signaling Technology, Denver, MA, USA), anti-acetyl-α-tubulin (Catalog# 5335, Cell Signaling Technology, Denver, MA, USA), or anti-GAPDH (Catalog# T0004, Affinity Biosciences, Cincinnati, OH, USA) antibody solutions in 1:1000-1:20000 dilutions at room temperature under slight agitation for 1 h, then put membranes at 4°C for overnight. Incubation with HRP-conjugated secondary anti-mouse (Catalog# sc-516102, Santa Cruz, Dallas, TX, USA) and anti-rabbit (Catalog# HAF008, R&D Systems Inc., Minneapolis, MN, USA) antibody solutions was performed for 1.5 h, and membranes were developed with clarity western ECL substrate. The ChemiDoc XRS+ System was used for detection, and Image Lab Software 6.1 (Bio-Rad, Hercules, CA, USA) for quantification [18-20].

4.2.3 | Celltiter-Glo Cell Viability Assay

The MM.1S cells $(2.5 \times 10^3 \text{ cells/well})$ were seeded in white 384-well plates and incubated with the respective compounds at increasing concentrations. For this purpose, the dilution series was prepared at 200× concentration in DMSO and then further diluted to 10× concentration in medium. The final DMSO concentration was 0.5%. The toxicity of compounds was assessed after 72 h using the CellTiter-Glo 2.0 cell viability

10 of 12

Archiv der Pharmazie, 2025

assay. Luminescence was then measured, and the IC_{50} was determined by plotting dose–response curves and performing nonlinear regression using GraphPad Prism [21].

4.2.4 | HDAC Enzyme Inhibition Assay

For test compounds and controls, serial dilutions of the respective DMSO stock solution in assay buffer (50 mM Tris-HCl, pH 8.0, 137 mM NaCl, 2.7 mM KCl, 1.0 mM MgCl₂·6H₂O, and 0.1 mg/mL BSA) were prepared, and 5.0 µL of this serial dilution was transferred into OptiPlate-96 black microplates (Revvity). A volume of 35 µL of the fluorogenic substrate ZMAL (Z-Lys(Ac)-AMC, 21.43 µM in assay buffer) [22] and 10 µL of enzyme solution were added. Human recombinant HDAC1 (BPS Bioscience, Catalog# 50051), HDAC2 (BPS Bioscience, Catalog# 50052), HDAC3/NcoR2 (BPS Bioscience, Catalog# 50003), or HDAC6 (BPS Bioscience, Catalog# 50006) was used. The total assay volume of 50 µL (HDAC2/3/6 max. 1% DMSO; HDAC1 max. 5% DMSO) was incubated at 37°C for 90 min. Subsequently, 50 µL of trypsin (0.4 mg/mL) in trypsin buffer (50 mM Tris-HCl, pH 8.0, 100 mM NaCl) was added, followed by an additional 30 min of incubation at 37°C. Fluorescence (excitation $\lambda = 355 \,\text{nm}$, emission $\lambda = 460 \,\text{nm}$) was measured using a FLUOstar OPTIMA microplate reader. The IC₅₀ was determined by plotting dose-response curves and performing nonlinear regression using GraphPad Prism [23-26].

4.2.5 | Annexin V/PI Assay

MM.1S cells (3×10^5 cells/well) were seeded in 24-well plates and treated with the indicated concentration of compound or DMSO for 48 h under cell culture conditions. Subsequently, cells were washed with cell staining buffer (HEPES 0.1 M, NaCl 1.4 M, CaCl₂·3H₂O 25 mM), resuspended in 300 μ L, and 150 μ L was transferred in a 96-well plate. The staining was performed using 5 μ L/well annexin V-FITC (Catalog#640945, Biolegend, San Diego, CA, USA) and 10 μ L/well PI (catalog# 421301, BioLegend, San Diego, CA, USA), incubated for 15 min and analyzed by flow cytometry (Guava easyCyte, Luminex, Austin, TX, USA) [22, 27].

Acknowledgments

S.L. and F.K.H. acknowledge financial support from the Deutsche Forschungsgemeinschaft (HA 7783/4-1). T.S. (grant no. 202107060004) and S.Z. (grant no. 202106150022) are funded by the China Scholarship Council. The new NMR console for the 500-MHz NMR spectrometer used in this research was funded by the Deutsche Forschungsgemeinschaft (DFG, German Research Foundation) under project number 507275896. M.M. and F.K.H. acknowledge financial support from the Deutsche Forschungsgemeinschaft (HA 7783/5-1). The work of M.M., I.H., and F.K.H. is funded by the Deutsche Forschungsgemeinschaft (DFG, German Research Foundation) — GRK2873 (494832089). The authors thank Daniel Stopper from our group for manuscript editing. Open Access funding enabled and organized by Projekt DEAL.

Conflicts of Interest

The authors declare no conflicts of interest.

Data Availability Statement

The data that support the findings of this study are available from the corresponding author upon reasonable request.

References

- 1. T. C. S. Ho, A. H. Y. Chan, and A. Ganesan, "Thirty Years of HDAC Inhibitors: 2020 Insight and Hindsight," *Journal of Medicinal Chemistry* 63 (2020): 12460–12484.
- 2. R. Parveen, D. Harihar, and B. P. Chatterji, "Recent Histone Deacetylase Inhibitors in Cancer Therapy," *Cancer* 129 (2023): 3372–3380.
- 3. S. Chen, Y. Zheng, B. Liang, et al., "The Application of PROTAC in HDAC," European Journal of Medicinal Chemistry 260 (2023): 115746.
- 4. Z. Huang, L. Zeng, B. Cheng, and D. Li, "Overview of Class I HDAC Modulators: Inhibitors and Degraders," *European Journal of Medicinal Chemistry* 276 (2024): 116696.
- 5. Y. N. Lamb, "Givinostat: First Approval," Drugs 84 (2024): 849-856.
- 6. K. Li and C. M. Crews, "PROTACs: Past, Present and Future," Chemical Society Reviews 51 (2022): 5214-5236.
- 7. J. Krönke, N. D. Udeshi, A. Narla, et al., "Lenalidomide Causes Selective Degradation of IKZF1 and IKZF3 in Multiple Myeloma Cells," *Science* 343 (2014): 301–305.
- 8. M. Słabicki, Z. Kozicka, G. Petzold, et al., "The CDK Inhibitor CR8 Acts as a Molecular Glue Degrader That Depletes Cyclin K," *Nature* 585 (2020): 293–297.
- 9. M. Słabicki, H. Yoon, J. Koeppel, et al., "Small-Molecule-Induced Polymerization Triggers Degradation of BCl6," *Nature* 588 (2020): 164–168.
- 10. G. Dong, Y. Ding, S. He, and C. Sheng, "Molecular Glues for Targeted Protein Degradation: From Serendipity to Rational Discovery," *Journal of Medicinal Chemistry* 64 (2021): 10606–10620.
- 11. V. Vetma, L. C. Perez, J. Eliaš, et al., "Confounding Factors in Targeted Degradation of Short-Lived Proteins," *ACS Chemical Biology* 19 (2024): 1484–1494.
- 12. M. Lim, T. D. Cong, L. M. Orr, et al., "DCAF16-Based Covalent Handle for the Rational Design of Monovalent Degraders," *ACS Central Science* 10 (2024): 1318–1331.
- 13. Y. Luan, J. Li, J. A. Bernatchez, and R. Li, "Kinase and Histone Deacetylase Hybrid Inhibitors for Cancer Therapy," *Journal of Medicinal Chemistry* 62 (2019): 3171–3183.
- 14. J. W. Walton, J. M. Cross, T. Riedel, and P. J. Dyson, "Perfluorinated HDAC Inhibitors as Selective Anticancer Agents," *Organic & Biomolecular Chemistry* 15 (2017): 9186–9190.
- 15. R. Jenke, N. Reßing, F. K. Hansen, A. Aigner, and T. Büch, "Anticancer Therapy With HDAC Inhibitors: Mechanism-Based Combination Strategies and Future Perspectives," *Cancers* 13 (2021): 634.
- 16. P. Ma and R. M. Schultz, "HDAC1 and HDAC2 in Mouse Oocytes and Preimplantation Embryos: Specificity Versus Compensation," *Cell Death & Differentiation* 23 (2016): 1119–1127.
- 17. C. Pu, Y. Liu, R. Deng, et al., "Development of PROTAC Degrader Probe of CDK4/6 Based on DCAF16," *Bioorganic Chemistry* 138 (2023): 106637.
- 18. L. Schäker-Hübner, R. Haschemi, T. Büch, et al., "Balancing Histone Deacetylase (HDAC) Inhibition and Drug-Likeness: Biological and Physicochemical Evaluation of Class I Selective HDAC Inhibitors," *ChemMedChem* 17 (2022): e202100755.
- 19. L. Sinatra, A. Vogelmann, F. Friedrich, et al., "Development of First-in-Class Dual Sirt2/HDAC6 Inhibitors as Molecular Tools for Dual Inhibition of Tubulin Deacetylation," *Journal of Medicinal Chemistry* 66 (2023): 14787–14814.

- 20. F. Feller and F. K. Hansen, "Targeted Protein Degradation of Histone Deacetylases by Hydrophobically Tagged Inhibitors," *ACS Medicinal Chemistry Letters* 14 (2023): 1863–1868.
- 21. I. A. Ahmed, S. Hafiz, S. van Ginkel, et al., "Augmentation of Docetaxel-Induced Cytotoxicity in Human PC-3 Androgen-Independent Prostate Cancer Cells by Combination With Four Natural Apoptosis-Inducing Anticancer Compounds," *Natural Product Communications* 18 (2023): 1934578X231175323, https://doi.org/10.1177/1934578X231175323.
- 22. F. B. Kraft, M. Hanl, F. Feller, L. Schäker-Hübner, and F. K. Hansen, "Photocaged Histone Deacetylase Inhibitors as Prodrugs in Targeted Cancer Therapy," *Pharmaceuticals* 16 (2023): 356.
- 23. N. Reßing, J. Schliehe-Diecks, P. R. Watson, et al., "Development of Fluorinated Peptoid-Based Histone Deacetylase (HDAC) Inhibitors for Therapy-Resistant Acute Leukemia," *Journal of Medicinal Chemistry* 65 (2022): 15457–15472.
- 24. F. B. Kraft, J. Enns, I. Honin, et al., "Groebke Blackburn Bienaymé-Mediated Multi-Component Synthesis of Selective HDAC6 Inhibitors With Anti-Inflammatory Properties," *Bioorganic Chemistry* 143 (2024): 107072.
- 25. L. Schäker-Hübner, R. Warstat, H. Ahlert, et al., "4-Acyl Pyrrole Capped HDAC Inhibitors: A New Scaffold for Hybrid Inhibitors of BET Proteins and Histone Deacetylases as Antileukemia Drug Leads," *Journal of Medicinal Chemistry* 64 (2021): 14620–14646.
- 26. B. König, P. R. Watson, N. Reßing, et al., "Difluoromethyl-1,3,4-Oxadiazoles Are Selective, Mechanism-Based, and Essentially Irreversible Inhibitors of Histone Deacetylase6," *Journal of Medicinal Chemistry* 66 (2023): 13821–13837.
- 27. K. Okubo, M. Isono, T. Asano, et al., "Ubiquitin-Proteasome System Is a Promising Target for Killing Cisplatin-Resistant Bladder Cancer Cells," *Anticancer Research* 41 (2021): 2901–2912.

Supporting Information

Additional supporting information can be found online in the Supporting Information section.

12 of 12 Archiv der Pharmazie, 2025

Supporting Information

DCAF16-based covalent molecular glues for targeted protein degradation of histone deacetylases

Tao Sun,¹ Shiyang Zhai,¹ Stephan Lepper,¹ Beate König,¹ Mateo Malenica,¹ Irina Honin,¹ Finn K. Hansen¹*

¹Department of Pharmaceutical and Cell Biological Chemistry, Pharmaceutical Institute, University of Bonn, 53121 Bonn, Germany

*Correspondence:

Prof. Dr. Finn K. Hansen, Department of Pharmaceutical and Cell Biological Chemistry, Pharmaceutical Institute, University of Bonn, An der Immenburg 4, 53121 Bonn, Germany Email: finn.hansen@uni-bonn.de

Table of Contents

1. Supplementary Figures and Scheme	S2
2. NMR data of synthesized compounds	S5
3 HPI C chromatograms	S22

1. Supplementary Figures and Scheme

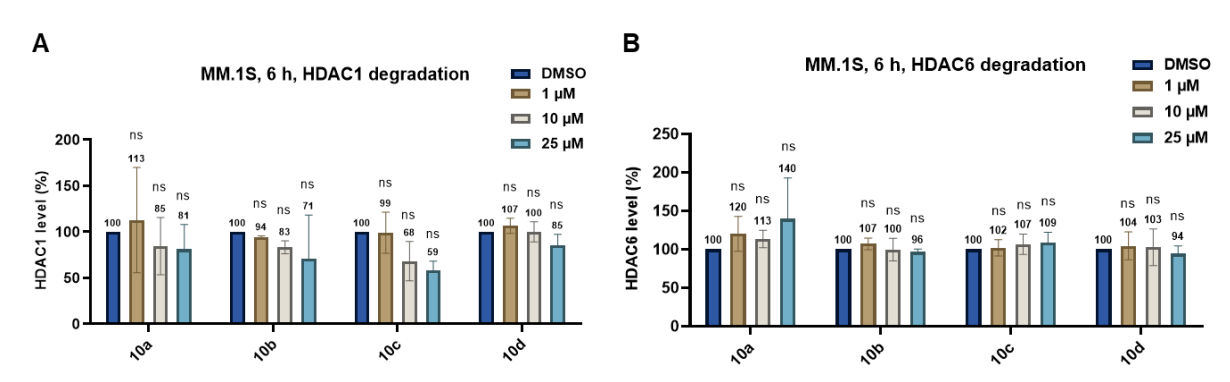


Figure S1. Densitometric analysis of HDAC1 (**A**) and HDAC6 (**B**) levels after treatment with **10a-d** for 6 h. Data from n = 2 replicates. Statistical analysis was performed by using one-way ANOVA in GraphPad Prism 8 (ns = no significance).

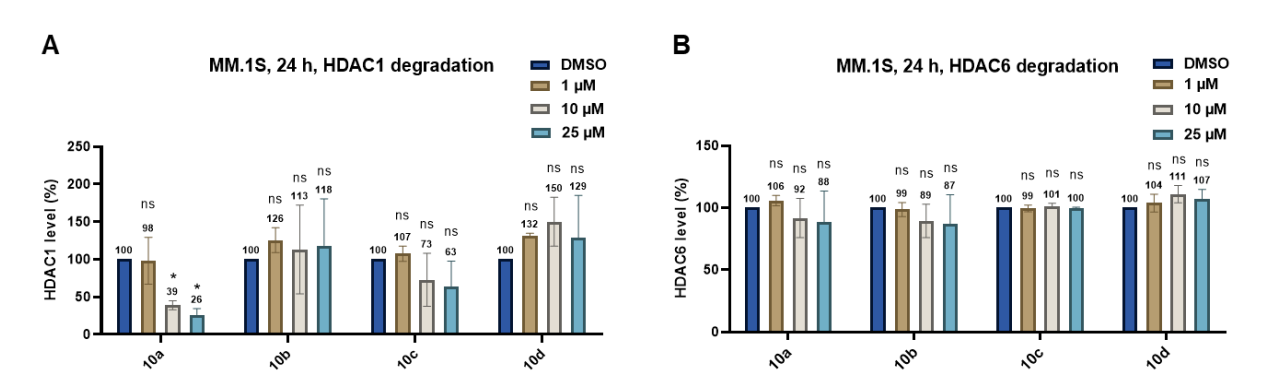


Figure S2. Densitometric analysis of HDAC1 (**A**) and HDAC6 (**B**) levels after treatment with **10a-d** for 24 h. Data from n = 2 replicates. Statistical analysis was performed by using one-way ANOVA in GraphPad Prism 8. Statistical significance was indicated with asterisks (ns = no significance; * = p < 0.05).

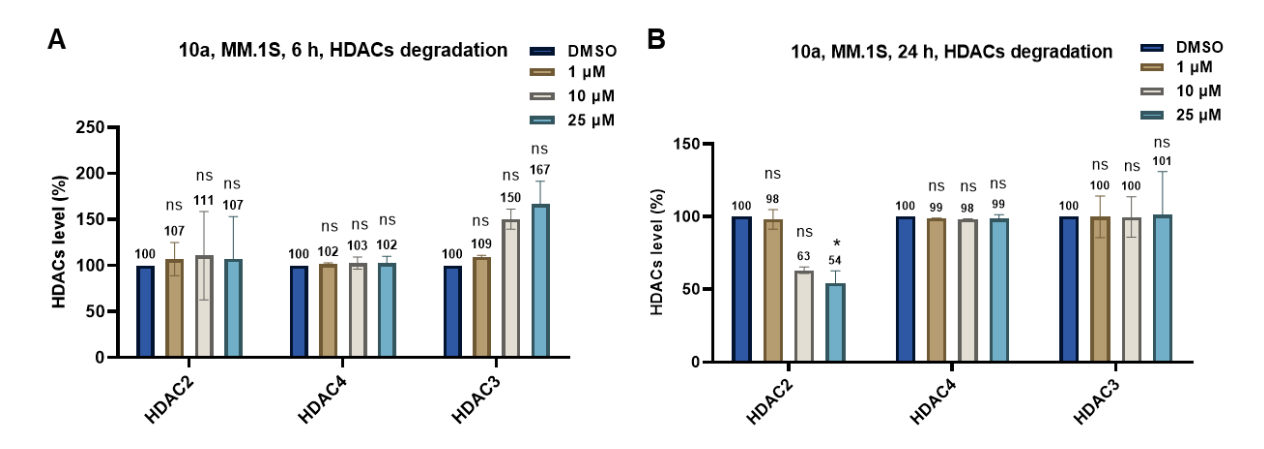


Figure S3. Densitometric analysis of HDAC2, HDAC3 and HDAC4 levels after treatment with **10a** for 6 h (**A**) or 24 h (**B**). Data from n = 2 replicates. Statistical analysis was performed by using one-way ANOVA in GraphPad Prism 8. Statistical significance was indicated with asterisks (ns = no significance; * = p < 0.05).

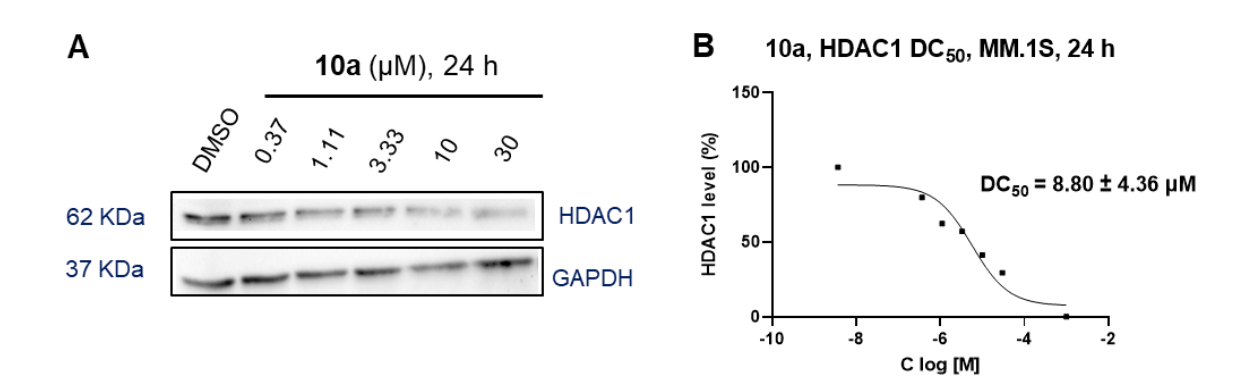
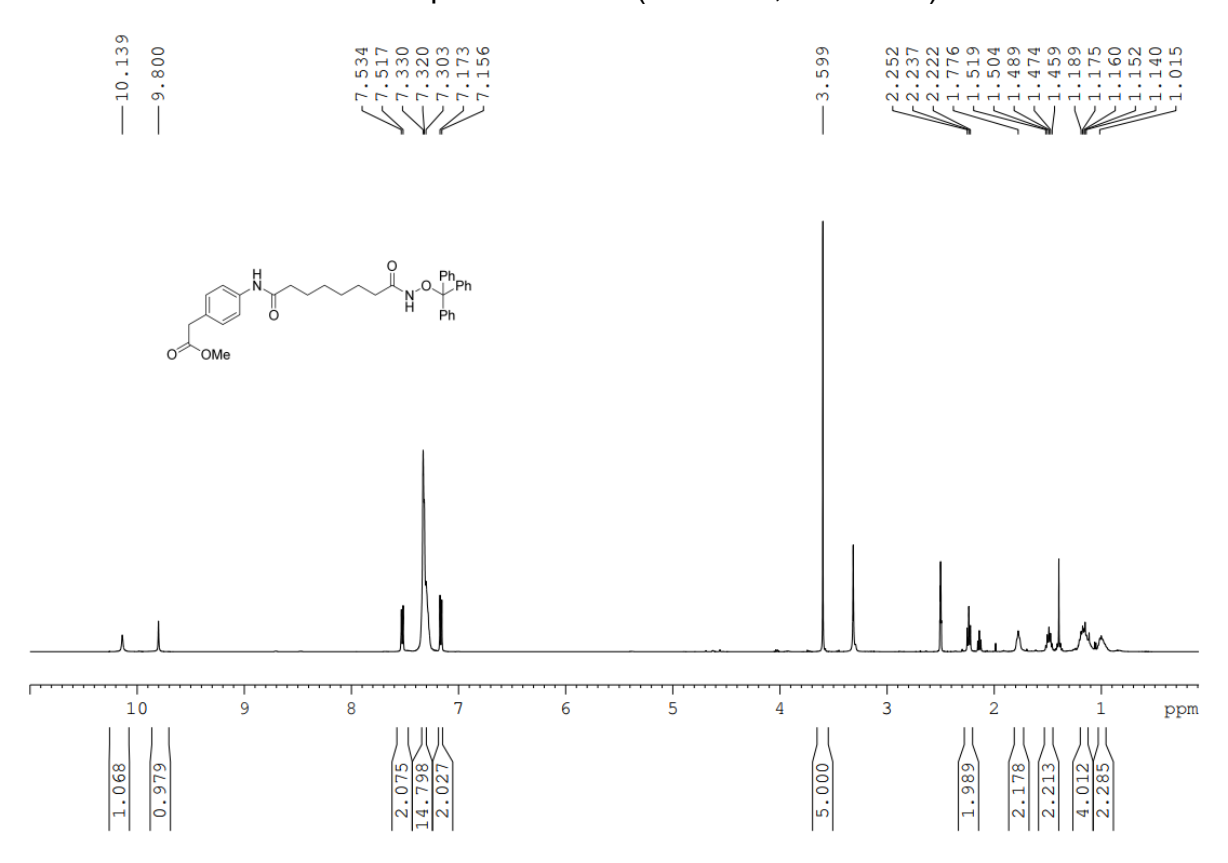


Figure S4. (**A**) Western blot analysis of HDAC1 in MM.1S cells treated for 24 h with **10a** at different concentrations ranging from 0.37 up to 30 μ M. GAPDH was selected as loading control. Representative image of n = 2 replicates. (**B**) DC₅₀ values were obtained by fitting D_{max} values to a variable slope response model. Representative curve of n = 2 replicates.

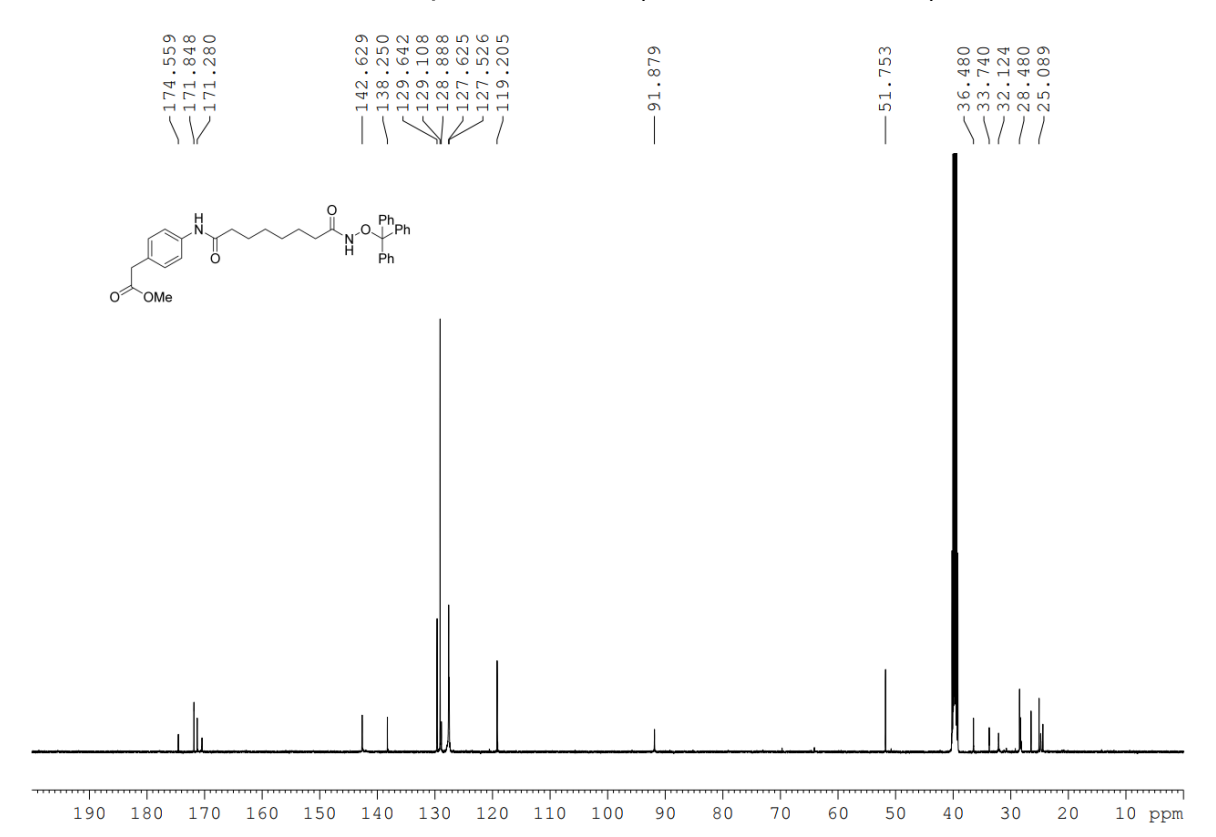
Scheme S1. Synthesis of negative control **10a-nc**. *Reagents and conditions*: **i)** HATU, DIPEA, DMF, rt, 16 h. **ii)** TFA, DCM, rt, 1 h, 10% yield (over two steps).

2. NMR data of synthesized compounds

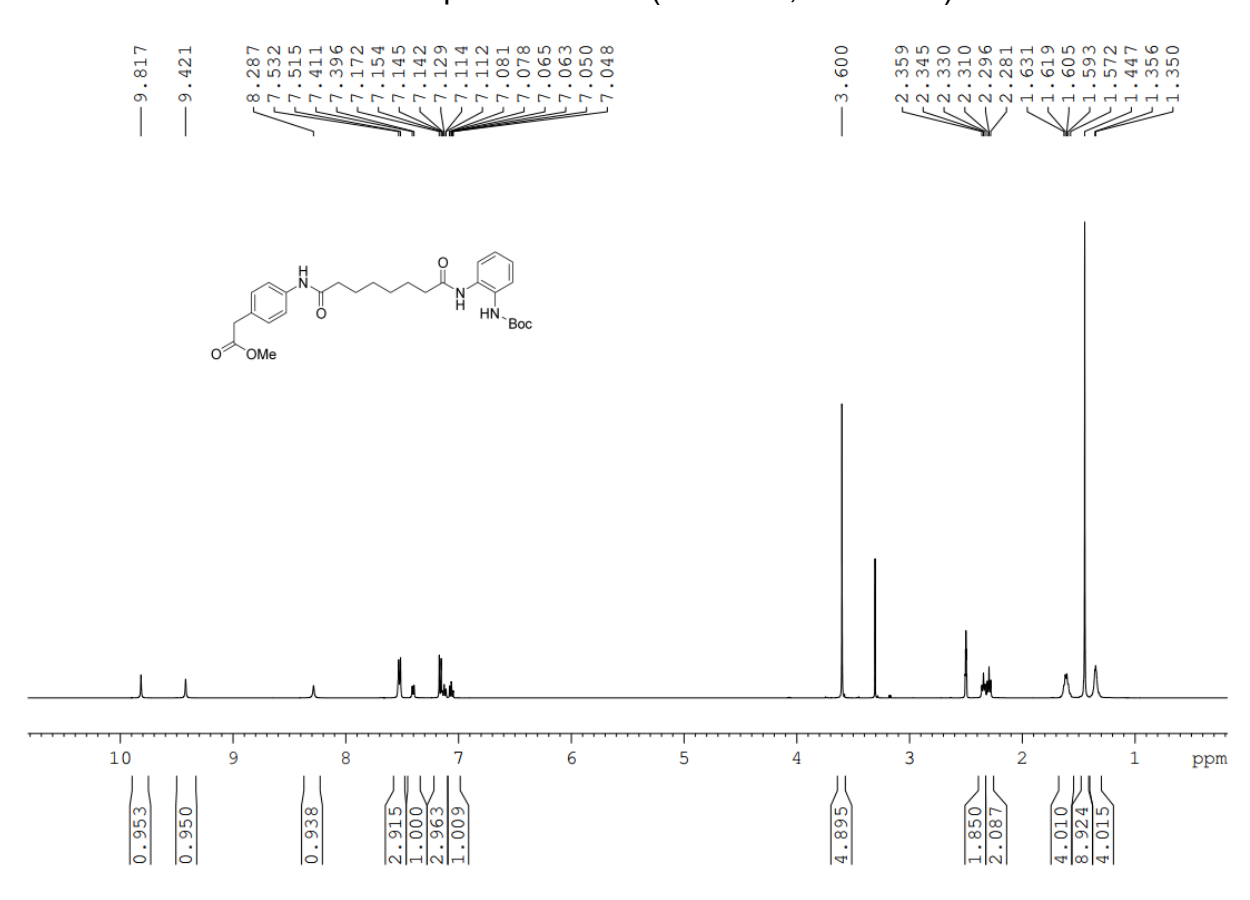
¹H NMR spectrum of **4a** (500 MHz, DMSO-*d*₆)



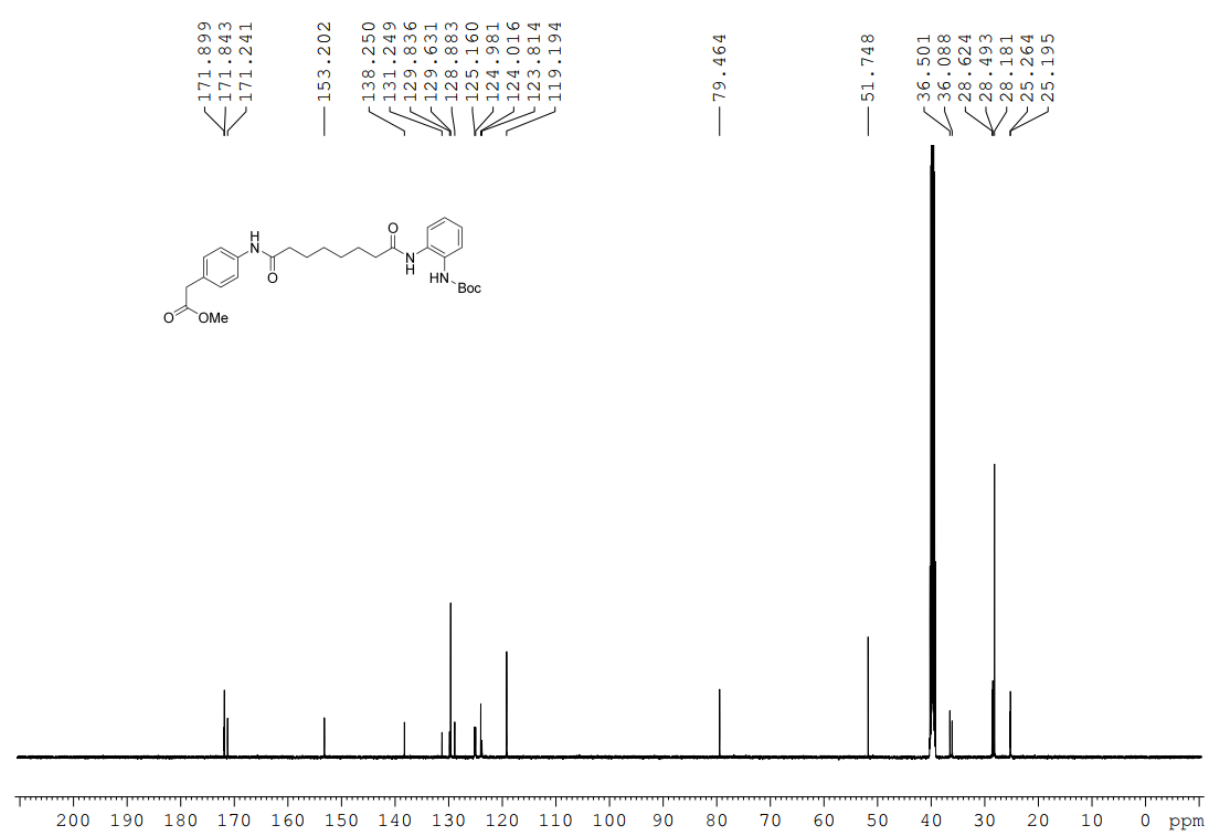
¹³C NMR spectrum of **4a** (126 MHz, DMSO-*d*₆)



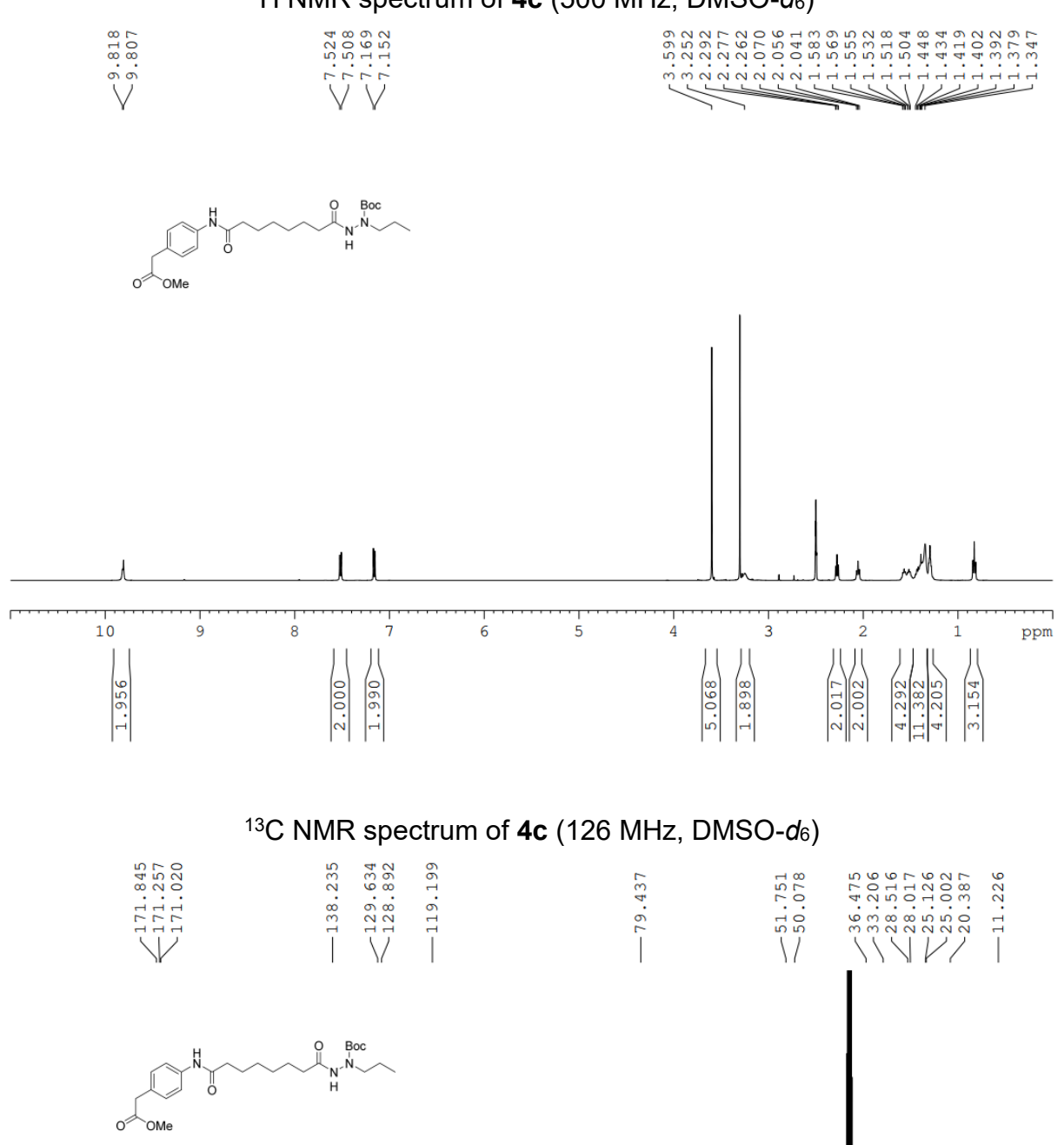
¹H NMR spectrum of **4b** (500 MHz, DMSO-*d*₆)



^{13}C NMR spectrum of **4b** (126 MHz, DMSO- d_6)







30

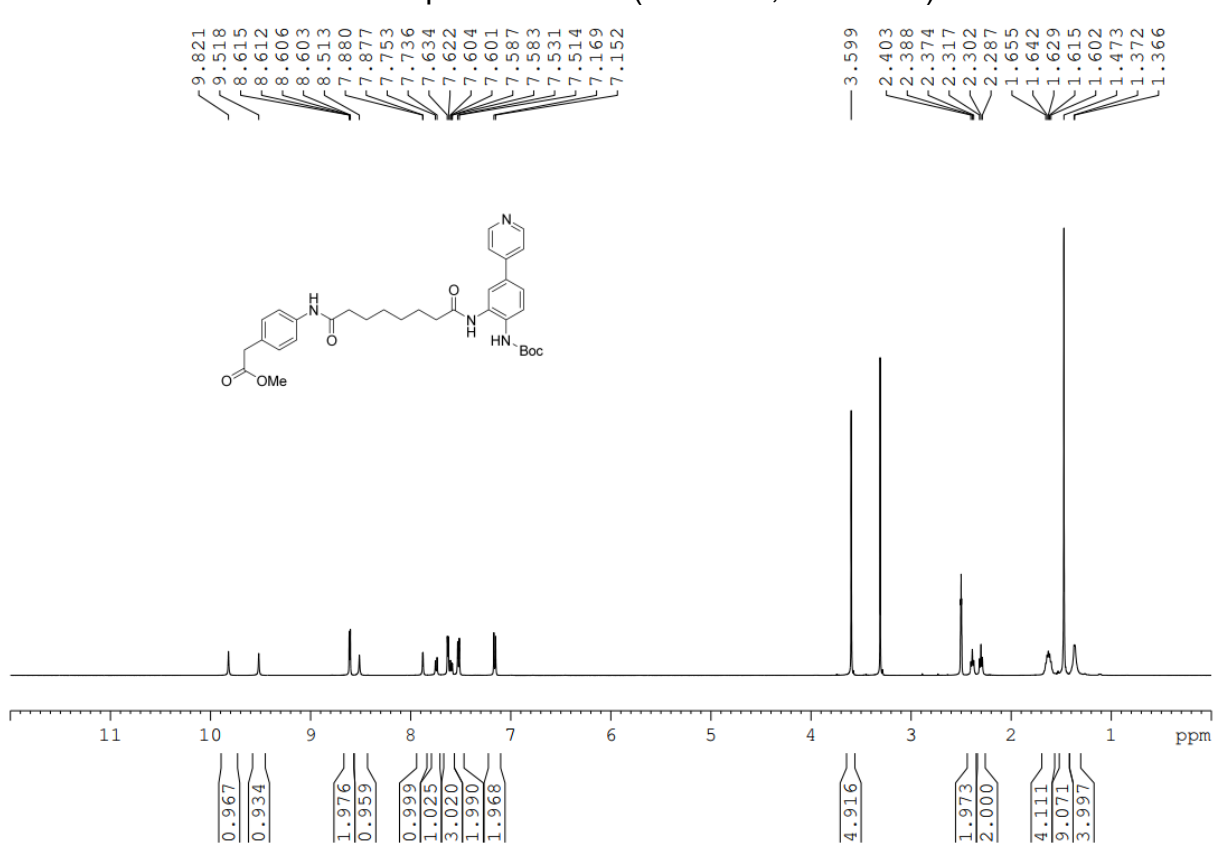
10 ppm

110

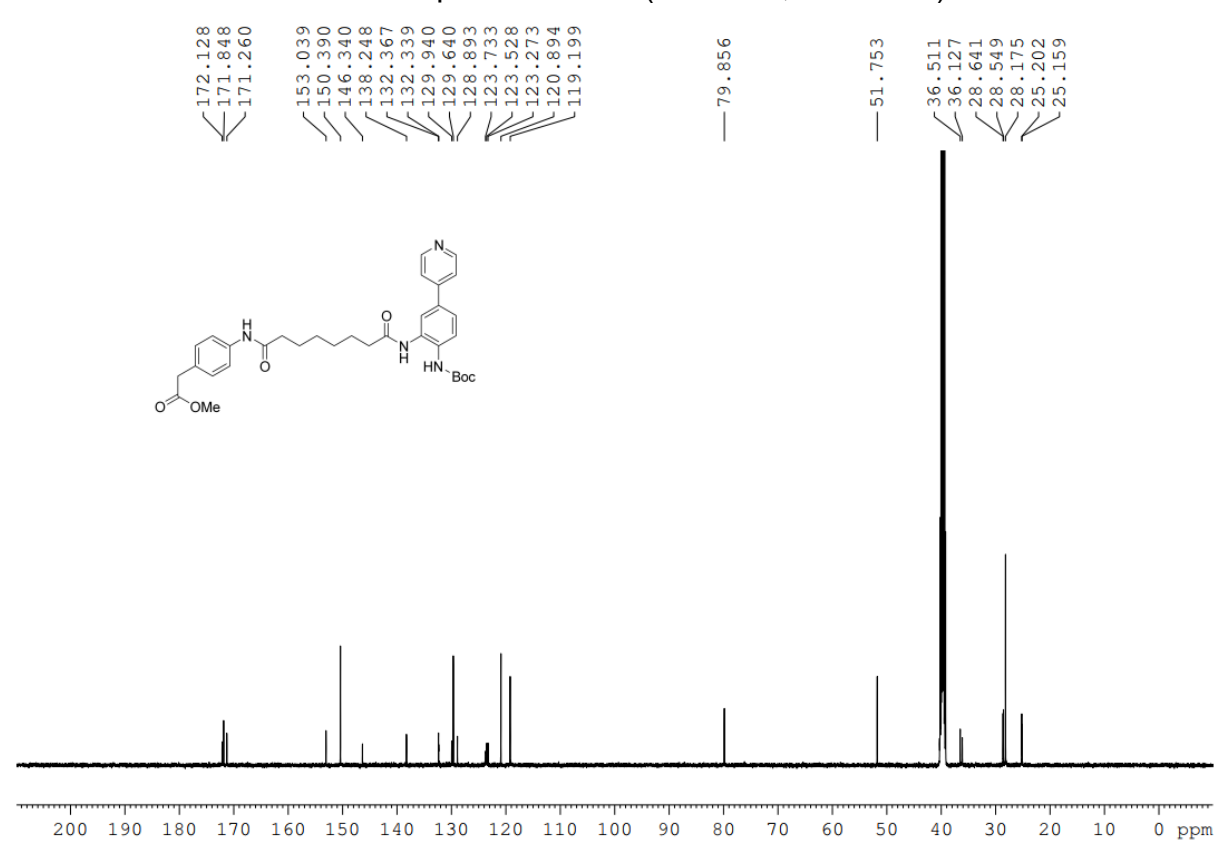
130 120

190 180 170 160 150 140

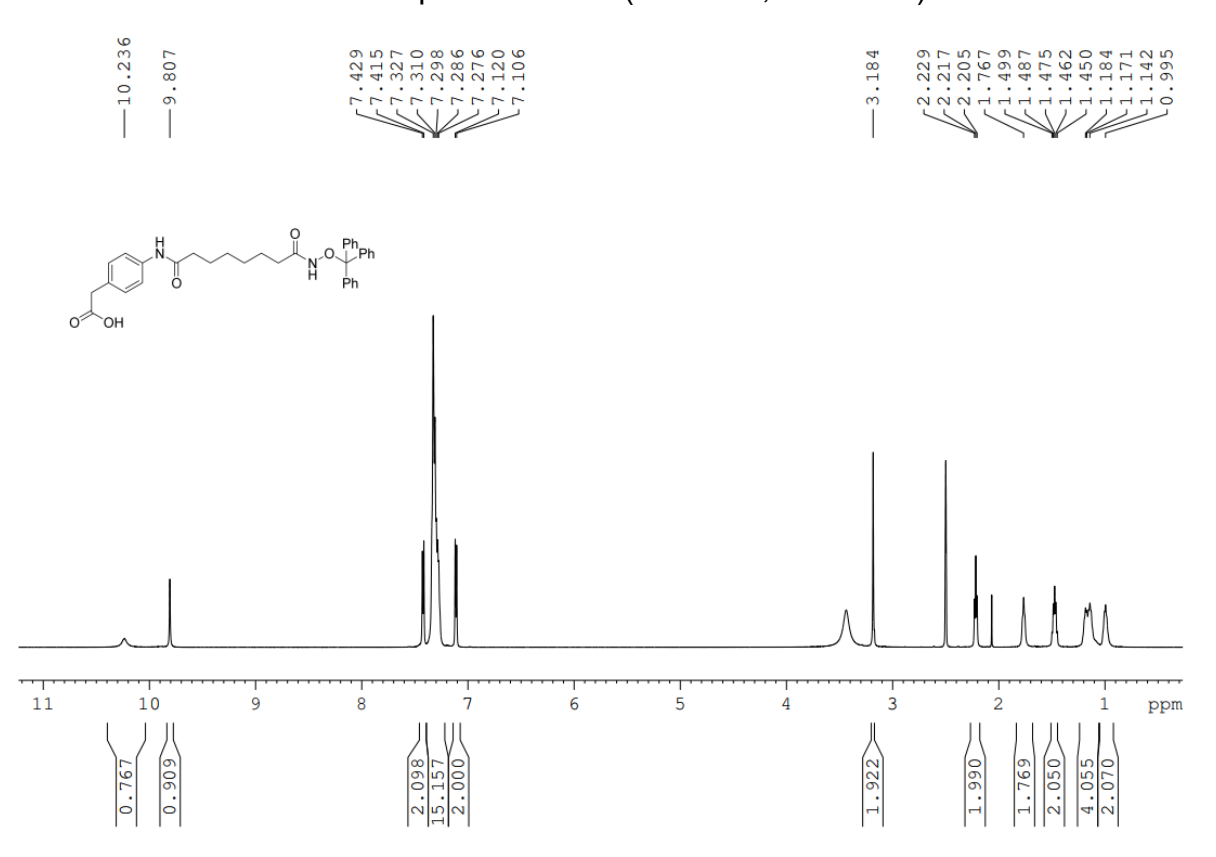
¹H NMR spectrum of **4d** (500 MHz, DMSO-*d*₆)



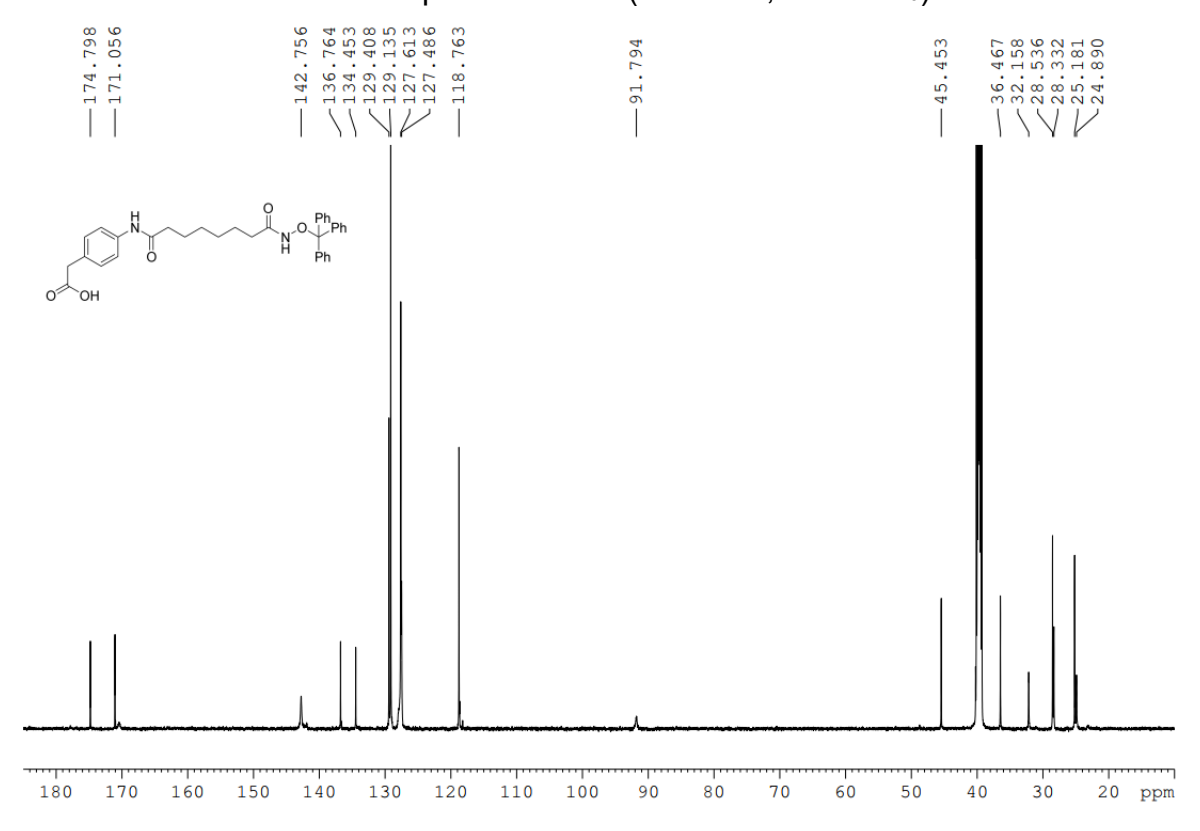
¹³C NMR spectrum of **4d** (126 MHz, DMSO-*d*₆)



¹H NMR spectrum of **5a** (600 MHz, DMSO-*d*₆)

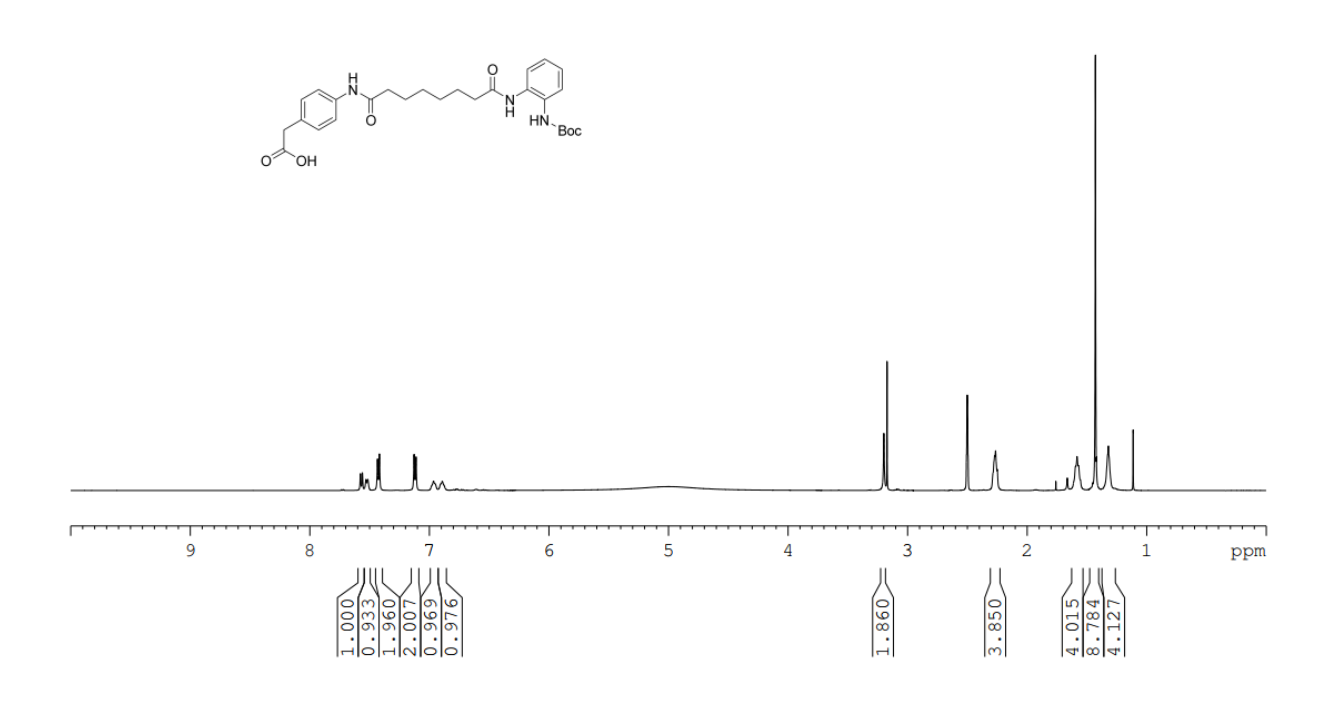


¹³C NMR spectrum of **5a** (151 MHz, DMSO-*d*₆)

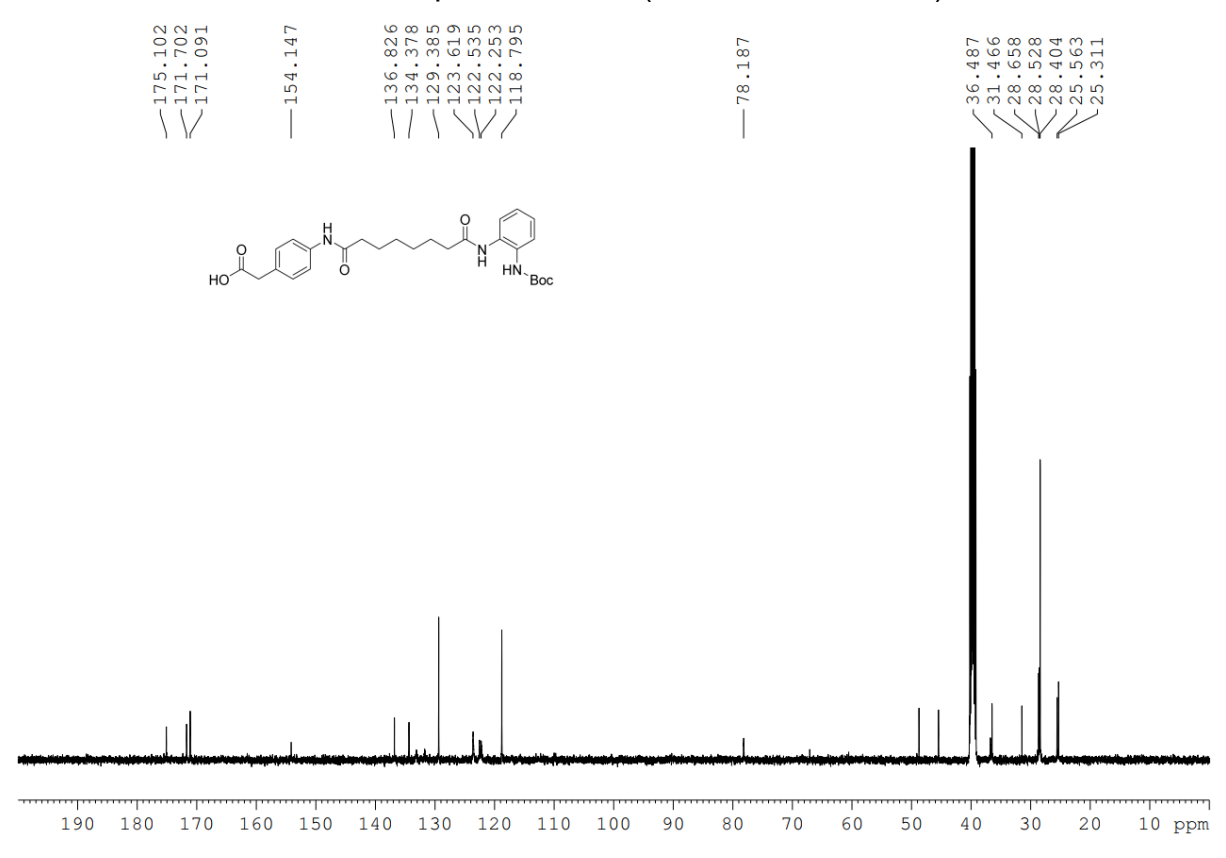






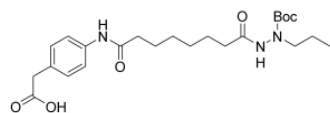


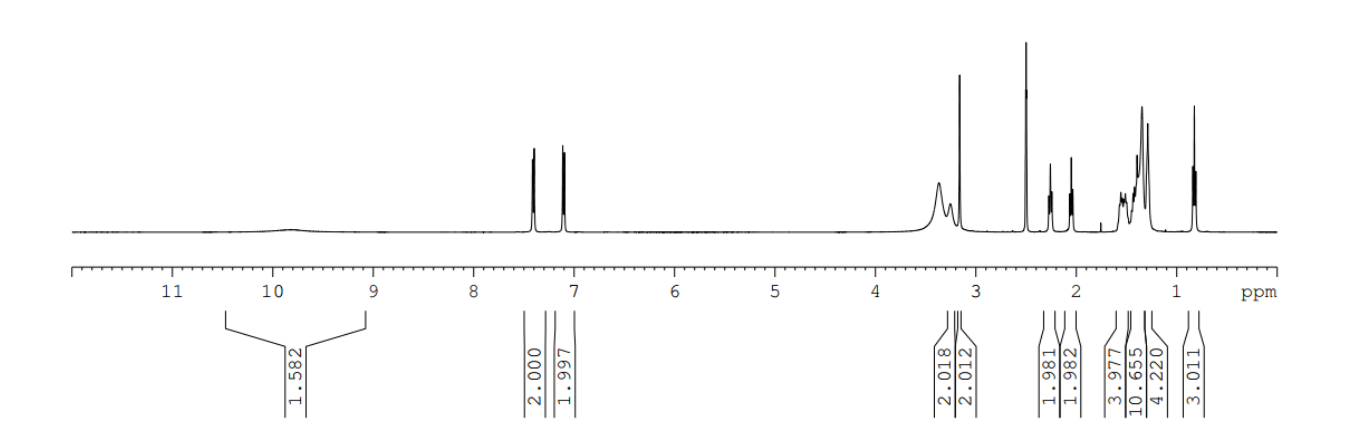
^{13}C NMR spectrum of **5b** (126 MHz, DMSO- d_6)



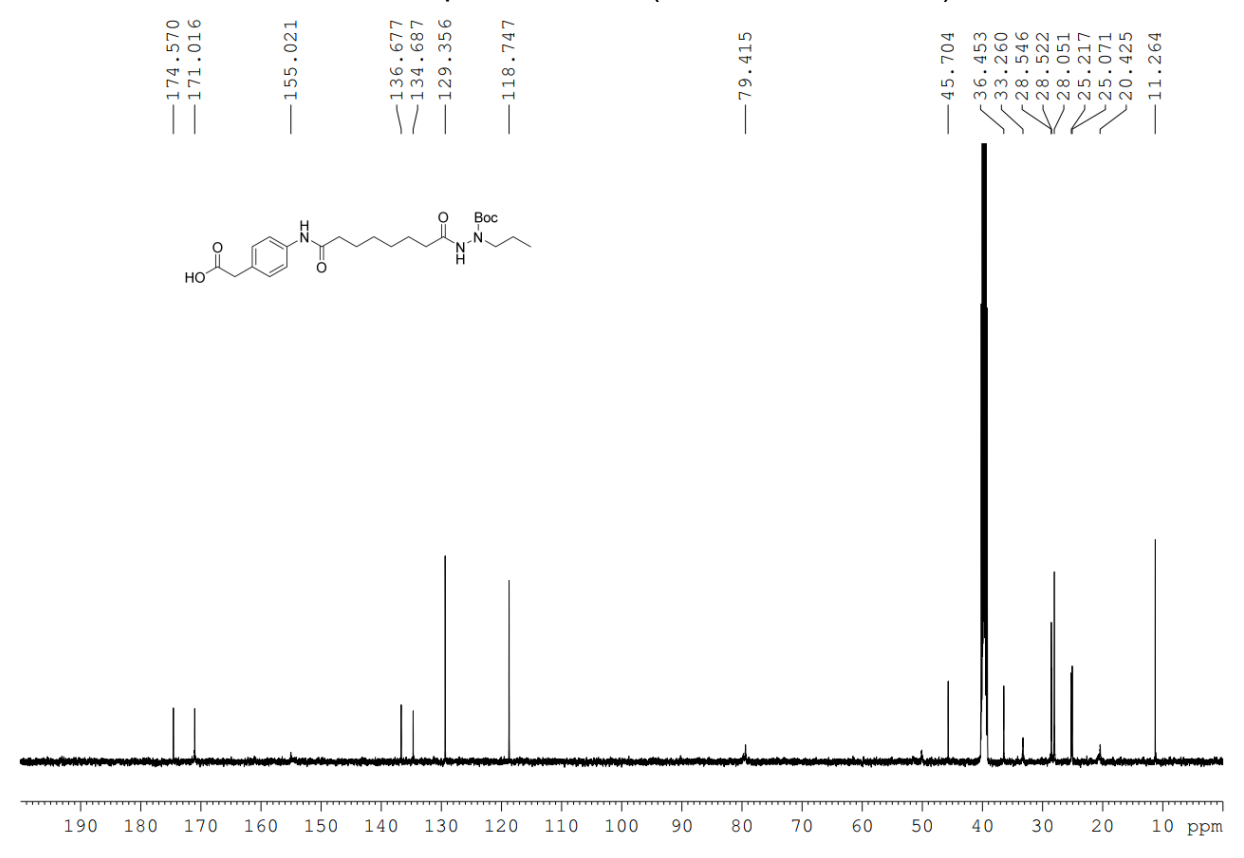
^{1}H NMR spectrum of **5c** (500 MHz, DMSO- d_{6})



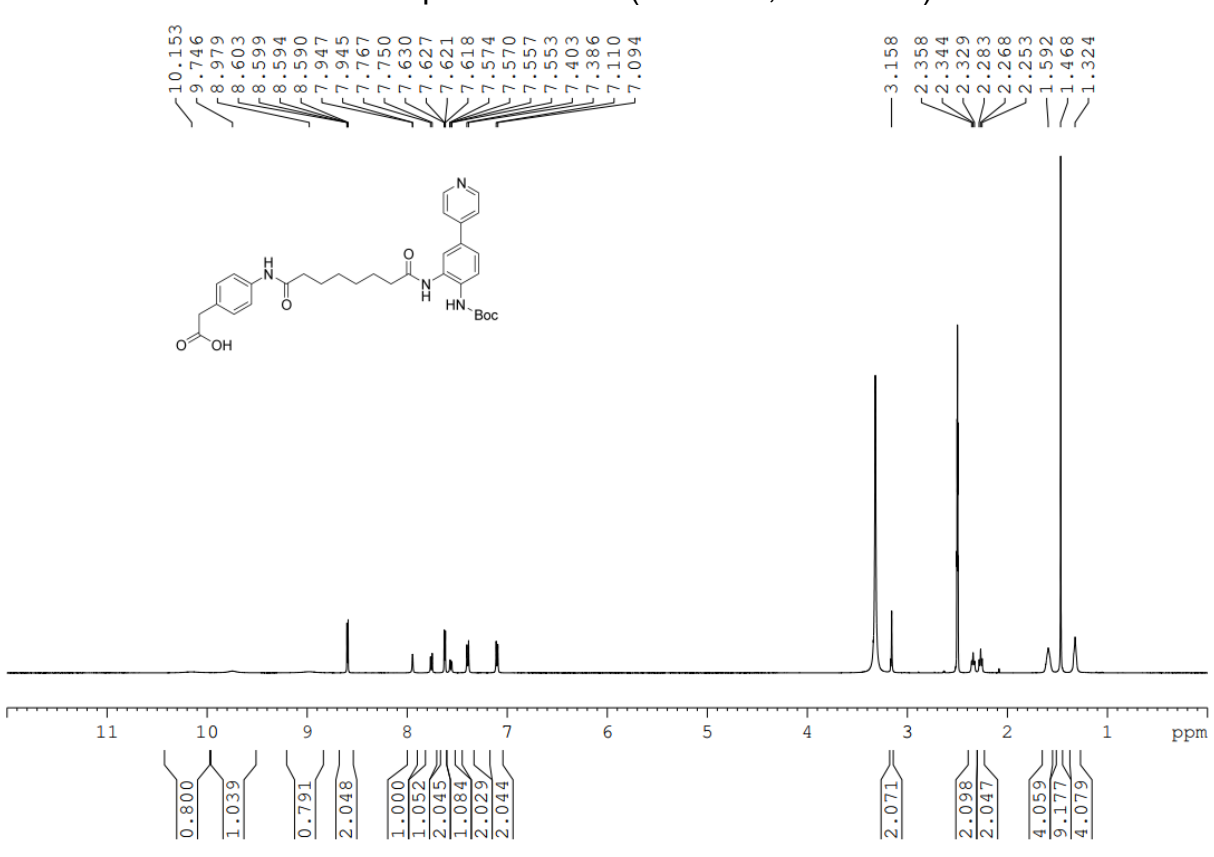




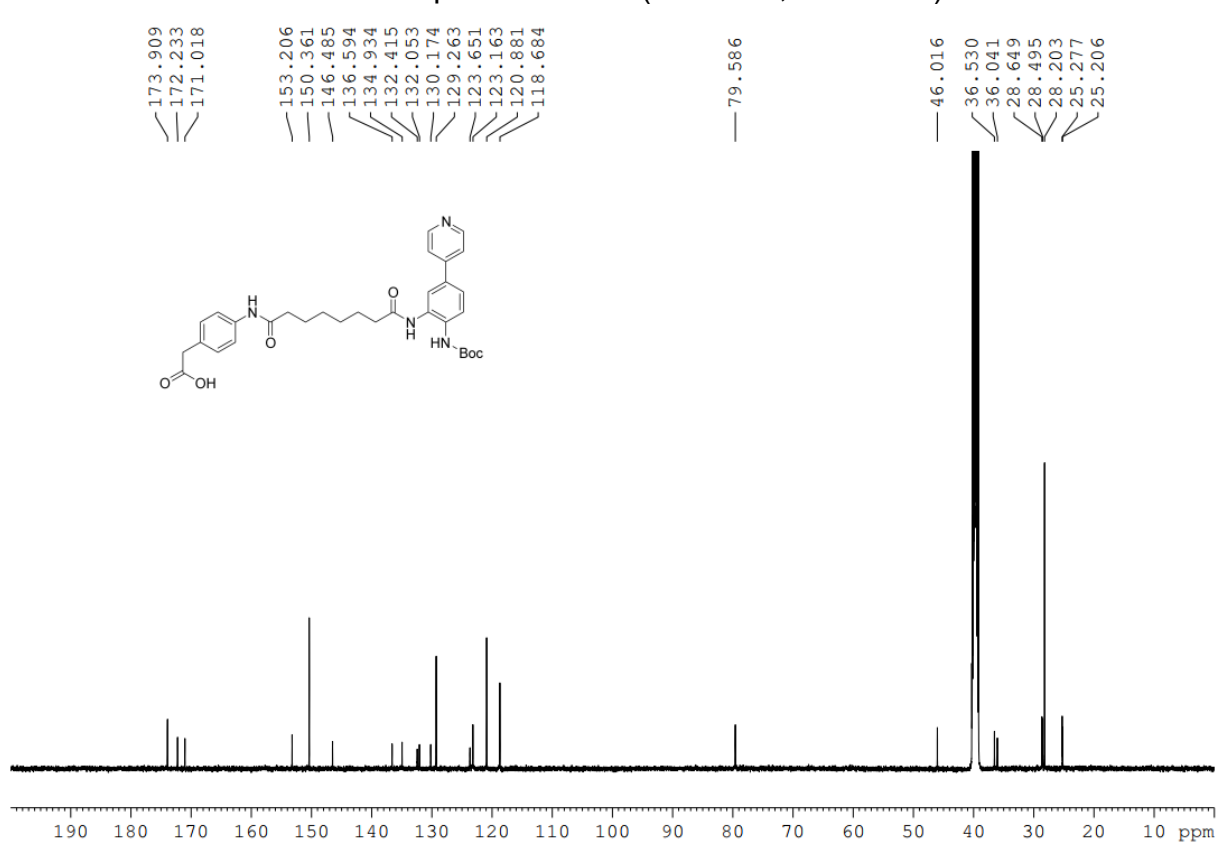
^{13}C NMR spectrum of **5c** (126 MHz, DMSO- d_6)



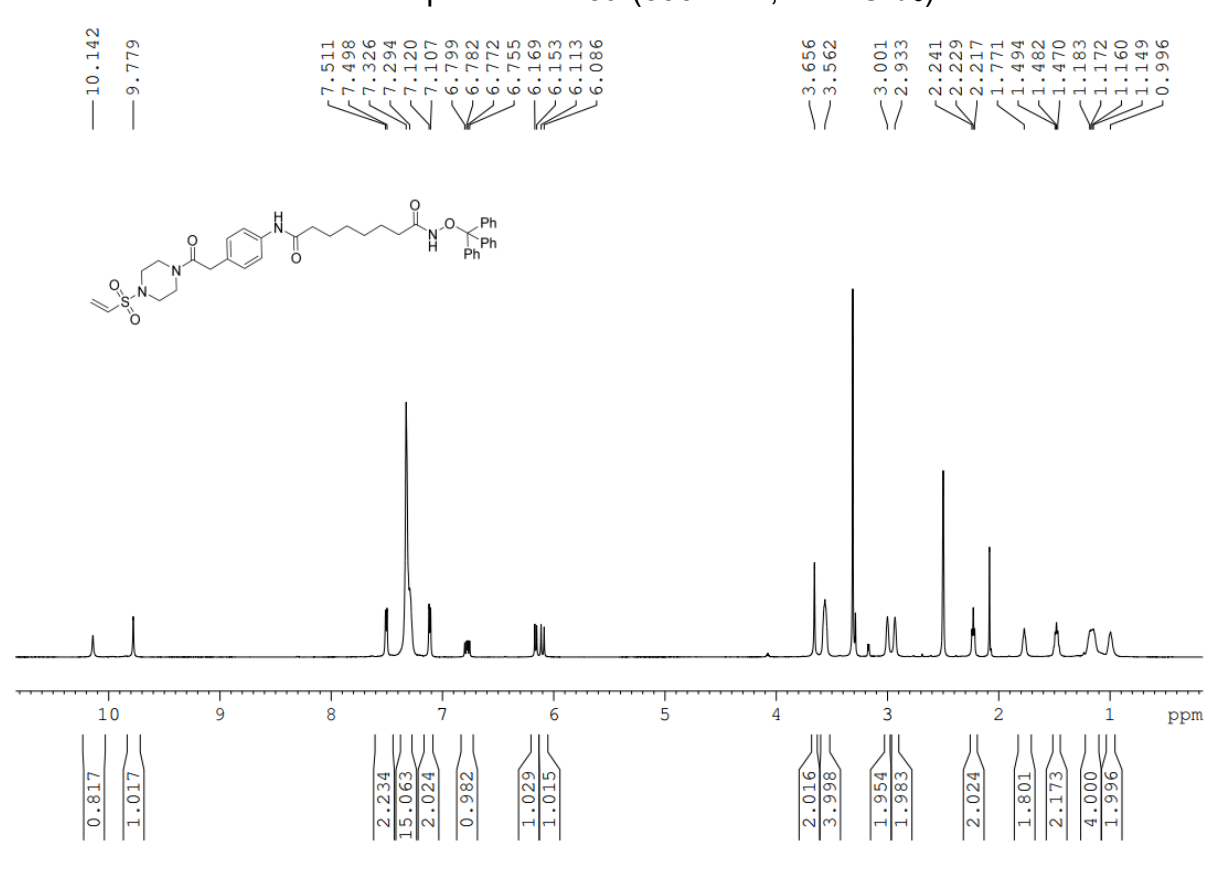
¹H NMR spectrum of **5d** (500 MHz, DMSO-*d*₆)



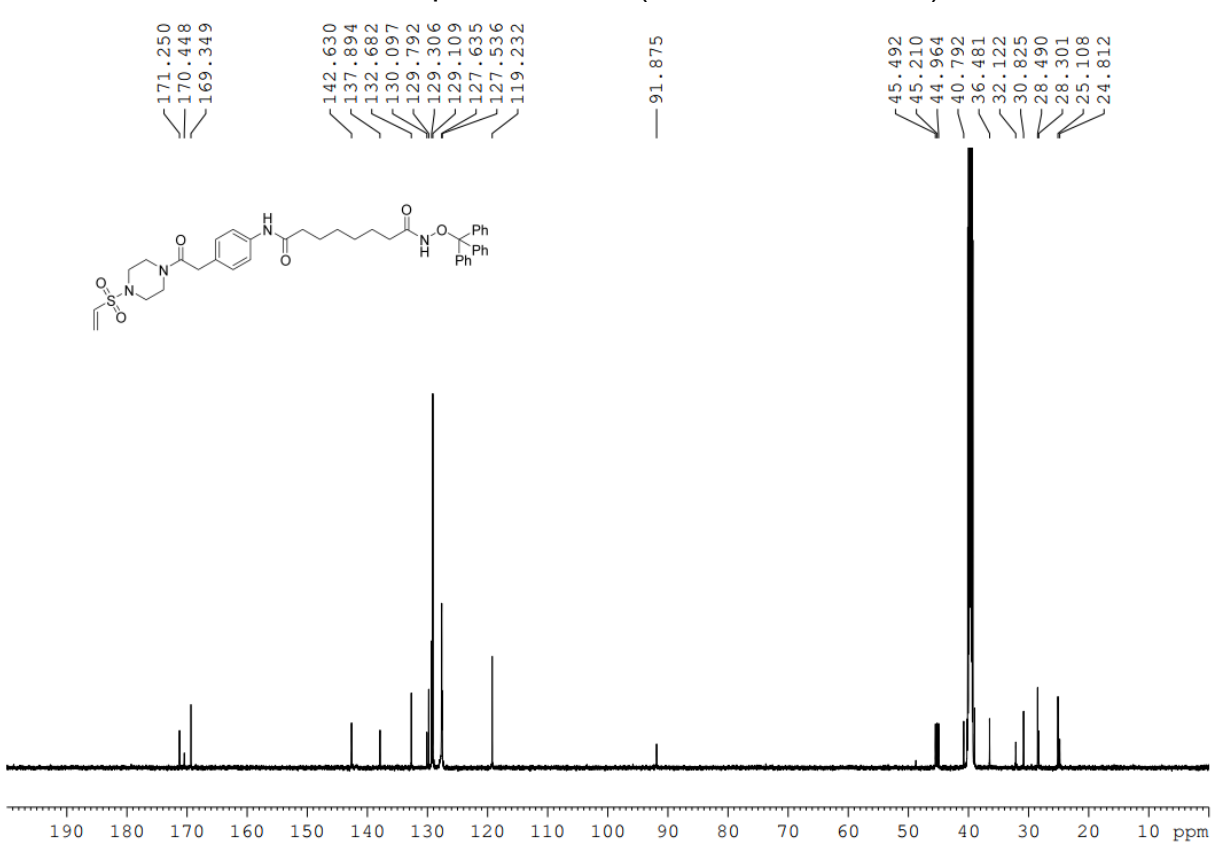
¹³C NMR spectrum of **5d** (126 MHz, DMSO-*d*₆)



¹H NMR spectrum of **9a** (600 MHz, DMSO-*d*₆)



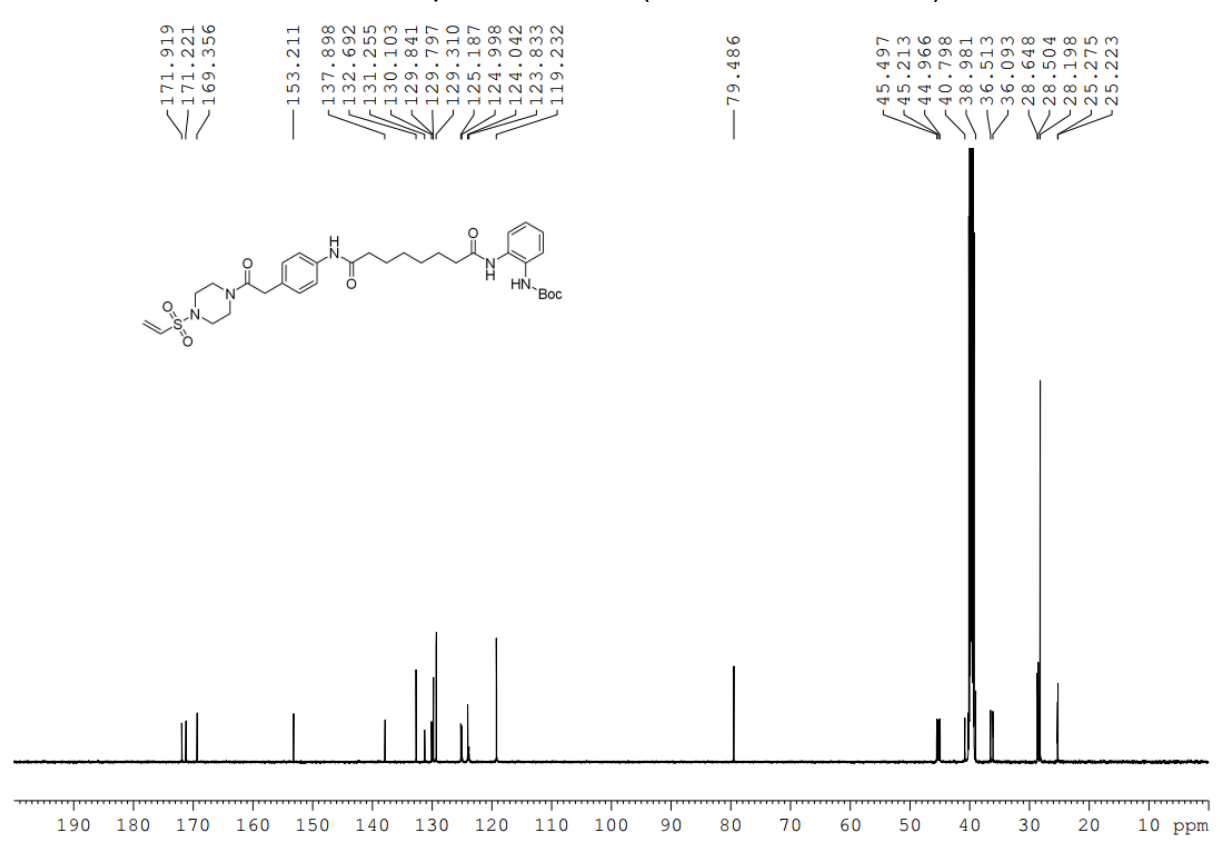
¹³C NMR spectrum of **9a** (151 MHz, DMSO-*d*₆)



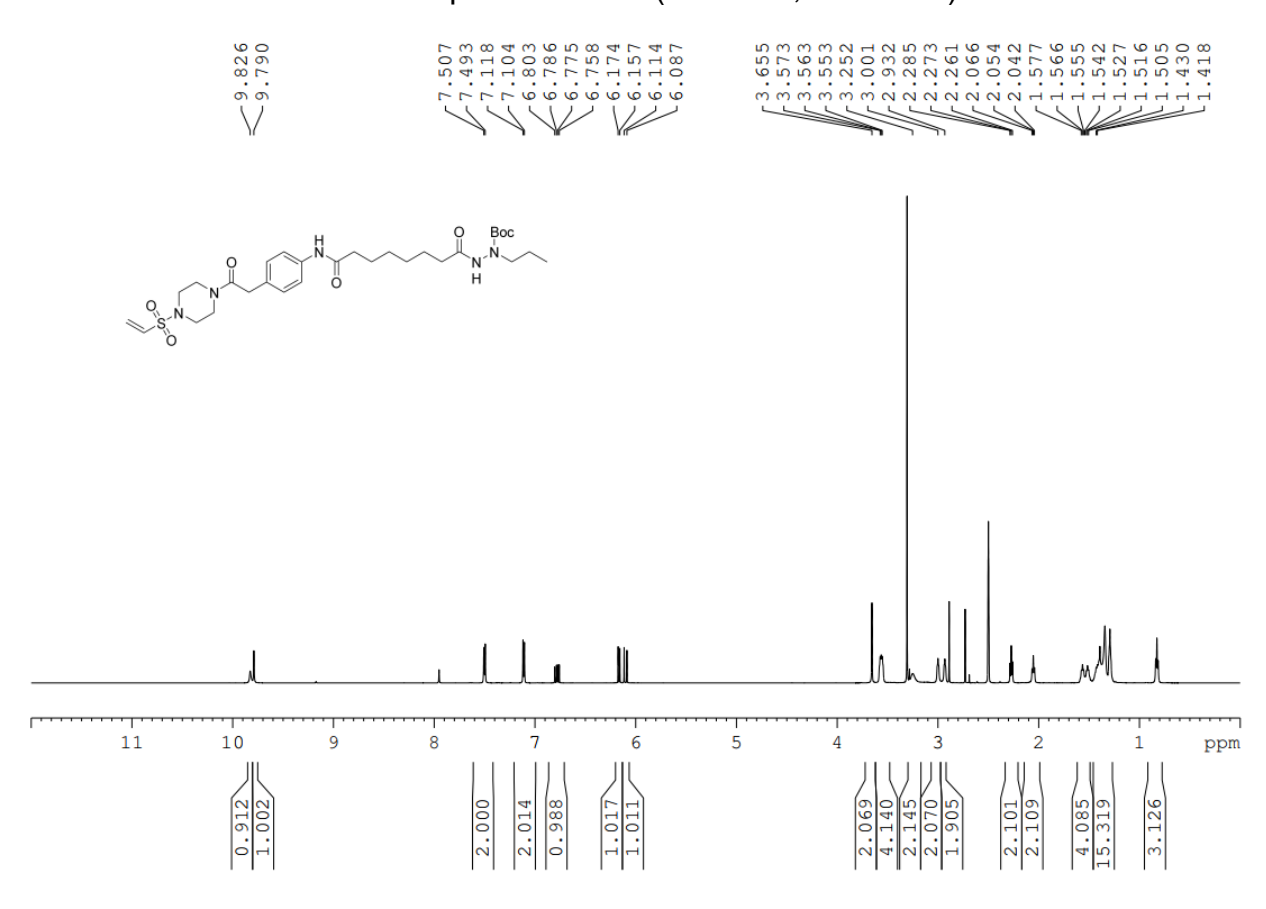
¹H NMR spectrum of **9b** (600 MHz, DMSO-*d*₆)



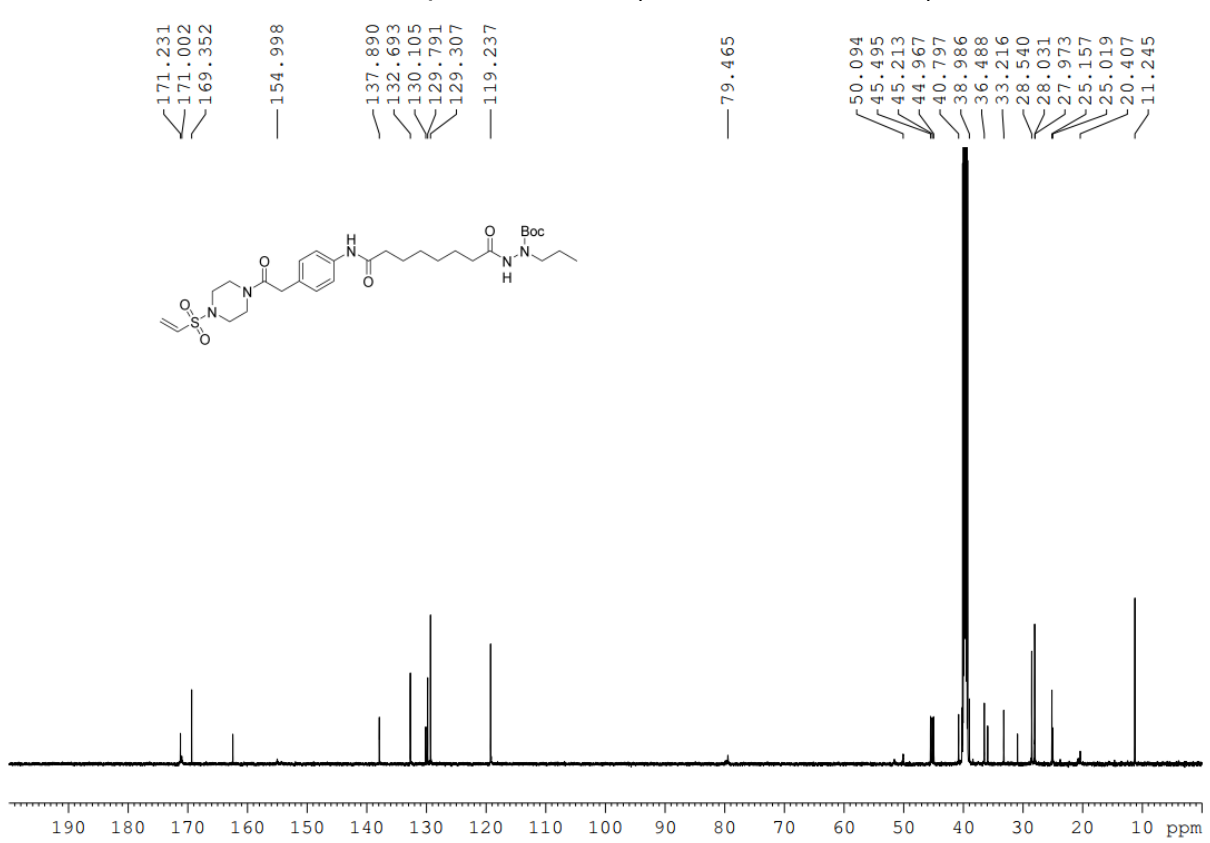
¹³C NMR spectrum of **9b** (151 MHz, DMSO-*d*₆)



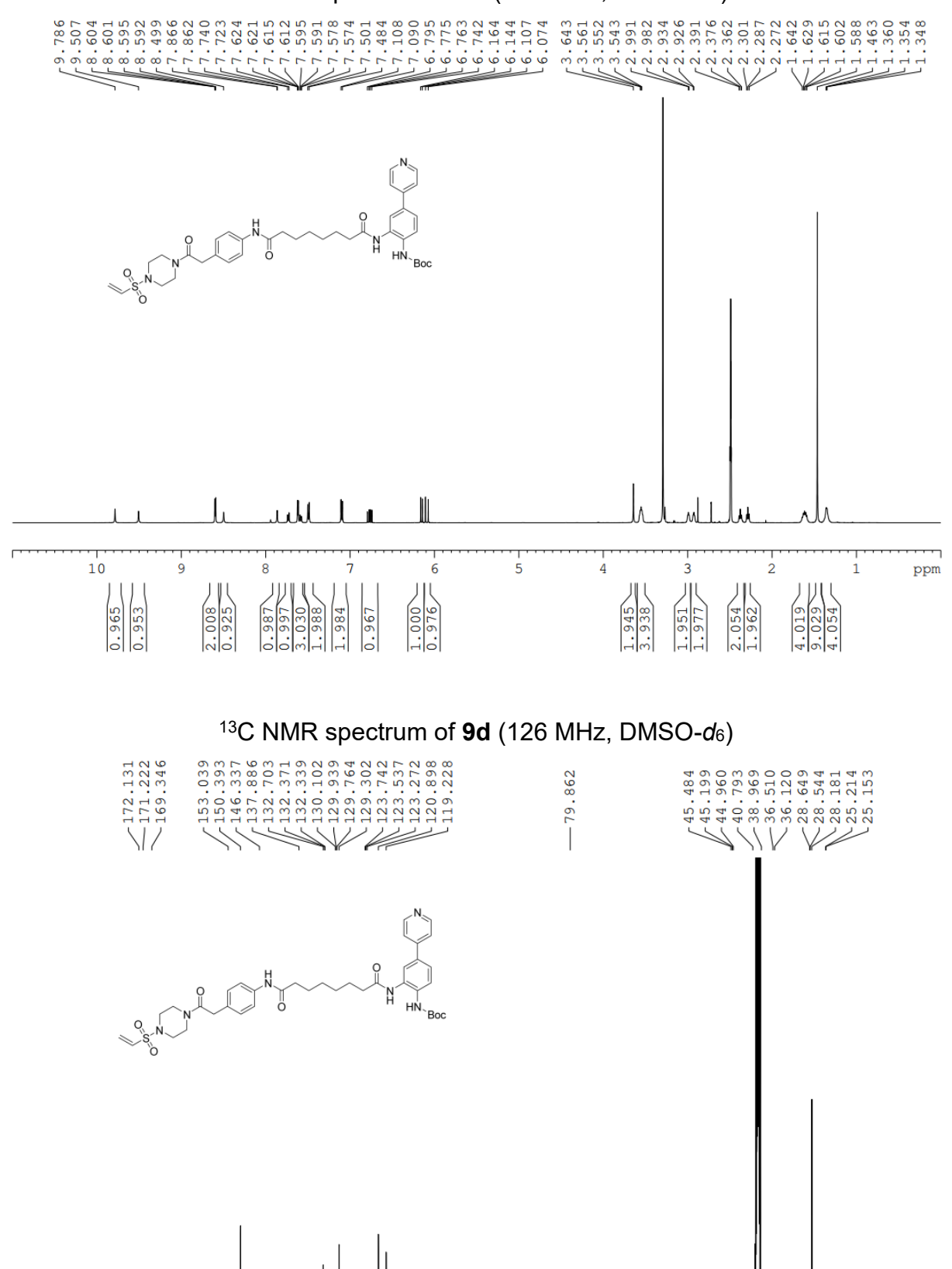
^{1}H NMR spectrum of **9c** (600 MHz, DMSO- d_{6})



^{13}C NMR spectrum of **9c** (151 MHz, DMSO- d_6)



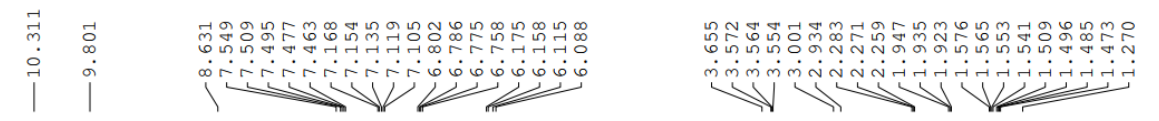
¹H NMR spectrum of **9d** (500 MHz, DMSO-*d*₆)

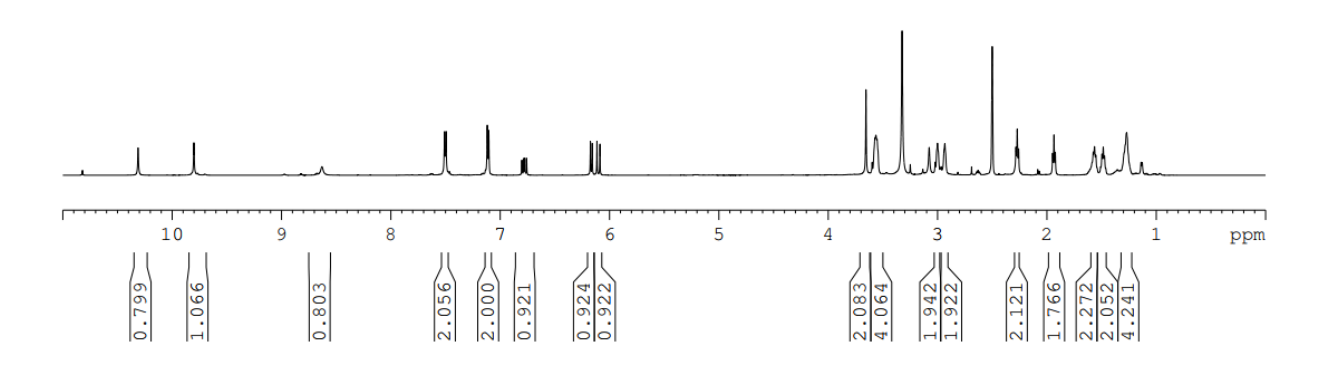


190 180 170 160 150 140 130 120 110

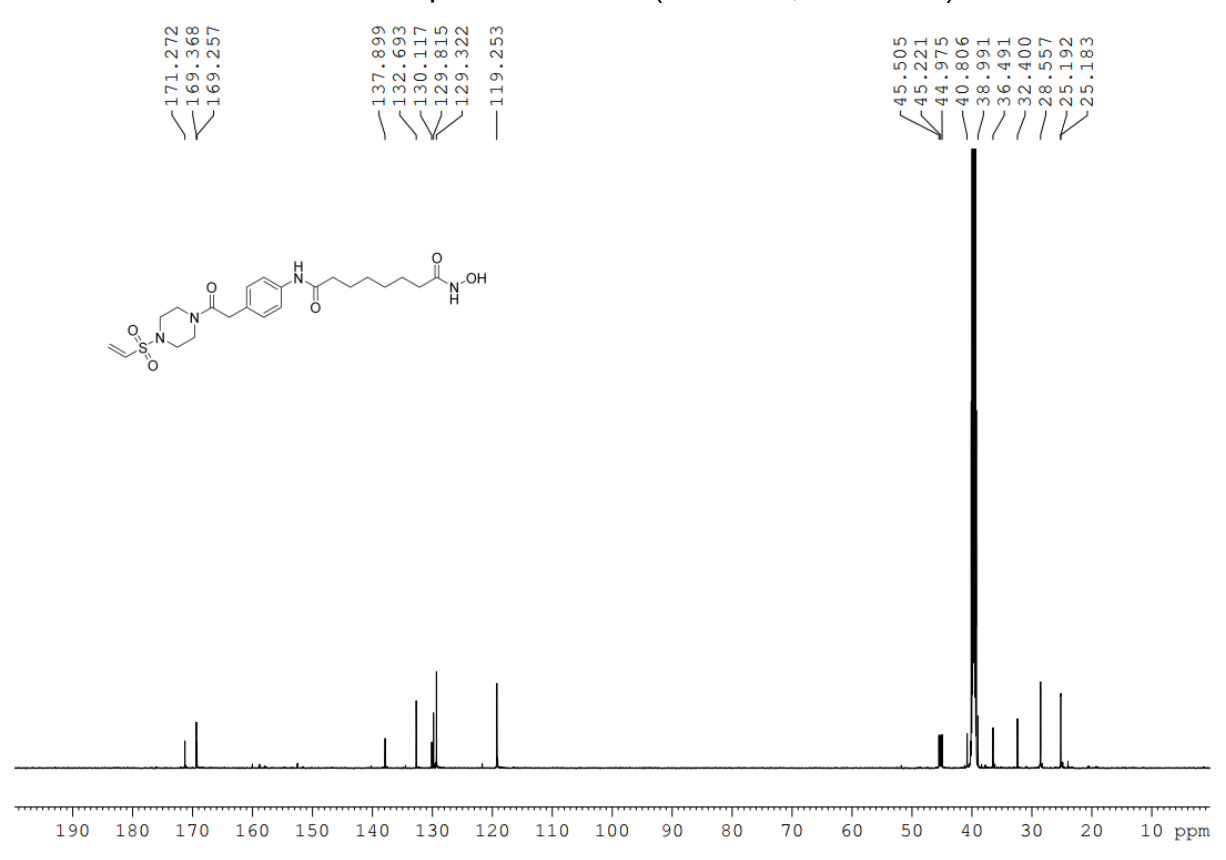
10 ppm

¹H NMR spectrum of **10a** (600 MHz, DMSO-*d*₆)

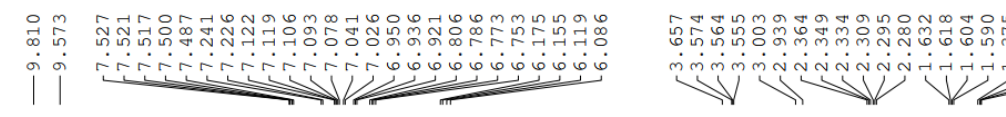


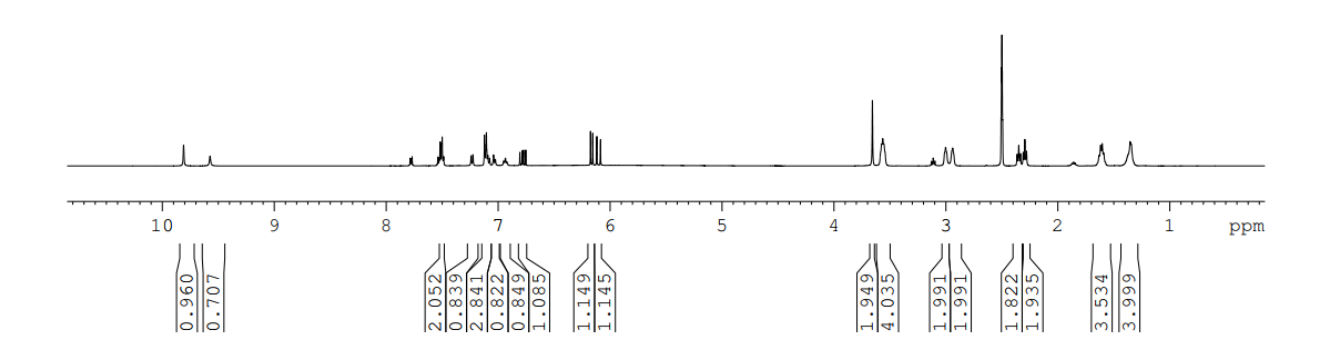


¹³C NMR spectrum of **10a** (151 MHz, DMSO-*d*₆)

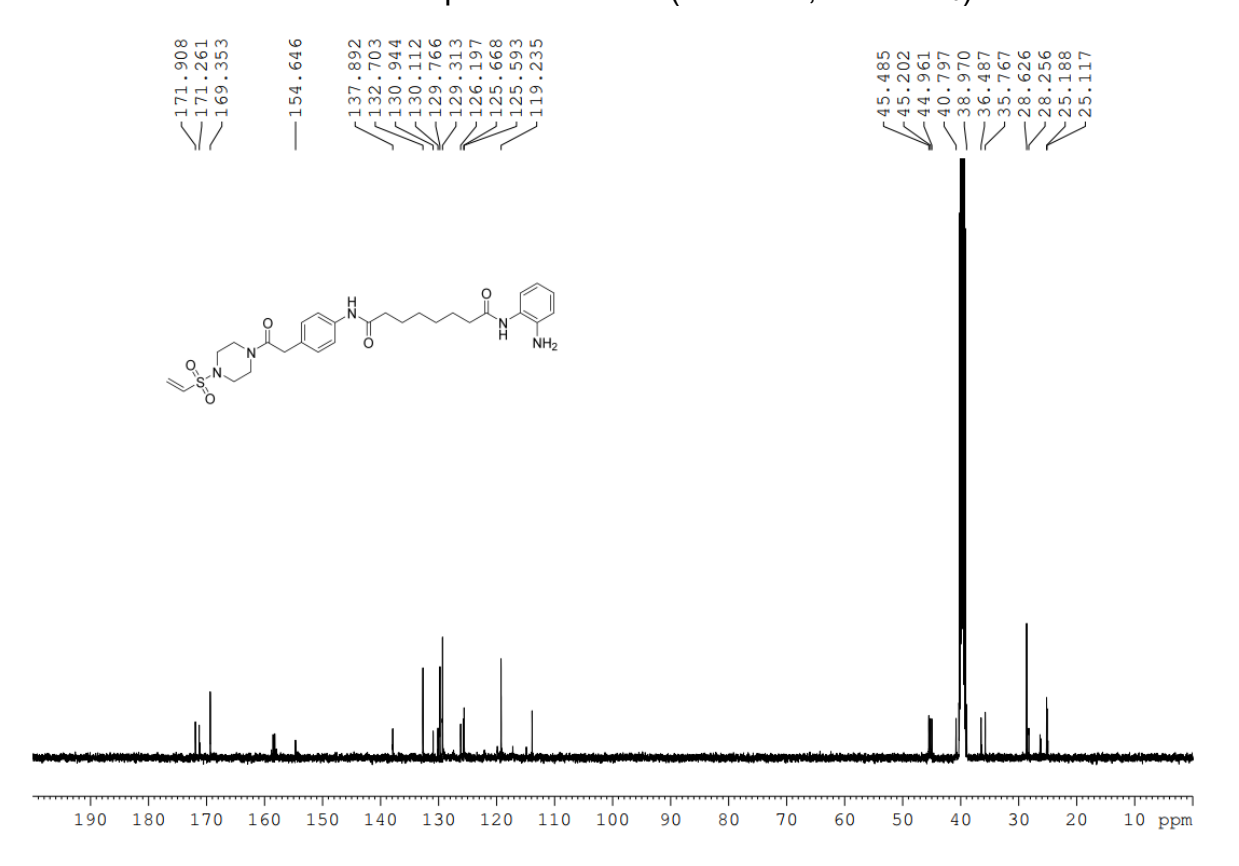


¹H NMR spectrum of **10b** (500 MHz, DMSO-*d*₆)



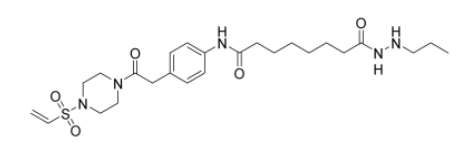


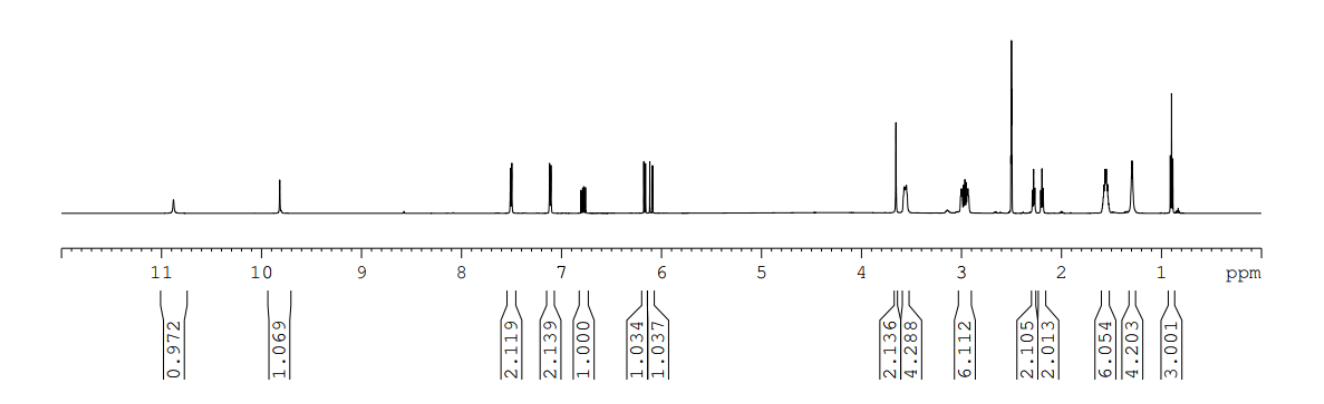
¹³C NMR spectrum of **10b** (126 MHz, DMSO-*d*₆)



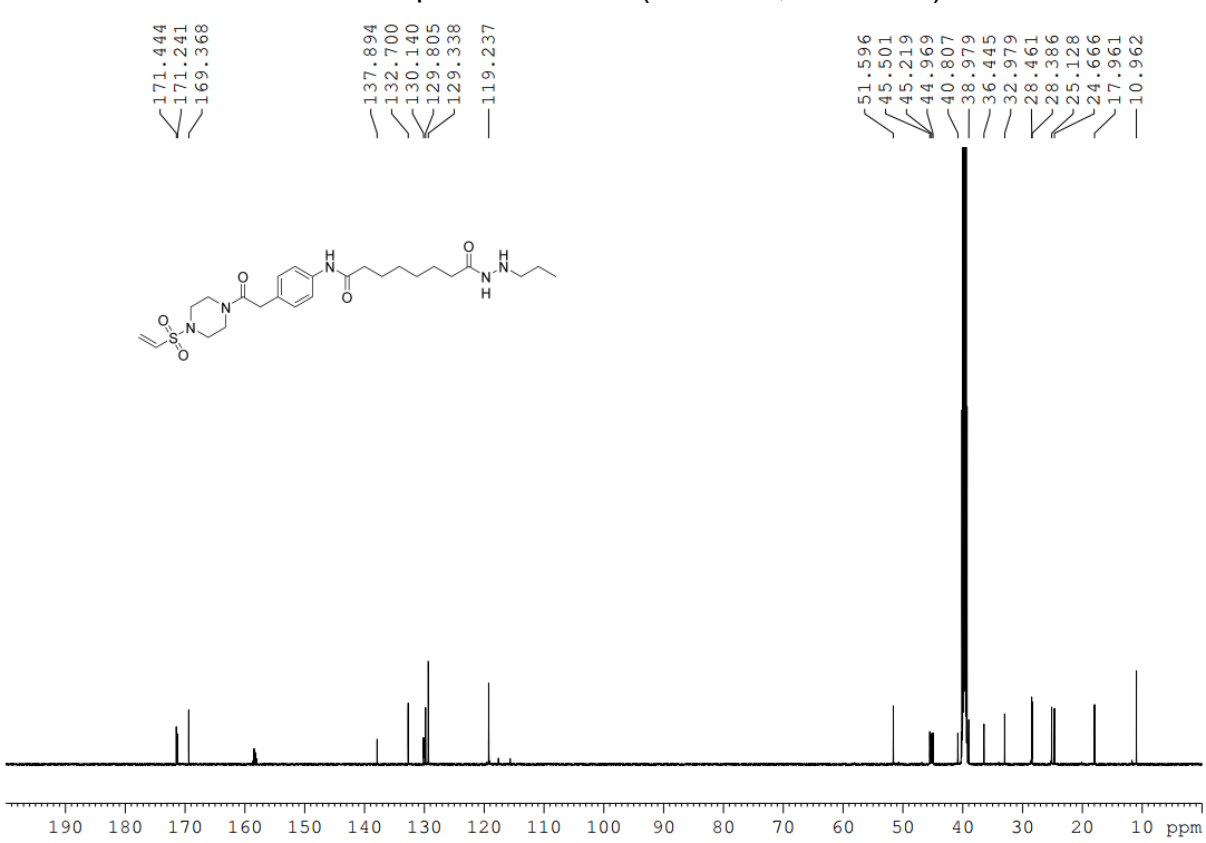




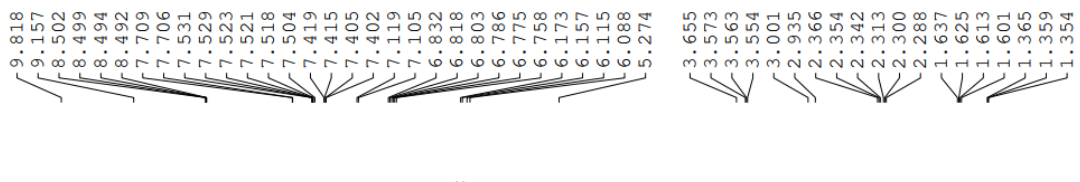


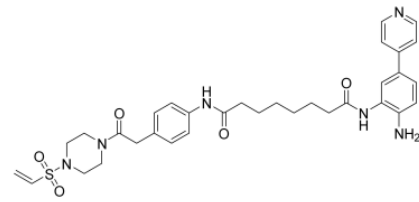


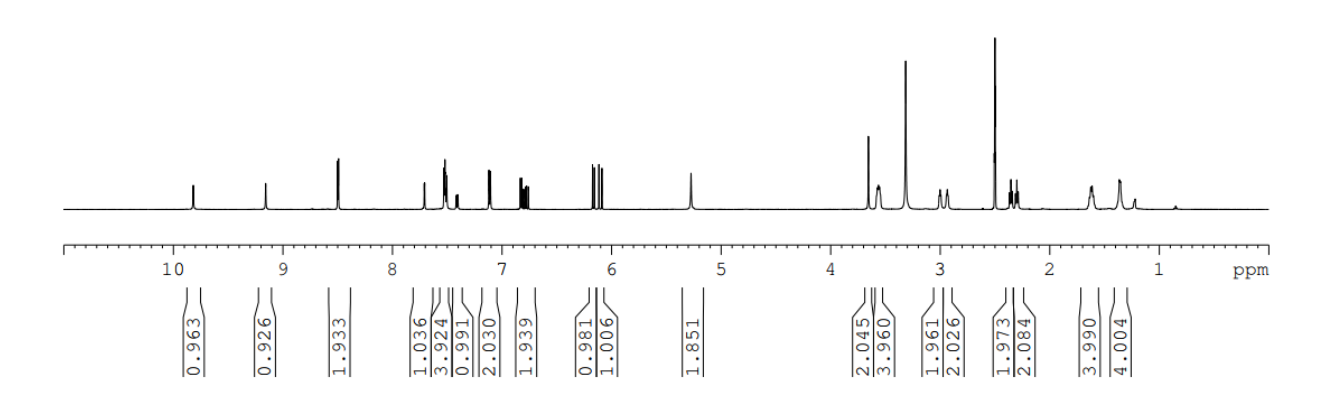
¹³C NMR spectrum of **10c** (151 MHz, DMSO-*d*₆)



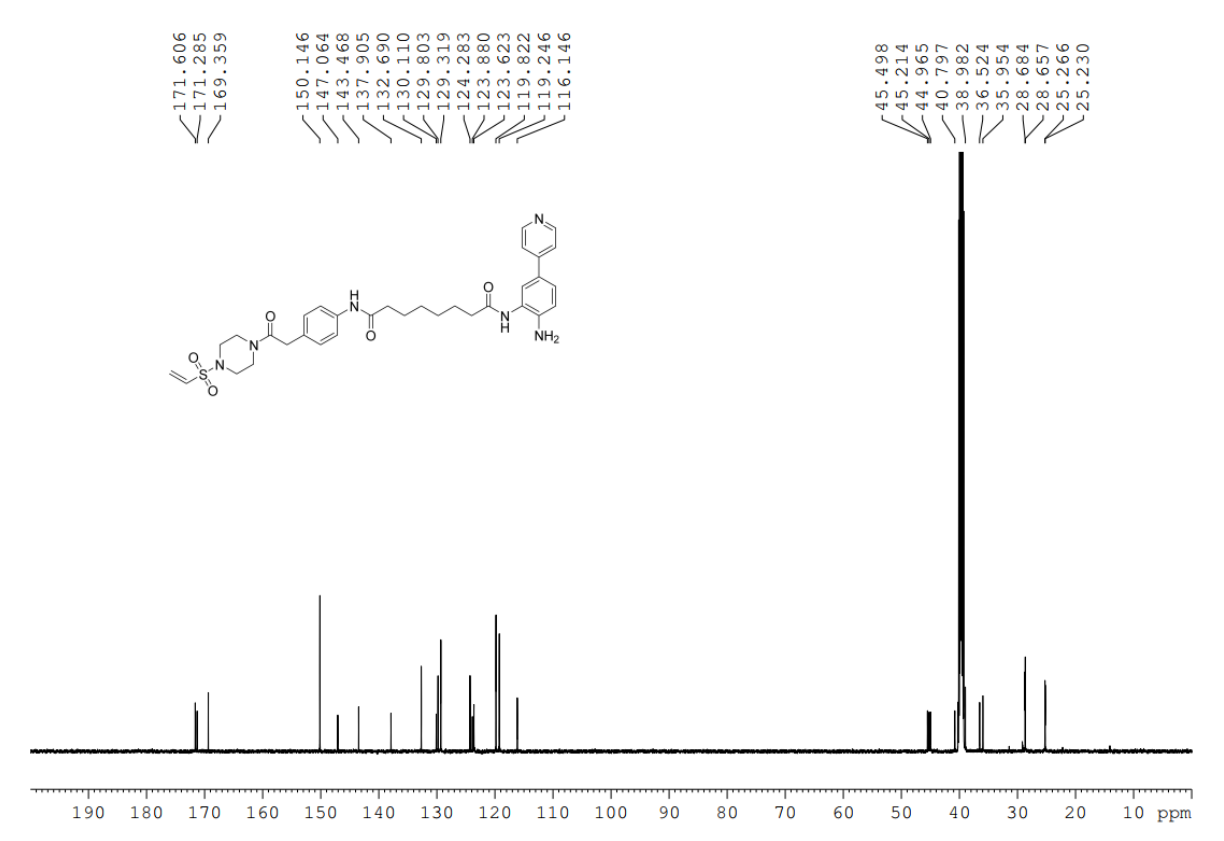
¹H NMR spectrum of **10d** (600 MHz, DMSO-*d*₆)





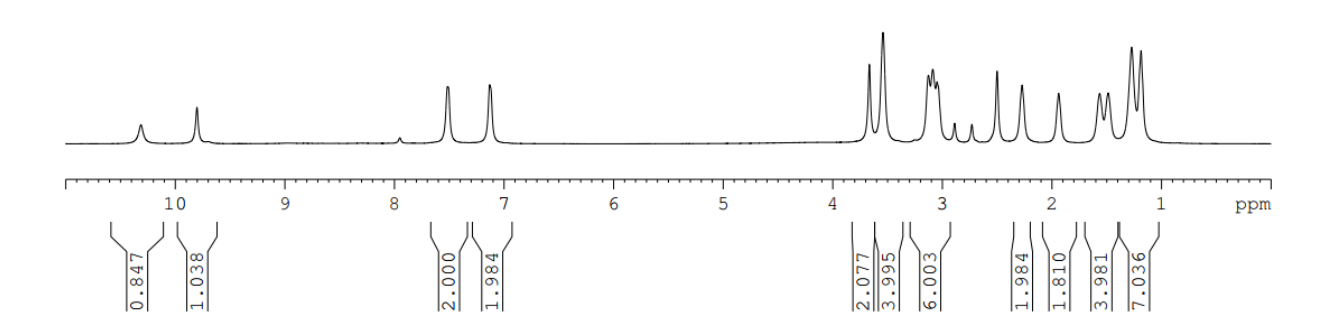


13 C NMR spectrum of **10d** (151 MHz, DMSO- d_6)

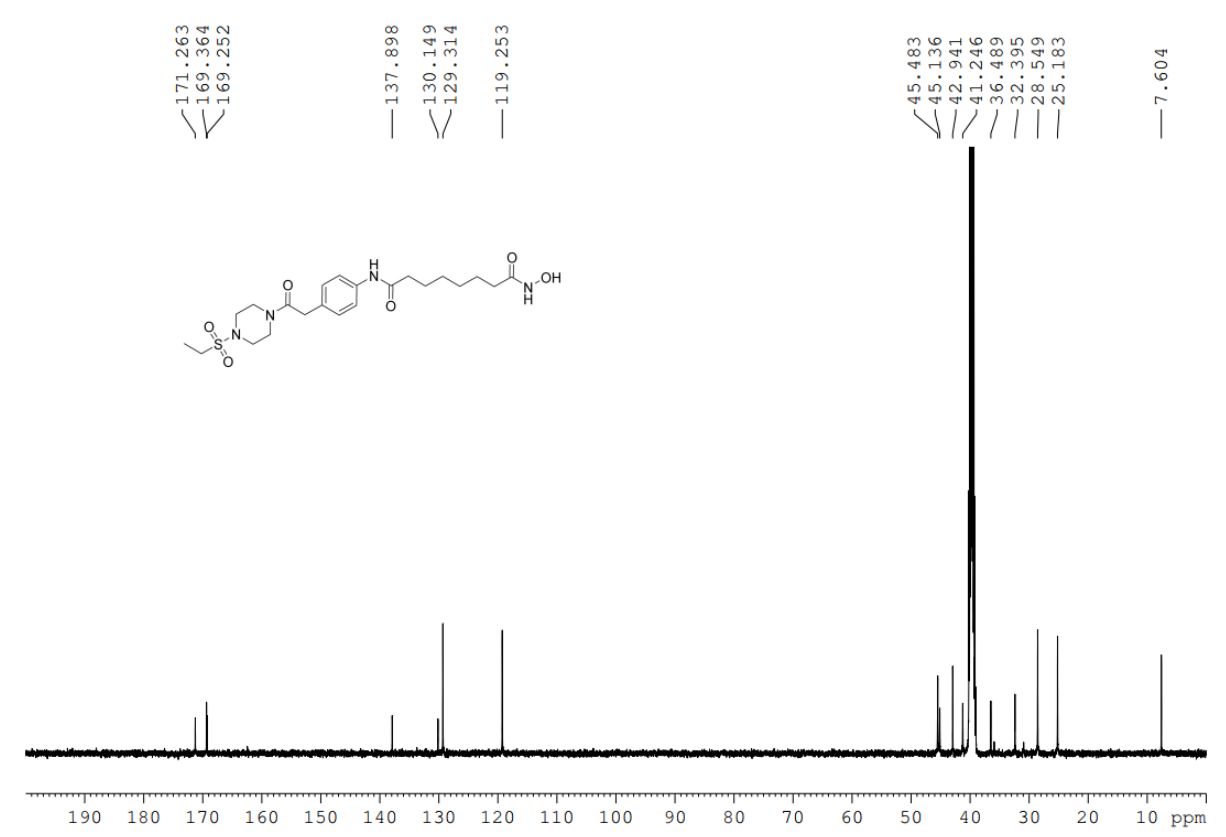


¹H NMR spectrum of **10a-nc** (500 MHz, DMSO-*d*₆)



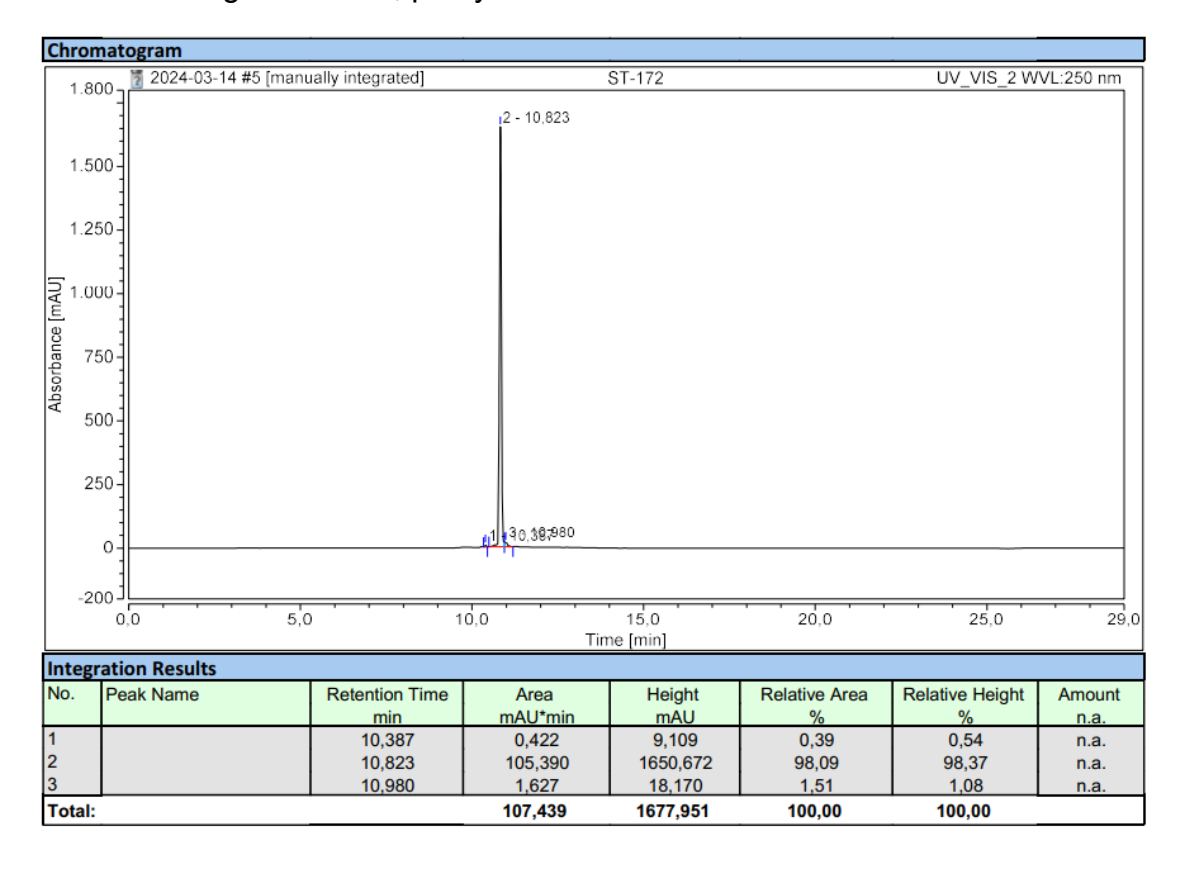


^{13}C NMR spectrum of **10a-nc** (126 MHz, DMSO- d_6)

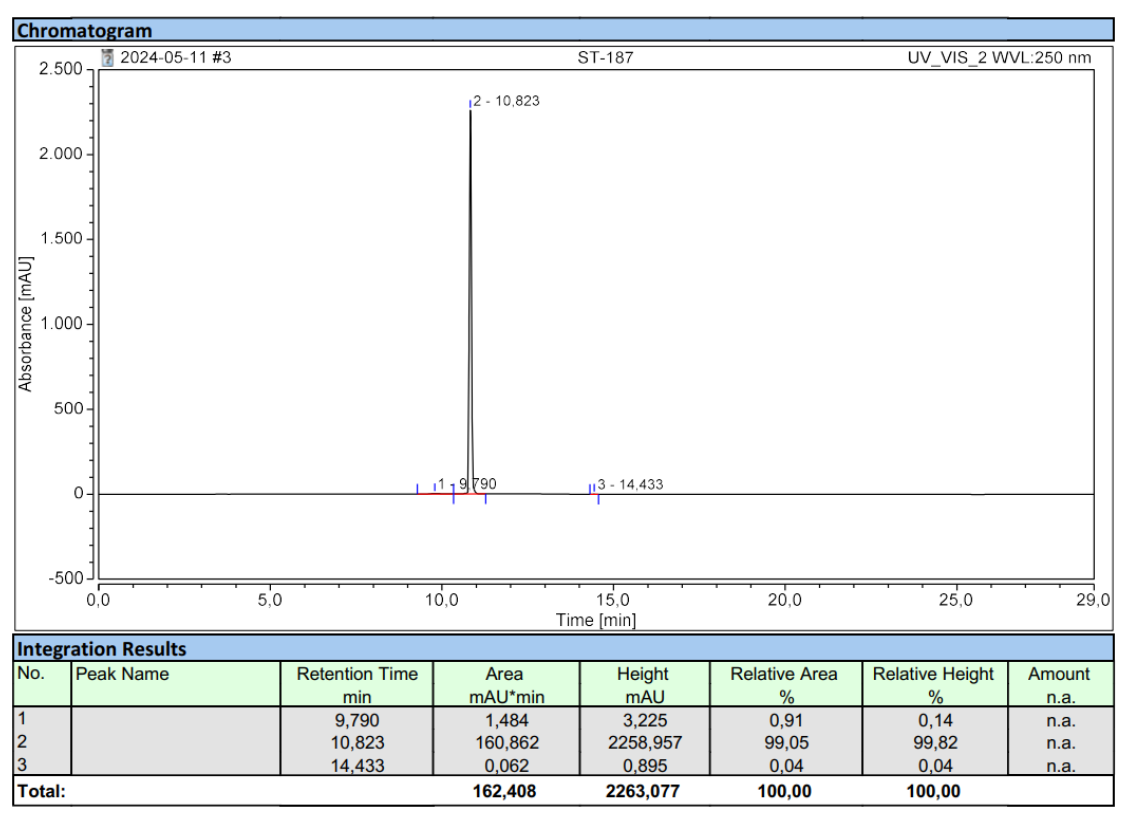


3. HPLC chromatograms

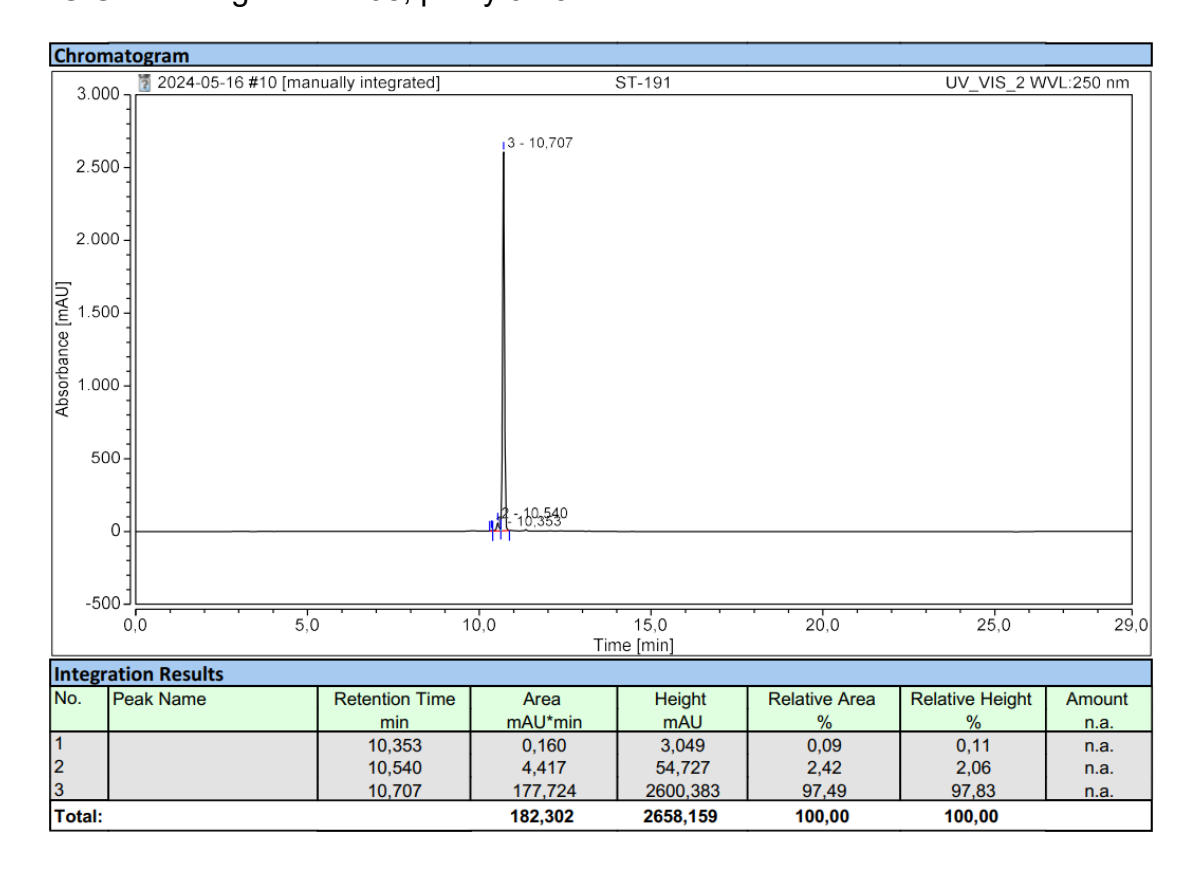
HPLC Chromatogram of 10a, purity 98.1%.



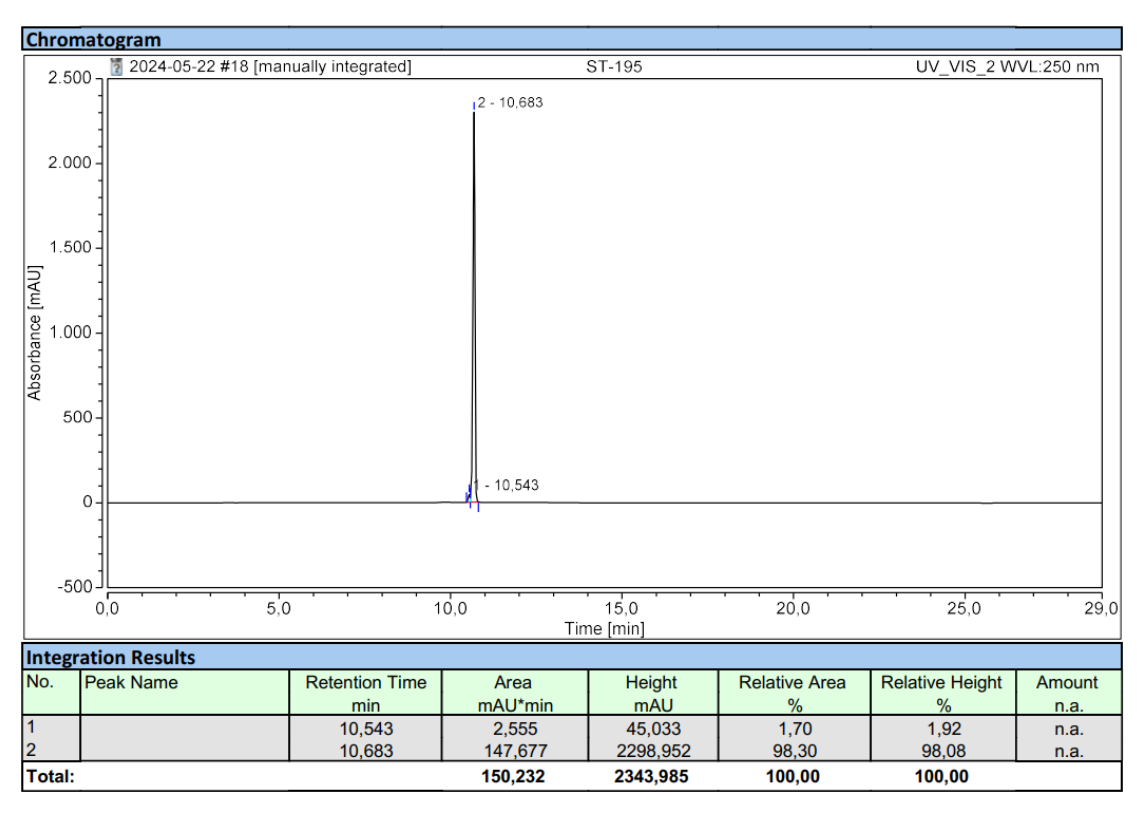
HPLC Chromatogram of **10b**, purity 99.1%.



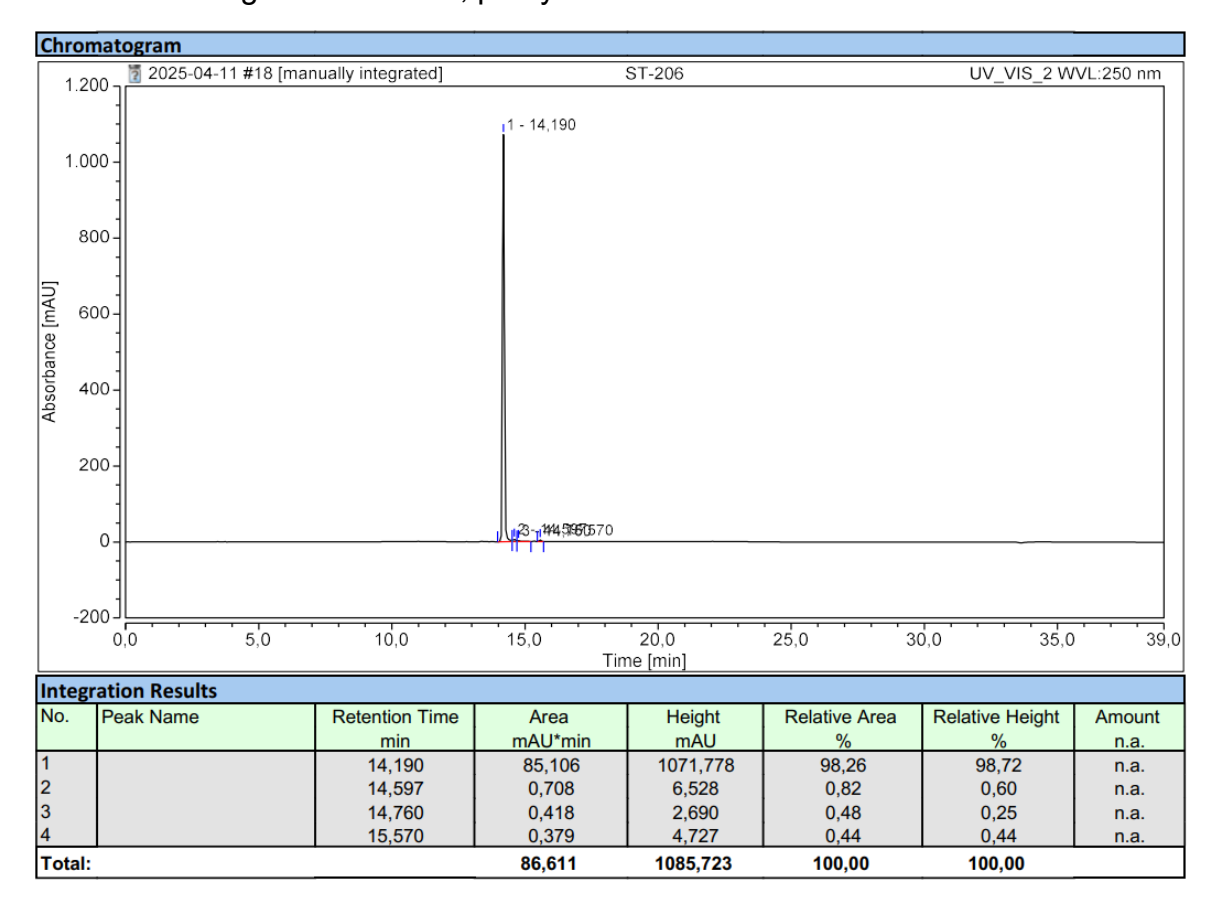
HPLC Chromatogram of 10c, purity 97.5%.



HPLC Chromatogram of 10d, purity 98.3%.



HPLC Chromatogram of 10a-nc, purity 98.3%.



6.2 Appendix II. Publication II: Targeted Degradation of Histone Deacetylases *via* Bypassing E3 Ligase Targeting Chimeras (BYETACs)

The following part contains the research article "Targeted Degradation of Histone Deacetylases *via* Bypassing E3 Ligase Targeting Chimeras (BYETACs)", including the supporting information, as it was published in *ACS Medicinal Chemistry Letters* by American Chemical Society.

The article is reprinted with permission from:

Sun T, Zhai S, König B, Honin I, Kponomaizoun CE, Hansen FK. Targeted Degradation of Histone Deacetylases *via* Bypassing E3 Ligase Targeting Chimeras (BYETACs). *ACS Med. Chem. Lett.* **2025**, *16*(6), 1155–1162. DOI: 10.1021/acsmedchemlett.5c00193

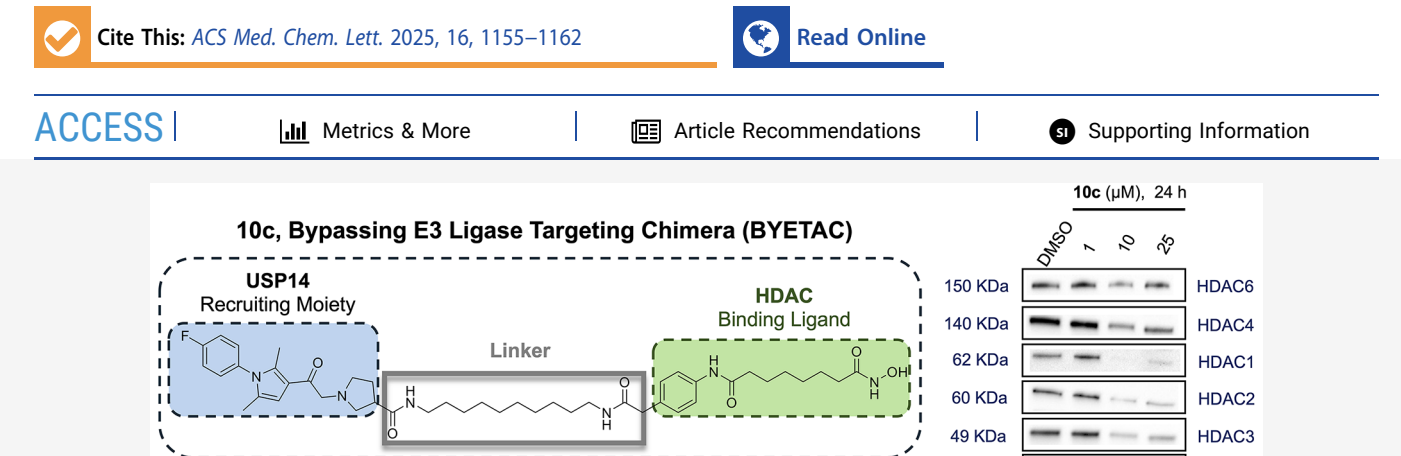
Copyright 2025. American Chemical Society.



pubs.acs.org/acsmedchemlett Letter

Targeted Degradation of Histone Deacetylases via Bypassing E3 Ligase Targeting Chimeras (BYETACs)

Tao Sun, Shiyang Zhai, Beate König, Irina Honin, Cindy-Esther Kponomaizoun, and Finn K. Hansen*



ABSTRACT: Targeted protein degradation (TPD) through heterobifunctional molecules to initiate ubiquitination and facilitate subsequent degradation has emerged as a powerful therapeutic strategy. Most heterobifunctional molecules designed for TPD function primarily through a limited set of E3 ligases, which restricts this therapeutic approach to specific tissues that express the necessary ligases. Herein, we have developed a novel series of heterobifunctional bypassing E3 targeting chimeras (BYETACs) for the targeted degradation of histone deacetylases (HDACs). To this end, a ubiquitin-specific protease 14 (USP14) inhibitor is utilized for the first time as a novel ligand that can directly bind to the 26S proteasome subunit RPN1. Subsequent conjugation of the USP14 ligand with the HDAC inhibitor vorinostat yielded HDAC BYETACs that effectively and preferentially reduced HDAC1 protein levels in multiple myeloma MM.1S cells.

KEYWORDS: Bypassing E3 targeting chimeras (BYETACs), cancer, histone deacetylases (HDACs), targeted protein degradation (TPD), ubiquitin-specific protease 14 (USP14)

ells rely primarily on the ubiquitin-proteasome system (UPS) to remove senescent or damaged proteins, thereby maintaining protein homeostasis. The proteasome, as the key component of the UPS, consists of two major regions: the 19S regulatory particle (19S RP) and the 20S core particle (20S CP). 2,3 Ubiquitinated proteins are recognized by the 19S RP via the three subunits RPN-1, RPN-10, and RPN-13, and are then transferred to the 20S CP for further degradation.4 Inspired by this well-understood mechanism, UPS-dependent degraders such as proteolysis-targeting chimeras (PROTACs) and molecular glues (MGs) have been developed for targeted protein degradation (TPD). 5,6 Compared to conventional small molecule inhibitors, UPSdependent degraders offer several advantages, including the ability to target undruggable proteins, act via a catalytic mode of action, and overcome drug resistance. Due to their robust and promising therapeutic potential, significant progress has been made in recent years, resulting in more than 25 UPSdependent degraders currently in clinical trials.^{7,8}

However, the identification of E3 ligases that can be leveraged for TPD has been largely limited to the cullin ligase family members Von Hippel-Lindau (VHL) and cereblon (CRBN). 9-13 Furthermore, the degradation efficacy depends

on the expression and subcellular localization of the E3 ligase in the relevant tissue. These limitations constrain the range of proteins that can be ubiquitinated and degraded by the UPS. Consequently, there is considerable interest in developing alternative degradation mechanisms that can be broadly applied to a wider array of target proteins.

37 KDa

To circumvent the need for interaction with E3 ligases, a viable approach is to bind directly to a subunit of the 26S proteasome to induce TPD. This novel strategy could provide a more universal degradation method for proteins that either lack ubiquitination sites or fail to interact with E3 ligases. Recent research first demonstrated the viability of this approach by establishing a binding interaction with the 26S proteasome subunit RPN1, thereby promoting the degradation of BRD4. Subsequently, another series of noncovalent

Received: April 4, 2025 Revised: May 8, 2025 Accepted: May 12, 2025 Published: May 20, 2025





GAPDH

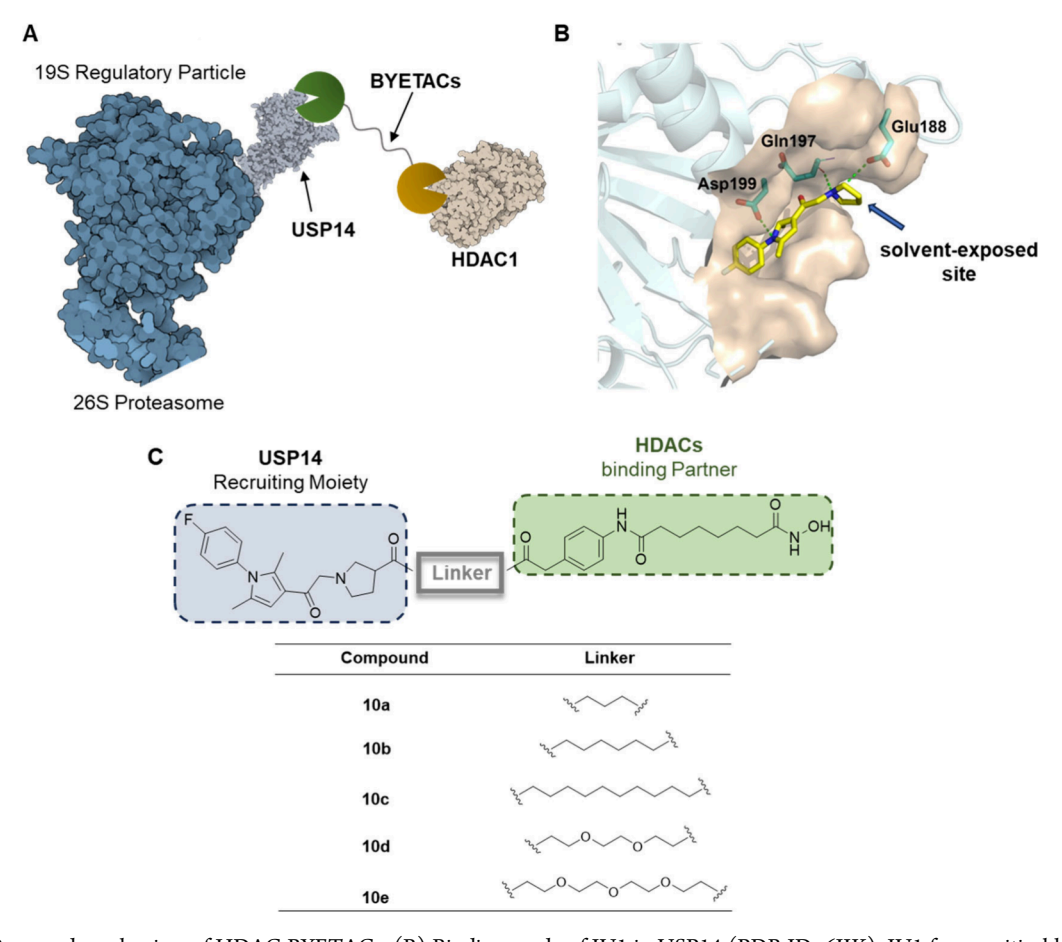


Figure 1. (A) Proposed mechanism of HDAC BYETACs. (B) Binding mode of IU1 in USP14 (PDB ID: 6IIK). IU1 forms critical hydrogen bonds with residues Gln197, Asp199 in the USP14 pocket, whereas the pyrrolidine group of IU1 is positioned in a solvent-exposed site. (C) General structure of the designed HDAC BYETACs with the USP14 recruiting moiety attached to the HDAC binding ligand via different linkers.

heterobifunctional molecules, termed bypassing E3 targeting chimeras (BYETACs), were proposed that led to the degradation of BRD4 through direct engagement of RPN13.¹⁵ These examples (see **Scheme S1**, Supporting Information for selected structures of BYETACs) validate the feasibility of directly binding to a 26S proteasome subunit for TPD.

To further expand the application of direct proteasome recruitment, we aimed to identify novel ligands to enrich the toolbox for TPD via the BYETAC approach. Initially, we found several proteasome activators in the literature that directly interact with the proteasome for degradation. Unfortunately, no cocrystal structures of these small molecules in complex with the respective proteasome subunit were reported, which hindered the design of functionalized compounds for protein degradation. Interestingly, we noticed that certain proteasome-associated enzymes can modulate proteasome activity and enhance protein degradation. Therefore, we hypothesized that ligands of these proteasome-associated enzymes could facilitate the direct recruitment of proteins to the proteasome for subsequent degradation. 22–24

A primary regulatory checkpoint involves the removal of ubiquitin chains from substrates by the ubiquitin-specific protease 14 (USP14), which reversibly binds the proteasome and confers the ability to edit and reject substrates. Furthermore, based on structures of human USP14 in complex with the 26S proteasome, USP14 interacts with RPN1 to form a complex that facilitates its localization to the regulatory

particle of the 26S proteasome, where it directly participates in the process of trimming polyubiquitin chains from ubiquitinated substrates.²⁵

Meanwhile, the small molecule IU1 was identified as a preferential USP14 inhibitor in a high-throughput screening campaign. The treatment of cells with IU1 resulted in enhanced degradation of several proteasome substrates implicated in neurodegenerative diseases. Moreover, based on the cocrystal structures of USP14 and IU1, the pyrrolidine group of IU1 is positioned in a solvent-exposed site, indicating the potential for chemical modifications in this region.

Histone acetylation is regulated by histone deacetylases (HDACs) and histone acetyltransferases (HATs). Modulation of HDAC activity and protein levels has been shown to affect many cellular processes including cell growth, cell cycle, and chromatin decondensation. The HDAC family encompasses 18 isoforms classified into four groups: class I (HDAC1, 2, 3 and 8), class IIa (HDAC4, 5, 7, and 9), class IIb (HDAC6 and 10), class III (Sirt1–7), and class IV (HDAC11).²⁷ HDACs are intriguing cancer targets due to their overexpression in many tumors. Therefore, targeting HDACs through inhibition or degradation holds great potential for advancing cancer treatment.

Building on the aforementioned research, we used the USP14 inhibitor IU1 as a direct proteasome recruiter. The conjugation of IU1 with an HDAC ligand generated HDAC BYETACs that effectively and preferentially degraded HDAC1

Scheme 1. Synthesis of the Trityl-Protected HDAC Ligand 5^a

^aReagents and conditions: i) SOCl₂, MeOH, 80 °C, 16 h, 97% yield. ii) Suberic anhydride, NaHCO₃, THF, rt, 16 h, 63% yield. iii) O-Tritylhydroxylamine, HATU, DIPEA, DMF, rt, 16 h, 28% yield. iv) LiOH·H₂O, THF/H₂O (v/v = 1:1), rt, 2 h, 71% yield.

Scheme 2. Synthesis of the IU1-Linker Conjugates 8a-e^a

^aReagents and conditions: v) Pyrrolidine-3-carboxylic acid, Et₃N, DMF, 85 °C, 2 h, 30% yield. vi) NH₂-R-NH-Boc, HATU, DIPEA, DMF, rt, 16 h, 58-90% yield.

Scheme 3. Synthesis of HDAC BYETAC 10a-ea

in multiple myeloma MM.1S cells. Thus, we present a proof of concept for the novel strategy of bypassing an E3 ligase, which may broaden the range of proteins suitable for TPD.

On the basis of a cocrystal structure of USP14 and IU1,²⁵ we rationally designed a novel class of BYETACs aimed at targeted degradation of HDACs through direct recruitment to

the proteasome (Figure 1A and 1B). The BYETACs incorporate a USP14 recruiter (IU1) and an HDAC ligand (vorinostat) connected by various linkers to induce HDAC degradation (Figure 1C).

The synthetic routes for the target compounds 10a-e are outlined in Schemes 1, 2, and 3. Briefly, 4-aminophenylacetic

[&]quot;Reagents and conditions: vii) TFA, DCM, rt, 1 h. viii) 5, HATU, DIPEA, DMF, rt, 16 h. ix) Triisopropylsilane, TFA, DCM, rt, 2 h, 4-12% yield (over three steps).

Table 1. HDAC1 and HDAC6 Enzyme Inhibition of 10a-e

Compound	IC ₅₀ (µM) HDAC1 ^a	$IC_{50} (\mu M) HDAC6^a$
10a	0.166 ± 0.020	0.034 ± 0.020
10b	0.208 ± 0.034	0.044 ± 0.028
10c	0.539 ± 0.086	0.100 ± 0.041
10d	0.133 ± 0.019	0.040 ± 0.004
10e	0.119 ± 0.010	0.040 ± 0.005
Vorinostat	0.064 ± 0.012	0.030 ± 0.017

 $^an=2$ biologically independent replicates. In all cases, mean \pm standard deviation is shown.

acid (1) was first activated with thionyl chloride and esterified with methanol to yield intermediate 2, which was further treated with suberic anhydride to afford 3. Subsequently, compound 3 was subjected to an amide coupling reaction with *O*-tritylhydroxylamine to produce the trityl-protected hydroxamic acid 4. The protected HDAC ligand 5 containing a free phenylacetic acid moiety was prepared by hydrolyzing 4 under basic conditions (Scheme 1).²⁸

The synthesis of the IU1-linker conjugates 8a-e is presented in Scheme 2. First, the commercially available chloroacetyl building block 6 was reacted with pyrrolidine-3-carboxylic acid in the presence of triethylamine (TEA) in dry DMF to give the key intermediate 7, which was then directly treated with various mono-Boc-protected diamine linkers to generate precursors 8a-e.

Next, the deprotection of 8a-e with trifluoroacetic acid (TFA) yielded the free amines 9a-e. Finally, 9a-e were conjugated with the trityl-protected HDAC ligand 5 using HATU and DIPEA as the amide coupling system, followed by acidolytic deprotection to afford the target compounds 10a-e (Scheme 3).

In addition, 6 was conjugated with pyrrolidine in the presence of TEA to afford the USP14 inhibitor IU1 (11) as a control (Scheme S2, Supporting Information).²⁵

As a first step in the biological evaluation of 10a-e, we evaluated their half-maximal inhibitory concentration (IC₅₀) values against HDAC1 and HDAC6 in biochemical HDAC inhibition assays using vorinostat as positive control. HDAC1 and HDAC6 were selected as representative isoforms due to their critical roles in several diseases including cancer.²⁹ As

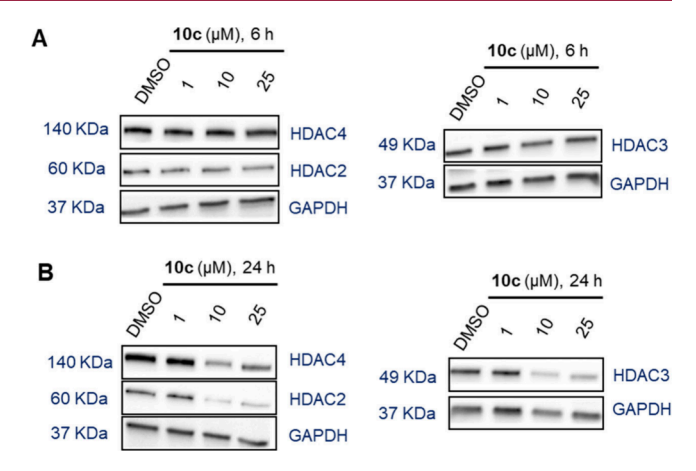


Figure 3. Degradation selectivity of **10c**. MM.1S cells were treated with compounds **10c** at concentrations of 1, 10, and 25 μ M for 6 h (A) or for 24 h (B). DMSO was used as vehicle control. HDAC2, HDAC3, and HDAC4 levels were detected by immunoblot analysis. GAPDH was used as loading control. Representative images from a total of n=2 replicates.

Table 2. HDAC2-4 Enzyme Inhibition of 10c

Compound	IC ₅₀ (µM) HDAC2 ^a	IC ₅₀ (µM) HDAC3 ^a	IC ₅₀ (µM) HDAC4 ^a
10c	0.703 ± 0.199	0.293 ± 0.065	n.i.
Vorinostat	0.203 ± 0.055	0.129 ± 0.002	n.d.
TMP269	n.d.	n.d.	0.458 ± 0.104

 an = 2 biologically independent replicates, mean \pm standard deviation is shown. n.i. = no inhibition (<30% inhibition up to 10 μ M). n.d. = not determined.

shown in Table 1, 10a–e exhibited substantial inhibitory activities against HDAC1 with IC $_{50}$ values ranging from 0.119 to 0.539 μ M. Additionally, HDAC6 inhibition by 10a–e was observed with IC $_{50}$ values ranging from 0.034 to 0.100 μ M. Consequently, our results confirm that all synthesized BYETACs are capable of binding to both HDAC1 and HDAC6.

To evaluate the ability of BYETACs 10a-e to degrade HDACs, the multiple myeloma cell line MM.1S was treated

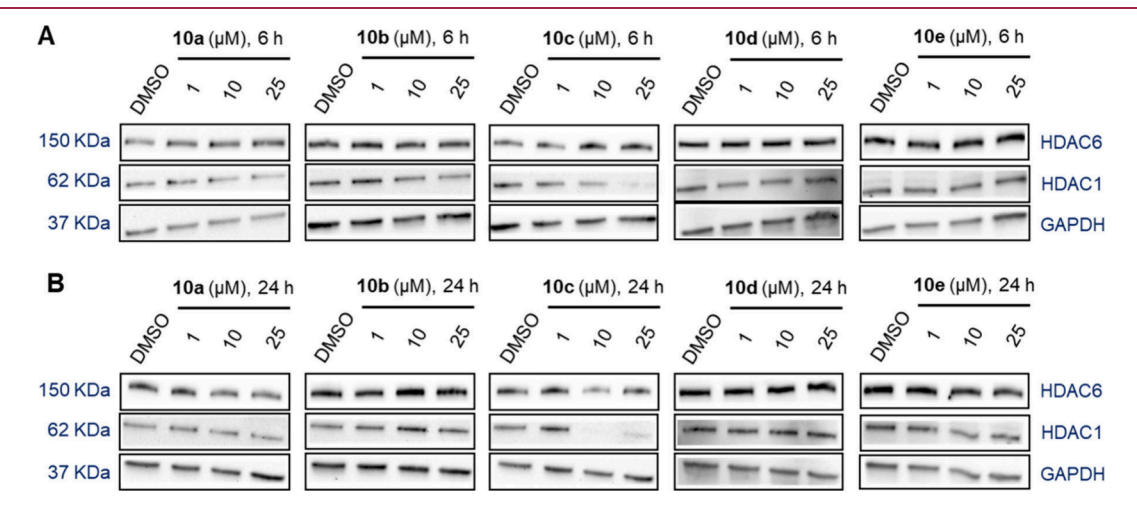


Figure 2. Degradation of HDAC1 and HDAC6 mediated by 10a-e. MM.1S cells were treated with compounds 10a-e at concentrations of 1, 10, and 25 μ M for 6 h (A) or for 24 h (B), with DMSO as vehicle control. HDAC1 and HDAC6 levels were detected by immunoblot analysis. GAPDH was used as the loading control. Representative images from a total of n=2 replicates.

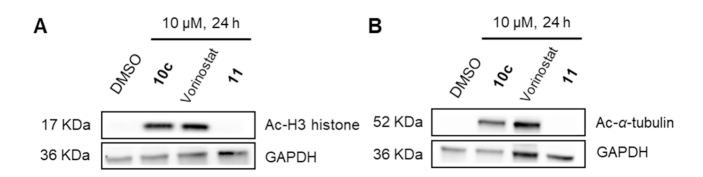


Figure 4. Cellular HDAC target engagement by **10c**, vorinostat, and **11**. Immunoblot analysis of acetylated histone H3 (A) and α -tubulin (B) in MM.1S cell lysates after treatment with the indicated compounds (10 μ M) or vehicle (DMSO) for 24 h. Representative images from a total of n=2 replicates.

with different concentrations (1, 10, and 25 μ M) of 10a-e for 6 and 24 h. In the next step, HDAC1 and HDAC6 protein levels were evaluated using immunoblot analysis. As summarized in Figure 2A and Figure S1 (Supporting Information), among all the BYETACs, only 10c achieved substantial degradation of HDAC1 with a maximal degradation (D_{max}) value of 81% at 25 μ M after a treatment time of 6 h. Meanwhile, all compounds exhibited weak degradation efficacy for HDAC6 at different concentrations after 6 h.

Next, the incubation time was extended to 24 h to investigate whether 10a-e displayed enhanced degradation of HDAC1 and HDAC6 after longer incubation times (Figure 2B and Figure S2, Supporting Information). None of the compounds showed significant degradation of HDAC6 at different concentrations after 24 h of treatment. Similarly, only degrader 10c still achieved significant and enhanced degradation of HDAC1 with a D_{max} value of 88% at $10~\mu{\rm M}$ compared to 6 h of treatment. Additionally, a hook effect was observed when MM.1S cells were treated with 10c at $25~\mu{\rm M}$ for 24 h, which is a typical phenomenon in TPD with heterobifunctional degraders. Based on these initial screening results, BYETAC 10c was selected for further biological evaluations.

Subsequently, degrader 10c was investigated at concentrations of 1, 10, and 25 μ M for its ability to degrade selected

other HDAC isoforms, namely, HDAC2, HDAC3, and HDAC4. As shown in Figure 3A and Figure S3A (Supporting Information), none of the used concentrations resulted in the degradation of HDAC2, HDAC3, or HDAC4 when MM.1S cells were treated with 10c for 6 h. However, treatment with 10c for 24 h had a significant effect on HDAC3 levels and a minimal impact on HDAC4 levels, HDAC2 levels were also noticeably affected (Figure 3B and Figure S3B, Supporting Information). In detail, 10c induced substantial degradation of HDAC2 ($D_{max} = 64\%$ at $10~\mu$ M), which may be a consequence of the high structural similarity between HDAC1 and HDAC2, especially within the catalytic domains.

The low degradation of HDAC4 and the significant degradation of HDAC2 and 3 are consistent with the extended HDAC isoform inhibition profile of **10c** (Table 2). While the compound showed submicromolar inhibition of HDAC2 and 3, it was inactive at HDAC4. In summary, our results indicate that **10c** exhibits potent degradation activity and a preference for HDAC1 among the HDAC isoforms tested.

After confirming that **10c** preferentially and effectively degrades HDAC1 in MM.1S cells, we determined its half-maximal degradation concentration (DC₅₀) value for HDAC1 (**Figure S4**, Supporting Information). A 24-h treatment with an increasing concentration of **10c** resulted in a dose-dependent reduction of HDAC1 levels (DC₅₀ = 4.0 \pm 1.0 μ M).

To investigate the cellular HDAC target engagement of degrader 10c in MM.1S cells, we performed immunoblot experiments to characterize the levels of acetylated histone H3 (an HDAC1-3 substrate) and acetylated α -tubulin (an HDAC6 substrate) using vorinostat as control. In good agreement with the results of the HDAC1 and HDAC6 inhibition assays, degrader 10c resulted in a pronounced hyperacetylation of acetylated histone H3 and acetylated α -tubulin after 24 h of treatment, indicating that 10c induced a strong reduction of both HDAC1 and HDAC6 activity in MM.1S cells. As expected, the USP14 inhibitor 11 had no

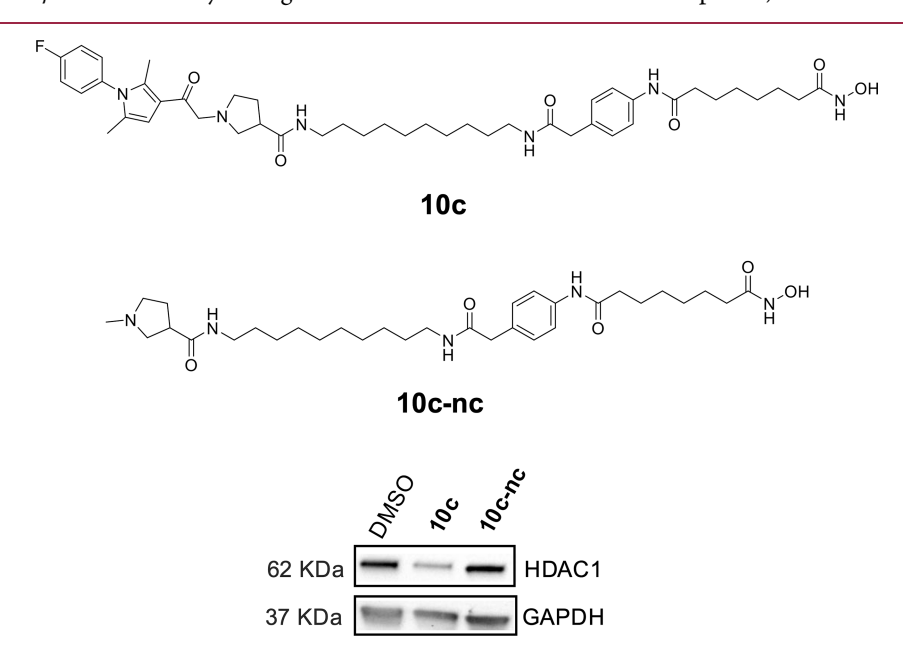


Figure 5. Degradation of HDAC1 mediated by 10c and negative control 10c-nc. MM.1S cells were treated with compounds 10c and 10c-nc at concentrations of 10 μ M for 24 h, with DMSO as vehicle control. HDAC1 levels were detected by immunoblot analysis. GAPDH was used as the loading control. Representative images from a total of n=2 replicates.

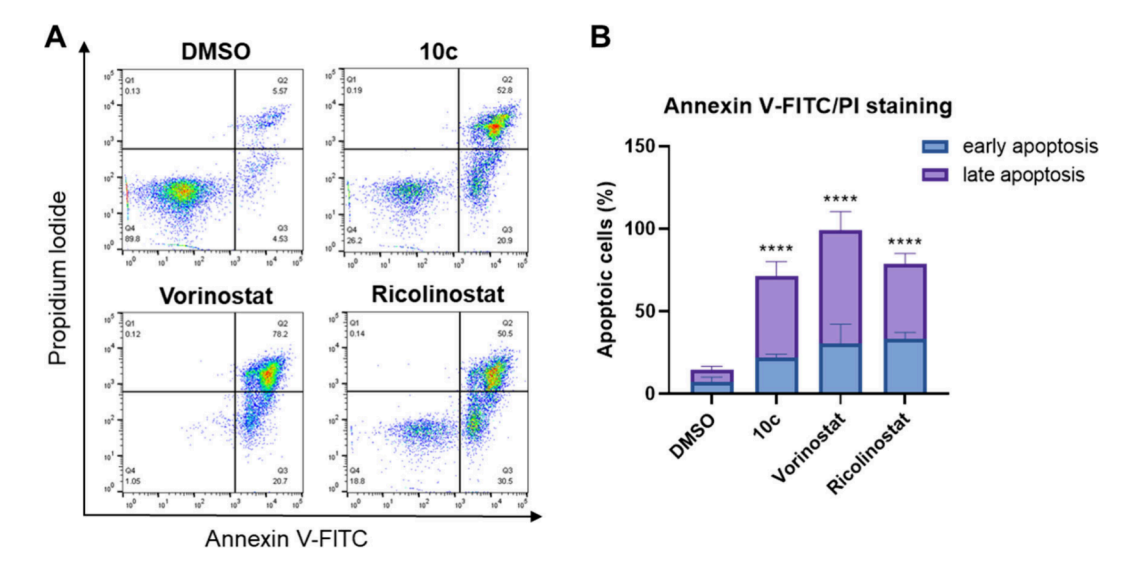


Figure 6. (A) Flow cytometry analysis of MM.1S cells stained with annexin V-FITC/PI after incubation with 5 μ M of the 10c, vorinostat, ricolinostat or vehicle (DMSO) for 48 h. Representative images from biologically independent n=2 replicates, each performed in duplicates. (B) Quantification of early and late apoptotic cells. The percentage of cells that were annexin V-positive but PI-negative was considered as early apoptotic, while the percentage of cells that were both annexin V- and PI-positive was considered as late apoptotic. Data are presented as mean \pm standard deviation (n=2 biological replicates, each performed in duplicates). Statistical analysis was performed by using one-way ANOVA followed by Dunnett's multiple comparisons test in GraphPad Prism 8. Statistical significance was indicated with asterisks (**** = $p \le 0.0001$).

effects on the levels of acetylated histone H3 and acetylated α -tubulin (Figure 4). To assess whether cotreatment with 10c and 11 affects the levels of acetylated histone H3 and acetylated α -tubulin, we conducted additional Western blot experiments. The combination treatment had minimal impact on the acetylation of both substrates compared to 10c alone (see Figure S5, Supporting Information). These results suggest that the effects observed in Figure 4 are not solely due to degradation, but that HDAC inhibition also contributes to the observed hyperacetylation.

To gain additional mechanistic insight, we synthesized a negative control compound, 10c-nc (see Scheme S3, Supporting Information for synthetic details), which lacks the 4-fluorophenyl-pyrrole moiety of 10c, which is critical for the interaction of IU1 (11) with USP14 (see Figure 1B). Immunoblot analysis confirmed that only 10c, and not 10c-nc, reduced HDAC1 levels. These results highlight the importance of an intact IU1 scaffold for the downregulation of HDAC1 protein levels.

Next, after 48 h of incubation of MM.1S cells with 10c, apoptosis induction was assessed by annexin V-FITC/propidium iodide (PI) staining and flow cytometry (Figure 6). Vorinostat and ricolinostat were included as positive controls. In contrast to the cell viability data which indicated weak antiproliferative activity (Figure S6, Supporting Information), 10c markedly increased the proportions of both early and late apoptotic cells, confirming its ability to induce apoptosis.

In summary, inspired by the interaction between USP14 and the 26S proteasome subunit RPN1, we have designed, synthesized, and characterized a new class of BYETACs aimed at the direct recruitment of the proteasome for HDAC degradation. Western blot analysis revealed that 10c effectively reduced HDAC1 levels in MM.1S cells in a potent and preferential manner. Furthermore, subsequent apoptosis induction analysis confirmed its promising anticancer activity. These results demonstrate that bypassing E3 ligases via BYETACs is a viable strategy for HDAC knockdown,

potentially expanding the scope of protein degradation in the future

ASSOCIATED CONTENT

Solution Supporting Information

The Supporting Information is available free of charge at https://pubs.acs.org/doi/10.1021/acsmedchemlett.5c00193.

Experimental procedures, Supplementary Scheme and Figures, ¹H NMR, ¹³C NMR, and ¹⁹F NMR spectra for all synthesized compounds, and HPLC data of test compounds (PDF)

■ AUTHOR INFORMATION

Corresponding Author

Finn K. Hansen — Department of Pharmaceutical and Cell Biological Chemistry, Pharmaceutical Institute, University of Bonn, 53121 Bonn, Germany; orcid.org/0000-0001-9765-5975; Phone: (+49) 228 73 5213; Email: finn.hansen@uni-bonn.de; Fax: (+49) 228 73 7929

Authors

Tao Sun – Department of Pharmaceutical and Cell Biological Chemistry, Pharmaceutical Institute, University of Bonn, 53121 Bonn, Germany

Shiyang Zhai — Department of Pharmaceutical and Cell Biological Chemistry, Pharmaceutical Institute, University of Bonn, 53121 Bonn, Germany; orcid.org/0009-0005-6840-3177

Beate König — Department of Pharmaceutical and Cell Biological Chemistry, Pharmaceutical Institute, University of Bonn, 53121 Bonn, Germany

Irina Honin — Department of Pharmaceutical and Cell Biological Chemistry, Pharmaceutical Institute, University of Bonn, 53121 Bonn, Germany; ⊙ orcid.org/0009-0009-7091-8419

Cindy-Esther Kponomaizoun – Department of Pharmaceutical and Cell Biological Chemistry,

Pharmaceutical Institute, University of Bonn, 53121 Bonn, Germany

Complete contact information is available at: https://pubs.acs.org/10.1021/acsmedchemlett.5c00193

Funding

T.S. (grant no. 202107060004) and S.Z. (grant no. 202106150022) are funded by China Scholarship Council. The new NMR console for the 500 MHz NMR spectrometer used in this research was funded by the Deutsche Forschungsgemeinschaft (DFG, German Research Foundation) under project number 507275896.

Notes

The authors declare no competing financial interest.

ACKNOWLEDGMENTS

Experimental support of Peng Chen and Prof. Dr. Ingo Schmidt-Wolf is gratefully acknowledged. The authors thank Daniel Stopper from our group for manuscript editing.

ABBREVIATIONS

UPS, Ubiquitin-proteasome system

19S RP, 19S regulatory particle

20S CP, 20S core particle

PROTAC(s), Proteolysis-targeting chimera(s)

MG(s), Molecular glue(s)

TPD, Targeted protein degradation

VHL, Von Hippel-Lindau

SD, Standard deviation

CRBN, Cereblon

BYETAC(s), bypassing E3 targeting chimera(s)

USP14, ubiquitin-specific protease 14

HDACs, Histone deacetylases

HATs, Histone acetyltransferases

MeOH, Methanol

THF, Tetrahydrofuran

HATU, 1-[Bis(dimethylamino)methylene]-1*H*-1,2,3-triazolo[4,5-*b*]pyridinium-3-oxide hexafluorophosphate

DIPEA, N,N-Diisopropylethylamine

DMF, *N*,*N*-Dimethylformamide

TEA, Triethylamine

rt, Room temperature

TFA, Trifluoroacetic acid

IC50, Half-maximal inhibitory concentration

 D_{max} , maximal degradation

DC₅₀, Half-maximal degradation concentration

PI, Propidium iodide

TLC, Thin-layer chromatography

NMR, Nuclear magnetic resonance spectroscopy

ppm, Parts per million

CDCl₃, Deuterated chloroform

DMSO- d_6 , Deuterated dimethyl sulfoxide

HPLC, High performance liquid chromatography

DAD, diodearray detector

REFERENCES

- (1) Kwon, Y. T.; Ciechanover, A. The Ubiquitin Code in the Ubiquitin-Proteasome System and Autophagy. *Trends Biochem. Sci.* **2017**, *42*, 873–886.
- (2) Coux, O.; Tanaka, K.; Goldberg, A. L. Structure and functions of the 20S and 26S proteasomes. *Annu. Rev. Biochem.* **1996**, *65*, 801–847.

- (3) Kimura, Y.; Tanaka, K. Regulatory mechanisms involved in the control of ubiquitin homeostasis. *J. Biochem.* **2010**, *147*, 793–798.
- (4) Martinez-Fonts, K.; Davis, C.; Tomita, T.; Elsasser, S.; Nager, A. R.; Shi, Y.; Finley, D.; Matouschek, A. The proteasome 19S cap and its ubiquitin receptors provide a versatile recognition platform for substrates. *Nat. Commun.* **2020**, *11*, 477.
- (5) Churcher, I. Protac-Induced Protein Degradation in Drug Discovery: Breaking the Rules or Just Making New Ones? *J. Med. Chem.* **2018**, *61*, 444–452.
- (6) Zhang, L.; Riley-Gillis, B.; Vijay, P.; Shen, Y. Acquired Resistance to BET-PROTACs (Proteolysis-Targeting Chimeras) Caused by Genomic Alterations in Core Components of E3 Ligase Complexes. *Mol. Cancer Ther.* **2019**, *18*, 1302–1311.
- (7) Liu, X.; Ciulli, A. Proximity-Based Modalities for Biology and Medicine. ACS Cent Sci. 2023, 9, 1269–1284.
- (8) Chirnomas, D.; Hornberger, K. R.; Crews, C. M. Protein degraders enter the clinic a new approach to cancer therapy. *Nat. Rev. Clin Oncol.* **2023**, *20*, 265–278.
- (9) Buckley, D. L.; Van Molle, I.; Gareiss, P. C.; Tae, H. S.; Michel, J.; Noblin, D. J.; Jorgensen, W. L.; Ciulli, A.; Crews, C. M. Targeting the von Hippel–Lindau E3 ubiquitin ligase using small molecules to disrupt the VHL/HIF-1 α interaction. *J. Am. Chem. Soc.* **2012**, *134*, 4465–4468.
- (10) Winter, G. E.; Buckley, D. L.; Paulk, J.; Roberts, J. M.; Souza, A.; Dhe-Paganon, S.; Bradner, J. E. Phthalimide conjugation as a strategy for in vivo target protein degradation. *Science* **2015**, *348*, 1376–1381.
- (11) Bondeson, D. P.; Mares, A.; Smith, I. E.; Ko, E.; Campos, S.; Miah, A. H.; Mulholland, K. E.; Routly, N.; Buckley, D. L.; Gustafson, J. L.; Zinn, N.; Grandi, P.; Shimamura, S.; Bergamini, G.; Faelth-Savitski, M.; Bantscheff, M.; Cox, C.; Gordon, D. A.; Willard, R. R.; Flanagan, J. J.; Casillas, L. N.; Votta, B. J.; den Besten, W.; Famm, K.; Kruidenier, L.; Carter, P. S.; Harling, J. D.; Churcher, I.; Crews, C. M. Catalytic in vivo protein knockdown by small-molecule PROTACs. *Nat. Chem. Biol.* **2015**, *11*, 611–617.
- (12) Raina, K.; Lu, J.; Qian, Y.; Altieri, M.; Gordon, D.; Rossi, A. M.; Wang, J.; Chen, X.; Dong, H.; Siu, K.; Winkler, J. D.; Crew, A. P.; Crews, C. M.; Coleman, K. G. PROTAC-induced BET protein degradation as a therapy for castration-resistant prostate cancer. *Proc. Natl. Acad. Sci. USA* **2016**, *113*, 7124–7129.
- (13) Zengerle, M.; Chan, K.-H.; Ciulli, A. Selective small molecule induced degradation of the BET bromodomain protein BRD4. *ACS Chem. Biol.* **2015**, *10*, 1770–1777.
- (14) Bashore, C.; Prakash, S.; Johnson, M. C.; Conrad, R. J.; Kekessie, I. A.; Scales, S. J.; Ishisoko, N.; Kleinheinz, T.; Liu, P. S.; Popovych, N.; Wecksler, A. T.; Zhou, L.; Tam, C.; Zilberleyb, I.; Srinivasan, R.; Blake, R. A.; Song, A.; Staben, S. T.; Zhang, Y.; Arnott, D.; Fairbrother, W. J.; Foster, S. A.; Wertz, I. E.; Ciferri, C.; Dueber, E. C. Targeted degradation via direct 26S proteasome recruitment. *Nat. Chem. Biol.* **2023**, *19*, 55–63.
- (15) Ali, E. M. H.; Loy, C. A.; Trader, D. J. ByeTAC: Bypassing an E3 Ligase for Targeted Protein Degradation. *bioRxiv* 2024, DOI: 10.1101/2024.01.20.576376.
- (16) Huang, L.; Ho, P.; Chen, C.-H. Activation and Inhibition of Proteasomes by Betulinic Acid and Its Derivatives. *FEBS Lett.* **2007**, *581*, 4955–4959.
- (17) Jones, C. L.; Njomen, E.; Sjögren, B.; Dexheimer, T. S.; Tepe, J. J. Small Molecule Enhancement of 20S Proteasome Activity Targets Intrinsically Disordered Proteins. *ACS Chem. Biol.* **2017**, *12*, 2240–2247.
- (18) Medina, D. X.; Caccamo, A.; Oddo, S. Methylene Blue Reduces $A\beta$ Levels and Rescues Early Cognitive Deficit by Increasing Proteasome Activity. *Brain Pathol.* **2011**, *21*, 140–149.
- (19) Njomen, E.; Osmulski, P. A.; Jones, C. L.; Gaczynska, M.; Tepe, J. J. Small Molecule Modulation of Proteasome Assembly. *Biochemistry* **2018**, *57*, 4214–4224.
- (20) Trader, D. J.; Simanski, S.; Dickson, P.; Kodadek, T. Establishment of a Suite of Assays That Support the Discovery of

- Proteasome Stimulators. Biochim. Biophys. Acta, Gen. Subj. 2017, 1861, 892-899.
- (21) Coleman, R. A.; Trader, D. J. Development and Application of a Sensitive Peptide Reporter to Discover 20S Proteasome Stimulators. *ACS Comb. Sci.* **2018**, *20*, 269–276.
- (22) Yao, T.; Cohen, R. E. A Cryptic Protease Couples Deubiquitination and Degradation by the Proteasome. *Nature* **2002**, 419, 403–407.
- (23) Lee, M. J.; Lee, B.-H.; Hanna, J.; King, R. W.; Finley, D. Trimming of Ubiquitin Chains by Proteasome-Associated Deubiquitinating Enzymes. *Mol. Cell. Proteomics* **2011**, *10*, No. R110.003871.
- (24) Zhang, S.; Zou, S.; Yin, D.; Zhao, L.; Finley, D.; Wu, Z.; Mao, Y. USP14-regulated allostery of the human proteasome by time-resolved cryo-EM. *Nature.* **2022**, *605*, 567–574.
- (25) Wang, Y.; Jiang, Y.; Ding, S.; et al. Small molecule inhibitors reveal allosteric regulation of USP14 via steric blockade. *Cell Res.* **2018**, 28, 1186–1194.
- (26) Lee, B.-H.; Lee, M. J.; Park, S.; Oh, D.-C.; Elsasser, S.; Chen, P.-C.; Gartner, C.; Dimova, N.; Hanna, J.; Gygi, S. P.; Wilson, S. M.; King, R. W.; Finley, D. Enhancement of Proteasome Activity by a Small-Molecule Inhibitor of USP14. *Nature* **2010**, *467*, 179–184.
- (27) Ho, T. C. S.; Chan, A. H. Y.; Ganesan, A. Thirty Years of HDAC Inhibitors: 2020 Insight and Hindsight. *J. Med. Chem.* 2020, 63, 12460–12484.
- (28) Walton, J. W.; Cross, J. M.; Riedel, T.; Dyson, P. J. Perfluorinated HDAC inhibitors as selective anticancer agents. *Org. Biomol Chem.* **2017**, *15*, 9186–9190.
- (29) Jenke, R.; Reßing, N.; Hansen, F. K.; Aigner, A.; Büch, T. Anticancer Therapy with HDAC Inhibitors: Mechanism-Based Combination Strategies and Future Perspectives. *Cancers (Basel)* **2021**, *13*, 634.
- (30) Pettersson, M.; Crews, C. M. Proteolysis TArgeting Chimeras (PROTACs) Past, present and future. *Drug Discov Today Technol.* **2019**, *31*, 15–27.
- (31) Ma, P.; Schultz, R. M. HDAC1 and HDAC2 in mouse oocytes and preimplantation embryos: Specificity versus compensation. *Cell Death Differ.* **2016**, 23, 1119–1127.

Supporting Information

Targeted Degradation of Histone Deacetylases *via*Bypassing E3 Ligase Targeting Chimeras (BYETACs)

Tao Sun, ¹ Shiyang Zhai, ¹ Beate König, ¹ Irina Honin, ¹ Cindy-Esther Kponomaizoun, ¹ Finn K. Hansen ¹*

¹ Department of Pharmaceutical and Cell Biological Chemistry, Pharmaceutical Institute, University of Bonn, 53121 Bonn, Germany

* Corresponding author:

Prof. Dr. Finn K. Hansen, Pharmaceutical and Cell Biological Chemistry, Pharmaceutical Institute, University of Bonn, An der Immenburg 4, 53121 Bonn, Germany. Tel.: (+49) 228 73 5213. Fax: (+49) 228 73 7929. E-mail: finn.hansen@uni-bonn.de.

Table of Contents

1. Experimental section	S2
1.1. Chemistry	S2
1.2. Biological assays	S12
2. Supplementary Schemes and Figures	S15
3. NMR spectra of synthesized compounds	S22
4. HPLC chromatograms	S42
5 References	S45

1. Experimental section

1.1 Chemistry

No unexpected or unusually high safety hazards were encountered.

1.1.1 General information

Chemicals were obtained from BLDpharm, Sigma-Aldrich, TCI Chemicals and abcr GmbH used without purification. Air-sensitive reactions were carried out under argon atmosphere utilizing standard *Schlenk* techniques. Thin-layer chromatography (TLC) was carried out on prefabricated plates (silica gel 60, F254, Merck). Components were visualized by irradiation with ultraviolet light (254 nm). Column Chromatography was carried out on silica gel (60 Å, 40–60 μ m, *Acros Organics*).

Nuclear magnetic resonance spectroscopy (NMR): Proton (¹H) and carbon (¹³C) NMR spectra were recorded either on a Bruker AvanceDRX 500 (500 MHz ¹H NMR, 126 MHz ¹³C NMR) or a BrukerAvance III 600 (600 MHz ¹H NMR, 151 MHz ¹³C NMR). The chemical shifts are given in parts per million (ppm). Deuterated chloroform (CDCl₃) and deuterated dimethyl sulfoxide (DMSO-*d*₆) were used as solvents.

High performance liquid chromatography (HPLC): A *Thermo Fisher Scientific* UltiMate 3000 UHPLC system with a Nucleodur 100–5 C18 (250 mm × 4.6 mm, *Macherey Nagel*) with a flow rate of 1 mL/min and a temperature of 25 °C or a 100–5 C18 (100 mm × 3 mm, *Macherey Nagel*) with a flow rate of 0.5 mL/min and a temperature of 25 °C with an appropriate gradient were used. For preparative purposes a AZURA Prep. 500/1000 gradient system with a Nucleodur 110–5 C18 HTec (250 mm × 32 mm, *Macherey Nagel*) column with 20 mL/min was used. Detection was implemented by UV absorption measurement at a wavelength of λ = 220 nm and λ = 250 nm. Bidest. H₂O (A) and CH₃CN (B) were used as eluents with an addition of 0.1% TFA for eluent A. The purity of all final compounds was 95% or higher. Purity was determined via HPLC with the Nucleodur 100–5 C18 (250mm × 4.6 mm, *Macherey Nagel*) at 250 nm.

Flash chromatography was performed on an Interchim puriFlash XS 520 Plus with a diodearray detector (DAD) from 200-400 nm using prepacked silica gel cartridges (PF-30SIHPF0012-F0040) or C18 reversed-phase cartridges (PF-30C18HP-F0004-F0012).

1.1.2 Synthesis

Synthesis of Methyl 2-(4-aminophenyl)acetate (2). Thionyl chloride (787 mg, 6.60 mmol, 1.0 eq.) was added dropwise to a solution of 4-aminophenylacetic acid (1, 1000 mg, 6.60 mmol, 1.0 eq.) in anhydrous methanol (25 mL). The mixture was stirred at 80°C for 16 h. The resulting solution was cooled and the solvent was removed under reduced pressure. The brown solid hydrochloride salt of the title compound was triturated with Et₂O (2 × 30 mL) to remove impurities. The free amine was liberated from its hydrochloride salt by addition of aqueous NaHCO₃, followed by extraction into CHCl₃ (3 × 30 mL). The organic layers were combined, dried over MgSO₄ and the solvent removed to afford compound 2 as a light brown oil (1.10 g, 97% yield). ¹H NMR (ppm, 500 MHz, DMSO- d_6): δ 6.88 (d, J = 8.5 Hz, 2H), 6.49 (d, J = 8.5 Hz, 2H), 4.94 (s, 2H), 3.58 (s, 3H), 3.43 (s, 2H). ESI-MS m/z: 166.1 [M + H]⁺.

Synthesis of 8-{[4-(2-Methoxy-2-oxoethyl)phenyl]amino}-8-oxooctanoic acid (3). Compound **2** (700 mg, 4.69 mmol, 1.0 eq.), suberic anhydride (560 mg, 3.59 mmol, 0.8 eq.) and NaHCO₃ (200 mg, 2.38 mmol, 0.5 eq.) were dissolved in anhydrous THF (25 mL) and stirred at room temperature for 16 h. Solid impurities were removed by filtration and the solvent was removed under reduced pressure. The obtained residue was purified by flash column chromatography (C18 reversed phase, MeCN/H₂O 5-95%) to obtain **3** as a white solid (860 mg, 63% yield). ¹H NMR (ppm, 600 MHz, CDCl₃): δ 7.47 (d, J = 8.4 Hz, 2H), 7.22 (d, J = 7.8 Hz, 2H), 3.68 (s, 3H), 3.59 (s, 2H), 2.34 (q, J = 7.2 Hz, 4H), 1.73 (t, J = 7.2 Hz, 2H), 1.65 (t, J = 6.6 Hz, 2H), 1.39-1.36 (m, 4H). ESI-MS m/z: 322.2, [M + H]⁺.

Synthesis of methyl 2-(4-{8-oxo-8-[(trityloxy)amino]octanamido}phenyl)acetate (4). To a mixture of **3** (321 mg, 1.0 mmol, 1.0 eq.) and DIPEA (522 μ L, 3.0 mmol, 3.0 eq.) in anhydrous DMF (25 mL) was added HATU (570 mg, 1.5 mmol, 1.5 eq.), and the reaction mixture was stirred at room temperature for 30 min. Then *O*-tritylhydroxylamine (275 mg, 1.0 mmol, 1.0 eq.) was added, and the mixture was stirred at room temperature for 16 h. The reaction mixture was distilled under vacuum to remove DMF. The obtained residue was purified by flash column chromatography (C18 reversed phase, MeCN/H₂O 5-95%) to obtain **4** as yellow solid (163 mg, 28% yield). ¹H NMR (ppm, 500 MHz, DMSO-*d*₆): δ 10.14 (s, 1H), 9.80 (s, 1H), 7.52 (d, J =

8.5 Hz, 2H), 7.32 (t, J = 8.0 Hz, 15H), 7.16 (d, J = 8.5 Hz, 2H), 3.60 (s, 5H), 2.24 (t, J = 7.5 Hz, 2H), 1.78 (s, 2H), 1.52-1.46 (m, 2H), 1.19-1.14 (m, 4H), 1.00 (t, J = 7.5 Hz, 2H). ¹³C NMR (ppm, 126 MHz, DMSO- d_6): 8 174.56, 171.85, 171.28, 170.45, 142.63, 138.25, 129.64, 129.11, 128.89, 127.62, 119.21, 91.88, 51.75, 36.48, 32.12, 28.48, 28.33, 25.09, 24.80. ESI-MS m/z: 577.5, [M - H]⁻.

Synthesis of 2-(4-{8-oxo-8-[(trityloxy)amino]octanamido}phenyl)acetic acid (5). 4 (578 mg, 1.0 mmol, 1.0 eq.) was dissolved in THF/H₂O (20 mL, v/v = 1:1). LiOH·H₂O (84 mg, 2.0 mmol, 2.0 eq.) was added and the homogenous solution was stirred at room temperature for 12 h. The solvent was removed under reduced pressure and purified by flash column chromatography (C18 reversed phase, MeCN/H₂O 5-95%) to obtain the 5 as white solid (401 mg, 71% yield). ¹H NMR (ppm, 600 MHz, DMSO- d_6): δ 10.24 (s, 1H), 9.81 (s, 1H), 7.42 (d, J = 8.4 Hz, 2H), 7.33-7.28 (m, 15H), 7.11 (d, J = 8.4 Hz, 2H), 3.18 (s, 2H), 2.22 (t, J = 7.2 Hz, 2H), 1.77 (s, 2H), 1.50-1.45 (m, 2H), 1.17 (t, J = 7.8 Hz, 4H), 0.99 (s, 2H). ¹³C NMR (ppm, 151 MHz, DMSO- d_6): δ 174.80, 171.06, 142.76, 136.76, 134.45, 129.41, 129.13, 127.61, 118.76, 91.79, 45.45, 36.47, 32.16, 28.54, 28.33, 25.18, 24.89. ESI-MS m/z: 563.4, [M - H]⁻.

Synthesis of 1-{2-[1-(4-fluorophenyl)-2,5-dimethyl-1H-pyrrol-3-yl]-2-oxoethyl}pyrrolidine-3-carboxylic acid (7). Pyrrolidine-3-carboxylic acid (260 mg, 2.26 mmol, 2.0 eq.) was added to a solution of 2-chloro-1-[1-(4-fluorophenyl)-2,5-dimethyl-1*H*-pyrrol-3-yl]ethan-1-one (6, 300 mg, 1.13 mmol, 1.0 eq.) and triethylamine (628 μL, 4.52 mmol, 4.0 eq.) in DMF (30 mL). The reaction mixture was heated to 85 °C for 2 h. The mixture was concentrated under vacuum and purified by flash column chromatography (C18 reversed phase, MeCN/H₂O 5-95%) to give 7 as yellow solid (116 mg, 30% yield). ¹H NMR (ppm, 500 MHz, DMSO- d_6): δ 7.39 (d, J = 1.0 Hz, 2H), 7.38 (s, 2H), 6.43 (d, J = 1.0 Hz, 1H), 3.66 (s, 2H), 2.96-2.86 (m, 2H), 2.75 (q, J = 2.5 Hz, 1H), 2.70-2.65 (m, 1H), 2.63-2.58 (m, 1H), 2.21 (s, 3H), 1.96 (t, J = 7.0 Hz, 2H), 1.93 (s, 3H). ¹³C NMR (ppm, 126 MHz, DMSO- d_6): δ 192.76, 175.87, 160.90, 135.23, 133.15, 130.43, 128.45, 118.69, 116.66, 116.47, 107.38, 62.51, 56.57, 53.52, 41.80, 27.37, 12.68, 12.50. ESI-MS m/z: 343.2, [M - H]⁻.

General procedures for the synthesis of 8a-e. To a mixture of 7 (344 mg, 1.0 mmol, 1.0 eq.) and DIPEA (523 μL, 3.0 mmol, 3.0 eq.) in anhydrous DMF (20 mL) was added HATU (570 mg, 1.5 mmol, 1.5 eq.), and the reaction mixture was stirred at room temperature for 30 min. Then, tert-butyl (3-aminopropyl)carbamate (174 mg, 1.0 mmol, 1.0 eq.), tert-butyl (6-aminohexyl)carbamate (216 mg, 1.0 mmol, 1.0 eq.), tert-butyl (10-aminodecyl)carbamate (272 mg, 1.0 mmol, 1.0 eq.), tert-butyl {2-[2-(2-aminoethoxy)ethoxy]ethyl}carbamate (248 mg, 1.0 mmol, 1.0 eq.), or tert-butyl N-(2-{2-[2-(2-aminoethoxy)ethoxy]ethoxy}ethyl)carbamate (292 mg, 1.0 mmol, 1.0 eq.) was added, and the mixture was stirred at room temperature overnight. The reaction mixture was distilled under vacuum to remove DMF. The obtained residue was purified by flash column chromatography (C18 reversed phase, MeCN/H₂O 5-95%) to obtain the products 8a-e.

[3-(1-{2-[1-(4-fluorophenyl)-2,5-dimethyl-1H-pyrrol-3-yl]-2-oxoethyl}pyrrolidine-3-carboxamido)propyl]carbamate (8a). 383 mg, yellow solid, 77% yield. 1 H NMR (ppm, 500 MHz, DMSO- d_6): δ 8.11 (t, J=5.0 Hz, 1H), 7.45-7.38 (m, 4H), 6.76 (s, 1H), 6.42 (s, 1H), 4.73 (s, 2H), 3.51 (q, J=5.0 Hz, 4H), 3.15 (t, J=7.5 Hz, 1H), 3.11-3.05 (m, 2H), 2.93 (q, J=6.0 Hz, 2H), 2.27 (s, 4H), 2.08 (s, 1H), 1.96 (s, 3H), 1.55-1.50 (m, 2H), 1.37 (s, 9H). 13 C NMR (ppm, 126 MHz, DMSO- d_6): δ 187.04, 171.20, 163.07, 161.11, 155.73, 137.08, 132.59, 130.31, 129.84, 116.87, 116.69, 106.92, 77.65, 60.91, 56.33, 54.37, 41.61, 37.72, 36.70, 29.55, 28.40, 27.95, 12.77, 12.47. ESI-MS m/z: 501.3, [M + H]⁺.

[6-(1-{2-[1-(4-fluorophenyl)-2,5-dimethyl-1H-pyrrol-3-yl]-2-oxoethyl}pyrrolidine-3-carboxamido)hexyl]carbamate (*8b*). 355 mg, yellow solid, 66% yield. 1 H NMR (ppm, 500 MHz, DMSO- d_6): δ 8.11 (t, J=5.5 Hz, 1H), 7.45-7.38 (m, 4H), 6.73 (s, 1H), 6.42 (s, 1H), 4.72 (q, J=6.5 Hz, 2H), 3.46 (br.s, 4H), 3.18-3.12 (m, 1H), 3.11-3.03 (m, 2H), 2.89 (q, J=6.0, 2H), 2.27 (s, 4H), 2.08 (s, 1H), 1.96 (s, 3H), 1.42-1.35 (m, 13H), 1.24 (d, J=3.5 Hz, 4H). 13 C NMR (ppm, 126 MHz, DMSO- d_6): δ 186.99, 171.05, 163.07, 161.11, 155.73, 137.10, 132.59, 130.34, 129.85, 116.86, 116.68, 106.91, 77.45, 60.89, 56.35, 54.37, 41.59, 38.87, 29.57, 29.05, 28.41, 27.99, 26.20, 12.77, 12.46. ESI-MS m/z: 543.4, [M + H]⁺.

oxoethyl}pyrrolidine-3-carboxamido)decyl]carbamate (8c). 349 mg, yellow solid, 58% yield. ¹H NMR (ppm, 500 MHz, DMSO- d_6): δ 8.11 (t, J = 5.5 Hz, 1H), 7.45-7.38 (m, 4H), 6.71 (s, 1H), 6.42 (d, J = 1.0 Hz, 1H), 4.72 (q, J = 7.0 Hz, 2H), 3.45 (br.s, 4H), 3.18-3.12 (m, 1H), 3.11-3.03 (m, 2H), 2.88 (q, J = 6.0 Hz, 2H), 2.27 (s, 4H), 2.06 (s, 1H), 1.96 (s, 3H), 1.42-1.34 (m,

[10-(1-{2-[1-(4-fluorophenyl)-2,5-dimethyl-1H-pyrrol-3-yl]-2-

Tert-butyl

13H), 1.24 (s, 12H). ¹³C NMR (ppm, 126 MHz, DMSO-*d*₆): δ 187.00, 171.05, 163.07, 161.11, 155.72, 137.09, 132.60, 130.34, 129.84, 116.86, 116.68, 106.91, 77.41, 60.89, 56.35, 54.38,

41.59, 38.90, 29.61, 29.09, 28.84, 28.41, 27.98, 26.49, 12.76, 12.46. ESI-MS m/z: 599.5, [M + H]⁺.

Tert-butyl (2-{2-[2-(1-{2-[1-(4-fluorophenyl)-2,5-dimethyl-1H-pyrrol-3-yl]-2-oxoethyl}pyrrolidine-3-carboxamido)ethoxy]ethoxy}ethyl)carbamate (8d). 517 mg, yellow oil, 90% yield. 1 H NMR (ppm, 600 MHz, DMSO- d_6): δ 8.25 (s, 1H), 7.44-7.39 (m, 4H), 6.74 (s, 1H), 6.42 (s, 1H), 4.74 (s, 2H), 3.51 (s, 4H), 3.44 (t, J = 6.0 Hz, 2H), 3.37 (t, J = 6.6 Hz, 2H), 3.28 (s, 2H), 3.25 (t, J = 3.6 Hz, 2H), 3.20 (s, 1H), 3.17 (s, 2H), 3.06 (q, J = 5.4 Hz, 2H), 2.27 (s, 4H), 2.08 (br.s, 1H), 1.96 (s, 3H), 1.37 (s, 9H). 13 C NMR (ppm, 151 MHz, DMSO- d_6): δ 186.98, 171.42, 162.92, 161.29, 155.76, 137.12, 132.60, 130.35, 129.86, 116.87, 116.71, 106.92, 77.78, 69.69, 69.32, 69.06, 60.90, 56.30, 41.50, 40.23, 39.02, 28.38, 27.97, 12.78, 12.48. ESI-MS m/z: 575.4, [M + H] $^+$.

Tert-butyl [1-(1-{2-[1-(4-fluorophenyl)-2,5-dimethyl-1H-pyrrol-3-yl]-2-oxoethyl}pyrrolidin-3-yl)-1-oxo-5,8,11-trioxa-2-azatridecan-13-yl]carbamate (8e). 357 mg, yellow oil, 58% yield. 1 H NMR (ppm, 600 MHz, DMSO- d_6): δ 8.24 (t, J = 4.8 Hz, 1H), 7.43-7.38 (m, 4H), 6.72 (s, 1H), 6.41 (s, 1H), 4.72 (q, J = 7.8 Hz, 2H), 3.51 (s, 4H), 3.49 (d, J = 3.6 Hz, 4H), 3.43 (t, J = 6.0 Hz, 2H), 3.36 (t, J = 6.0 Hz, 2H), 3.27 (s, 3H), 3.25-3.22 (m, 2H), 3.18 (q, J = 6.6 Hz, 2H), 3.04 (q, J = 6.0 Hz, 2H), 2.26 (s, 4H), 2.05 (br.s, 1H), 1.95 (s, 3H), 1.36 (s, 9H). 13 C NMR (ppm, 151 MHz, DMSO- d_6): δ 187.02, 171.46, 162.92, 161.28, 155.75, 137.10, 132.61, 130.35, 129.85, 116.87, 116.71, 106.92, 77.76, 69.89, 69.75, 69.67, 69.32, 69.07, 60.91, 56.31, 41.51, 40.23, 39.02, 28.38, 27.98, 12.78, 12.48. ESI-MS m/z: 619.4, [M + H]+.

General procedure for the synthesis of 9a-e. TFA (2 mL) was added dropwise to a solution of 8a-e in DCM (8 mL) and the reaction mixture was stirred at room temperature for 1 h. The solvent was removed under reduced pressure to afford the crude compounds 9a-e, which were used directly in the next step without further purification.

General procedure for the synthesis of 10a-e. To a mixture of 5 (564 mg, 1.0 mmol, 1.0 eq.) and DIPEA (1.74 mL, 10.0 mmol, 10.0 eq.) in anhydrous DMF (25 mL) was added HATU (760 mg, 2.0 mmol, 2.0 eq.). The reaction mixture was stirred at room temperature for 30 min. Then, 9a (400 mg, 1.0 mmol, 1.0 eq.), 9b (442 mg, 1.0 mmol, 1.0 eq.), 9c (498 mg, 1.0 mmol, 1.0 eq.), 9d (474 mg, 1.0 mmol, 1.0 eq.), or 9e (518 mg, 1.0 mmol, 1.0 eq.) was added, and the mixture was stirred at the room temperature for 12 h. The reaction mixture was distilled under vacuum to remove DMF. The obtained residue was redissolved in DCM (10 mL), triisopropylsilane (TIPS, 1 mL) and TFA (1 mL) were added gradually and the mixture was stirred at room temperature for 1 h. DCM was removed under reduced pressure and the crude product was purified by preparative HPLC (MeCN/H₂O 5-95%) to obtain the final products 10a-e.

 N^1 -[4-(2-{[3-(1-{2-[1-(4-fluorophenyl)-2,5-dimethyl-1H-pyrrol-3-yl]-2-oxoethyl}pyrrolidine-3-carboxamido)propyl]amino}-2-oxoethyl)phenyl]- N^8 -

hydroxyoctanediamide (10a). 33 mg, brown solid, 5% yield. 1 H NMR (ppm, 600 MHz, DMSO-d₆): δ 10.29 (s, 1H), 9.76 (s, 1H), 8.61 (s, 1H), 7.91 (t, J = 5.4 Hz, 1H), 7.79 (t, J = 5.4 Hz, 1H), 7.47 (d, J = 8.4 Hz, 2H), 7.40-7.37 (m, 4H), 7.13 (d, J = 8.4 Hz, 2H), 6.42 (s, 1H), 3.65 (s, 2H), 3.31 (s, 2H), 3.27 (s, 2H), 3.04-3.00 (m, 4H), 2.91 (t, J = 8.4 Hz, 1H), 2.82-2.77 (m, 2H), 2.25 (t, J = 7.2 Hz, 2H), 2.20 (s, 3H), 1.93-1.86 (m, 7H), 1.57-1.53 (m, 2H), 1.52-1.45 (m, 4H), 1.27-1.24 (m, 4H). 13 C NMR (ppm, 151 MHz, DMSO-d₆): δ 171.21, 170.34, 169.23, 162.79, 161.16, 137.82, 131.09, 130.39, 129.23, 119.14, 116.74, 116.59, 107.19, 54.00, 42.00, 36.59, 32.39, 29.33, 28.55, 27.95, 25.17, 12.74, 12.50. 19 F NMR (ppm, 565 MHz, DMSO-d₆): δ -113.64. ESI-MS m/z: 705.5, [M + H]⁺. HRMS (ESI): calcd for C₃₈H₄₉FN₆O₆, [M + H]⁺ 705.3770; found, 705.3747. HPLC: t_R= 10.75 min (96.9% purity).

 N^1 -[4-(2-{[6-(1-{2-[1-(4-fluorophenyl)-2,5-dimethyl-1H-pyrrol-3-yl]-2-oxoethyl}pyrrolidine-3-carboxamido)hexyl]amino}-2-oxoethyl)phenyl]- N^8 -

hydroxyoctanediamide (*10b*). 31 mg, light yellow solid, 4% yield. 1 H NMR (ppm, 600 MHz, DMSO- 2 d₆): δ 10.31 (s, 1H), 9.78 (s, 1H), 8.10 (d, 2 = 25.8 Hz, 1H), 7.92 (s, 1H), 7.47 (d, 2 = 8.4 Hz, 2H), 7.45-7.40 (m, 4H), 7.13 (d, 2 = 8.4 Hz, 2H), 6.41 (d, 2 = 12.6 Hz, 1H), 4.78 (dd, 2 = 7.8, 10.2 Hz, 2H), 3.77 (t, 2 = 57.6 Hz, 2H), 3.31 (s, 2H), 3.20 (t, 2 = 7.8 Hz, 3H), 3.08 (s, 2H), 3.01 (d, 2 = 6.0 Hz, 2H), 2.26 (t, 2 = 7.8 Hz, 5H), 1.93 (q, 2 = 7.2 Hz, 5H), 1.56 (t, 2 = 7.2 Hz, 2H), 1.48 (t, 2 = 7.2 Hz, 2H), 1.38 (s, 5H), 1.25 (s, 9H). 13 C NMR (ppm, 151 MHz, DMSO- 2 d₆): δ 187.06, 171.22, 170.18, 169.25, 162.92, 161.28, 137.79, 137.14, 132.60, 131.21, 130.35, 129.88, 129.20, 119.13, 116.87, 116.72, 106.94, 61.03, 56.39, 54.70, 54.16, 42.02, 41.57, 38.63, 36.47, 32.39, 29.17, 29.00, 28.55, 27.88, 26.15, 25.17, 12.78, 12.49. 19 F NMR (ppm, 565 MHz, DMSO- 2 d₆): δ -113.27. ESI-MS m/z: 745.5, [M - H]- HRMS (ESI): calcd for C₄₁H₅₅FN₆O₆, [M + H]+ 747.4240; found, 747.4211. HPLC: t_R= 15.54 min (96.0% purity).

 N^1 -[4-(2-{[10-(1-{2-[1-(4-fluorophenyl)-2,5-dimethyl-1H-pyrrol-3-yl]-2-oxoethyl}pyrrolidine-3-carboxamido)decyl]amino}-2-oxoethyl)phenyl]- N^8 -

hydroxyoctanediamide (*10c*). 33 mg, light yellow solid, 4% yield. ¹H NMR (ppm, 600 MHz, DMSO-*d*₆): δ 10.30 (s, 1H), 9.77 (s, 1H), 8.13 (q, J= 4.8 Hz, 1H), 7.89 (t, J= 5.4 Hz, 1H), 7.46 (d, J= 8.4 Hz, 2H), 7.43-7.38 (m, 4H), 7.12 (d, J= 9.0 Hz, 2H), 6.39 (d, J= 13.2 Hz, 1H), 4.78-4.67 (m, 2H), 3.86-3.64 (m, 2H), 3.29 (s, 2H), 3.24-3.16 (m, 3H), 3.04 (q, J= 6.0 Hz, 2H), 2.99 (q, J= 6.0 Hz, 2H), 2.25 (t, J= 7.8 Hz, 5H), 1.92 (q, J= 7.2 Hz, 5H), 1.57-1.52 (m, 2H), 1.50-1.45 (m, 2H), 1.40-1.35 (m, 5H), 1.22 (s, 17H). ¹³C NMR (ppm, 151 MHz, DMSO-*d*₆): δ 187.05, 171.20, 170.15, 169.24, 162.91, 161.28, 137.80, 137.14, 132.59, 131.22, 130.34, 129.88, 129.19, 119.09, 116.87, 116.71, 106.93, 61.02, 56.39, 54.69, 54.15, 42.03, 41.57, 38.70, 36.47, 32.39, 29.22, 29.07, 28.83, 28.55, 27.87, 26.49, 25.17, 12.78, 12.48. ¹⁹F NMR (ppm, 565 MHz, DMSO-*d*₆): δ -113.26. ESI-MS m/z: 801.6, [M - H]⁻. HRMS (ESI): calcd for C₄₅H₆₃FN₆O₆, [M + H]⁺ 803.4866; found, 803.4865. HPLC: t_R= 16.63 min (95.6% purity).

 N^{l} -{4-[1-(1-{2-[1-(4-fluorophenyl)-2,5-dimethyl-1H-pyrrol-3-yl]-2-oxoethyl}pyrrolidin-3-yl)-1,12-dioxo-5,8-dioxa-2,11-diazatridecan-13-yl]phenyl}- N^{8} -hydroxyoctanediamide (10d).

45 mg, white solid, 6% yield. 1 H NMR (ppm, 500 MHz, DMSO- d_6): δ 10.31 (s, 1H), 9.79 (s, 1H), 8.29-8.23 (m, 1H), 8.02 (t, J = 5.5 Hz, 1H), 7.52-7.38 (m, 6H), 7.15 (t, J = 8.5 Hz, 2H), 6.40 (d, J = 8.5 Hz, 1H), 4.81-4.65 (m, 2H), 3.60 (s, 4H), 3.50 (s, 4H), 3.45-3.39 (m, 5H), 3.25 (d, J = 5.0 Hz, 2H), 3.19 (q, J = 6.0 Hz, 2H), 2.31-2.25 (m, 5H), 1.93 (t, J = 10.5 Hz, 5H), 1.62-1.54 (m, 4H), 1.51-1.45 (m, 2H), 1.39-1.34 (m, 2H), 1.33-1.22 (m, 4H). 13 C NMR (ppm, 126 MHz, DMSO- d_6): δ 187.00, 171.25, 170.53, 169.23, 163.07, 161.11, 137.83, 137.12, 132.58, 131.04, 130.34, 129.85, 129.23, 119.20, 116.86, 116.68, 106.92, 69.70, 69.19, 69.04, 61.03, 56.34, 54.69, 54.13, 41.86, 41.50, 39.01, 38.80, 36.46, 32.38, 28.54, 27.87, 25.17, 12.76, 12.46. 19 F NMR (ppm, 471 MHz, DMSO- d_6): δ -113.28. ESI-MS m/z: 777.3, [M - H]-. HRMS (ESI): calcd for C₄₁H₅₅FN₆O₈, [M + H]+ 779.4138; found, 779.4134. HPLC: t_R= 15.05 min (98.2% purity).

 N^1 -{4-[1-(1-{2-[1-(4-fluorophenyl)-2,5-dimethyl-1H-pyrrol-3-yl]-2-oxoethyl}pyrrolidin-3-yl)-1,15-dioxo-5,8,11-trioxa-2,14-diazahexadecan-16-yl]phenyl}- N^8 -hydroxyoctanediamide (10e). 100 mg, white solid, 12% yield. 1 H NMR (ppm, 500 MHz, DMSO- 4 6): δ 10.31 (s, 1H), 9.78 (s, 1H), 8.26 (q, J = 5.0 Hz, 1H), 8.01 (t, J = 5.5 Hz, 1H), 7.48-7.37 (m, 6H), 7.13 (d, J = 8.5 Hz, 2H), 6.40 (d, J = 9.5 Hz, 1H), 4.80-4.64 (m, 2H), 3.83 (t, J = 13.0 Hz, 4H), 3.65 (s, 2H), 3.49 (d, J = 6.5 Hz, 8H), 3.43-3.38 (m, 4H), 3.24 (s, 3H), 3.20-3.15 (m, 4H), 2.25 (t, J = 9.0 Hz, 5H), 1.92 (t, J = 7.5 Hz, 5H), 1.61-1.52 (m, 2H), 1.50-1.44 (m, 2H), 1.26 (t, J = 3.0 Hz, 4H). 13 C NMR (ppm, 126 MHz, DMSO- 4 6): δ 187.01, 171.30, 170.51, 169.24, 163.07, 161.11, 137.83, 137.12, 132.60, 131.04, 130.34, 129.86, 129.23, 119.12, 116.87, 116.67, 106.93, 69.88, 69.74, 69.19, 69.04, 61.02, 56.34, 54.69, 54.13, 41.86, 41.51, 39.01, 38.81, 36.47, 32.38, 28.54, 27.88, 25.17, 12.77, 12.47. 19 F NMR (ppm, 471 MHz, DMSO- 4 6): δ -113.28. ESI-MS m/z: 821.3, [M - H]⁻. HRMS (ESI): calcd for C43H59FN6O9, [M + H]⁺ 823.4400; found, 823.4395. HPLC: 18 1 HRMS (ESI): calcd for C43H59FN6O9, [M + H]⁺ 823.4400; found, 823.4395.

Synthesis of 1-[1-(4-fluorophenyl)-2,5-dimethyl-1H-pyrrol-3-yl]-2-(pyrrolidin-1-yl)ethan-1-one (11). 2-chloro-1-[1-(4-fluorophenyl)-2,5-dimethyl-1H-pyrrol-3-yl]ethan-1-one (6, 300 mg, 1.13 mmol, 1.0 eq.) was added to a solution of pyrrolidine (189 μ L, 2.26 mmol, 2.0 eq.) and triethylamine (314 μ L, 4.52 mmol, 4.0 eq.) in DMF (20 mL). The resulting mixture was heated

to 85 °C for 2 h. The mixture was concentrated under a vacuum and purified by flash column chromatography (C18 reversed phase, MeCN/H₂O 5-95%) to give **11** as light yellow solid (142 mg, 42% yield). ¹H NMR (ppm, 500 MHz, DMSO- d_6): δ 7.45-7.38 (m, 4H), 6.43 (d, J = 0.5 Hz, 1H), 4.71 (s, 2H), 3.31 (s, 4H), 2.26 (s, 3H), 1.97 (s, 4H), 1.96 (s, 3H). ESI-MS m/z: 301.3, [M + H]⁺.

 N^{1} - $(4-\{2-[(10-aminodecyl)amino]-2-oxoethyl\}phenyl)-<math>N^{8}$ -Synthesis of (benzyloxy)octanediamide (13). To a mixture of 12 (412 mg, 1.0 mmol, 1.0 eq.) and DIPEA (522 μL, 3.0 mmol, 3.0 eq.) in anhydrous DMF (25 mL) was added HATU (570 mg, 1.5 mmol, 1.5 eq.) and the reaction mixture was stirred at room temperature for 30 min. Then, tert-butyl (10-aminodecyl)carbamate (408 mg, 1.5 mmol, 1.5 eq.) was added and the mixture was stirred at room temperature for 16 h. The reaction mixture was distilled under vacuum to remove DMF. The obtained residue was directly dissolved in DCM (10 mL) without further purification. Trifluoroacetic acid (1 mL) was added dropwise and reaction was stirred at room temperature for 1 h. Solvents were removed in vacuo and the residue was purified by flash column chromatography (C18 reversed phase, MeCN/H₂O 5-95%) to obtain 13 as yellow oil (127 mg, 23% yield over two steps). ¹H NMR (ppm, 600 MHz, DMSO- d_6): δ 9.79 (s, 1H), 7.91 (t, J =4.8 Hz, 1H), 7.65 (s, 1H), 7.48 (d, J = 7.8 Hz, 2H), 7.38-7.33 (m, 5H), 7.13 (d, J = 7.8 Hz, 2H), 4.77 (s, 2H), 3.01 (q, J = 6.6 Hz, 2H), 2.89 (s, 2H), 2.78-2.73 (m, 2H), 2.26 (t, J = 7.2 Hz, 2H), 1.94 (t, J = 7.2 Hz, 2H), 1.56 (t, J = 6.6 Hz, 2H), 1.53-1.48 (m, 4H), 1.37 (t, J = 6.0 Hz, 2H), 1.23 (d, J = 16.8 Hz, 18H). ¹³C NMR (ppm, 151 MHz, DMSO- d_6): δ 171.25, 170.20, 169.49, 137.82, 136.28, 131.24, 129.21, 128.90, 128.43, 119.12, 116.72, 114.79, 76.90, 42.05, 39.03, 38.72, 36.48, 32.37, 29.23, 28.89, 28.54, 27.14, 26.49, 25.90, 25.18, 25.00. ESI-MS *m/z*: 566.8, $[M + H]^+$.

Synthesis of N^1 -hydroxy- N^8 -[4-(2-{[10-(1-methylpyrrolidine-3-carboxamido)decyl]amino}-2-oxoethyl)phenyl]octanediamide (10c-nc). To a mixture of 1-methylpyrrolidine-3-carboxylic acid (258 mg, 2.0 mmol, 2.0 eq.) and DIPEA (695 μ L, 4.0 mmol, 4.0 eq.) in anhydrous DMF (30 mL) was added HATU (1140 mg, 3.0 mmol, 3.0 eq.) and the reaction mixture was stirred at room temperature for 30 min. Then, 13 (566 mg, 1.0 mmol, 1.0 eq.) was added and the

mixture was stirred at room temperature for 16 h. The reaction mixture was distilled under vacuum to remove DMF. The obtained residue was directly dissolved in MeOH (20 mL) without further purification. Pd/C (5% palladium on carbon, 0.05 eq.) was added. The flask was evacuated and flushed with H₂. Afterwards, the reaction mixture was stirred at room temperature for another 16 h. The resulting reaction solution was filtered over celite and solvents were removed *in vacuo*. Finally, the residue was purified by flash column chromatography (C18 reversed phase, MeCN/H₂O 5-95%) to obtain **10c-nc** as light yellow solid (213 mg, 36% yield over two steps). ¹H NMR (ppm, 600 MHz, DMSO- d_6): δ 10.32 (s, 1H), 9.78 (s, 1H), 7.90 (s, 2H), 7.47 (d, J = 7.8 Hz, 2H), 7.13 (d, J = 8.4 Hz, 2H), 3.30 (s, 2H), 3.04-2.99 (m, 6H), 2.87-2.77 (m, 2H), 2.52 (s, 3H), 2.27 (t, J = 7.2 Hz, 2H), 2.07-2.01 (m, 1H), 1.95-1.91 (m, 2H), 1.56 (s, 2H), 1.48 (t, J = 7.2 Hz, 2H), 1.37 (d, J = 6.0 Hz, 4H), 1.27 (t, J = 1.8 Hz, 4H), 1.22 (s, 14H). ¹³C NMR (ppm, 151 MHz, DMSO- d_6): δ 172.48, 171.21, 170.15, 169.25, 137.80, 131.22, 129.18, 119.09, 58.30, 55.48, 42.49, 42.03, 41.17, 38.76, 36.47, 32.39, 29.21, 29.05, 28.83, 28.55, 28.43, 26.48, 25.18. ESI-MS m/z: 586.5, [M - H]. HPLC: t_R = 10.64 min (96.4% purity).

1.2 Biological assays

No unexpected or unusually high safety hazards were encountered.

1.2.1 Cell culture

The MM.1S cell line was obtained from ATCC (Manassas, VA, USA). MM.1S cells were cultivated in RPMI 1640 medium supplemented with 10% FBS, 100 IU/mL penicillin, 0.1 mg/mL streptomycin, and 1 mM sodium pyruvate at 37 °C in a 5% CO₂ atmosphere.

1.2.2 HDAC enzymes inhibition assay

For test compounds and controls, 3-fold serial dilutions of the test compounds were prepared in assay buffer (50 mM Tris-HCl, pH 8.0, 137 mM NaCl, 2.7 mM KCl, 1.0 mM MgCl₂·6H₂O, 0.1 mg/mL BSA), and 5.0 µL of this serial dilution were transferred into black OptiPlate-96 black microplates (PerkinElmer). Then 35 µL of the fluorogenic substrate ZMAL (Z-Lys(Ac)-AMC, 21.43 µM in assay buffer) and 10 µL enzyme solution diluted in assay buffer were added. In the case of HDAC4, 35 µL of the fluorogenic substrate Boc-Lys(Tfa)-AMC (42.86 µM in assay buffer) and 10 µL HDAC4 enzyme solution diluted in assay buffer were added.^[1] Human recombinant HDAC1 (BPS Bioscience, Catalog# 50051), HDAC2 (BPS Bioscience, Catalog# 50052), HDAC3/NcoR2 (BPS Bioscience, Catalog# 50003), HDAC4 (BPS Bioscience, Catalog# 50004), or HDAC6 (BPS Bioscience, Catalog# 50006) were used. The total assay volume of 50 µL (HDAC2/3/4/6 max. 1% DMSO; HDAC1 max. 5% DMSO) was incubated at 37 °C for 90 min. Subsequently, 50 µL of trypsin (HDAC1-3, 6 = 0.4 mg/mL; HDAC4 = 1.0 mg/mL) in trypsin buffer (50 mM Tris-HCl, pH 8.0, 100 mM NaCl) was added, followed by additional incubation at 37 °C for 30 min Fluorescence (excitation $\lambda = 355$ nm, emission $\lambda = 460$ nm) was measured using a FLUOstar OPTIMA microplate reader. The IC₅₀ was determined by plotting normalized dose response curves using a three-parameter logistic equation with GraphPad Prism. All compounds were tested in duplicates and IC50 values were calculated from at least two independent experiments.^[2-5]

1.2.3 Western blot assay

The MM.1S cells (3×10^6 cells/mL) were seeded into cell culture flasks and after 72 h treated

with the indicated concentration of compound or DMSO for the given time. Cell lysis was performed with Cell Extraction Buffer and addition of Halt Protease Inhibitor Cocktail and phenylmethanesulfonyl fluoride. Protein content was determined by PierceTM BCA Protein Assay Kit. Samples were denatured by Laemmli 2× Concentrate, and Precision Plus Protein Unstained Standard was used as molecular weight marker in all cases. SDS-PAGE was performed with 10% Mini-PROTEAN TGX Stain-Free Gel (Catalog# 458035, Bio-Rad, Hercules, CA, USA) at 200 V for 50 min (Catalog# 458035, Bio-Rad). Afterwards, proteins were transferred with the Trans-Blot Turbo Transfer System to Immobilon-FL PVDF membranes at 1.0 A for 30 min and incubated with 5% milk-powder solution for 1 h at room temperature under slight agitation. Subsequently, the membranes were incubated with anti-HDAC1 (Catalog# 5356S, Cell Signaling Technology, Denver, MA, USA), anti-HDAC2 (Catalog# 9959S, Cell Signaling Technology, Denver, MA, USA), anti-HDAC3 (Catalog# 85057S, Cell Signaling Technology, Denver, MA, USA), anti-HDAC4 (Catalog# 7628S, Cell Signaling Technology, Denver, MA, USA), anti-HDAC6 (Catalog# 7558S, Cell Signaling Technology, Denver, MA, USA), anti-acetyl-histone H3 (Catalog# 9677S, Cell Signaling Technology, Denver, MA, USA), anti-acetyl-α-tubulin (Catalog# 5335, Cell Signaling Technology, Denver, MA, USA) or anti-GAPDH (Catalog# T0004, Affinity Biosciences, Cincinnati, OH, USA) antibody solutions in 1:1000-1:20000 dilutions at room temperature under slight agitation for 1 h, and at 4°C for overnight. Incubation with HRP-conjugated secondary anti-mouse (Catalog# sc-516102, Santa Cruz, Dallas, TX, USA) and anti-rabbit (Catalog# HAF008, R&D Systems, Inc., Minneapolis, MN, USA) antibody solutions were performed for 1.5 h, and membranes were developed with clarity western ECL substrate. The ChemiDoc XRS+ System was used for detection and Image Lab Software 6.1 (Bio-Rad, Hercules, CA, USA) for quantification. [6-8]

1.2.4 CellTiter-Glo® cell viability assay

The MM.1S cells (2.5×10^3 cells/well) were seeded in white 384-well plates and incubated with the respective compounds at increasing concentrations. For this purpose, the dilution series were prepared at $200 \times$ concentration in DMSO and then further diluted to $10 \times$ concentration in medium. The final DMSO concentration was 0.5%. The toxicity of compounds was assessed

after 72 h using the CellTiter-Glo 2.0 cell viability assay. Luminescence was then measured, and the IC₅₀ was determined by plotting concentration-response curves and performing nonlinear regression using GraphPad Prism.^[9]

1.2.5 Annexin V/PI assay

MM.1S cells (3 \times 10⁵ cells/well) were seeded in 24-well plates and treated with indicated concentration of compound or DMSO for 48 h under cell culture conditions. Subsequently, cells were washed with cell staining buffer (HEPES 0.1 M, NaCl 1.4 M, CaCl₂ \times 3 H₂O 25 mM), resuspended in 300 μ L cell staining buffer and 150 μ L was transferred in a 96-well plate. The staining was performed using 5 μ L/well annexin V-FITC and 10 μ L/well propidium iodide, followed by incubation for 15 min and analysis by flow cytometry.^[1,10]

2. Supplementary Schemes and Figures

Scheme S1. Selected structures of reported Bypassing E3 Ligase Targeting Chimeras (BYETACs). (A) Macrocyclic BYETAC: the peptidic macrocycle binds to the 26S proteasome subunit PSMD2, while the small molecule ligand is a BRD4 ligand. (B) Small molecule BYETAC capable of inducing a RPN13:BYETAC:BRD4 ternary complex for E3 ligase independent targeted protein degradation.

Scheme S2. Synthesis of USP14 inhibitor IU1 (11). Reagents and conditions: i) Pyrrolidine, Et₃N, DMF, 85 °C, 42% yield.

Scheme S3. Synthesis of the negative control **10c-nc**. Reagents and conditions: i) *tert*-butyl (10-aminodecyl)carbamate, HATU, DIPEA, DMF, rt, 16 h. ii) TFA, DCM, rt, 1 h, 23% yield (over two steps). iii) 1-Methylpyrrolidine-3-carboxylic acid, HATU, DIPEA, DMF, rt, 16 h. iv) H₂, Pd/C, CH₃OH, rt, 16 h, 36% yield (over two steps).

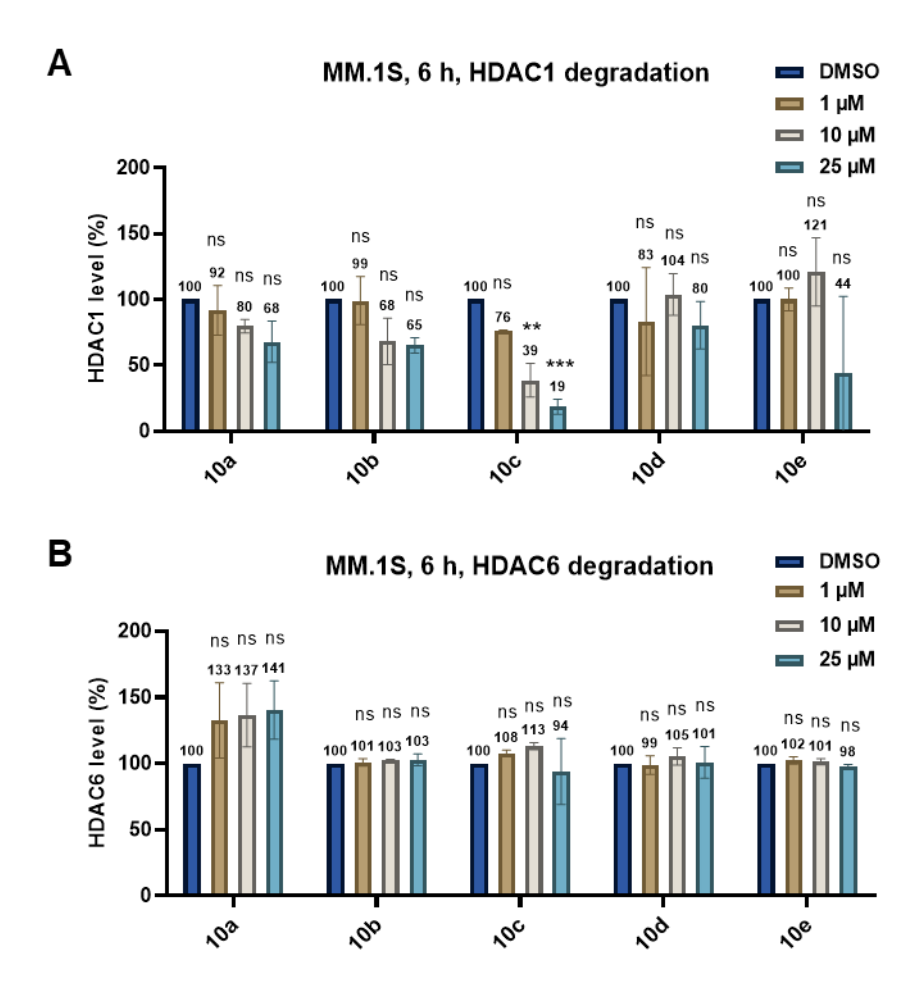


Figure S1. Densitometric analysis of HDAC1 (**A**) and HDAC6 (**B**) levels after treatment with **10a-e** for 6 h. Data from n = 2 replicates. Statistical analysis was performed by using one-way ANOVA in GraphPad Prism 8. Statistical significance was indicated with asterisks (ns = no significance; ** = p < 0.01; *** = p < 0.001).

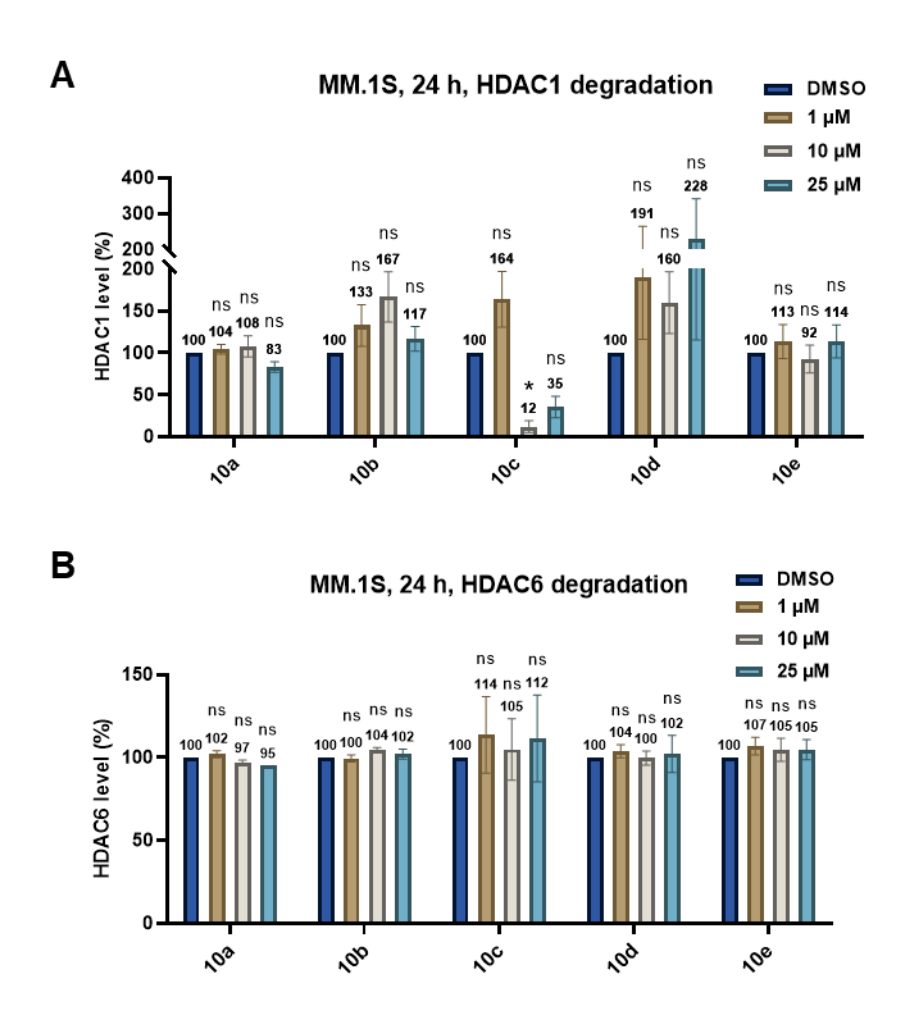


Figure S2. Densitometric analysis of HDAC1 (**A**) and HDAC6 (**B**) levels after treatment with **10a-e** for 24 h. Data from n = 2 replicates. Statistical analysis was performed by using one-way ANOVA in GraphPad Prism 8. Statistical significance was indicated with asterisks (ns = no significance; * = p < 0.05).

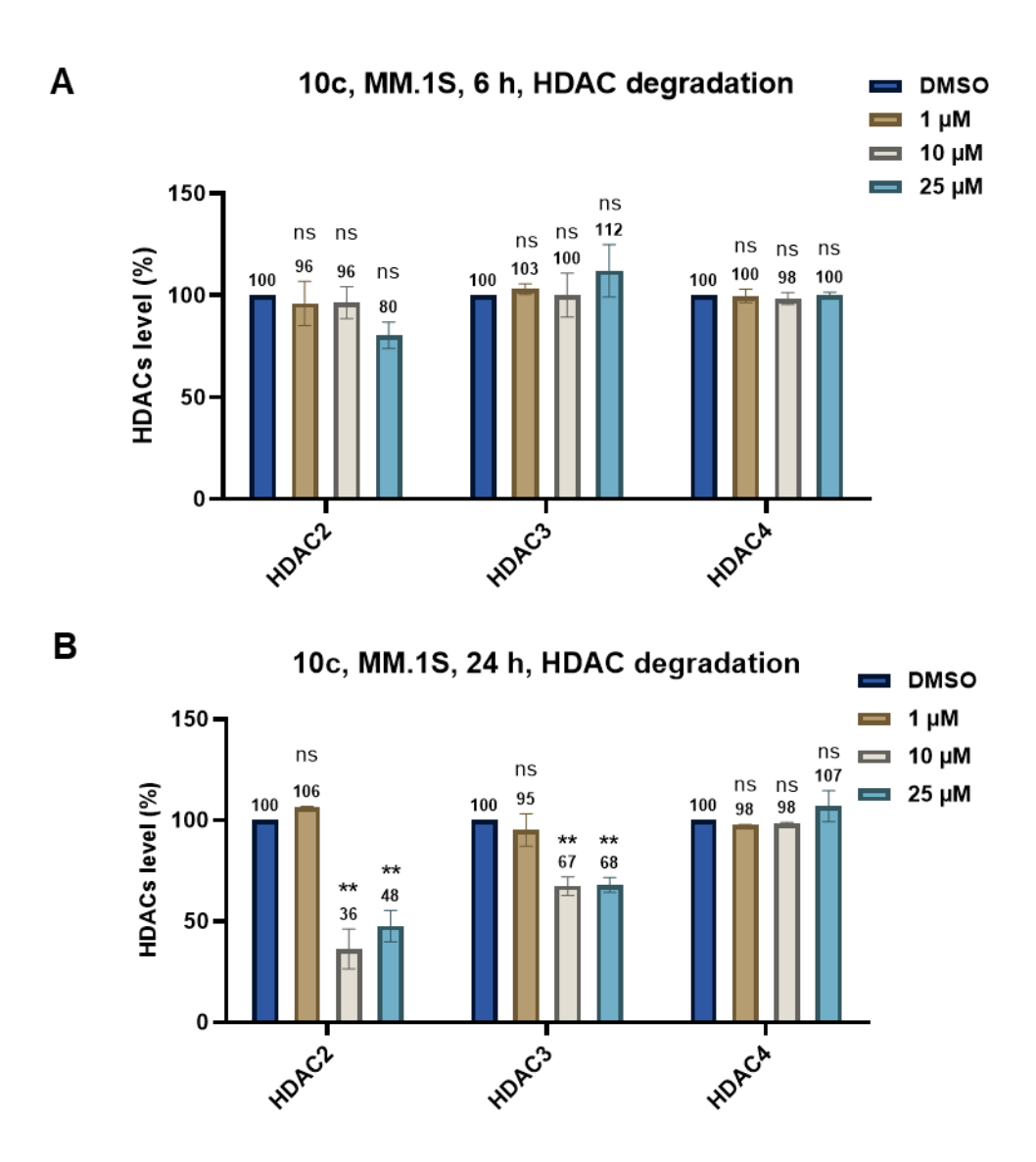


Figure S3. Densitometric analysis of HDAC2, HDAC3 and HDAC4 levels after treatment with **10c** for 6 h (**A**) or 24 h (**B**). Data from n = 2 replicates. Statistical analysis was performed by using one-way ANOVA in GraphPad Prism 8. Statistical significance was indicated with asterisks (ns = no significance; ** = p < 0.01).

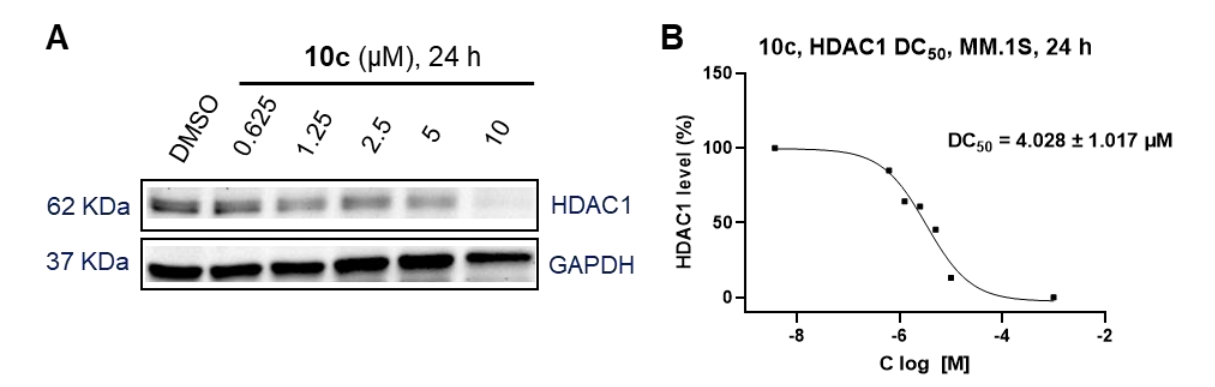


Figure S4. (A) Western blot analysis of HDAC1 levels in MM.1S cells treated for 24 h with 10c at different concentrations ranging from 0.625 to 10 μ M. GAPDH was selected as loading control. Representative image of n = 2 replicates. (B) DC₅₀ values were obtained by fitting D_{max} values to a variable slope response model. Representative curve of n = 2 replicates.

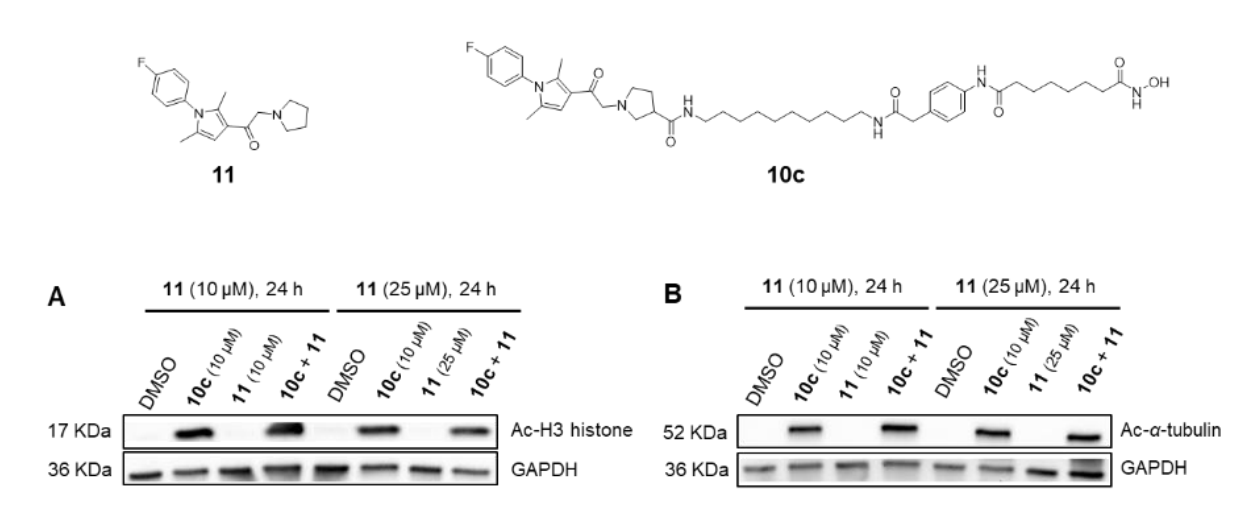


Figure S5. Cellular target engagement by 10c, 11 and co-treatment of 11 and 10c. Immunoblot analysis of acetylated histone H3 (A) and α-tubulin (B) in MM.1S cell lysates after 1 h of pre-treatment with 11 at concentration of 10 μM or 25 μM followed by 24 h of treatment with 10c (10 μM) or vehicle (DMSO). Representative images from a total of n = 2 replicates.

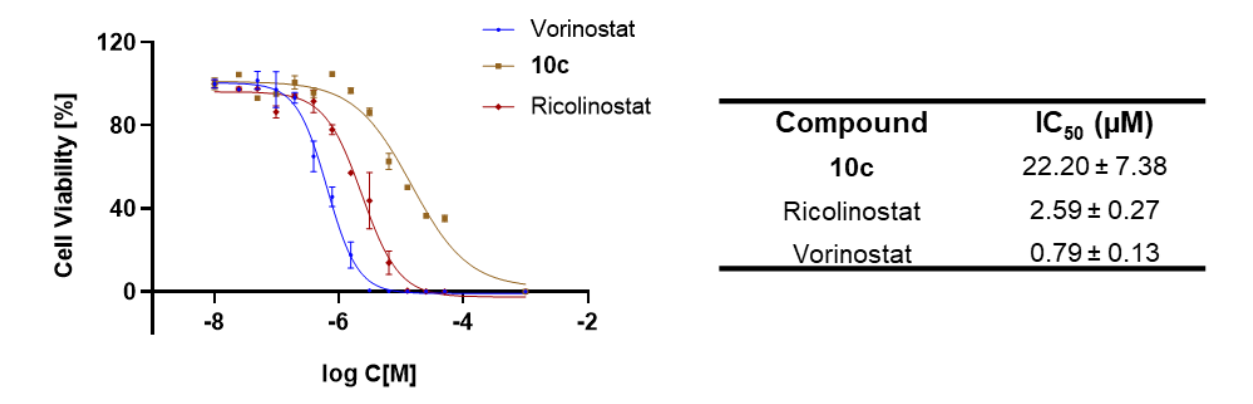
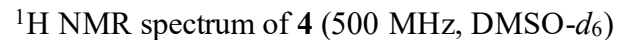
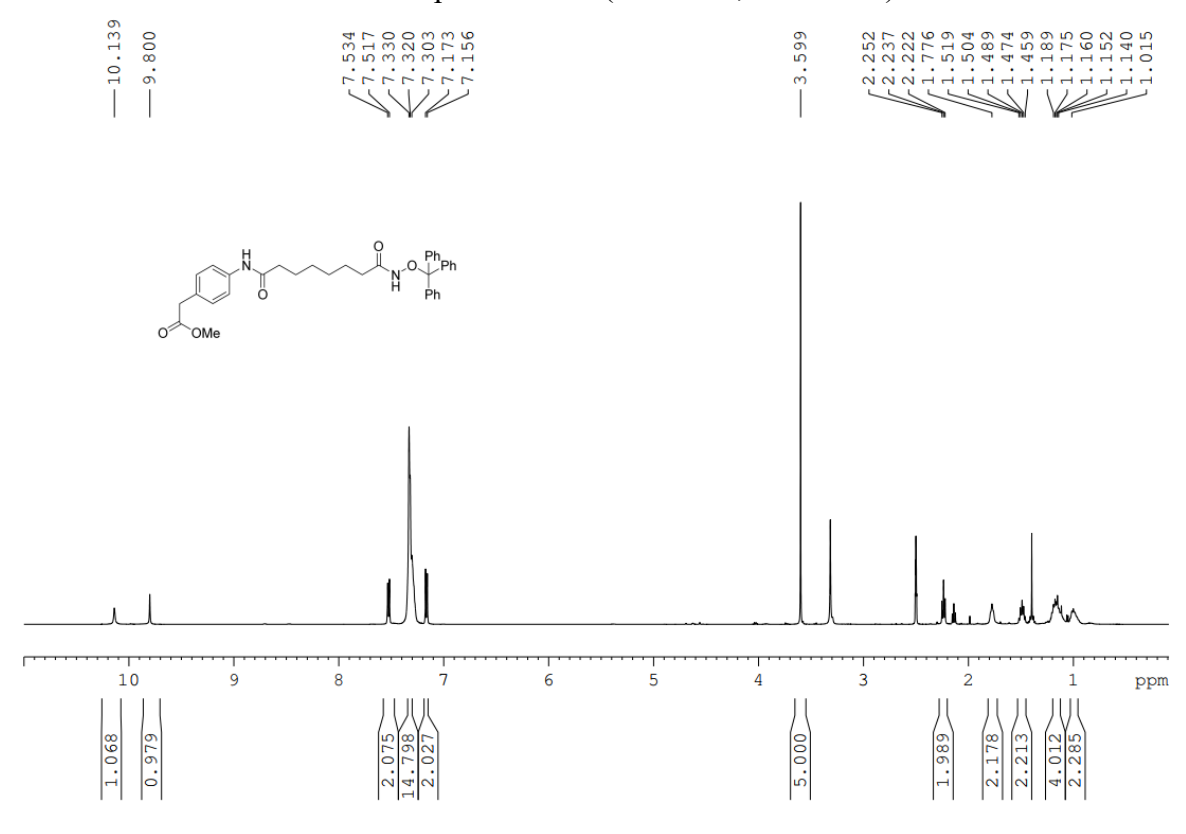


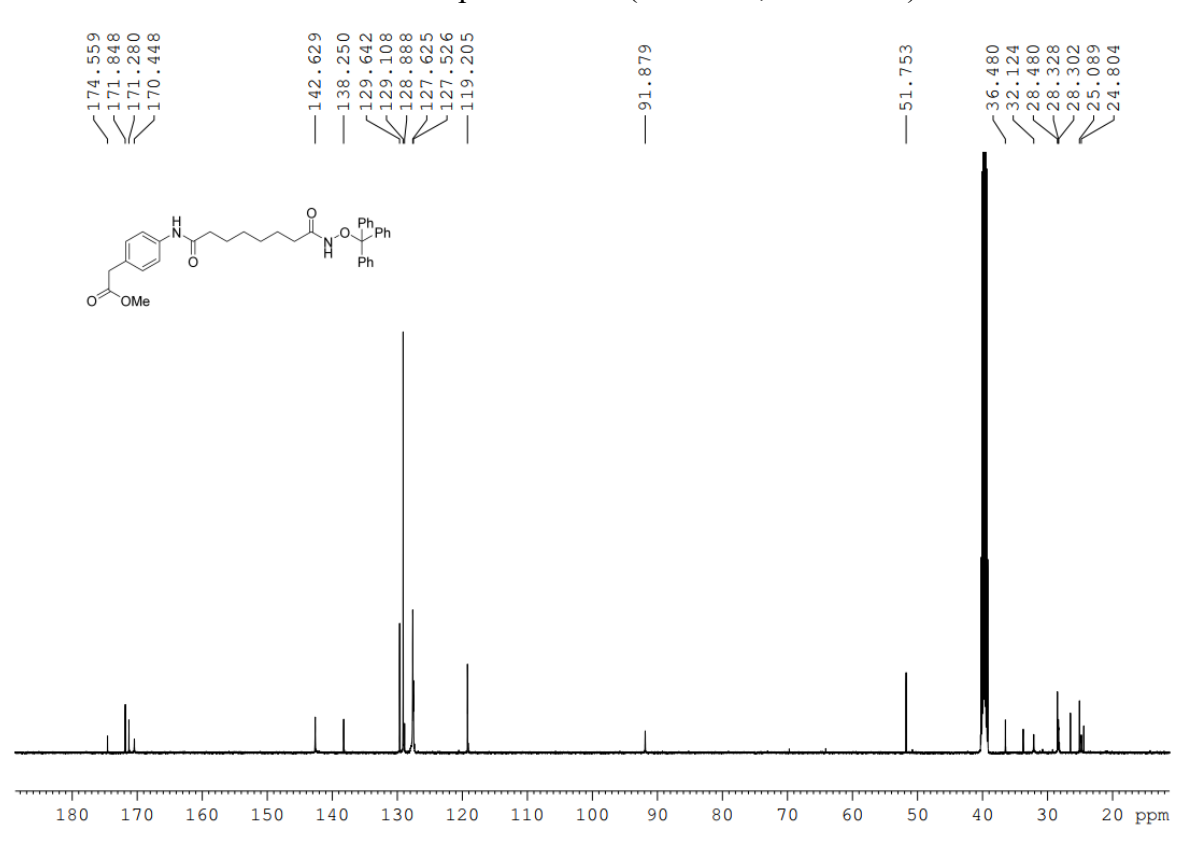
Figure S6. Antiproliferative activities of 10c against MM.1S cells. MM.1S cells were treated with the indicated compounds in increasing concentration for 72 h followed by a CellTiter-Glo® cell viability assay. n = 3 biologically independent experiments.

3. NMR data of synthesized compounds

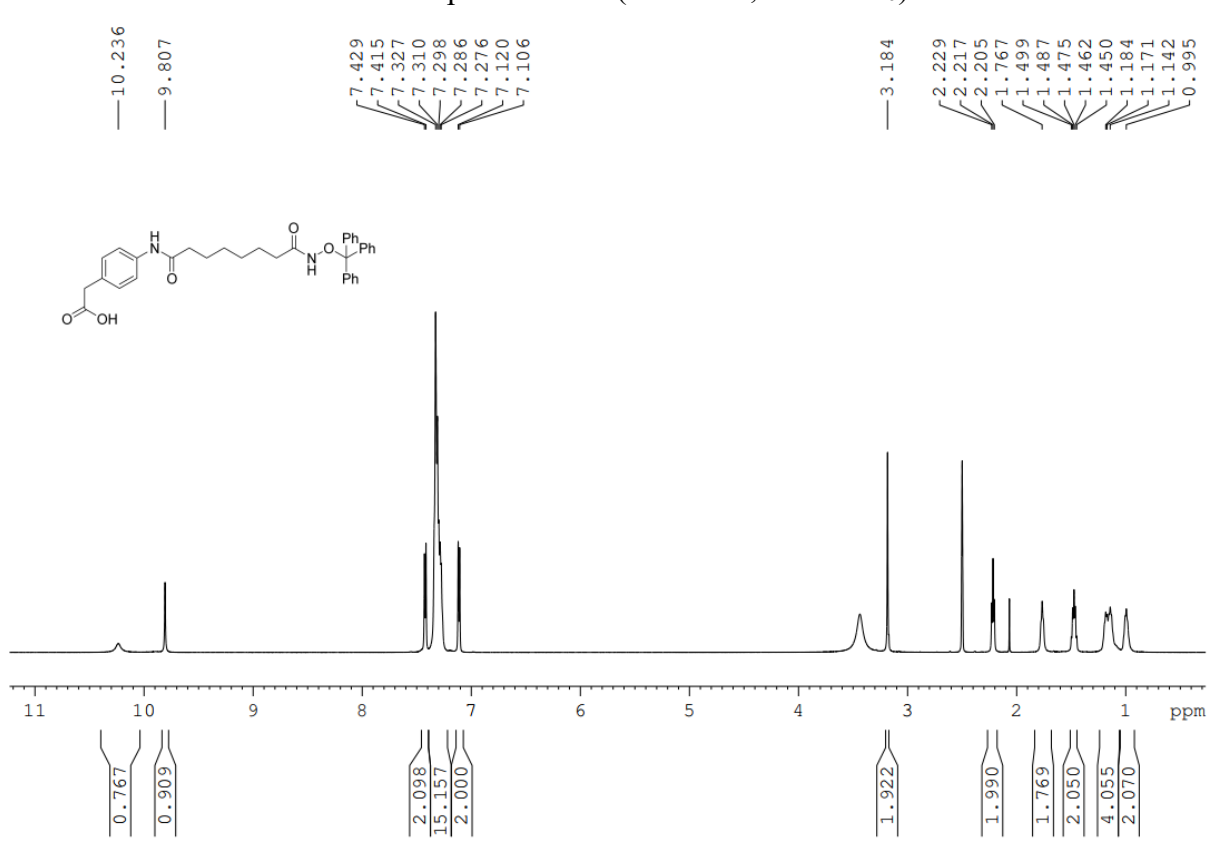




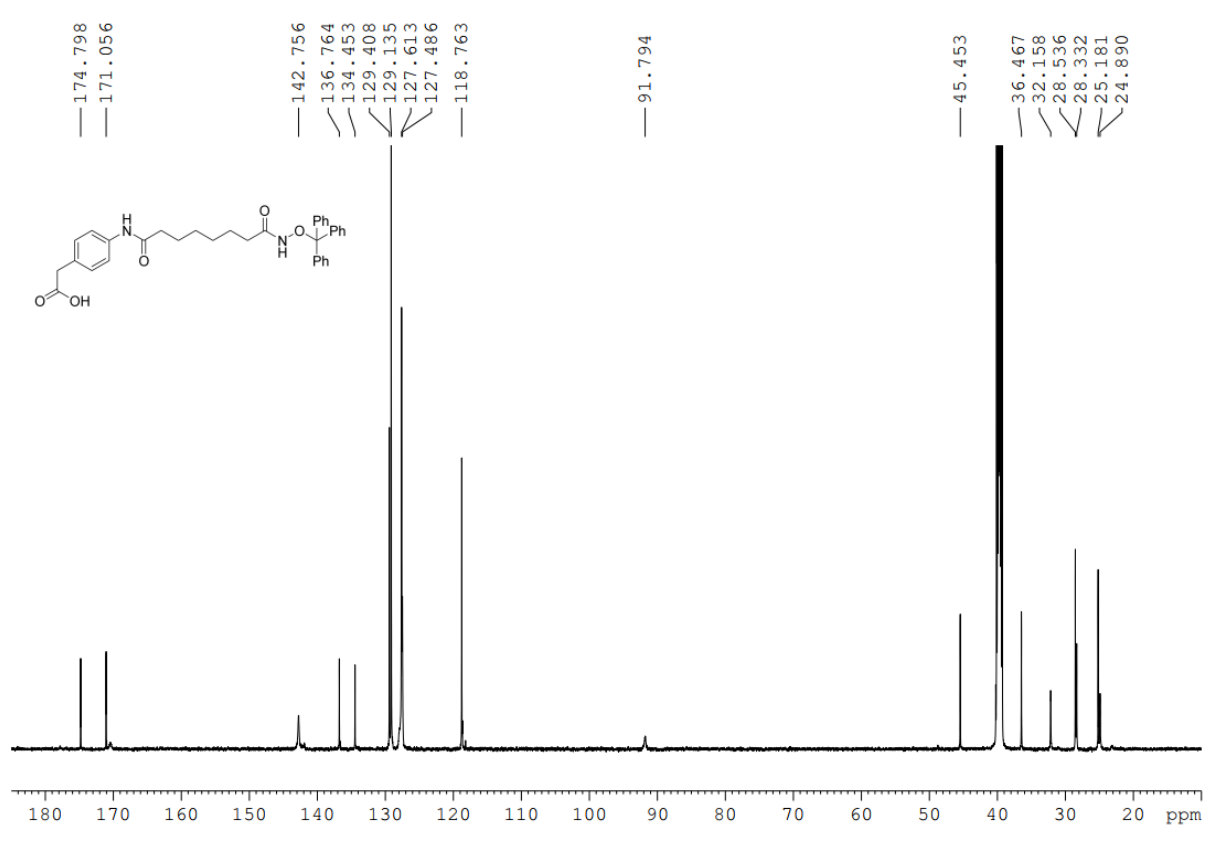
¹³C NMR spectrum of 4 (126 MHz, DMSO-*d*₆)



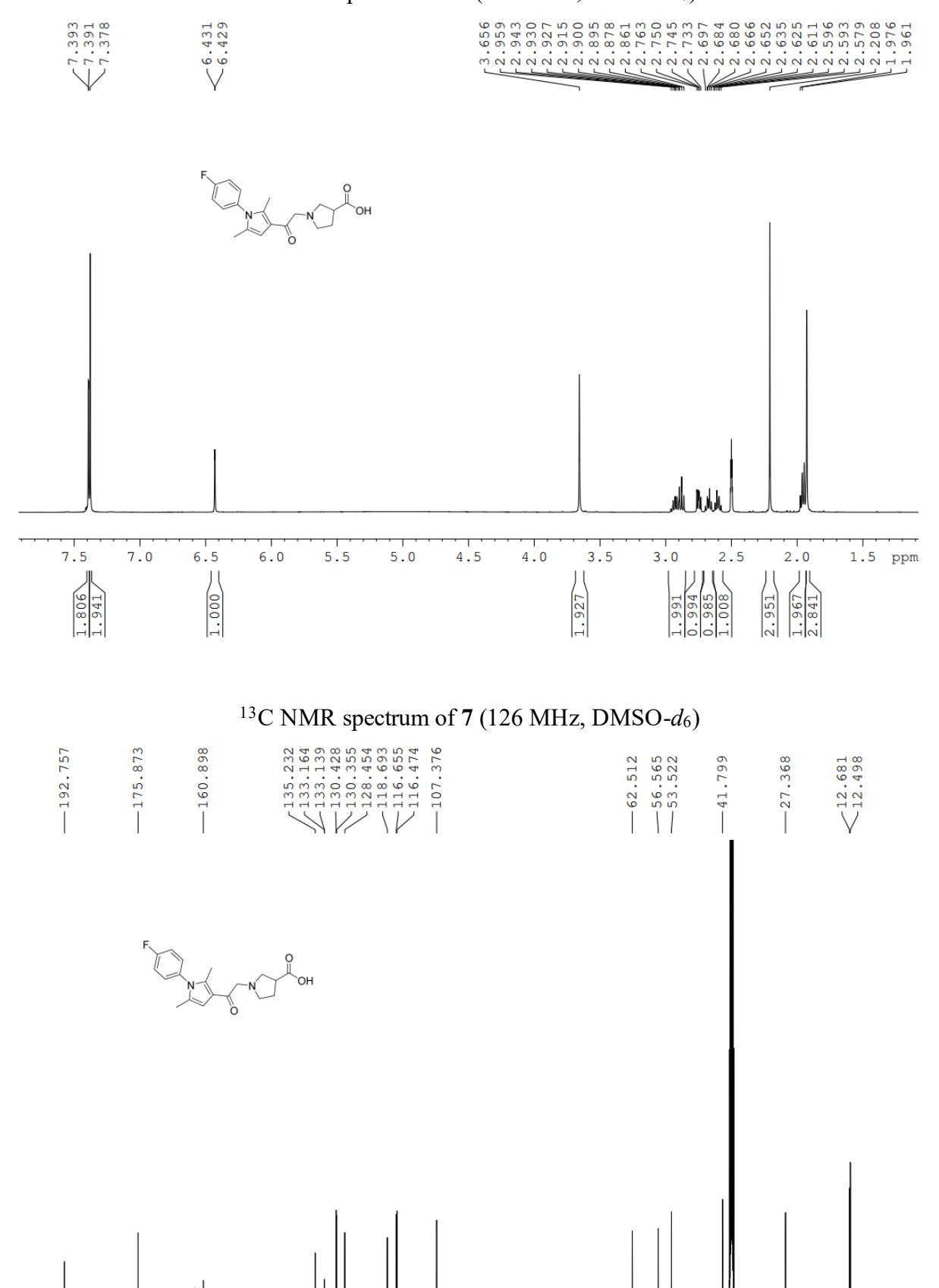
¹H NMR spectrum of **5** (600 MHz, DMSO-*d*₆)



13 C NMR spectrum of **5** (151 MHz, DMSO- d_6)



1 H NMR spectrum of **7** (500 MHz, DMSO- d_{6})



80 70

50

60

40

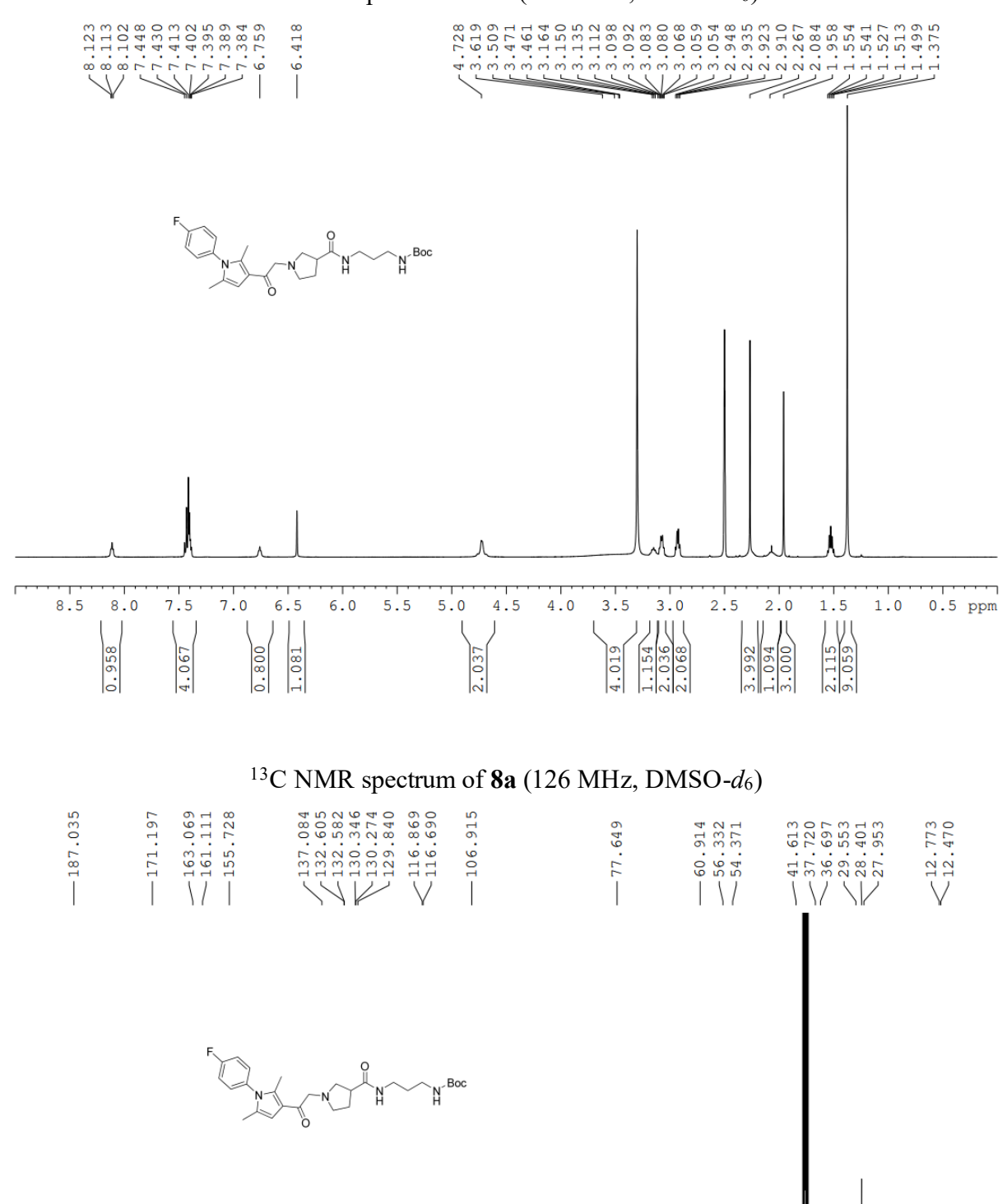
30

20

10 ppm

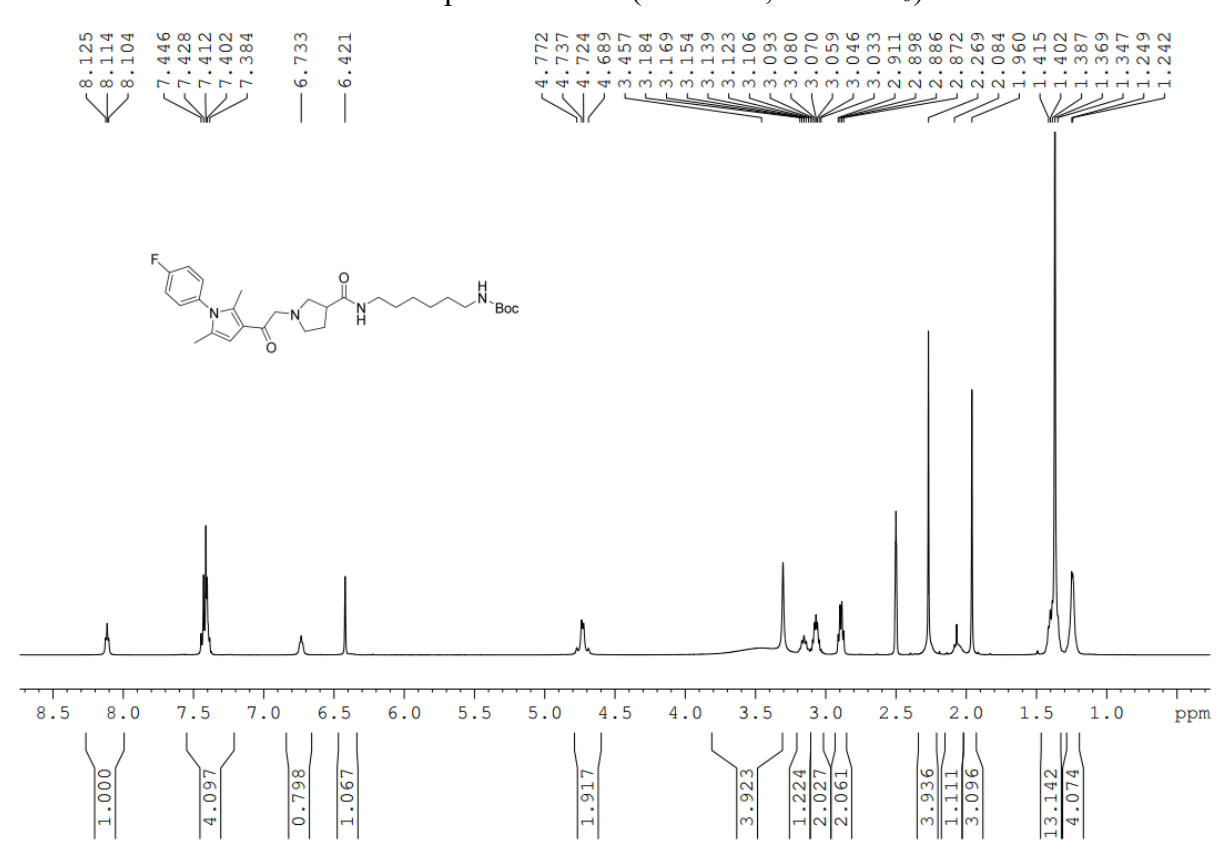
190 180 170 160 150 140 130 120 110 100 90

¹H NMR spectrum of **8a** (500 MHz, DMSO-*d*₆)

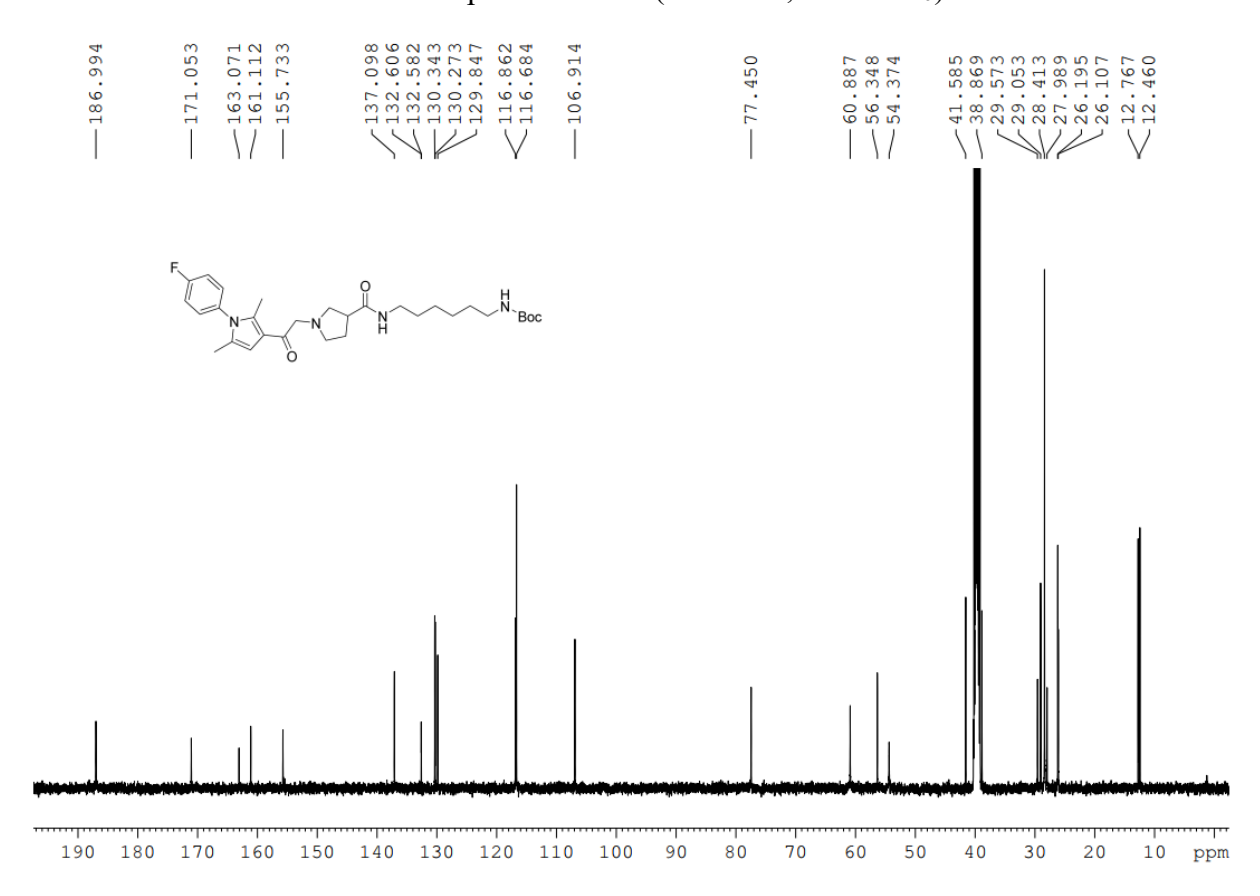


190 180 170 160 150 140 130 120 110

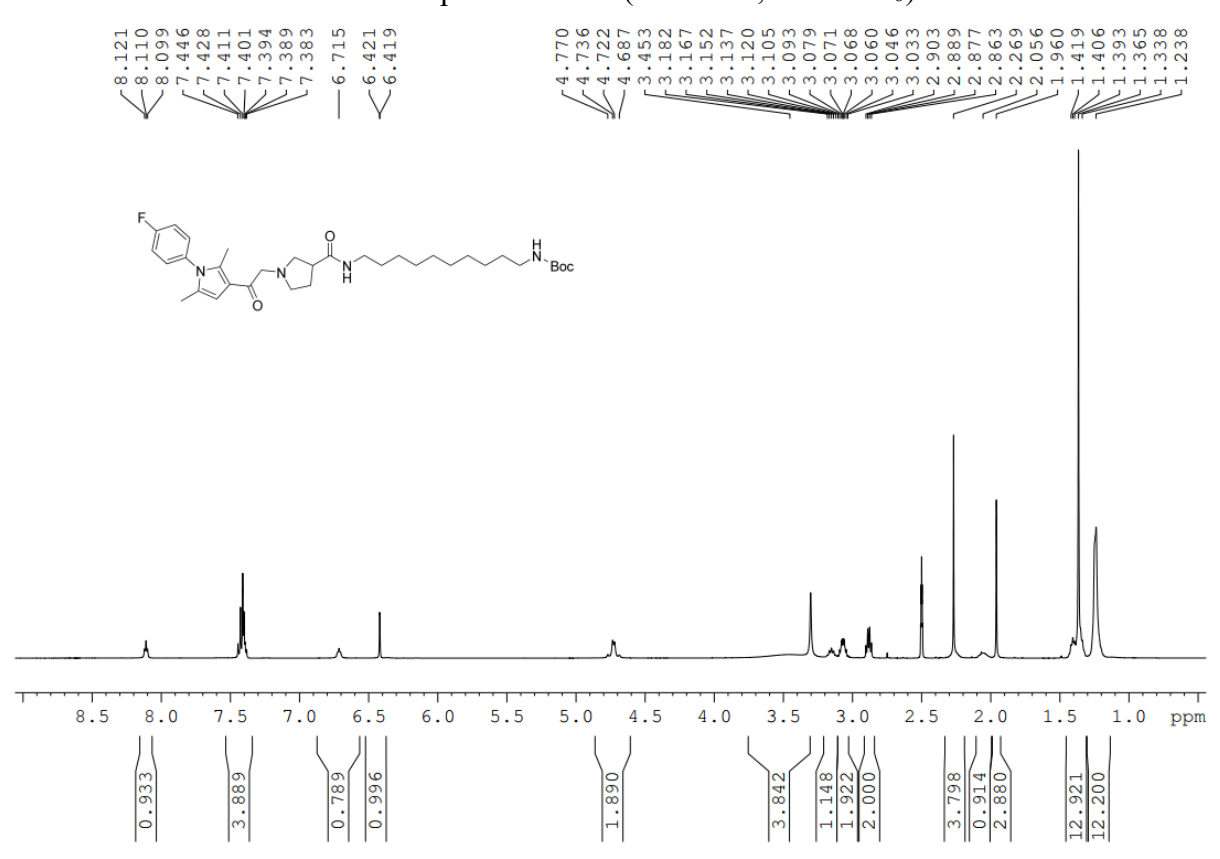
¹H NMR spectrum of **8b** (500 MHz, DMSO-*d*₆)



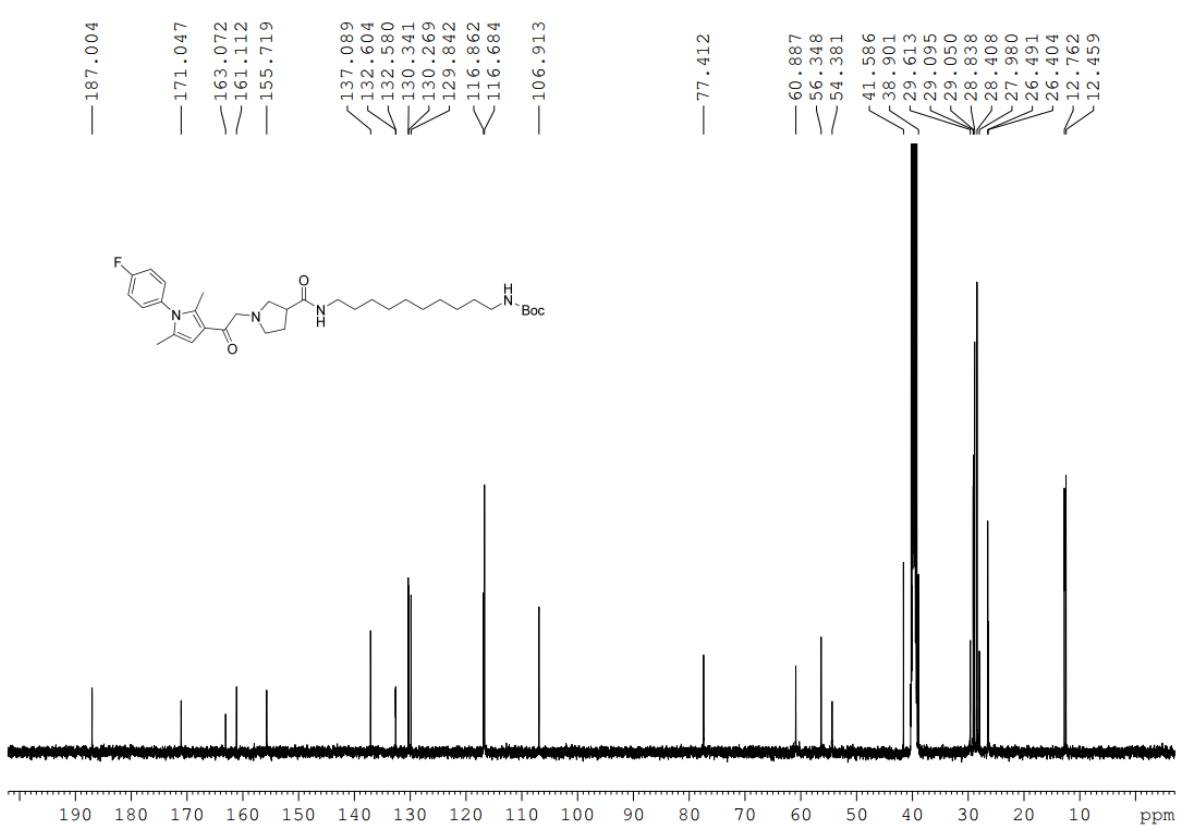
¹³C NMR spectrum of **8b** (126 MHz, DMSO-*d*₆)



¹H NMR spectrum of **8c** (500 MHz, DMSO-*d*₆)

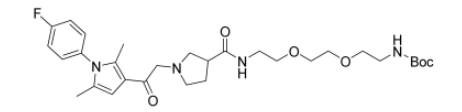


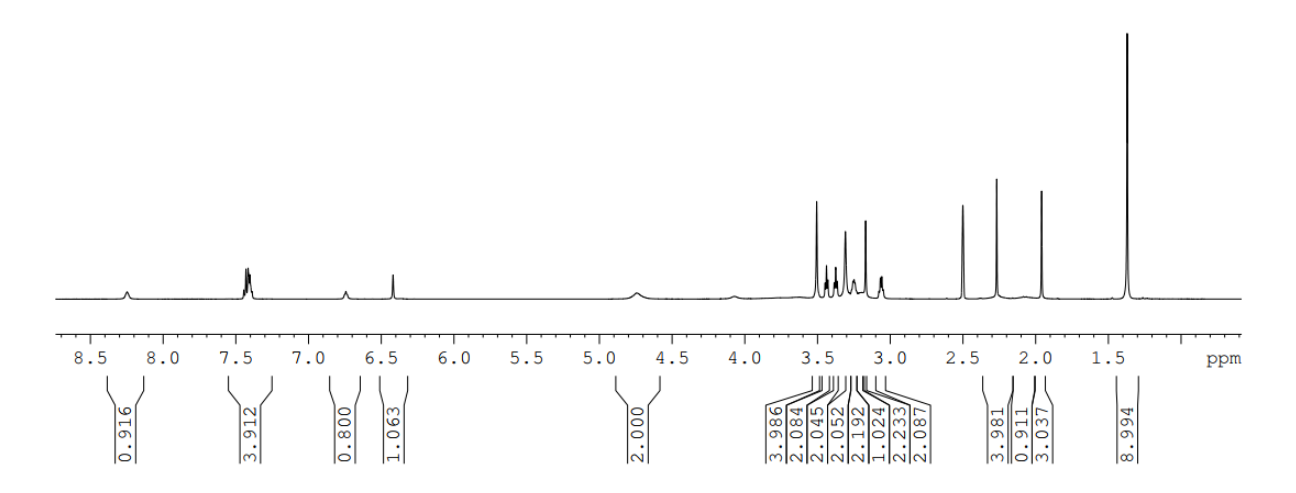
13 C NMR spectrum of **8c** (126 MHz, DMSO- d_6)



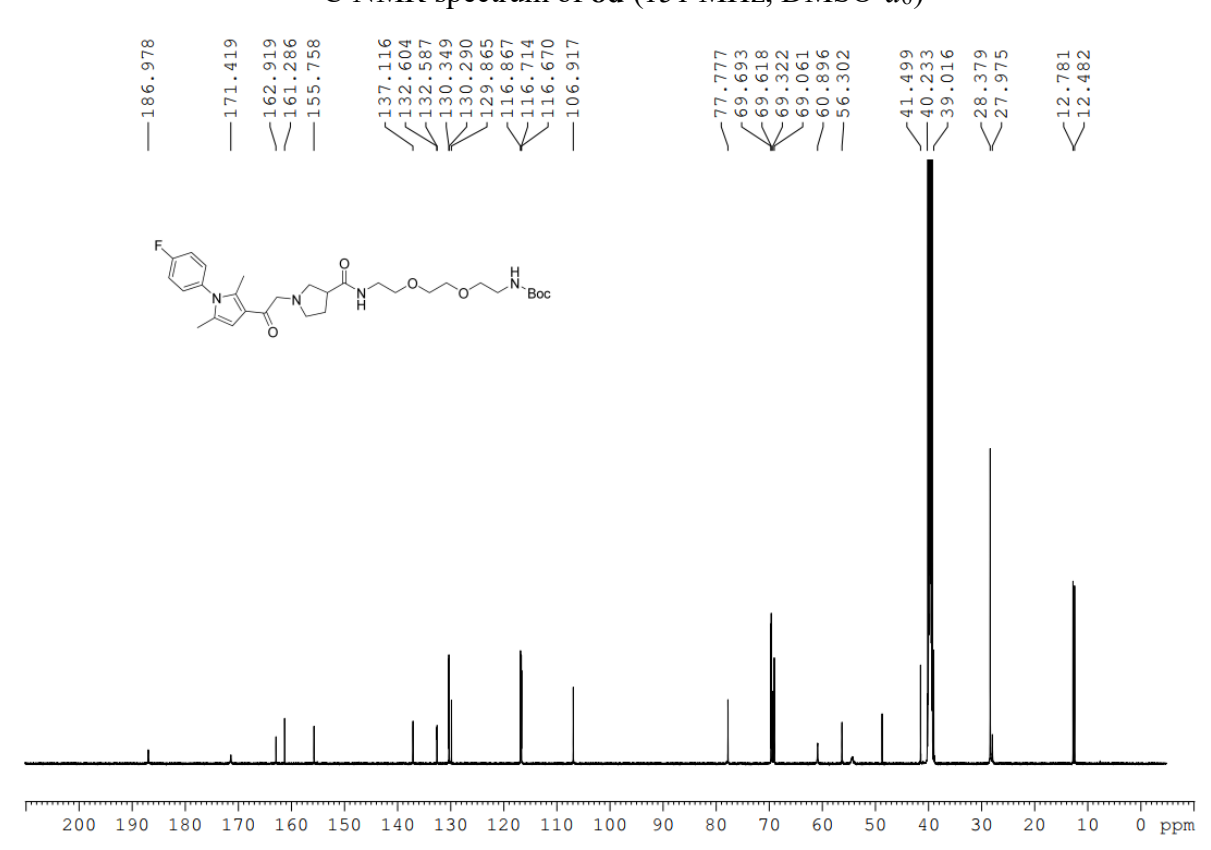
¹H NMR spectrum of **8d** (600 MHz, DMSO-*d*₆)



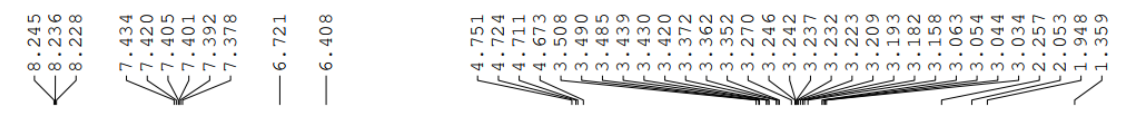


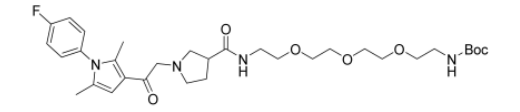


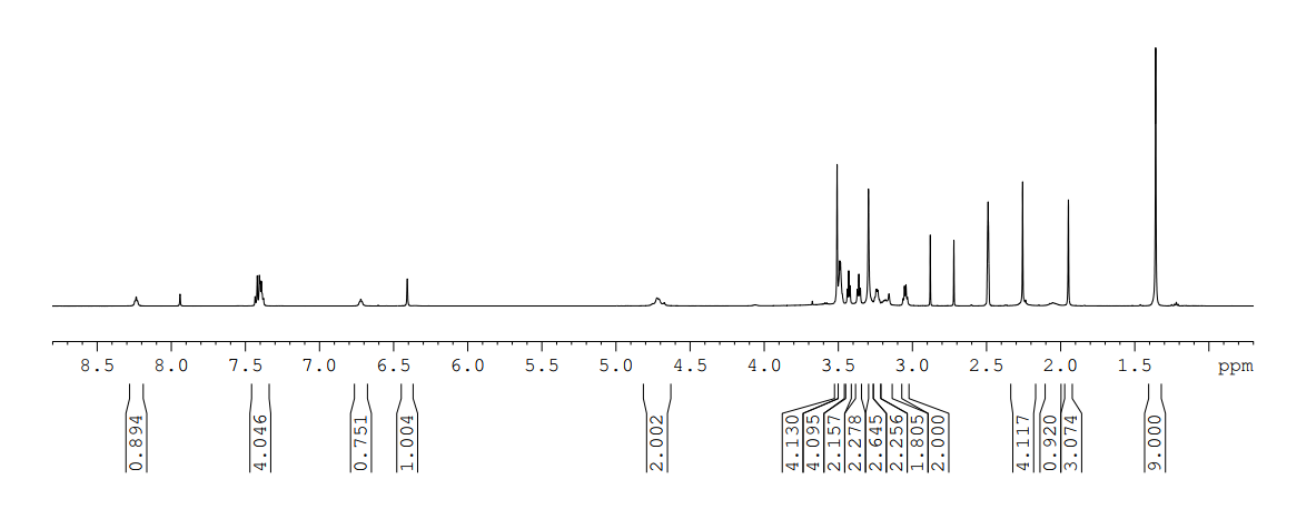
13 C NMR spectrum of **8d** (151 MHz, DMSO- d_6)



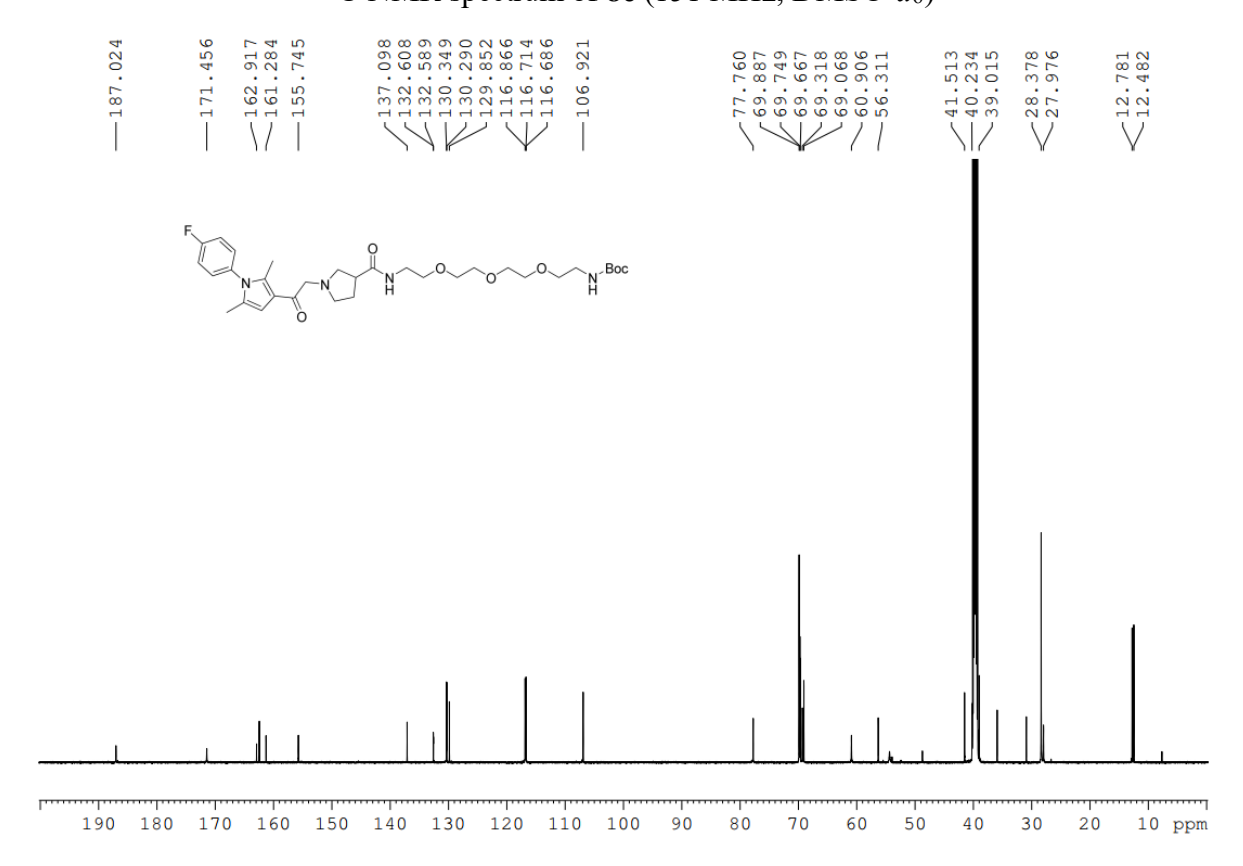
¹H NMR spectrum of **8e** (600 MHz, DMSO-*d*₆)



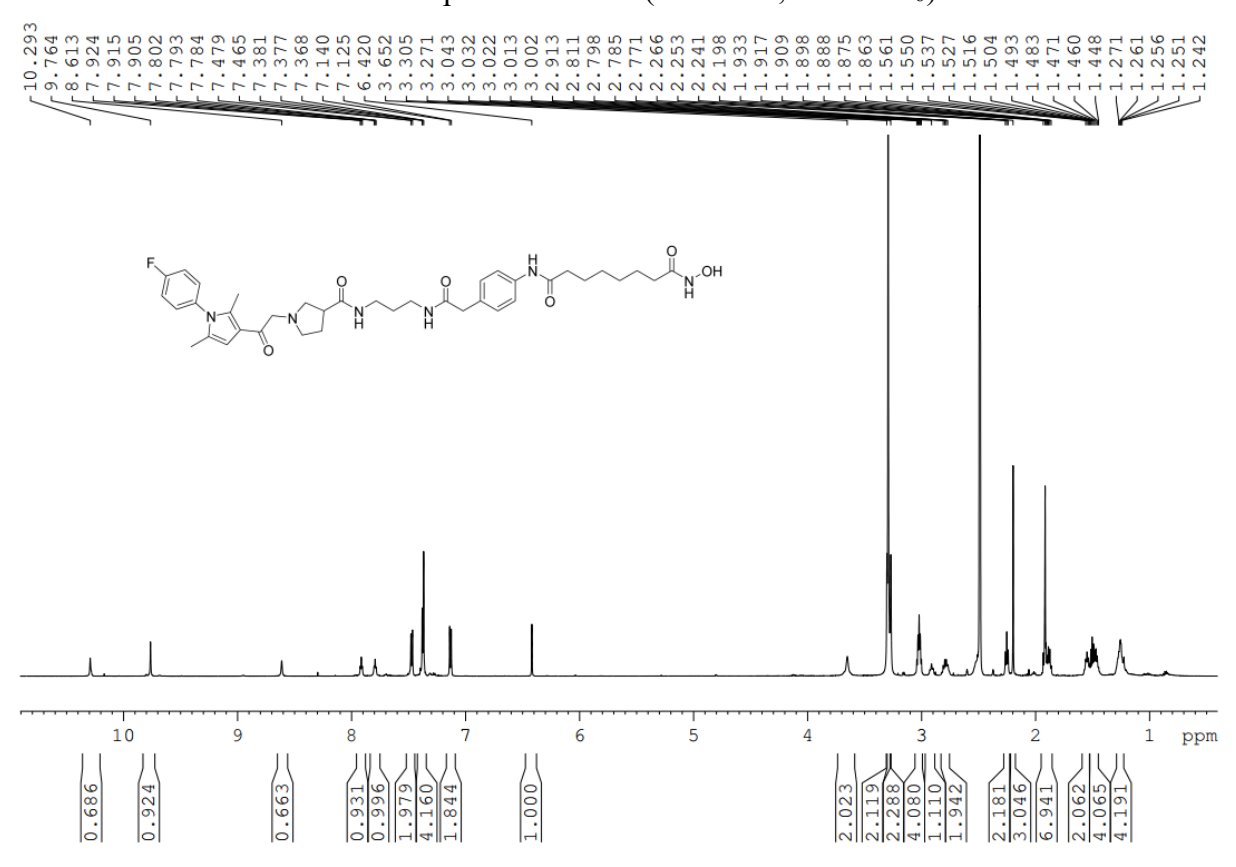




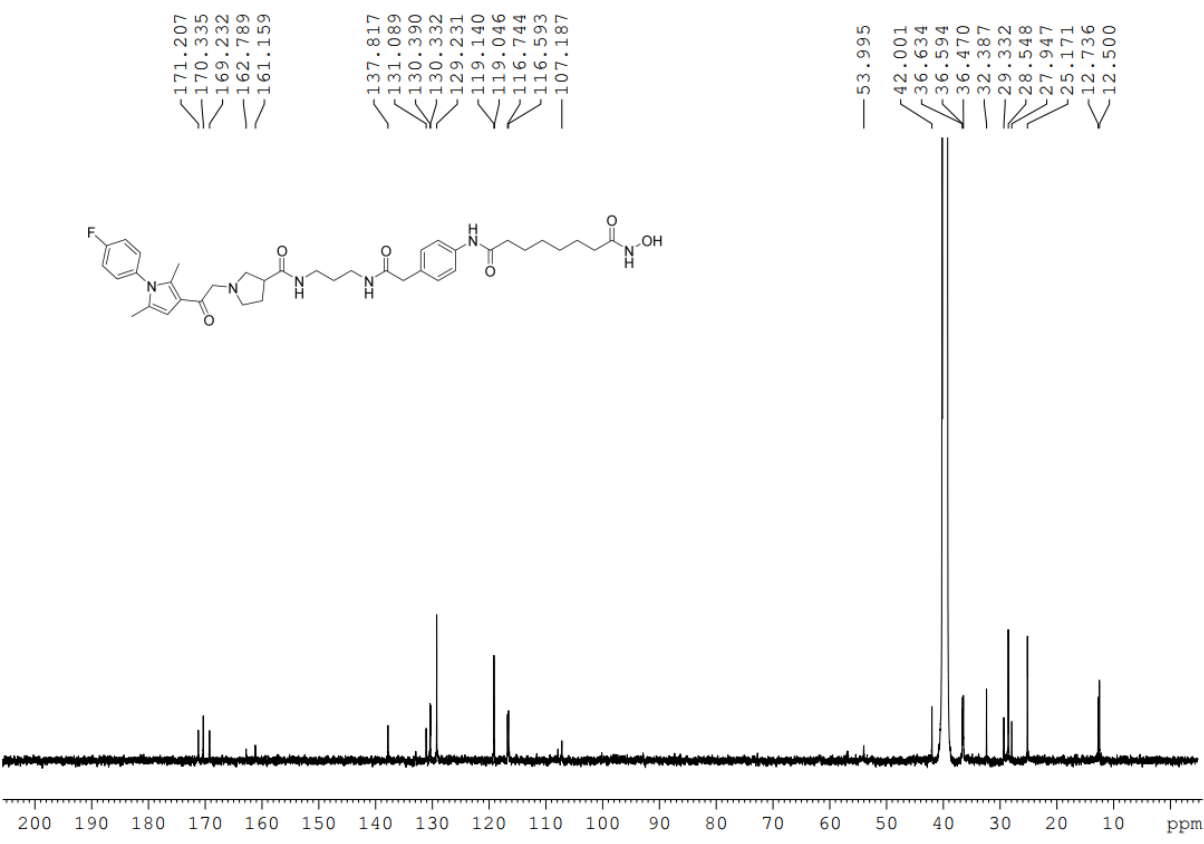
¹³C NMR spectrum of **8e** (151 MHz, DMSO-*d*₆)



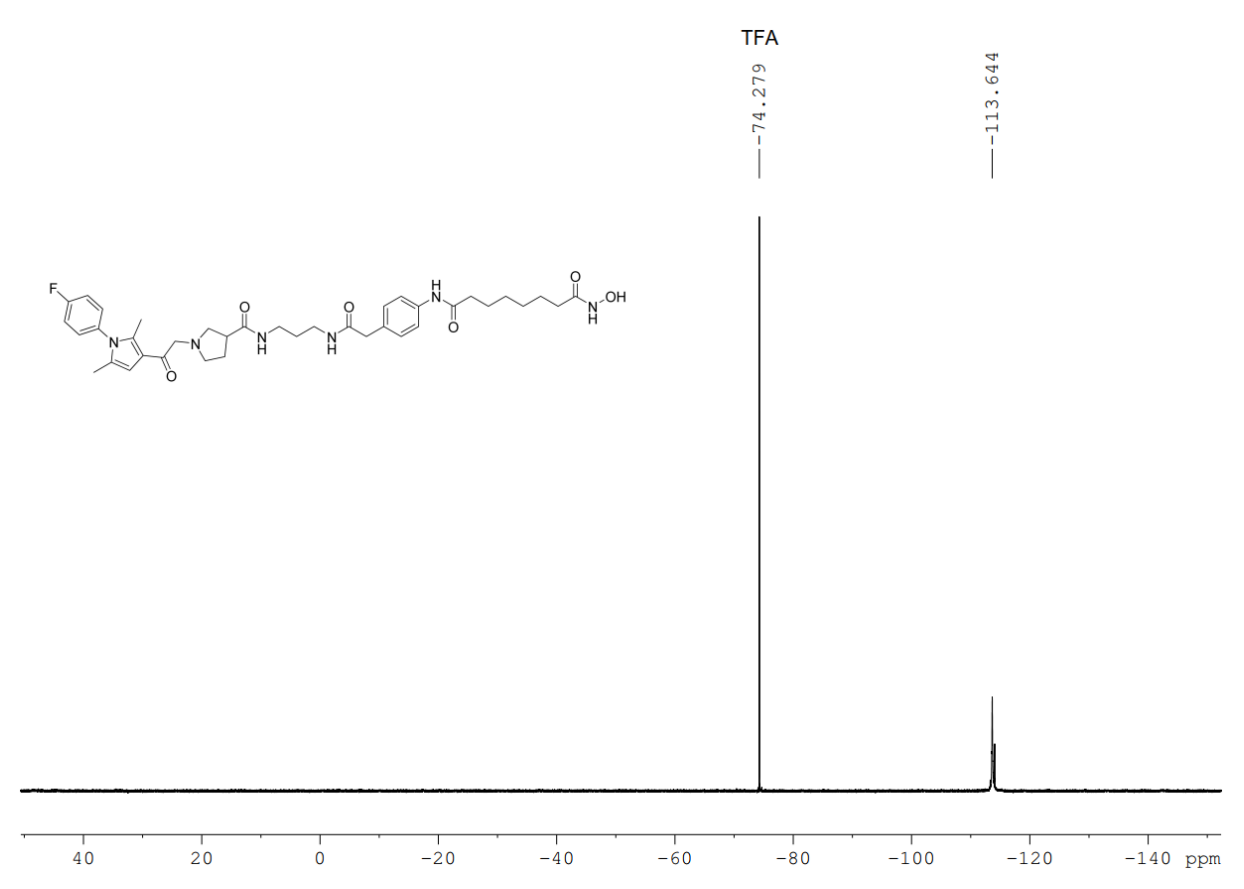
¹H NMR spectrum of **10a** (600 MHz, DMSO-*d*₆)



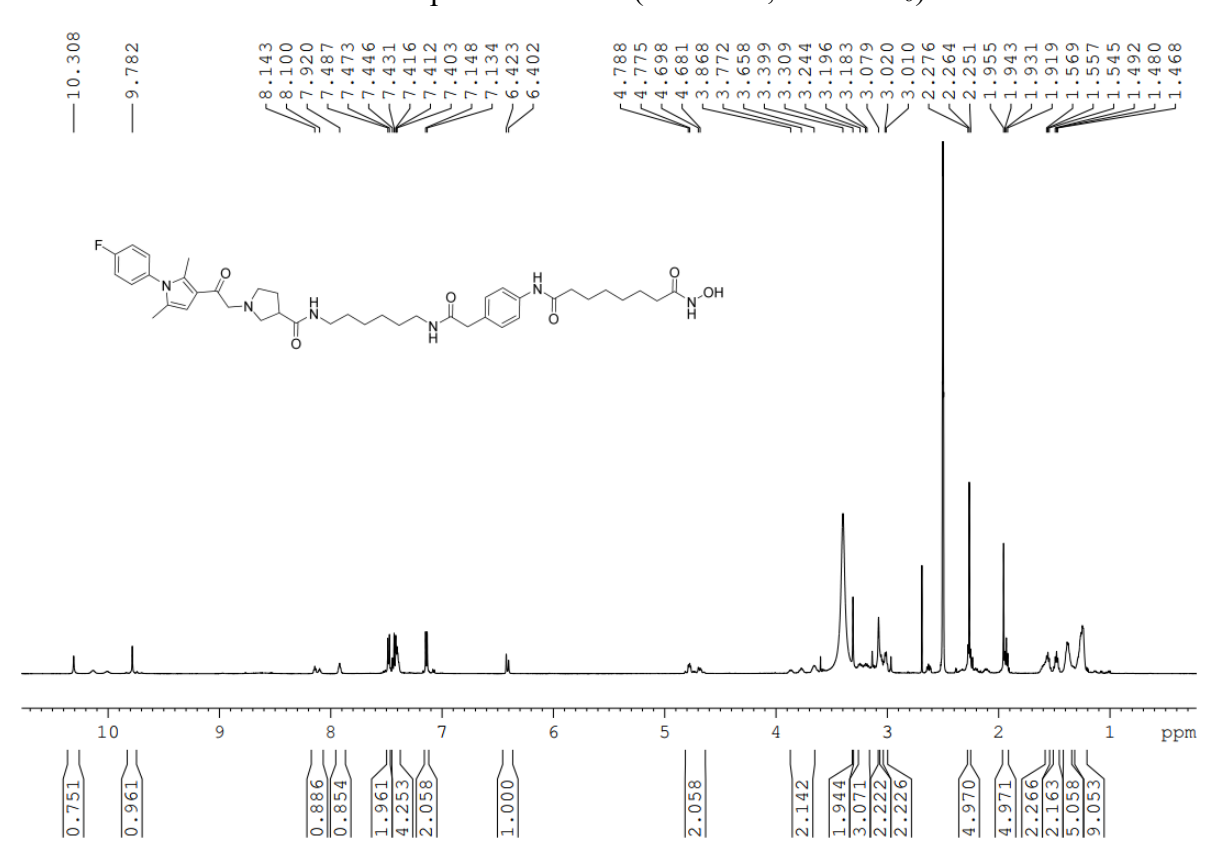
13 C NMR spectrum of **10a** (151 MHz, DMSO- d_6)



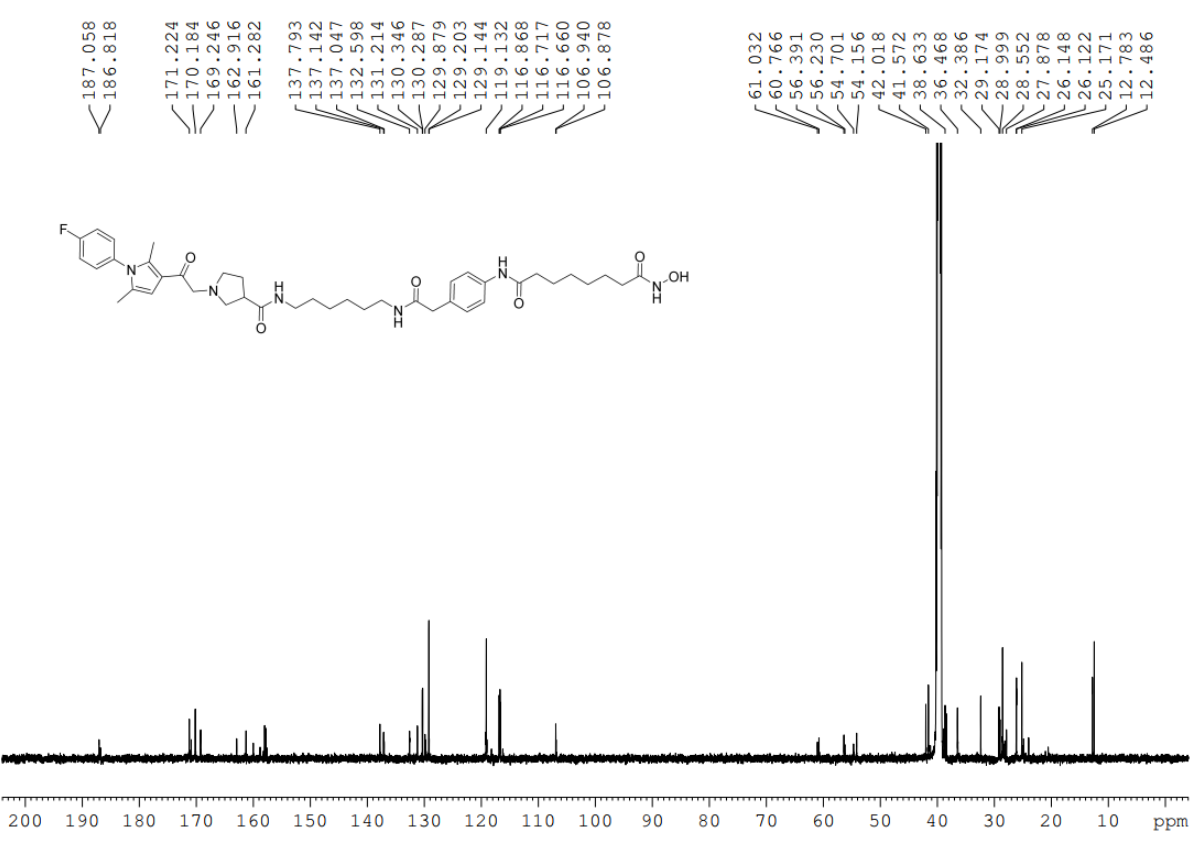
19 F NMR spectrum of **10a** (565 MHz, DMSO- d_6)



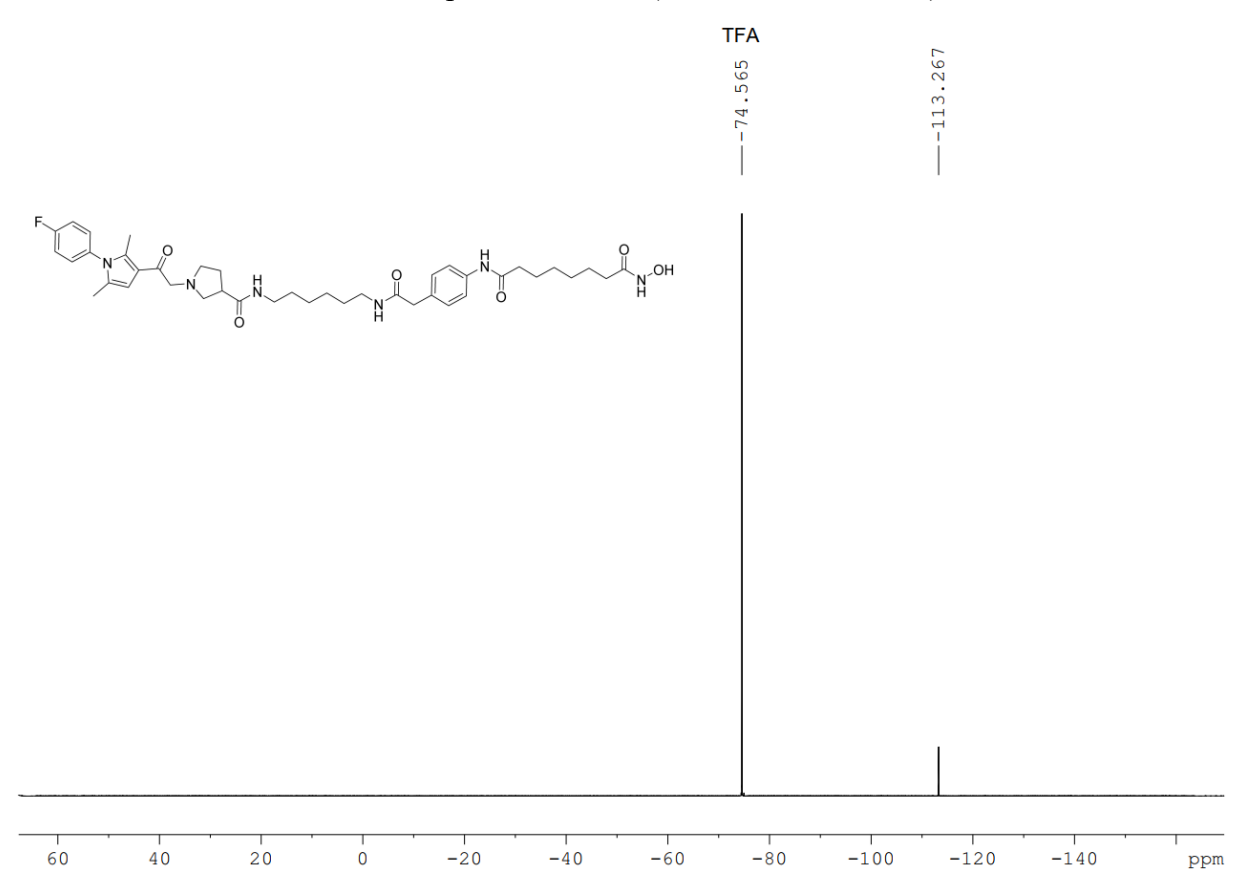
¹H NMR spectrum of **10b** (600 MHz, DMSO-*d*₆)



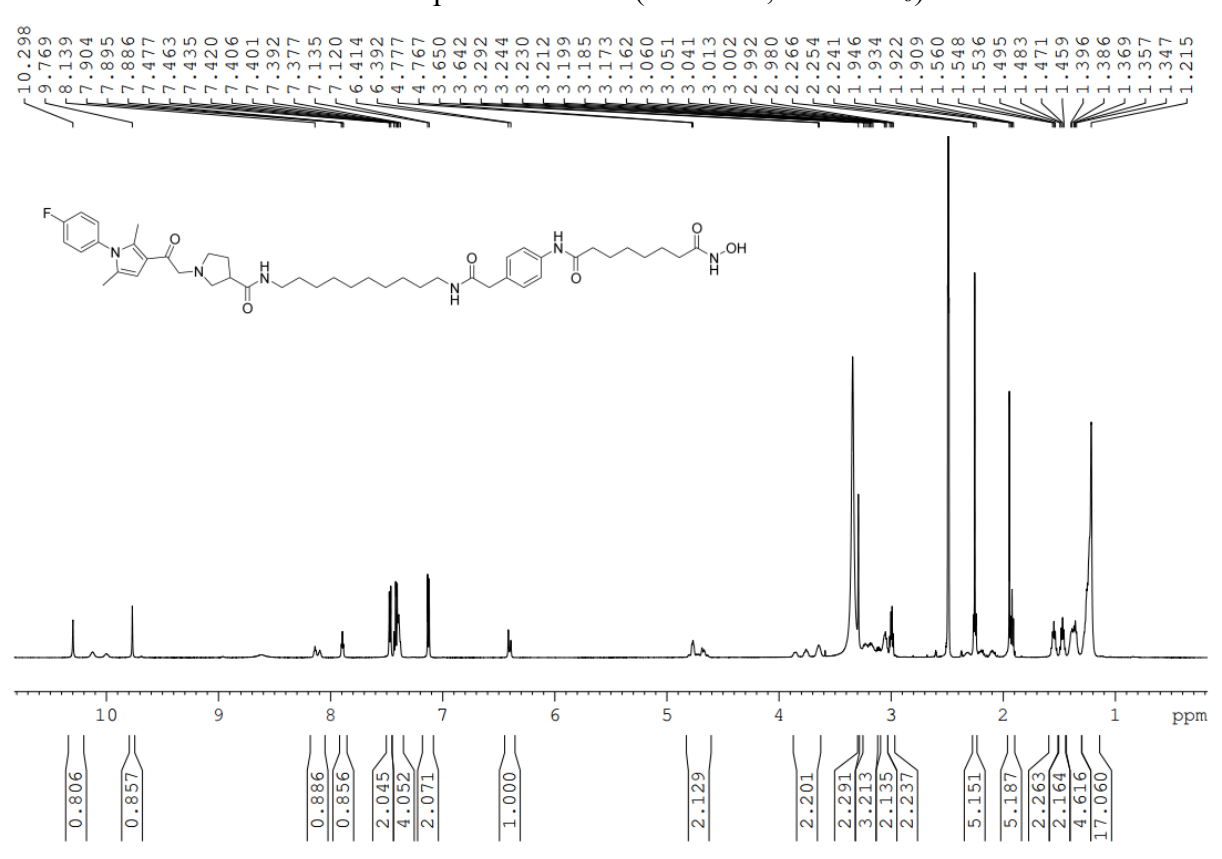
13 C NMR spectrum of **10b** (151 MHz, DMSO- d_6)



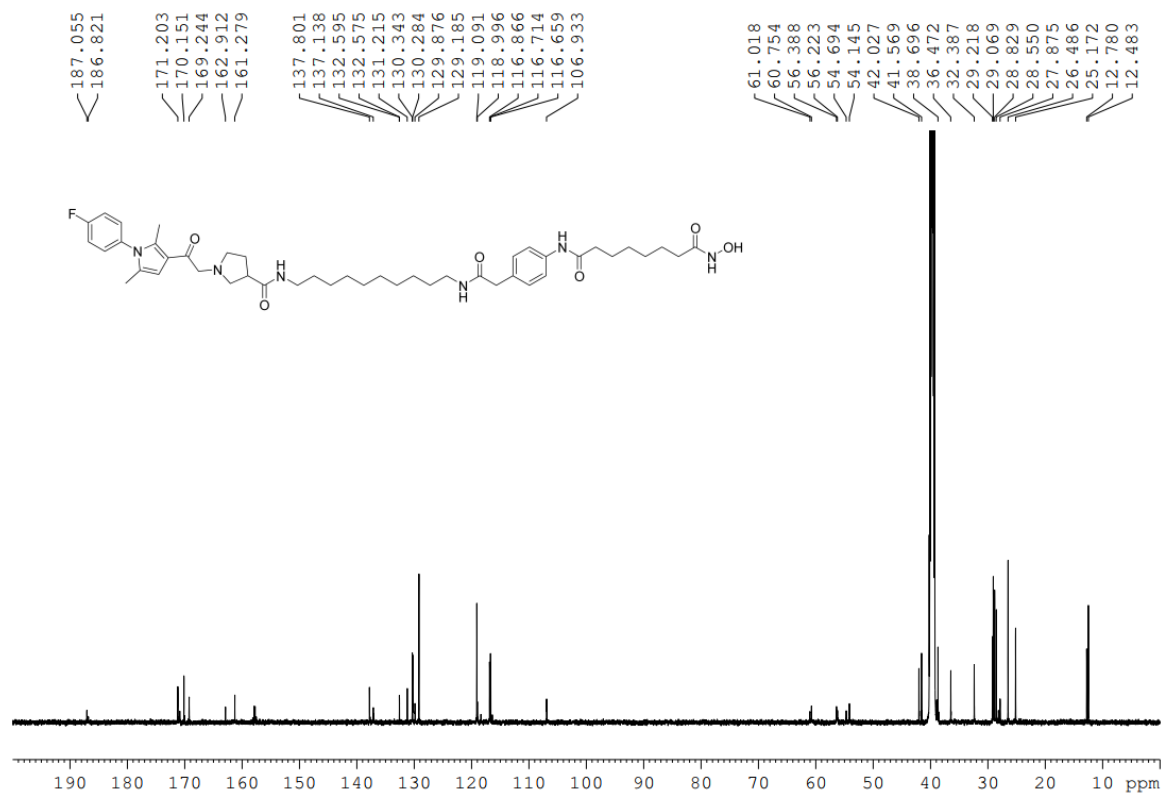
19 F NMR spectrum of **10b** (565 MHz, DMSO- d_6)



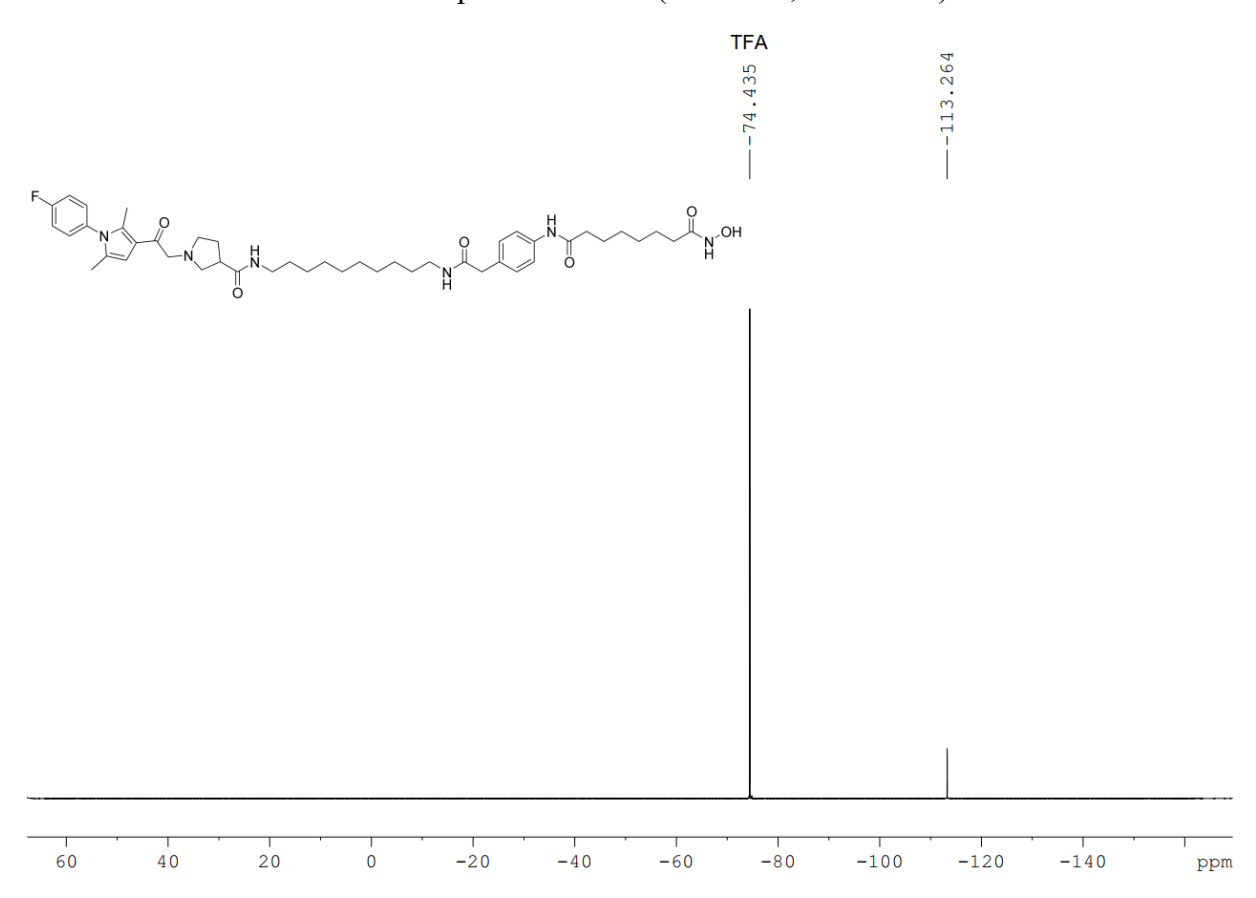
¹H NMR spectrum of **10c** (600 MHz, DMSO-*d*₆)



13 C NMR spectrum of **10c** (151 MHz, DMSO- d_6)

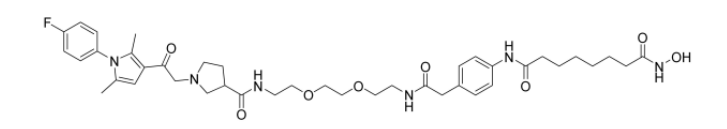


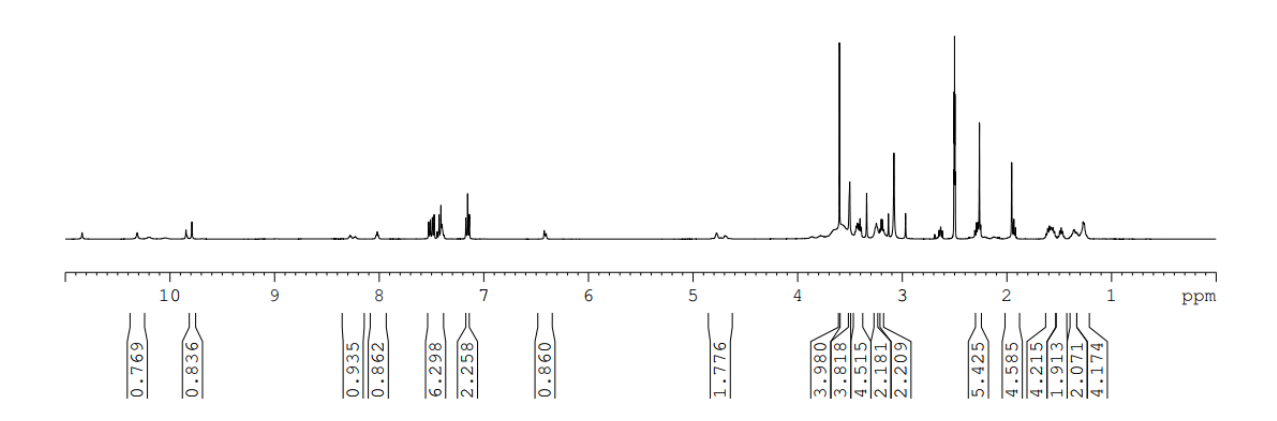
19 F NMR spectrum of **10c** (565 MHz, DMSO- d_6)



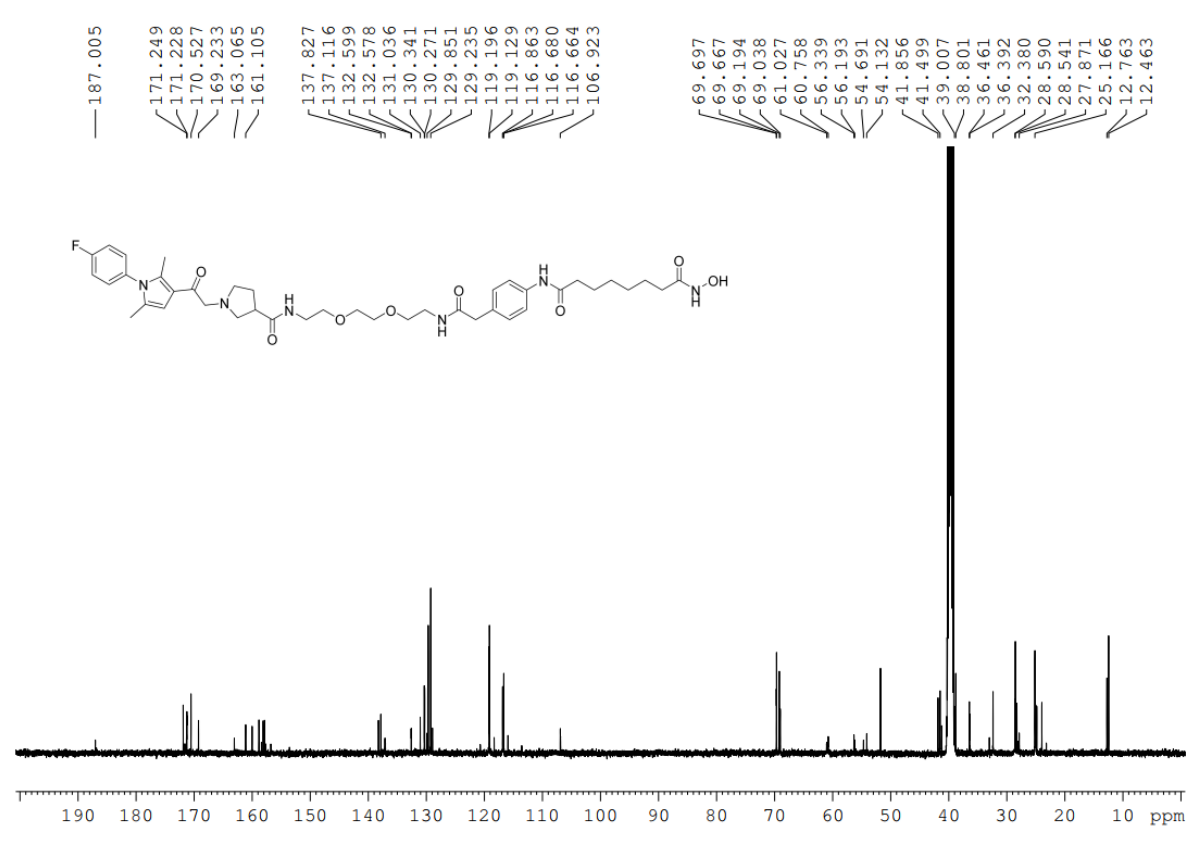
¹H NMR spectrum of **10d** (500 MHz, DMSO-*d*₆)



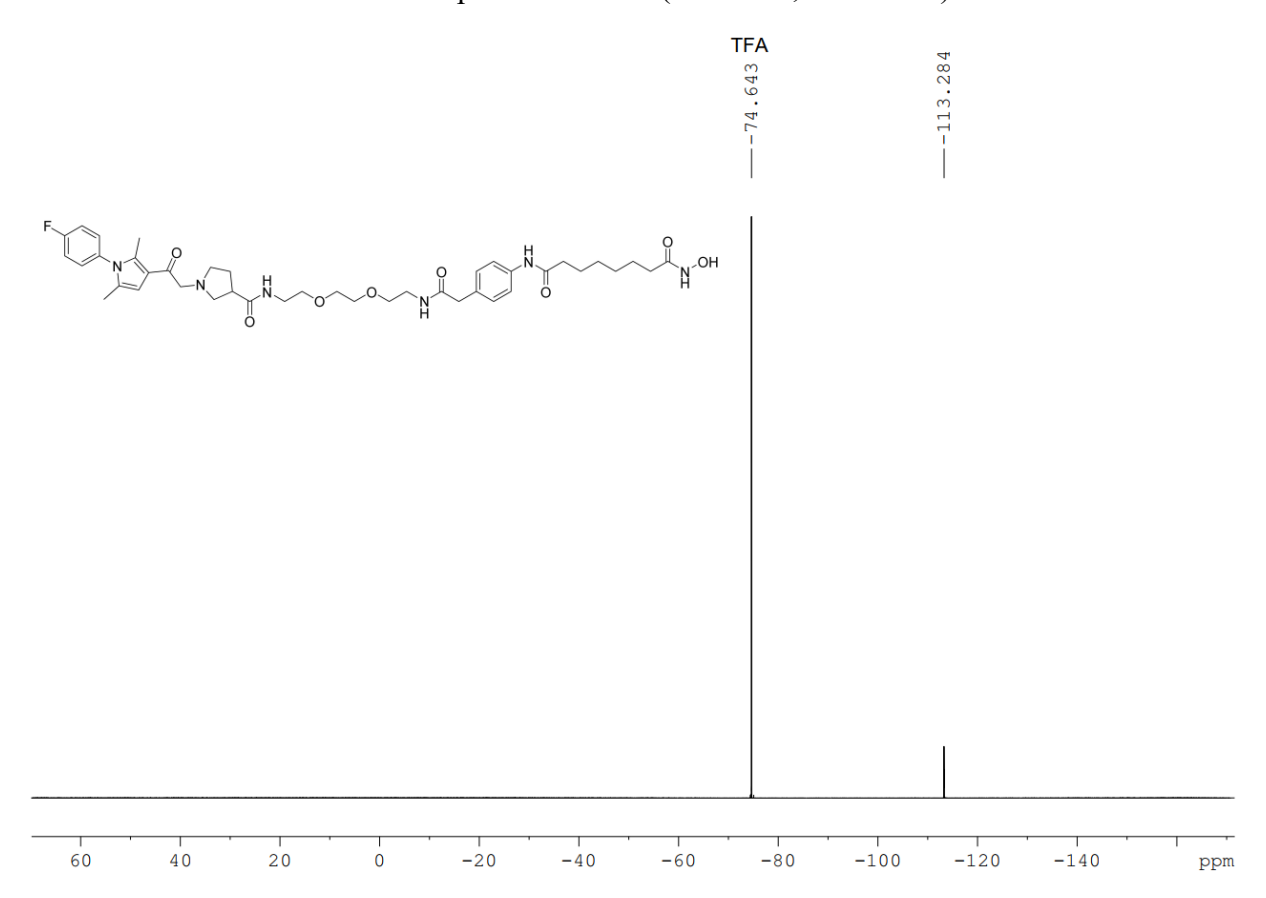




13 C NMR spectrum of **10d** (126 MHz, DMSO- d_6)

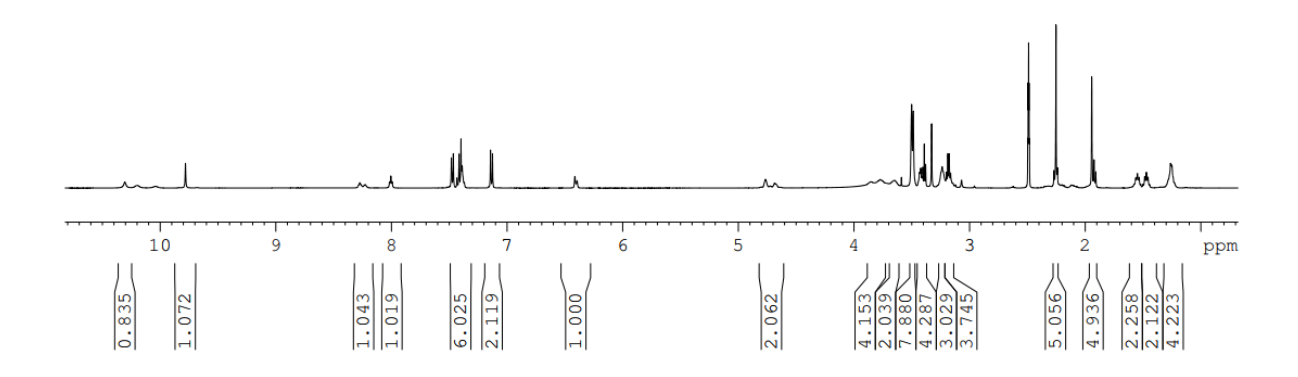


19 F NMR spectrum of **10d** (471 MHz, DMSO- d_6)

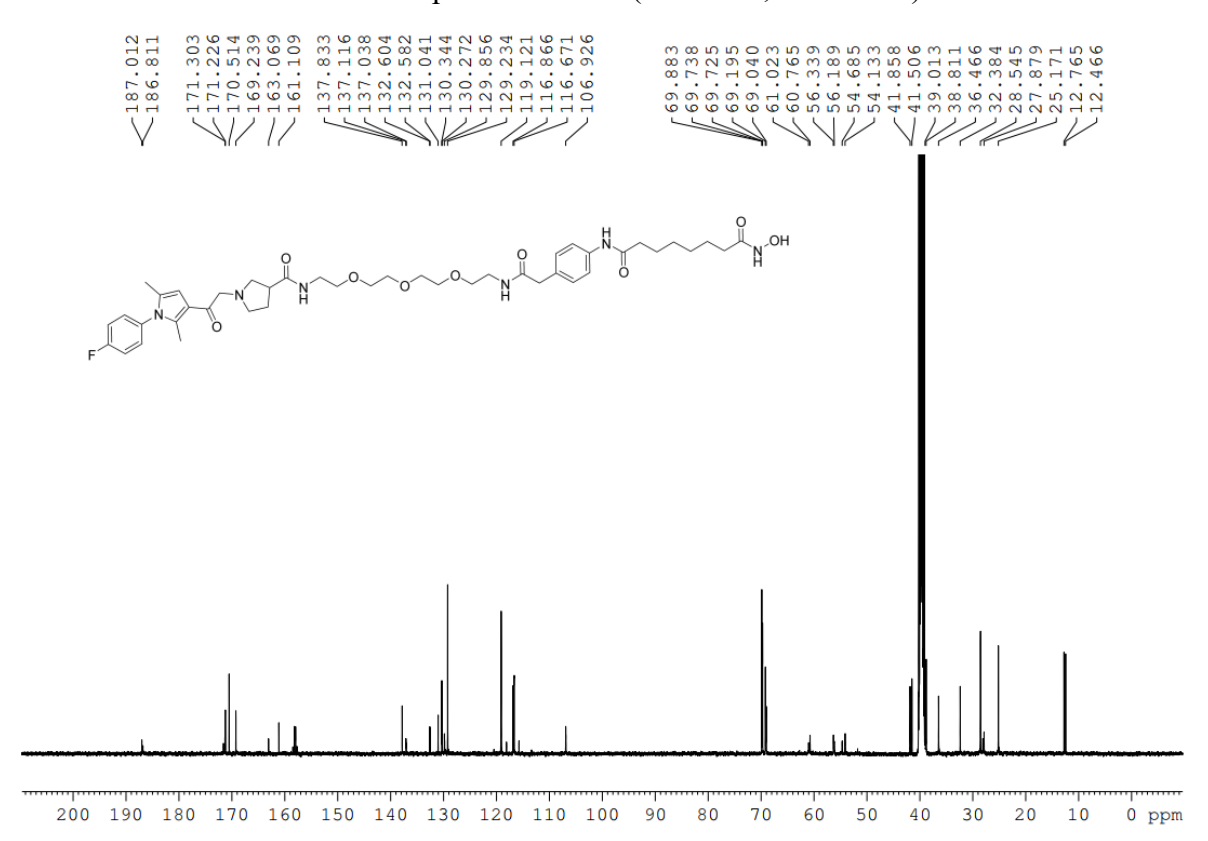


¹H NMR spectrum of **10e** (500 MHz, DMSO-*d*₆)

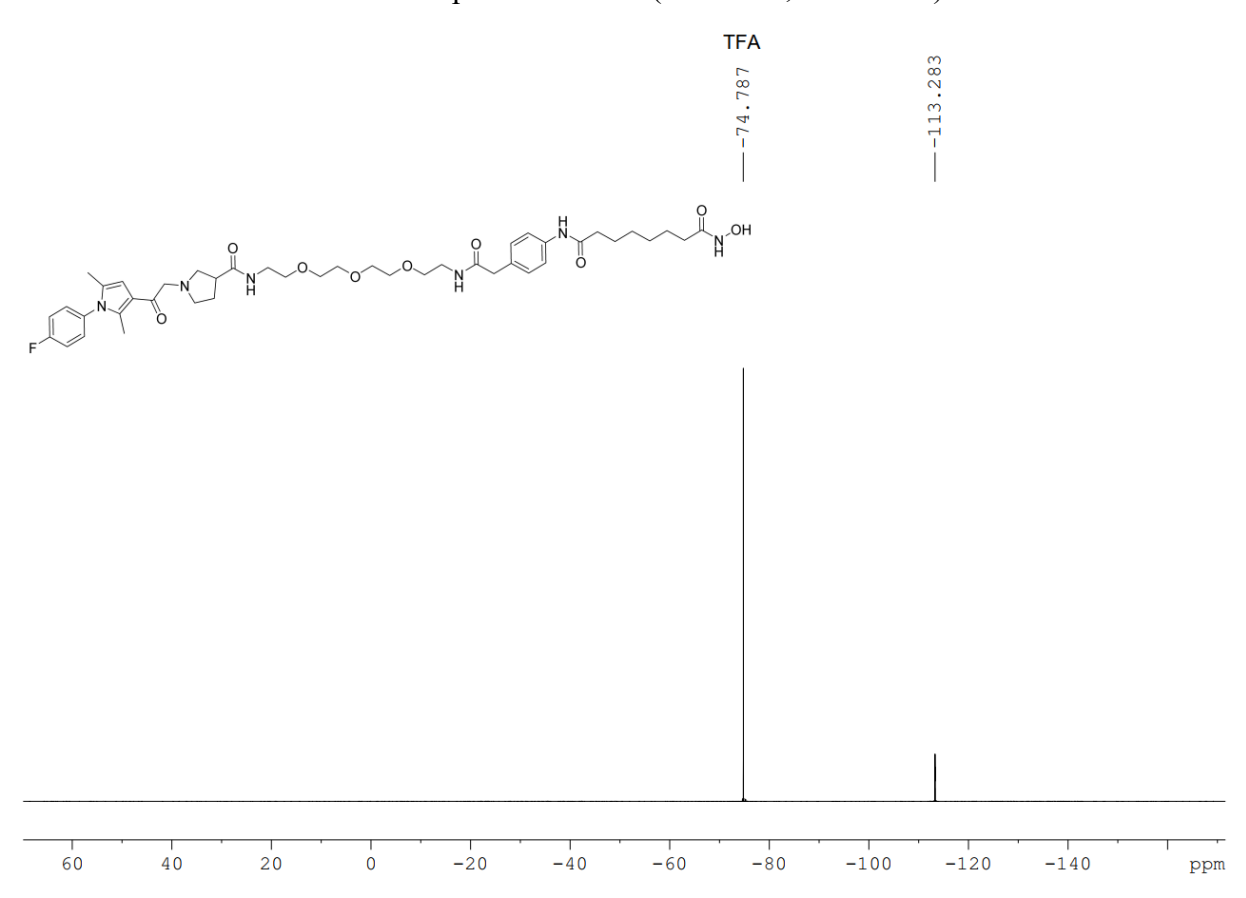




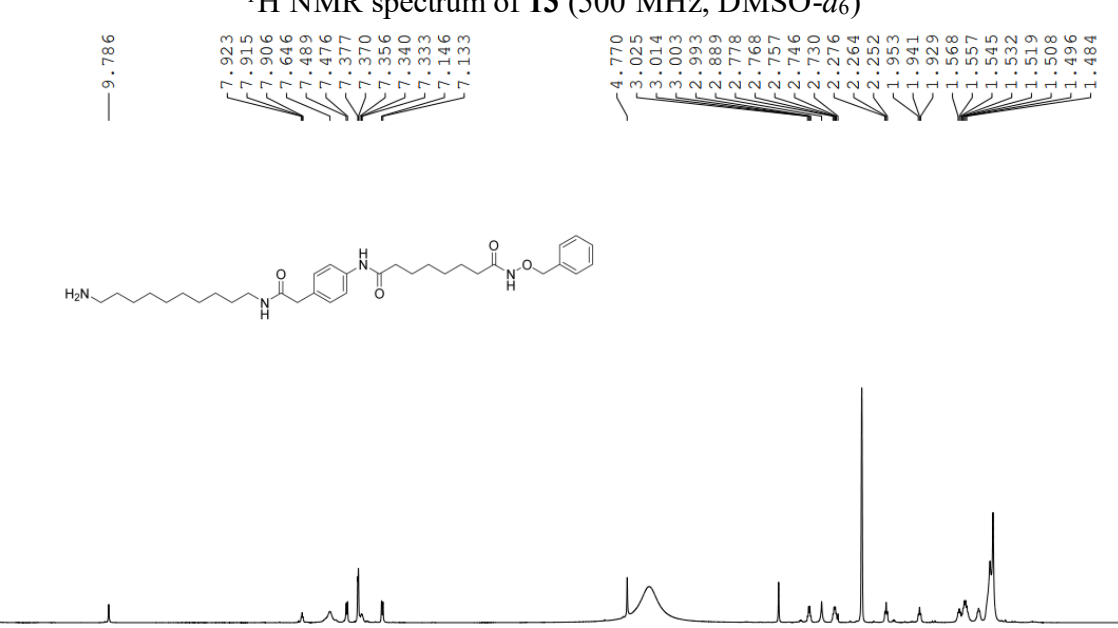
13 C NMR spectrum of **10e** (126 MHz, DMSO- d_6)



¹⁹F NMR spectrum of **10e** (471 MHz, DMSO-*d*₆)



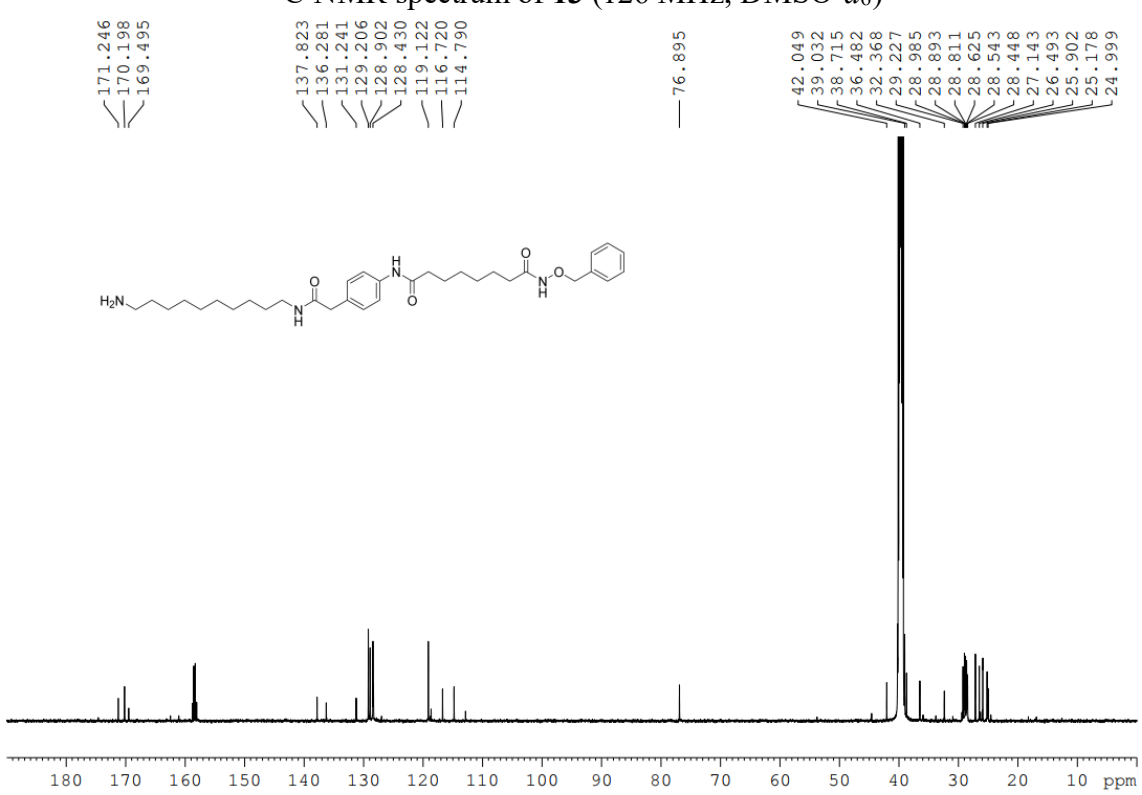
¹H NMR spectrum of **13** (500 MHz, DMSO-*d*₆)



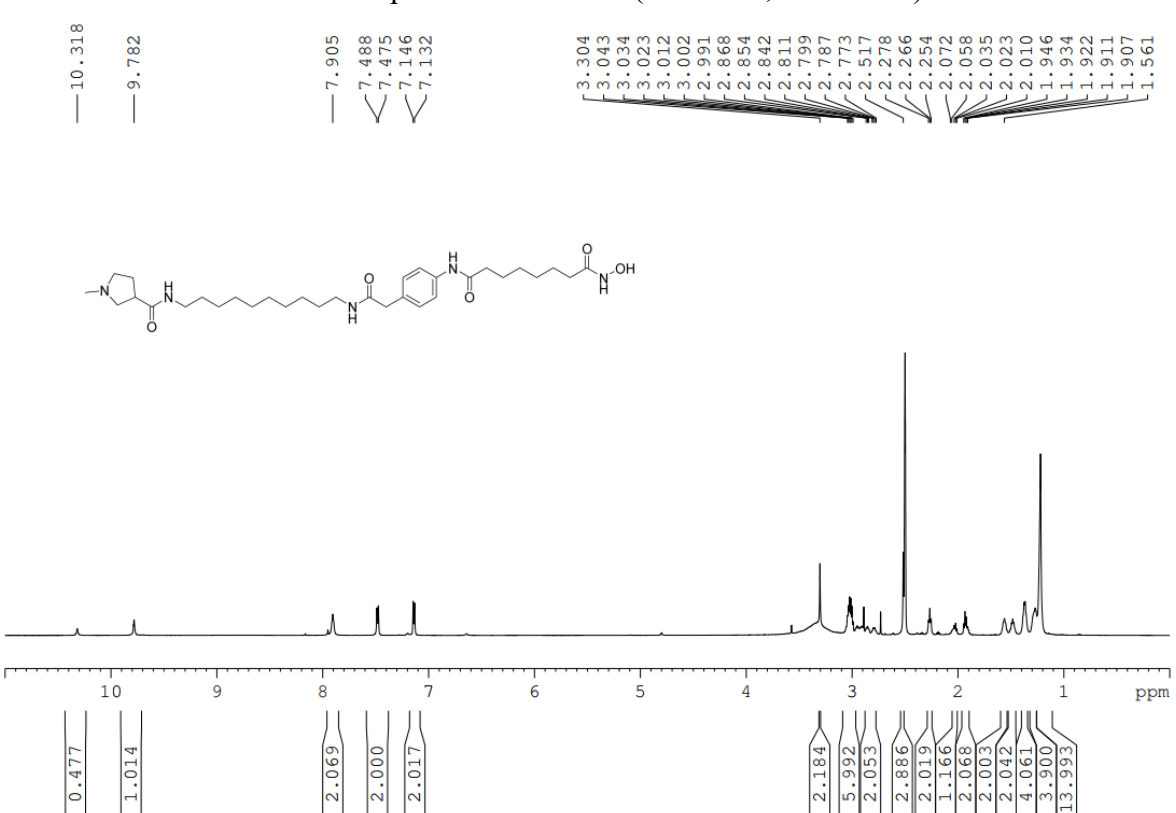
¹³C NMR spectrum of **13** (126 MHz, DMSO-*d*₆)

ppm

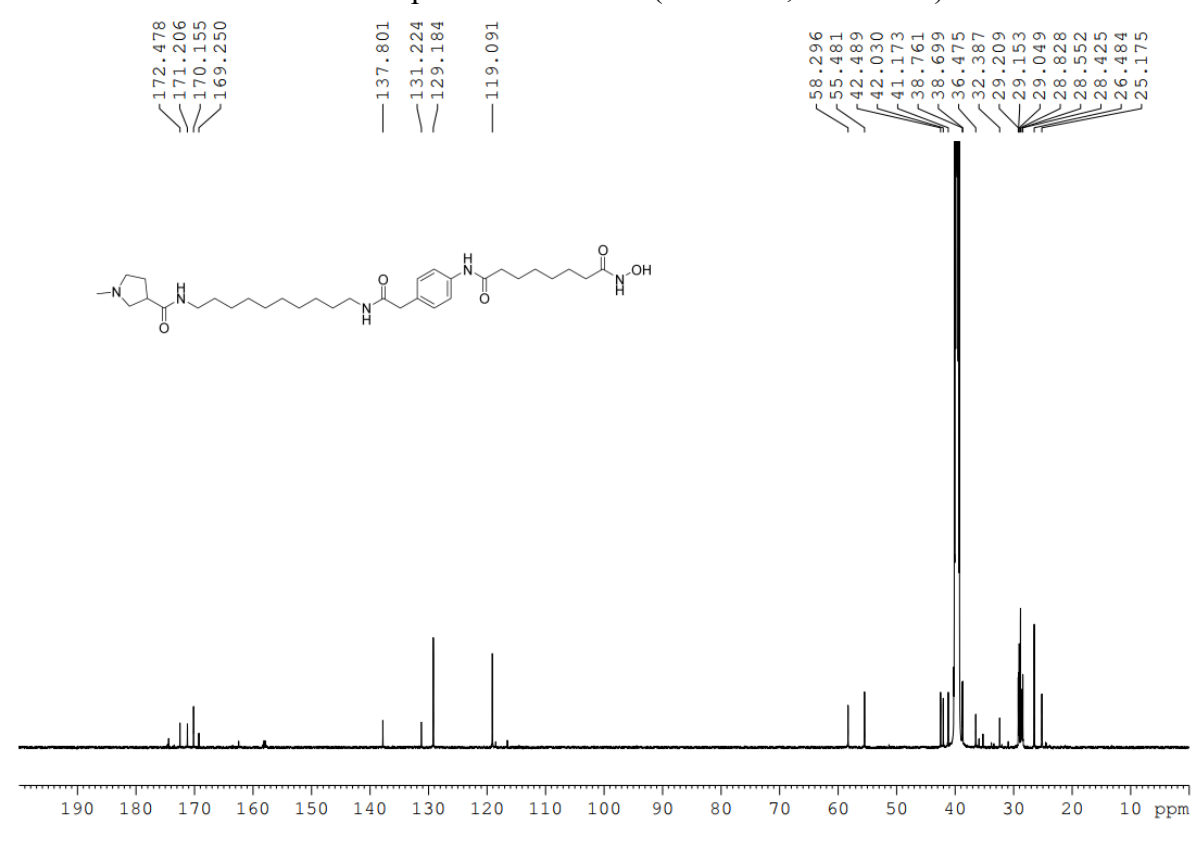
10



¹H NMR spectrum of **10c-nc** (500 MHz, DMSO-*d*₆)

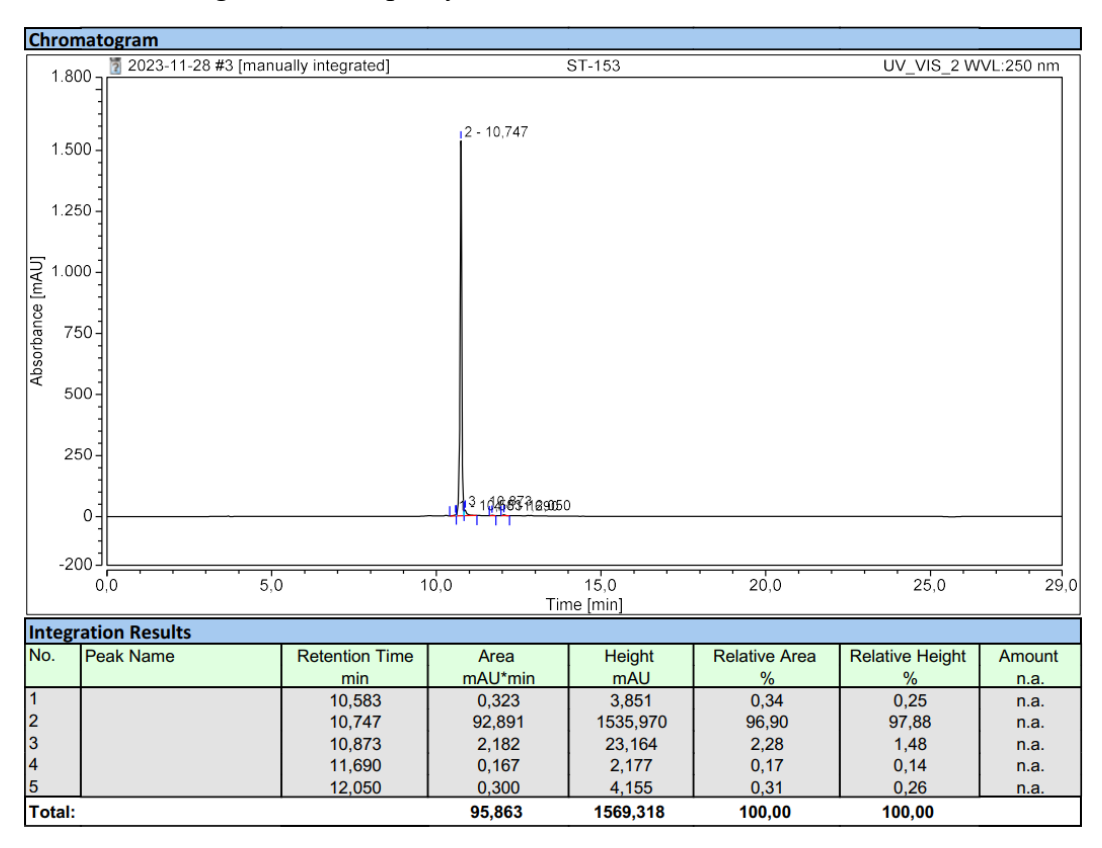


¹³C NMR spectrum of **10c-nc** (126 MHz, DMSO-*d*₆)

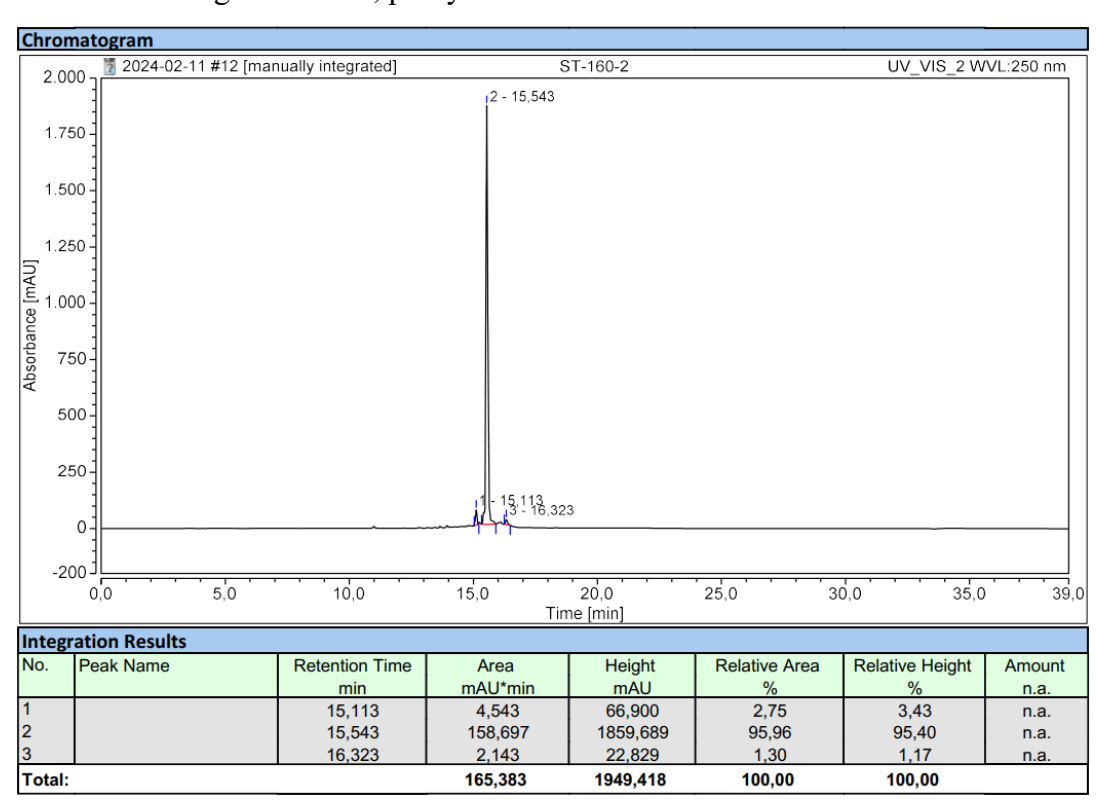


4. HPLC chromatograms

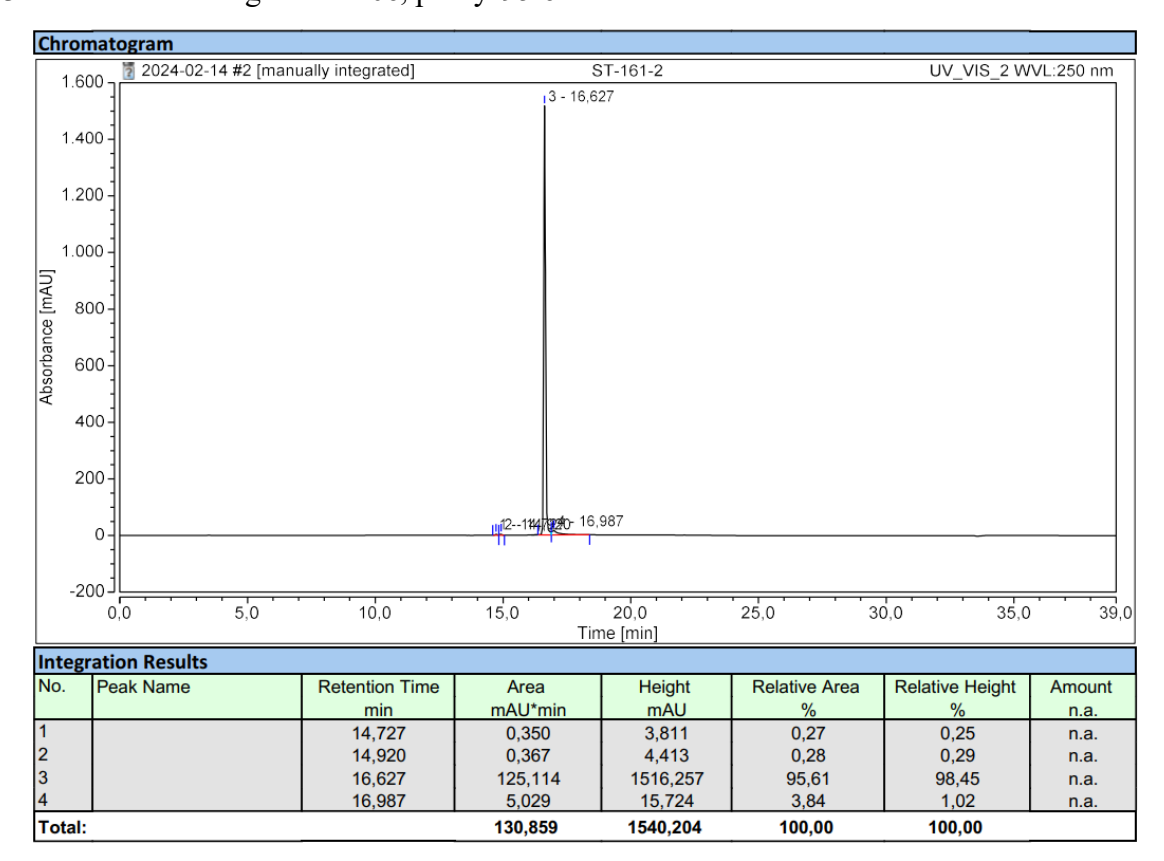
4.1 HPLC Chromatogram of 10a, purity 96.9%.



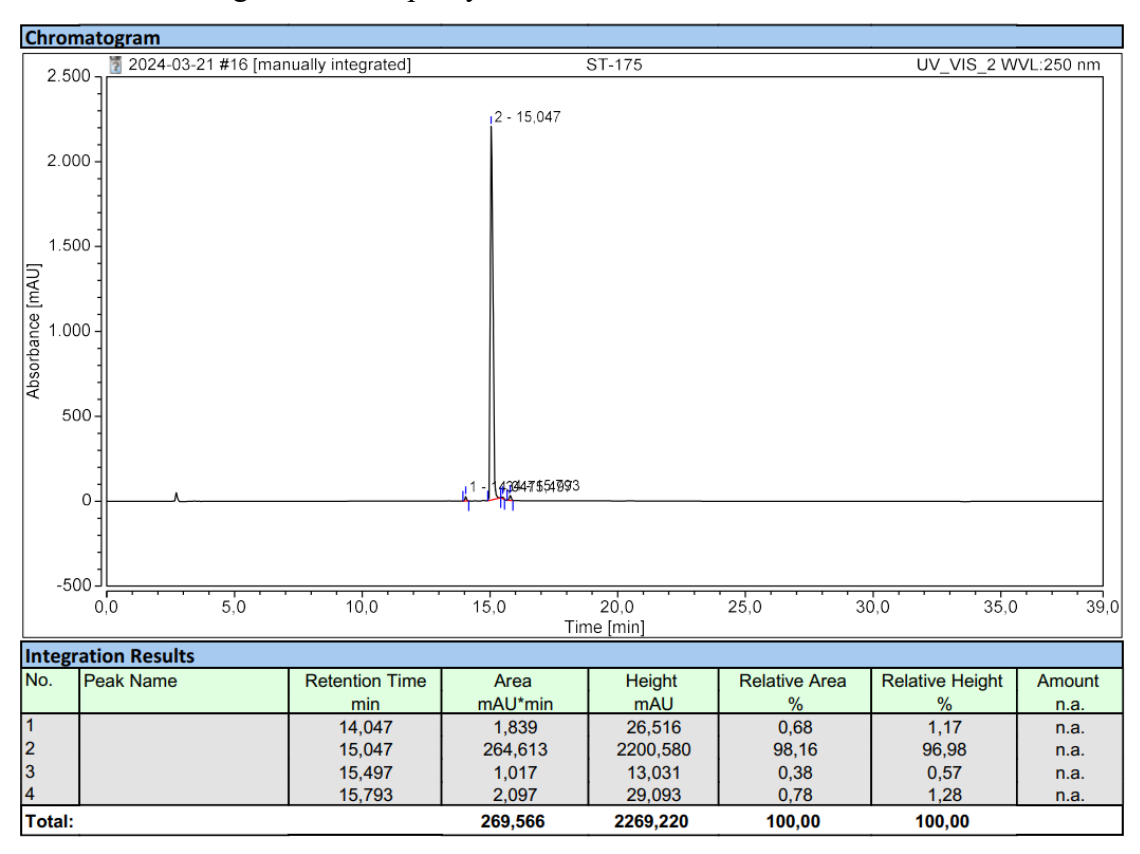
4.2 HPLC Chromatogram of 10b, purity 96.0%.



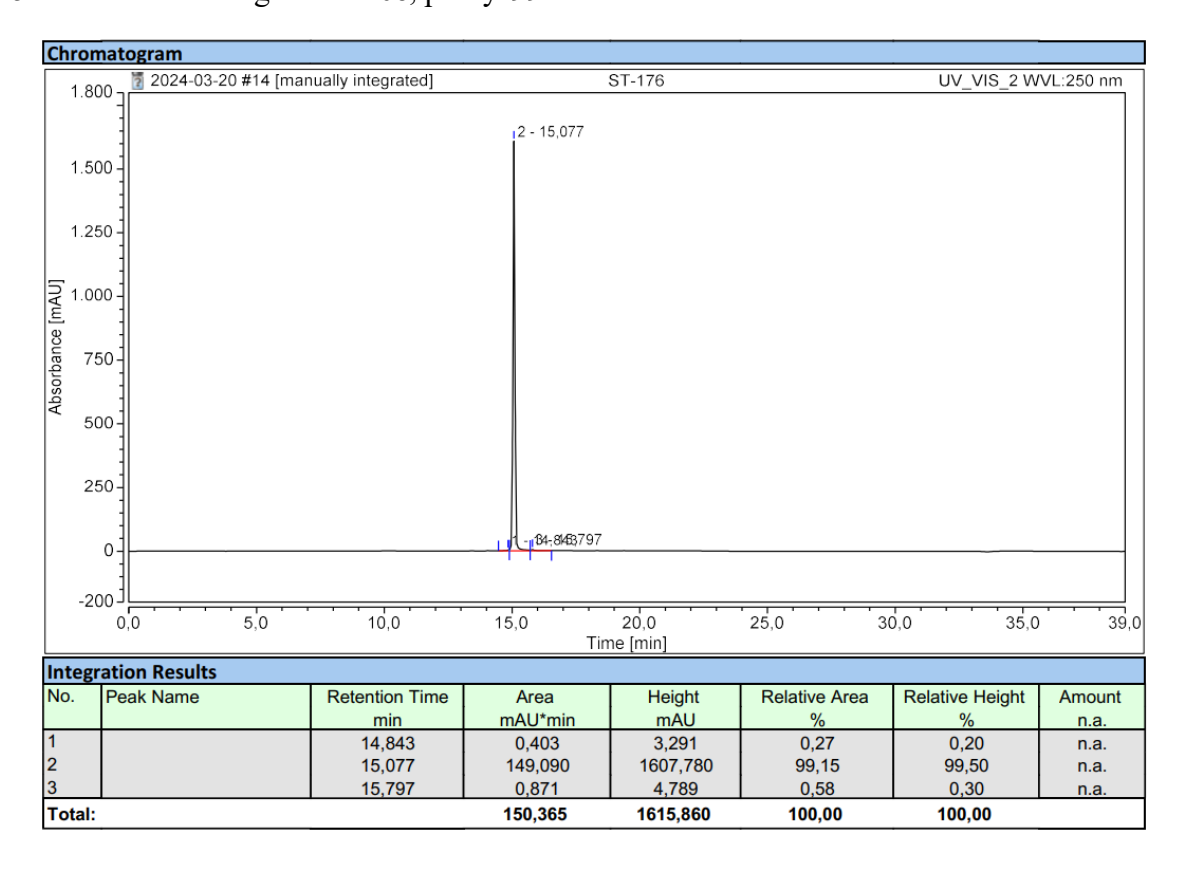
4.3 HPLC Chromatogram of 10c, purity 95.6%.



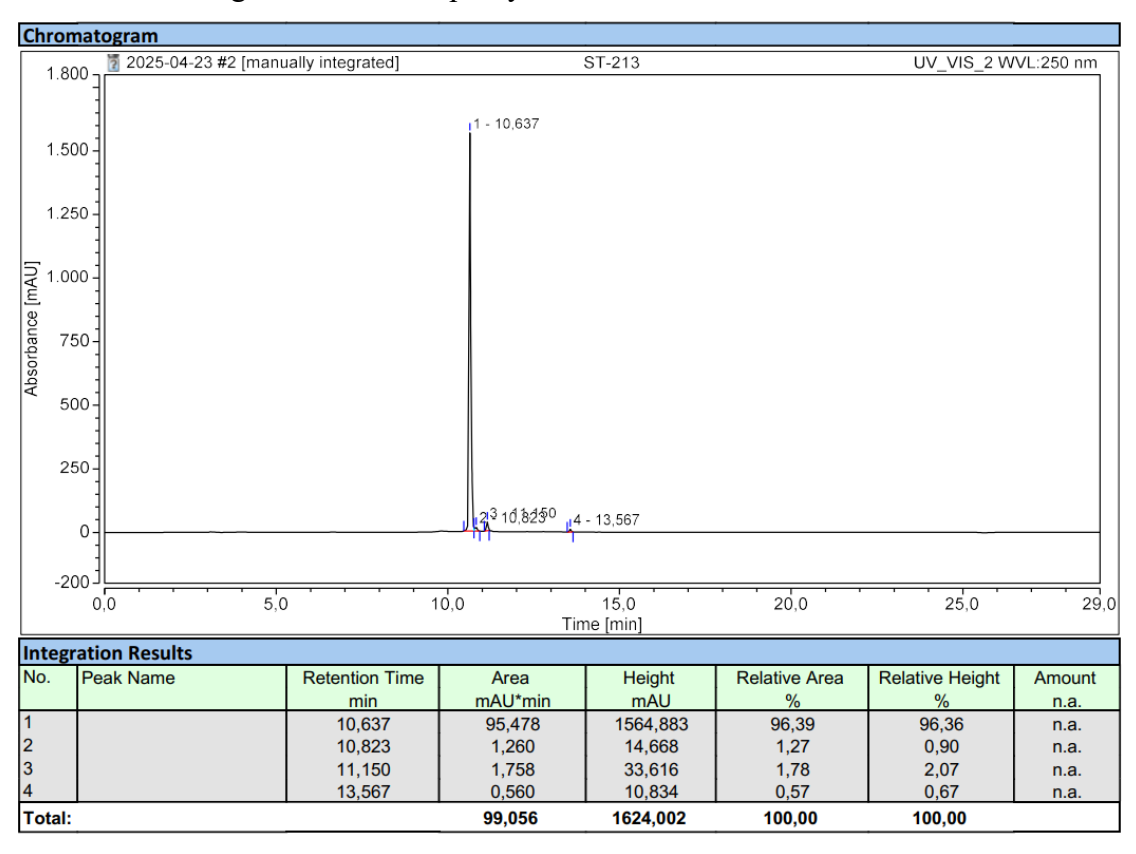
4.4 HPLC Chromatogram of 10d, purity 98.2%.



4.5 HPLC Chromatogram of 10e, purity 99.2%.



4.6 HPLC Chromatogram of 10c-nc, purity 96.4%.



5. References

- (1) Kraft FB, Hanl M, Feller F, Schäker-Hübner L, Hansen FK. Photocaged Histone Deacetylase Inhibitors as Prodrugs in Targeted Cancer Therapy. *Pharmaceuticals (Basel)*. **2023**, *16*, 356.
- (2) Reßing, N.; Schliehe-Diecks, J.; Watson, P. R.; Sonnichsen, M.; Cragin, A. D.; Schöler, A.; Yang, J.; Schäker-Hübner, L.; Borkhardt, A.; Christianson, D. W.; Bhatia, S.; Hansen, F. K. Development of Fluorinated Peptoid-Based Histone Deacetylase (HDAC) Inhibitors for Therapy-Resistant Acute Leukemia. *J Med Chem.* **2022**, *65*, 15457-15472.
- (3) Kraft, F. B.; Enns, J.; Honin, I.; Engelhardt, J.; Scholer, A.; Smith, S. T.; Meiler, J.; Schäker-Hübner, L.; Weindl, G.; Hansen, F. K. Groebke Blackburn Bienaymé-mediated multi-component synthesis of selective HDAC6 inhibitors with anti-inflammatory properties. *Bioorg Chem* **2024**, *143*, 107072.
- (4) Schäker-Hübner, L.; Warstat, R.; Ahlert, H.; Mishra, P.; Kraft, F. B.; Schliehe-Diecks, J.; Schöler, A.; Borkhardt, A.; Breit, B.; Bhatia, S.; Hügle, M.; Günther, S.; Hansen, F. K. 4-Acyl Pyrrole Capped HDAC Inhibitors: A New Scaffold for Hybrid Inhibitors of BET Proteins and Histone Deacetylases as Antileukemia Drug Leads. *J Med Chem.* **2021**, *64*, 14620-14646.
- (5) König B, Watson PR, Reßing N, Cragin AD, Schäker-Hübner L, Christianson DW, Hansen FK. Difluoromethyl-1,3,4-oxadiazoles Are Selective, Mechanism-Based, and Essentially Irreversible Inhibitors of Histone Deacetylase 6. *J Med Chem.* 2023, 66, 13821-13837.
- (6) Schäker-Hübner, L.; Haschemi, R.; Buch, T.; Kraft, F. B.; Brumme, B.; Scholer, A.; Jenke, R.; Meiler, J.; Aigner, A.; Bendas, G.; Hansen, F. K. Balancing Histone Deacetylase (HDAC) Inhibition and Druglikeness: Biological and Physicochemical Evaluation of Class I Selective HDAC Inhibitors. ChemMedChem 2022, 17, e202100755.
- (7) Sinatra, L.; Vogelmann, A.; Friedrich, F.; Tararina, M. A.; Neuwirt, E.; Colcerasa, A.; König, P.; Toy, L.; Yesiloglu, T. Z.; Hilscher, S.; Gaitzsch, L.; Papenkordt, N.; Zhai, S.; Zhang, L.; Romier, C.; Einsle, O.; Sippl, W.; Schutkowski, M.; Gross, O.; Bendas, G.; Christianson, D. W.; Hansen, F. K.; Jung, M.; Schiedel, M. Development of First-in-Class Dual Sirt2/HDAC6 Inhibitors as Molecular Tools for Dual Inhibition of Tubulin Deacetylation. *J Med Chem.* 2023, 66, 14787-14814.
- (8) Feller, F.; Hansen, F. K. Targeted Protein Degradation of Histone Deacetylases by Hydrophobically Tagged Inhibitors. *ACS Med Chem Lett.* **2023**, *14*, 1863-1868.
- (9) Ahmed IA, Hafiz S, van Ginkel S, Pondugula SR, Abdelhaffez AS, Sayyed HG, El-Aziz EAA, Mansour MM. Augmentation of Docetaxel-Induced Cytotoxicity in Human PC-3 Androgen-Independent Prostate

- Cancer Cells by Combination With Four Natural Apoptosis-Inducing Anticancer Compounds. *Nat Prod Commun.* **2023**, *18*, 10.1177/1934578x231175323.
- (10) Okubo K, Isono M, Asano T, REßING N, Schulz WA, Hansen FK, Sato A. Ubiquitin-proteasome System Is a Promising Target for Killing Cisplatin-resistant Bladder Cancer Cells. *Anticancer Res.* **2021**, *41*, 2901-2912.

6.3 Appendix III. Supporting Information of chapter 4 "Deubiquitinase-targeting Chimeras (DUBTACs) for Targeted Stabilization of SIRT6"

The following part contains ¹H- and ¹³C-NMR spectra of synthesized compounds, and HPLC chromatograms of all final compounds reported in chapter 4.

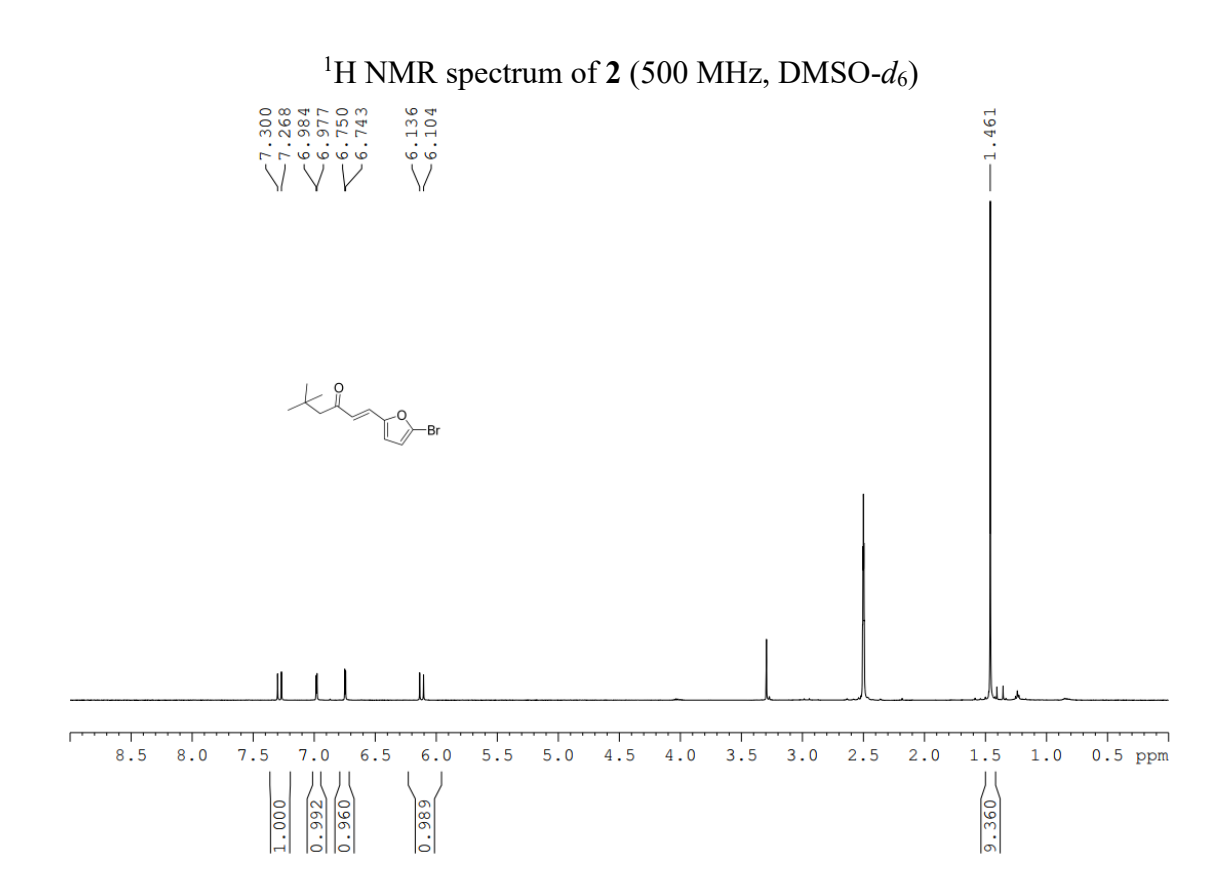
Supporting Information

Deubiquitinase-targeting Chimeras (DUBTACs) for Targeted Stabilization of SIRT6

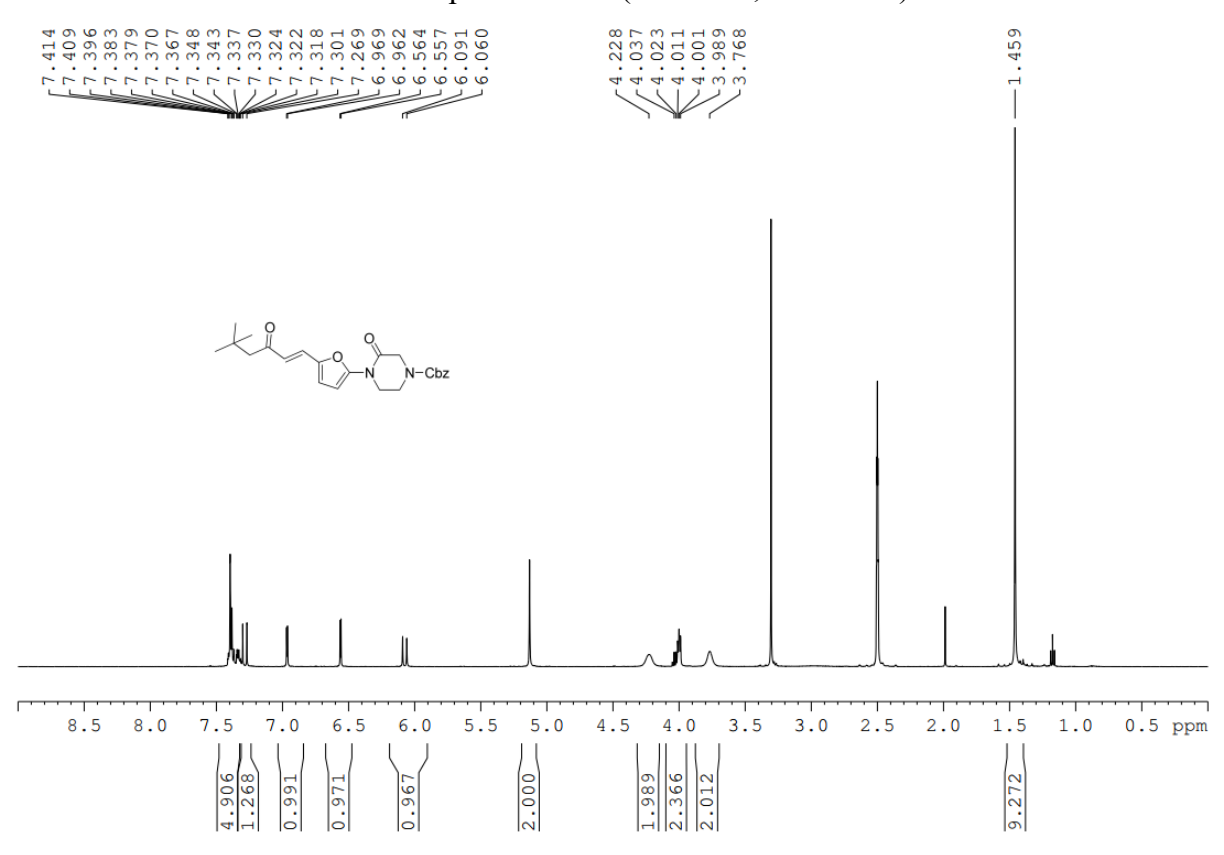
Table of Contents

1. NMR data of synthesized compounds	S1
3. HPLC chromatograms	S34

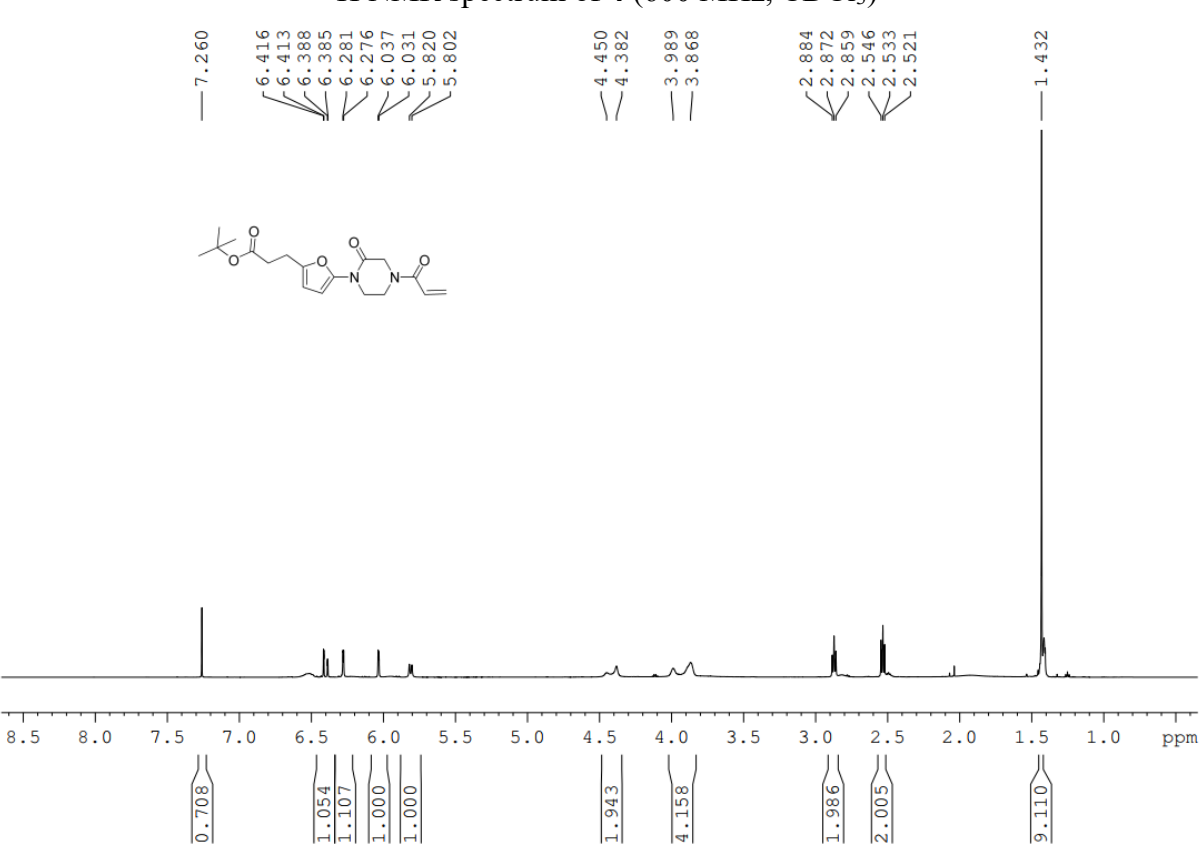
1. NMR data of synthesized compounds

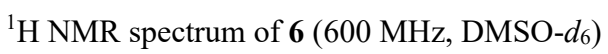


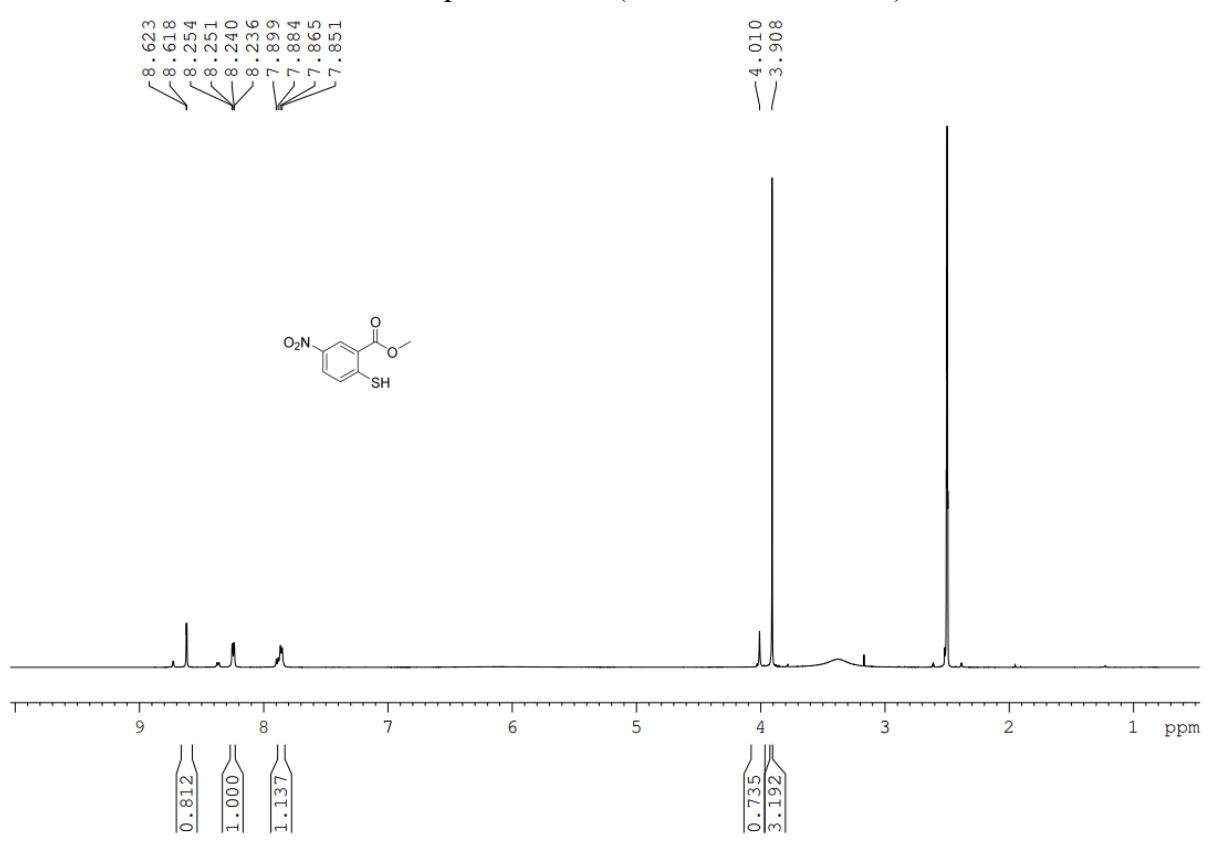
¹H NMR spectrum of **3** (500 MHz, DMSO-*d*₆)



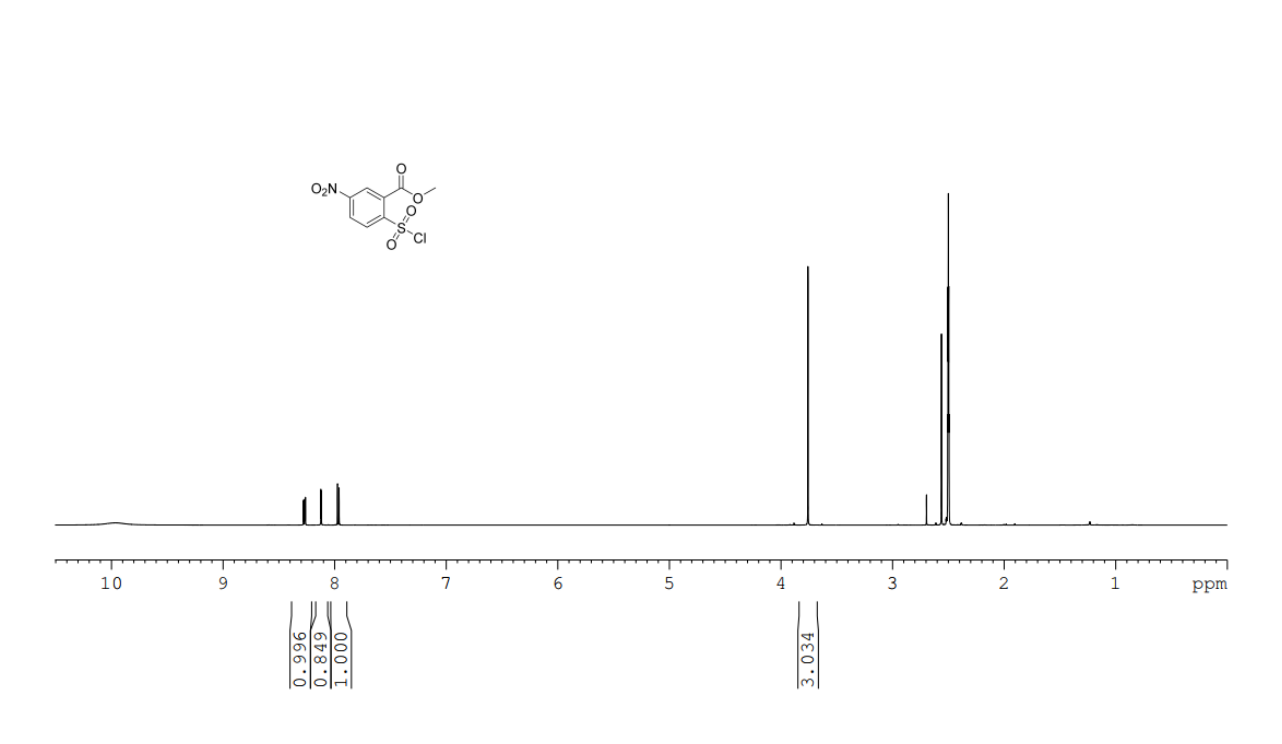
¹H NMR spectrum of **4** (600 MHz, CDCl₃)

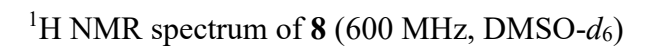




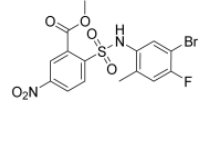


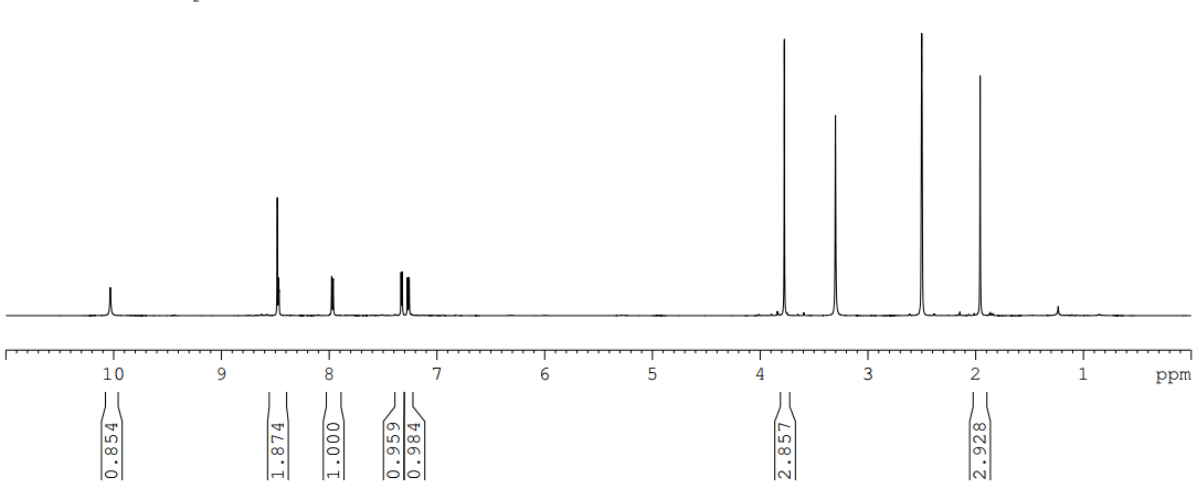
1 H NMR spectrum of 7 (600 MHz, DMSO- d_{6})





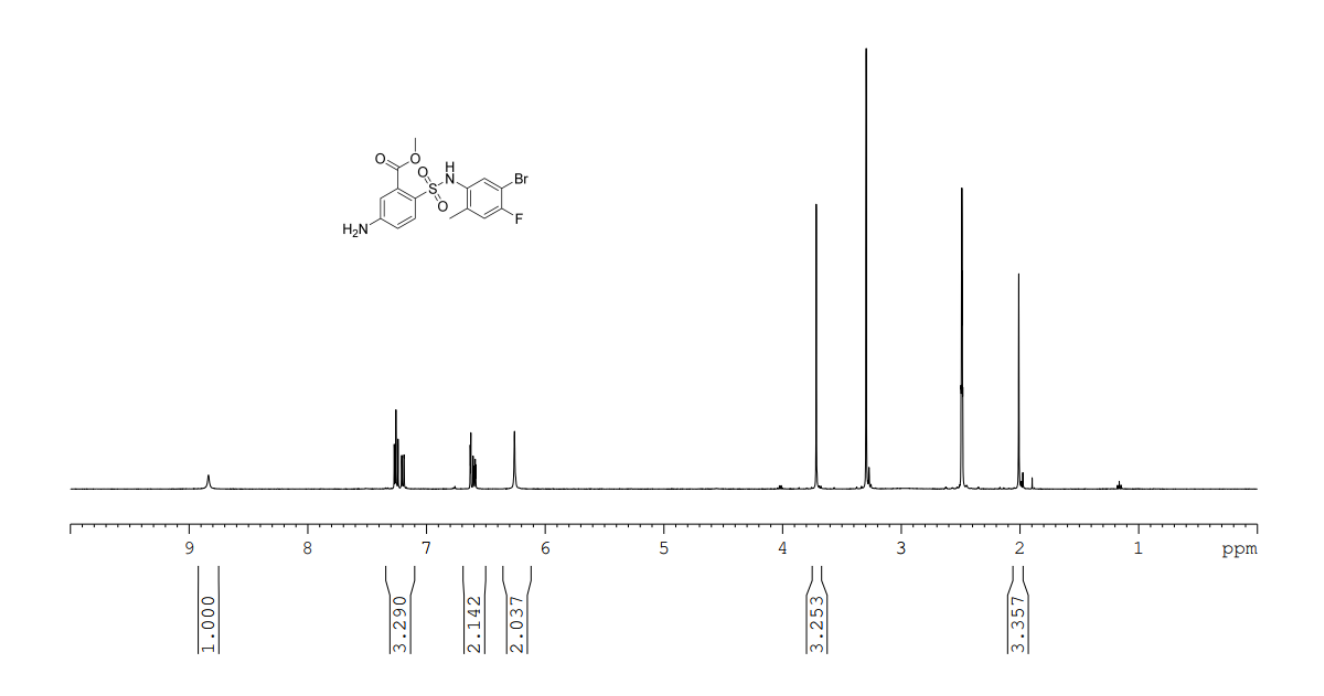


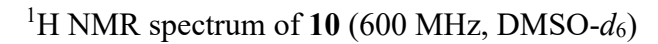


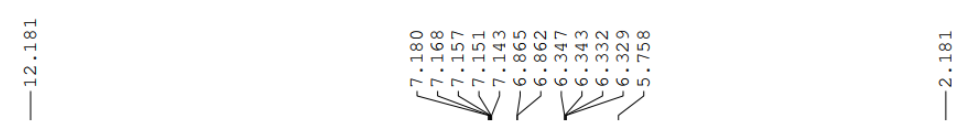


1 H NMR spectrum of **9** (500 MHz, DMSO- d_{6})

837	272 272 240 240 258 663 258 258	716	011
	77777	e m	2.

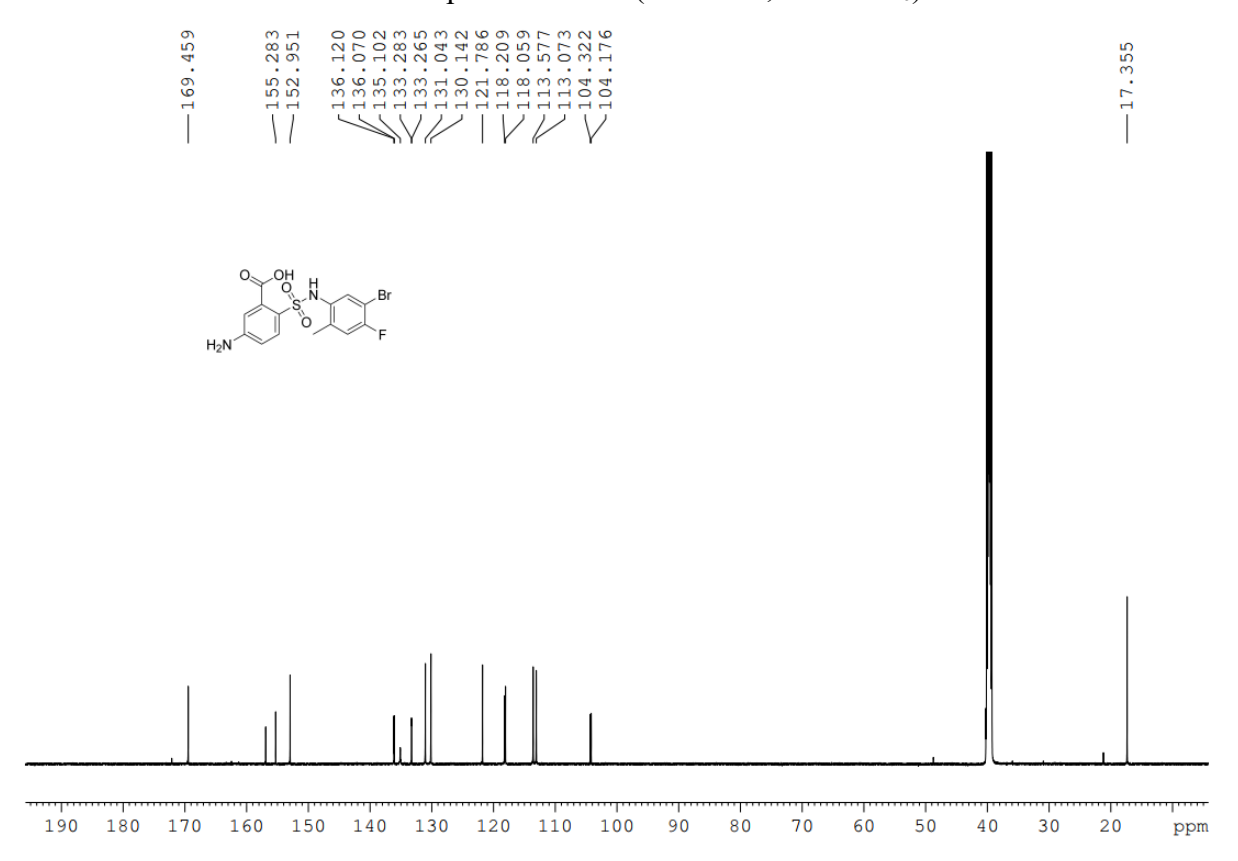




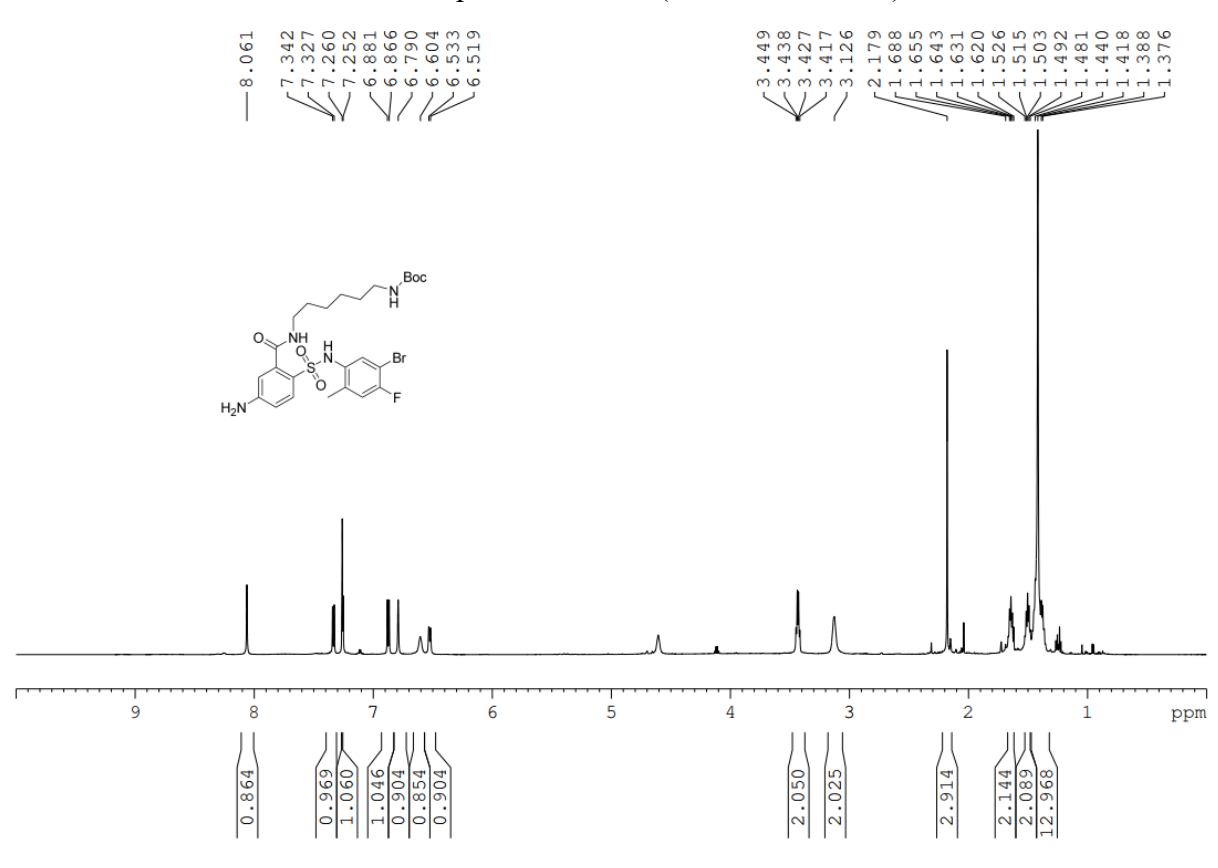




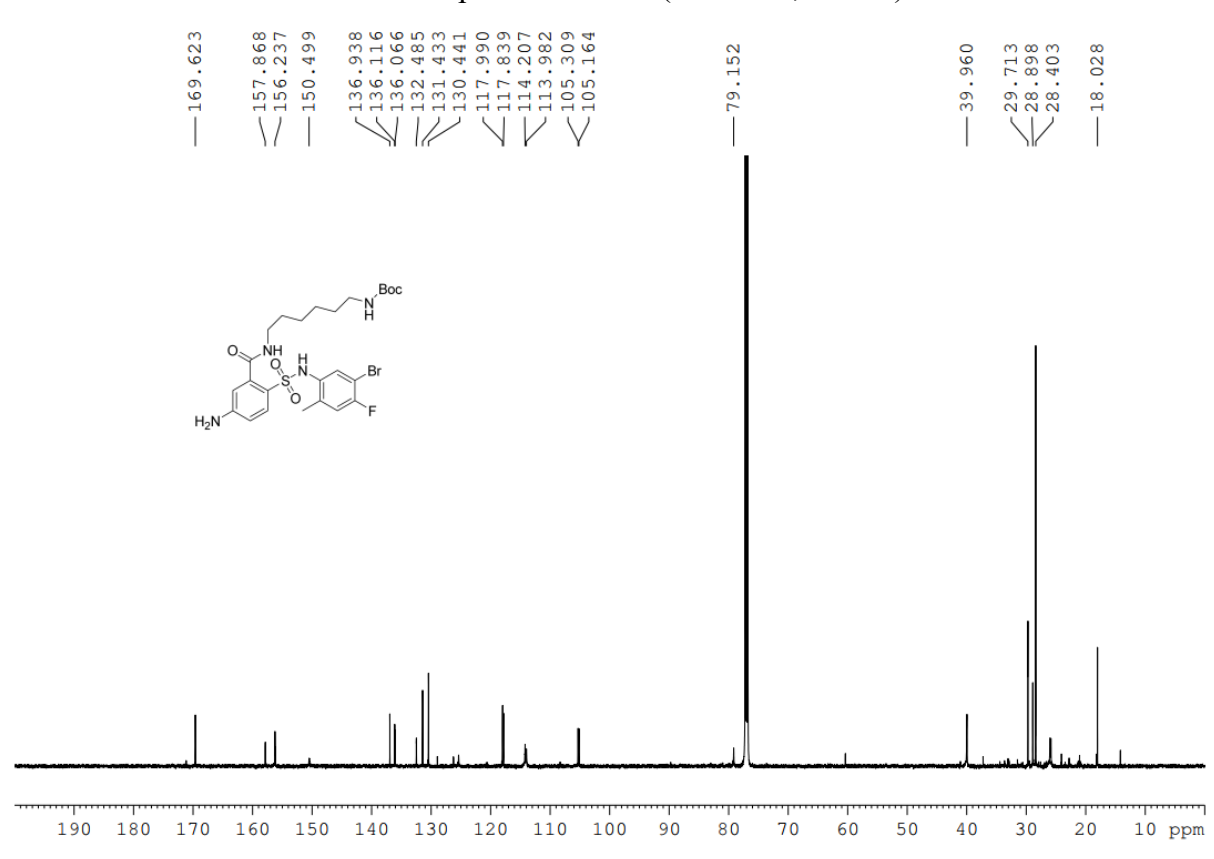
13 C NMR spectrum of **10** (151 MHz, DMSO- d_6)



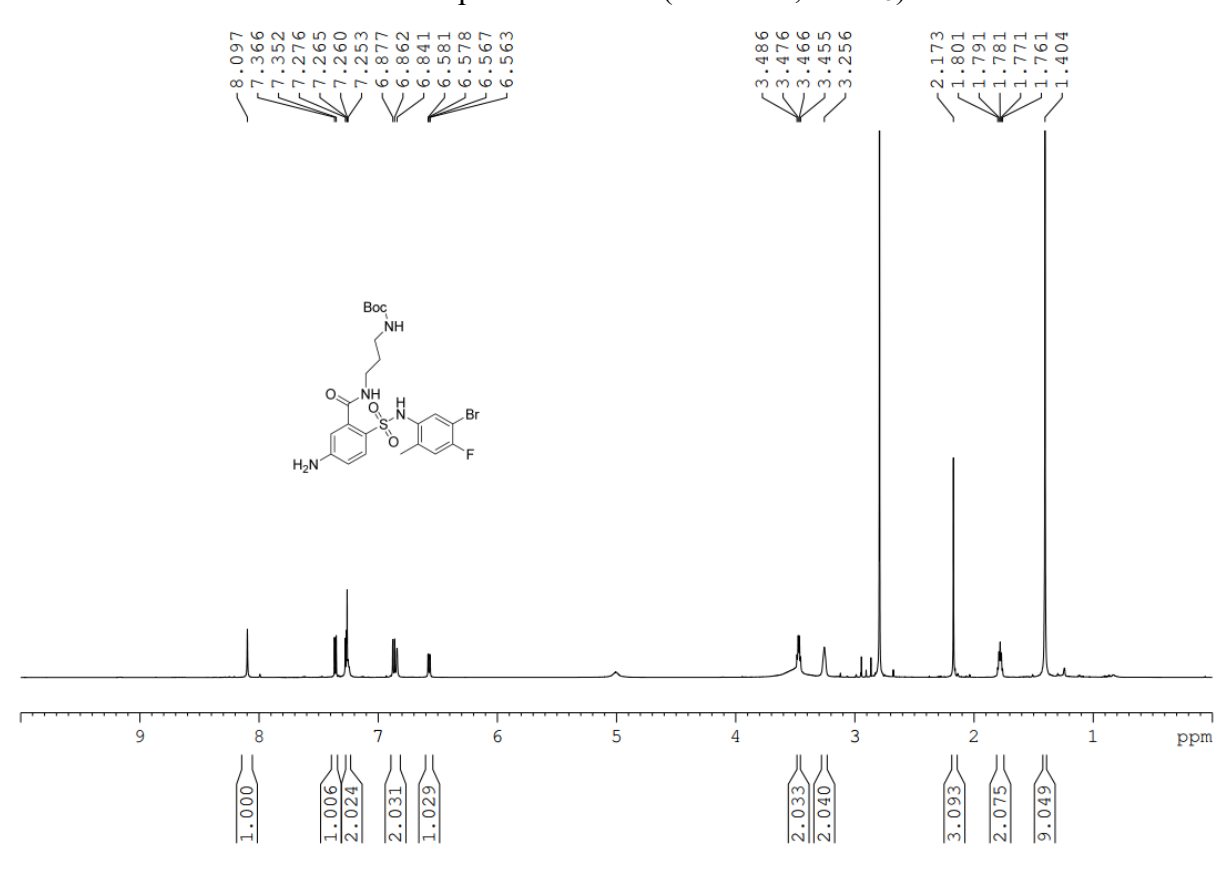
¹H NMR spectrum of **11a** (600 MHz, CDCl₃)



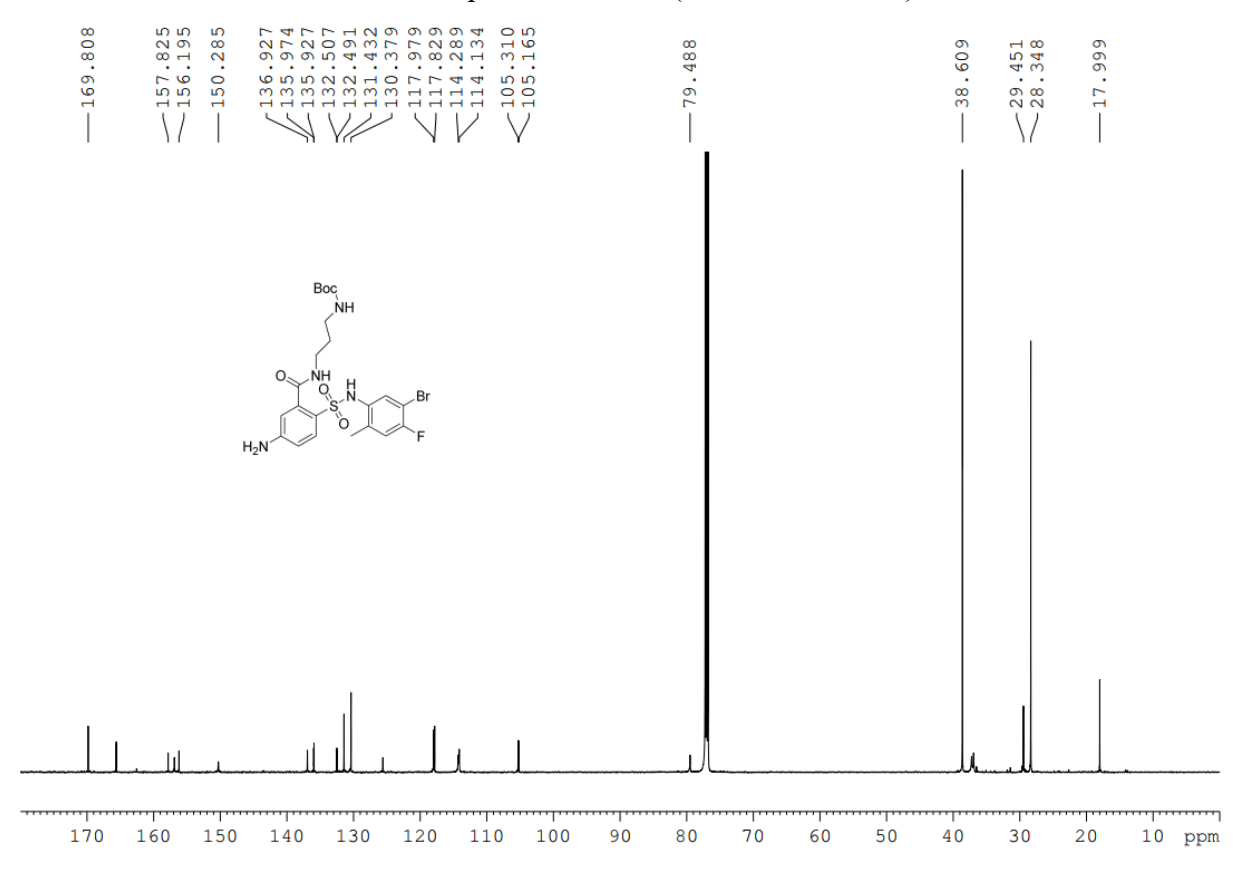
^{13}C NMR spectrum of 11a (151 MHz, CDCl₃)



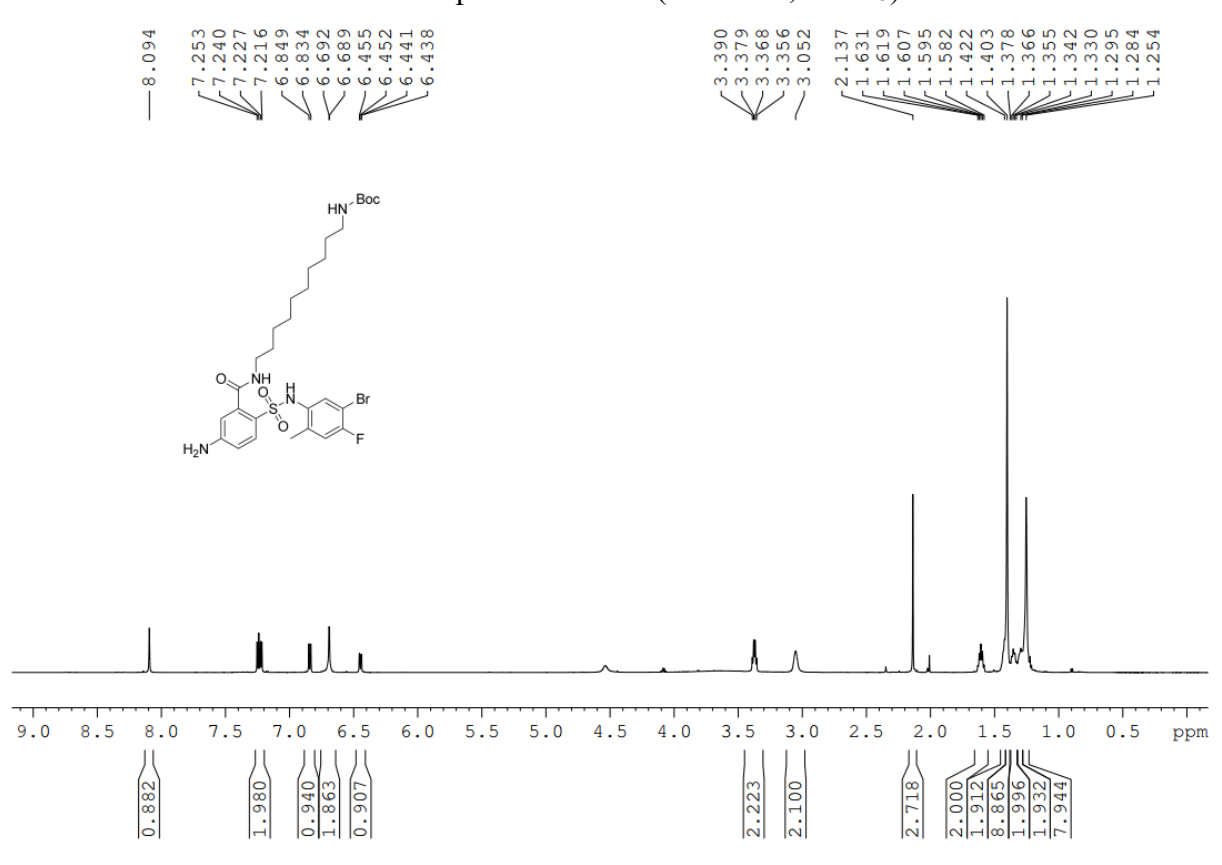
¹H NMR spectrum of **11b** (600 MHz, CDCl₃)



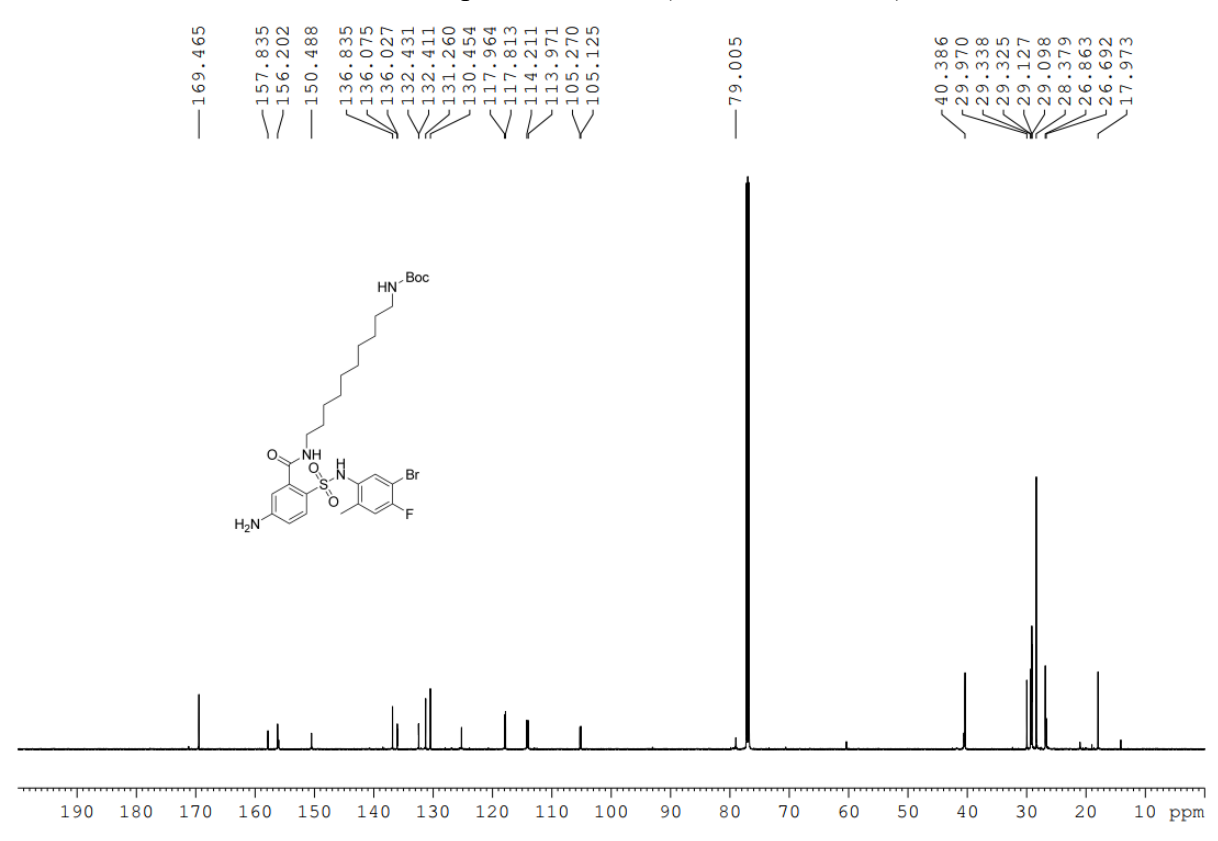
13 C NMR spectrum of 11b (151 MHz, CDCl₃)



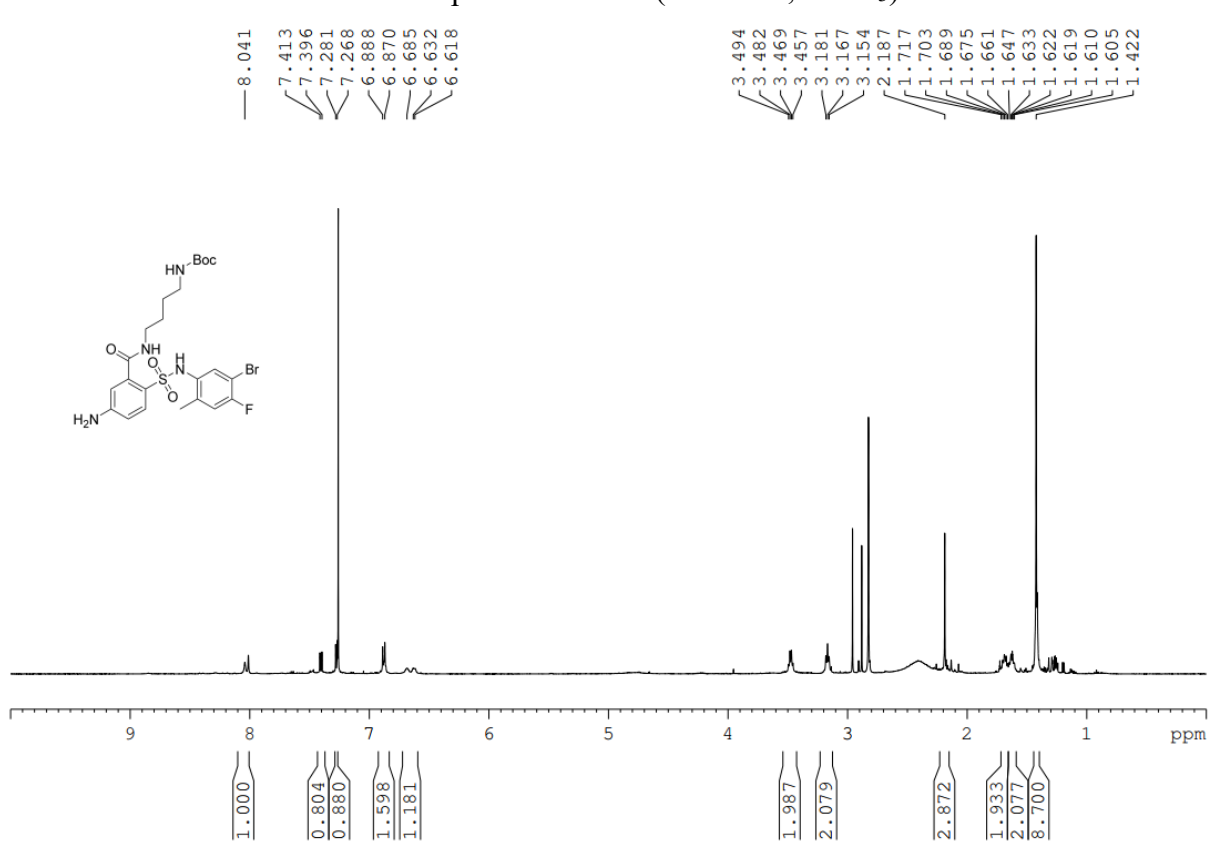
¹H NMR spectrum of **11c** (600 MHz, CDCl₃)



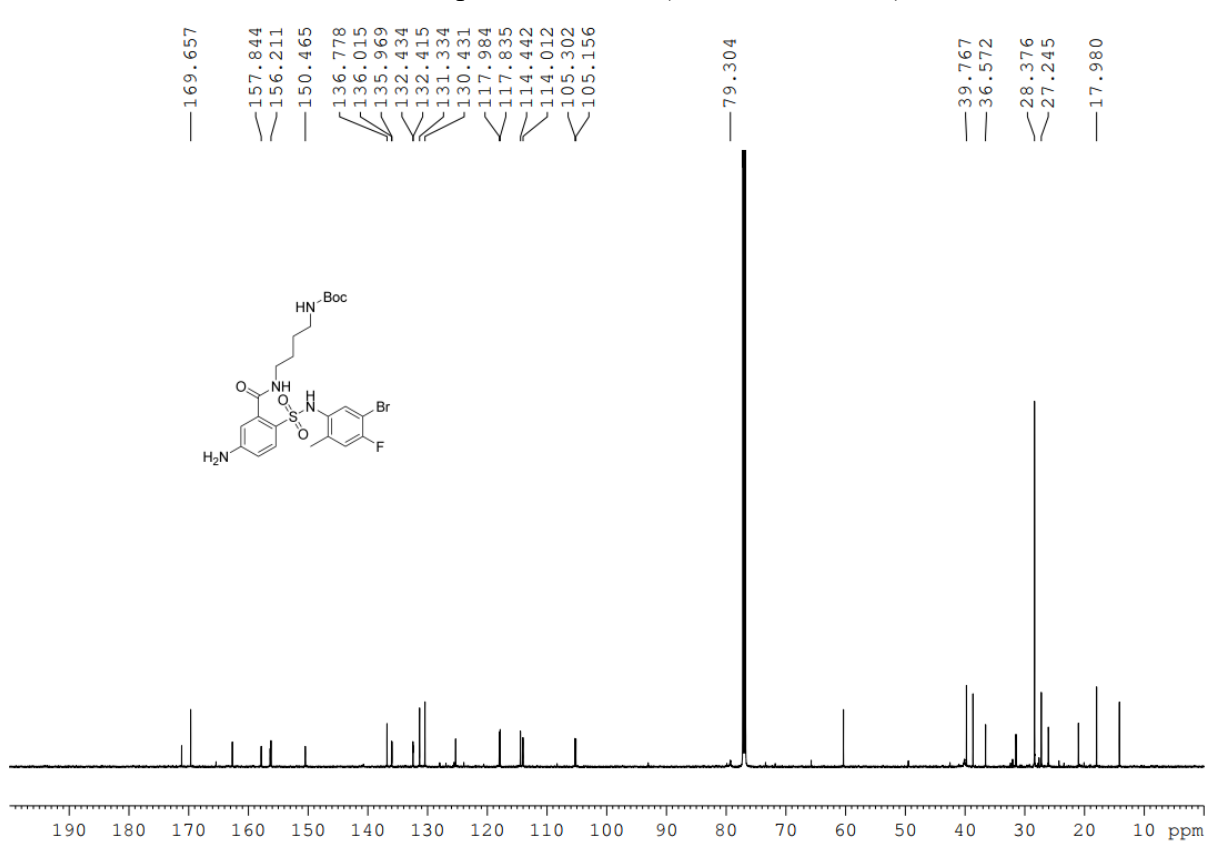
13 C NMR spectrum of **11c** (151 MHz, CDCl₃)



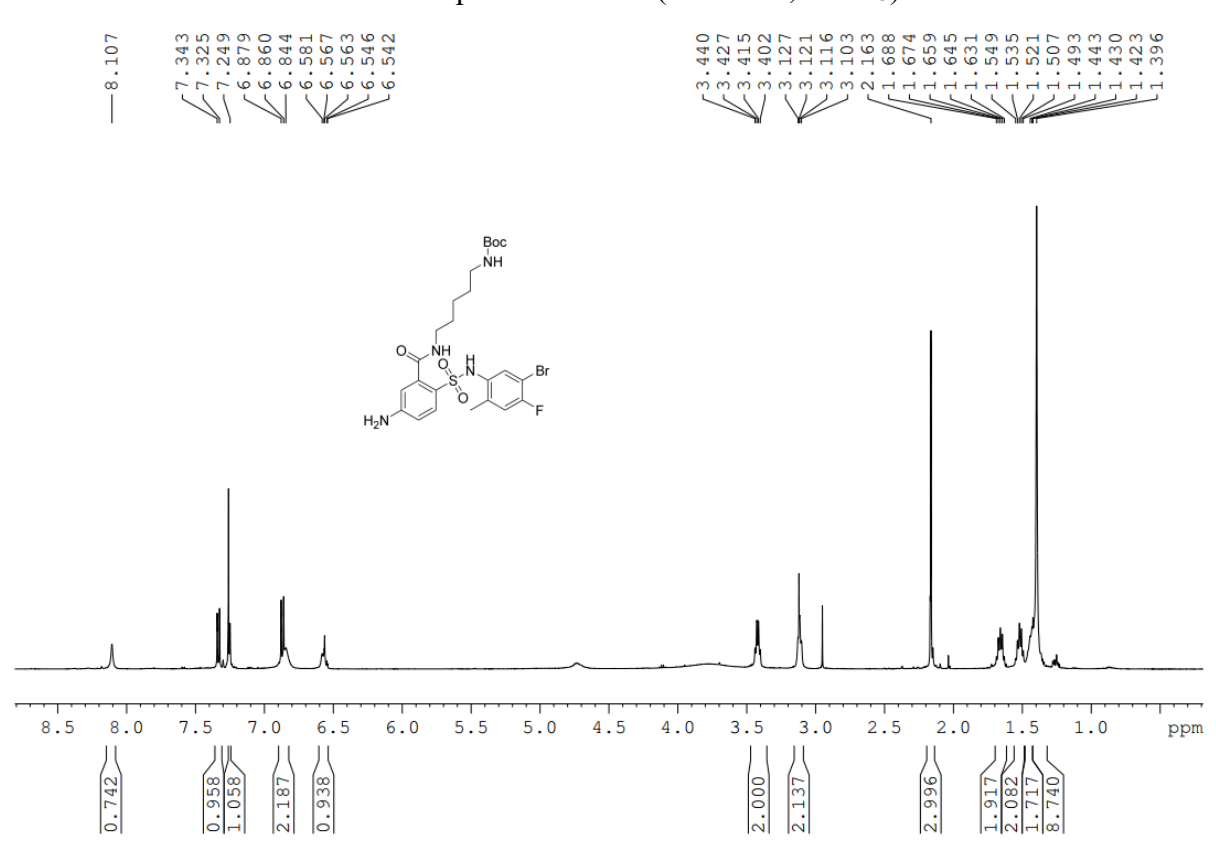
¹H NMR spectrum of **11d** (500 MHz, CDCl₃)



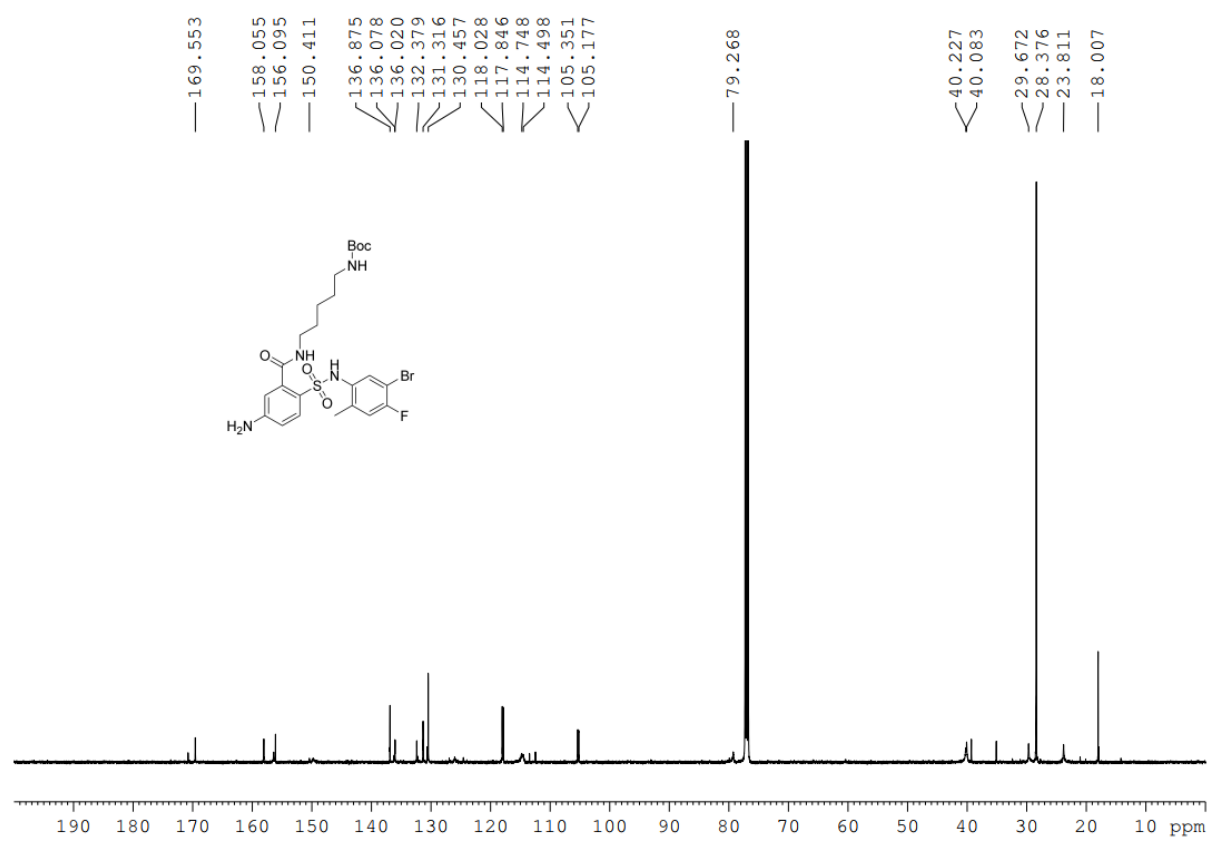
13 C NMR spectrum of **11d** (151 MHz, CDCl₃)



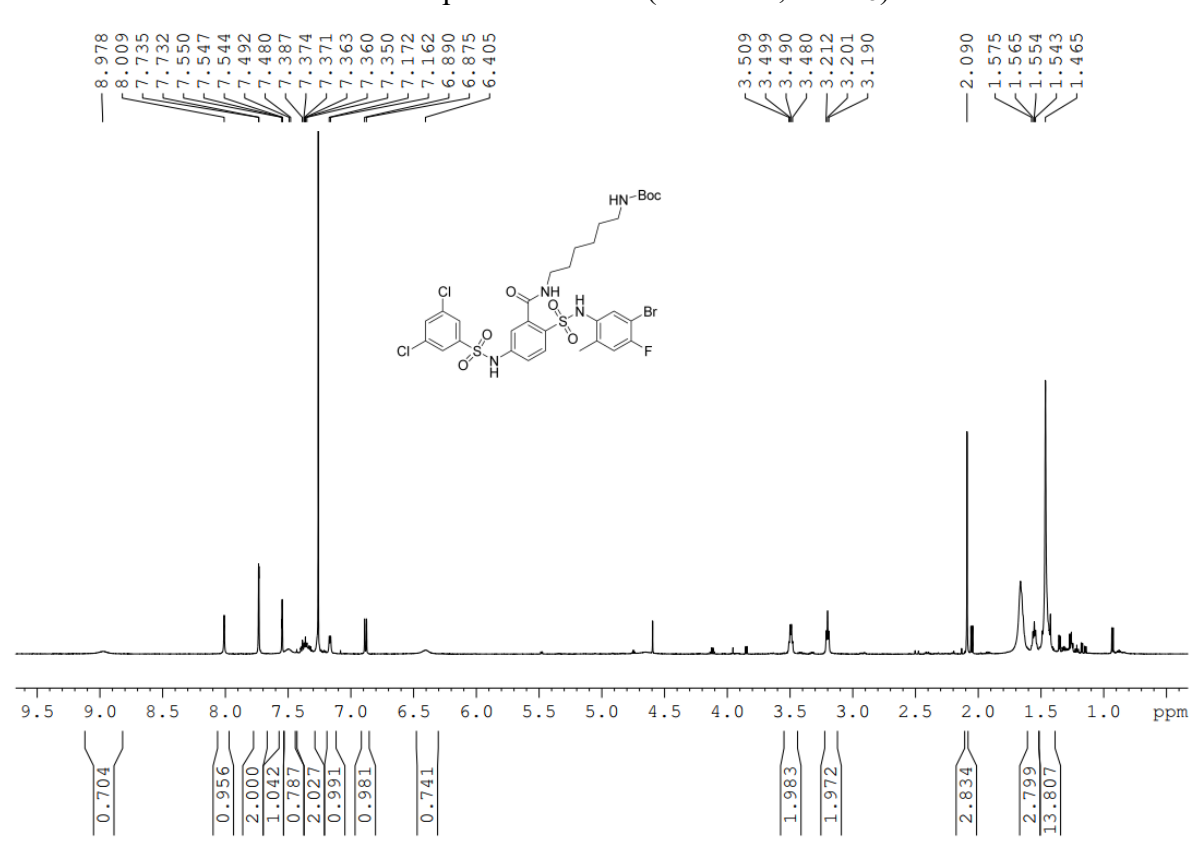
¹H NMR spectrum of **11e** (500 MHz, CDCl₃)



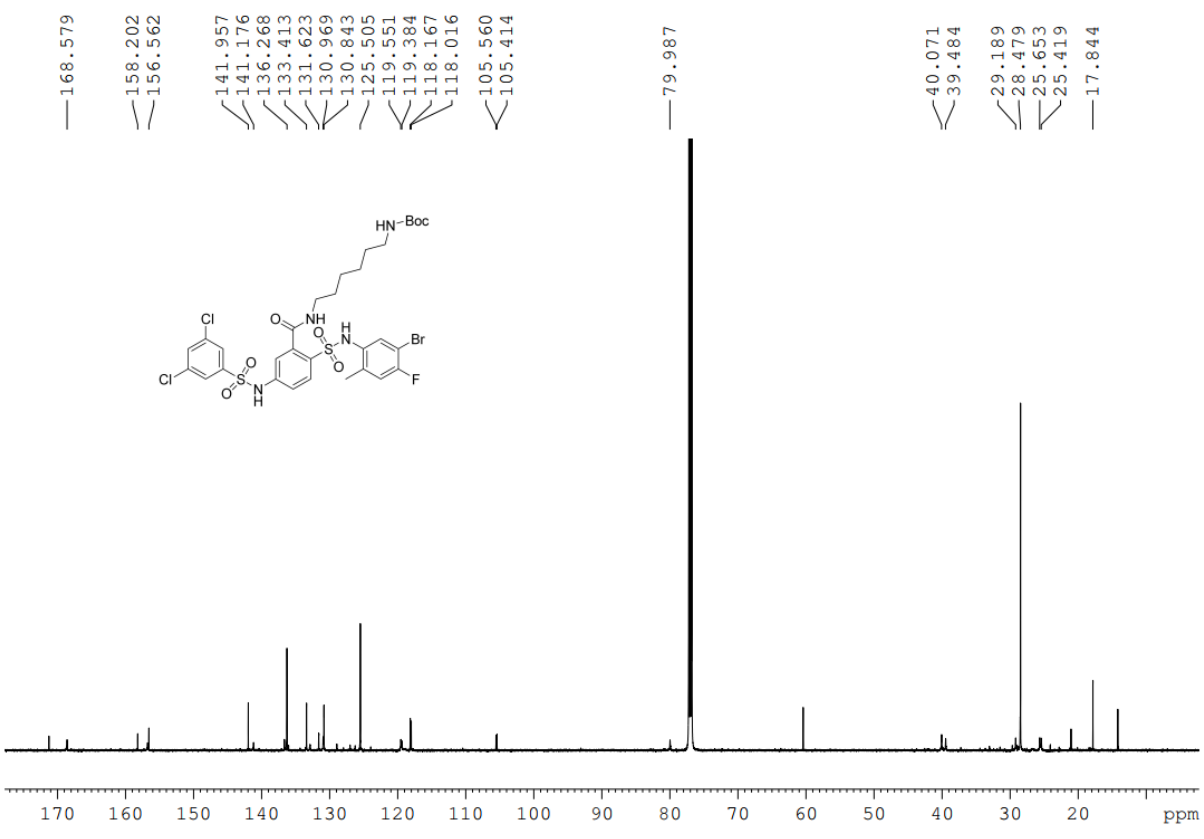
13 C NMR spectrum of 11e (126 MHz, CDCl₃)



¹H NMR spectrum of **12a** (600 MHz, CDCl₃)

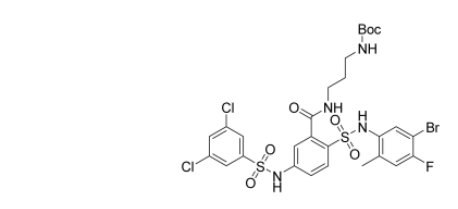


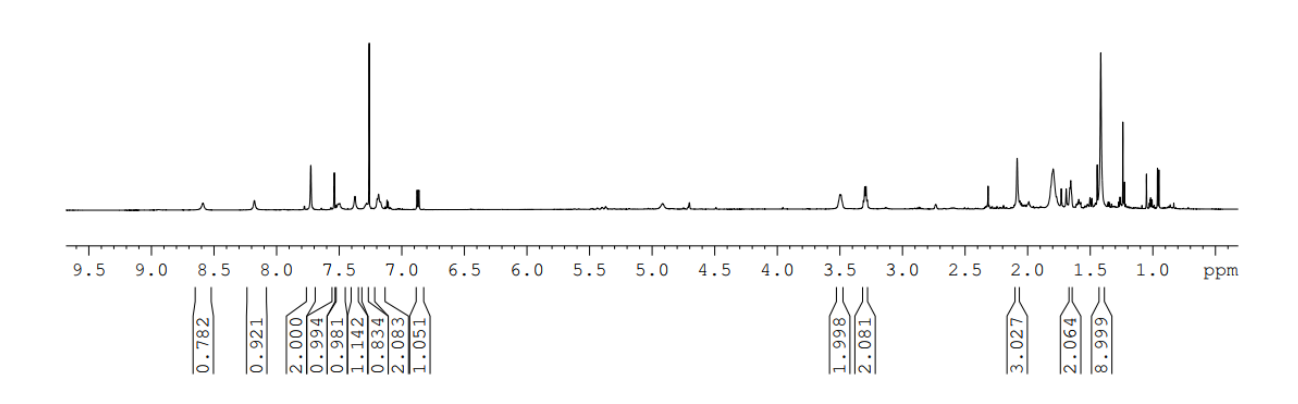
¹³C NMR spectrum of **12a** (151 MHz, CDCl₃)



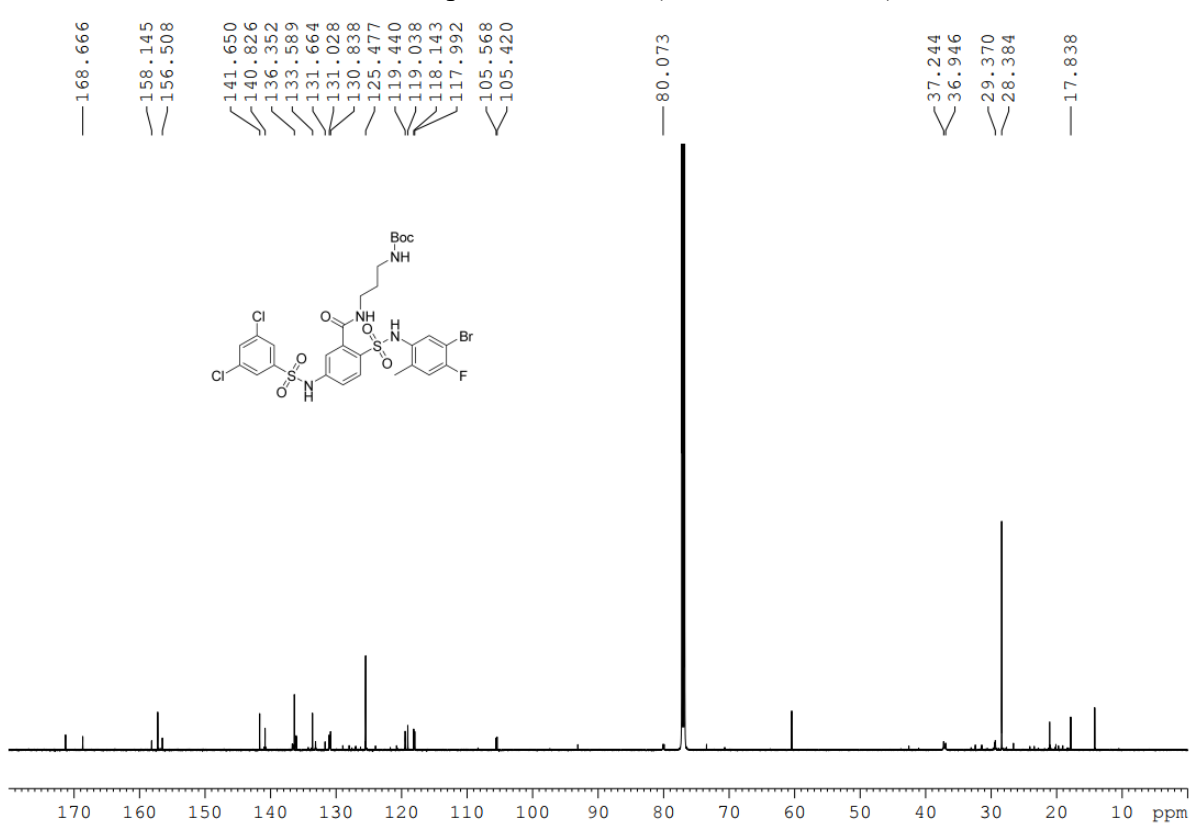
¹H NMR spectrum of **12b** (600 MHz, CDCl₃)



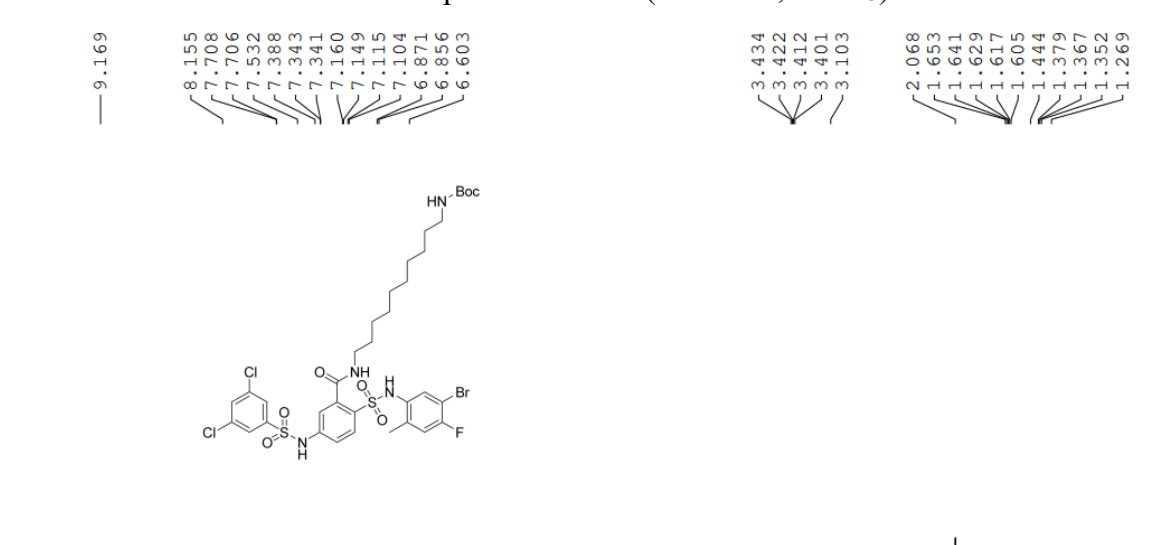


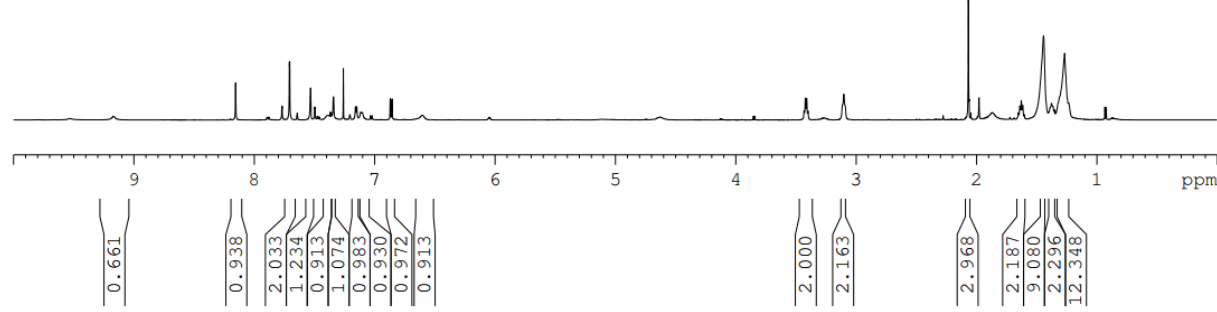


¹³C NMR spectrum of **12b** (151 MHz, CDCl₃)

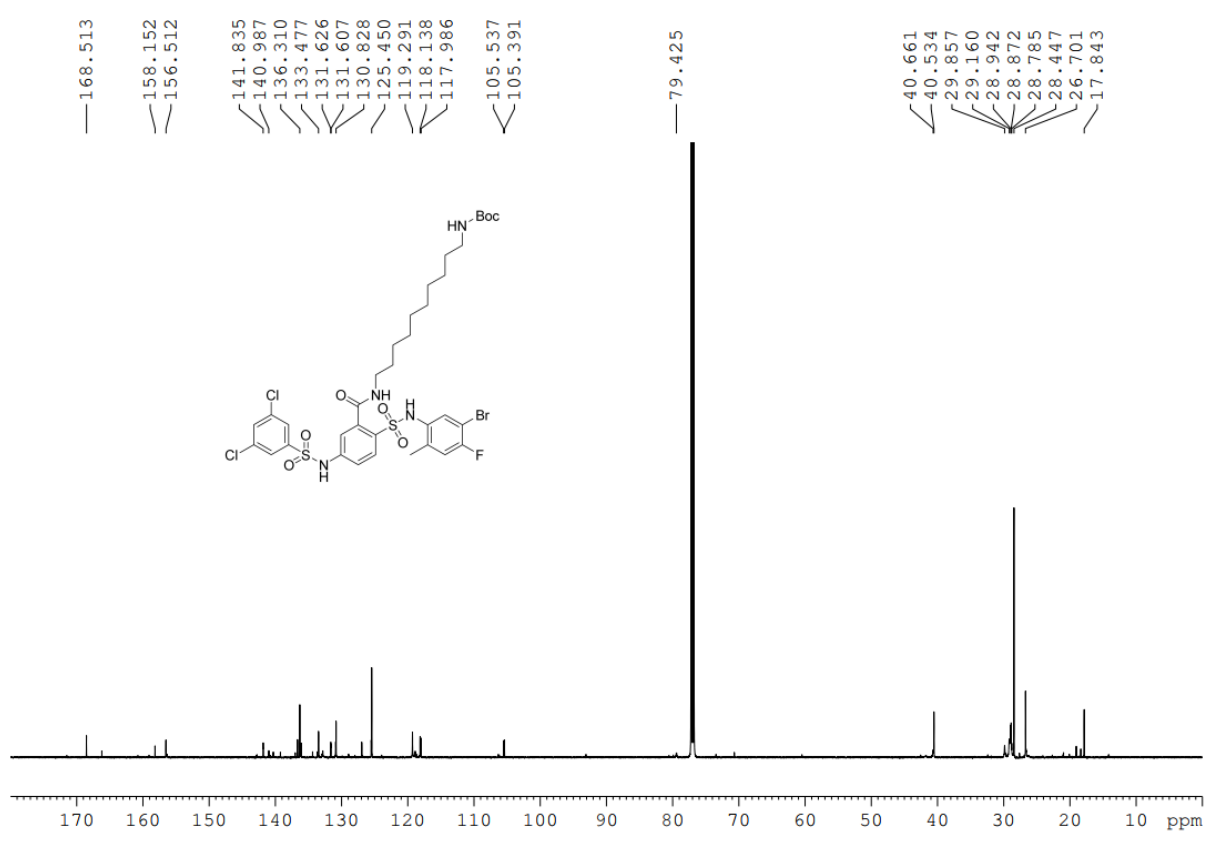


¹H NMR spectrum of **12c** (600 MHz, CDCl₃)



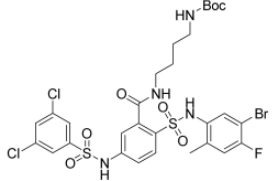


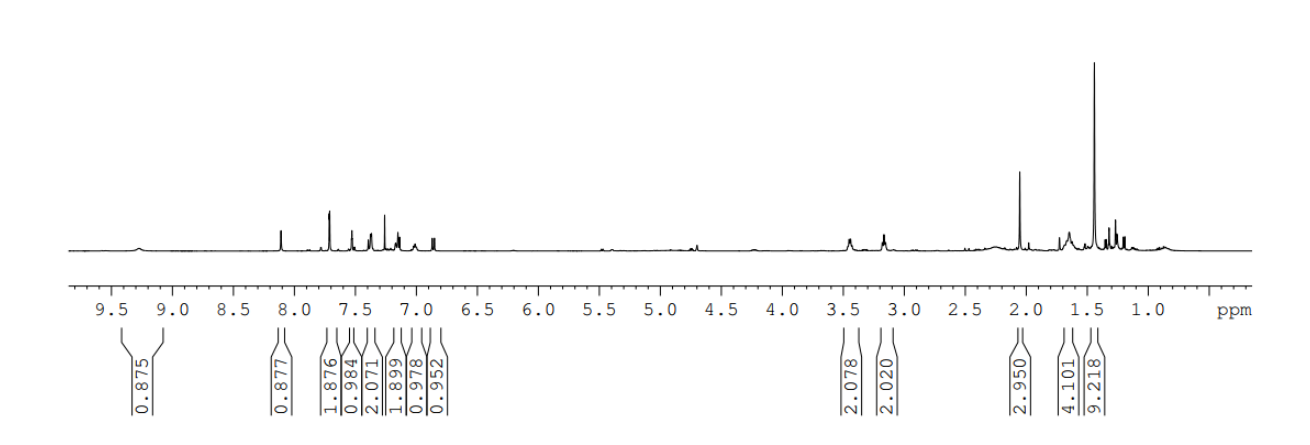
13 C NMR spectrum of 12c (151 MHz, CDCl₃)



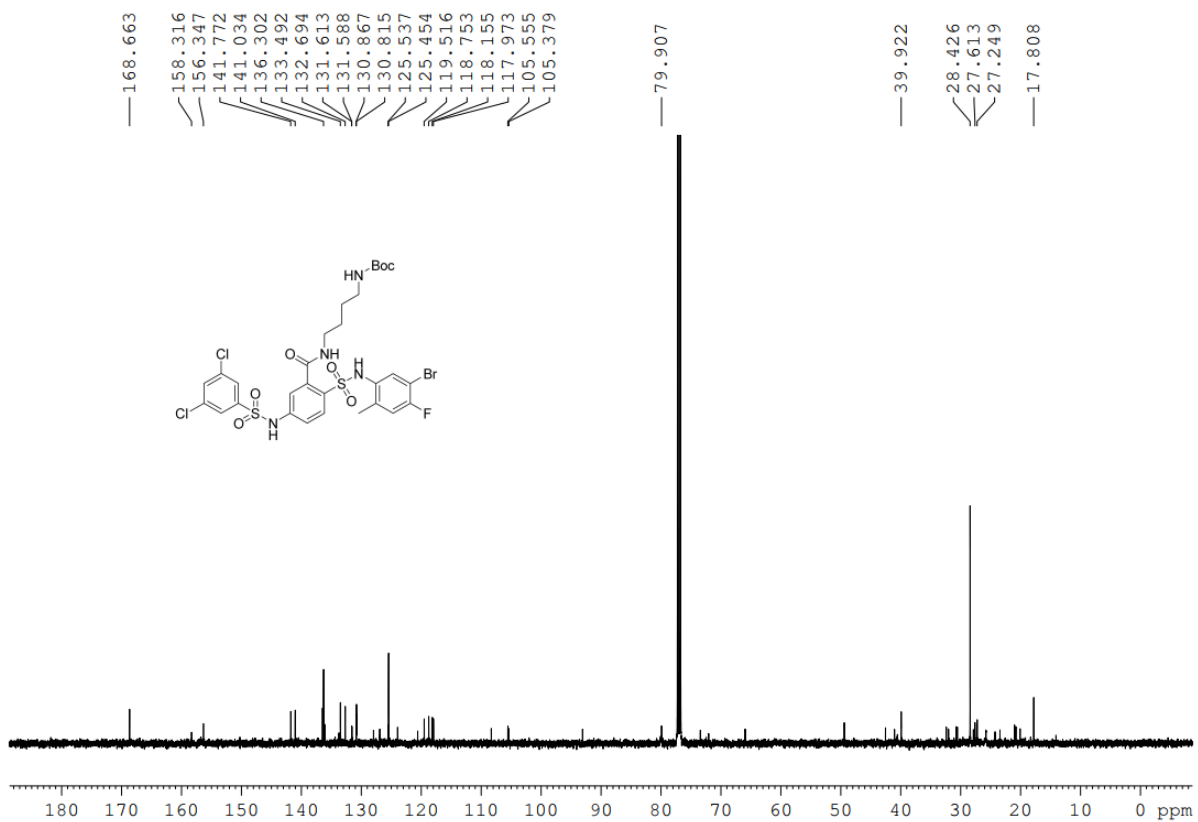
¹H NMR spectrum of **12d** (500 MHz, CDCl₃)



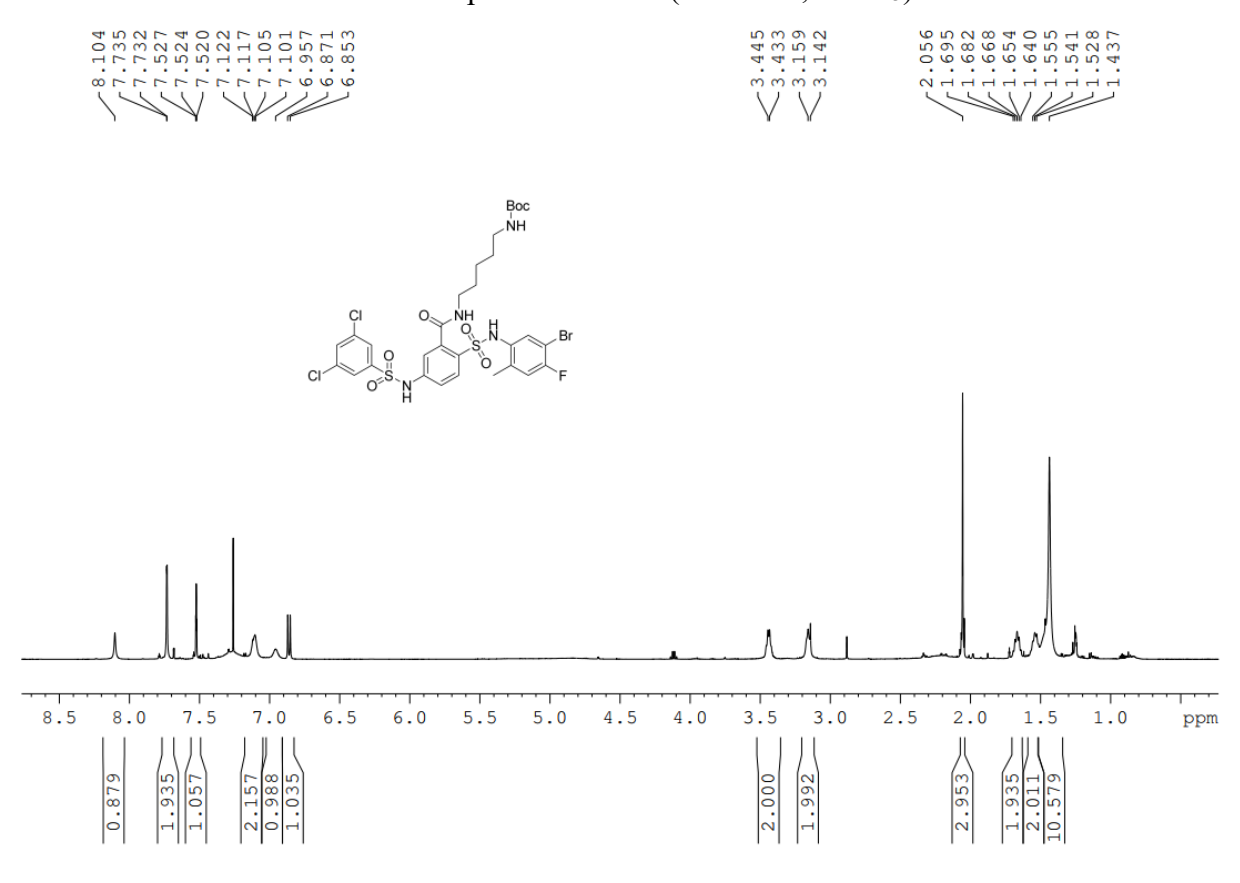




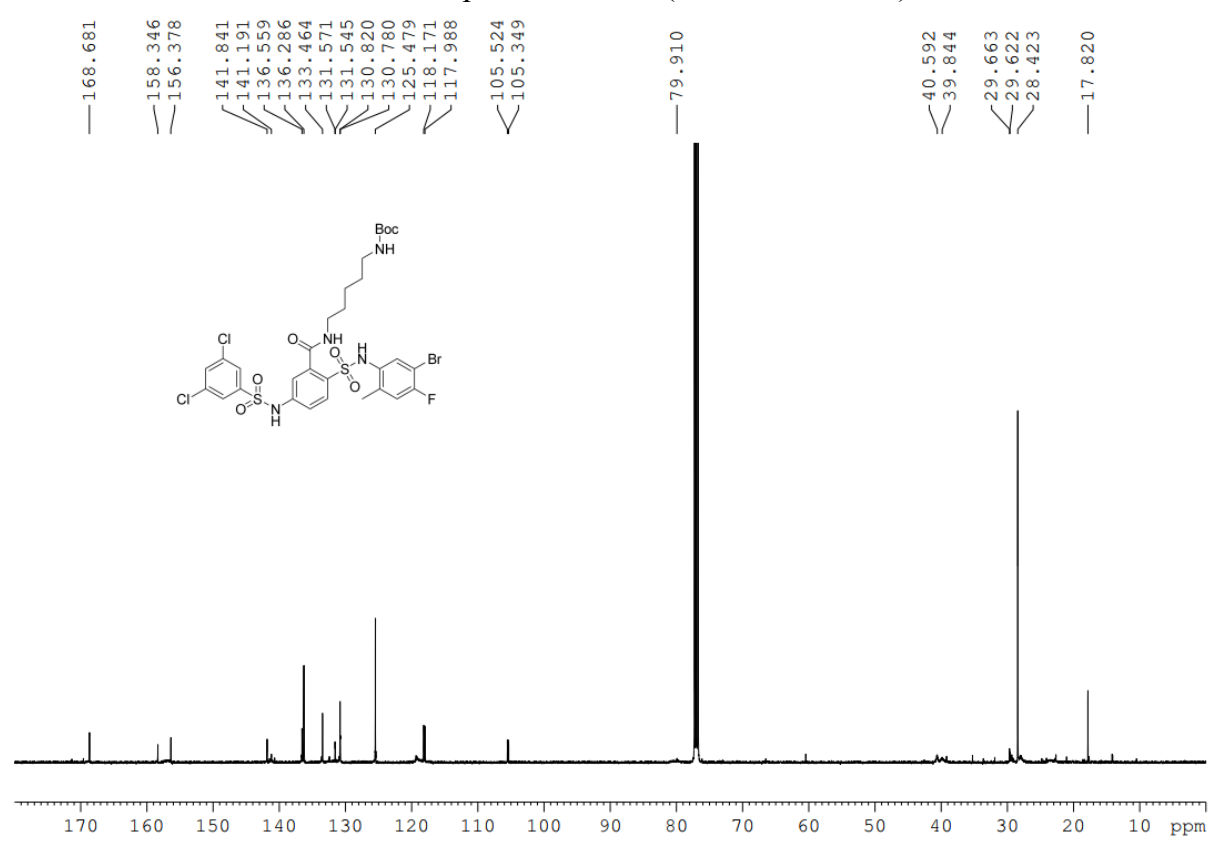
^{13}C NMR spectrum of **12d** (126 MHz, CDCl₃)

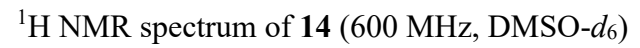


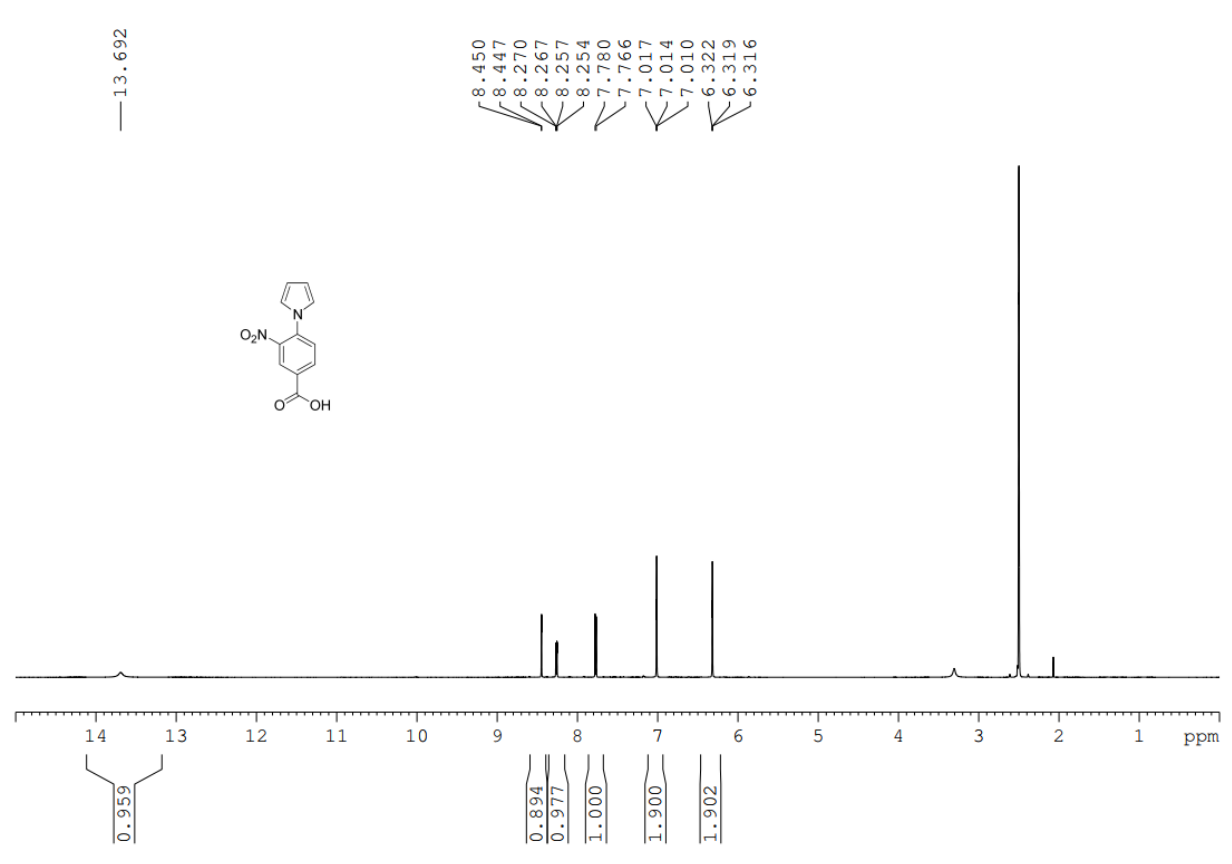
¹H NMR spectrum of **12e** (500 MHz, CDCl₃)



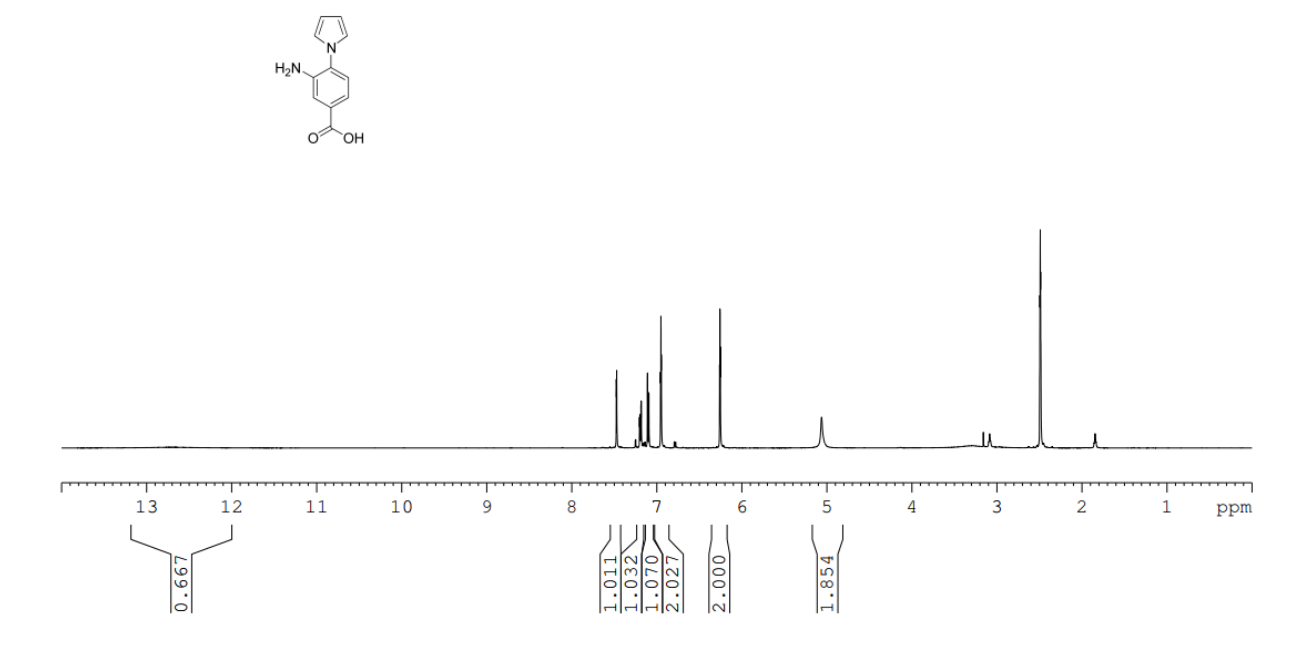
¹³C NMR spectrum of **12e** (126 MHz, CDCl₃)

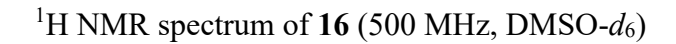


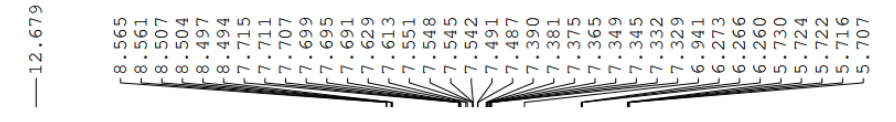




1 H NMR spectrum of **15** (500 MHz, DMSO- d_{6})

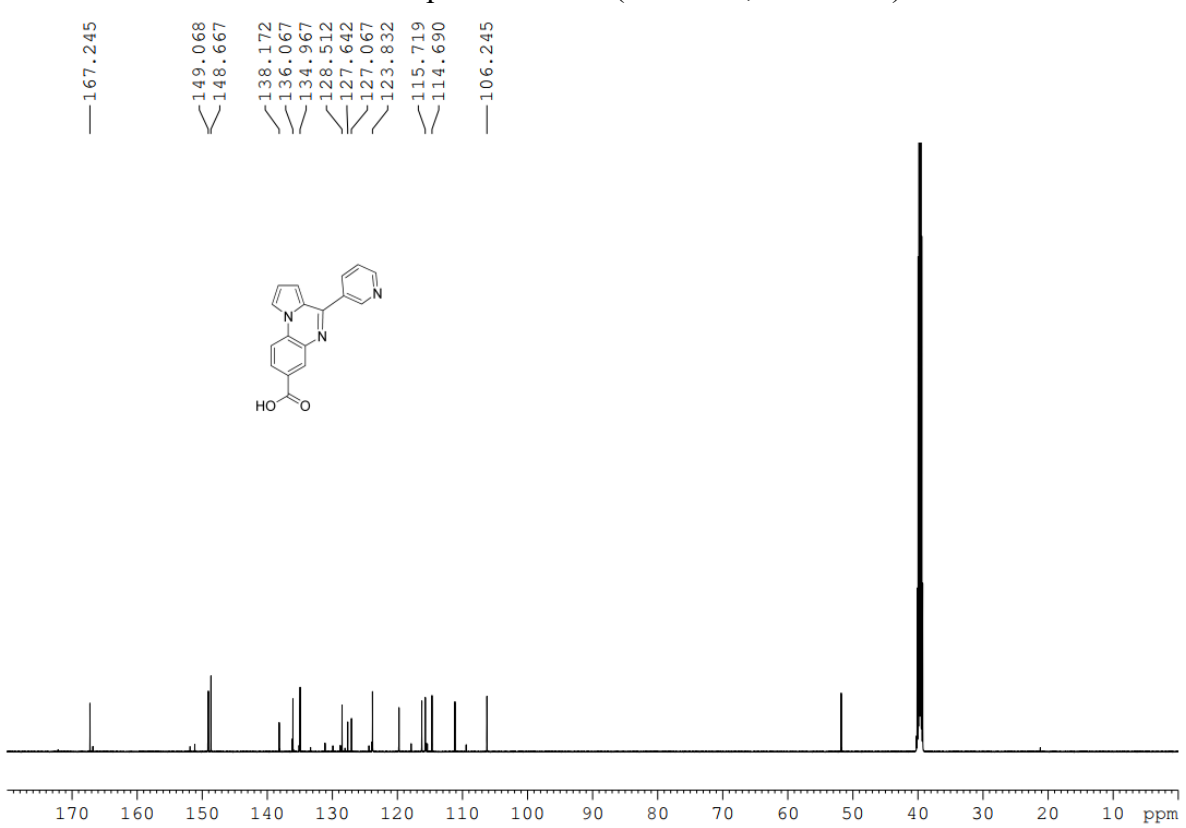




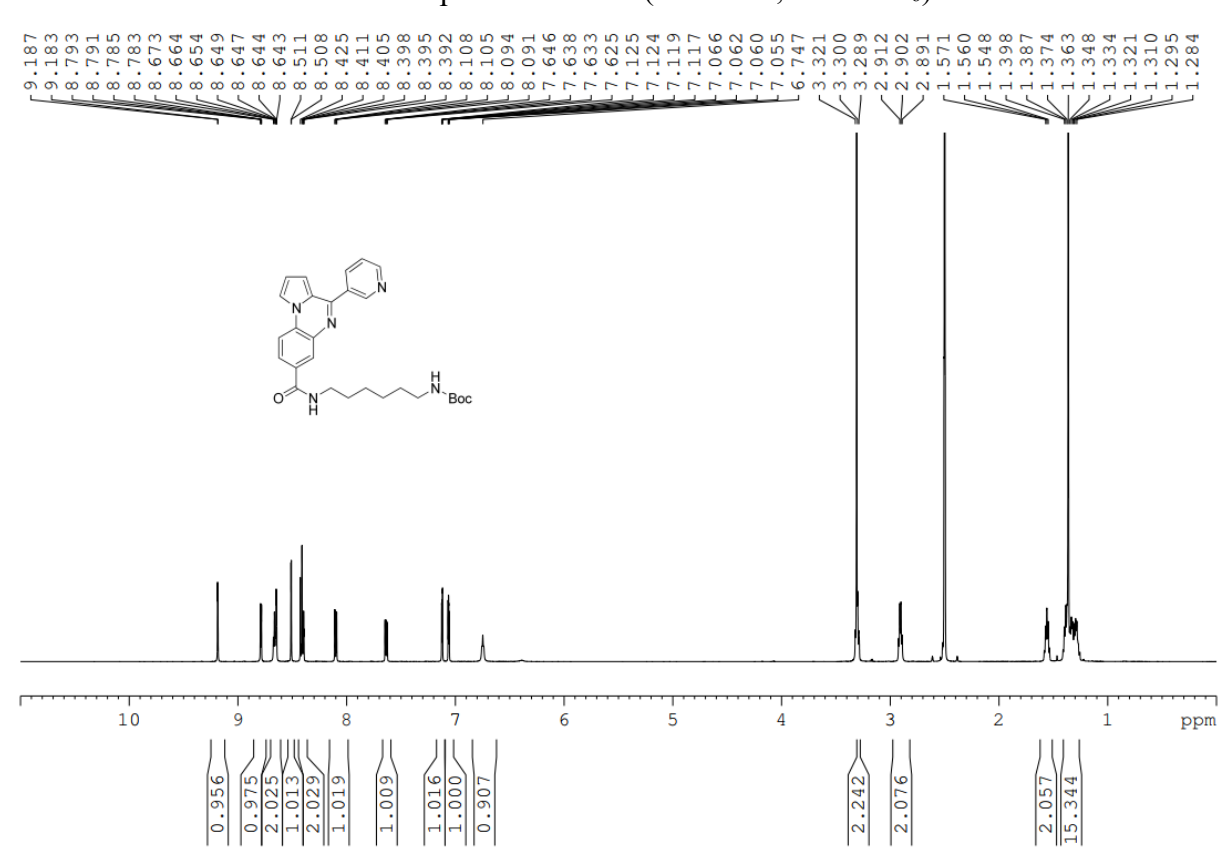




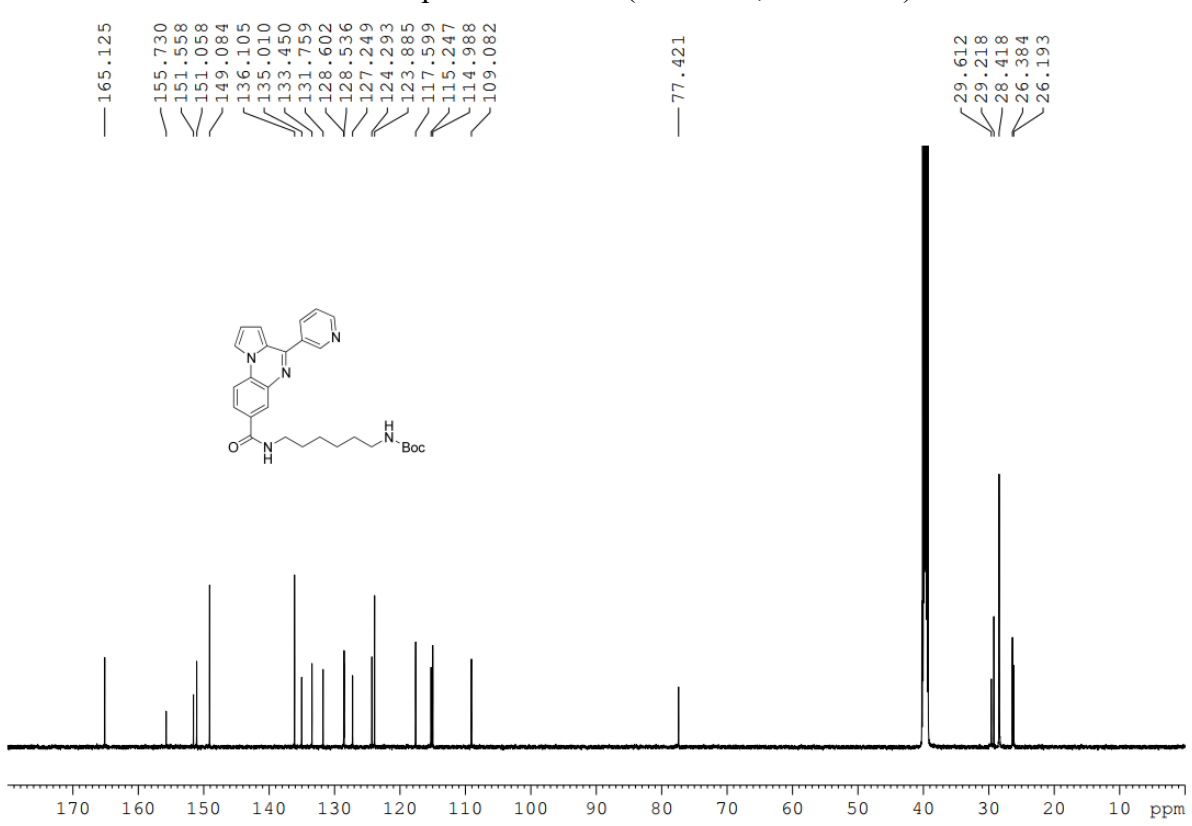
13 C NMR spectrum of **16** (151 MHz, DMSO- d_6)



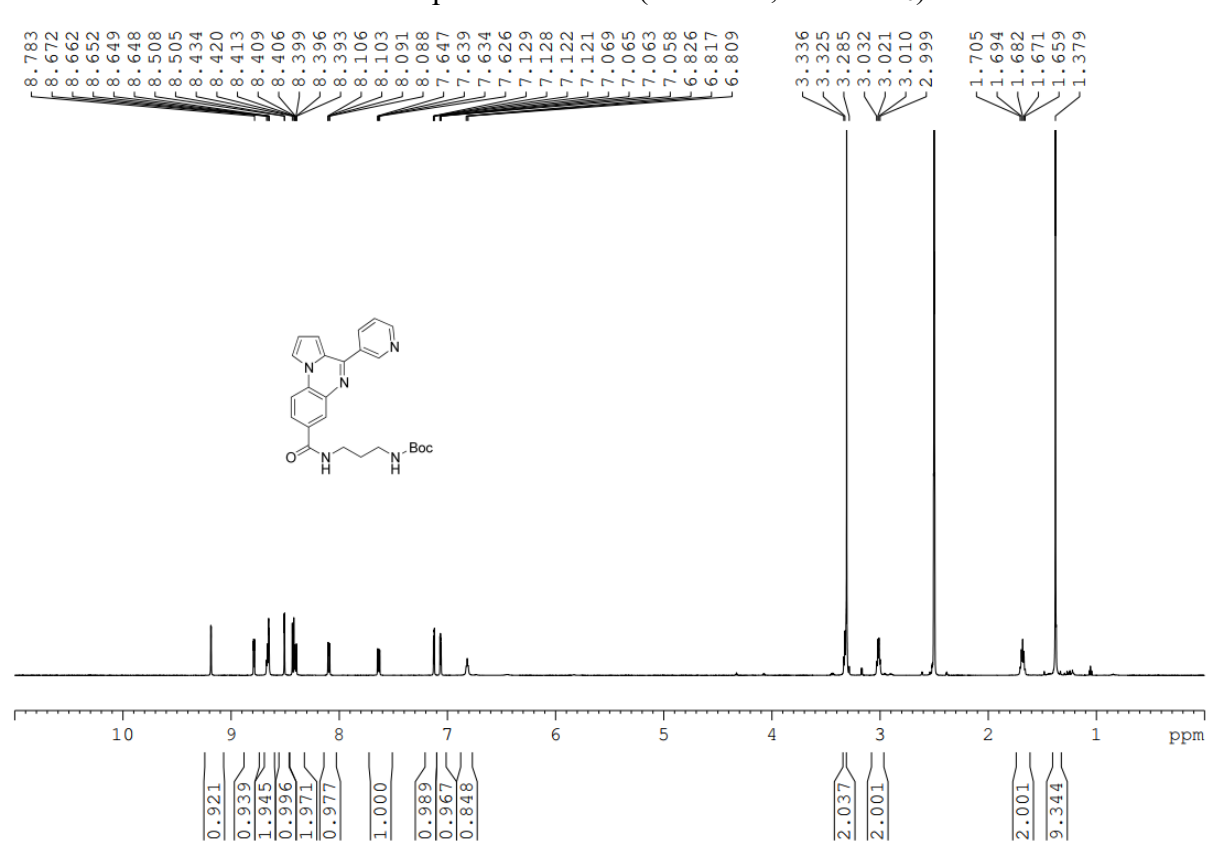
¹H NMR spectrum of **17a** (600 MHz, DMSO-*d*₆)



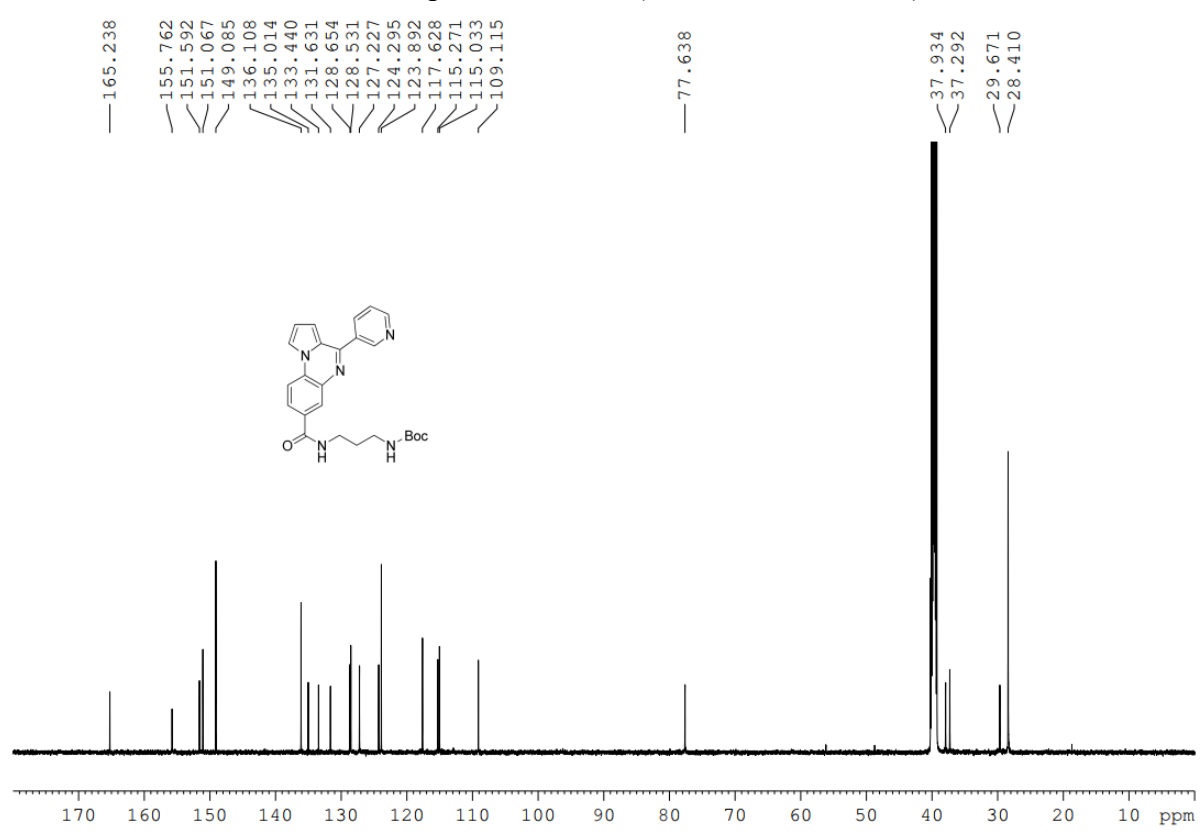
13 C NMR spectrum of **17a** (151 MHz, DMSO- d_6)



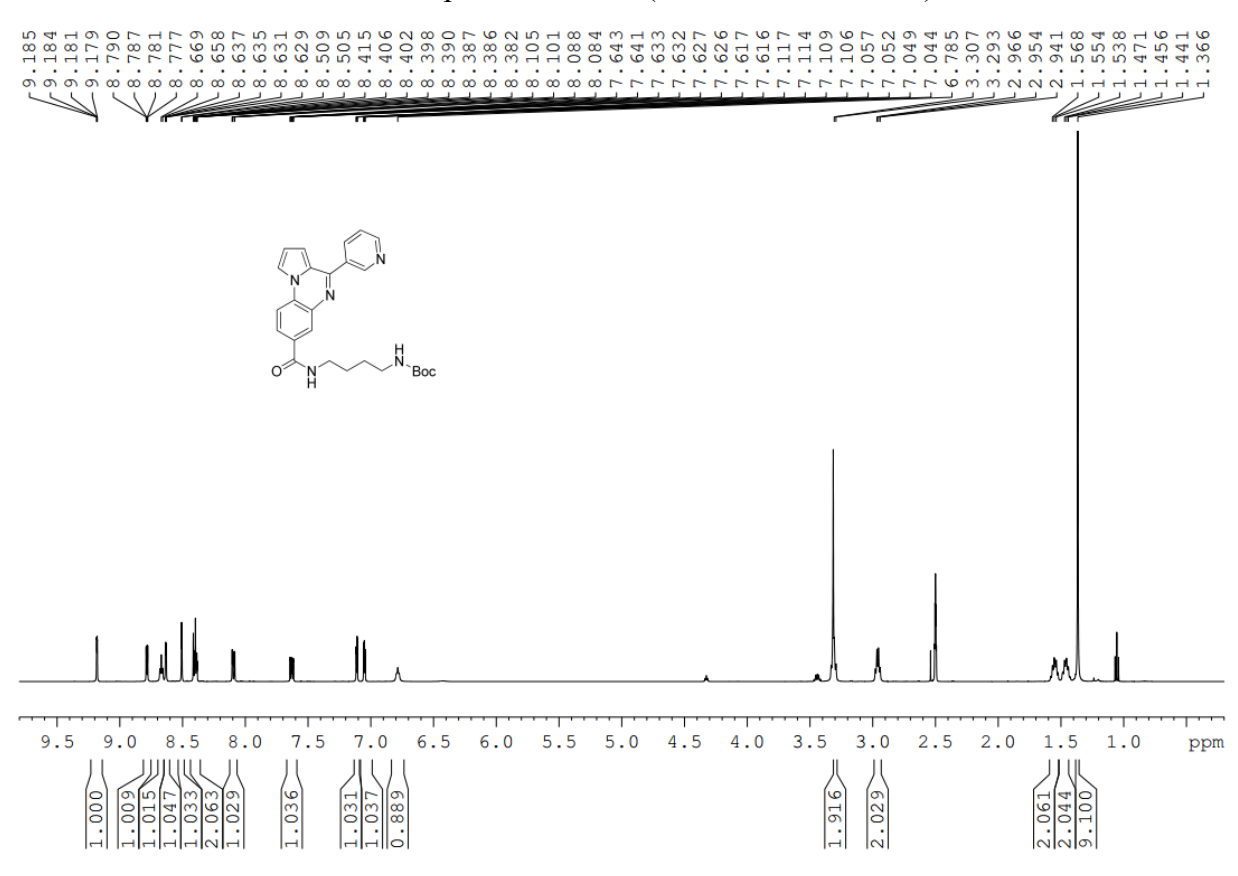
¹H NMR spectrum of **17b** (600 MHz, DMSO-*d*₆)



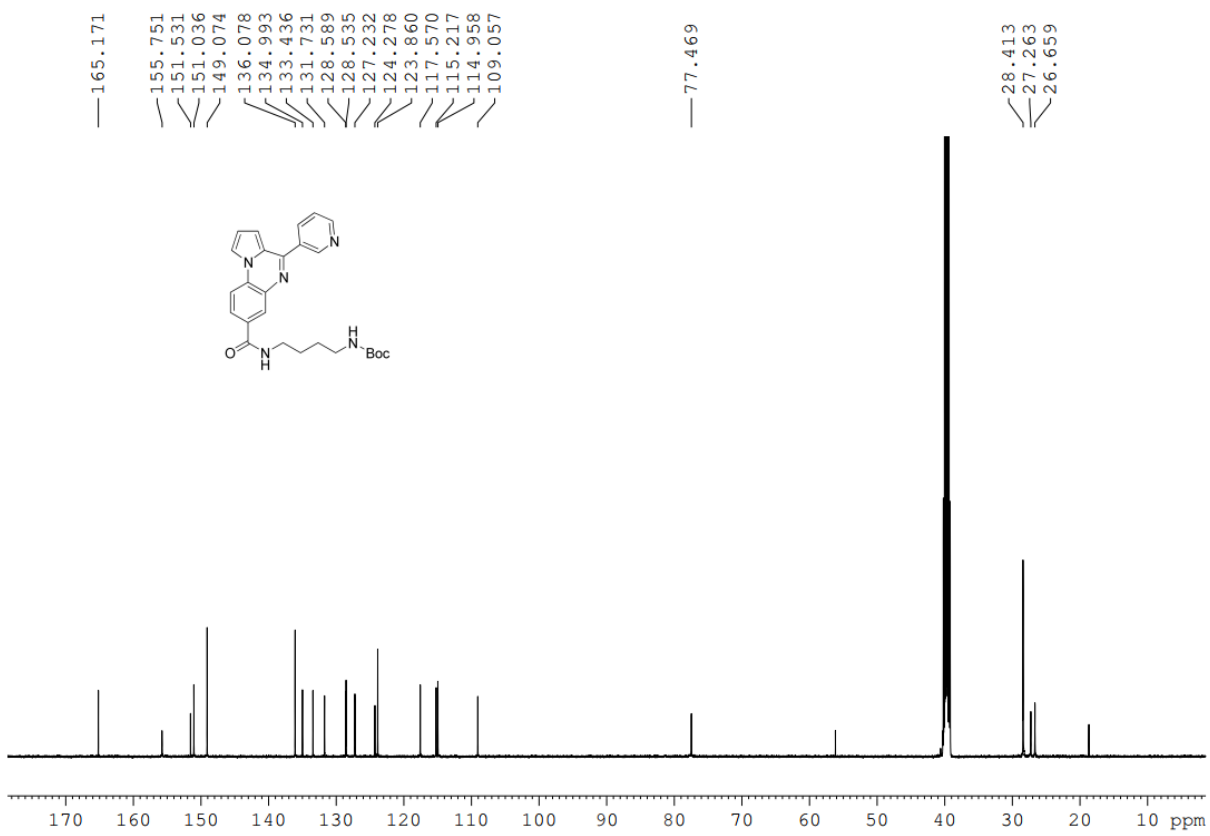
¹³C NMR spectrum of **17b** (151 MHz, DMSO-*d*₆)



¹H NMR spectrum of **17c** (500 MHz, DMSO-*d*₆)



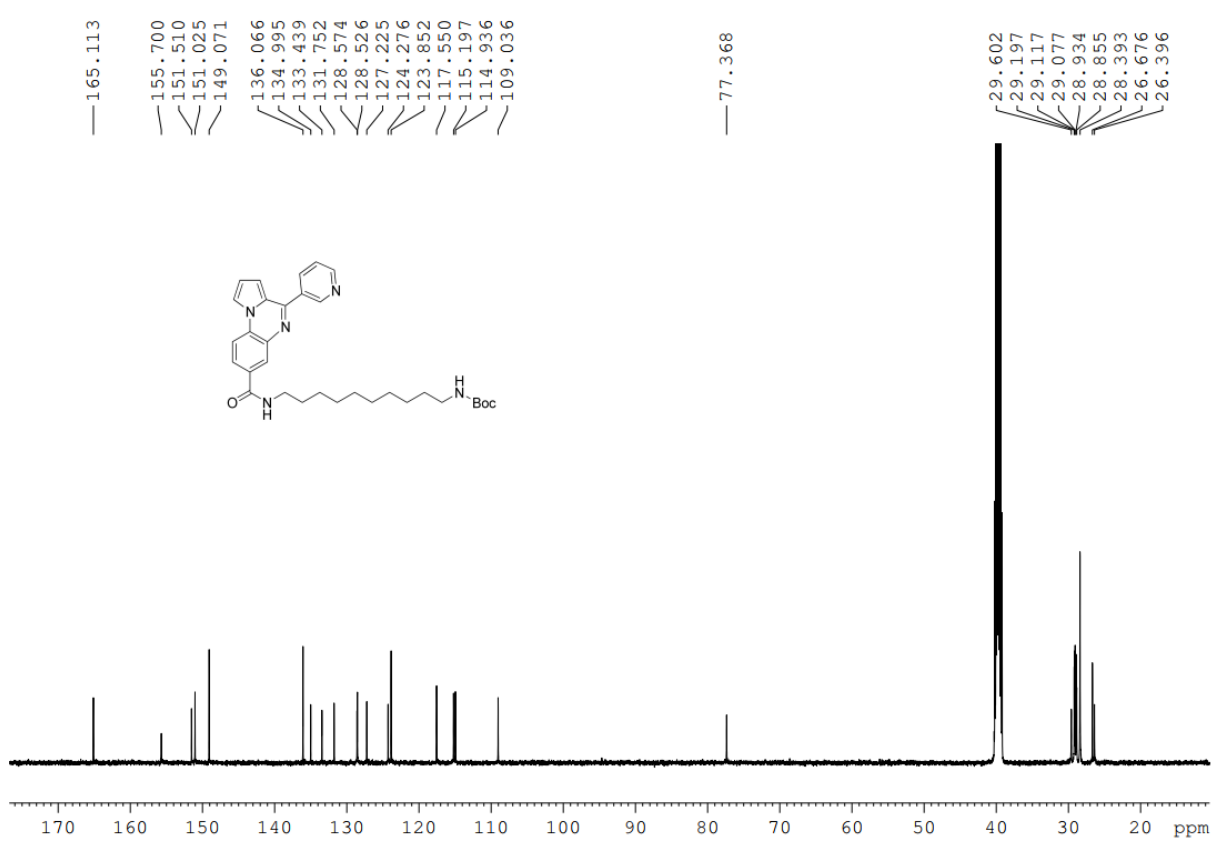
13 C NMR spectrum of **17c** (126 MHz, DMSO- d_6)



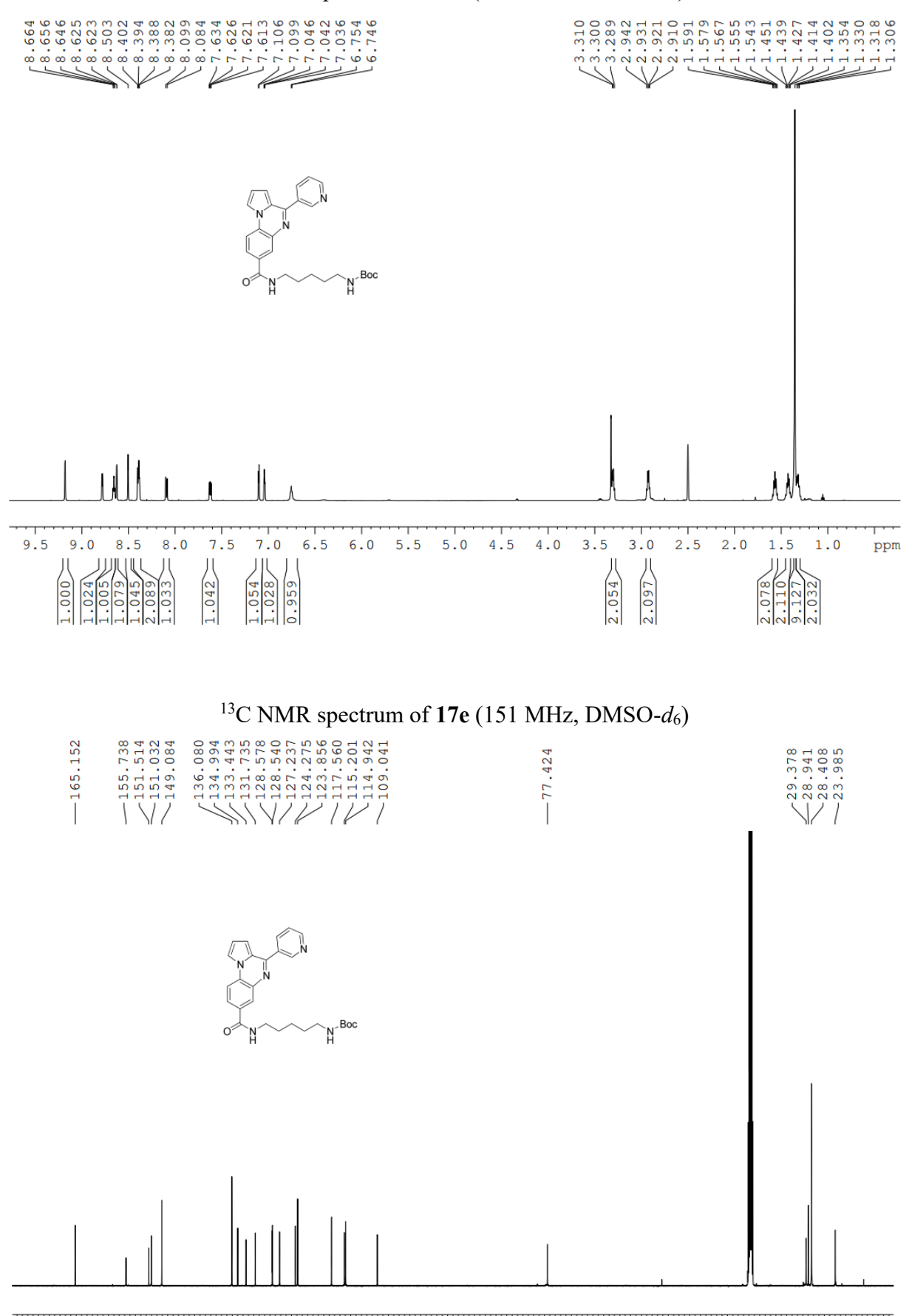
¹H NMR spectrum of **17d** (500 MHz, DMSO-*d*₆)



13 C NMR spectrum of **17d** (126 MHz, DMSO- d_6)

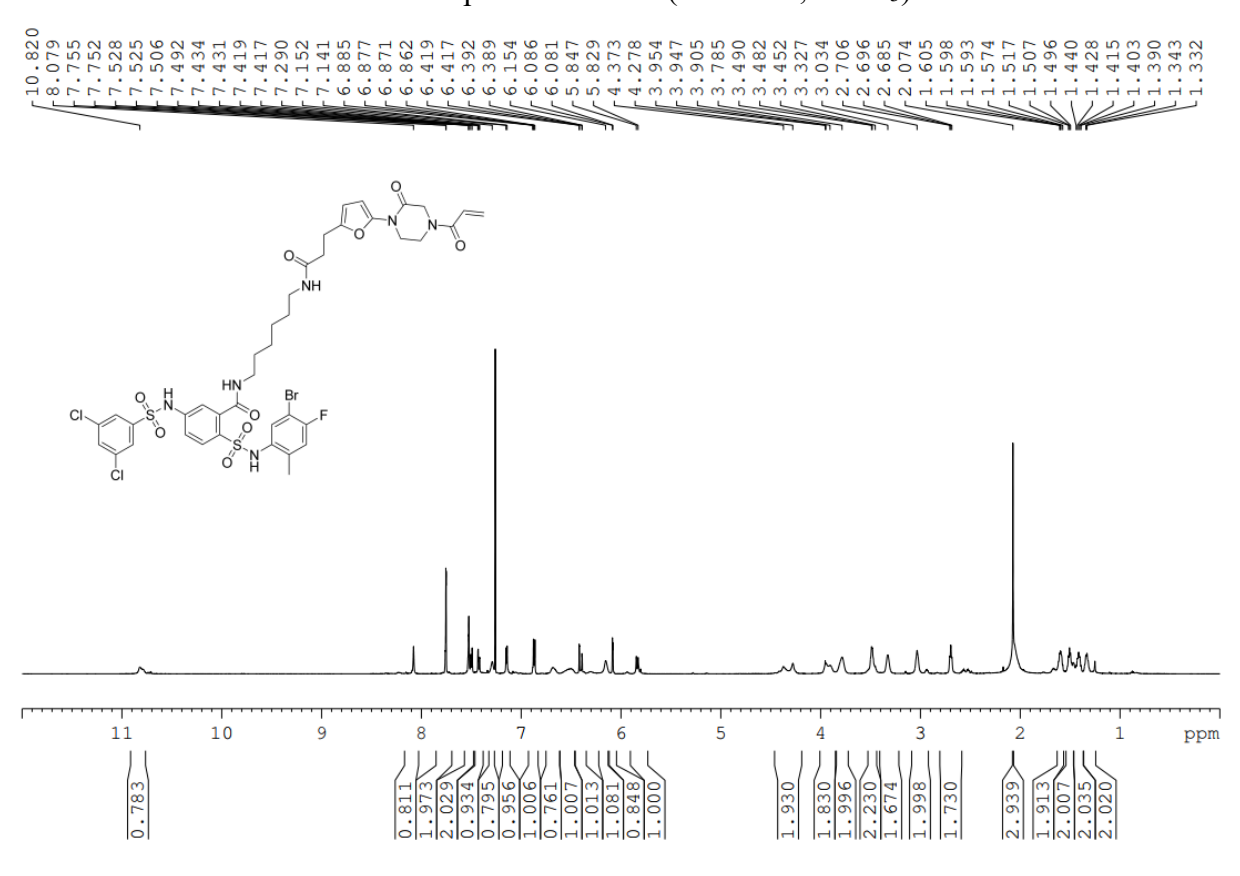


¹H NMR spectrum of **17e** (600 MHz, DMSO-*d*₆)

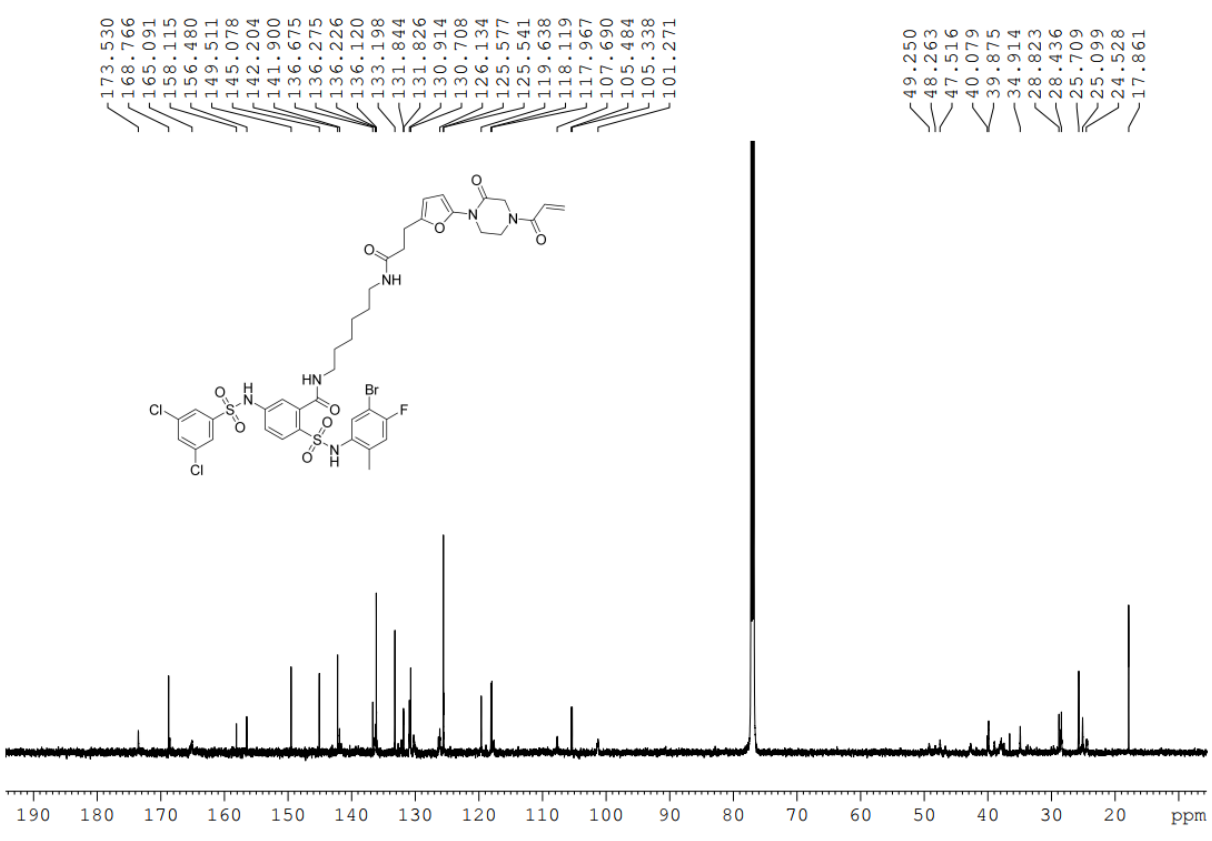


ppm

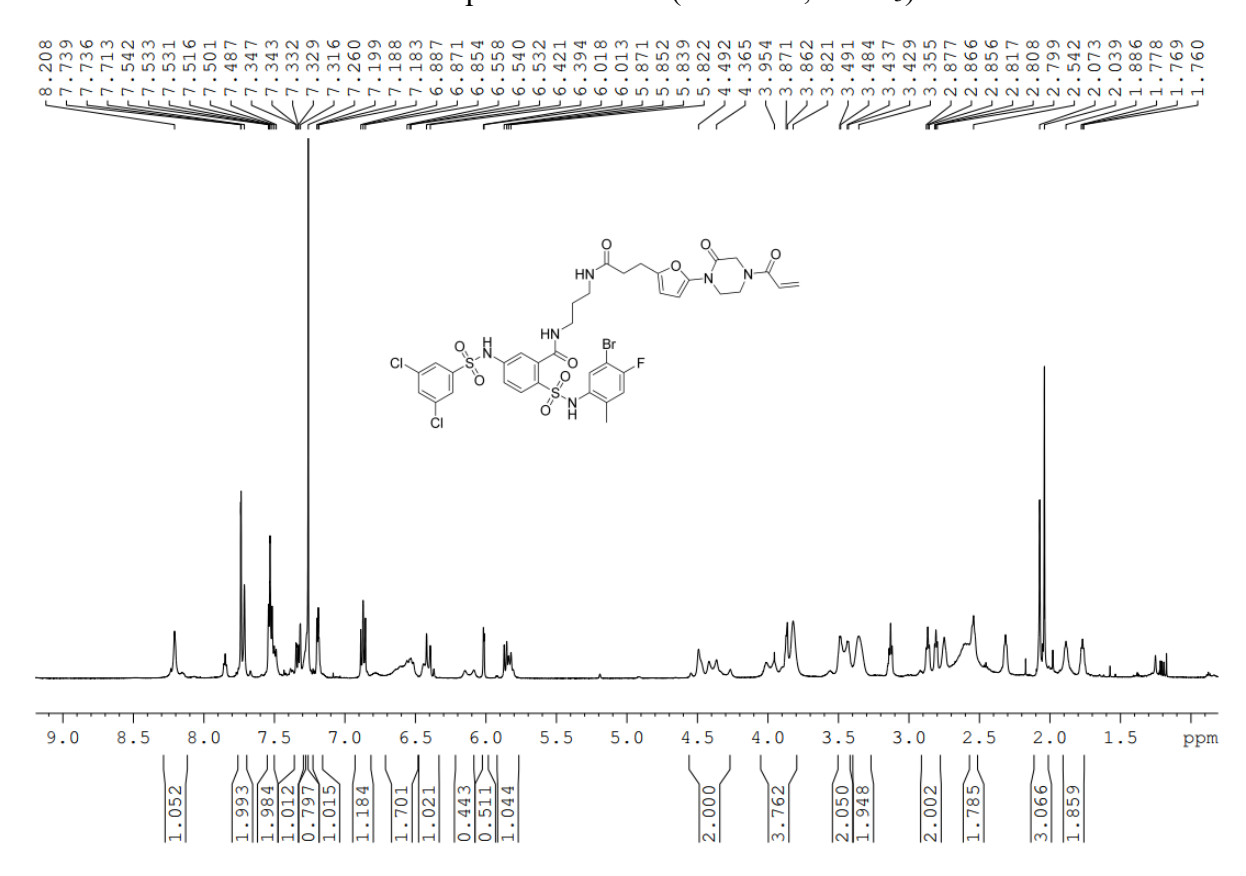
¹H NMR spectrum of **18a** (600 MHz, CDCl₃)



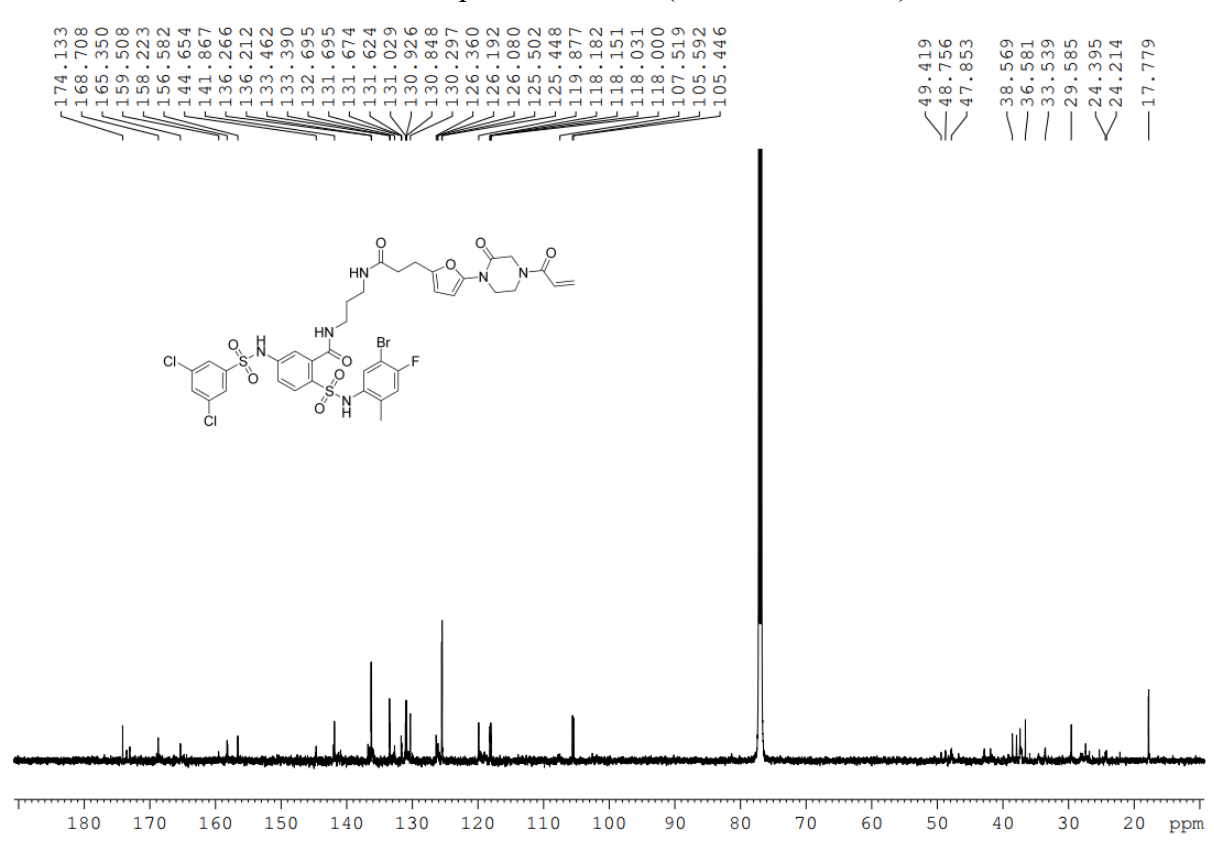
¹³C NMR spectrum of **18a** (151 MHz, CDCl₃)



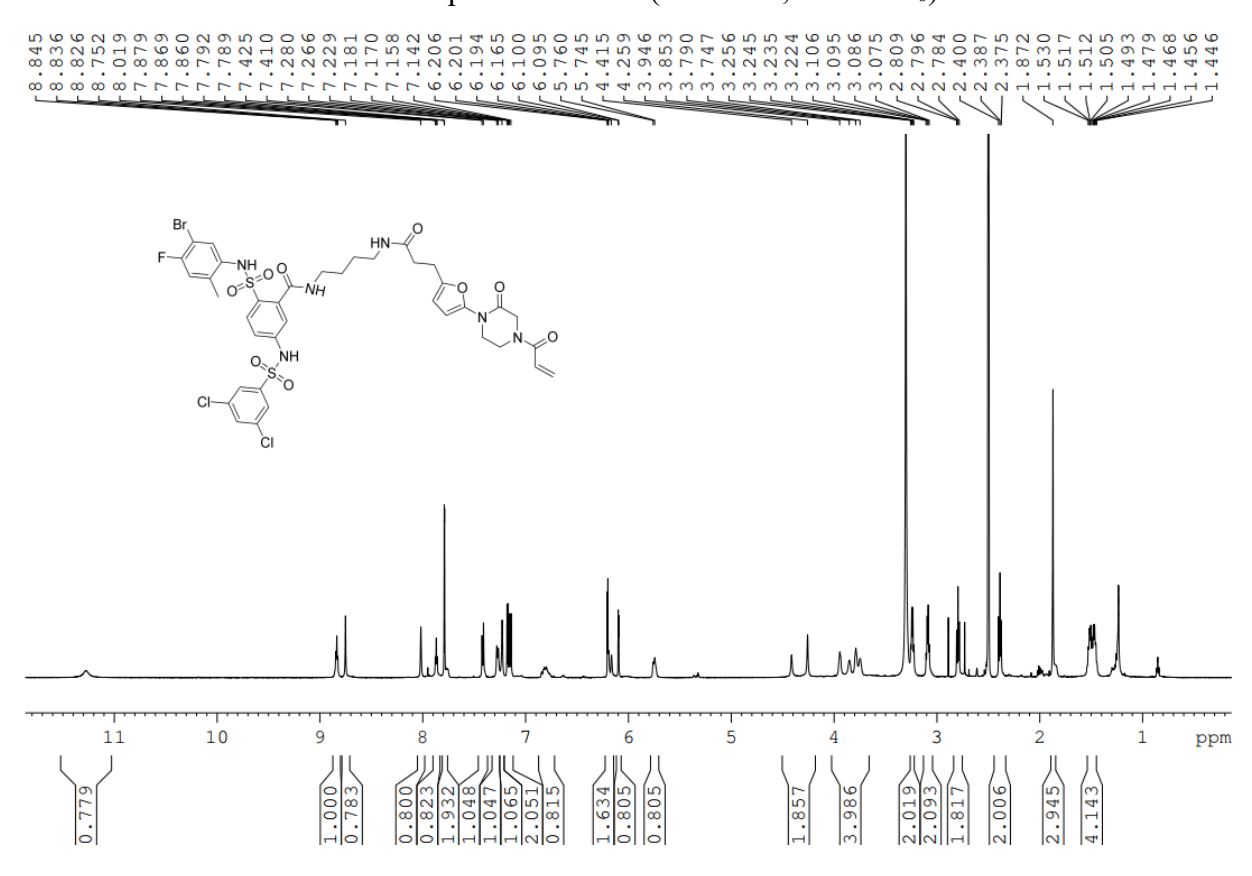
¹H NMR spectrum of **18b** (600 MHz, CDCl₃)



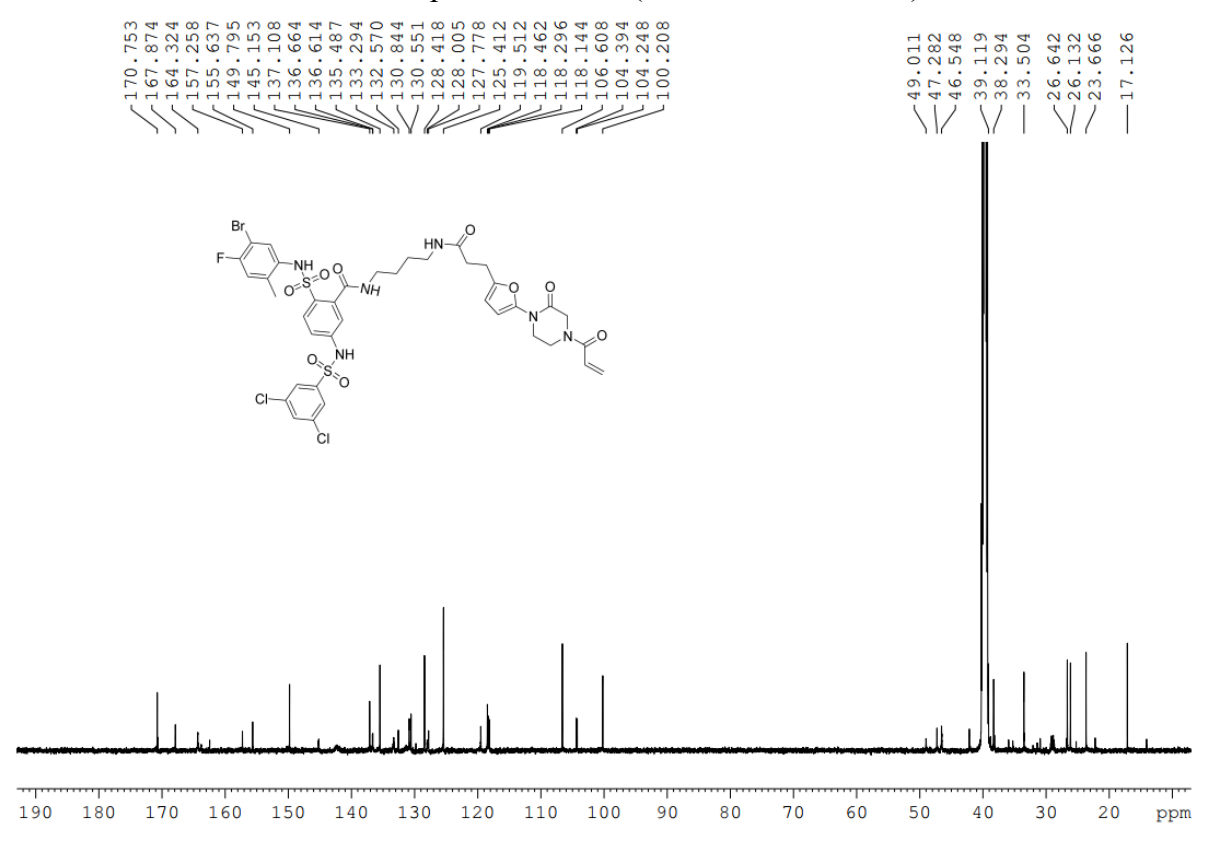
13 C NMR spectrum of **18b** (151 MHz, CDCl₃)



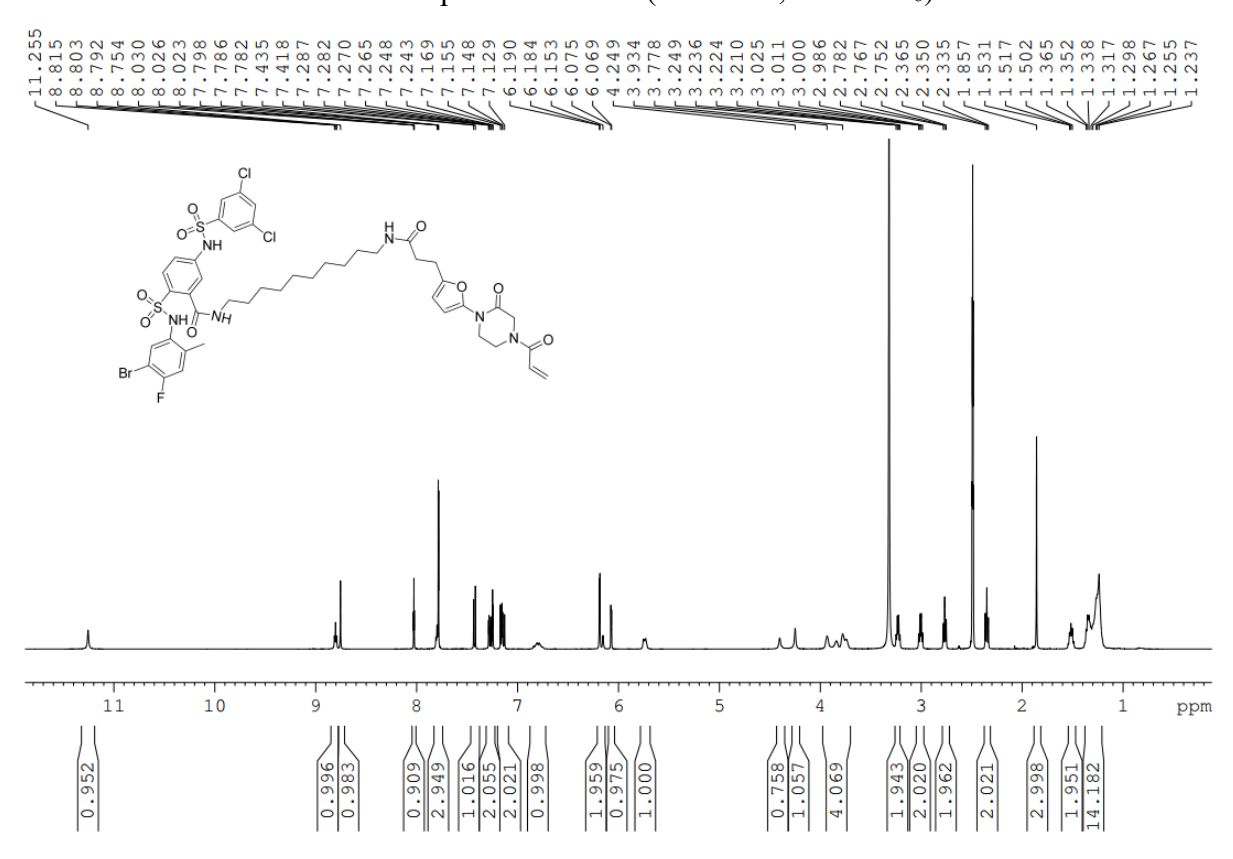
¹H NMR spectrum of **18c** (600 MHz, DMSO-*d*₆)



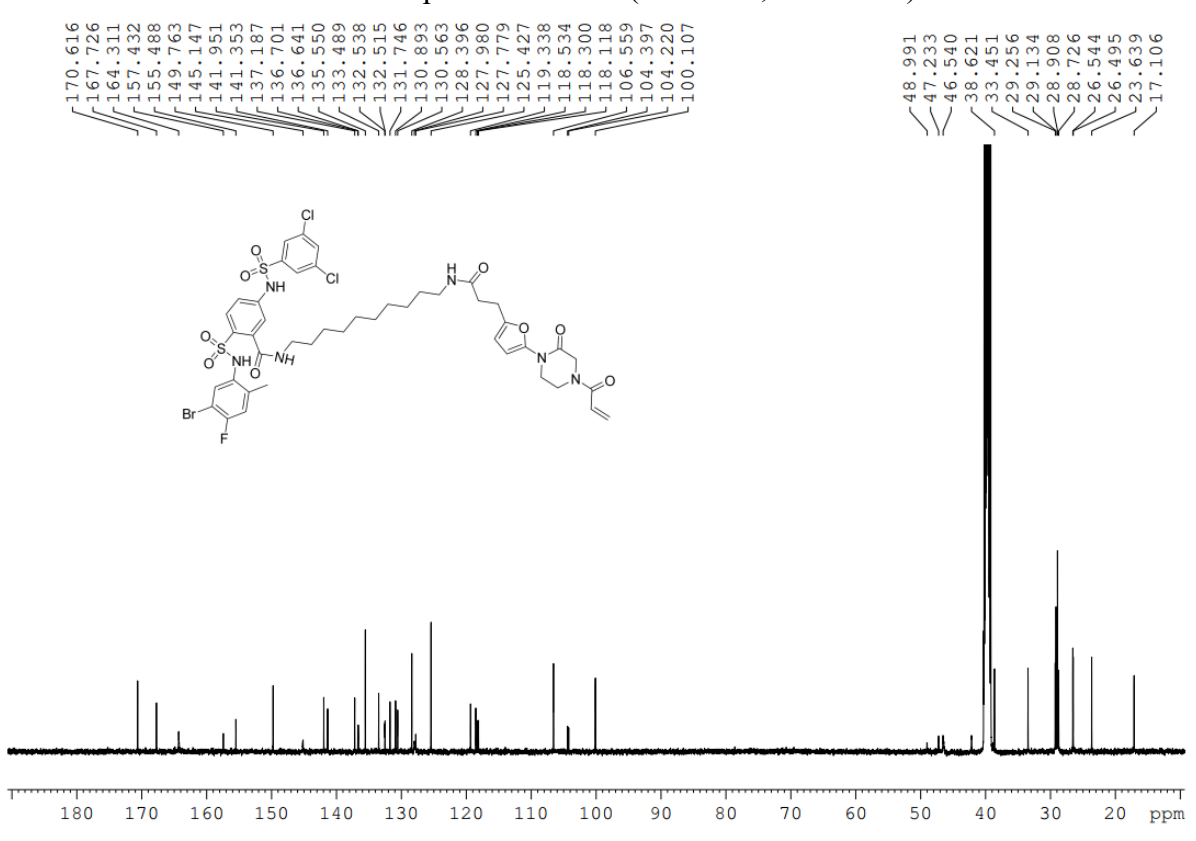
13 C NMR spectrum of **18c** (151 MHz, DMSO- d_6)



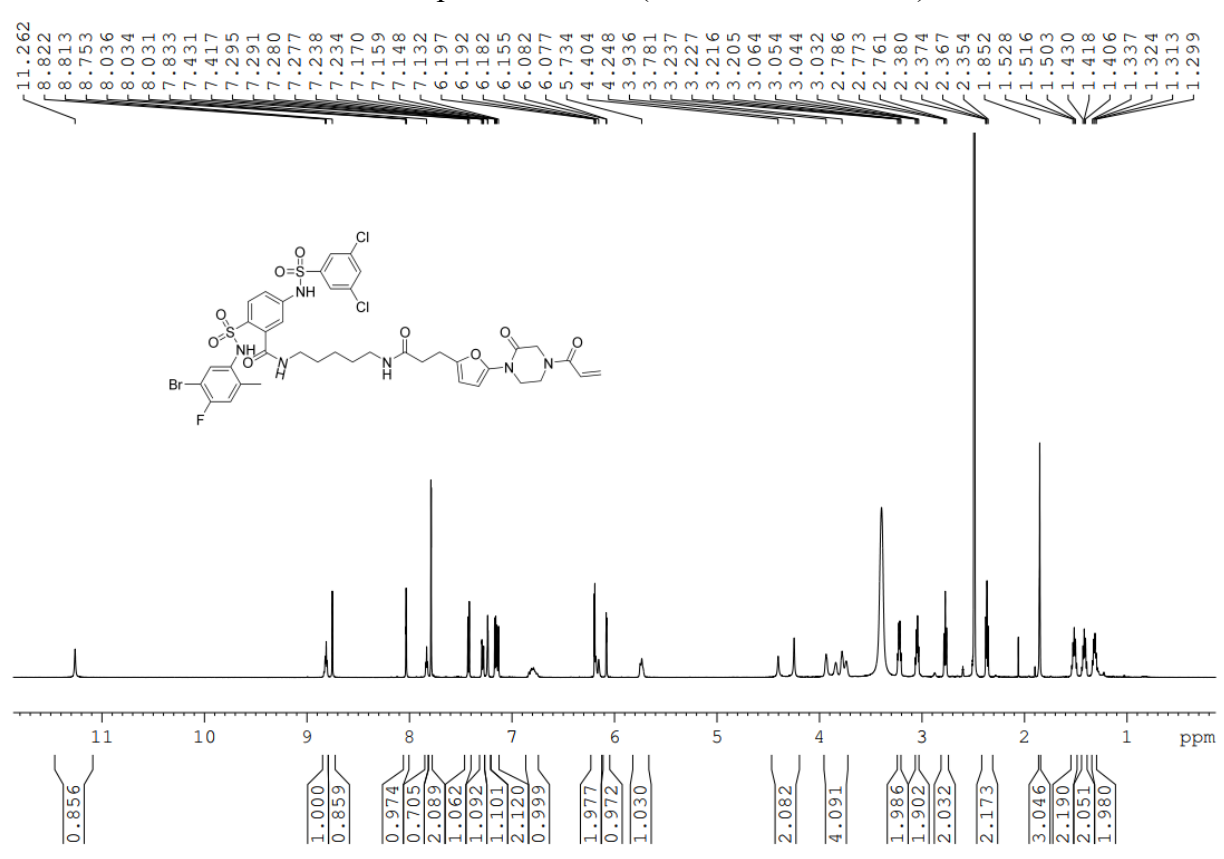
1 H NMR spectrum of **18d** (500 MHz, DMSO- d_{6})



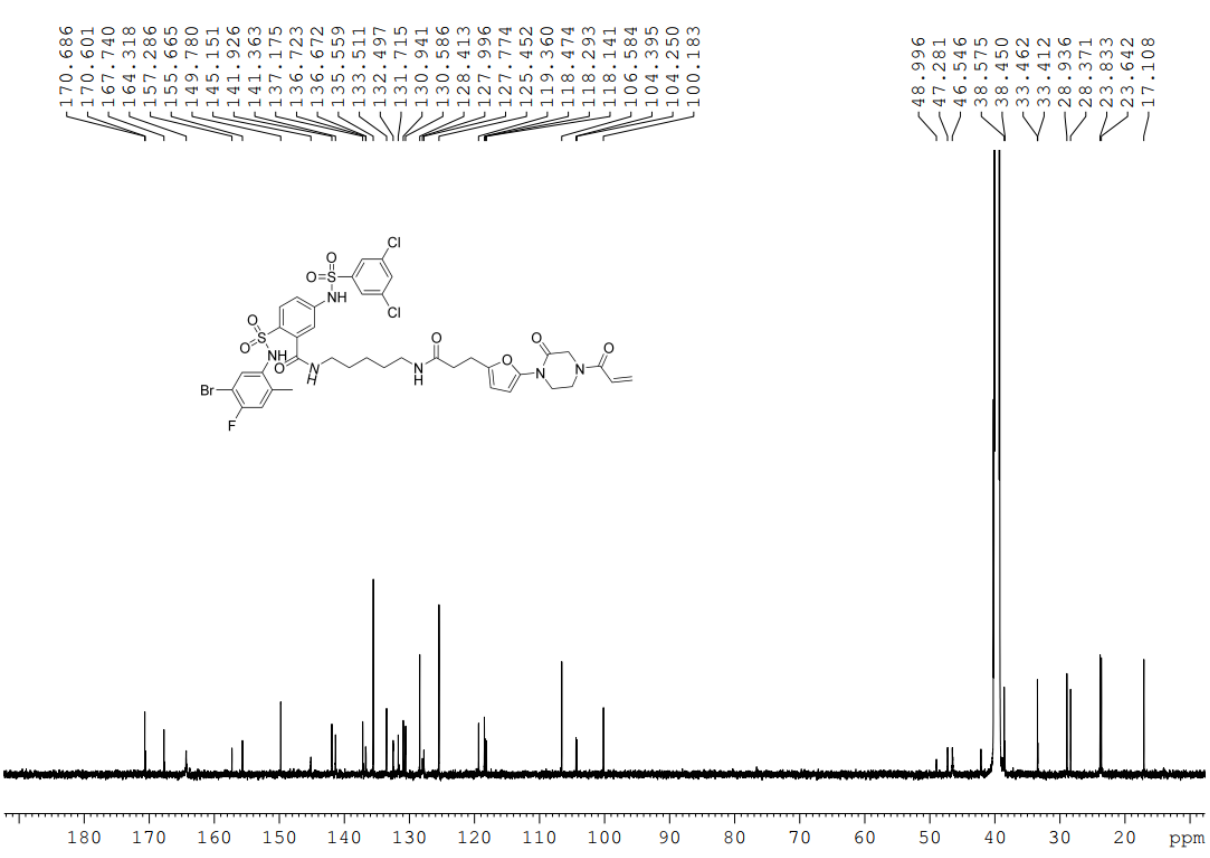
13 C NMR spectrum of **18d** (126 MHz, DMSO- d_6)



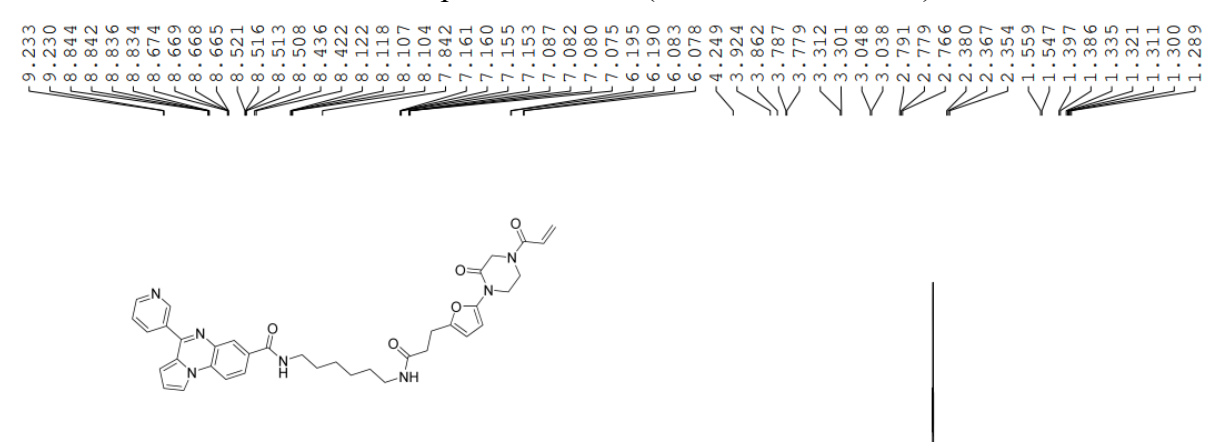
1 H NMR spectrum of **18e** (600 MHz, DMSO- d_{6})

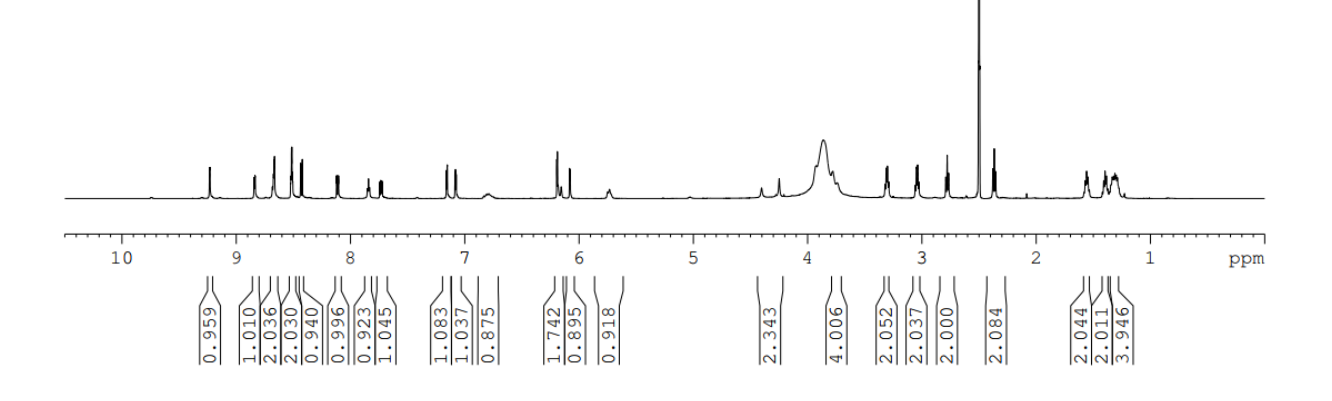


13 C NMR spectrum of **18e** (151 MHz, DMSO- d_6)

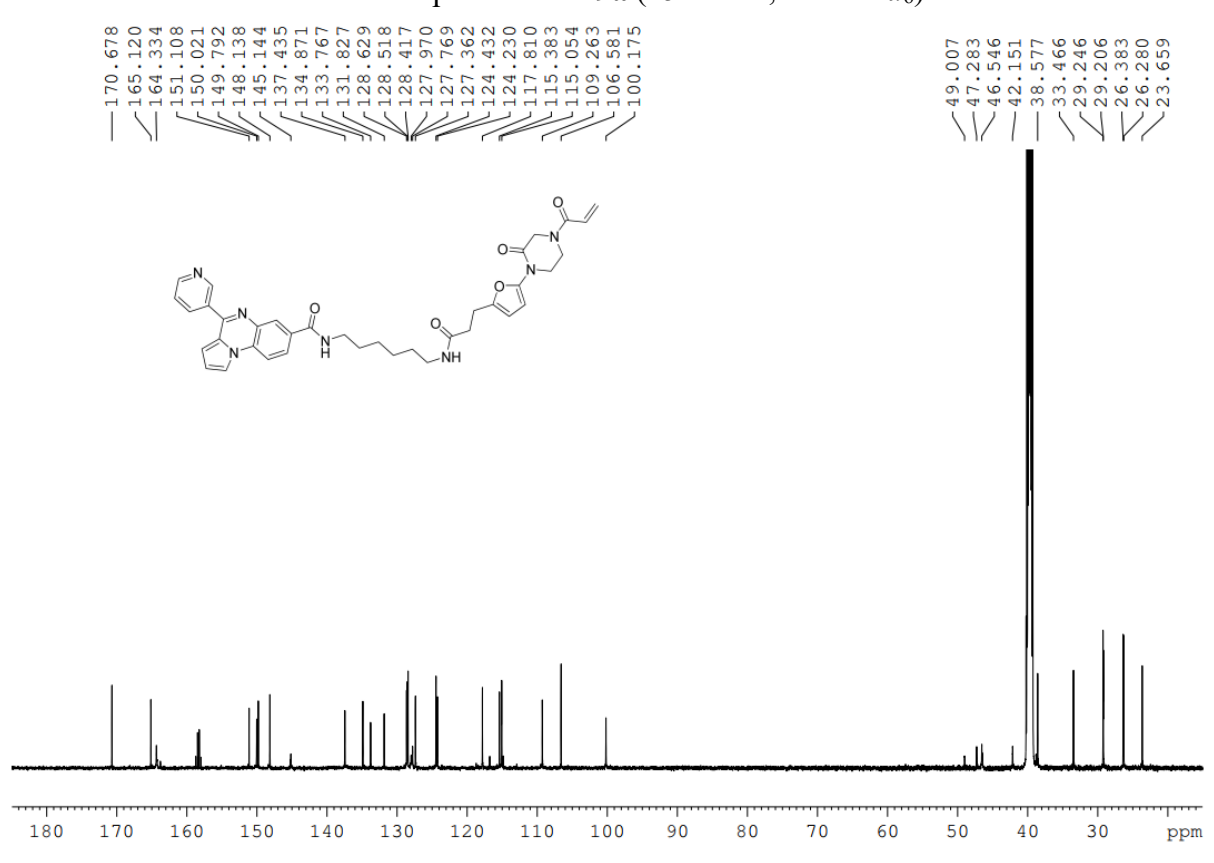


1 H NMR spectrum of **19a** (600 MHz, DMSO- d_{6})

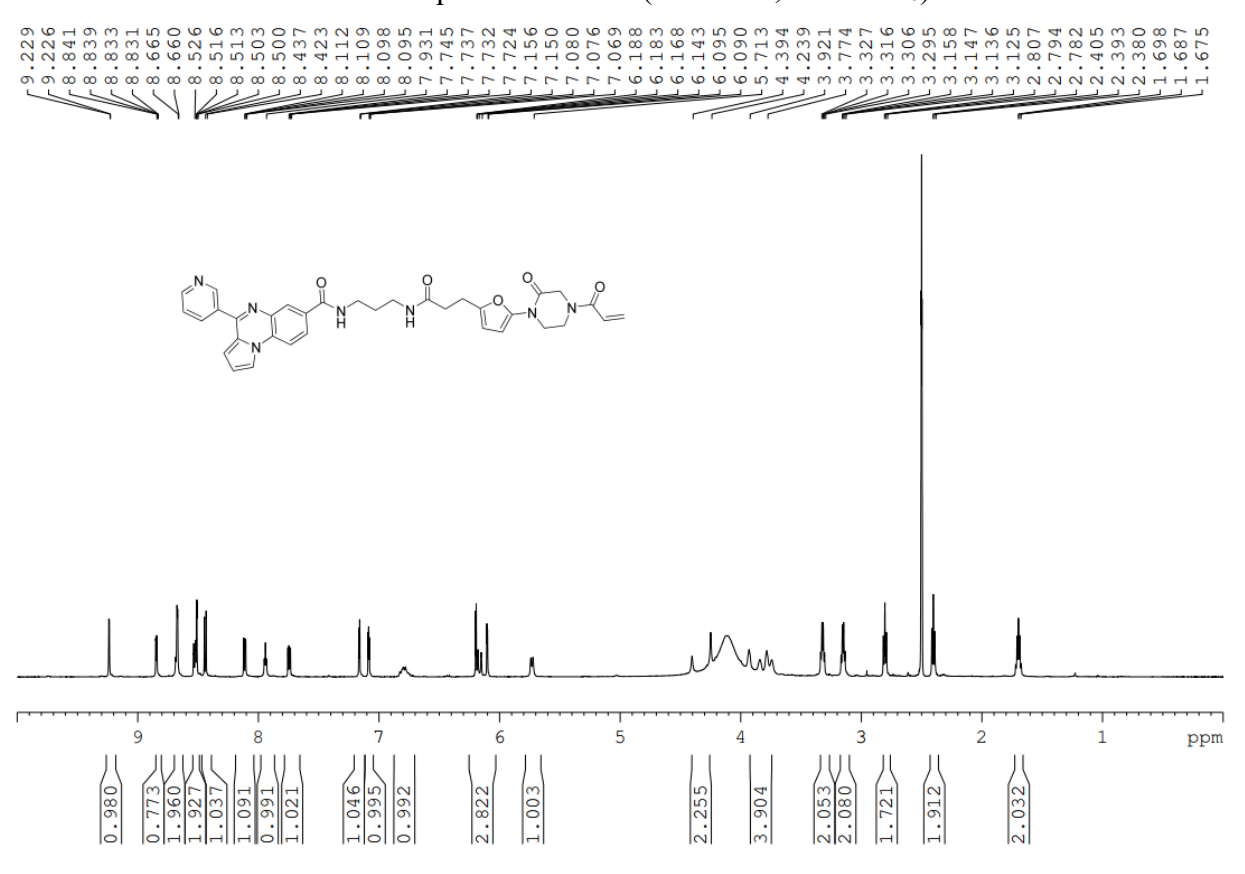




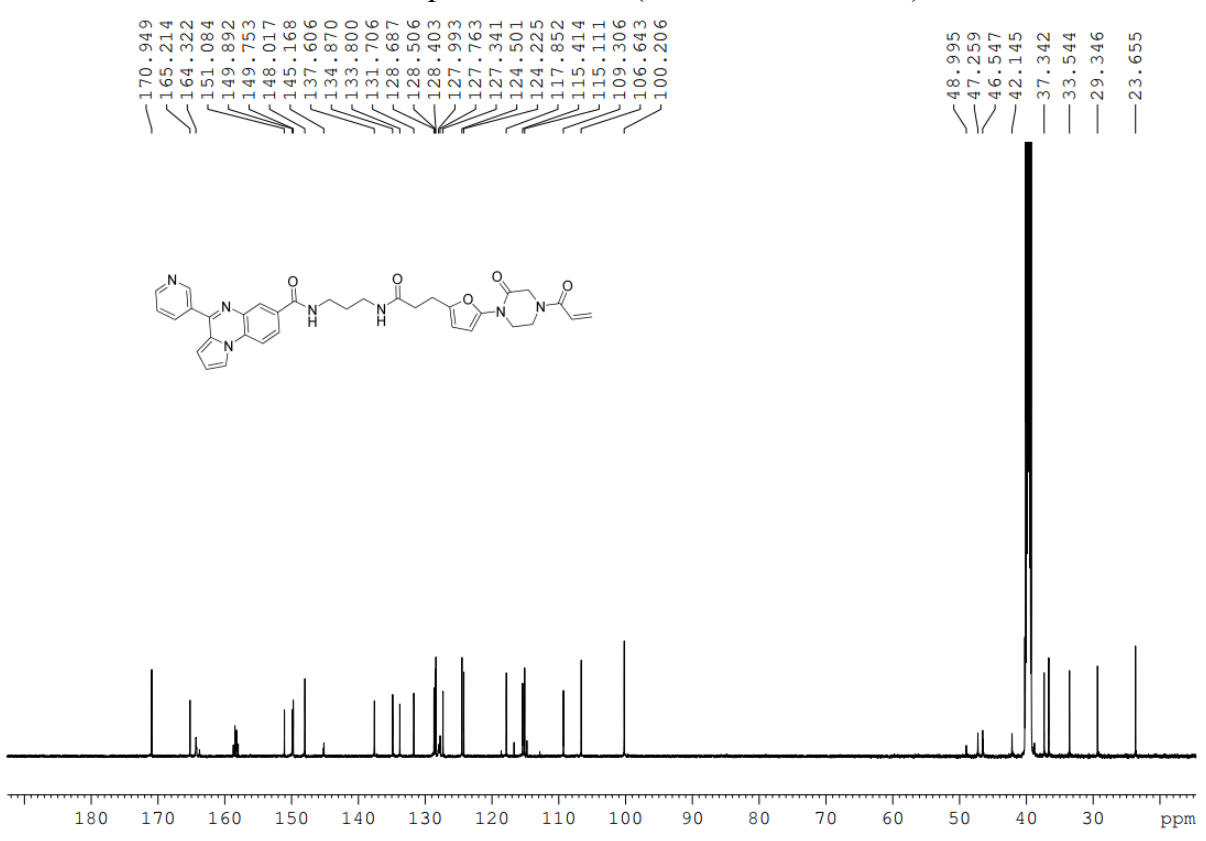
13 C NMR spectrum of **19a** (151 MHz, DMSO- d_6)



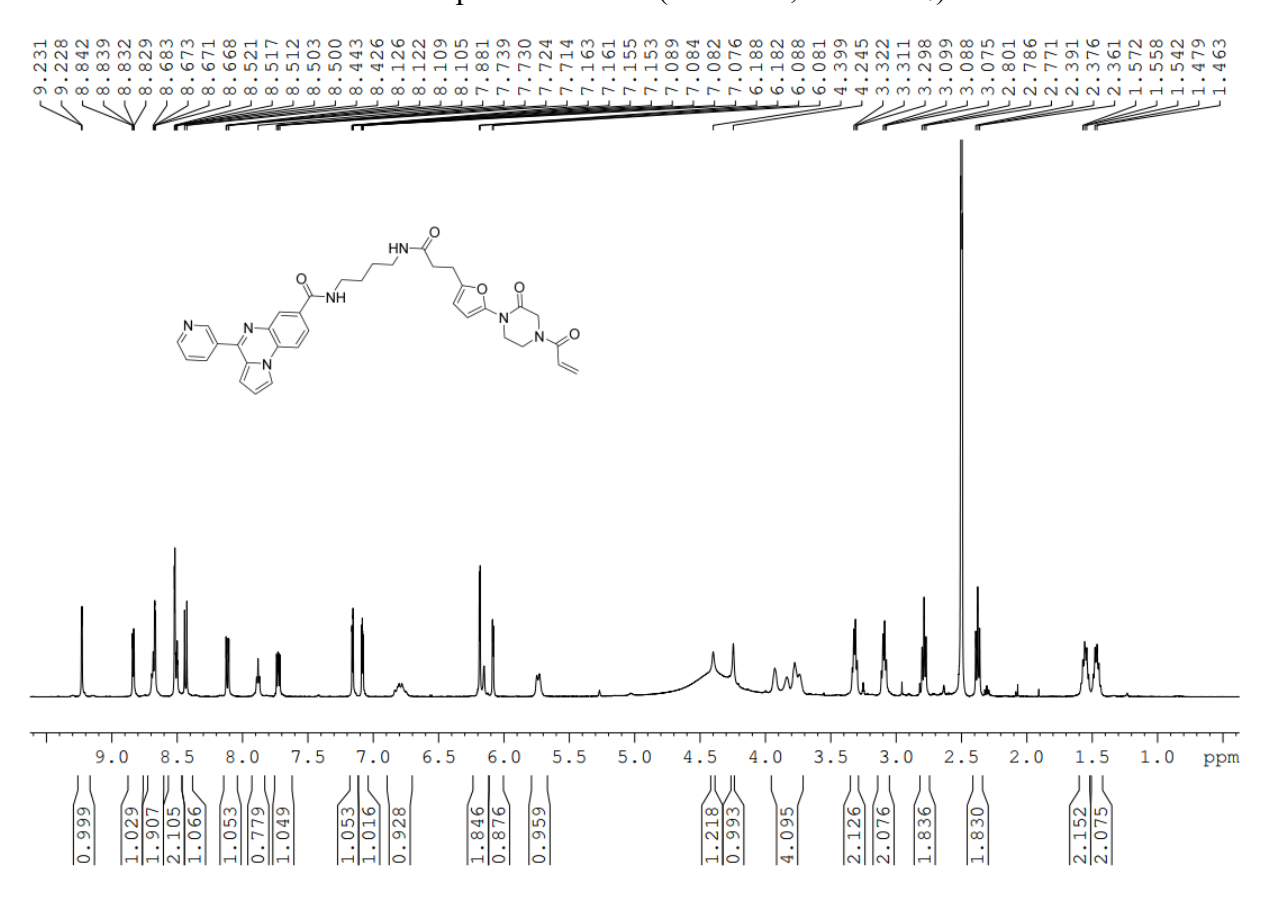
¹H NMR spectrum of **19b** (600 MHz, DMSO-*d*₆)



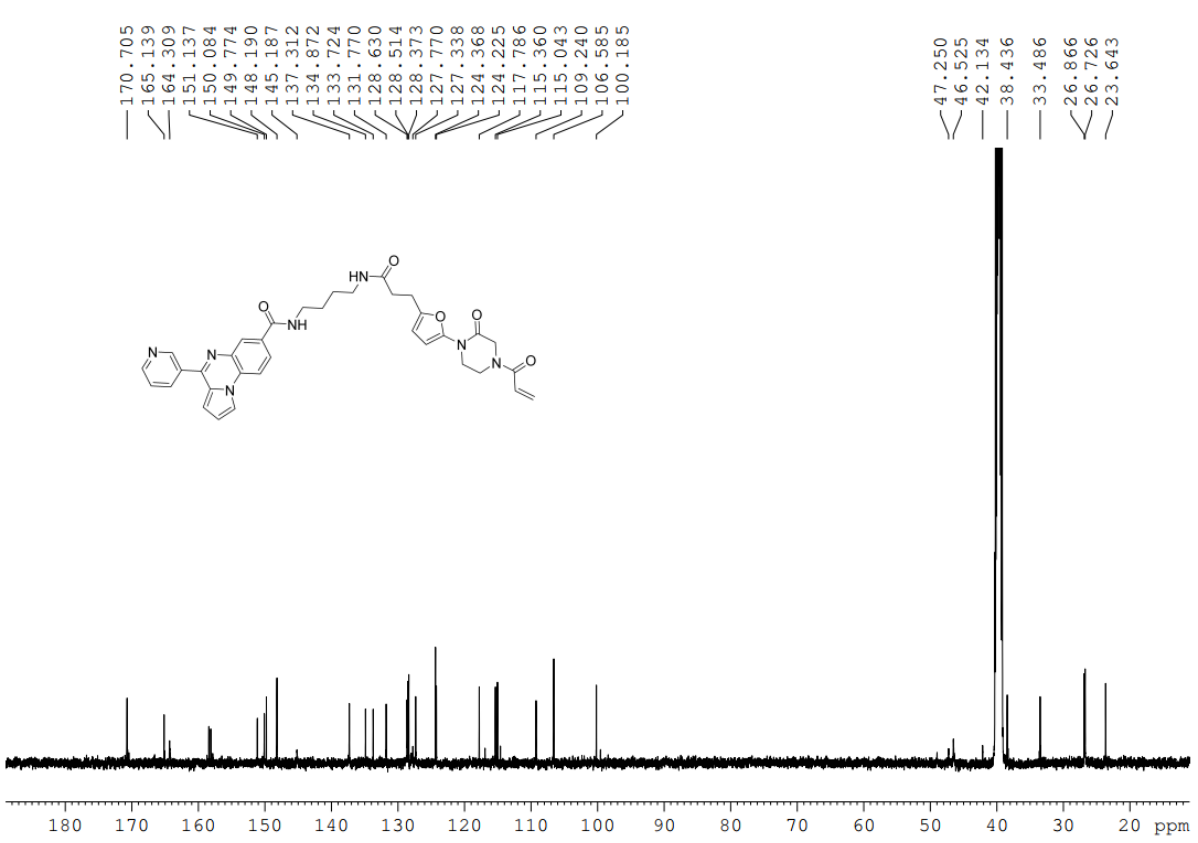
¹³C NMR spectrum of **19b** (151 MHz, DMSO-*d*₆)



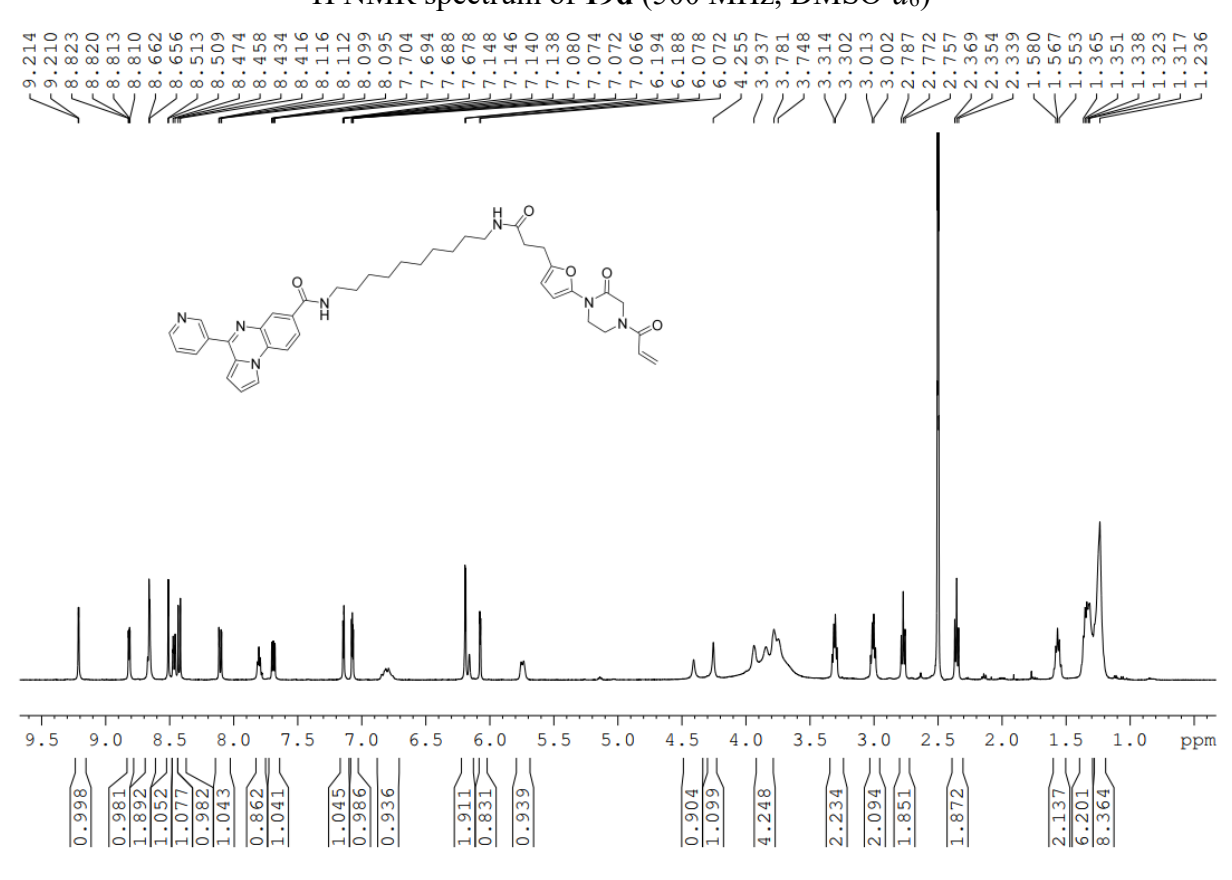
¹H NMR spectrum of **19c** (500 MHz, DMSO-*d*₆)



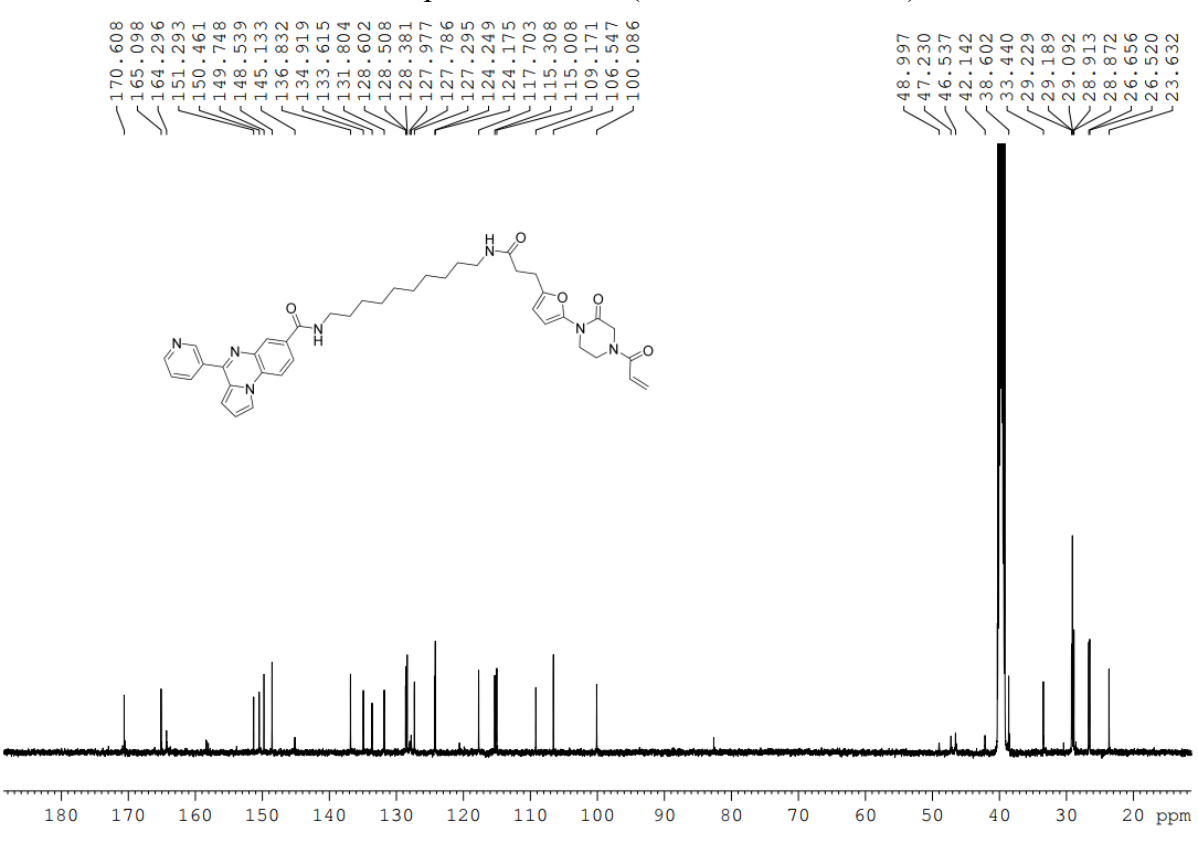
13 C NMR spectrum of **19c** (126 MHz, DMSO- d_6)



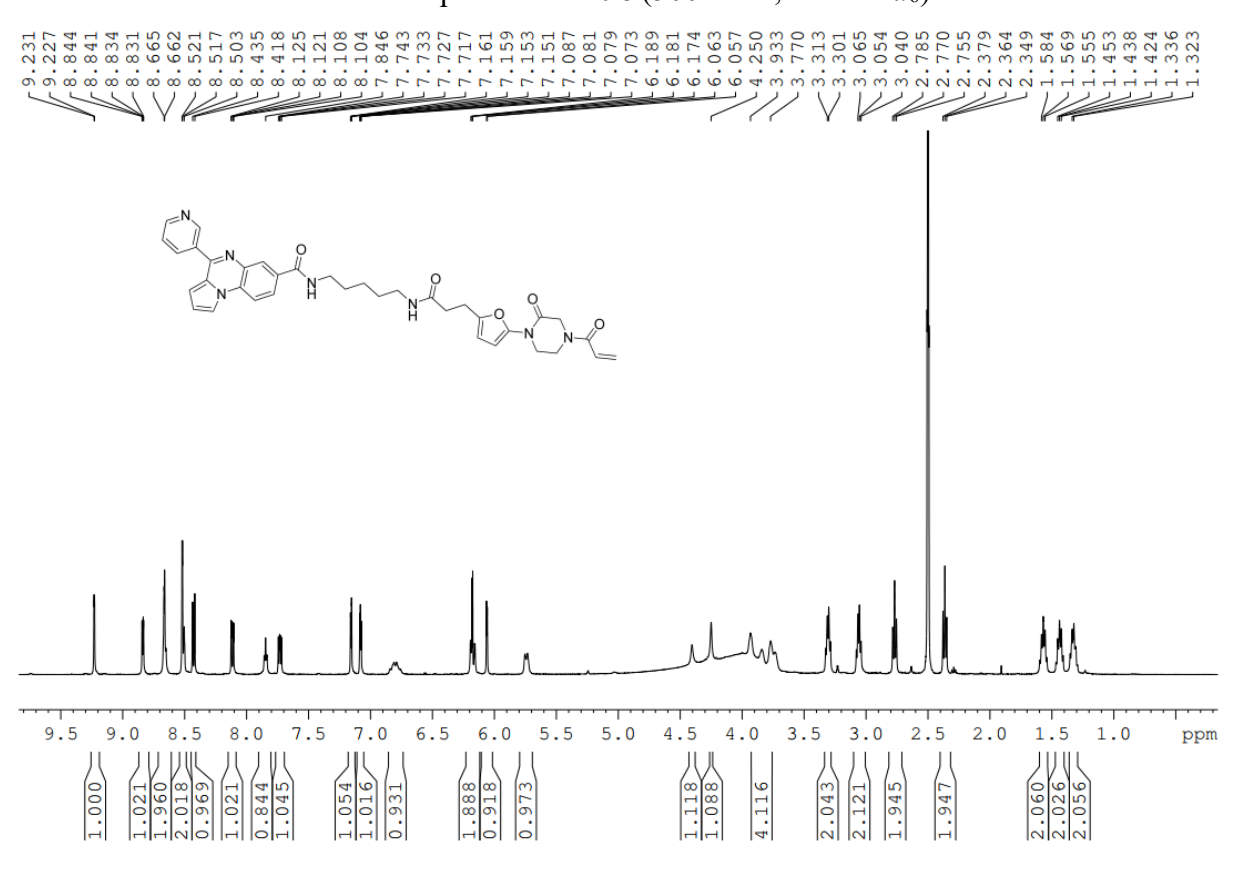
¹H NMR spectrum of **19d** (500 MHz, DMSO-*d*₆)



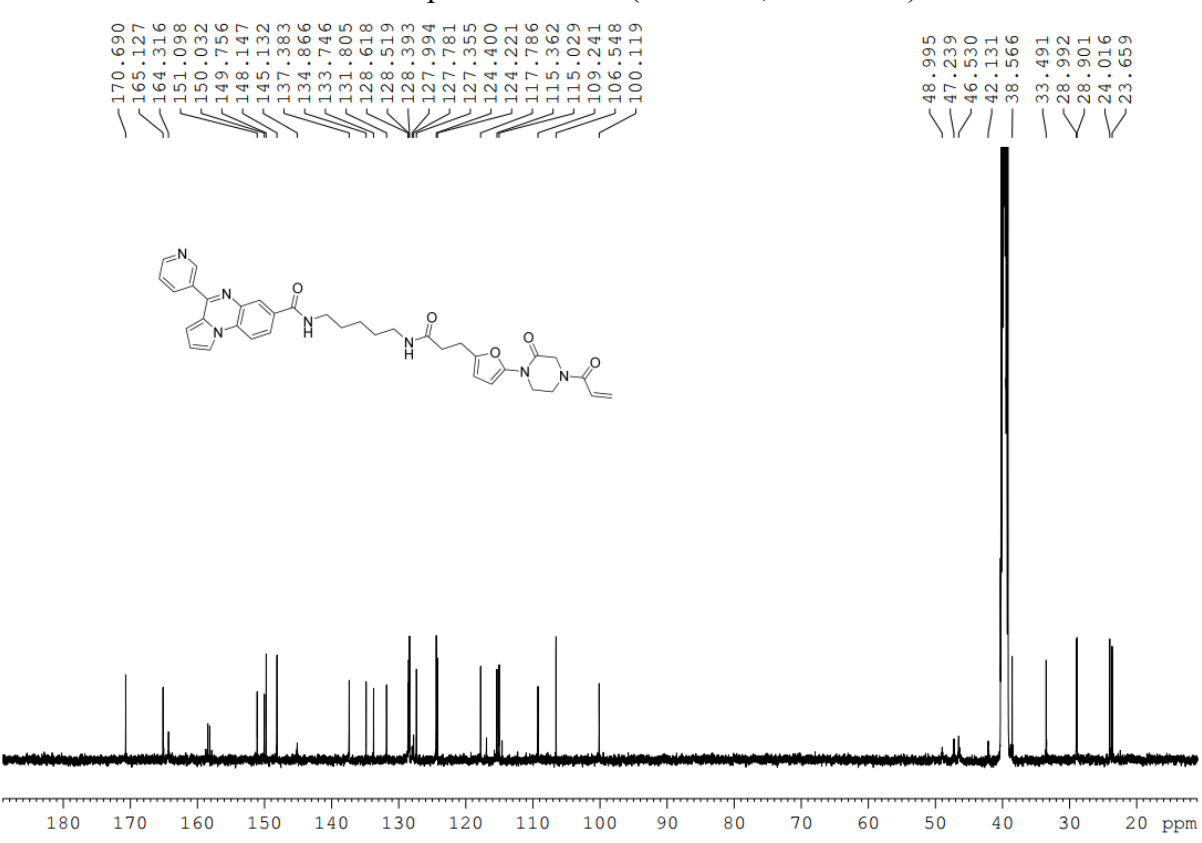
13 C NMR spectrum of **19d** (126 MHz, DMSO- d_6)



¹H NMR spectrum of **19e** (500 MHz, DMSO-*d*₆)

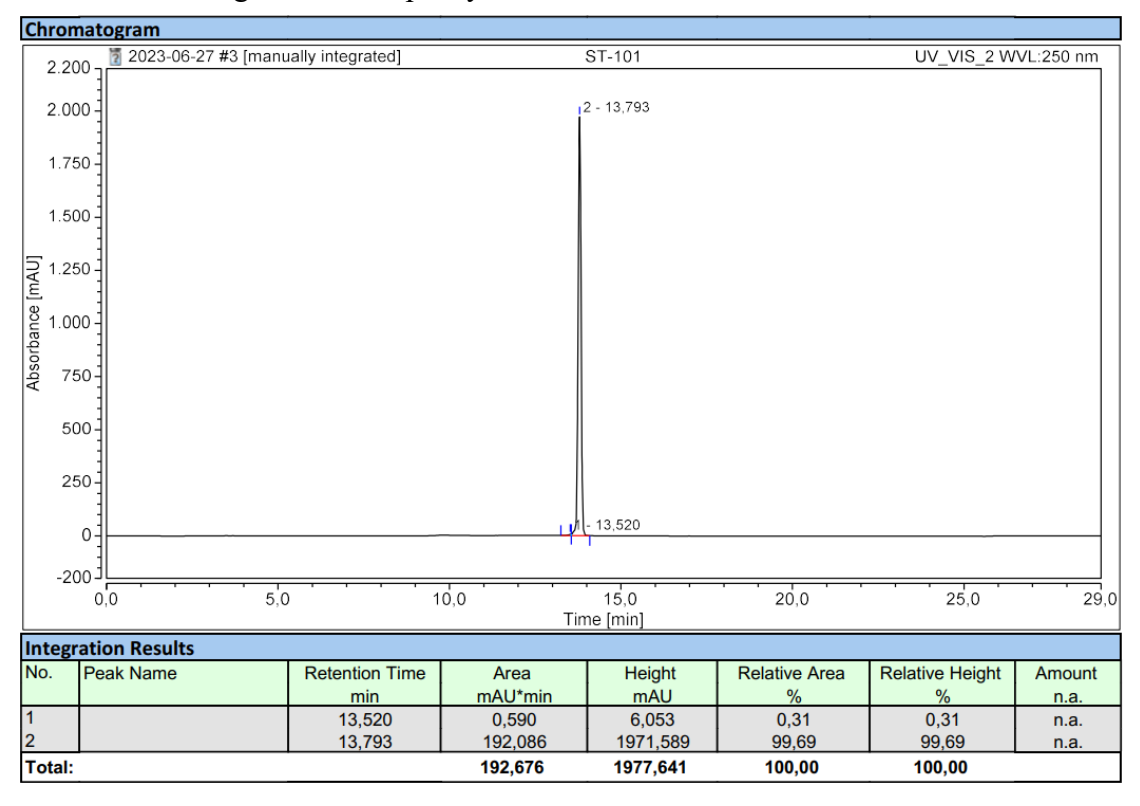


13 C NMR spectrum of **19e** (126 MHz, DMSO- d_6)

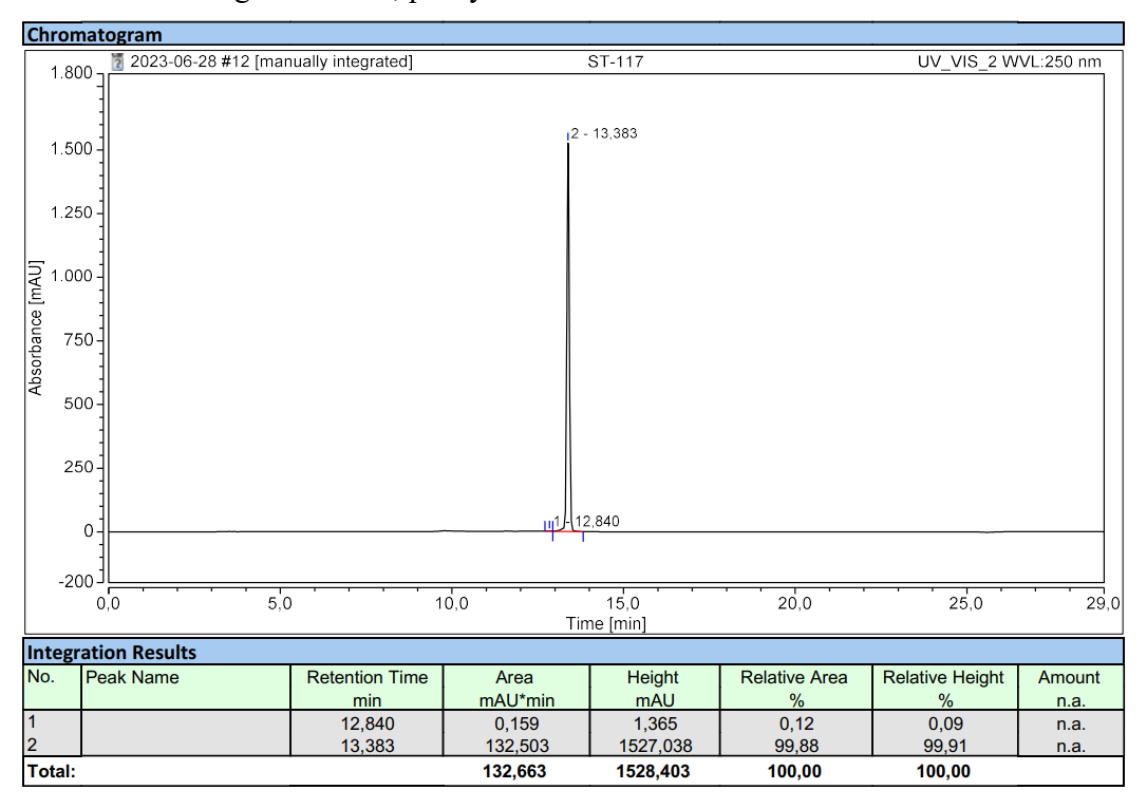


2. HPLC chromatograms

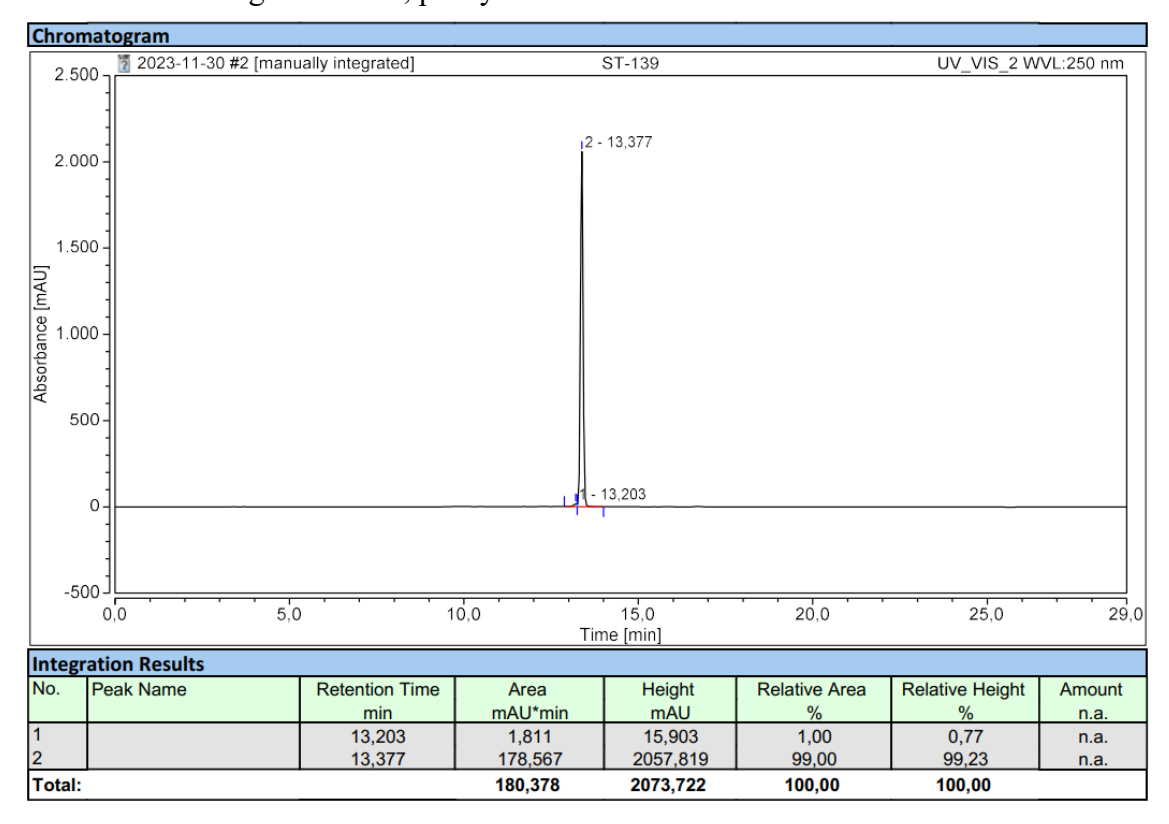
2.1 HPLC Chromatogram of 18a, purity 99.69%.



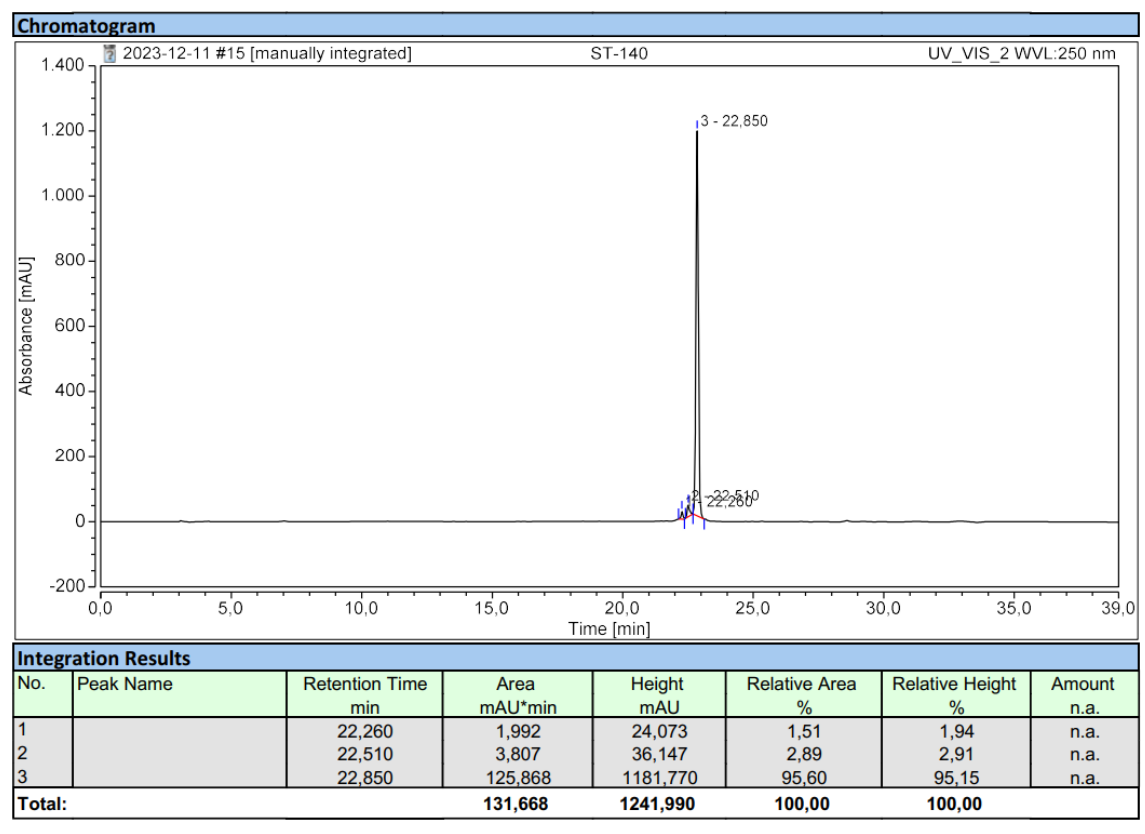
2.2 HPLC Chromatogram of 18b, purity 99.88%.



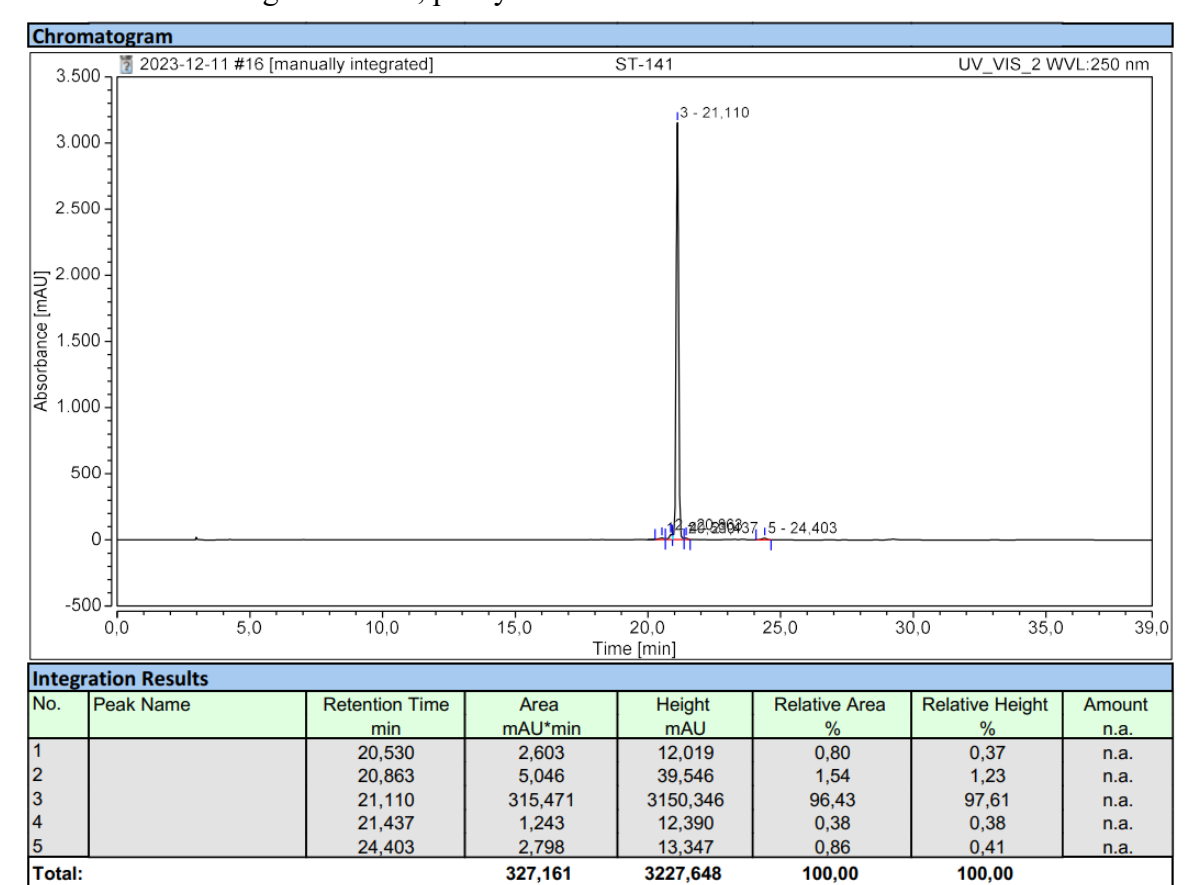
2.3 HPLC Chromatogram of 18c, purity 99.00%.



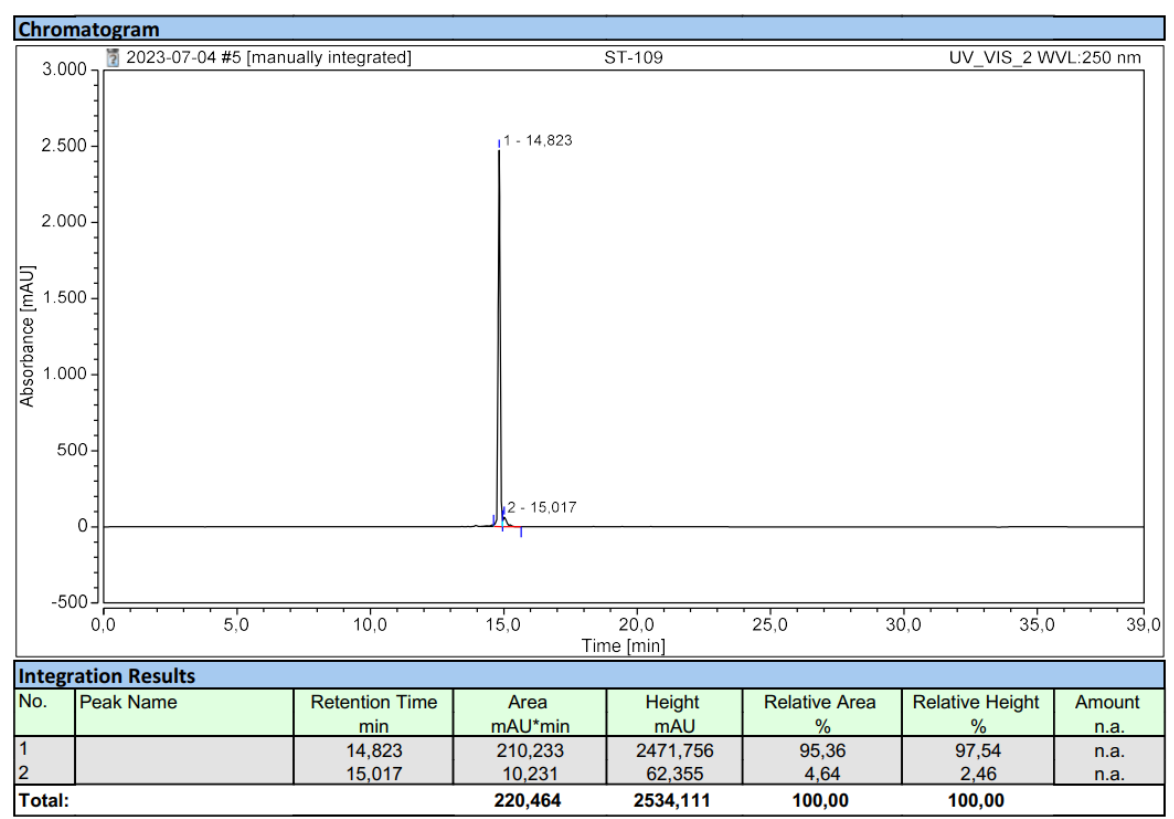
2.4 HPLC Chromatogram of 18d, purity 95.60%.



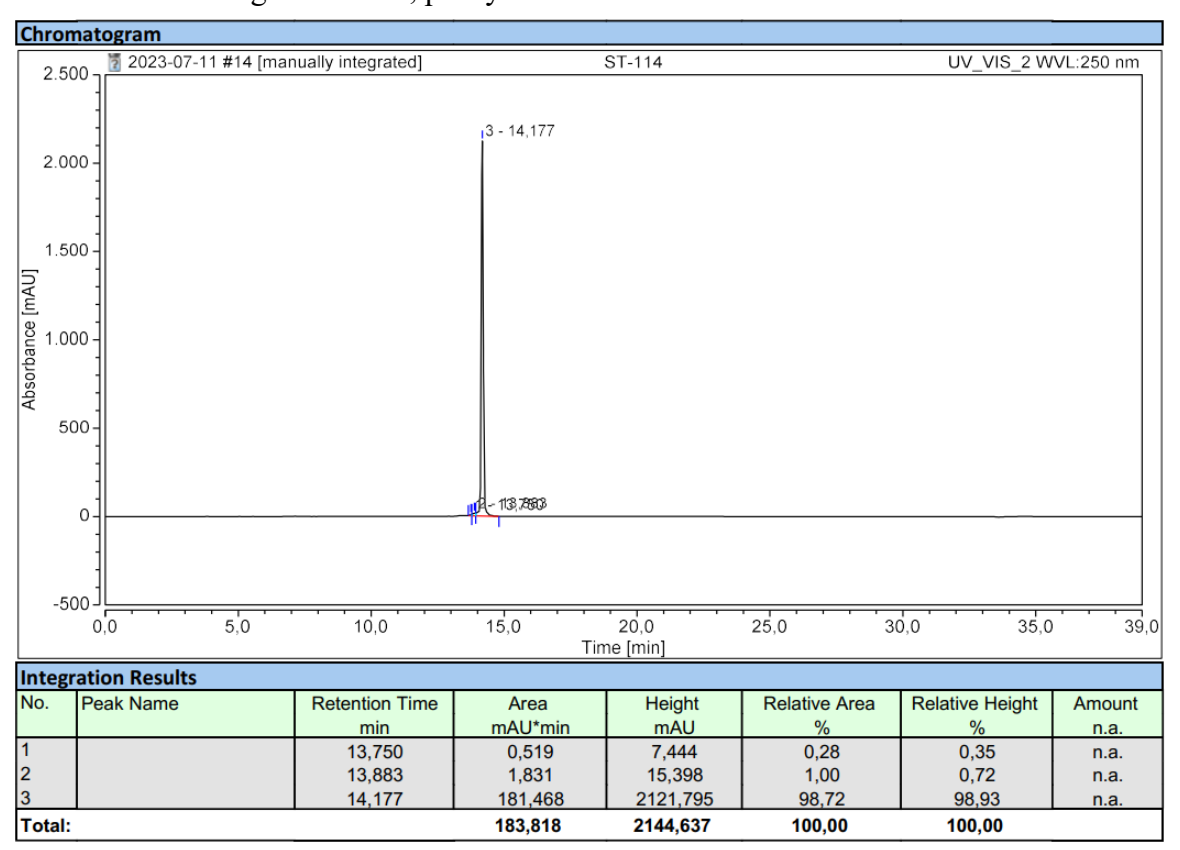
2.5 HPLC Chromatogram of 18e, purity 96.43%.



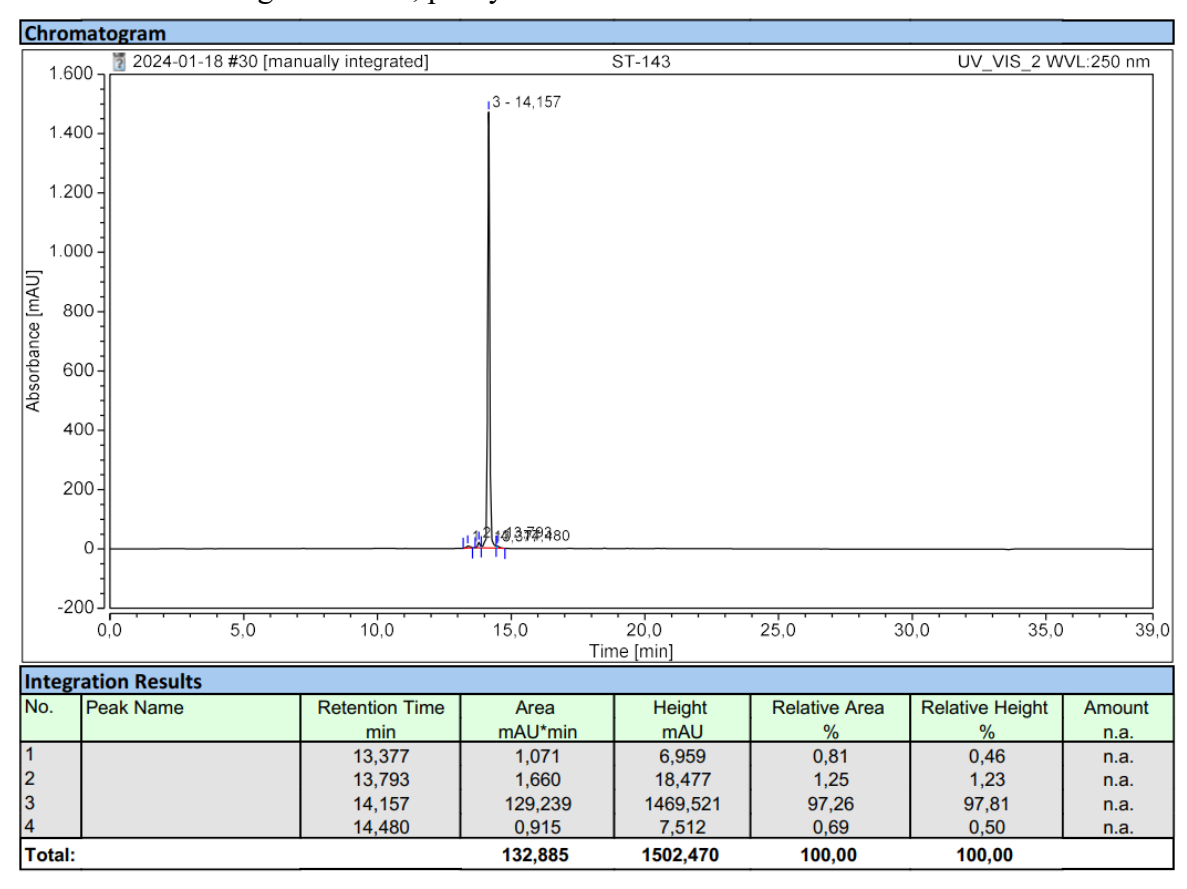
2.6 HPLC Chromatogram of 19a, purity 95.36%.



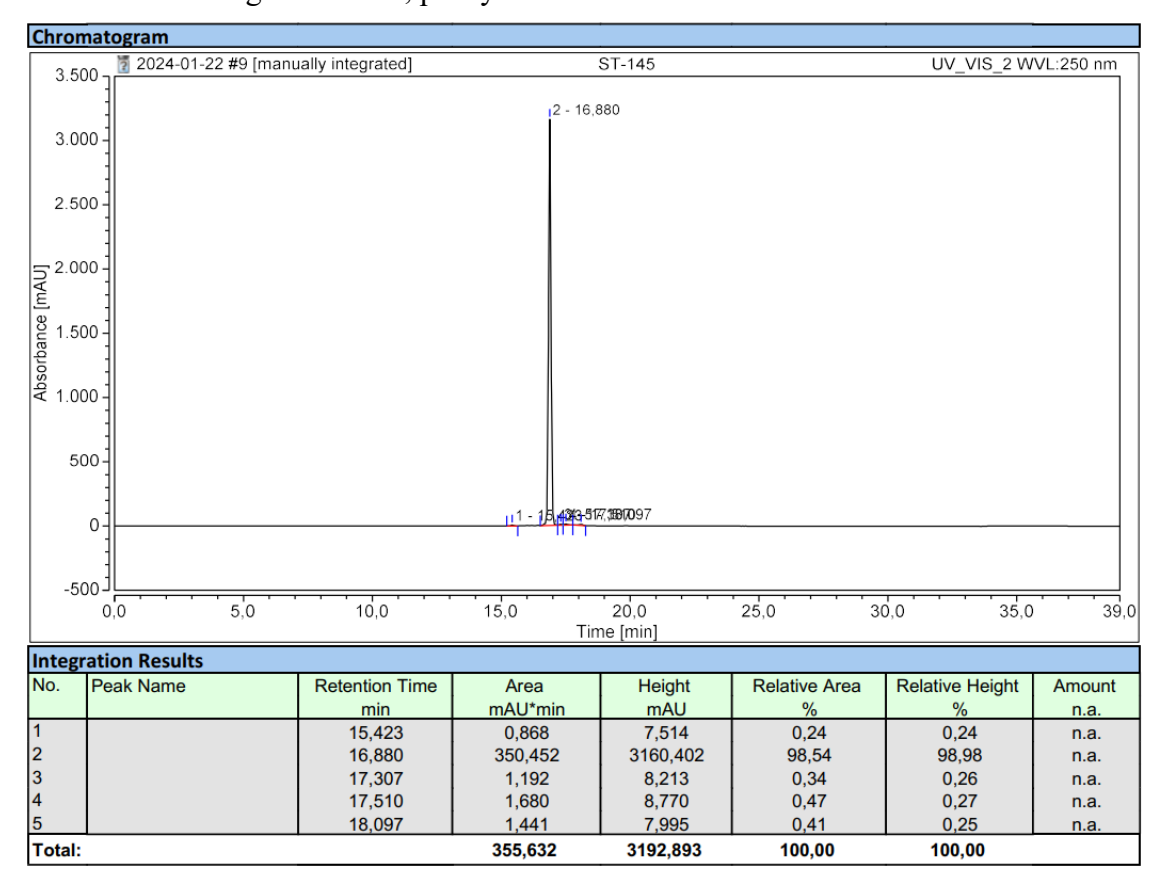
2.7 HPLC Chromatogram of 19b, purity 98.72%.



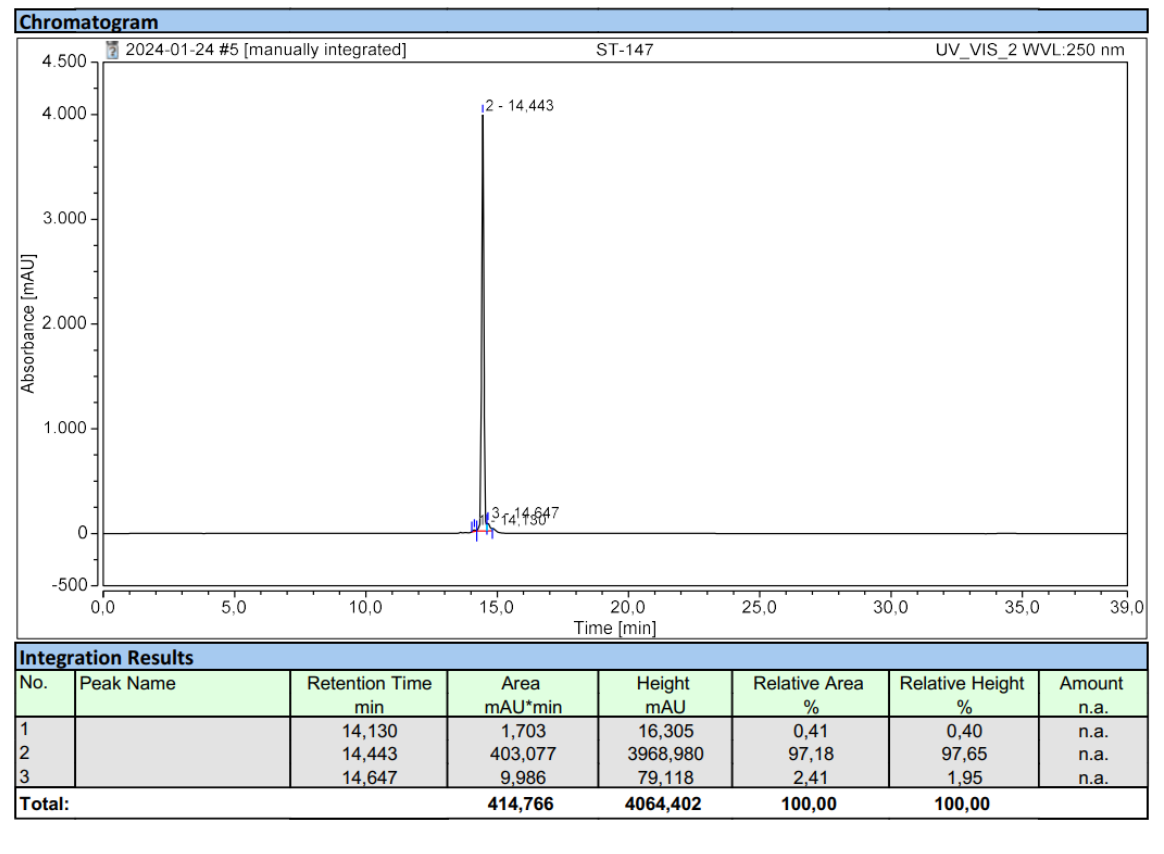
2.8 HPLC Chromatogram of 19c, purity 97.26%.



2.9 HPLC Chromatogram of 19d, purity 98.54%.



2.10 HPLC Chromatogram of 19e, purity 97.18%.



Acknowledgments

I still remember the first time I arrived in Germany four years ago, beginning my PhD journey, and now it's almost time to say goodbye. My experiences in Prof. Hansen's group feel like a beautiful dream. The friends I made here have been incredibly kind and supportive, leaving a lasting impression on me.

First, I want to express my deep appreciation to Prof. Hansen for accepting me as a PhD student in his group. He provided me with immense, selfless support in every aspect of my life. Starting a new life in an unfamiliar country was a significant challenge, but I consider myself fortunate to have had Prof. Hansen as my supervisor.

I'd like to share two stories from my time in his group. Since I had never been to Germany before, I didn't speak the language. One day, while discussing an experiment with Prof. Hansen, I wanted to show him some data, but my keyboard is a German keyboard. I struggled to type and joked that I wasn't used to a German keyboard. A few days later, I found a new English keyboard on my desk. I was genuinely touched by this gesture, even though it happened four years ago.

The second story involves my experiments. I chose challenging projects at the beginning. Although I successfully synthesized the final compounds, the biological aspects proved to be tough for me. After struggling with my initial two projects, I felt depressed and worried about my graduation. In that moment of despair, Prof. Hansen offered his support, reassuring me that I didn't need to stress about graduation and encouraging me to relax, reminding me that I had already done a good job. His words renewed my confidence and motivation. I am truly grateful to Prof. Hansen for everything he has done for me, his support has made my PhD experience fulfilling and rewarding.

Next, I want to thank all the members of Hansen's group. Their help throughout my PhD journey has been invaluable. Shiyang and Felix taught me how to perform western blots and apoptosis experiments. Irina assisted with MTT assays, and Cindy tested my DUBTACs compounds. Stephan, Daniel, Kathrin, Beate and others helped me with synthesis. Mattias always help me with IT problem. I will never forget the assistance you all provided.

I also want to thank Prof. Bendas and his group members. Thank you to Nico,

Philip, Marie, Michael, Leno and everyone else for your support.

Special thanks to Marion, Chris and other fellows for helping me with MS and NMR analysis.

Meanwhile, I've received so much help from my Chinese friends as well. Your support helped me through the tough days during my PhD.

Many thanks for China Scholarship Council, I can't finish my PhD study without your support!

Many thanks for Bonn International Graduate School of Drug Sciences (BIGS DrugS) for supporting my attendance at the conferences in Basel and Cambridge.

Lastly, I want to express my heartfelt gratitude to my family. Thank you for your nurturing and unwavering support over the years. Whenever I felt lost, you were always there to guide and comfort me, helping me regain my confidence. Throughout this long journey of study, you have been my strongest support.

Tao Sun 2025.07.01, Bonn